

Geometallurgical characterization of samples from Aitolampi graphite ore

Simon P. Michaux

Jesal Hirani

Alona Nad

Tero Korhonen

Sauli Rytkönen

Lorenza Sardisco

Johanna Tepsell

Nikos Apeiranthitis

Max Franzel

Duncan Pirrie

Dave Wray

Ester M. Jolis

Morven Davidson

Alan R. Butcher

GEOLOGICAL SURVEY OF FINLAND**DOCUMENTATION PAGE**

Authors Simon P. Michaux GTK Jesal Hirani X-Ray Minerals Services Finland Alona Nad GTK Tero Korhonen GTK Lorenza Sardisco X-Ray Minerals Services Finland Sauli Rytönen GTK Johanna Tepsell X-Ray Minerals Services Finland Nikos Apeiranthitis X-Ray Minerals Services Finland Max Franzel X-Ray Minerals Services Finland Duncan Pirrie University of South Wales Dave Wray Analytical Services Laboratory, University of Greenwich at Medway Ester M. Jolis GTK Morven Davidson X-Ray Minerals Services Finland Alan R. Butcher GTK	Date 8 th March 2023 Type of report Open File Work Report Commission by BATCircle 2.0 Project WP3.1
Title of report Geometallurgical characterization of samples from Aitolahti graphite ore	
Abstract <p>This report documents the characterization results from tests done on drill core samples from the Aitolahti graphite deposit. A Principal Component Analysis was done on the Aitolahti drill hole chemical assay data base. Based on these outcomes, 5 ore types were defined, which were sampled by Fennoscandian geologists and supplied to GTK Mintec. In addition to this, a further two samples from a pilot scale test tails were supplied. A total of 7 samples were characterized with the following:</p> <ul style="list-style-type: none"> • Chemical assays LECO S and LECO C • Inductively coupled plasma optical emission spectroscopy (ICP-OES) • Scanning micro-XRF analysis • Quantitative X-ray Diffraction Analysis (QXRD) • Energy Dispersive X-ray Fluorescence Spectroscopy (ED-XRF) • Laser Induced Breakdown Spectroscopy (LIBS) • Raman Spectroscopy • Fourier Transform Infrared Spectroscopy (FTIR) • Automated Mineralogy SEM analysis • Acid Mine Drainage (AMD) 	

Keywords Graphite, Aitolahti, Characterization, ore, pilot tailings			
Geographical area			
Map sheet N/A			
Other information			
Report serial 17/2023	Archive code		
Total pages 235	Language English	Price N/A	Confidentiality Public Domain
Unit and section Circular Economy Solutions KTR	Project code		
Jouko Nieminen - Circular Economy Solutions KTR Unit Head 	Associate Professor Simon P. Michaux - Circular Economy Solutions KTR 		

TABLE OF CONTENTS

1	Introduction	6
1.1	Work Package 3.1.1 Geometallurgical characterization of samples from Finnish graphite ore	6
1.2	Natural graphite	6
2	The Aitolahti deposit	7
2.1	Mineralization and metallurgy	8
3	Local community concerns	10
4	Environmental aspects	10
5	PCA Analysis of Chemical Assay database to Support Sample Selection	11
6	Data Correlation Pattern to Support Sample Selection	14
7	Sample Selection	20
7.1	The Five Orientation Samples Selected	20
8	Experimental Design for a Geometallurgical Program	23
9	Sample Preparation	26
10	Scanning Micro-XRF	28
11	Chemical assays	36
11.1	<i>Inductively coupled plasma optical emission spectroscopy (ICP-OES)</i>	36
12	Quantitative X-ray Diffraction Analysis (QXRD)	38
12.1	QXRD Whole-rock analysis	38
12.2	QXRD Clay fraction analysis	39
13	Energy Dispersive X-ray Fluorescence Spectroscopy (ED-XRF)	41
14	Laser Induced Breakdown Spectroscopy (LIBS)	44
14.1	Instrument parameters	45
14.2	Graphite ore samples	45
14.3	Graphite Tailings	47
15	Raman Spectroscopy	49
16	Fourier Transform Infrared Spectroscopy (FTIR)	53
17	Automated Mineralogy SEM analysis	56
17.1	Sample preparation to produce SEM polished blocks	56
17.2	Sample PA1-CAM	57
17.3	Sample QA2-CAM	60
17.4	Sample XA3-CAM	63
17.5	Sample YA4-CAM	65
17.6	Sample ZA5-CAM	68
18	Acid Mine Drainage	70
18.1	Soil contamination	74

18.2	Sulfide sulfur	74
18.3	ABA test	75
18.4	NAG test	75
18.5	NAPP	75
19	References	.81
20	Appendix A – BATCircle 2.0 Project Description	83
20.1	BATcircle Work Package Structure	84
20.2	How this report relates to the rest of the BATCircle 2 project	87
21	Appendix B - Sample Labelling Protocol	88
21.1	Unique rock type sample tag to help prevent labelling mistakes between sample groups	88
21.2	Deposit name	88
21.3	Rock types selected for study	88
21.4	First pass crush -3.35mm sub-sampling	88
21.5	Process path sub-group	88
21.6	Examples	89
22	Appendix C - Sample Preparation	91
23	Appendix D – Correlation Matrix analysis of Aitolahti assay	93
24	Appendix E – Principle component analysis of Aitolahti assay database	96
24.1	Principal component Method:	96
25	Appendix F - Class Selection of Ore Types in Aitolahti Chemical Assay Data	104
26	Appendix G – Scanning Micro-XRF Mapping	116
26.1	Sample PA1 Scanning Micro-XRF	116
26.2	Sample QA2 Scanning Micro-XRF	122
26.3	Sample XA3 Scanning Micro-XRF	133
26.4	Sample YA4 Scanning Micro-XRF	139
26.5	Sample ZA5 Scanning Micro-XRF	150
27	Appendix H - Major and Trace Elements (ICP-OES / MS - XMS)	156
28	Appendix I – X-Ray Diffraction (QXRD) spectra of samples measured	158
29	Appendix J – Comparsion of different XRF methods	172
30	Appendix K - Raman analysis of Graphite ore samples and tailings	181
30.1	Method	182
30.1.1	Ore samples	182
30.1.2	Tailings	182
30.2	Results	183
30.2.1	PA1-C	184
30.2.2	QA2-C	186

30.2.3	XA3-C	188
30.2.4	YA4-C	190
30.2.5	ZA5-C	193
30.2.6	Aitolahti Pilot Tailings West APTW-C	195
30.2.7	Aitolahti Pilot Tailings East APTE-C	196
30.3	Appendix K - Conclusions	198
31	Appendix L - Automated Mineralogy SEM	199

1 INTRODUCTION

This report documents the characterization results from tests done on drill core samples from the Aitolampi graphite deposit. This report is Deliverable D3.1.1 (Report on characterization results of collected samples) from Work Package 3.1 in the BATCircle 2.0 project (see Appendix A).

1.1 Work Package 3.1.1 Geometallurgical characterization of samples from Finnish graphite ore

Partners: GTK, Fennو

Aim of this Task is to find most efficient environmentally safe purification methods for floated graphite concentrates. The approach for this is a geometallurgical study to identify the key geological and mineralogical factors that affect the processing of the graphite. Characterization will be done at each process using analysis methods as XRD, Raman, ICP-MS, SEM/EDS and Optical Microscopy. This will be done to support Task 3.1.2.

1.2 Natural graphite

NG is mined from deposits in metamorphic rocks such as marble, schist, and gneiss, as well as vein deposits. Under long-term high temperature and pressure geological environments in sedimentary rocks, NG is formed from carbon-rich organics (Zhao, et al., 2022; Robinson Jr., Hammarstrom, & Olson, 2017). Commercial deposits occur in three different geologic settings, which are discussed next.

Amorphous graphite is a commercial term for earthy to compact fine-grained graphite that is typically formed during the thermal metamorphism of coal. Commercial deposits typically contain over a million metric tons of ore with a carbon grade of up to 75%. Amorphous graphite can be used to produce lubricants (Robinson Jr., Hammarstrom, & Olson, 2017).

Flake graphite is the commercial classification for well-developed crystal platelets with sizes between 40 micrometers (μm) and 4 centimeters (cm). These platelets are disseminated in beds of carbonaceous sediments and have been subjected to amphibolite-facies or higher-grade regional metamorphism. Commercial deposits typically contain over 200,000 tons of ore with a grade of more than 8%, although lower grade deposits are also known. This type of deposit can be found in belts of crystalline metamorphic rock from the Archean or late Proterozoic age. The flake graphite is classified into four different sizes, which are jumbo, large, medium, and fine. Flake graphite is used, for example, in the battery and refractory industries (INN, 2021; Robinson Jr., Hammarstrom, & Olson, 2017).

Lump or chip graphite, also known as vein graphite, is the commercial classification for interlocking aggregates of rough graphite crystals located in veins of fractures in igneous and crystalline metamorphic rocks from the Precambrian age. This type of deposit is rare, and no reliable data on the tonnages is available. Vein graphite is used in lubricants (Robinson Jr., Hammarstrom, & Olson, 2017).

Next the mining methods are discussed. Flake graphite is often found in deposits that are close to the surface, and depending on how much weathering has occurred, it can be mined using either hard-rock or soft-rock mining techniques. The extraction of amorphous graphite involves using methods often used in coal mining. Open-pit or traditional shaft mining techniques can be used to extract vein graphite (Damm & Zhou, 2020).

2 THE AITOLAMPI DEPOSIT

The Aitolampi graphite prospect is owned by Beowulf Mining plc, which is a UK registered exploration and development company. In 2016, a deposit was discovered 40 km southwest of Outokumpu at Heinävesi (Beowulf Mining, 2022). The location on the Finnish map is shown in Figure 1.



Figure 1. Aitolampi graphite prospect location (modified from (Google Earth, 2022)

The project is still in the exploration stage. In 2021, the Finnish Safety and Chemicals Agency (TUKES) authorized an extension for the previous exploration permit, and now ongoing exploration can continue till 2024. The 407.4 ha exploration area (Pitkäjärvi, ML2016:0040) is shown in Figure 2.

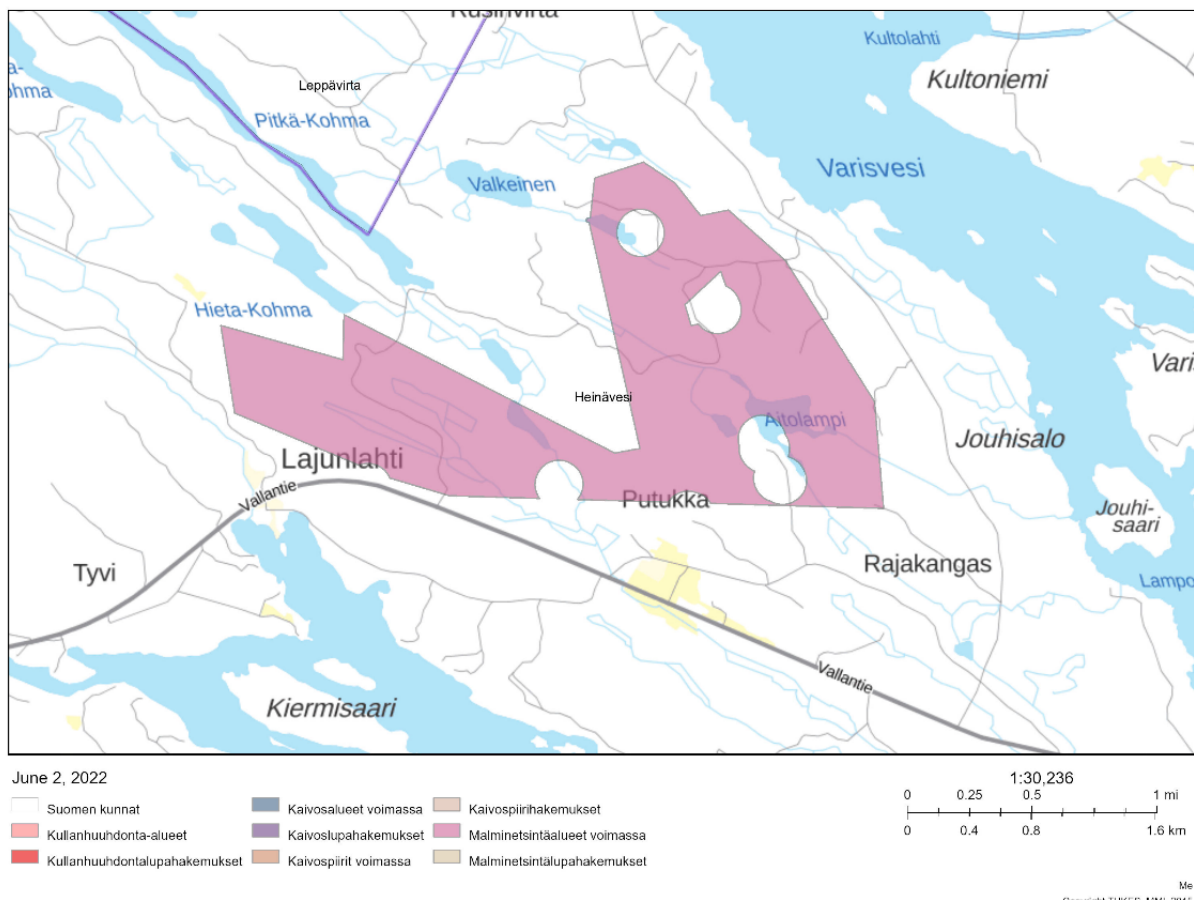
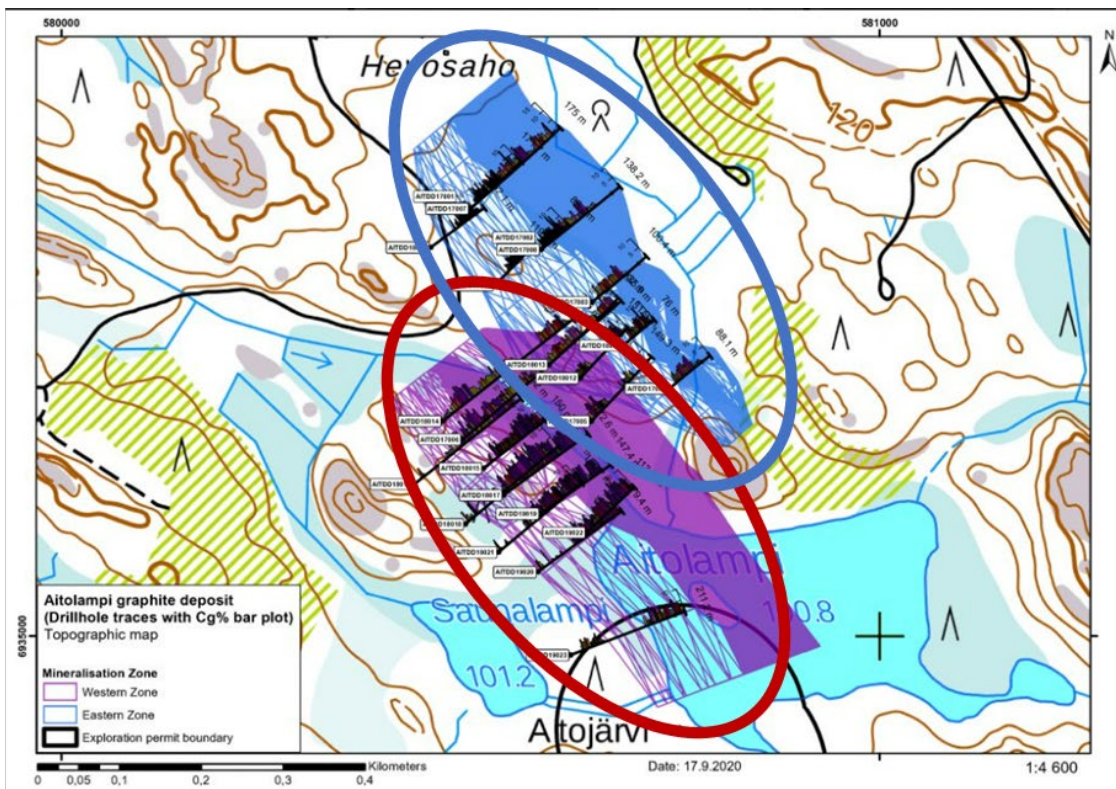


Figure2. Aitolampi exploration area marked on red (TUKES; MML, 2015)

The latest mineral resource estimation (MRE) was conducted on August 28th, 2019. According to the global JORC Code (2012 edition), the indicated and inferred resource of 26.7 Mt at 4.8% Total Graphitic Carbon (TGC) for 1275000 tons of contained graphite was estimated. For the whole deposit, the estimated sulfur (S) content was 4.7% (Beowulf Mining, 2022).

2.1 Mineralization and metallurgy

The Aitolampi graphite schist occurs on a folding limb within a high-metamorphic quartz-feldspar-biotite gneiss. The graphite mineralization is found in two zones, which are referred to as the eastern and western lenses. The drill program has confirmed a strike length of at least 525 m for the eastern zone and 530 m for the western zone (Beowulf Mining, 2022). The mineralization zones with MRE data are presented in Figure 3.



■ Western zone: Indicated + Inferred = 17.2 Mt @TGC 5.2%; S 4.8%

■ Eastern zone: Indicated + Inferred = 9.5 Mt @TGC 4.1%; S 4.5%

Figure3. Aitolampi mineralization zones (modified from Beowulf Mining, 2022)

Metallurgical test-work including purification and characterization tests for three composited quarter drill core samples MET-17001, MET-17002, and MET-17003 was conducted in 2017. Metallurgical test-work was performed by SGS Minerals Services in Canada and characterization was performed by ProGraphite GmbH in Germany (Beowulf Mining, 2022). The metallurgical test work result for drill core samples is shown in Table 5. In the table, the flake size is shown in μm and in Mesh, and the C(t) stands for total carbon grade.

Table 1. Metallurgical test results of Aitolampi ore (Beowulf Mining, 2022)

Flake type			Fraction in %		
Flake size	Size in μm	Size in Mesh	MET-17001	MET-17002	MET-17003
Jumbo	> 300	> 48	1.6	0.6	0.6
Large	180–300	80–50	17	12.2	13.4
Medium	150–180	150–80	30	26.8	29.2
Fine	< 106	< 150	51.4	60.4	56.8
C(t) concentrate (%)			96.8	97.2	97.5
Open Circuit Graphite Recovery (%)			87.3	77.8	91.4

Based on the results (see Table 5.) the graphite ore contains 0.6–1.6% jumbo sized flakes, 12.2–17% large flakes, and 26.8–30% medium sized flakes. The fines ranged from 51.4 to 60.4%. The overall recovery was

77.8-91.4% with a 96.8-97.5% carbon grade. According to Beowulf Mining (2022), there are multiple aspects which are benefiting the explored deposit in the LIB graphite markets. For example, with process optimization, the 99.95 % purity, which is required for the LIB markets, may be possible to achieve. The studied graphite also shows high crystallinity, with a degree of graphitization of 98%, and the specific surface area is similar to that of high-quality flake graphite from China. In addition, Aitolampi graphite also has some other good features suitable for other applications like refractories, lubricants, and foundries.

3 LOCAL COMMUNITY CONCERNS

Even though the project is in the exploration stage, multiple concerns have been raised. As in the case of any project of this size, most concerns are related to how the mine affects the surrounding nature and local fauna. Non-governmental organizations, Pro Heinävesi, and the Finnish Association for Nature Conservation have summarized their concerns as statements against the mining project, which are presented in Table 6.

Table 2. Concerns related to Aitolampi graphite project

Concern	Reason
Small particle pollution	Small particle pollution may have an impact on local fauna and the environment by causing heavy metal enrichment.
Noise, ground vibration and odour nuisance	People and fauna near the possible mine can become disturbed.
Beneficiation and tailings	Beneficiation by flotation will cause process waters and tailings containing sulfides and heavy metals, which can pollute local environment.
Asbestos	In similar kinds of deposits, tremolite and actinolite have been present.
Sulfidic sulfur	Acid mine drainage and lack of neutralization capacity. As example, consider the Särkiniemi mine (Leppävirta, Finland) (Leskinen, 2020).

Source: Lehtinen (2020); PRO Heinävesi (2018); ISY-2004-Y-210 (2005)

4 ENVIRONMENTAL ASPECTS

In this section, the focus is put on environmental problems related to the waste created in mines. Also, waste types and environmental aspects related to open-pit mining, graphite deposits, and beneficiation processing will be discussed. The focus will be put more on the sulfidic tailings, as in this study the raw material is sulfidic tailings.

As the target material grade is usually low in the known deposit, high volumes of waste are generated during different processing stages. The generated waste can cause multiple environmental problems, including acid mine drainage (AMD) and runoff waters containing dissolved metals (Blowes, et al., 2014). The risks are real before, during, and after the operations, of which there are multiple examples around the world like Brumadinho dam disaster in Brazil and case Talvivaara in Finland. It is hard to estimate the amount of waste created, but one estimate is that over 100 billion tons of solid waste are generated annually worldwide by the mining industry alone (Tayebi-Khorami et al., 2019).

The studied deposits occur in black schist, which is a common rock type in Finland. In addition to graphite, the host rock usually contains 5-10 wt.% sulfur, some metals like zinc and nickel, and small amounts of copper and cobalt. Typically, the metal grades are less than 0.1 wt.%. The main sulfide minerals are pyrite and pyrrhotite, with some minor amounts of other sulfides like sphalerite. (Törmänen & Tuomela, 2021).

5 PCA ANALYSIS OF CHEMICAL ASSAY DATABASE TO SUPPORT SAMPLE SELECTION

A Principal Component Analysis was done on the Aitolampi drill hole chemical assay data base (shown in Appendix E). The correlation matrix of this data is shown in Appendix D. This analysis was done using the IoGAS analysis software. Figure 4 shows the first and second principal component made up from Eigen values calculated (Appendix G). Based on this analysis, the Aitolampi drill hole chemical assay data set was split up into five Classes. Figures 4 to 8 shows the principal components plotted against each other, by Class.

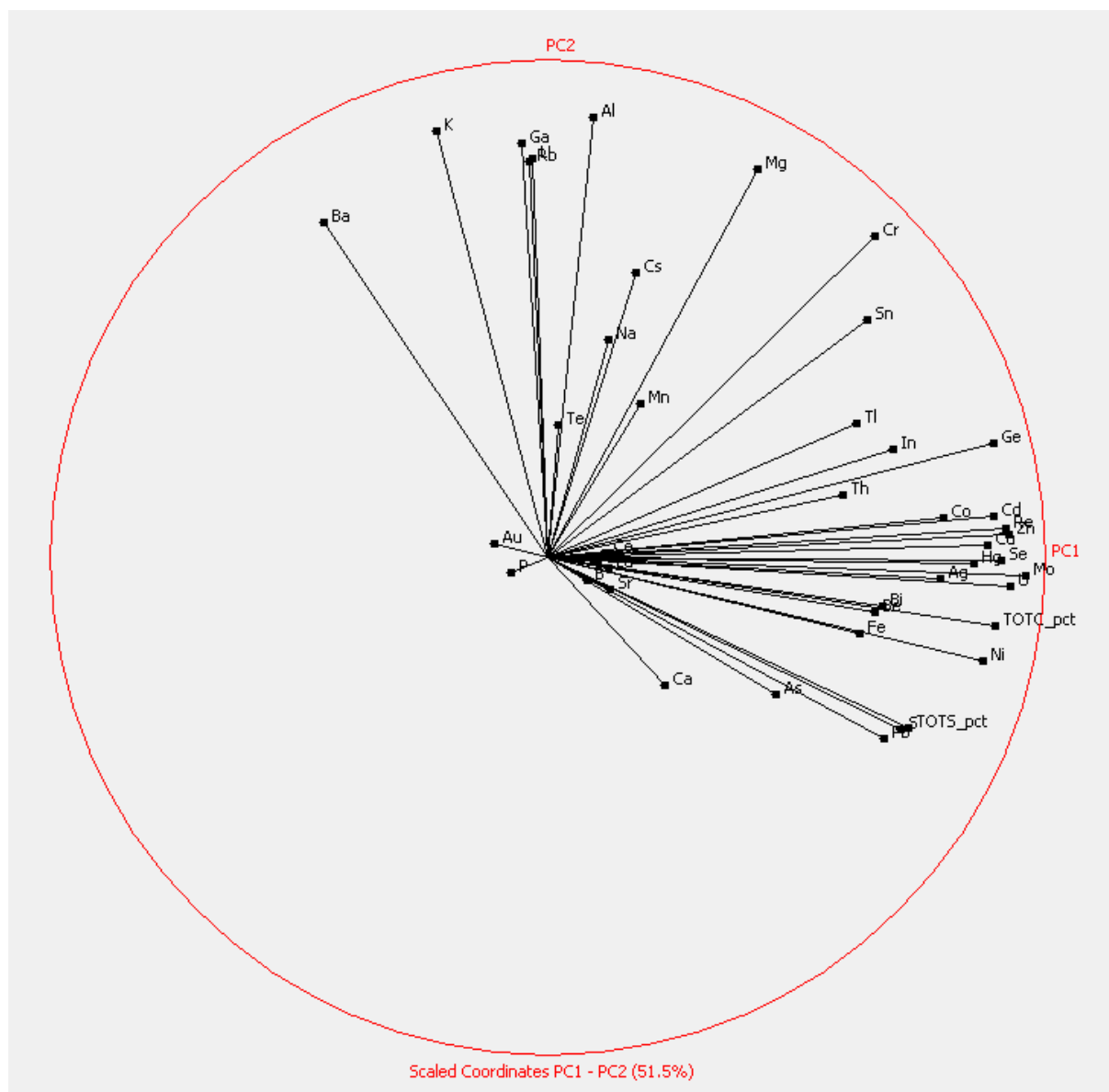


Figure 4. PC1 vs. PC2 (Drill Hole chemical assay database)

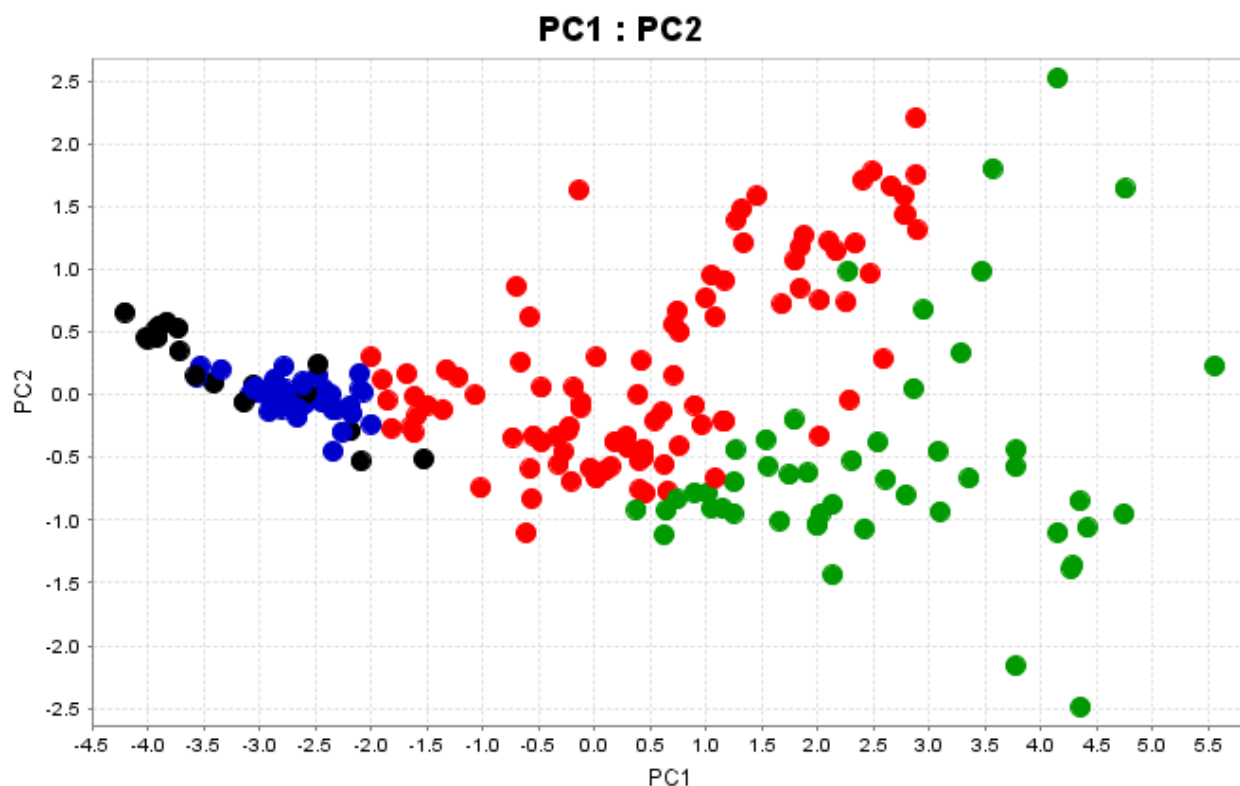


Figure 5. PC1 vs. PC2, by Class (Drill Hole chemical assay database)

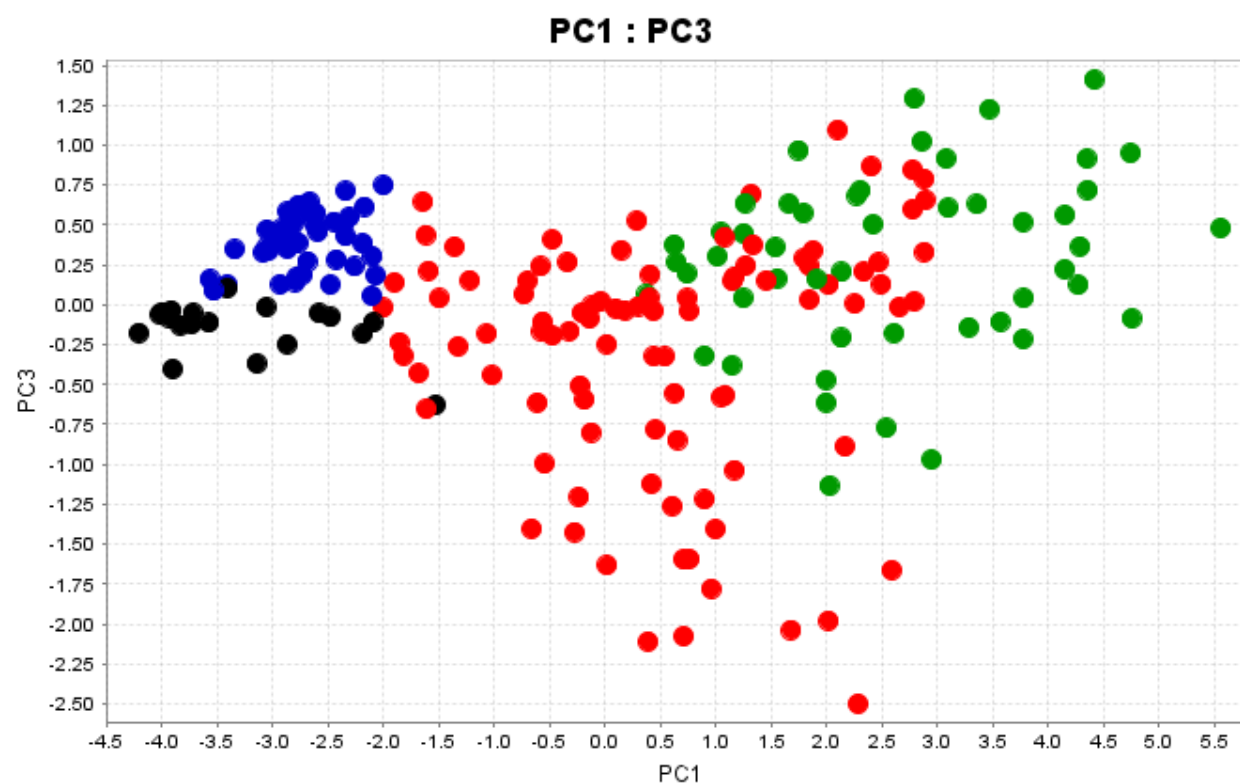


Figure 6. PC1 vs. PC3, by Class (Drill Hole chemical assay database)

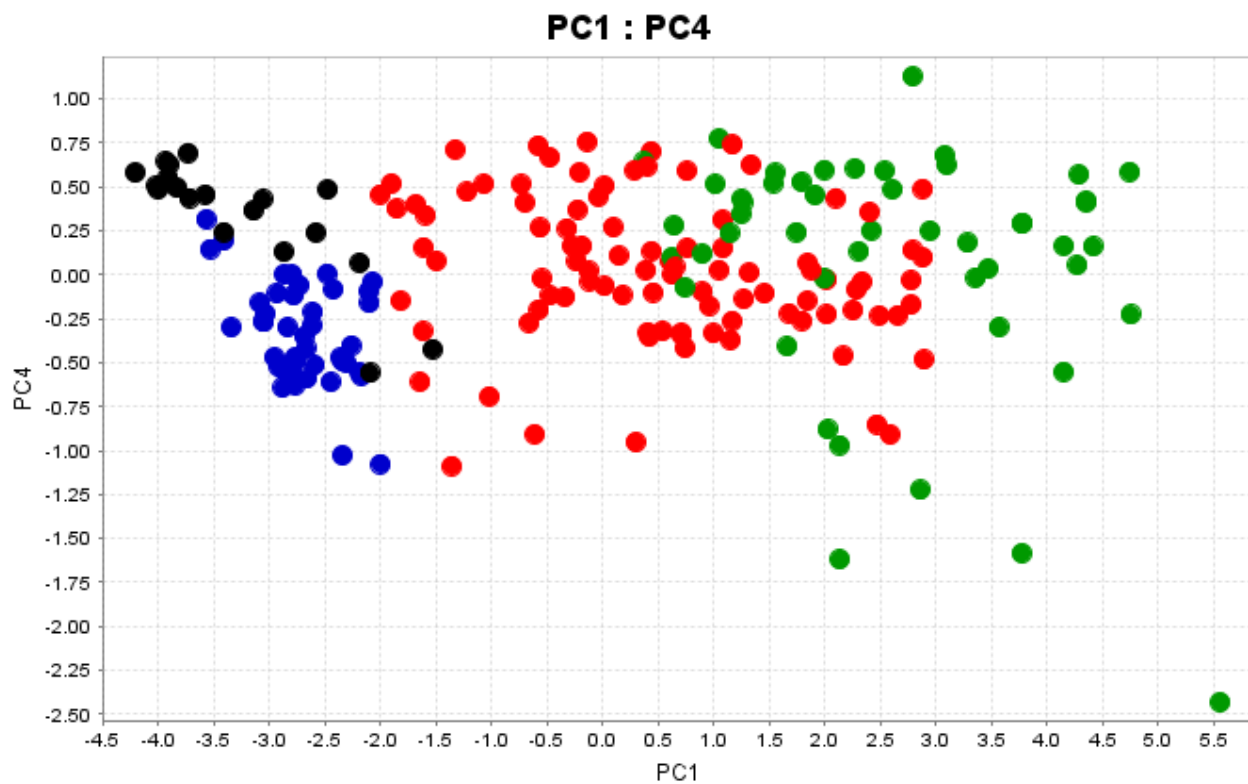


Figure 7. PC1 vs. PC2, by Class (Drill Hole chemical assay database)

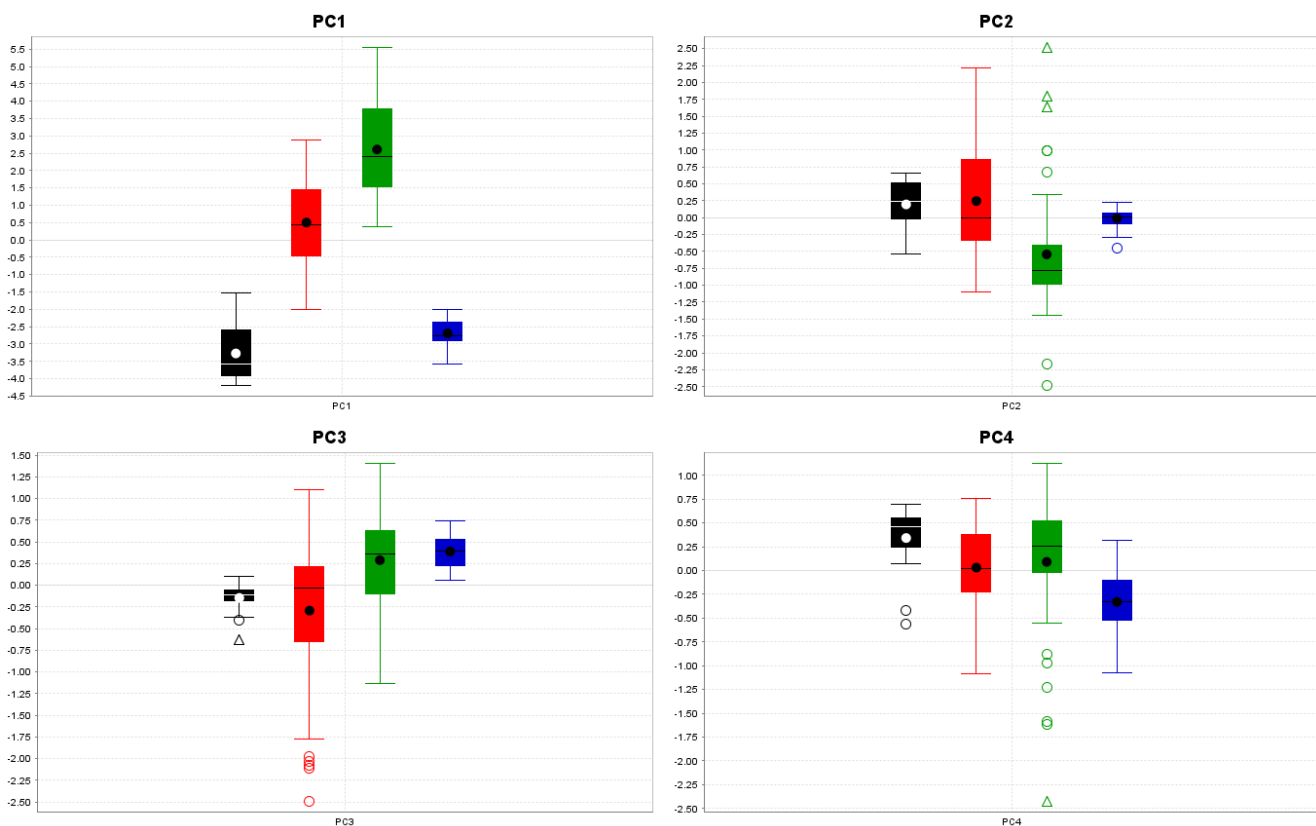


Figure 8. Principal Component Eigen Values, by Class (Drill Hole chemical assay database)

6 DATA CORRELATION PATTERN TO SUPPORT SAMPLE SELECTION

Using the PCA plots in Figures 9 to 17, in Appendices E & F, and the correlation matrix in Appendix D, the elements that had greater influence and control over variability in the data set were extracted from the full data set to be examined more closely. Table 7 shows a second correlation matrix to examine how these influential elements might relate to each other.

Table 7. Correlation matrix of the elements that control variability in the Aitolampi Drill Hole chemical assay database

Correlation	TOTC_pct	TOTS_pct	Co_ppm	Cu_ppm	Fe_pct	Mg_pct	Mo_ppm	Zn_ppm
TOTC_pct	1	0.84	0.78	0.68	0.77	0.28	0.87	0.75
TOTS_pct	0.84	1	0.78	0.48	0.94	0.045	0.63	0.49
Co_ppm	0.78	0.78	1	0.66	0.81	0.41	0.69	0.61
Cu_ppm	0.68	0.48	0.66	1	0.36	0.37	0.85	0.87
Fe_pct	0.77	0.94	0.81	0.36	1	0.16	0.52	0.37
Mg_pct	0.28	0.045	0.41	0.37	0.16	1	0.33	0.38
Mo_ppm	0.87	0.63	0.69	0.85	0.52	0.33	1	0.95
Zn_ppm	0.75	0.49	0.61	0.87	0.37	0.38	0.95	1
Ba_ppm	-0.5	-0.6	-0.25	-0.33	-0.37	0.25	-0.42	-0.35
Bi_ppm	0.7	0.73	0.62	0.5	0.65	0.2	0.59	0.51
Ni_ppm	0.92	0.91	0.83	0.68	0.87	0.19	0.82	0.71
U_ppm	0.85	0.61	0.65	0.82	0.5	0.31	0.96	0.9
Se_ppm	0.73	0.53	0.67	0.95	0.4	0.34	0.89	0.9
Ge_ppm	0.75	0.57	0.77	0.83	0.55	0.56	0.83	0.81
Cd_ppm	0.69	0.41	0.55	0.88	0.28	0.41	0.92	0.99

Correlation	Ba_ppm	Bi_ppm	Ni_ppm	U_ppm	Se_ppm	Ge_ppm	Cd_ppm
TOTC_pct	-0.5	0.7	0.92	0.85	0.73	0.75	0.69
TOTS_pct	-0.6	0.73	0.91	0.61	0.53	0.57	0.41
Co_ppm	-0.25	0.62	0.83	0.65	0.67	0.77	0.55
Cu_ppm	-0.33	0.5	0.68	0.82	0.95	0.83	0.88
Fe_pct	-0.37	0.65	0.87	0.5	0.4	0.55	0.28
Mg_pct	0.25	0.2	0.19	0.31	0.34	0.56	0.41
Mo_ppm	-0.42	0.59	0.82	0.96	0.89	0.83	0.92
Zn_ppm	-0.35	0.51	0.71	0.9	0.9	0.81	0.99
Ba_ppm	1	-0.51	-0.48	-0.41	-0.38	-0.23	-0.31
Bi_ppm	-0.51	1	0.65	0.53	0.56	0.56	0.46
Ni_ppm	-0.48	0.65	1	0.81	0.72	0.74	0.64
U_ppm	-0.41	0.53	0.81	1	0.84	0.81	0.87
Se_ppm	-0.38	0.56	0.72	0.84	1	0.86	0.9
Ge_ppm	-0.23	0.56	0.74	0.81	0.86	1	0.8
Cd_ppm	-0.31	0.46	0.64	0.87	0.9	0.8	1

This smaller set of elements was imported in the IoGAS software, where each element was examined against all other elements in a variety of ways. The purpose was to determine patterns and relationships between elements. This included, cross correlation, probability plots, box & whisker plots and multivariate dimensional analysis.

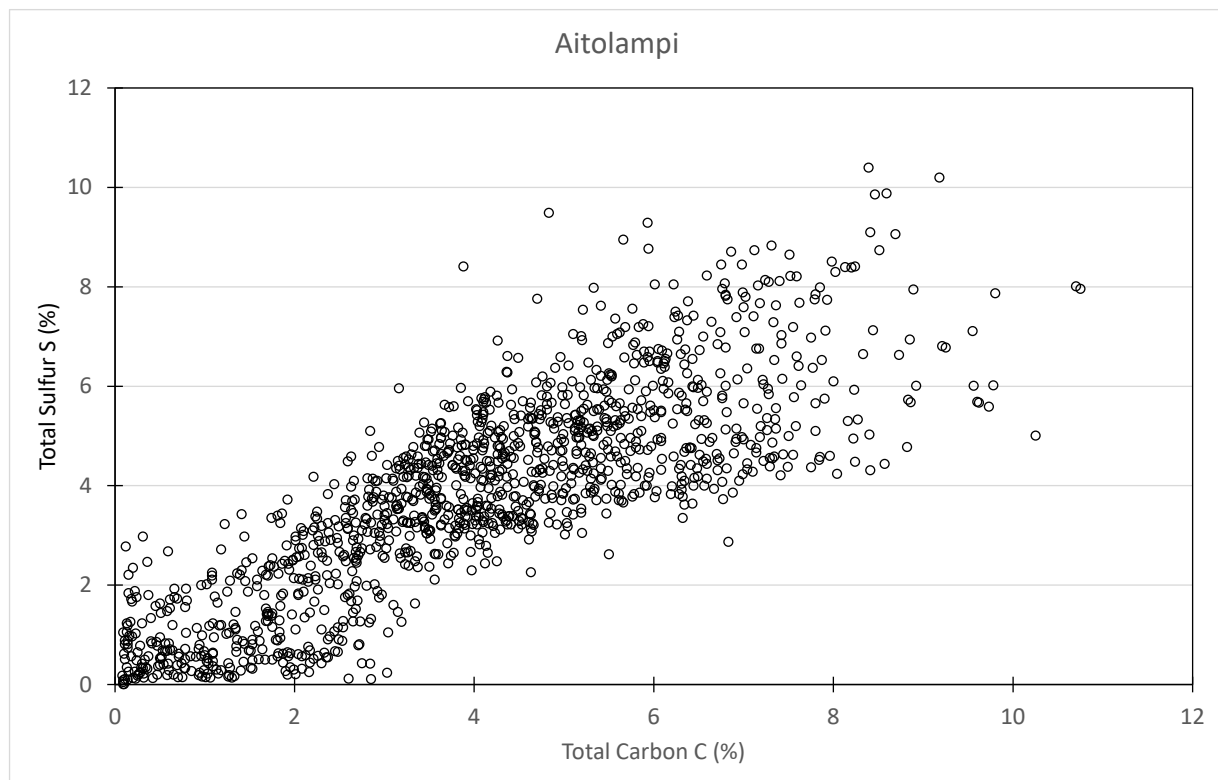


Figure 9. Aitolahti Carbon C vs. Sulfur S (Drill Hole chemical assay database)

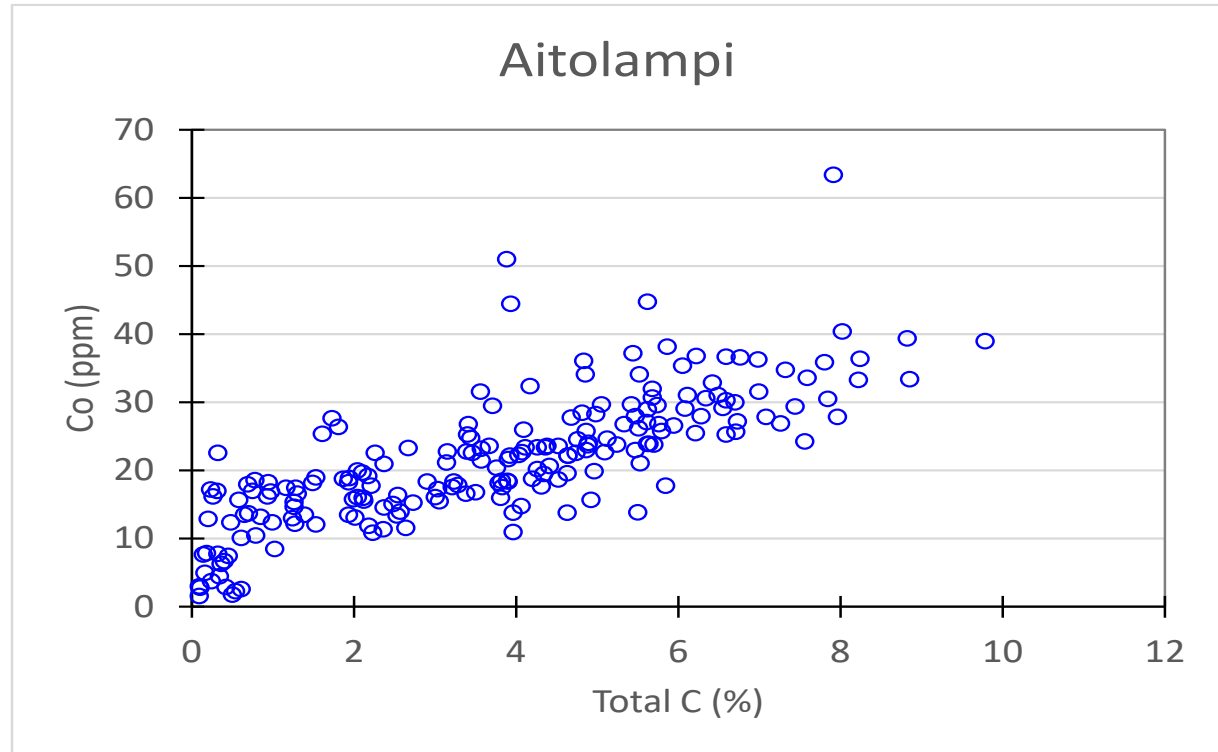


Figure 10. Aitolahti Carbon C vs. Sulfur S (Drill Hole chemical assay database)

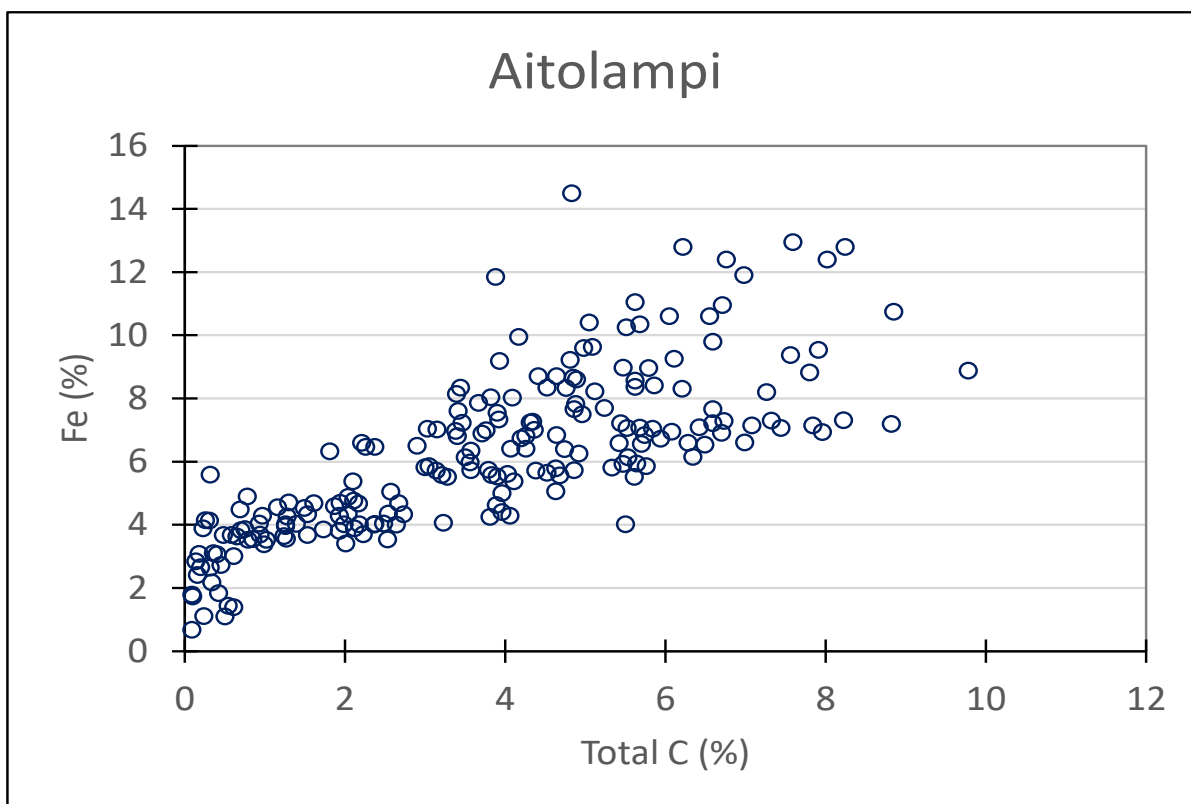


Figure 11. Aitolampi Carbon C vs. Sulfur S (Drill Hole chemical assay database)

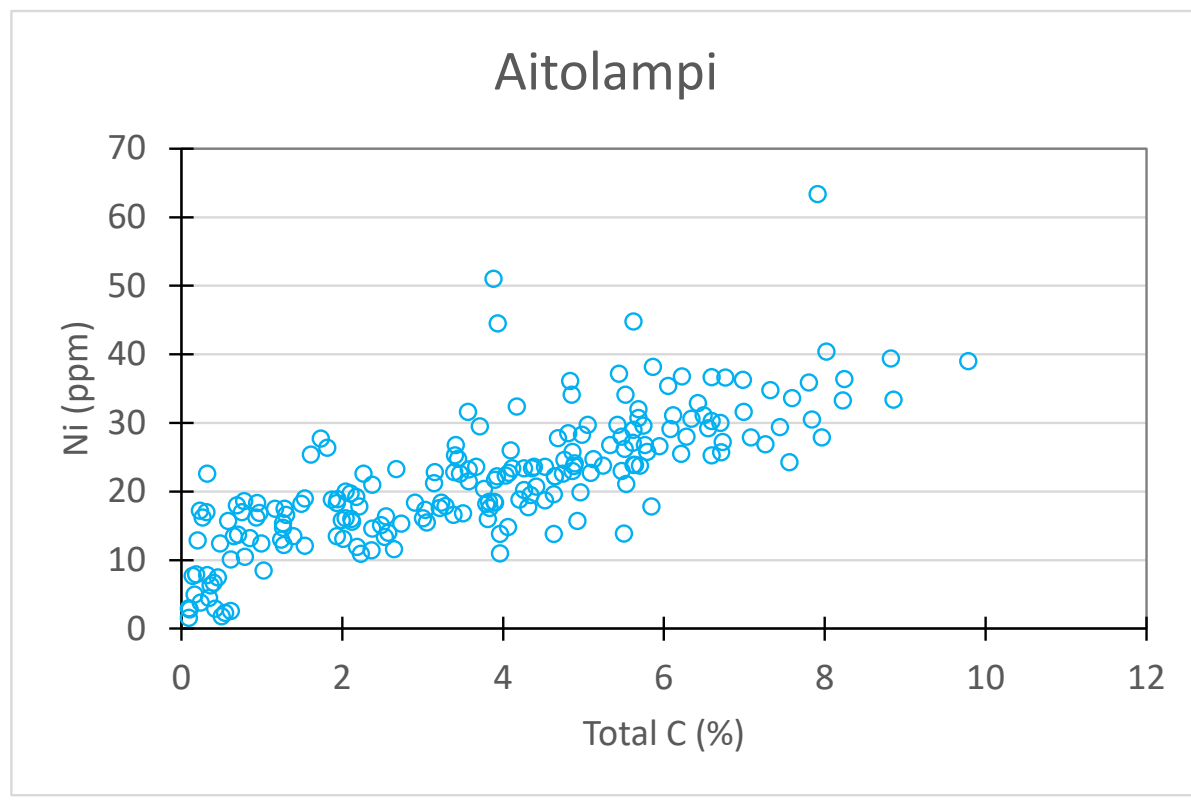


Figure 12. Aitolampi Carbon C vs. Sulfur S (Drill Hole chemical assay database)

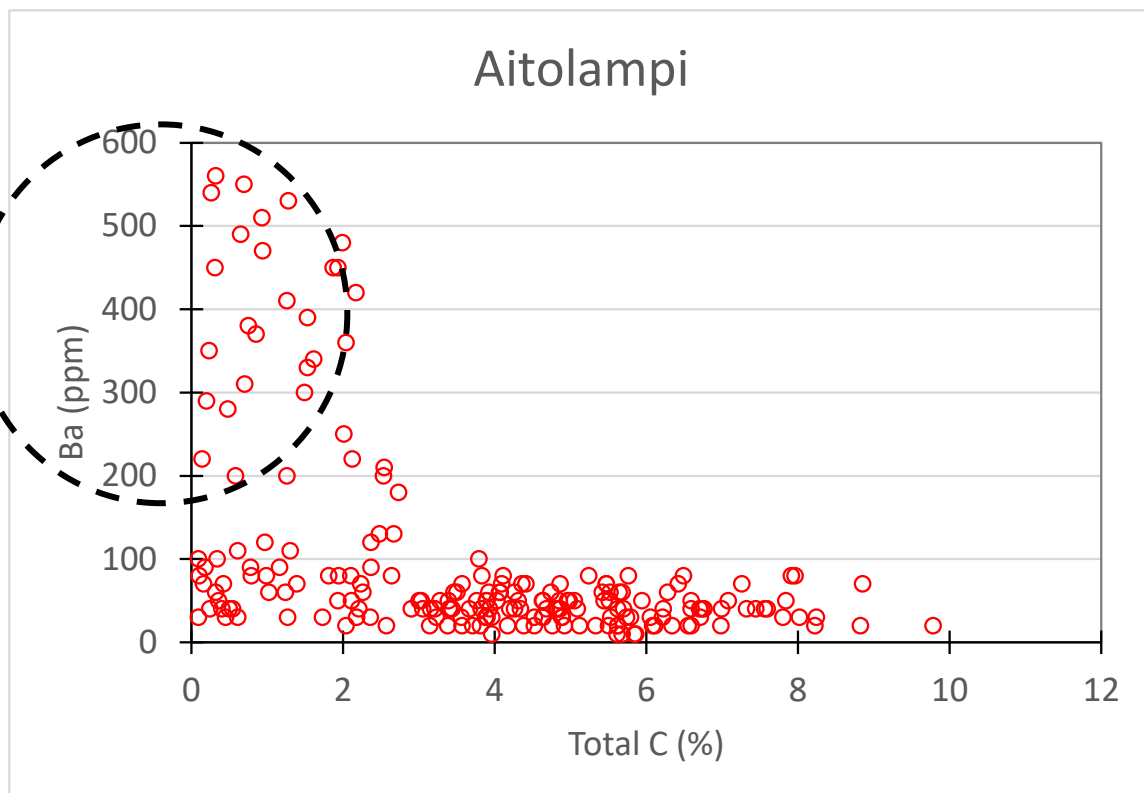


Figure 13. Aitolahti Carbon C vs. Sulfur S (Drill Hole chemical assay database)

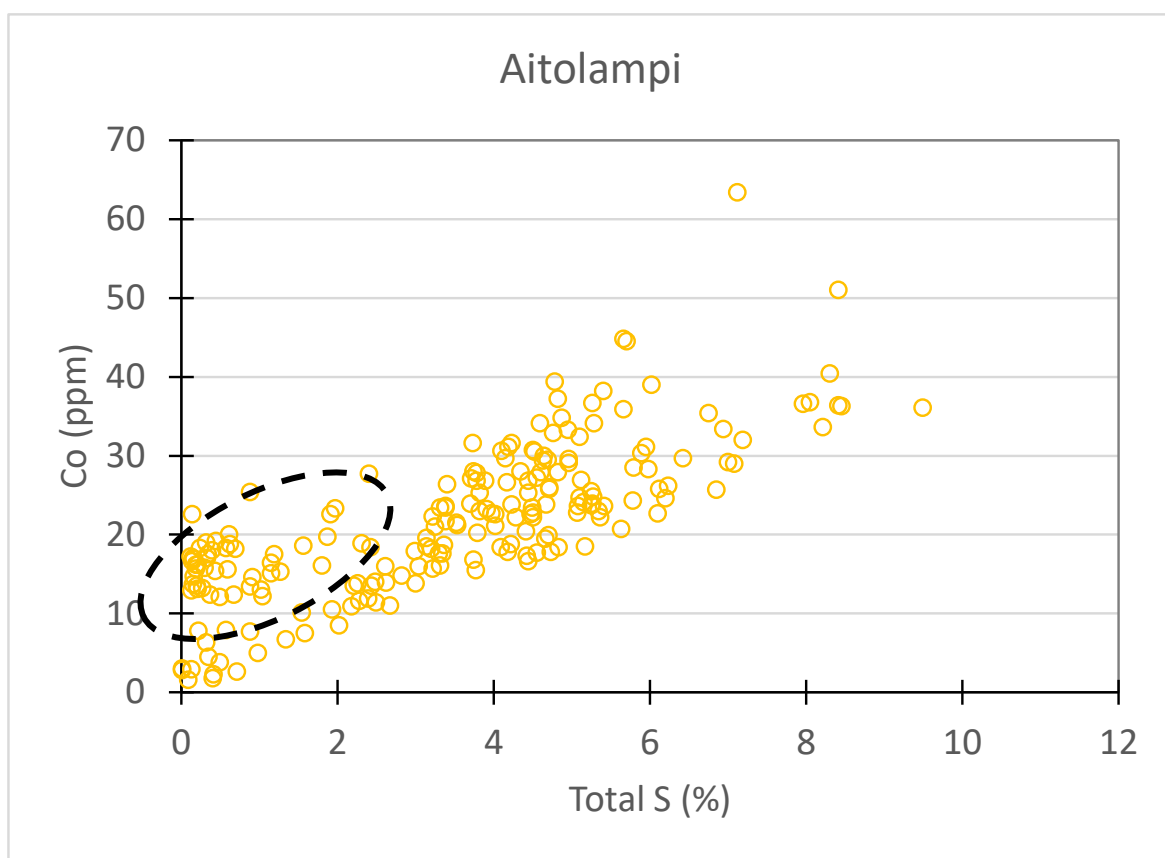


Figure 14. Aitolahti Carbon C vs. Sulfur S (Drill Hole chemical assay database)

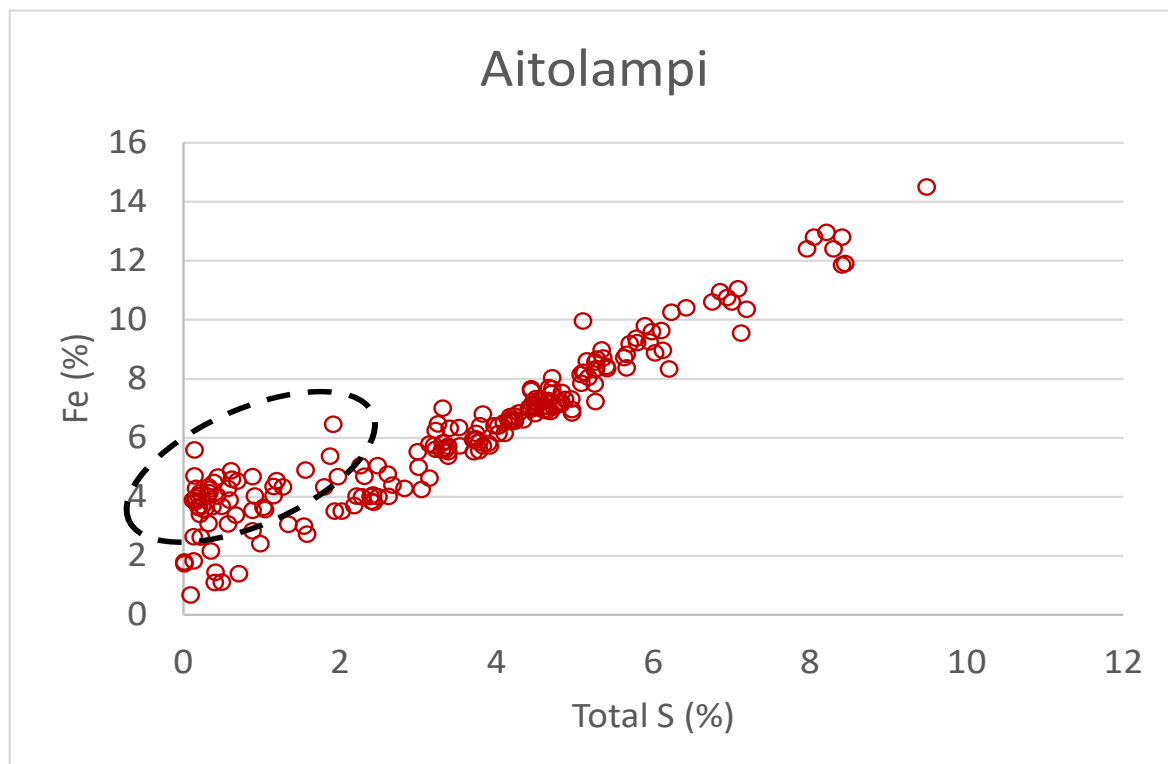


Figure 15. Aitolahti Carbon C vs. Sulfur S (Drill Hole chemical assay database)

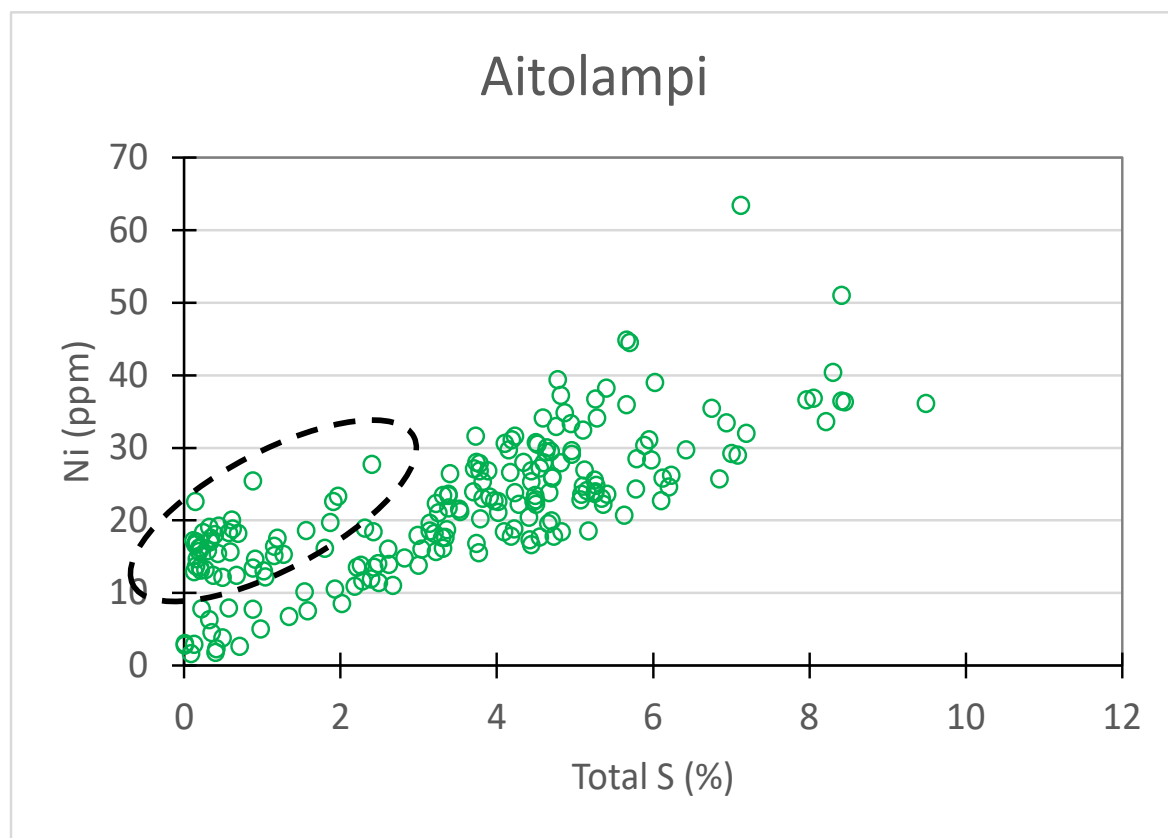


Figure 16. Aitolahti Carbon C vs. Sulfur S (Drill Hole chemical assay database)

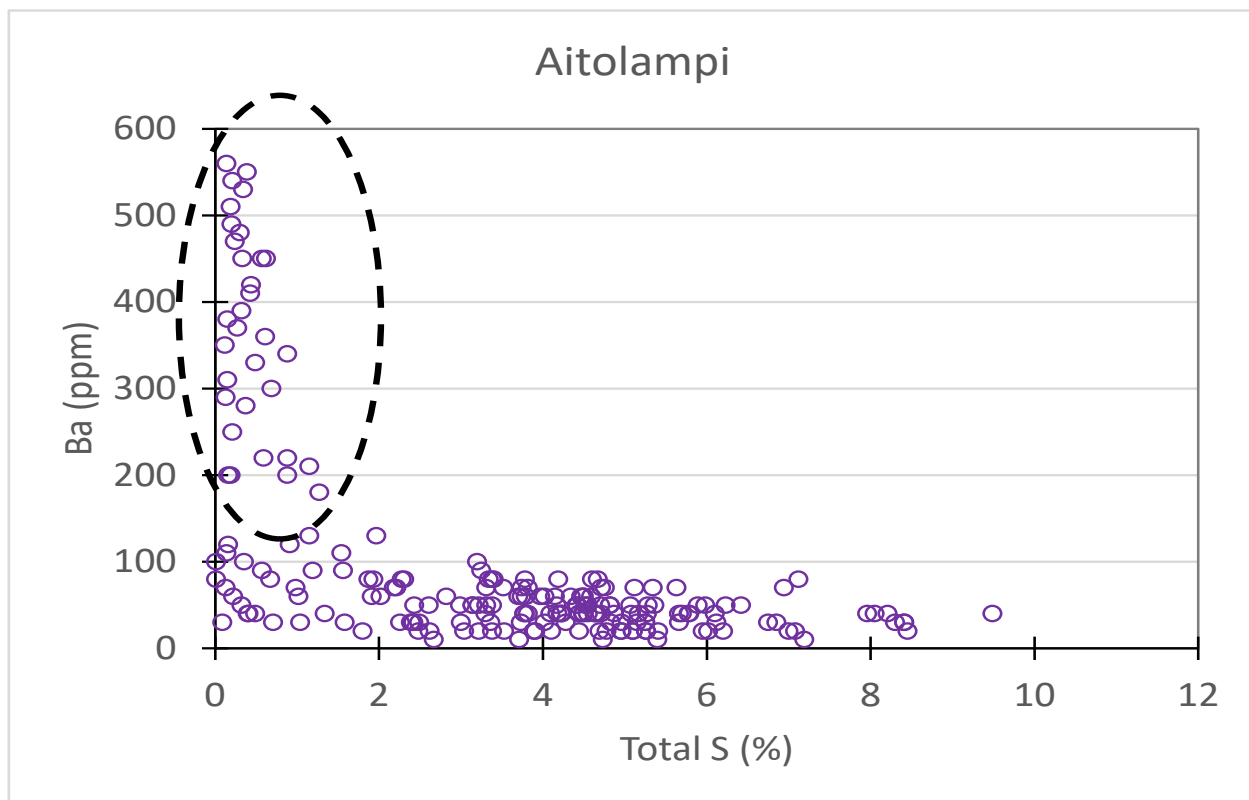


Figure 17. Aitolahti Carbon C vs. Sulfur S (Drill Hole chemical assay database)

The conclusions from this study were as follows:

- Graphite correlates well with sulfides
- Correlation of Fe with sulphur suggest we have Fe sulphides present – either pyrite and/or pyrrhotite. How do we float the sulphides but suppress the graphite?! (Dugald River analogy)
- Correlation of sulphur with carbon is very interesting – high grade graphite ore is also high in Fe sulphides! There might be an AMD issue?!
- Correlation of Ni and Co with sulphur suggests that cobaltian pentlandite is present along with pyrite/pyrrhotite – could be an interesting side stream for Beowulf?!
- Barium is not at all correlated with carbon – so it is not present in the ore but might be in hanging wall or footwall!
 - Or is it an internal structure that is not part of the graphite deposition

A more detailed discussion is shown in Appendix G.

7 SAMPLE SELECTION

A series of samples from the Aitolahti (owned and operated by Fennoscandian Minerals) were selected after discussions with Fennoscandian Minerals staff. These samples were to represent each of the major rock type end member of the deposit. The purpose of this work was to attempt to contribute and advance the effective and efficient extraction of graphite from these ores. The required samples were selected and were delivered to the GTK-Mintec laboratory at Outokumpu.

Appendix B shows the labelling protocol used for these samples. The following sampling recommendations were used by Fennoscandian Minerals staff.

Select samples with as close to similar rock textures as you can, approximately 25kg of:

- High grade C, S, Fe, Ni Co, low grade Ba
- Low grade C, S, Fe, Ni Co, low grade Ba
- High grade C, S, Fe, Ni Co, high grade Ba
- If you can find a texture that has lots of contaminants embedded into the graphite grains
- If you can find a texture that no contaminants embedded into the graphite grains

7.1 The Five Orientation Samples Selected

Five samples were selected and delivered to GTK Mintec pilot plant at Outokumpu.



Figure 18. Five orientation samples selected for Aitolahti geometallurgy study

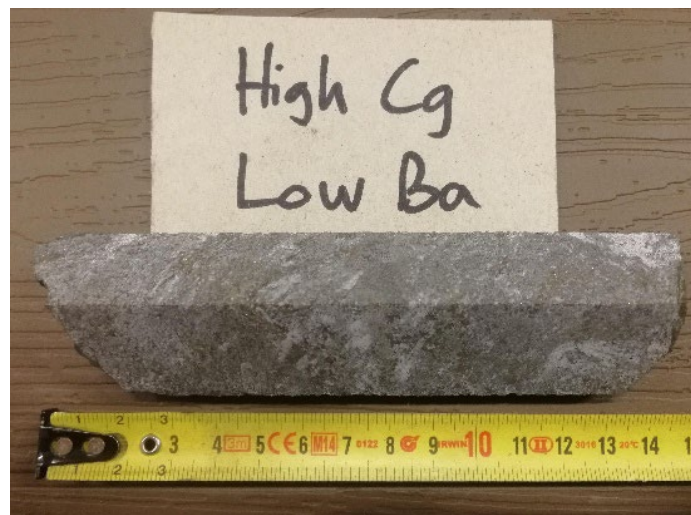


Figure 19. Aitolampi ore type, High Carbon, Low Barium – PA1



Figure 20. Aitolampi ore type, High Carbon, Low Sulfur – QA2



Figure 21. Aitolampi ore type, Medium Carbon, Medium Sulfur – XA3



Figure 22. Aitolahti ore type, Low Carbon, Low Barium – YA4



Figure 23. Aitolahti ore type, High Carbon, High Barium – ZA5

In addition to the five graphite ore samples taken from drill core (as per Figures 19 to 23), two samples from a metallurgical pilot test were also made available. The metallurgical testwork was split into two runs, to represent two parts of the deposit, Eastern Zone and Western Zone (see Figure 3).

This Metallurgical test-work including purification and characterization tests for three composited quarter drill core samples MET-17001, MET-17002, and MET-17003 was conducted in 2017. Metallurgical test-work was performed by SGS Minerals Services in Canada and characterization was performed by ProGraphite GmbH in Germany (Beowulf Mining, 2022). These two samples were labeled Pilot Rougher Tails East and Pilot Rougher Tails West. The seven samples for this study were:

- Drill core ore: High Carbon, Low Barium – PA1
- Drill core ore: High Carbon, Low Sulfur – QA2
- Drill core ore: Medium Carbon, Medium Sulfur – XA3
- Drill core ore: Low Carbon, Low Barium – YA4
- Drill core ore: High Carbon, High Barium – ZA5
- Pilot Rougher Tails East
- Pilot Rougher Tails West

8 EXPERIMENTAL DESIGN FOR A GEOMETALLURGICAL PROGRAM

The experimental objective was to find most efficient environmentally safe purification methods for floated graphite concentrates.

1. Select an appropriate set of orientation samples
2. Representative divide each sample into sub-samples for further testwork
3. Take one sub-sample and sub-divide it further for extensive characterization
4. Conduct a series of process separation tests on the sub-samples
5. Examine the results on what works
6. Conduct a series of process tests in combination of what has been learned

Each sample was representative subdivided based on the planned process test work (Figures 24 & 25). At all times, care was taken to ensure that each sub-sample was representative. Based on past experience, flotation was considered to be the most effective method, but other separation methods could improve recovery.

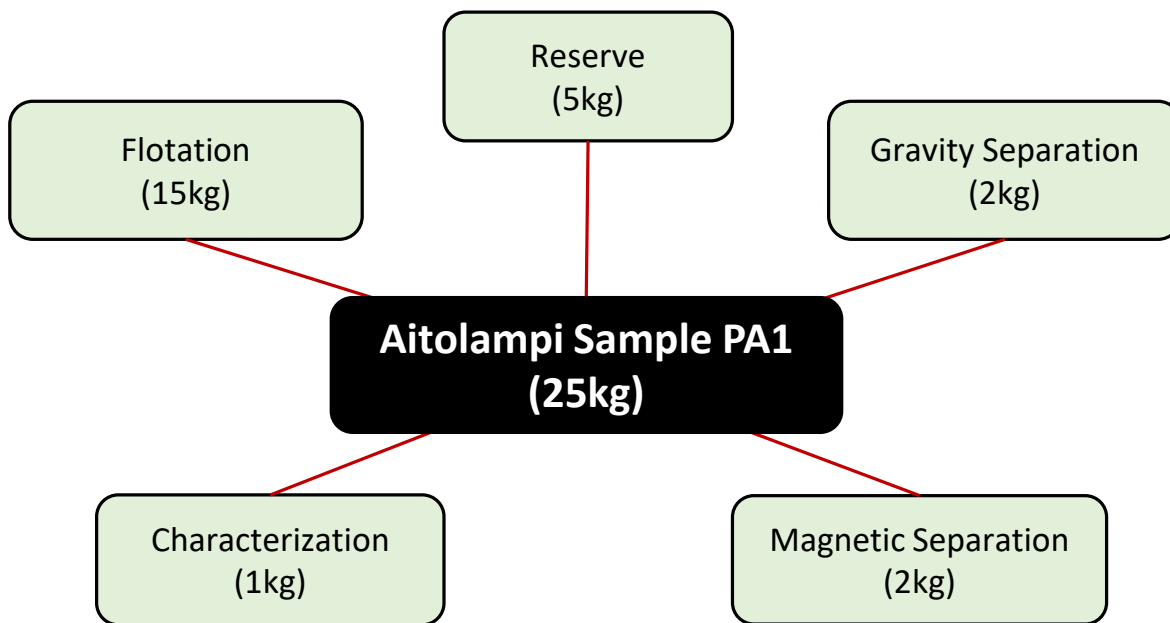


Figure 24. Each sample was riffled into representative sub fractions to be tasked for process test work

The characterization sub-sample was then further sub-divided representative (see Appendix D) and was characterized with a series of tests. This characterization was the focus of this report.

Each of the samples received was to be prepared, characterized and subject to process separation in as close to the same way as practical. A number of process separation methods were examined, and the products characterized. This was done in a way where a mineralogical mass balance could be done for each process test (Figure 26). What minerals reported which process product? In doing so, different process paths could be meaningfully compared.

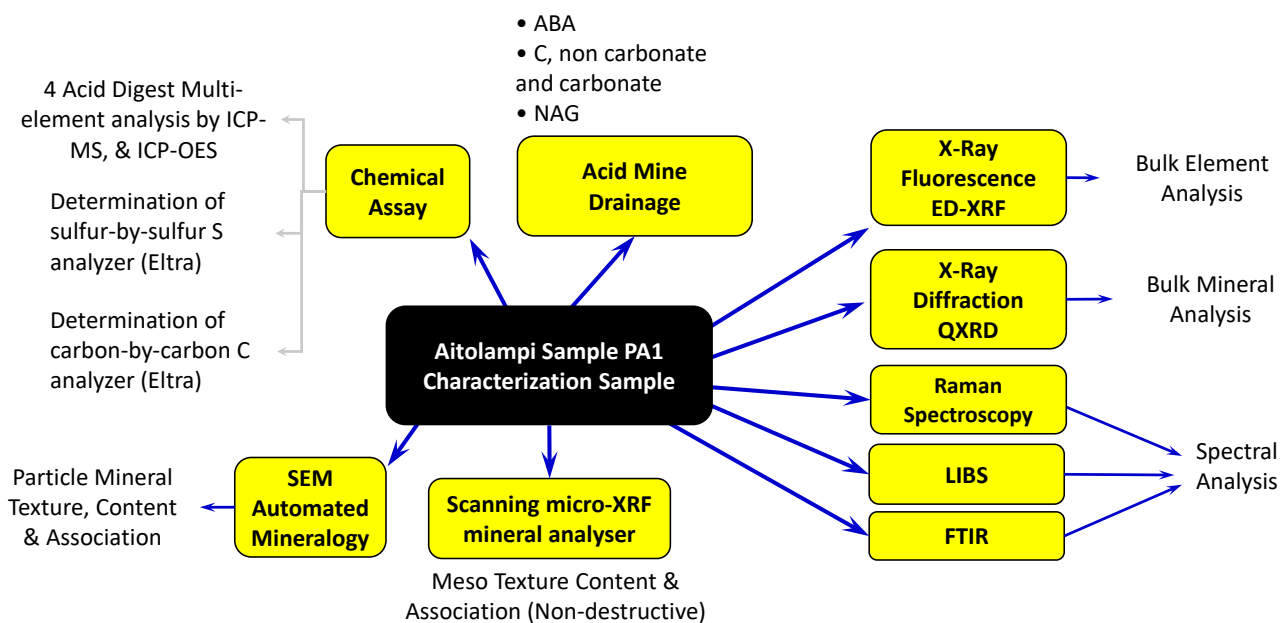


Figure 25. Characterization tests done on each sample

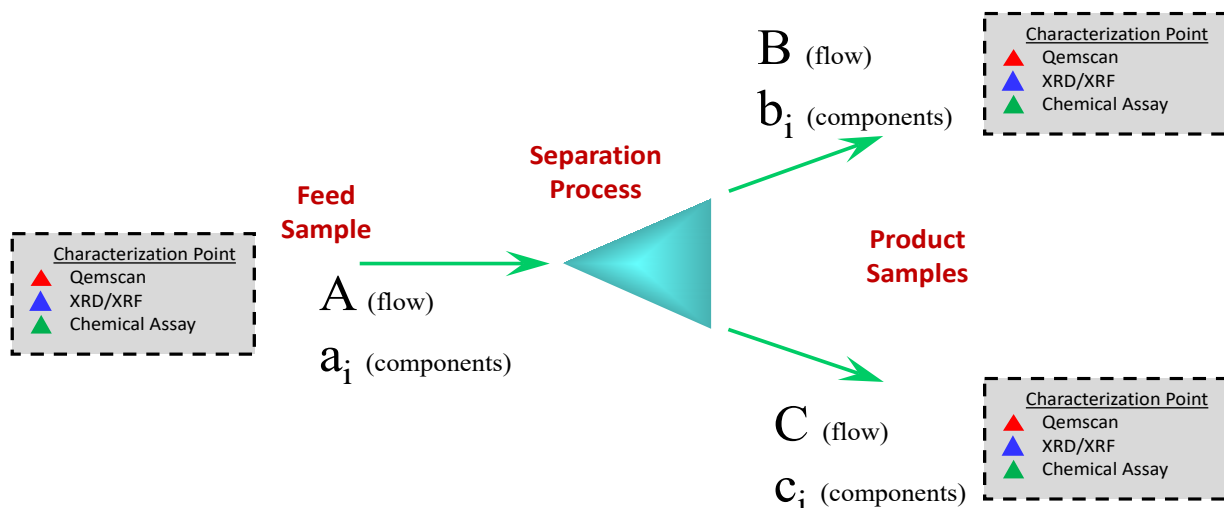


Figure 26. Each process separation test is experimentally designed so a mineralogical mass balance can be done

Once the sample has been characterized, a series of process separation tests were to be conducted, and the products were compared against the baseline unprocessed sample (Figure 27) in an experimental stage called Part I. The data from Part I was analyzed and what works and what does not was determined. Based on this outcome, the experimental stage Part II was planned (Figure 28).

The purpose of this report was to fully characterize the unprocessed feed samples with multiple methods of characterization. Each method serves a purpose.

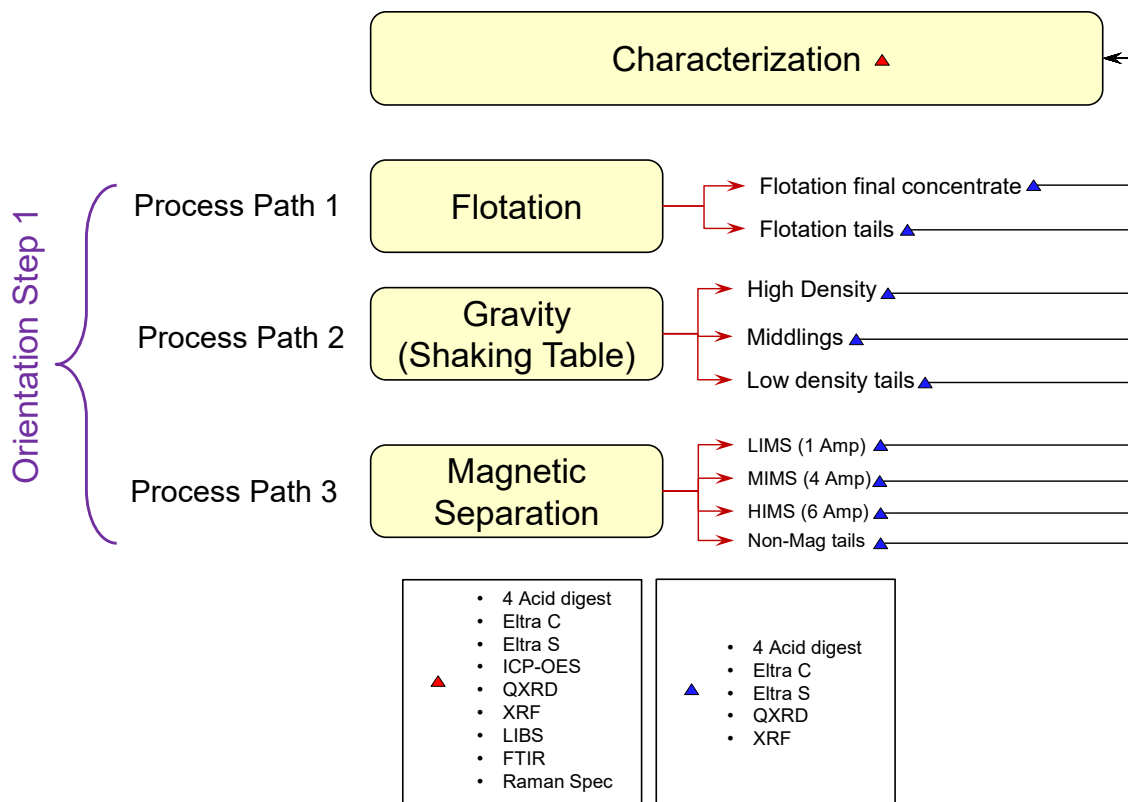


Figure 27. Orientation Study experimental design – Part 1

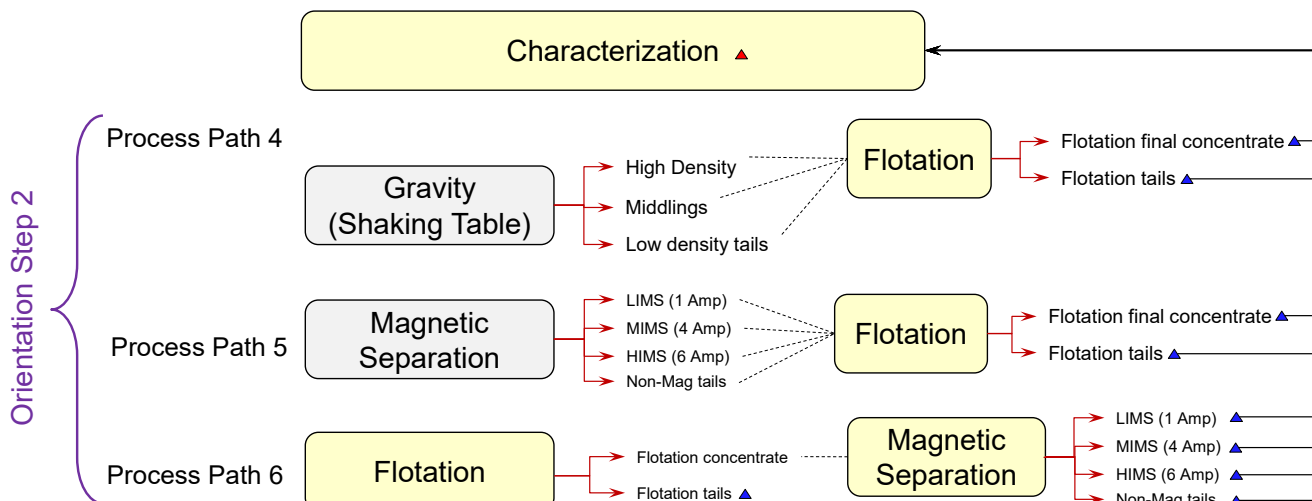


Figure 28. Orientation Study experimental design – Part II

9 SAMPLE PREPARATION

All sample residues are to be kept and returned to GTK Mintec where possible. All samples that are still representative are to be kept after tests done as an orientation sample specific reserve sample. The following sample preparations were conducted for each of the Aitolahti samples:

- **Step 0:** Clean down all equipment with compressed air and sweep floor.
- **Step 1:** Check label protocol (see Appendix B).
- **Step 2:** Select 2-3 intact core section examples that are reasonably representative of the rest of the sample (say 50 to 100mm long). Weigh, bag and label this sample with the label coding PA1-CSMX (using PA1 rock type as an example). This is to be sent to Espoo office to be analyzed by the Scanning Micro-XRF mineral analyzer.
- **Step 3:** Measure remaining sample mass as received (to 0.1g precision)
- **Step 4:** Crush the sample in large crusher with approximately CSS setting of around 15mm
- **Step 5:** Measure the sample mass (to 0.1g precision), post coarse crush. Aim for 0.5% sample loss or less.
- **Step 6:** Crush the sample to 99% mass passing 3.35mm
- **Step 7:** Measure the sample mass (to 0.1g precision), post fine crush. Aim for 0.5% sample loss or less.
- **Step 8:** Rotary divide or riffle the sample into representative sub-samples that would be tasked to specific characterization and process separation tests. Divide the approximate 25 kg sample into approximate sub-samples as shown:

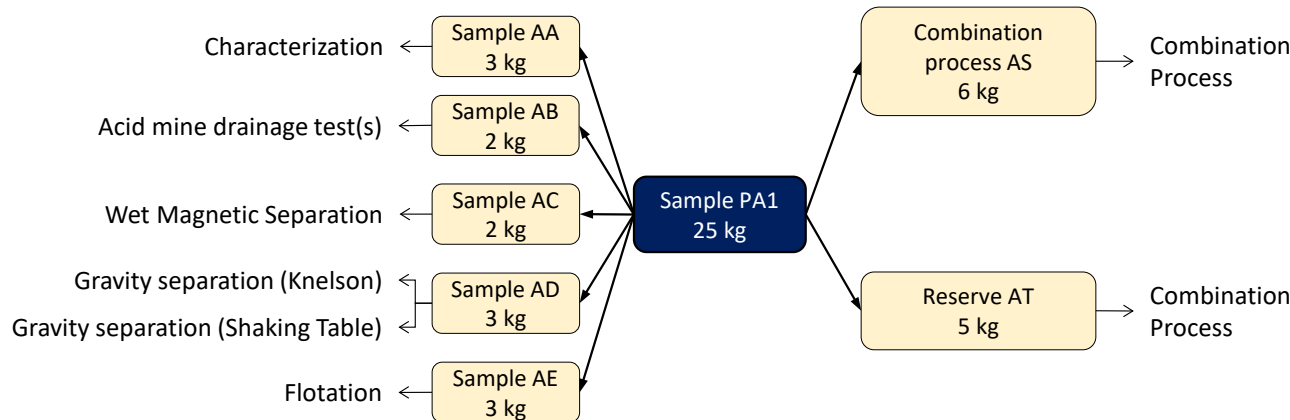


Figure 29. Sample sub dividing – first stage

- **Step 9:** Measure sample mass (to 0.1g precision) of each sub-sample. Mathematically combine all sub-samples and compare to the mass in Step 6. Aim for 0.5% sample loss or less.
- **Step 10:** Label the sub-samples according to the protocol in Appendix B

- **Step 11:** Take Sample AA (approximately 3 kg) and rotary divide it into 4 sub-samples. Measure sample mass (to 0.1g precision) of each sub-sample. Mathematically combine all sub-samples and compare to the mass in Step 9. Aim for 0.5% sample loss or less. Take the four AA sub samples and label them for mailout.
- **Step 12:** Take Sample AB (approximately 2 kg) and rotary divide it into 4 sub-samples. Measure sample mass (to 0.1g precision) of each sub-sample. Mathematically combine all sub-samples and compare to the mass in Step 9. Aim for 0.5% sample loss or less. Take the four AB sub samples and label them for mailout.
- **Step 13:** Mail out the samples in Table 8 to the required destination.

Table 8. Sub-sampling for characterization and acid mine drainage tests

Step	Source Sub-sample	Relabelling	Target Mass	Test	Mail to
2	PA1	PA1-CSMX	2-3 intact core sections	Scanning Micro-XRF mineral analyzer	GTK Espoo office
11	PA1-AA1	PA1-CA	600-700g	Chemical Assay	ALS Finland
11	PA1-AA2	PA1-CXF	600-700g	XRF	X-Ray Mineral Services Finland
11	PA1-AA3	PA1-CXD	600-700g	XRD	X-Ray Mineral Services Finland
11	PA1-AA4	PA1-CAM	600-700g	Automated Mineralogy	-
12	PA1-AB1	PA1-AMD-1		Acid Mine Drainage	-
12	PA1-AB2	PA1-AMD-2		Acid Mine Drainage	-
12	PA1-AB3	PA1-AMD-3		Acid Mine Drainage	-
12	PA1-AB4	PA1-AMD-4		Acid Mine Drainage	-

All sample residues are to be kept and returned to GTK Mintec where possible. All samples that are still representative are to be kept after tests done as an orientation sample specific reserve sample.

10 SCANNING MICRO-XRF

The micro-XRF analysis were performed at the GTK Espoo laboratory using a Tornado plus (with AMICS) instrument from Bruker on a 2D surface of the samples. The system has an Rh X-ray 30-Watt Rh anode target, two simultaneously operating 30mm² XFlash® silicon drift detectors (SDD) with an energy resolution of < 145 eV at 275 kcps (measured on MnK α) via beryllium windows and poly-capillary optics. Scanning and sample navigation is carried out via a motorized stage which moves the sample beneath the static X-ray beam. All data acquisition was performed with an accelerating voltage of 50 kV, a beam current of 600 μ A using a fixed spot size of 20 μ m under 2 mbar vacuum. The samples were mapped in separate runs using different step size varying from 28 to 41 μ m and a pixel dwell time of 10 ms/pixel. Appendix G shows a more complete scope of this mapping technique.

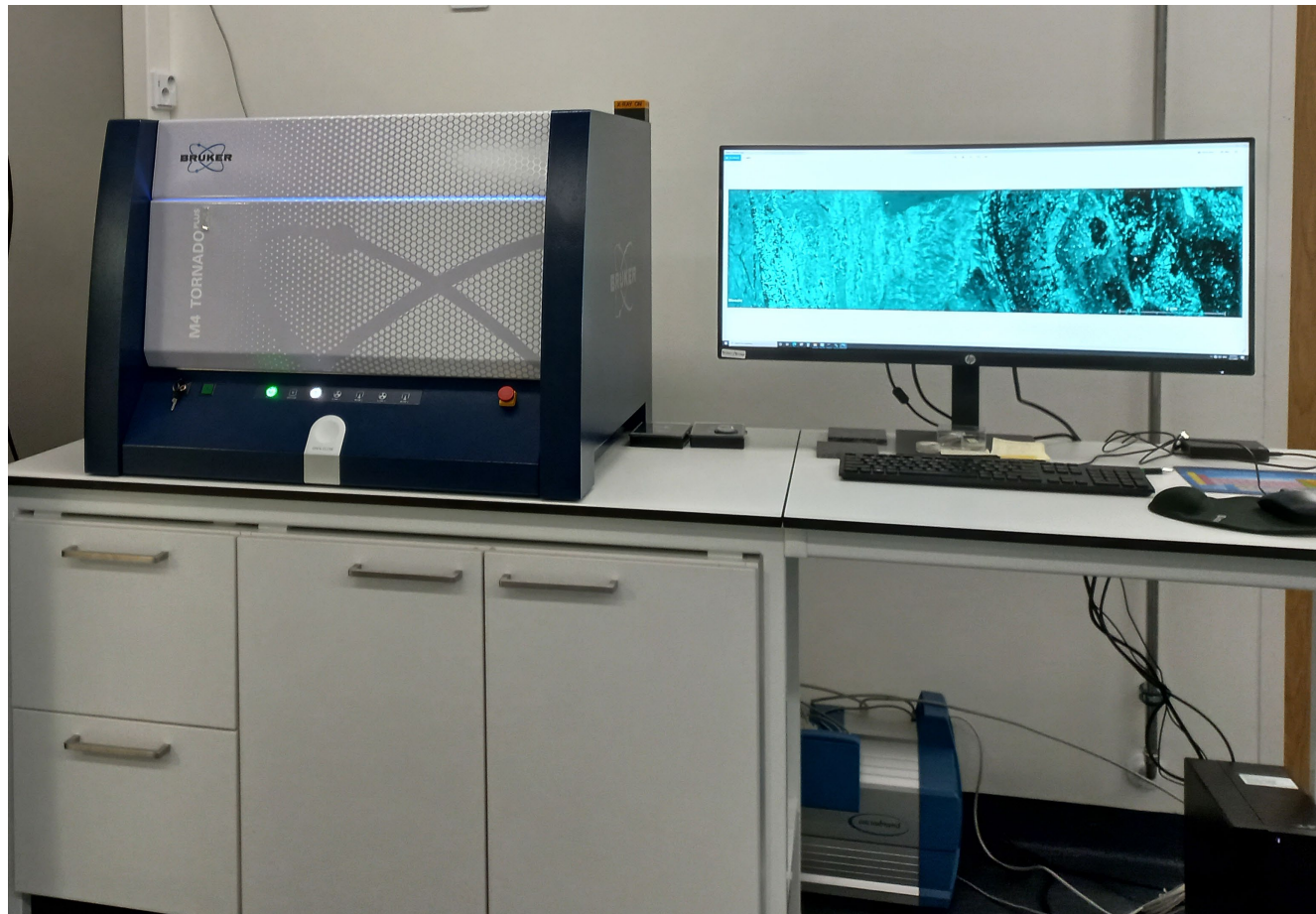


Figure 30. Tornado plus (with AMICS) instrument from Bruker

Appendix G shows the full suite of Scanning Micro-XRF results.

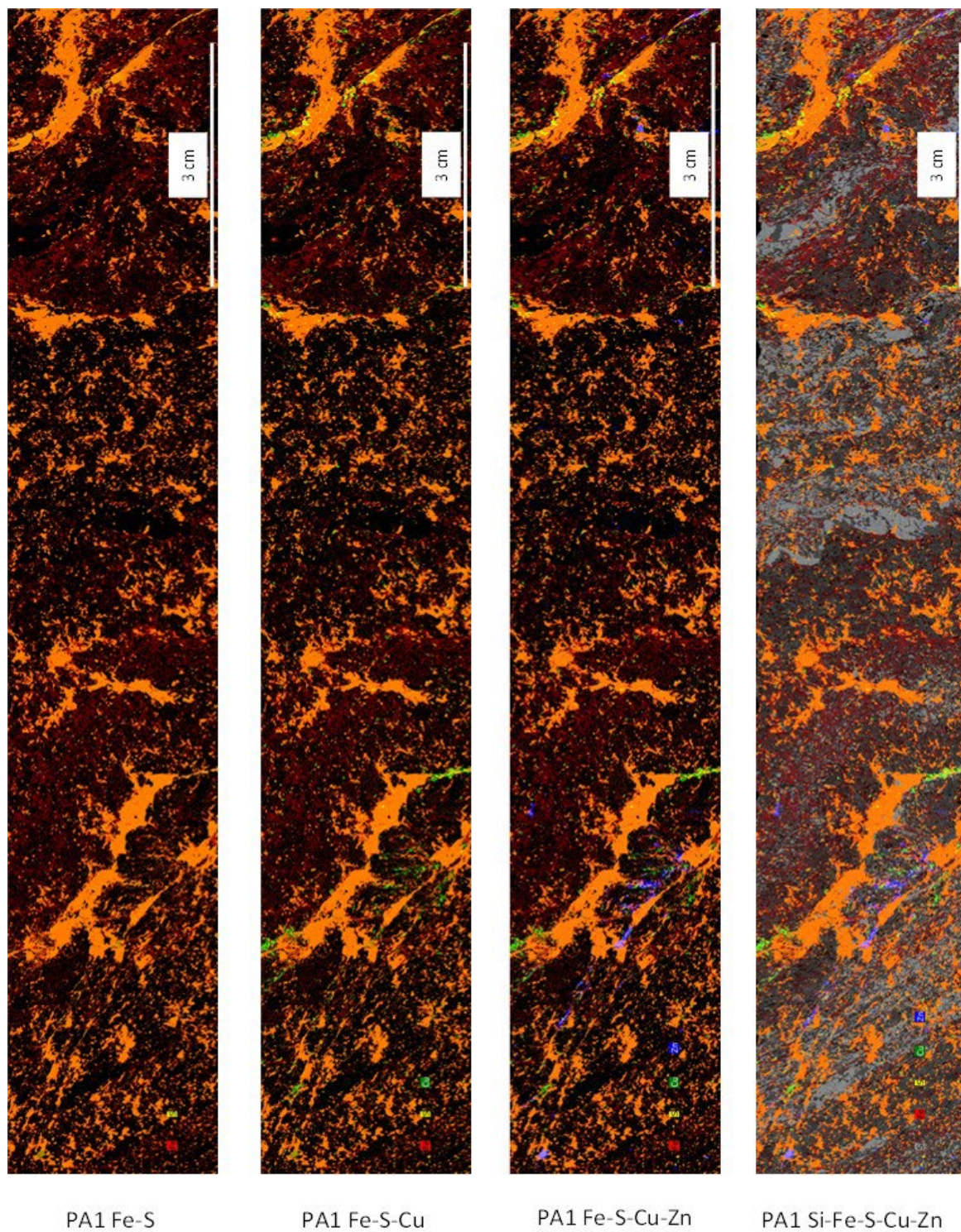
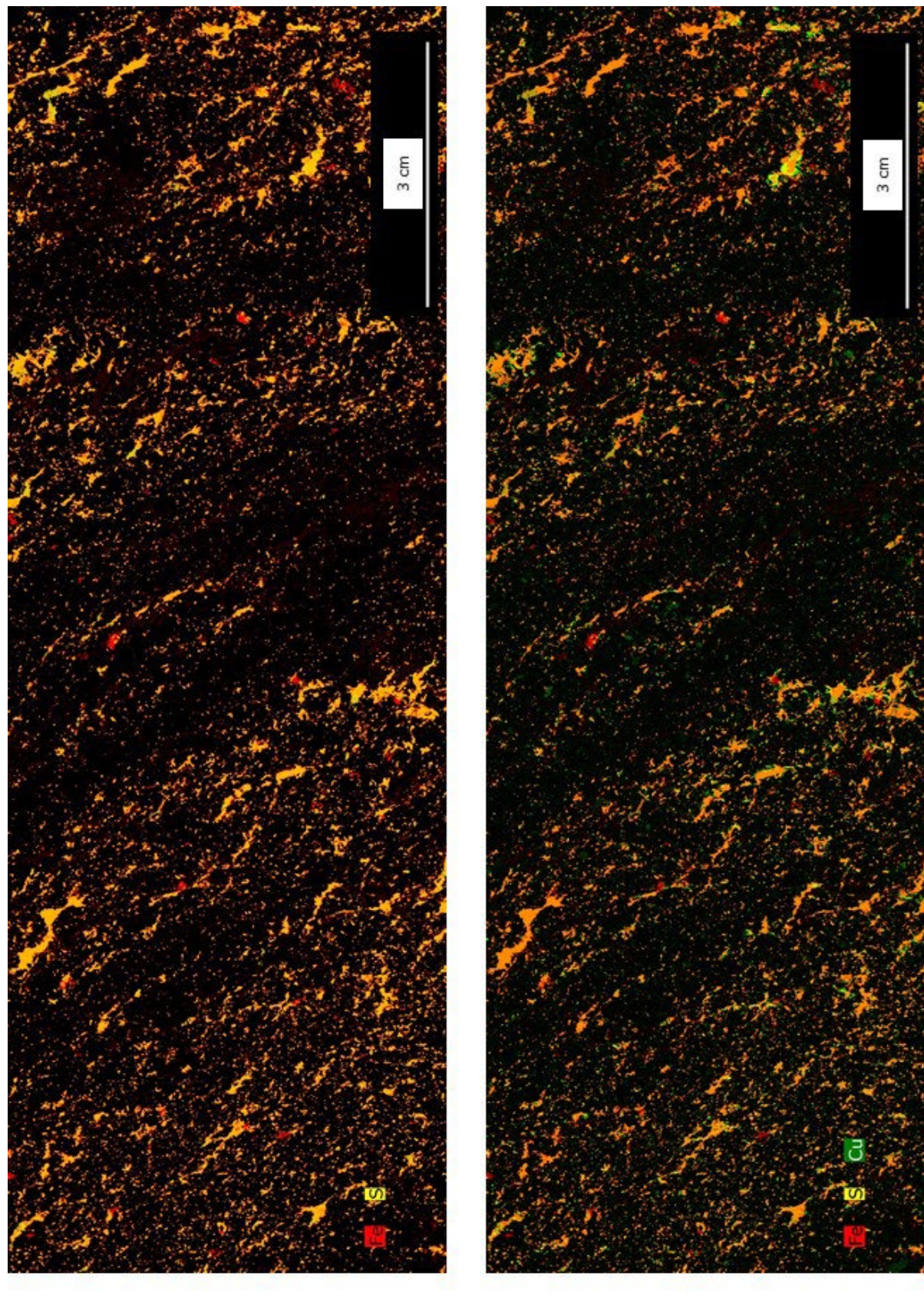


Figure 31. Sample PA1 Composite maps



QA2 Fe-S

QA2 Fe-S-Cu

Figure 32. Sample QA2 Composite maps - 1

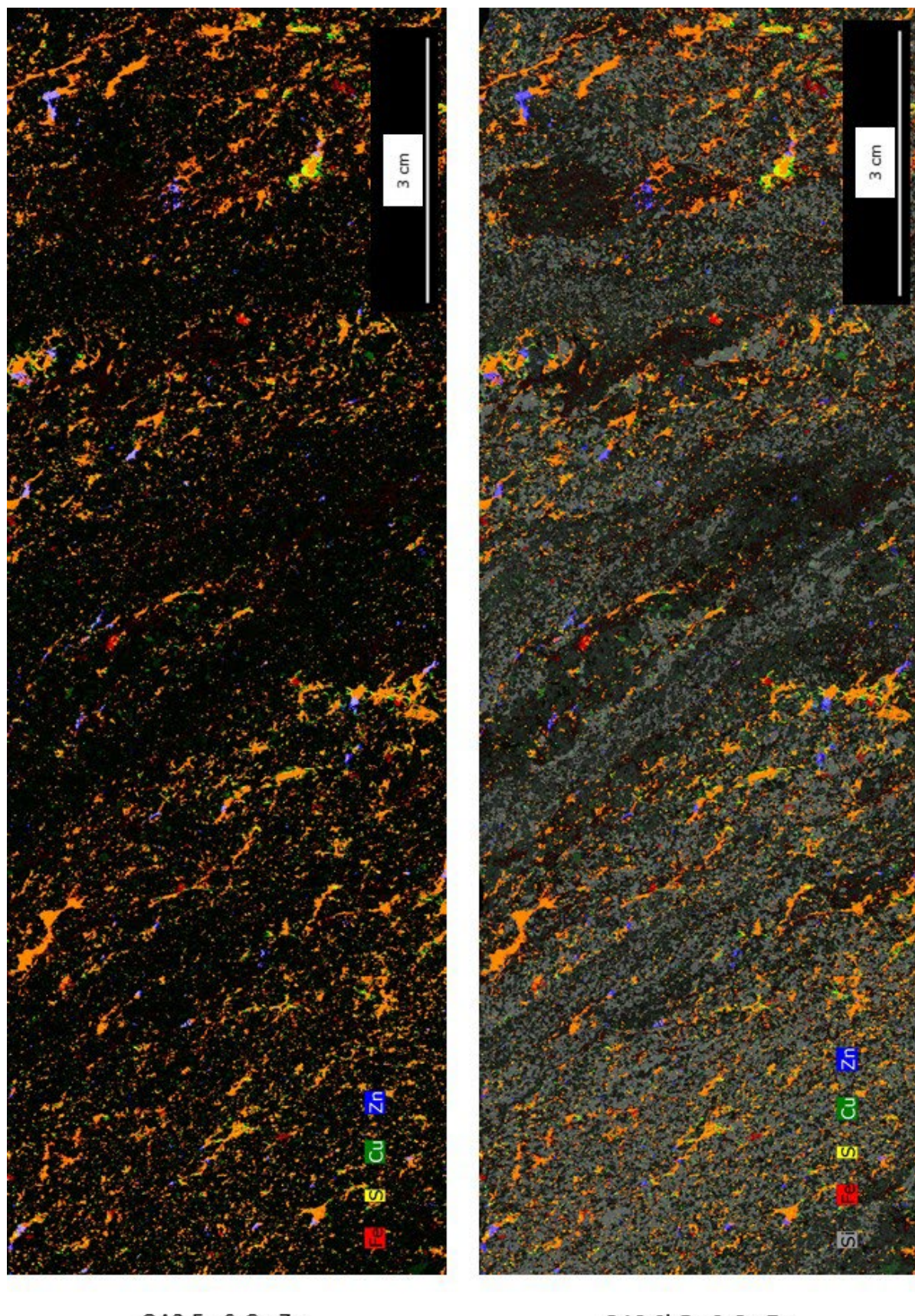


Figure 33. Sample QA2 Composite maps - 2

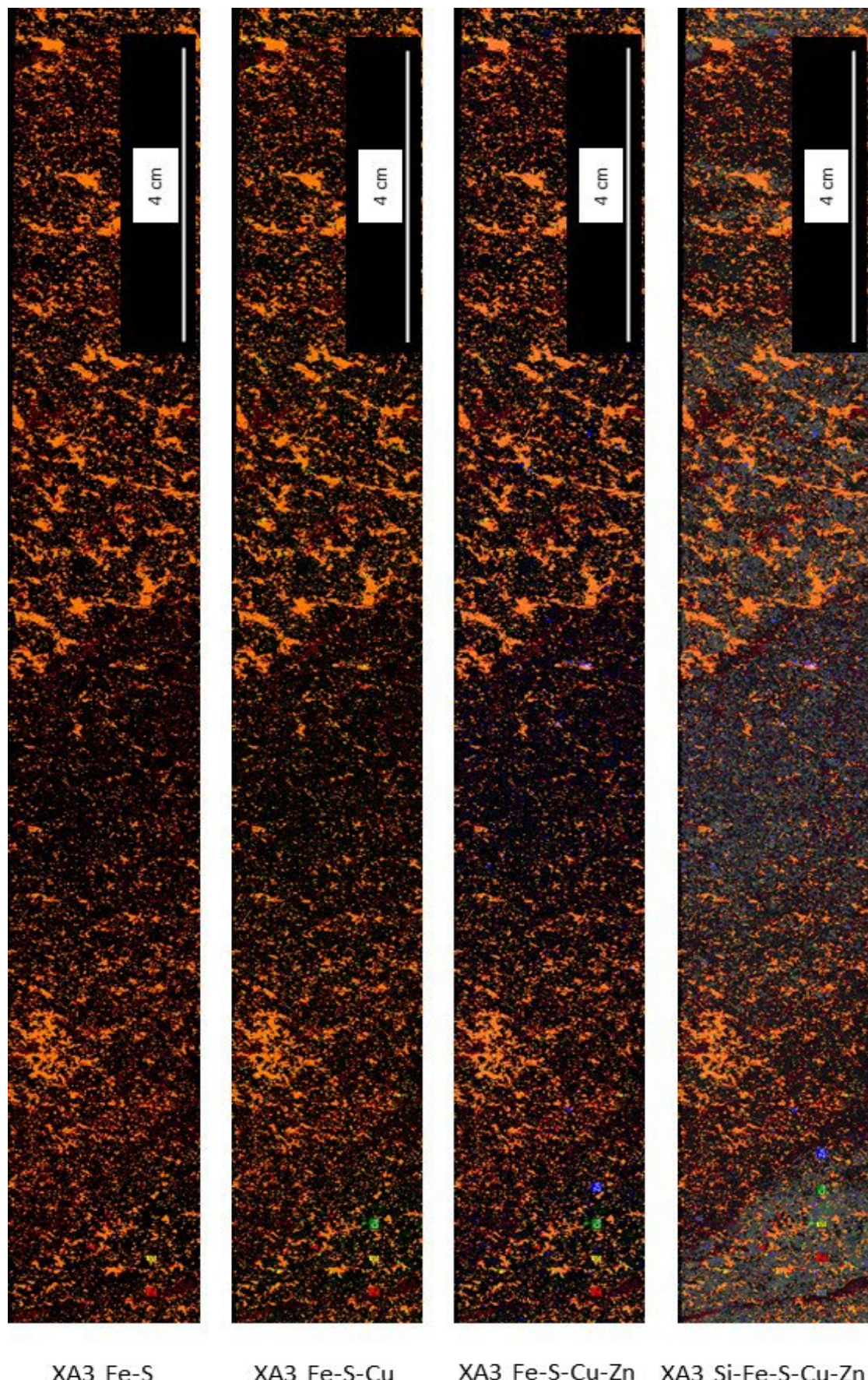


Figure 34. Sample XA3 Composite maps

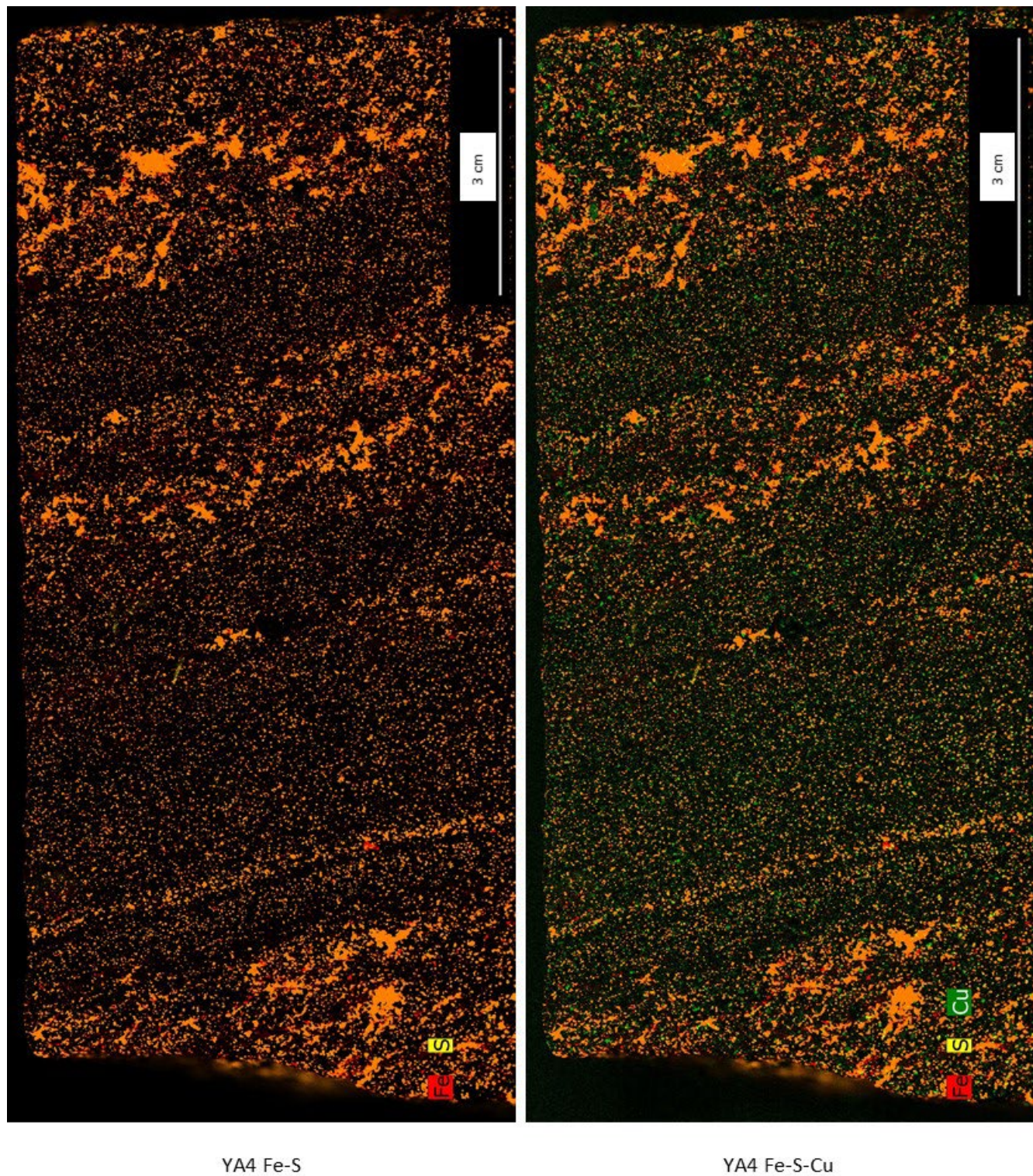


Figure 35. Sample YA4 Composite maps - 1

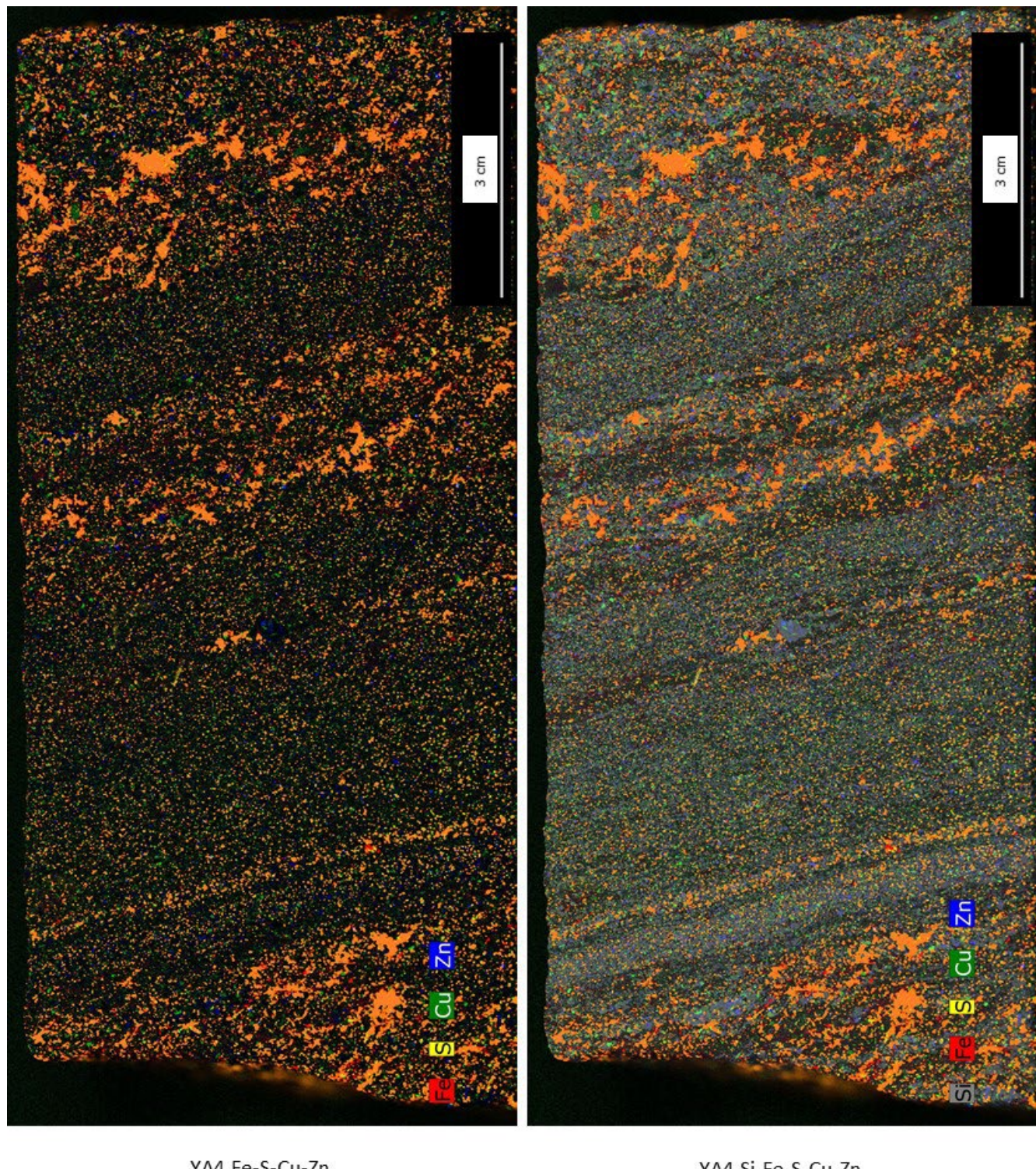


Figure 36. Sample YA4 Composite maps - 2

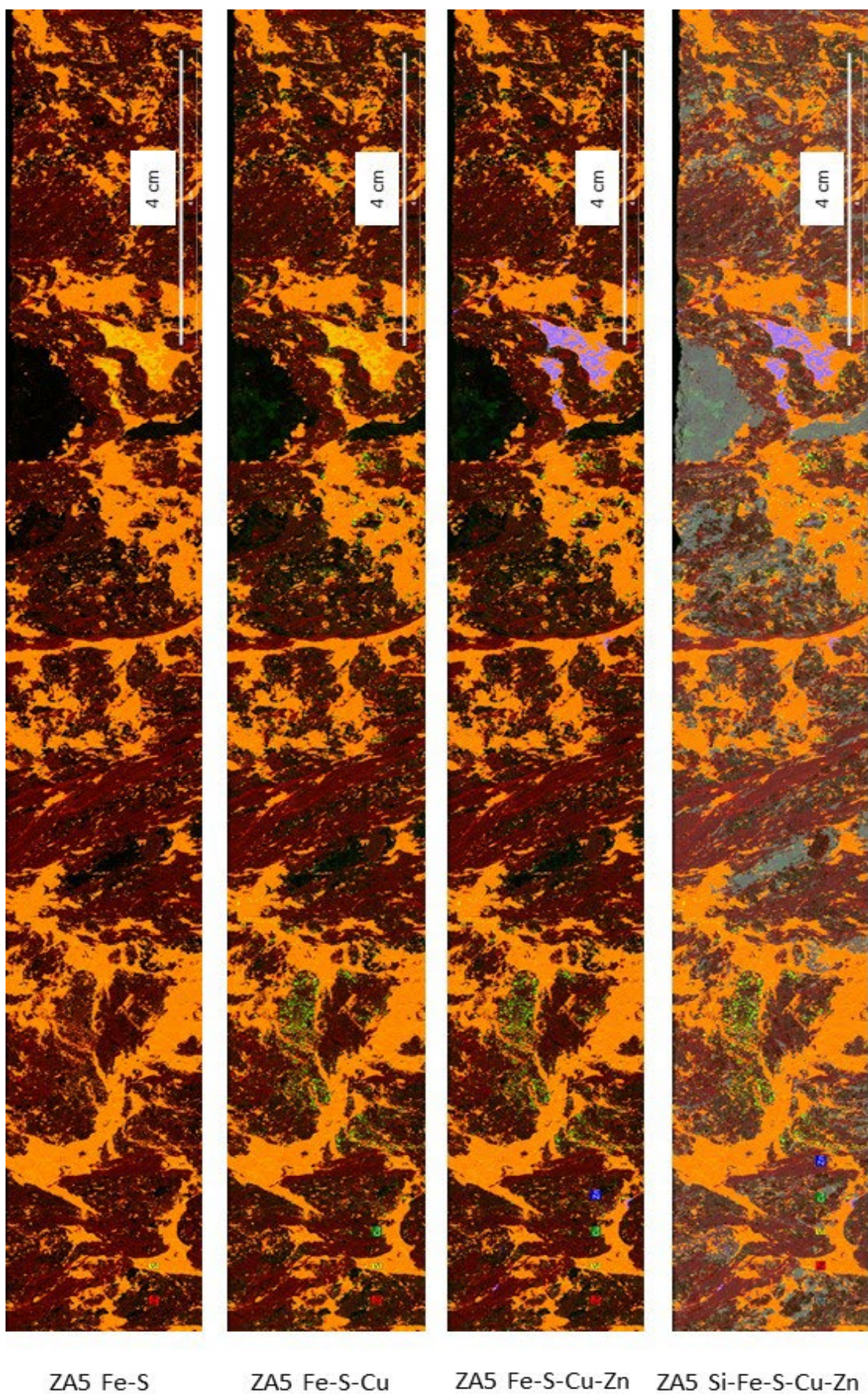


Figure 37. Sample ZA5 Composite maps

11 CHEMICAL ASSAYS

The geochemical assays were performed by CRS Laboratories Oy (Outokumpu, Finland) by using a four-acid digestion method and inductively coupled plasma mass spectrometry (ICP-MS) to get multielement analysis of the elements present in the samples.

Four-acid digestion dissolve the most minerals with minimized loss of elements. In the test the sample is digested with combination of nitric, perchloric, and hydrofluoric acid with a final dissolution stage using hydrochloric acid (ALS, 2021).

The bomb combustion method was used to analyze the total carbon (C) and total sulfur (S) present in the sample. The analysis was performed using Leco analyzer. In the analysis the sample is combusted in high temperature furnace with oxygen. The combustion oxidizes the S to sulfur di-oxide (SO_2) and C to carbon dioxide (CO_2) which quantities are measured with IR detection (Leco, 2021; Punkkinen, et al., 2019).

The LECO analysis has been also subcontracted by X-Ray Mineral Services Finland OY to Wheal Jane Services Ltd. The Sulphur and TOC analysis were measured on a LECO SC-144DRPC analyzer. 0.2 g of sample is weighed into a combustion boat, which is then inserted into the furnace. The sample is roasted at 1350°C and the sulfur and carbon are vaporized and detected by the instrument and reported as a concentration.

Table 9. LECO analysis (X-Ray Mineral Services Finland OY)

Sample	Label	%S (tot)	%C (tot)
Graphite Ore	PA1-CXD	6.47	7.96
Graphite Ore	QA2-CXD	4.60	5.96
Graphite Ore	XA3-CXD	5.22	4.99
Graphite Ore	YA4-CXD	3.83	2.85
Graphite Ore	ZA5-CXD	5.51	6.82
Pilot run tailings	APTE-C	4.19	0.15
Pilot run tailings	APTW-C	4.24	0.44

11.1 Inductively coupled plasma optical emission spectroscopy (ICP-OES)

Inductively coupled plasma optical emission spectroscopy (ICP-OES) is a technique used to analyze a sample for its elemental content. This technique has a wide linear dynamic range, a high matrix tolerance, and the speed of analysis is enhanced as opposed to techniques such as inductively coupled plasma mass spectrometry (ICP-MS) or atomic absorption spectrometry (AAS).

ICP-OES involves the analysis of the optical spectra produced by samples as they pass into an excitation source or high temperature plasma. ICP-MS utilises a similar plasma excitation source, but instead of viewing the optical spectra, it passes the emission into a mass spectrometer for analysis. Both instruments analyse samples in solution, therefore any rock samples need to be dissolved prior to analysis.

ICP-MS / OES data measured on the Aitolampi Graphite Ore and Tailings samples were undertaken at the X-Ray Welshpool lab by Lithium Metaborate Fusion. .

Solid samples were first digested by alkali fusion with lithium metaborate (LiBO_2) flux. The flux was mixed with the 0.25 g of sample in a carbon crucible with a 5:1 ratio and heated to 1050°C using a furnace. The molten bead was then tipped into dilute nitric acid (2%) and allowed to dissolve. The chemical composition of the dissolved samples was determined by ICP-OES with a Thermo ICAP 7200 and by inductively ICP-MS with a Thermo ICAP RQ-ICP-MS.



Figure 38. Thermo ICAP 7200 (LHS), Thermo ICAP RQ-ICP-MS (RHS)

The digested solutions were serially diluted to enter the quantification range of the instrument and calibration was achieved using matrix matched synthetic standards made from traceable single element stock standards.

Table 10. Major elements (ICP-OES/MS-XMS)

Method Sample	Al ₂ O ₃ ICP-OES %	SiO ₂ ICP-OES %	TiO ₂ ICP-OES %	Fe ₂ O ₃ ICP-OES %	MnO ICP-OES %	MgO ICP-OES %	CaO ICP-OES %	Na ₂ O ICP-OES %	K ₂ O ICP-OES %	P ₂ O ₅ ICP-OES %
PA1-C	10.95	51.86	0.50	12.34	0.06	3.96	3.04	1.48	2.15	0.13
QA2-C	12.29	55.51	0.55	9.89	0.06	3.44	2.96	1.99	2.49	0.16
XA3-C	11.76	59.71	0.54	9.50	0.05	2.57	2.83	2.43	1.96	0.18
YA4-C	12.34	60.42	0.62	8.62	0.05	2.62	2.41	2.68	2.31	0.18
ZA5-C	11.93	54.24	0.54	10.25	0.06	3.79	2.98	1.81	2.35	0.13
Pilot Tails Eastern	12.51	64.54	0.48	9.53	0.05	2.50	2.51	2.48	2.28	0.15
Pilot Tails Western	12.74	62.02	0.53	9.61	0.06	3.07	2.64	2.38	2.52	0.18

Note: Sulphur values can be treated as semi-quantitative.

More data from this characterization method is shown in Appendix H.

12 QUANTITATIVE X-RAY DIFFRACTION ANALYSIS (QXRD)

X-Ray diffraction (XRD) is an analytical technique used for the quantitative determination of the minerals present in crystalline material such as rocks. The method depends upon the unique structural properties of the analyzed crystals and measures the intensities and scattering of the X-rays leaving the sample. Appendix I shows the x-ray spectra for QXRD.

12.1 QXRD Whole-rock analysis

The samples were first disaggregated gently using a pestle and mortar. After quartering, three splits of 2 g for each triplicate sample and one for non-triplicate sample were micronized in water using a McCrone Micronising Mill to obtain an X-ray diffraction powder with a mean particle diameter of between 5 – 10 microns. The slurry was dried overnight at 80°C, re-crushed to a fine powder and backpacked into a steel sample holder, producing a randomly orientated sample for presentation to the X-ray beam.

The goal of the whole-rock sample preparation is to have a random orientation of the grains, allowing unbiased phase quantification and minimizing the error caused by preferred orientation of certain minerals (e.g., mica flakes, feldspar, amphibole). The study of a randomly oriented powder will give an approximate proportion of clay minerals present in the sample.

Whole-rock samples were scanned on a PANalytical X'Pert3 diffractometer using a CuK α radiation at 40 kV and 40 mA. The diffractometer is equipped with Automatic Divergence Slits (10 mm irradiated area), sample spinner and PIXcel 1-D detector. Whole-rock samples were scanned from 4.5 to 75° (2θ) at a step size of 0.013 for 4 hours. The longer scan time improves the resolution of the data, which is particularly important for graphite bearing samples within a quartz rich matrix..

Qualitative analysis on bulk rock samples has been carried out using two commercial software packages associated with the ICDD PDF-4 Minerals database: Traces (v.6) by GBC Scientific Equipment and HighScore Plus (v.4) by PANalytical. For this project XRD quantitative phase analysis on whole rock samples has been performed using the Rietveld method with either BGmn AutoQuan or HighScore Plus software. The Rietveld method is based upon a full-pattern analysis (rather than single peaks) where a computer model allows a theoretical diffractogram to be calculated for any phase mixture (Post & Bish, 1989).



Figure 11. The PANalytical X'Pert3 diffractometer diffractometer using a CuK α radiation at 40 kV and 40 mA

Table 11. Whole rock XRD analysis Aitolampi drill core ore and pilot tailings

Aitolampi Sample	Mass (g)	Biotite (%)	Muscovite (%)	Kaolinite (%)	Chlorite (%)	Quartz (%)	K Feldspar (%)
PA1-CXD	717.1	0.1	5.0	0.0	9.3	27.7	13.7
QA2-CXD	692.5	1.5	0.7	0.0	8.0	34.8	12.0
XA3-CXD	724.1	3.0	0.4	0.0	3.8	36.6	12.4
YA4-CXD	716.6	0.7	2.1	0.0	7.2	37.8	14.2
ZA5-CXD	703.8	8.7	0.0	0.0	2.9	30.2	9.9

Rougher Tails Eastern		6.8	2.3	0.2	3.1	37.7	6.1
Rougher Tails Western		6.6	1.6	0.0	11.6	37.3	4.8

Aitolampi Sample	Plagioclase (%)	Calcite (%)	Amphibole (%)	Graphite (%)	Sphalerite (%)	Pyrite (%)	Pyrrhotite (%)	Total (%)
PA1-CXD	15.5	TR	5.4	10.9	0.6	0.3	11.5	100 %
QA2-CXD	22.9	0.0	TR	11.5	0.6	2.2	5.8	100 %
XA3-CXD	24.8	0.0	0.0	10.8	0.0	TR	8.2	100 %
YA4-CXD	30.4	TR	0.0	0.0	TR	1.4	6.2	100 %
ZA5-CXD	22.5	0.0	TR	14.8	0.6	0.2	10.2	100 %

Rougher Tails Eastern	33.1	0.0	0.0	3.1	0.0	TR	7.6	100 %
Rougher Tails Western	31	TR	0.0	0.0	0.1	1.1	5.9	100 %

Note:

Quantification using the Rietveld method (HighScore software)

Plagioclase is andesine

Quantification of graphite in sample YA4-CXD not possible because below the detection limit considering the high quartz content.

12.2 QXRD Clay fraction analysis

Although clay minerals may be evident in whole rock diffractograms, the most satisfactory method for their quantification is to extract and analyze the clay fraction separately. A 5 g split of the sample that was disaggregated at the first stage of the whole rock preparation (see above) was taken and weighed accurately. The weight was recorded in a central register for later reference. Separating the <2-micron fraction was achieved by ultrasound and centrifugation. The total weight of clay extracted was determined by removing a 20-25g aliquot of the final clay suspension and evaporating to dryness at 80°C. The initial and final weights of the beaker used were also recorded in the register. The clay XRD mount was obtained by filtering the clay suspension through a Millipore glass micro-fiber filter and drying the filtrate on the filter paper. The samples were analyzed as an untreated clay, after saturation with ethylene glycol vapor overnight and following heating at 380°C for 2 hours, with a further heating to 550°C for one hour.

Identification and characterization of clay minerals in the <2 µm fraction has been performed following the guidelines described by Moore & Reynolds (1997) overlaying the diffractograms from the four clay treatments. Clay filters were scanned on a Philips PW1730 Generator using a CuK α radiation at 40 kV and 40 mA. Clay filters were scanned from 3 to 35° (2θ) at a step size of 0.05° and 2 s step time.

The clay quantification has been performed on the oriented samples using a Reference Intensity Ratio based method. Peak intensities are measured and incorporated in a formula to indicate the relative amounts of clay minerals present. This data is then used to quantify the clay minerals with respect to the whole rock by reference to the total amount of <2-micron clay fraction, which is calculated from the aliquot previously

extracted and dried. An indication of the clay minerals crystallinity was given by assessment of the peak width for each component.



Figure 40. Philips PW1730 Generator using CuK α radiation at 40 kV and 40 mA.

Table 12. Clay analysis (<2 µm) XRD analysis Aitolampi drill core ore and pilot tailings

Aitolampi Sample	Mass (g)	Wt. % <2µm	Illite/smectite				Mica		
			% A	% B	Order	% Illite	% A	% B	Crys
PA1-CXD	717.10	2.0	0.0	0.0			26.6	0.5	P
QA2-CXD	692.50	2.1	0.0	0.0			33.5	0.7	P
XA3-CXD	724.10	1.9	0.0	0.0			41.2	0.8	P
YA4-CXD	716.60	2.2	0.0	0.0			33.7	0.7	P
ZA5-CXD	703.80	2.2	0.0	0.0			27.6	0.6	P
Rougher Tails Eastern		2.7	0.0	0.0			54.6	1.5	P
Rougher Tails Western		3.2	0.0	0.0			42.6	1.4	P

Aitolampi Sample	Kaolinite			Chlorite			Y	Quartz	
	% A	% B	Crys	% A	% B	Crys		% A	% B
PA1-CXD	0.0	0.0		34.5	0.7	M	0	38.8	0.8
QA2-CXD	0.0	0.0		27.6	0.6	M	0	38.9	0.8
XA3-CXD	0.0	0.0		23.2	0.4	M	0	35.6	0.7
YA4-CXD	0.0	0.0		38.5	0.8	M	0	27.8	0.6
ZA5-CXD	0.0	0.0		11.0	0.2	M	0	61.5	1.4
Rougher Tails Eastern	5.9	0.2	P	8.7	0.2	M		30.8	0.8
Rougher Tails Western	0.0	0.0		35.8	1.2	M		21.6	0.7

A = Weight % relevant size fraction

B = Weight % bulk sample

Mixed-layer Ordering:

R I = Randomly Interstratified (R0)

Crystallinity:

VW = Very Well Crystallised

O = Ordered Interstratification (R1)

W = Well Crystallised

LR = Long-range Ordering (R3)

M = Moderately Crystallised

P = Poorly Crystallised

Y = No. of Fe atoms in six octahedral sites

13 ENERGY DISPERITIVE X-RAY FLUORESCENCE SPECTROSCOPY (ED-XRF)

Energy dispersive X-ray fluorescence (ED-XRF) spectrometry is a non-destructive analytical technique used to obtain elemental information from e.g., pellets, cuttings, or powders. Portable ED-XRD allows analysis of ca. 30 geologically important major and trace elements in the field with limit of detection <10 ppm for most of the elements.

The elemental composition of samples was analyzed on powdered material with the measurements undertaken on a portable benchtop Spectroscout (by Spectro) ED-XRF spectrometer. Approximately four grams of loose powder was measured into an XRF cup consisting of double open ended plastic rings with a thin chemically inert polypropylene film at the base. Samples were run under a vacuum for 6 minutes to achieve full characterization. During the analysis, the sample was rotated to mitigate any voids creased within the sample. Standards were run in the beginning and at the end of the analytical session, and after every ten samples to monitor the stability of the instrument (drift).



Figure 41. The portable benchtop Spectroscout (by Spectro) ED-XRF spectrometer

Table 13. XRF Major Elements (Scout) in Aitolampi samples

Aitolampi Sample	Na ₂ O %	MgO %	Al ₂ O ₃ %	SiO ₂ %	P ₂ O ₅ %	K ₂ O %	CaO %	TiO ₂ %	MnO ₂ %	Fe ₂ O ₃ %	S %	Total %
PA1-CXD	0.50	5.77	11.70	52.63	0.18	2.84	4.31	0.61	0.08	10.82	4.23	93.7
QA2-CXD	0.85	4.67	12.08	54.47	0.16	3.40	3.18	0.74	0.07	8.79	3.22	91.6
XA3-CXD	1.00	3.84	11.74	61.16	0.20	2.81	2.87	0.78	0.07	8.89	3.59	96.9
YA4-CXF	1.48	3.88	12.48	61.16	0.16	3.08	2.56	0.81	0.06	6.76	2.39	94.8
ZA5-CXF	0.97	5.46	11.93	55.93	0.18	3.14	3.62	0.77	0.08	9.07	4.00	95.1
Rougher Tails Eastern	2.7	4.8	12.7	63.8	0.1	3.2	2.9	0.7	0.1	7.2	3.1	101
Rougher Tails Western	2.1	6.3	13.0	59.4	0.2	3.1	3.1	0.7	0.1	8.5	3.6	100

Table 14. XRF Trace Elements (Scout) in Aitolampi samples - 1

Aitolampi Sample	V ppm	Cr ppm	Co ppm	Ni ppm	Cu ppm	Zn ppm	Ga ppm	As ppm	Se ppm	Rb ppm	Sr ppm	Y ppm
PA1-CXD	~1276	237.3	60.4	319.1	833.8	2553.0	20.8	<LOD	45.2	109.1	148.6	47.6
QA2-CXD	~1100	229.1	35.1	284.9	406.2	1375.0	20.9	<LOD	38.2	109.0	202.2	43.0
XA3-CXD	469.0	144.3	39.9	157.0	159.0	524.0	15.6	<LOD	8.2	89.0	209.3	29.5
YA4-CXF	234.0	128.4	25.6	96.3	114.6	150.3	17.2	1.8	3.1	88.9	197.5	22.7
ZA5-CXF	~1237	276.4	50.6	226.2	873.4	2595.0	26.4	<LOD	50.2	117.6	196.7	32.1
Rougher Tails Eastern	560.5	230.4	<LOD	112.0	84.2	687.8	15.1	<LOD	12.4	88.5	201.2	31.5
Rougher Tails Western	~908	257.7	<LOD	191.5	296.5	1550.0	17.1	<LOD	27.4	100.0	205.9	36.4

Note: Values prefixed with ~ can be considered as semi-quantitative only.

<LOD = Less than Limit of Detection

Table 15. XRF Trace Elements (Scout) in Aitolampi samples - 2

Aitolampi Sample	Zr ppm	Nb ppm	Mo ppm	Sn ppm	Sb ppm	Cs ppm	Ba ppm	La ppm	Hf ppm	Pb ppm	Th ppm	U ppm
PA1-CXD	152.7	6.6	173.8	<LOD	<LOD	56.2	477.5	130.3	8.0	18.3	5.9	10.1
QA2-CXD	194.1	8.3	148.1	<LOD	<LOD	43.3	593.8	164.3	8.2	17.6	6.8	8.0
XA3-CXD	174.6	5.9	46.1	<LOD	<LOD	49.2	471.9	147.1	13.3	8.3	1.5	<LOD
YA4-CXF	175.3	9.0	15.1	<LOD	11.1	58.9	578.8	142.0	1.4	9.1	2.2	<LOD
ZA5-CXF	138.9	5.7	162.8	<LOD	12.2	40.7	489.1	133.5	6.4	13.0	2.4	8.0
Rougher Tails Eastern	146.2	10.7	22.7	<LOD	<LOD	<LOD	561.8	54.1	<LOD	21.8	7.4	7.9
Rougher Tails Western	168.6	11.0	62.9	<LOD	<LOD	<LOD	549.4	96.9	<LOD	22.9	12.8	12.7

Note: Values prefixed with ~ can be considered as semi-quantitative only.

<LOD = Less than Limit of Detection

Table 16. XRF Trace Elements (Scout) in Aitolampi samples – 3

Aitolampi Sample	Bi ppm	Br ppm	Cd ppm	Hg ppm	Ta ppm	W ppm
PA1-CXD	<LOD	<LOD	0.0	<LOD	<LOD	7.9
QA2-CXD	<LOD	<LOD	0.0	<LOD	<LOD	10.4
XA3-CXD	<LOD	<LOD	0.0	<LOD	<LOD	10.4
YA4-CXF	<LOD	<LOD	0.0	<LOD	<LOD	<LOD
ZA5-CXF	<LOD	<LOD	0.0	<LOD	<LOD	9.7
Rougher Tails Eastern	<LOD	<LOD	0.0	1.7	19.4	<LOD
Rougher Tails Western	<LOD	<LOD	0.0	2.0	14.1	<LOD

Note: Values prefixed with ~ can be considered as semi-quantitative only.

<LOD = Less than Limit of Detection

Appendix J shows a comparison of different XRF methods.

14 LASER INDUCED BREAKDOWN SPECTROSCOPY (LIBS)

Laser Induced Breakdown Spectroscopy (LIBS) is an atomic emission spectroscopy technique that provides elemental data using high energy laser pulses to excite the sample. The excited sample emits light with discrete spectral peaks that can be used to define elemental concentrations qualitatively or quantitatively. LIBS is a technology that is similar to ED-XRF that is capable of analyzing up to 30 elements in rock samples. The technique is complimentary to ED-XRF whereby the LIBS is capable of replicating the major and trace elements but it can also detect light elements (e.g. Na, Mg and Li). The LIBS instrument operates by measuring light emission from a plasma which is generated by a laser. The LIBS is capable of direct analysis of a material, in contrast, ICP-OES requires the dissolution of the sample.

Samples were homogenized and prepared into pressed pellets using an in-house technique. 1 g of the micronized sample powder (as described for XRD whole rock preparation) was mixed with 0.1 g of binder and pressed using a 15T press for 1min, producing a 13 mm diameter pellet.

Pressed pellets were analyzed with a J200 LIBS instrument manufactured by Applied Spectra. The instrument utilizes a Nd:YAG femtosecond laser with a wavelength of 343 nm for ablating the samples. The femtosecond nature of the laser means that it has ultrashort pulse duration, which allows firing at very high repetition rates, with minimum heating effects (melting) on the sample, as opposed to a nanosecond laser. The laser is coupled with two spectrometers of high sensitivity, in the ranges of:

- Spectrometer 1 (Spec 1): 180 – 600 nm (UV – Visible range)
- Spectrometer 2 (Spec 2): 470 - 800 nm (Visible – IR range)

A 10-spot analysis experiment was utilised to acquire a full spectroscopic LIBS range from 180 nm (UV) to 800 nm (N-IR), in order to acquire the (major) elemental fingerprint of these samples. 200 spectral measurements (number of shots) were taken per spot under an argon environment assuring a low spectral intensity variability.

Spectra are qualitatively interpreted, annotating major elements' vibration wavelength, using the existing chemical composition. When more samples are available, more advanced statistical analysis can be applied for classifying samples with different chemical compositions, potentially linked to different processes.

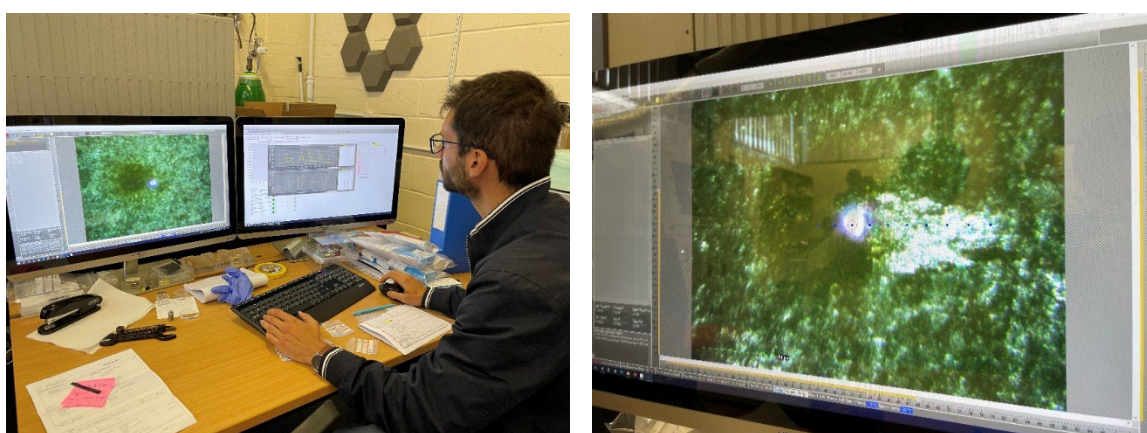


Figure 42. The J200 LIBS instrument manufactured by Applied Spectra

Five samples of graphite ore and two sample of graphite tailings were analyzed with LIBS for their spectral signal. Samples have different graphite content along with other aluminosilicate minerals present. ED-XRF analysis showed some relative enrichment in some of the transition metals such as Zn, Ni, Cu, V, Mo etc.



Figure 43. Graphite ore samples, PA1-C, QA2-C, XA3-C, YA4-C, ZA5-C and graphite tailings APTE-C and APTW-C.

14.1 Instrument parameters

LIBS analysis parameters were:

- Spectral resolution (Grating): 1200
- Gate Delay and gate width: 0.11 & 3 usec
- Energy at 70%
- Number of shots: 200 @ 40Hz repetition rate
- Spot size 30um

14.2 Graphite ore samples

The 5 graphite ore samples showed high similarity in their spectral pattern, as it can be seen in Figure 44 & 45 for Spec 1 and Figure 46 for Spec2.

In Figure 44 and Figure 45 some of the major elements are annotated such as Si, Mg, Al, Ca and Fe, corresponding the aluminosilicate phases in those samples. Carbon absorption line is at 193 nm, according to the literature, but in the case of these samples and the parameters tested, C was not identified. Other observations that can be made is that, in the particular set of samples, LIBS spectra can be used for a qualitative analysis as the changes at the intensities of elemental absorption are clear across the five samples. Similar interpretation can be made for spectral patterns in Figure 46, where Na and K dominate the spectral signal, with relative minor Ca and Mg also appearing, as annotated respectively in the graph.

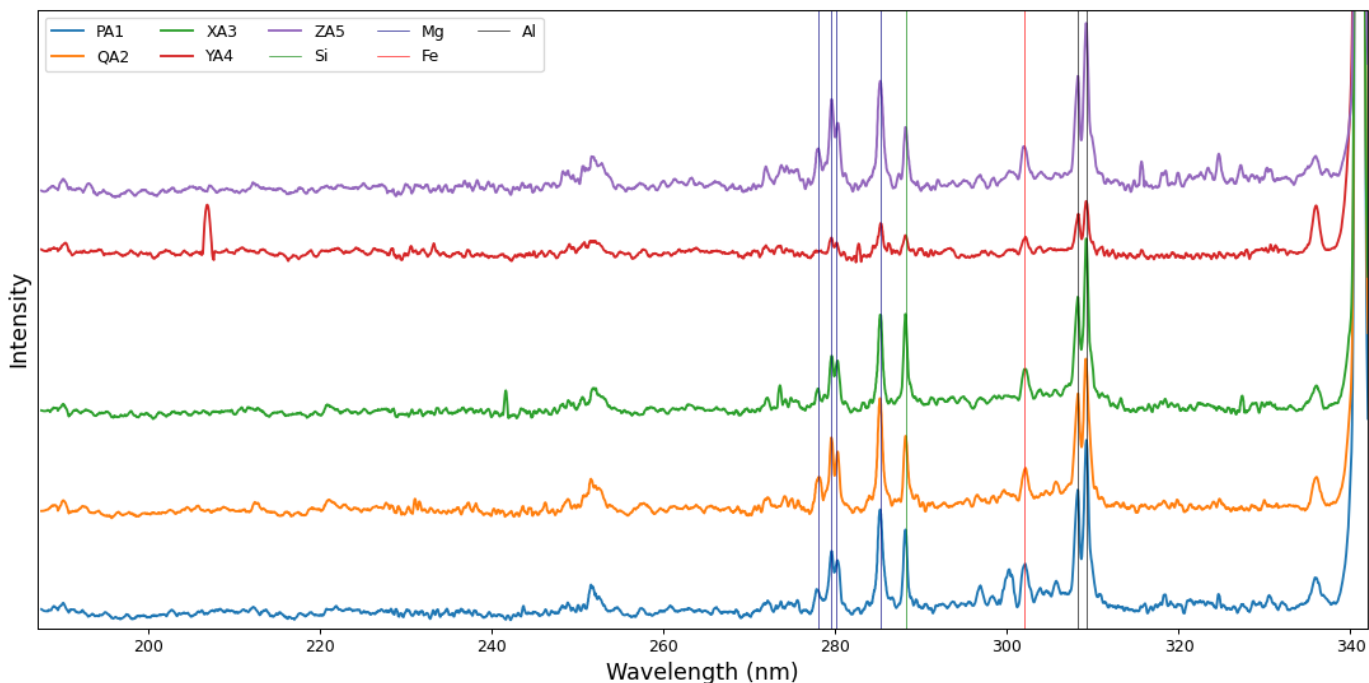


Figure 44. LIBS spectra of graphite ore samples in the Spec1 subregion of 187-340 nm. Annotated are the major elements that occur in the region

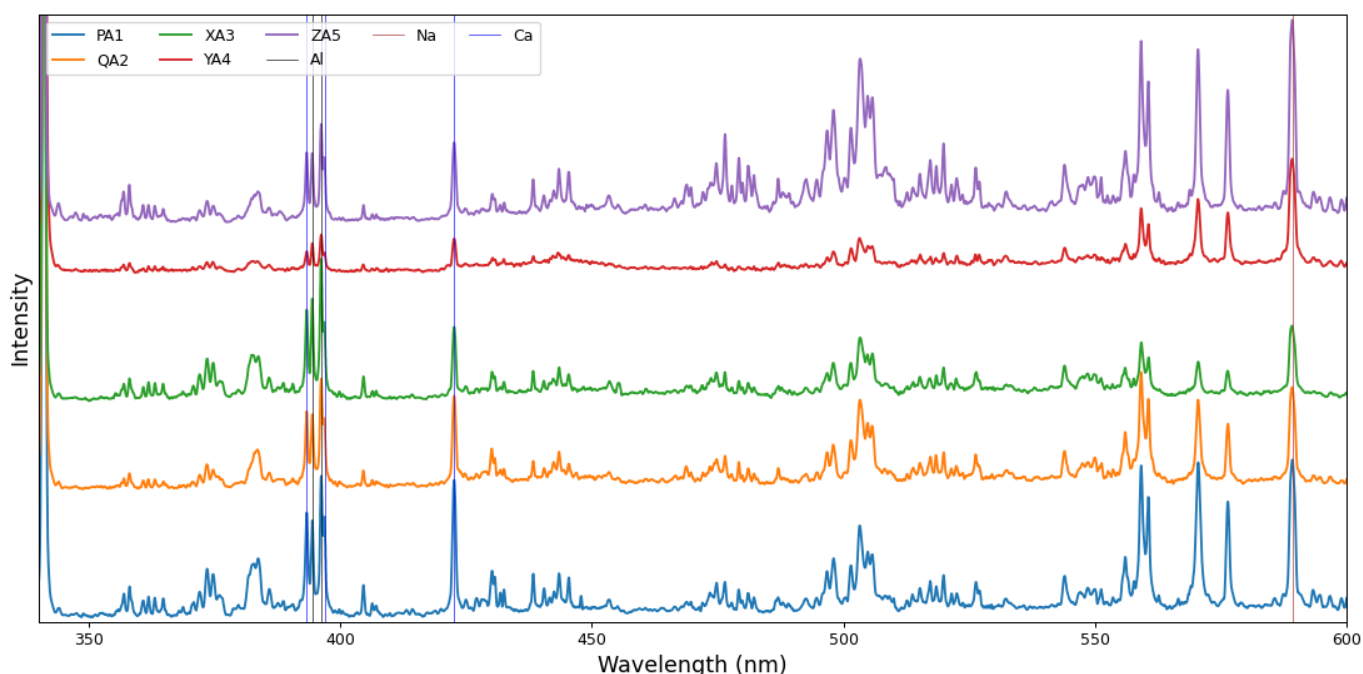


Figure 45. LIBS spectra of graphite ore samples in the Spec1 subregion of 340-600 nm. Annotated are the major elements that occur in the region.

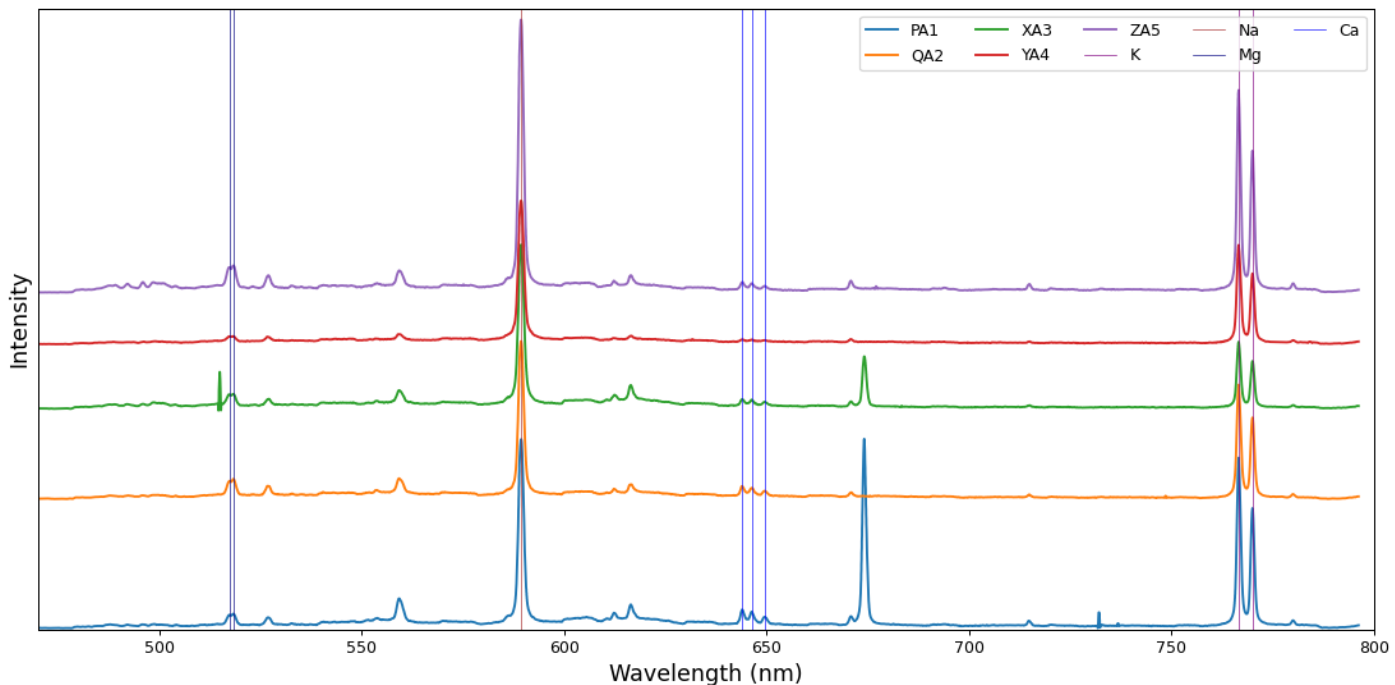


Figure 16. LIBS spectra of graphite ore samples in the Spce2 region of 450-800 nm. Annotated are the major elements that occur in the region

14.3 Graphite Tailings

Tailing samples have very similar spectral pattern as the graphite ore samples. Since the signal comes primarily from the elements incorporated in the alumino-silicate minerals, no big changes should be expected in the actual spectra (Figures 47 to 49) when compared to those of the graphite ore above. The lack of C peak identification, which would be the distinction factor between graphite ore and tailings is under further examination and parameters optimization.

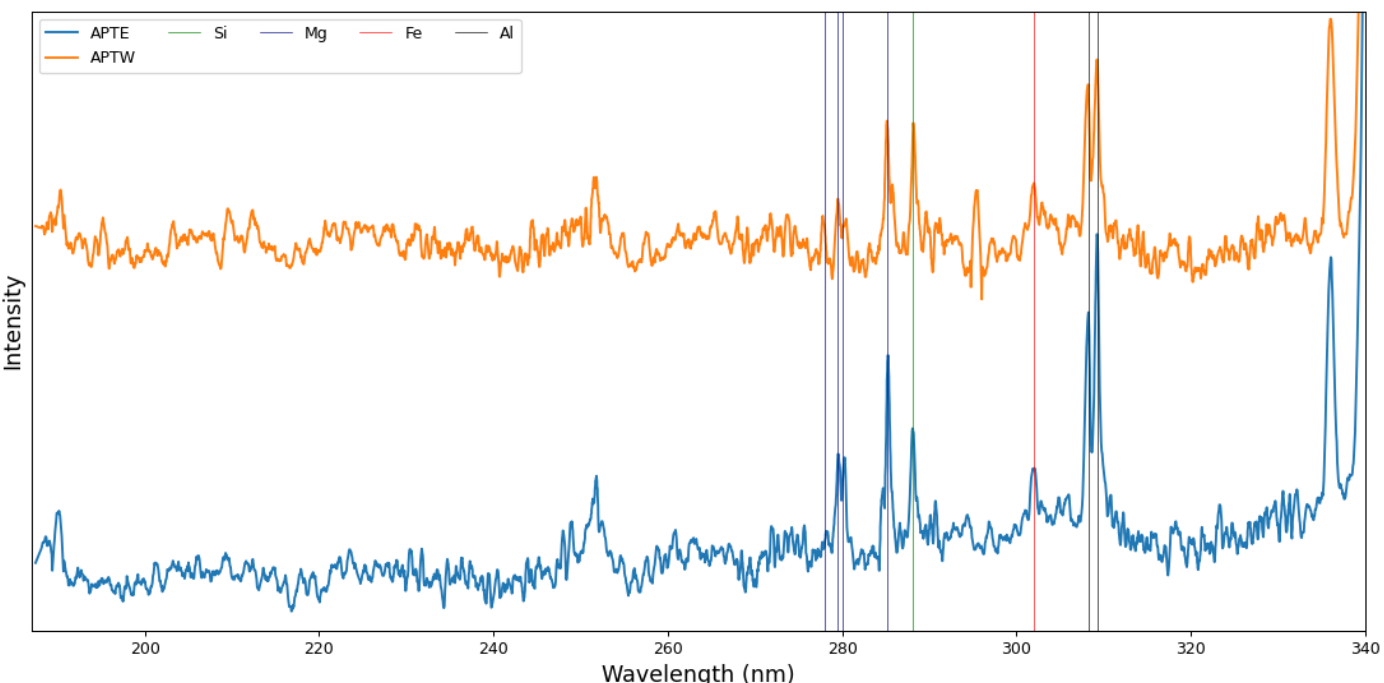


Figure 47. LIBS spectra of graphite tailings samples in the Spce1 subregion of 187-340 nm. Annotated are the major elements that occur in the region

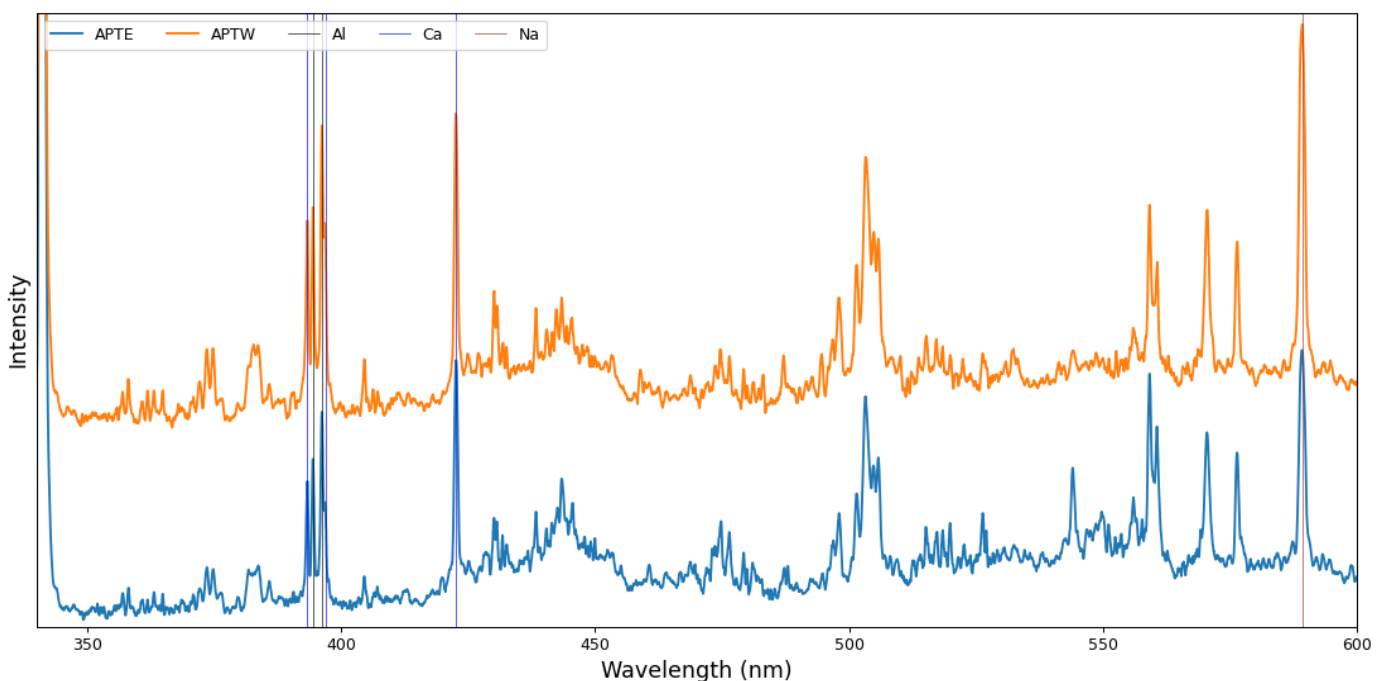


Figure 48. LIBS spectra of graphite tailings samples in the Spce1 subregion of 340-600 nm. Annotated are the major elements that occur in the region

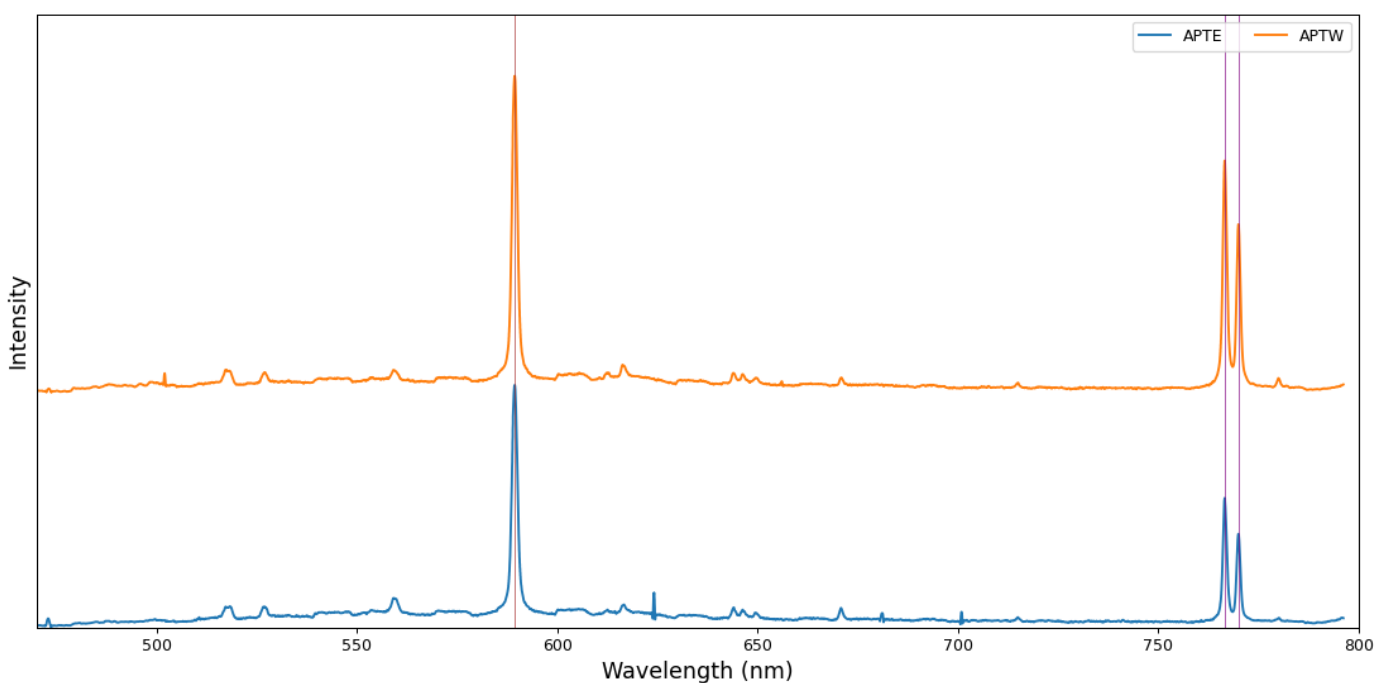


Figure 49. LIBS spectra of graphite tailings samples in the Spce2 region of 450-800 nm. Annotated are the major elements that occur in the region

15 RAMAN SPECTROSCOPY

Raman spectroscopy is an automated mineral identification technique that is based upon inelastic scattering of light when sample is irradiated with laser (Raman effect). It is used to characterize the chemistry and structure of a grain to identify the mineral, but it can also provide information on texture, size, liberation and relationships between phases. The technology is routinely used to quantify the accessory mineral composition in sandstones or coarse silt to sand sized materials. The effective constraint on analysis is the grain-size of the analyte.

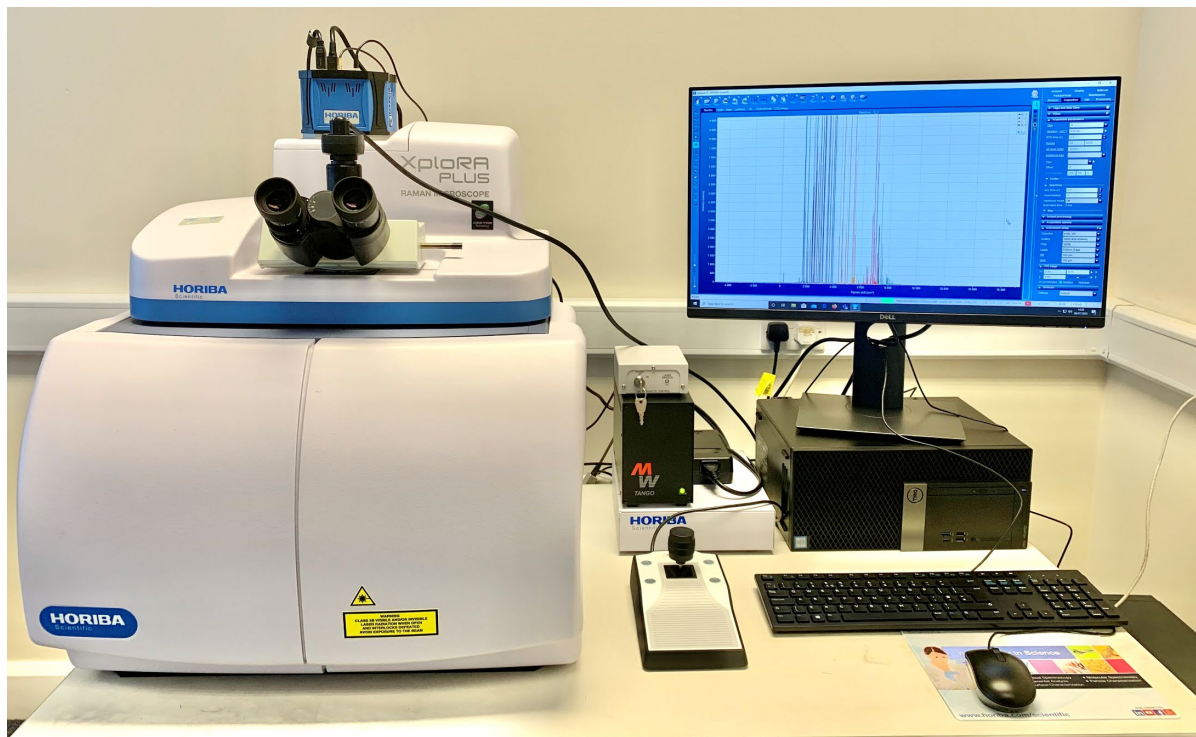


Figure 50. Horiba Xplora Plus spectrometer with a continuous window and 532 nm laser

For interpreting the Raman data, database Raman shift spectra were taken from the RRUFF database as well as the literature available on some of the phases present in the samples analyzed (Xiaojian *et al* 2012, Su Kyoung *et al* 2019, Sharma *et al* 2006 and Singh *et al* 2017). An example of Raman spectrum from the literature is shown in Figure 51.

On the Raman shift spectra in the samples for this section, the main wavelength bands are annotated and assigned to the mineral phases associated. Shifting, at lower or higher wavelengths, of these main bands was observed, as the position can be dependent by the elemental variation as well as the process (P/T/water conditions) these phases were created from.

Five ore graphite samples were analyzed with Raman microscopy for their spectral fingerprint. PA1-C, QA2-C, XA3-C, YA4-C, ZA5-C were received as smashed rock chips. In order to perform the Raman analysis, resin blocks were prepared and polished for each sample, revealing a granular representation of the rock. Within these grains, it was possible to identify the main mineralogy as well as the presence of graphite. Textural information can also be drawn by the analytical approach developed.

Raman microscopy workflow analysis:

- Point analysis of present mineral phases within 2 grains for each sample
- Map scans of the same two grains for acquiring a cumulative spectrum

Raman analysis parameter setting:

Point and map scan analysis

- Laser: 532 nm
- Energy: 25%
- Acquisition time: 1 sec
- Acquisition accumulation: 1 spectrum
- Magnification lenses: 10X (unless otherwise specified)

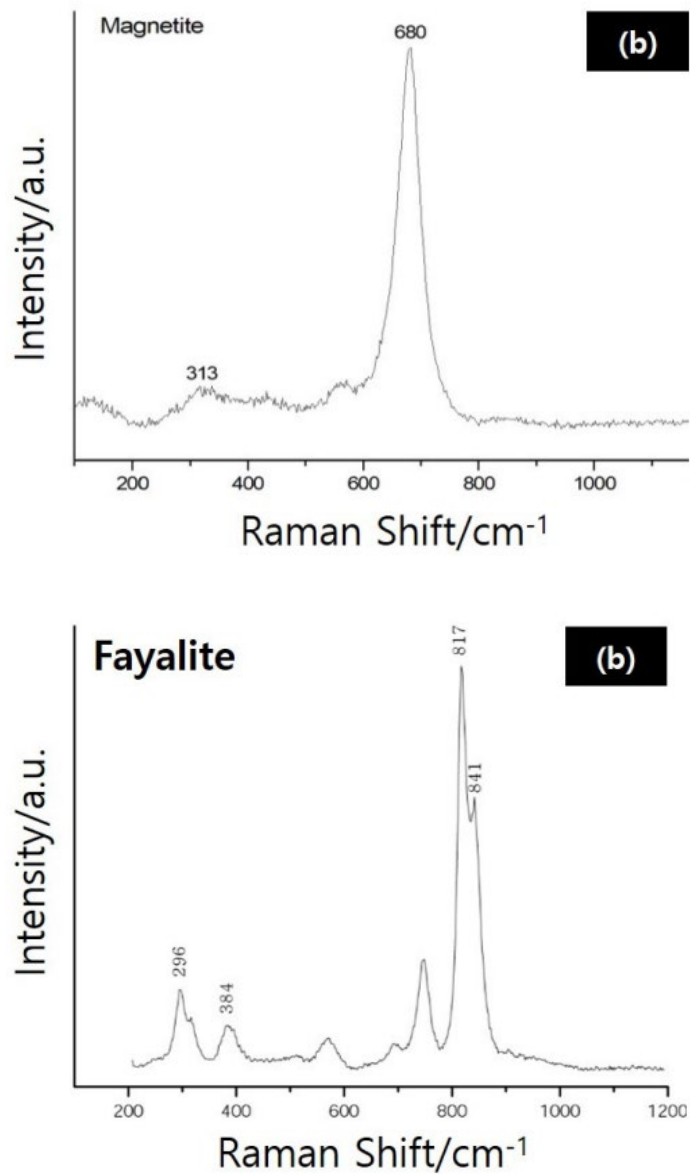


Figure 51. Examples of Raman spectrums (Source: Su Kyoung et al 2019)

In addition to this workflow, 4 high resolution scans were performed only for sample YA4-C. Three of the scans were performed on three different grains under 10X magnification while the fourth scan was performed under 50X for configuring the texture in more detail.

It is important to note that the way all samples were presented for analysis (as centimeter rock chips), introduces a degree of bias to the analysis, as some grains would contain only silicates, while others may have opaque phases or graphite grains. An example of the general view of the ore resin blocks is shown in Figure 52.

Two tailings samples, APTE-C and APTE-W, were analyzed with Raman microscopy, after preparing resin polished packs. Similarly to the ore samples, point analysis was performed for acquiring individual mineral phases spectra. Due to the finer grain size of both of these samples, map scans were not possible to acquire, as the resin material would interfere with the grains. For that reason, a higher amount of point analysis was done. These were added to acquire the cumulative spectrum for the non-opaque minerals. A second cumulative spectra for the non-opaque mineral phases is given, where possible.

All spectra presented are corrected for the resin background signal. However, resin material signal interference may still be present. Figures # to # show samples YA4 as an example. Appendix K has a more complete showing of all 5 ore samples and the 2 tailings samples.

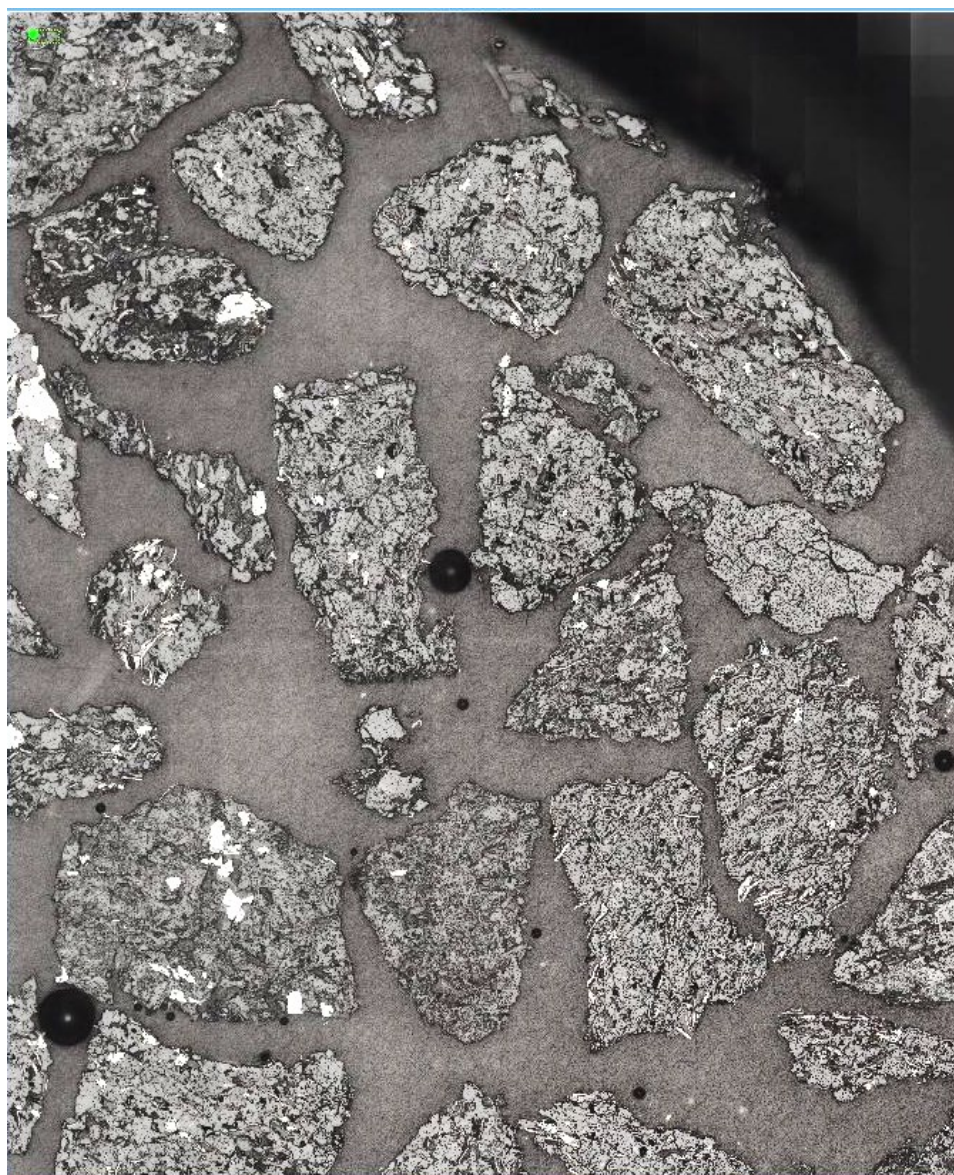


Figure 52. Grain size and sample representation in YA4-C graphite ore sample.

High resolution maps were constructed for the YA4-C ore sample, as an example of textural analysis by Raman microscopy. In this case, three different grains were scanned, using a grid of over 9000 point analyses, producing a mineralogical map. The information of the initial grain, grid, and identified mineral location was compiled in Spotfire, producing a mineralogy map as shown in Figures 53, 54 and (Appendix K). This Raman analysis configuration can give the textural context of the analyzed area/grain, illustrating the relationship between graphite and other mineral phases present.

It can be observed that graphite has an elongated crystal structure in the majority of the cases, with no preferential proximity to other minerals. It appears to occur adjacent to any of the silicate minerals, e.g. quartz, plagioclases or micas, as well as the Ti-rich phases.

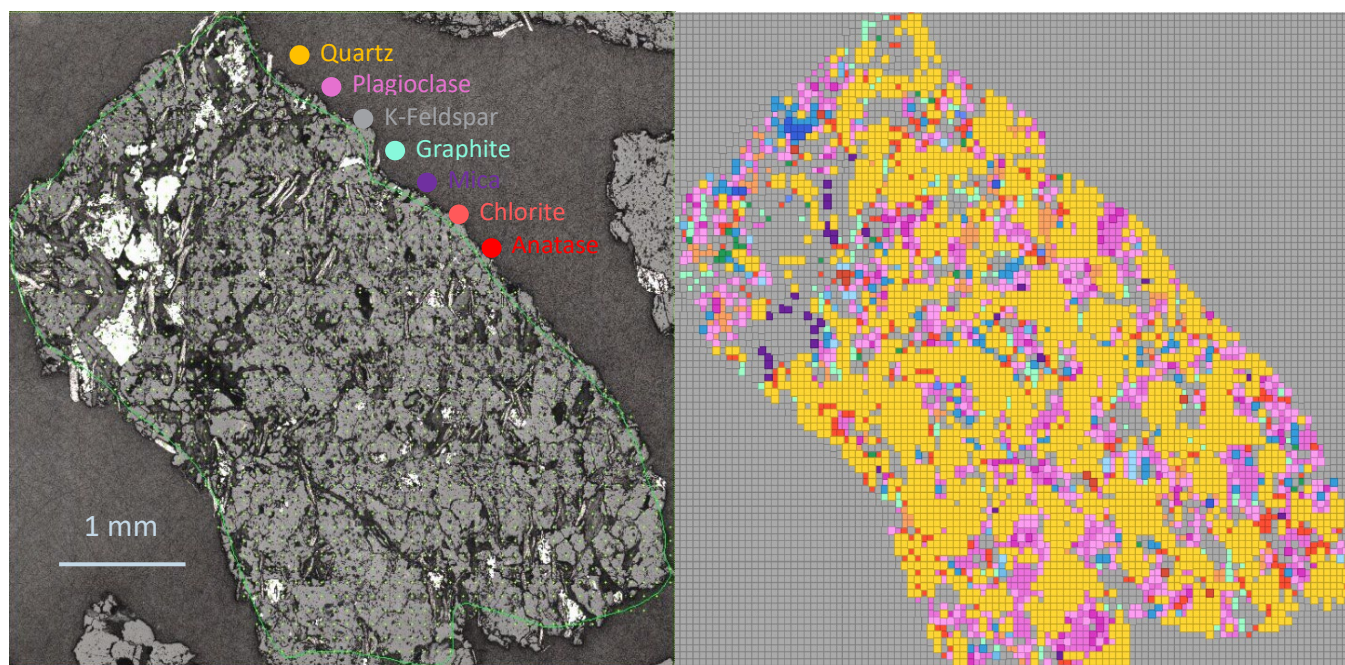


Figure 53. High resolution map scan of a selected grain in YA4-C, under 10X magnification lense, (left-hand side). A compilation of the mineralogy according to the gridding reference of the map scan using Spotfire (right-hand side)

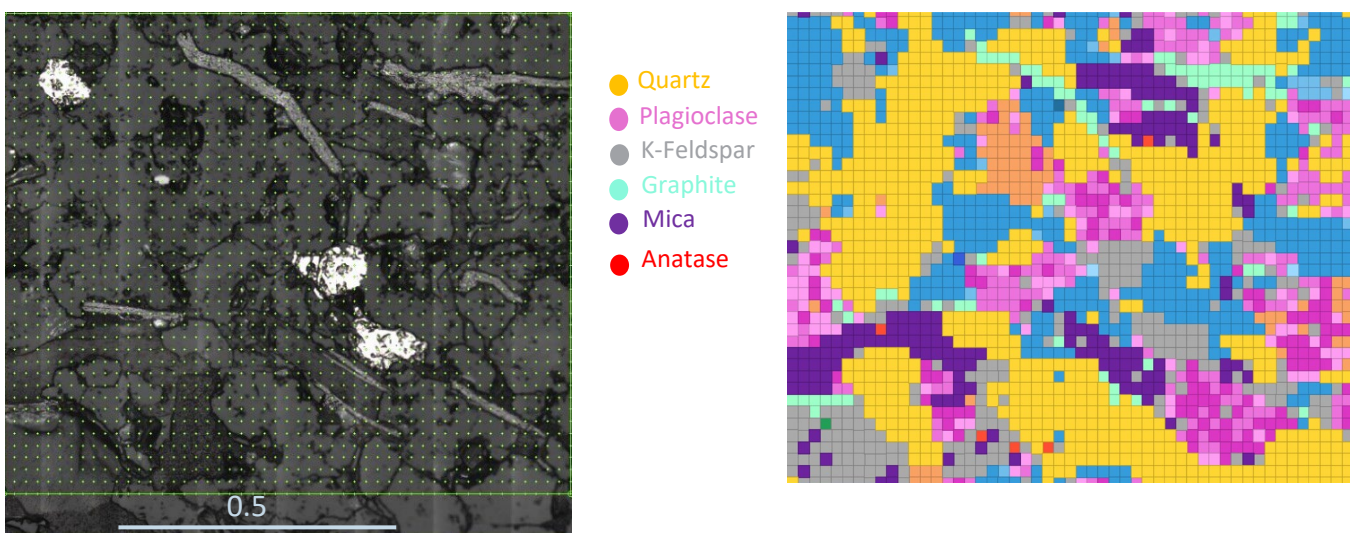


Figure 54. High resolution map scan of a small grain area in YA4-C, under 50X magnification lense, (left-hand side). A compilation of the mineralogy according to the gridding reference of the map scan using Spotfire (right-hand side)

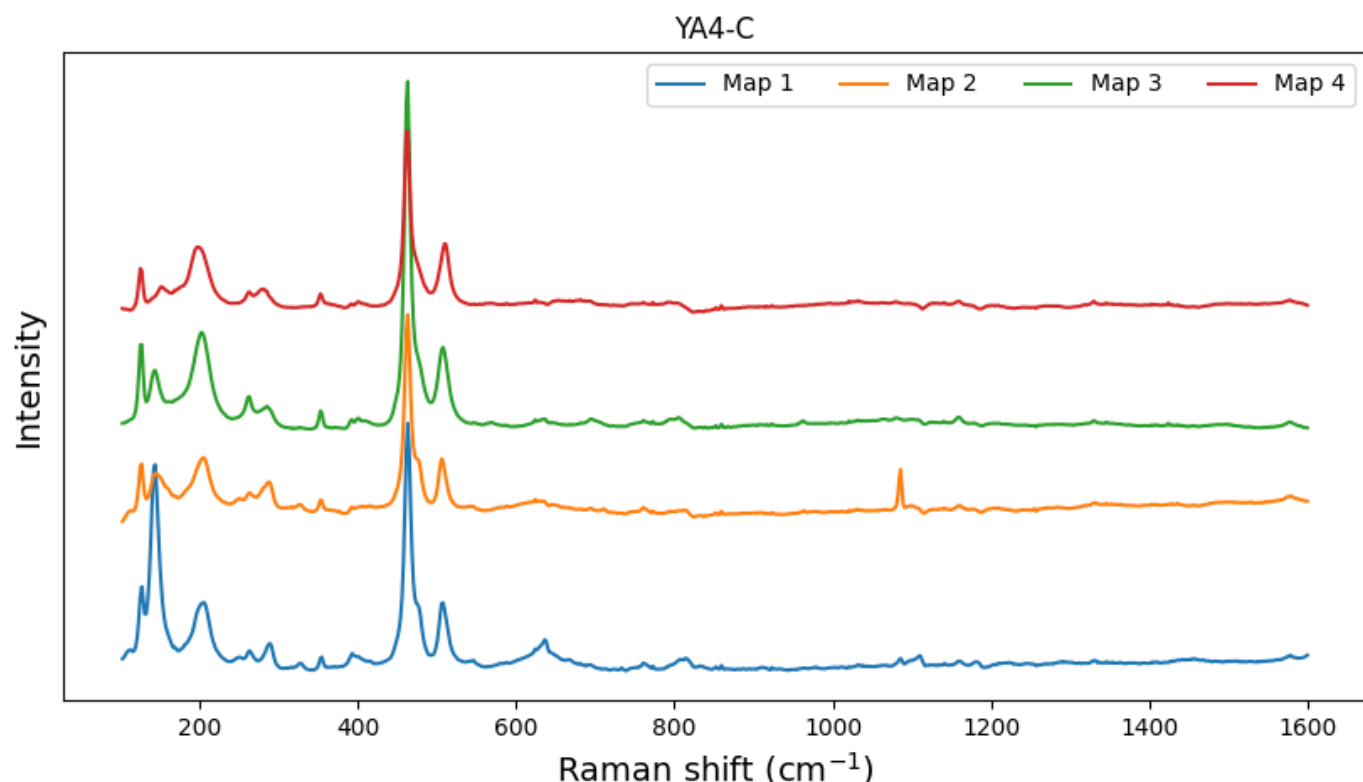


Figure 55. Cumulative spectra for 4 different high resolution grain scans. Map 3 corresponds to scan in Figure 8 and Map 4 from scan shown in Figure 9. See Appendix for Grain 1 – Map 1, and Grain 2 – Map 2.

16 FOURIER TRANSFORM INFRARED SPECTROSCOPY (FTIR)

Fourier Transform Infrared Spectroscopy (FTIR) is a technique used to obtain an infrared spectrum from a broad spectral range. The technology is used to detect different functional groups with characteristic absorption or emission lines. FTIR can provide mineralogical data as percentage with minimal sample requirements from small sample amounts when based on a model built from XRD data.

The analyses here were run on the same split that was first used for the XRD analyses. This is to ensure that the FTIR results are comparable to the XRD results. The sample is analyzed with a compact Bruker Alpha FTIR spectrometer. The instrument is first set-up to collect a background spectrum with a clear sample plate. Once this is collected, a small amount (<50 mg) of the powdered sample is put on the sample window and analyzed. The instrument then calculates and presents the spectrum.

Upon data collection, the different bands vibrating are assigned to the structures / stretching and bending vibrations of molecules that should be present, according to the XRD results, e.g. Si-O for silicates, CO₃ for carbonates, Al-O for aluminosilicates, etc.

For mono-mineralogical samples, database FTIR spectra are used to compare between nominal and the ‘unknown’ spectra, which can lead to identification of structural interferences due to cations substituting key structural sites of the minerals. Although these changes are not unique to one or two substitutions, the chemical breakdown of those samples can be indicative of these changes.

For more quantitative analysis, a number of samples are needed to build a FTIR-XRD calibration, which can help the quantification of the minerals present in unknown samples, and with more advanced and bespoke modelling, the structural changes can also be identified.



Figure 56. Bruker Alpha instrument with an ATR stage and a M-IR range of 4000-400 1/cm

FTIR analysis was conducted on five Aitolampi graphite drill core ore (Figures 57 & 58) and two pilot tailings samples (Figures 59 & 60), using the XRD powder split. Upon data acquisition, spectra are corrected for the scattering background, and then interpreted according to the QXRD analysis for presence of quantified minerals. The interpretation is based on nominal/database spectra of those minerals taking into account any relevant rock matrix shifting of the main vibrating bands.

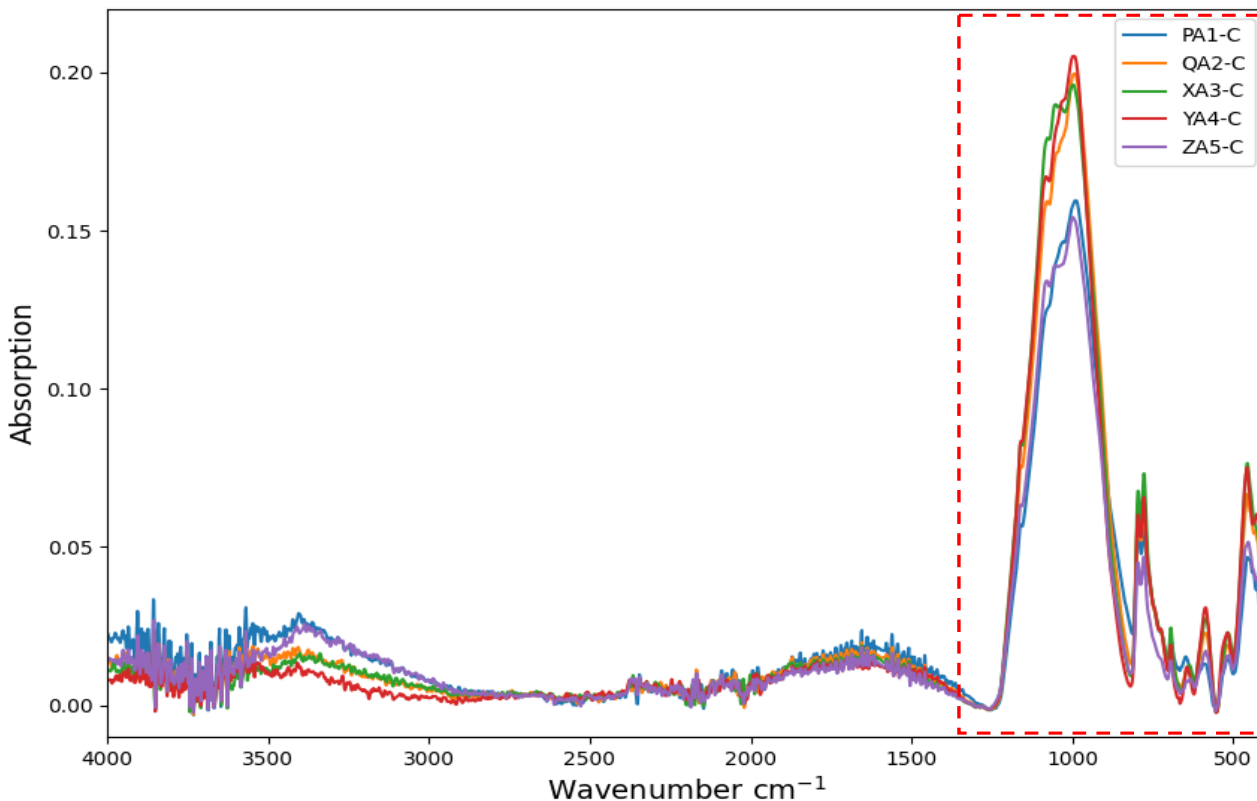


Figure 57. Graphite ore spectra from 4000 cm⁻¹ to 400 cm⁻¹. Annotated is the area of C-H bond presence and red box refers to Figure 58.

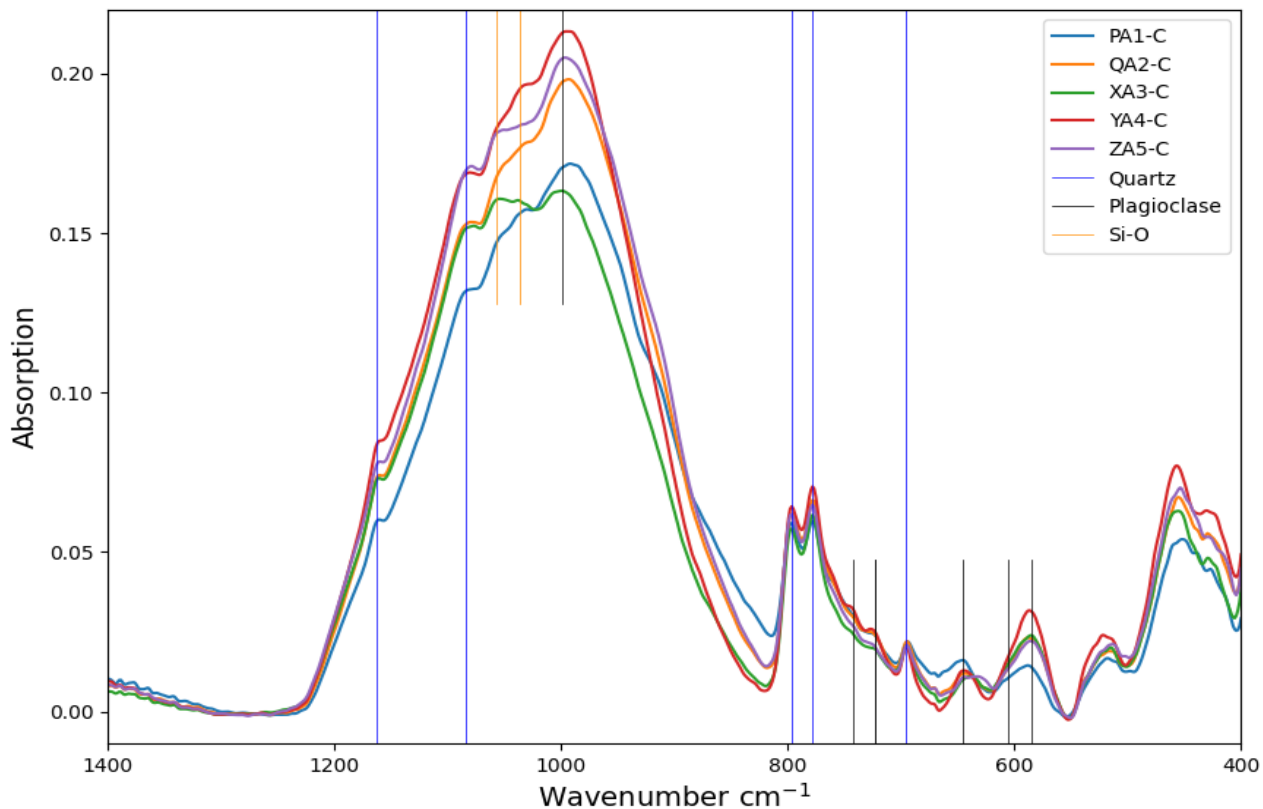


Figure 58. Graphite ore spectra from 1400 cm⁻¹ to 400 cm⁻¹. Annotated are the main wavenumber bands corresponding to quartz, plagioclase and Si-O bonds related to the other aluminosilicates present.

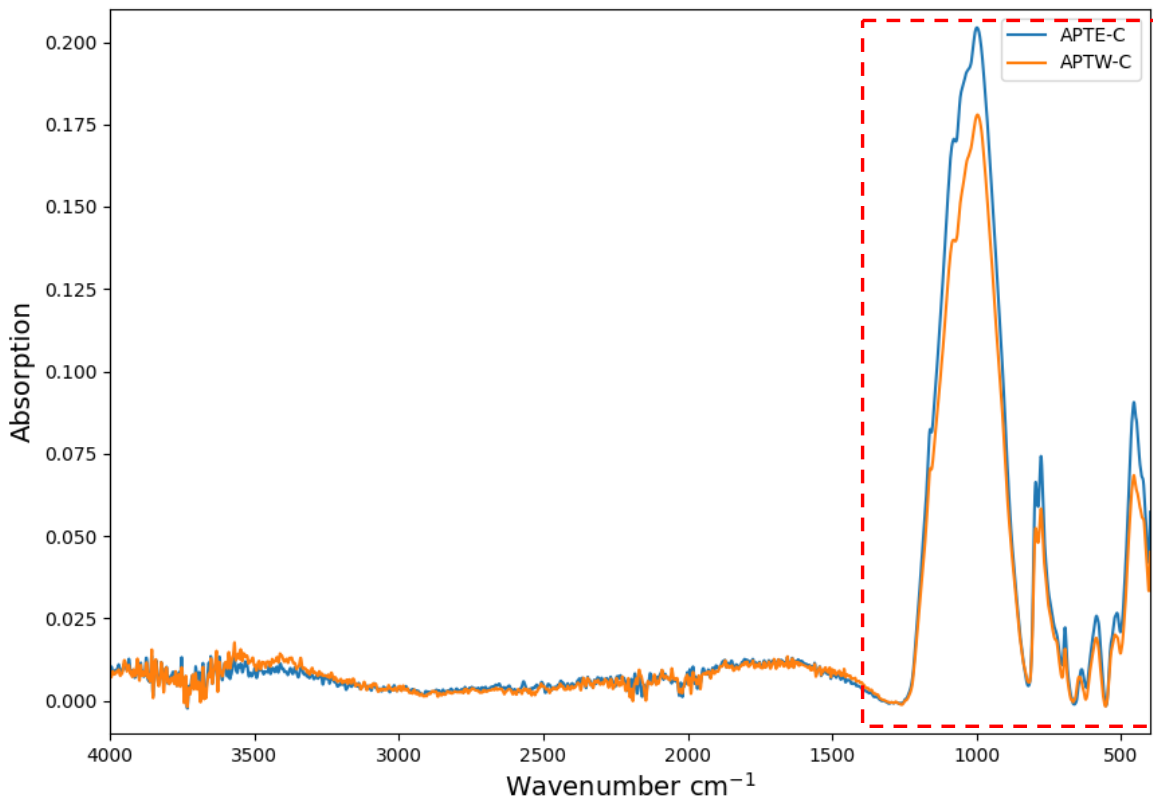


Figure 59. Graphite tailings spectra from 4000 cm⁻¹ to 400 cm⁻¹. Annotated is the area of C-H bond presence and red box refers to Figure 60.

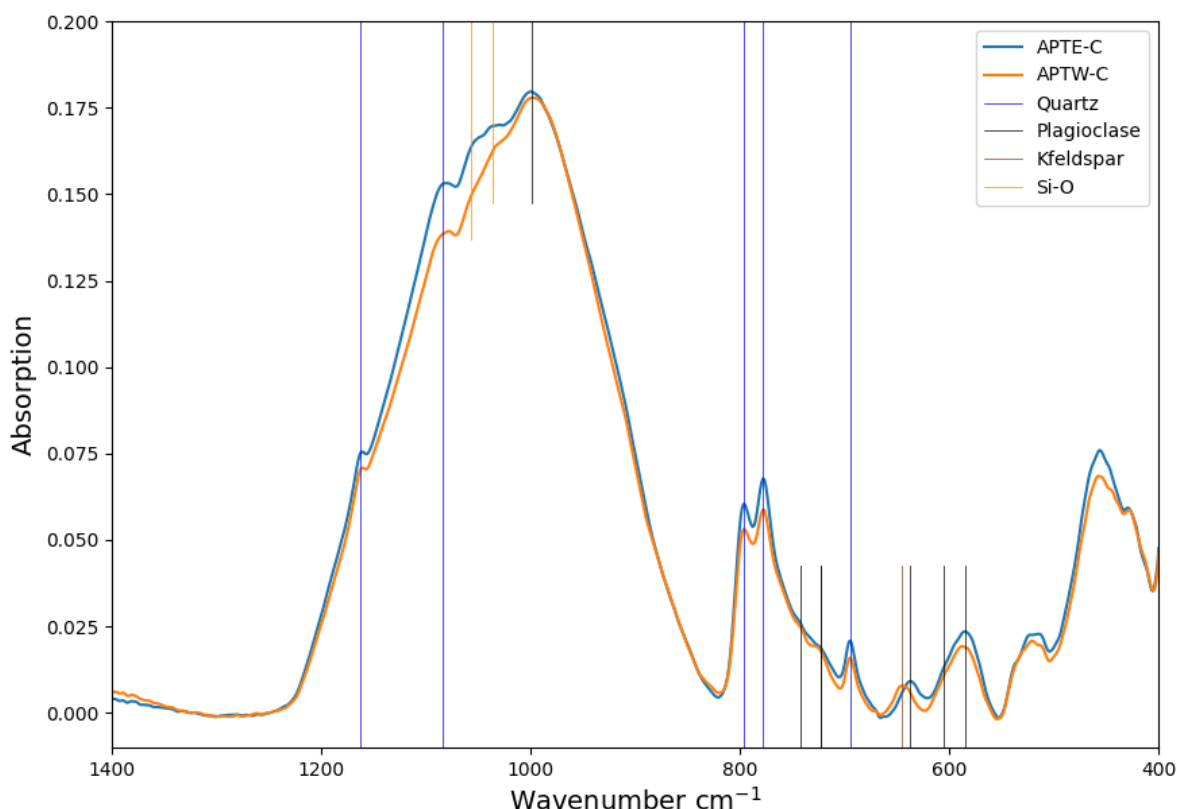


Figure 60. Graphite tailings spectra from 1400 cm⁻¹ to 400 cm⁻¹. Annotated are the main wavenumber bands corresponding to quartz, plagioclase and Si-O bonds related to the other aluminosilicates present.

17 AUTOMATED MINERALOGY SEM ANALYSIS

Samples were prepared and investigated by Duncan Pirrie, Helford Geoscience LLP), using automated SEM-EDS along with individual spot chemical analyses using EDS (this work was conducted as a subcontractor through X-Ray Mineral Services Oy). The aim of the analysis is to gain an understanding of how the metals are occurring within the sample along with what form any Br, Bi and Se present is occurring in.

17.1 Sample preparation to produce SEM polished blocks

On receipt the samples were sealed within labelled plastic zip lock sample bags. The samples were digitally photographed and then subsampled, with an approximately 1 g aliquot of each sample dispersed with a filler and then resin impregnated. On curing, the resin blocks were then cross sectioned, and the cross sectioned surfaces remounted within a resin block, and then polished, so that both areas of the cross section were within the polished face for analysis. This preparation method was used to test for particle segregation within the resin. The surface of the blocks were polished and carbon coated prior to analysis.

The composition and texture of the sample was quantified through automated SEM-EDS analysis (Schultz et al., 2020). Analysis was undertaken using a Hitachi SU3900 scanning electron microscope fitted with a single large area (60 mm²) Bruker SDD energy dispersive spectrometer and running the AMICS automated mineralogy software package. Beam conditions are optimized for analysis and therefore an accelerating voltage of 20kV coupled with a beam current of approximately 15 nA were used. The sample was measured with a segmented field image mode of analysis. This analytical mode subdivides the BSE image into domains (segments) of similar brightness which represent different particle compositions and then acquires a representative EDS X-ray spectrum from a point within the segment; the phase identified is then assigned to

the entire segment. Measurements are optimized to highlight both textural and modal mineralogical information and so an effective image resolution of 1.1 µm is achieved.

The ED spectra acquired during the measurement are compared with a library of measured and synthetic standards and a phase identification is made on a closest match basis. Phases which are not represented in the standards list at the time of measurement are added either by acquiring reference spectra directly from the sample, or by creating a reference spectrum from the measurement itself. As the standards list can comprise hundreds of reference spectra, the data are grouped into a final, reported compositional list (Table L1, Appendix L). These samples are likely to contain predominantly man-made phases, along with less abundant naturally occurring mineral species; the man-made phases are given compositional names and the phases included within each category are described in Table L1. Modal data expressed as area % are provided. During the automated analysis a full area SEM-BSE montage is also captured of the analyzed area. The modal compositional data are provided in excel file HG-22-11b. In addition, “association” data are provided for both samples; these data are based on the measured numbers of transitions between one compositional group and another. Where the association is with “background” it means that the measured phase is adjacent to the mounting medium (resin).

17.2 Sample PA1-CAM

The modal mineralogy data for Sample PA1-CAM for the three size fractions and replicate analyses are presented in Table L3 in Appendix L as mass %. In this summary major minerals form >10%, minor minerals 1-10% and trace minerals (<1%).

The -250/+150 µm size fraction for Sample PA1-CAM is composed of major quartz (22.79-23.50%), plagioclase (15.08-15.62%) and pyrrhotite (14.56-17.57%) along with minor orthoclase, muscovite, biotite, phlogopite, vermiculite, chlorite, clinopyroxene and amphibole, CaAl silicates, graphite (2.07-6.11%) and pyrite (1.62-2.11%). Trace phases present are: kaolinite, calcite, chalcopyrite (0.13-0.29%), sphalerite (0.42-0.56%), molybdenite (0.01%), Fe oxides, Ti oxides, titanite, apatite, zircon and monazite and “undifferentiated” (Table L3 in Appendix L, Figures 61 and 63).

The -150/+75 µm size fraction for Sample PA1-CAM is composed of major quartz (24.74-25.47%), plagioclase (13.07-13.40%) and pyrrhotite (15.11-15.84%) along with minor orthoclase, muscovite, biotite, phlogopite, vermiculite, chlorite, clinopyroxene and amphibole, CaAl silicates, graphite (7.47-7.81%) and pyrite (2.02-2.06%). Trace phases present are: kaolinite, calcite, chalcopyrite (0.19-0.21%), sphalerite (0.53-0.61%), molybdenite (0.02%), Fe oxides, Ti oxides, titanite, apatite, zircon and monazite and “undifferentiated” (Table L3, Figures 61 and 63).

The -75 µm size fraction for Sample PA1-CAM is composed of major quartz (25.97%), plagioclase (13.68%) and pyrrhotite (15.38%) along with minor orthoclase, muscovite, biotite, phlogopite, vermiculite, chlorite, clinopyroxene and amphibole, CaAl silicates, graphite (3.22%) and pyrite (2.81%). Trace phases present are: kaolinite, calcite, chalcopyrite (0.31%), sphalerite (0.83%), molybdenite (0.02%), Fe oxides, Ti oxides, titanite, apatite, zircon and monazite and “undifferentiated” (Table L3, Figures 61 and 63).

Modal Abundance Ore Phases PA1-CAM

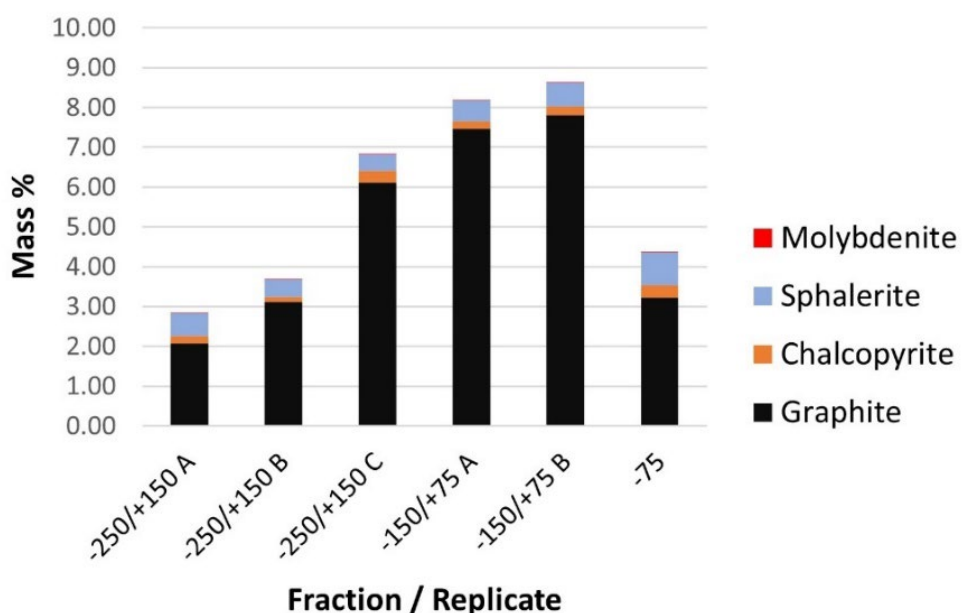


Figure 61. Modal mineralogy (mass %) ore phases for Sample PA1-CAM.

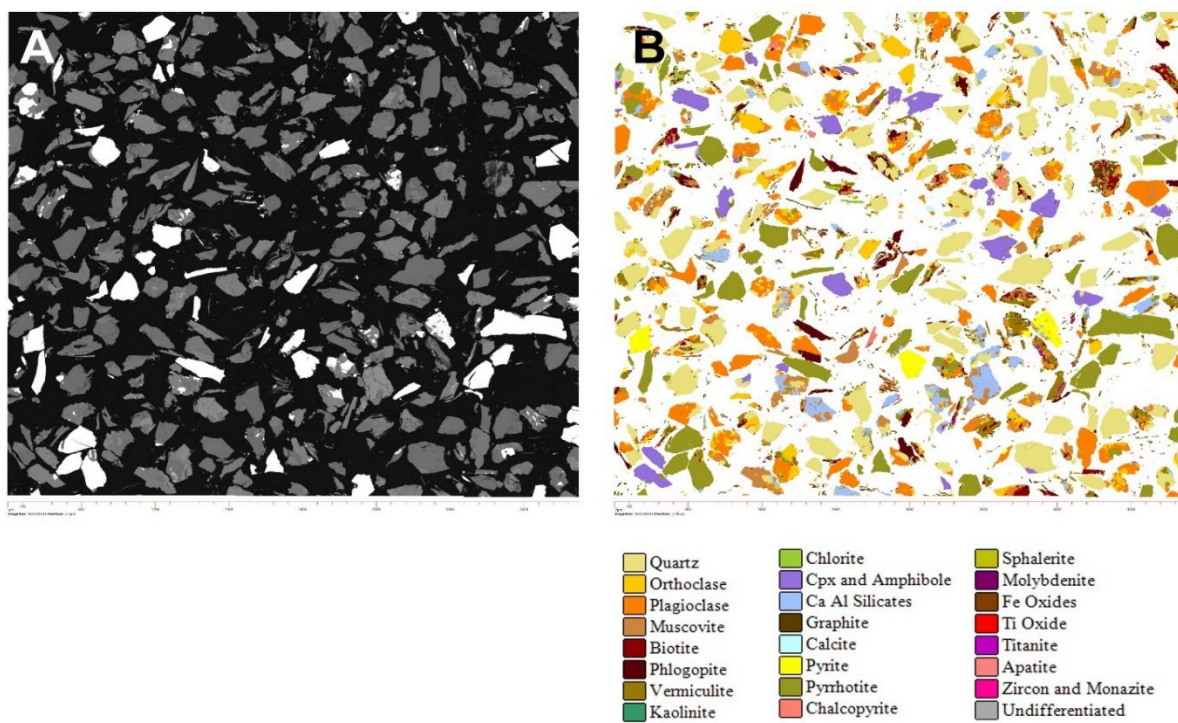


Figure 62. Higher magnification SEM-BSE image (A) and AMICS particle image (B) for the corresponding area Sample PA1-CAM - 250/+150 µm size fraction replicate A. Note the clear correspondence between the AMICS and the SEM-BSE images.

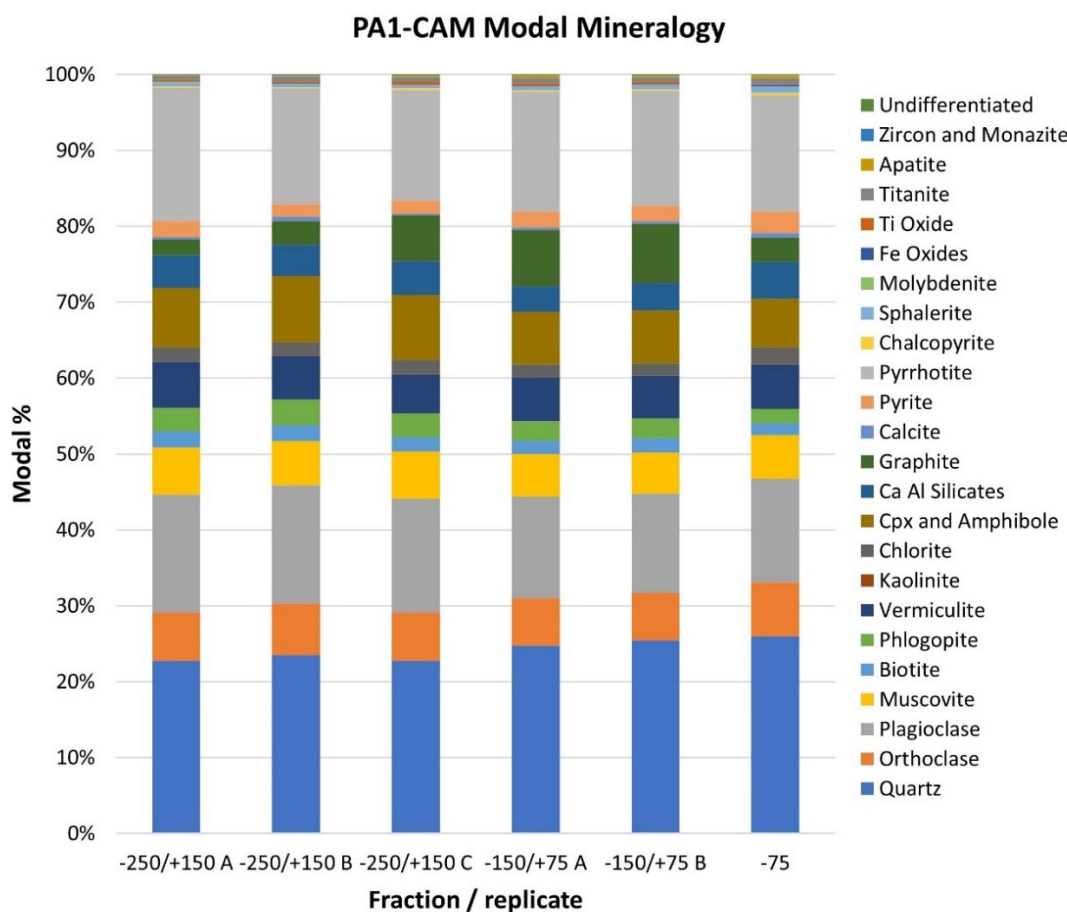


Figure 63. Modal mineralogy (mass %) all phases for Sample PA1-CAM

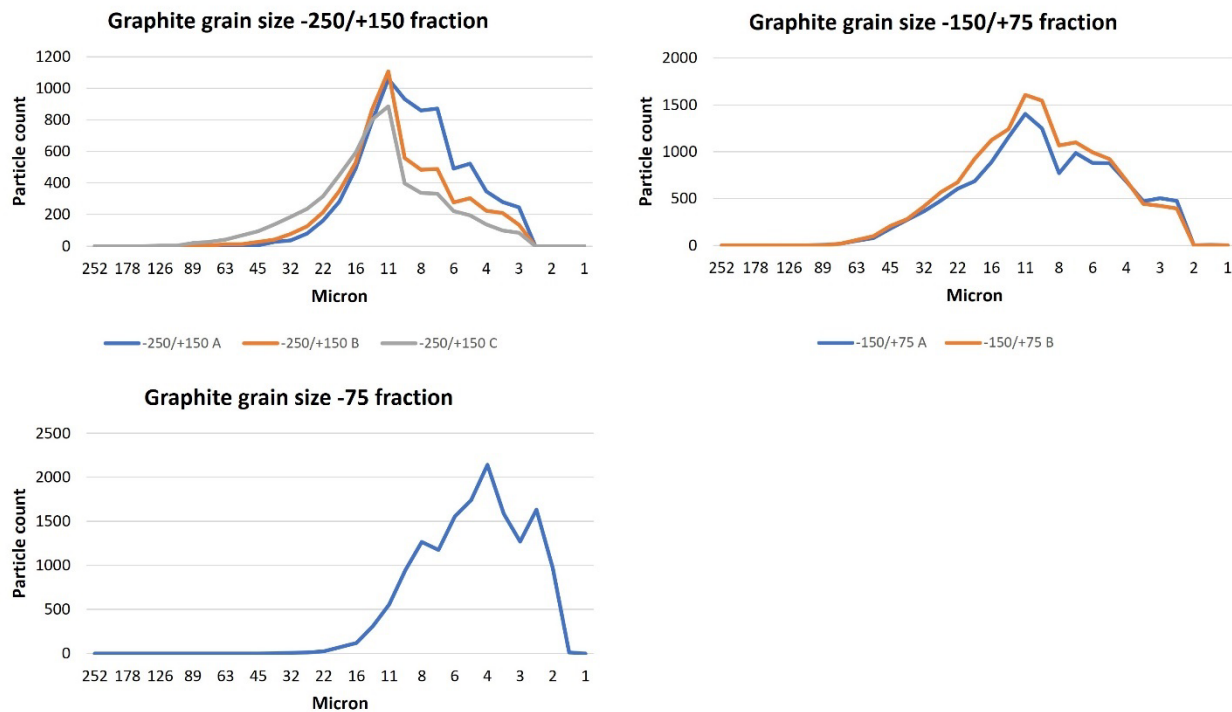


Figure 64. Graphs highlighting the grain size distribution data for graphite in the three size fractions analyzed from Sample PA1-CAM.

17.3 Sample QA2-CAM

The modal mineralogy data for Sample QA2-CAM for the three size fractions and replicate analyses are presented in Table 5 in Appendix L as mass %. In this summary major minerals form >10%, minor minerals 1-10% and trace minerals (<1%).

The -250/+150 µm size fraction for Sample QA2-CAM is composed of major quartz (27.38-29.52%), plagioclase (23.21-24.66%), phlogopite (11.00-12.36%) and pyrrhotite (9.55-11.55%) along with minor orthoclase, muscovite, biotite, vermiculite, chlorite, clinopyroxene and amphibole, CaAl silicates, graphite (1.68-1.95%) and pyrite (2.09-2.82%). Trace phases present are: kaolinite, calcite, chalcopyrite (0.09-0.27%), sphalerite (0.27-0.73%), molybdenite (0.01-0.02%), Fe oxides, Ti oxides, titanite, apatite, zircon and monazite and “undifferentiated” (Table L5 in Appendix L, Figures 67 and 65).

The -150/+75 µm size fraction for Sample QA2-CAM is composed of major quartz (32.18-32.58%), plagioclase (21.07-22.54%), phlogopite (10.60-10.62%) and pyrrhotite (9.45-11.11%) along with minor orthoclase, muscovite, biotite, vermiculite, chlorite, clinopyroxene and amphibole, CaAl silicates, graphite (1.44-1.53%) and pyrite (1.76-1.96%). Trace phases present are: kaolinite, calcite, chalcopyrite (0.12-0.18%), sphalerite (0.42-0.72%), molybdenite (0.01-0.02%), Fe oxides, Ti oxides, titanite, apatite, zircon and monazite and “undifferentiated” (Table L5, Figures 67 and 65).

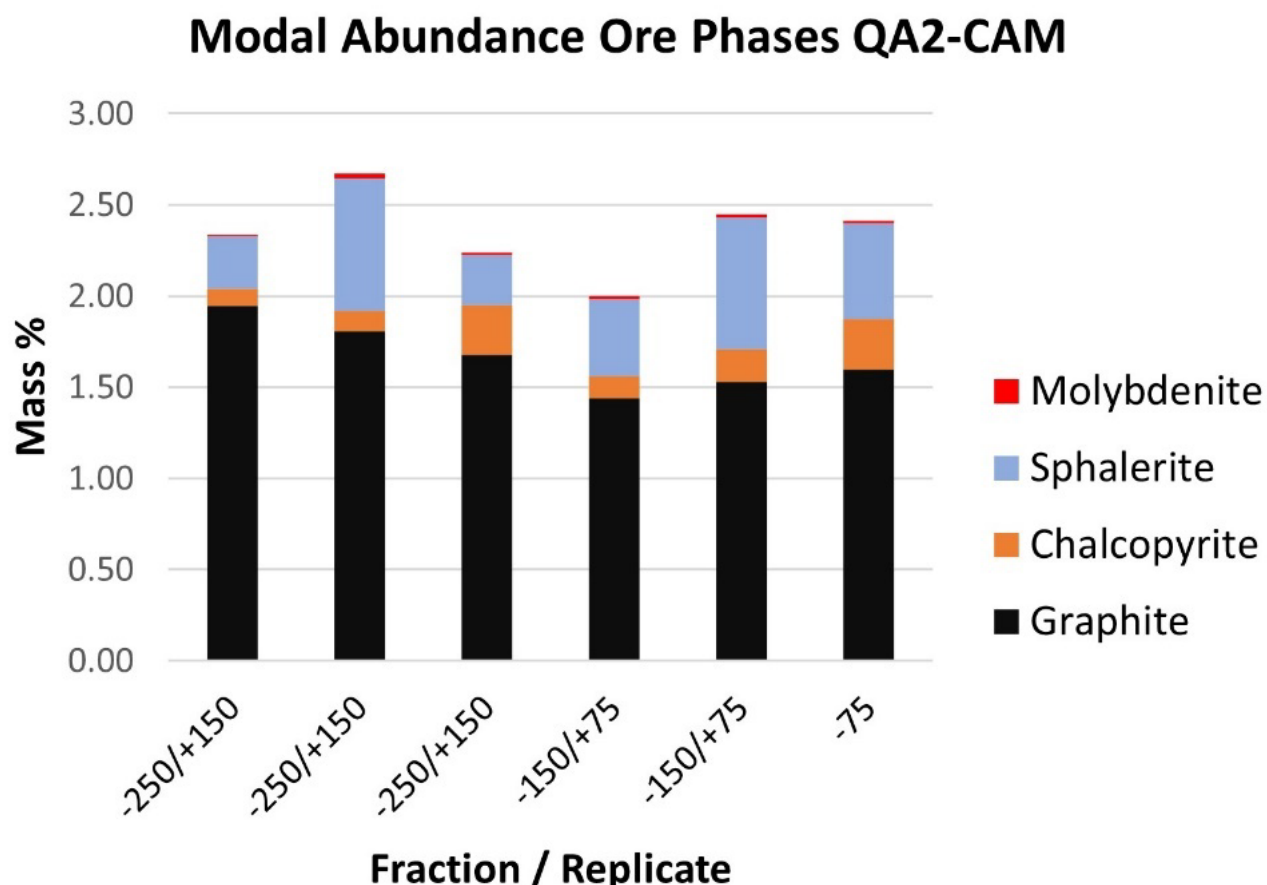


Figure 65. Modal mineralogy (mass %) ore phases for Sample QA2-CAM.

The -75 µm size fraction for Sample QA2-CAM is composed of major quartz (30.69%), plagioclase (22.68%) and pyrrhotite (10.98%) along with minor orthoclase, muscovite, biotite, phlogopite, vermiculite, chlorite, clinopyroxene and amphibole, CaAl silicates, graphite (1.60%) and pyrite (3.24%). Trace phases present are: kaolinite, calcite, chalcopyrite (0.28%), sphalerite (0.52%), molybdenite (0.02%), Fe oxides, Ti oxides, titanite, apatite, zircon and monazite and “undifferentiated” (Table L5, Figures 67 and 65).

(A) SEM-BSE and (B) AMICS particle images sample QA2-CAM A -250/+150 (enlarged)

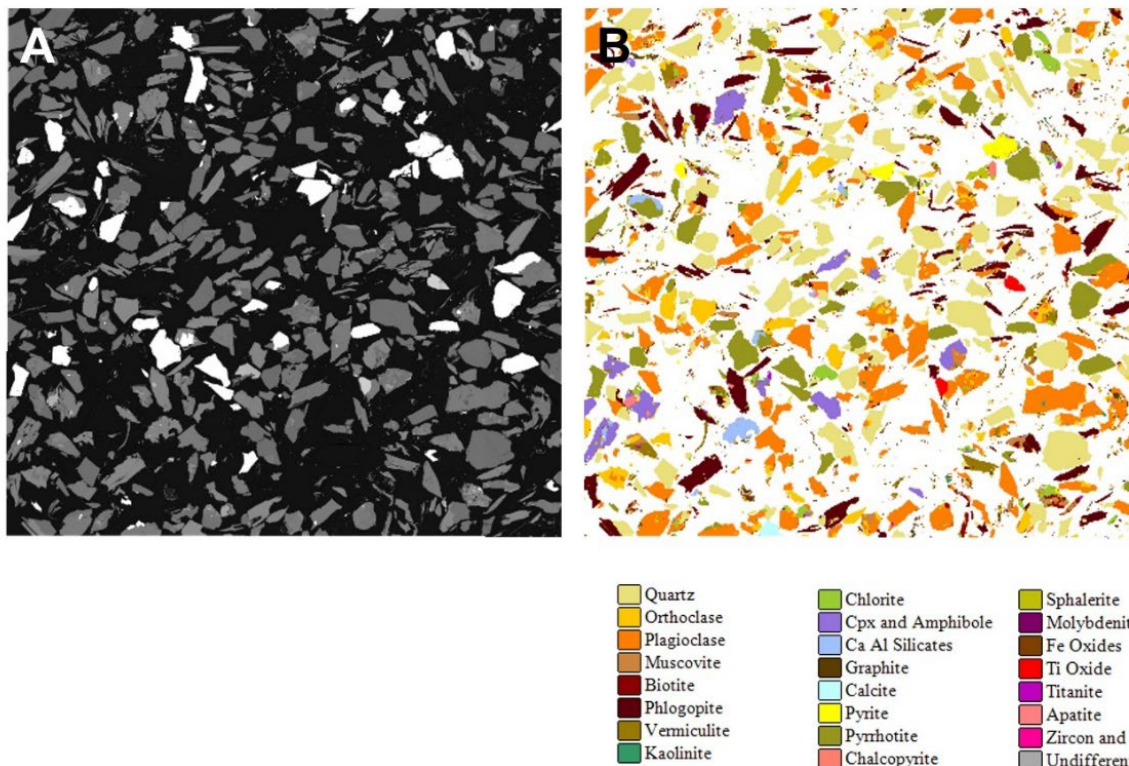


Figure 66. Higher magnification SEM-BSE image (A) and AMICS particle image (B) for the corresponding area Sample QA2-CAM - 250/+150 µm size fraction replicate A. Note the clear correspondence between the AMICS and the SEM-BSE images.

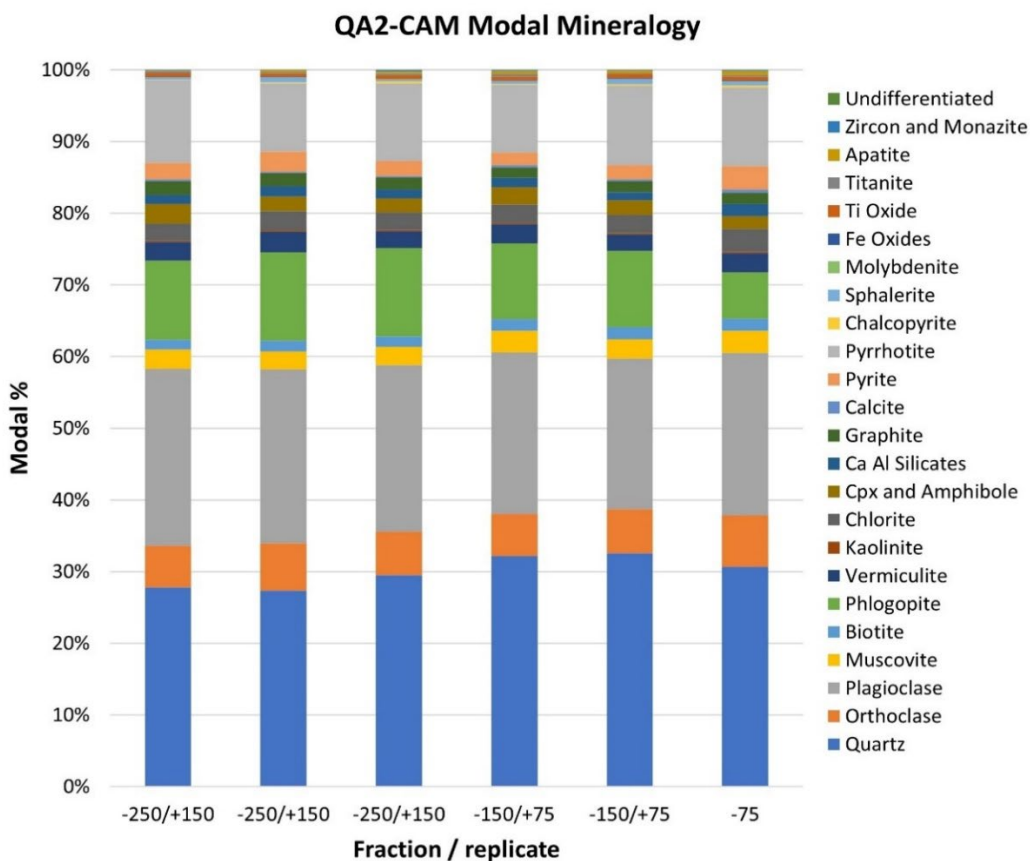


Figure 67. Modal mineralogy (mass %) all phases for Sample QA2-CAM

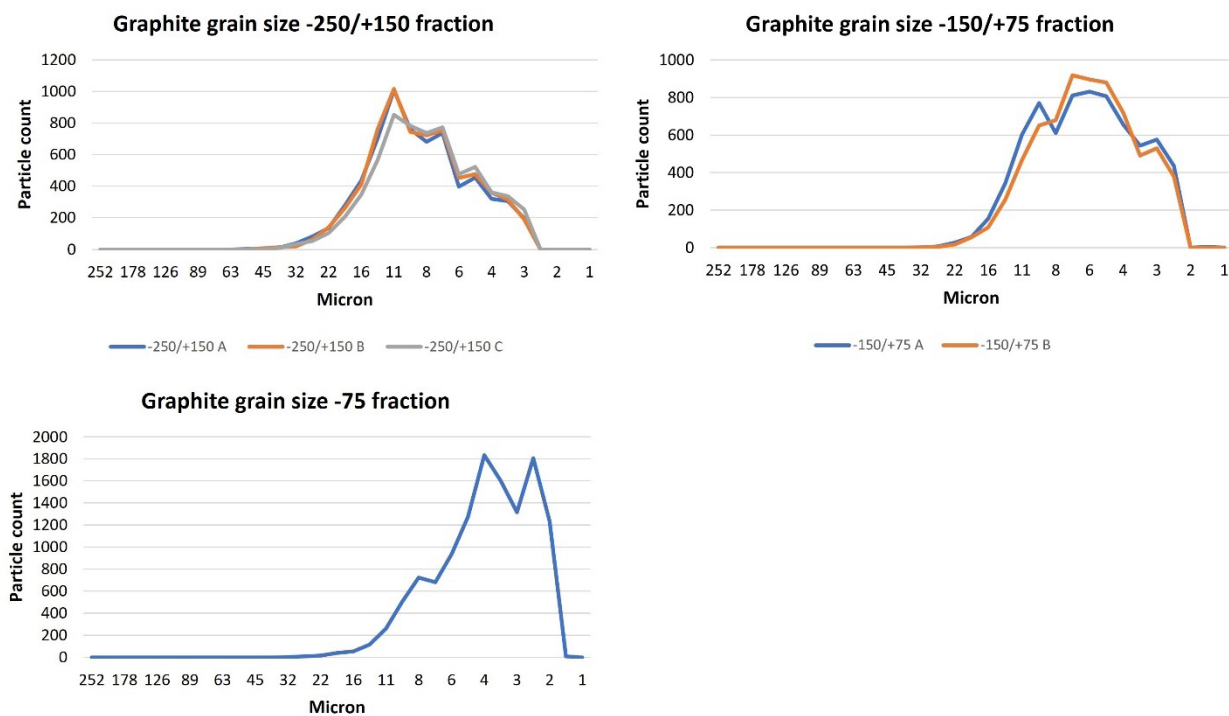


Figure 68. Graphs highlighting the grain size distribution data for graphite in the three size fractions analyzed from Sample QA2-CAM.

17.4 Sample XA3-CAM

The modal mineralogy data for Sample XA3-CAM for the three size fractions and replicate analyses are presented in Table L7 in Appendix L as mass %. In this summary major minerals form >10%, minor minerals 1-10% and trace minerals (<1%).

The -250/+150 µm size fraction for Sample XA3-CAM is composed of major quartz (30.53-30.93%), plagioclase (27.96-30.48%) and pyrrhotite (14.07-16.67%) along with minor orthoclase, muscovite, phlogopite, vermiculite, graphite (2.81-5.51%) and pyrite (0.76-1.12%). Trace phases present are: biotite, kaolinite, chlorite, clinopyroxene and amphibole, CaAl silicates, calcite, chalcopyrite (0.03-0.04%), sphalerite (0.01-0.21%), molybdenite (0.01%), Fe oxides, Ti oxides, titanite, apatite, zircon and monazite and “undifferentiated” (Table L7 in Appendix L, Figures 71 and 70).

The -150/+75 µm size fraction for Sample XA3-CAM is composed of major quartz (35.05-35.35%), plagioclase (25.06-25.47%) and pyrrhotite (13.12-13.99%) along with minor orthoclase, muscovite, phlogopite, vermiculite and graphite (4.20-4.60%). Trace phases present are: biotite, kaolinite, chlorite, clinopyroxene and amphibole, CaAl silicates, calcite, pyrite (0.79%) chalcopyrite (0.02-0.08%), sphalerite (0.07-0.09%), molybdenite (0.01%), Fe oxides, Ti oxides, titanite, apatite, zircon and monazite and “undifferentiated” (Table L7, Figures 71 and 70).

The -75 µm size fraction for Sample XA3-CAM is composed of major quartz (34.31%), plagioclase (27.10%) and pyrrhotite (13.71%) along with minor orthoclase, muscovite, biotite, phlogopite, vermiculite, chlorite, CaAl silicates, graphite (1.66%) and pyrite (1.81%). Trace phases present are: kaolinite, clinopyroxene and amphibole, calcite, chalcopyrite (0.08%), sphalerite (0.14%), Fe oxides, Ti oxides, titanite, apatite, zircon and monazite and “undifferentiated” (Table L7, Figures 71 and 70).

(A) SEM-BSE and (B) AMICS particle images sample XA3-CAM A -250/+150 (enlarged)

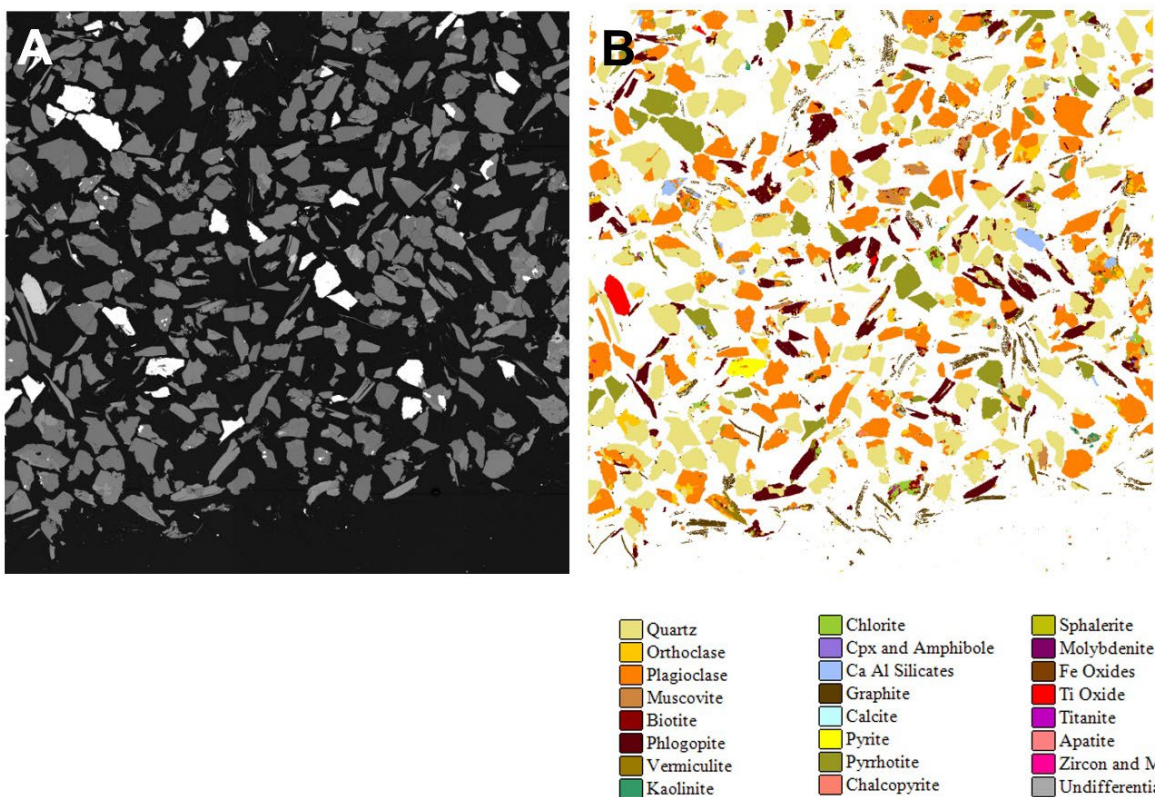


Figure 69. Higher magnification SEM-BSE image (A) and AMICS particle image (B) for the corresponding area Sample XA3-CAM - 250/+150 µm size fraction replicate A. Note the clear correspondence between the AMICS and the SEM-BSE images.

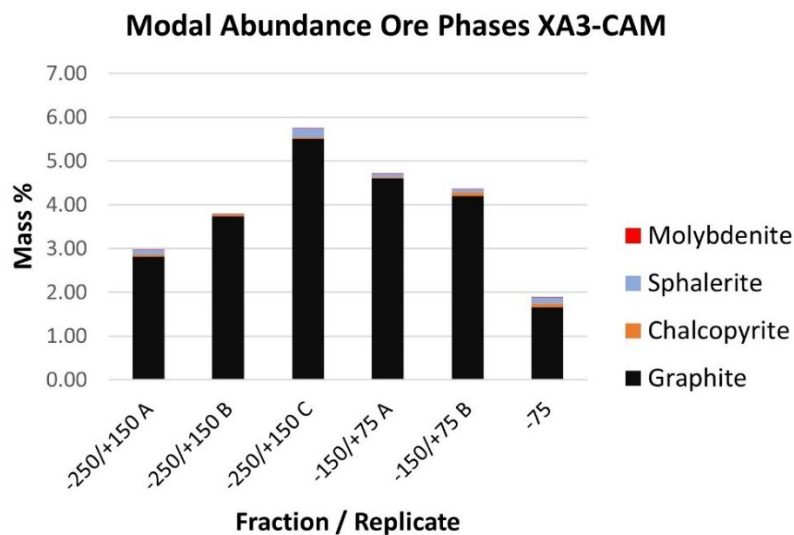


Figure 70. Modal mineralogy (mass %) ore phases for Sample XA3-CAM.

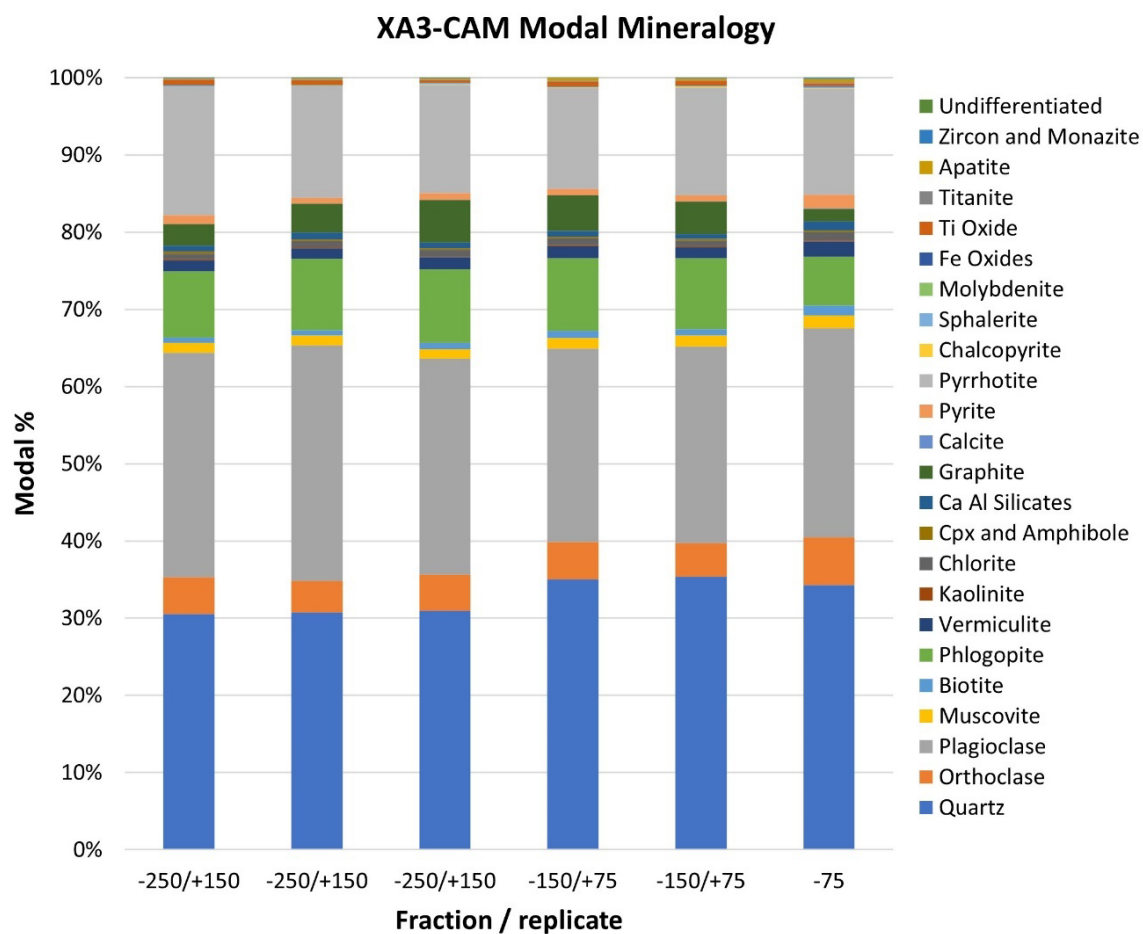


Figure 71. Modal mineralogy (mass %) all phases for Sample XA3-CAM

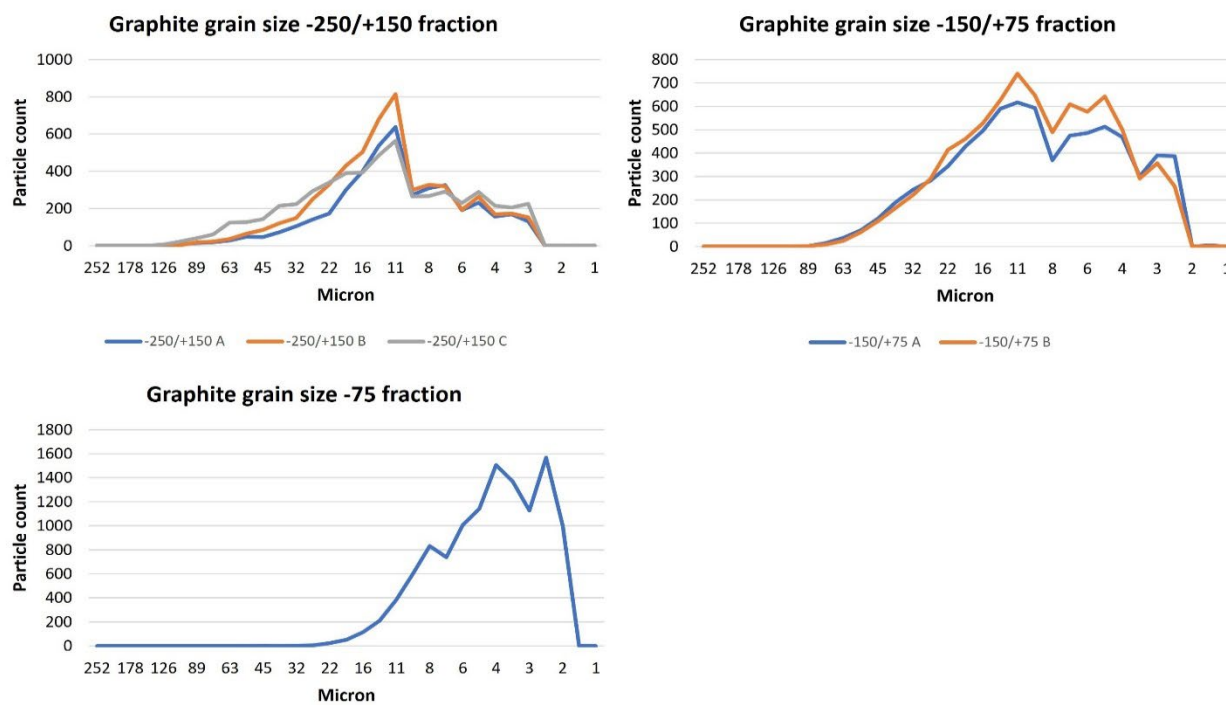


Figure 72. Graphs highlighting the grain size distribution data for graphite in the three size fractions analyzed from Sample XA3-CAM.

17.5 Sample YA4-CAM

The modal mineralogy data for Sample YA4-CAM for the three size fractions and replicate analyses are presented in Table 9 as mass % in Appendix L. In this summary major minerals form >10%, minor minerals 1-10% and trace minerals (<1%).

The -250/+150 µm size fraction for Sample YA4-CAM is composed of major quartz (29.95-30.57%) and plagioclase (30.52-31.15%) along with minor orthoclase, muscovite, phlogopite, vermiculite, chlorite, graphite (0.71-1.31%), pyrite (1.97-2.62%) and pyrrhotite (9.76-11.07%). Trace phases present are: biotite, kaolinite, clinopyroxene and amphibole, CaAl silicates, calcite, chalcopyrite (0.03-0.07%), sphalerite (0-0.08%), Fe oxides, Ti oxides, titanite, apatite, zircon and monazite and “undifferentiated” (Table L9 in Appendix L, Figures 74 and 73).

The -150/+75 µm size fraction for Sample YA4-CAM is composed of major quartz (32.98-34.06%), plagioclase (25.86-28.04%) and pyrrhotite (8.91-10.78%) along with minor orthoclase, muscovite, phlogopite, vermiculite, chlorite and pyrite (1.80-2.09%). Trace phases present are: biotite, kaolinite, clinopyroxene and amphibole, CaAl silicates, graphite (0.56-0.57%) calcite, chalcopyrite (0.04%), sphalerite (0.03-0.04%), Fe oxides, Ti oxides, titanite, apatite, zircon and monazite and “undifferentiated” (Table L9, Figures 74 and 73).

The -75 µm size fraction for Sample YA4-CAM is composed of major quartz (31.96%) and plagioclase (27.71%) along with minor orthoclase, muscovite, biotite, phlogopite, vermiculite, chlorite, graphite (1.91%), calcite, pyrite (2.81%) and pyrrhotite (8.41%). Trace phases present are: kaolinite, clinopyroxene and amphibole, CaAl silicates, chalcopyrite (0.11%), sphalerite (0.10%), Fe oxides, Ti oxides, titanite, apatite, zircon and monazite and “undifferentiated” (Table L9, Figures 74 and 73).

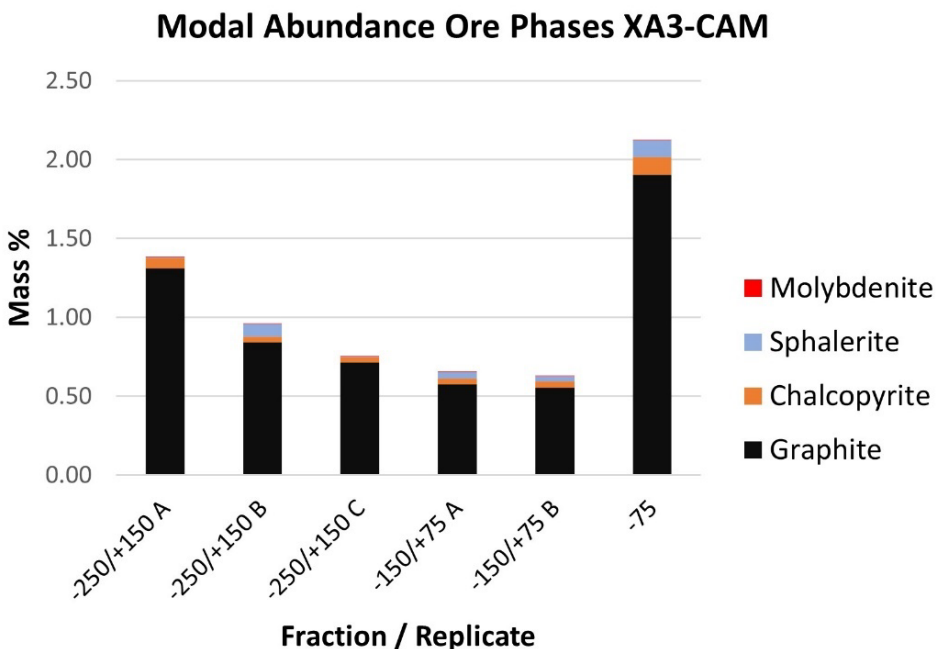


Figure 73. Modal mineralogy (mass %) ore phases for Sample YA4-CAM.

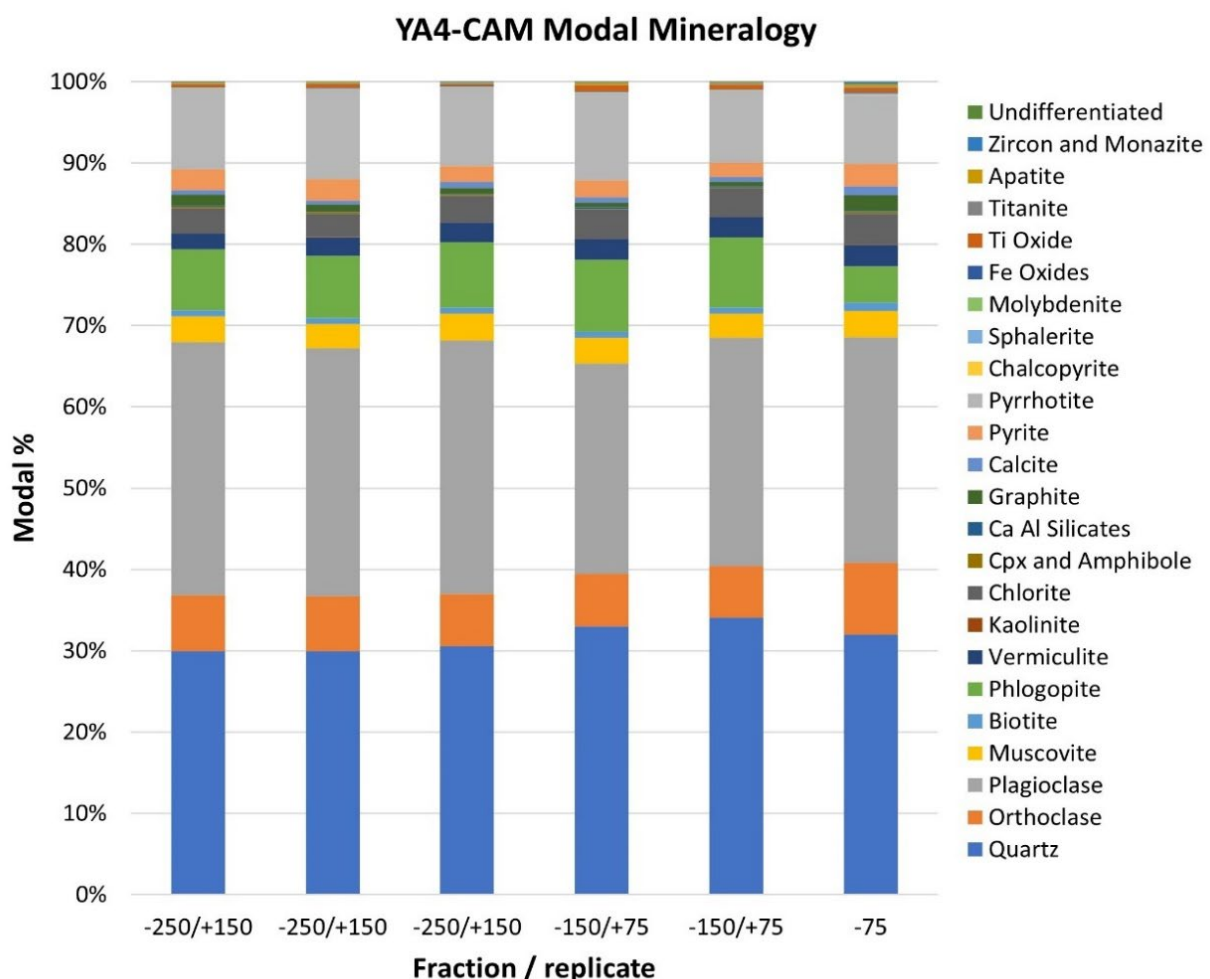


Figure 74. Modal mineralogy (mass %) all phases for Sample YA4-CAM

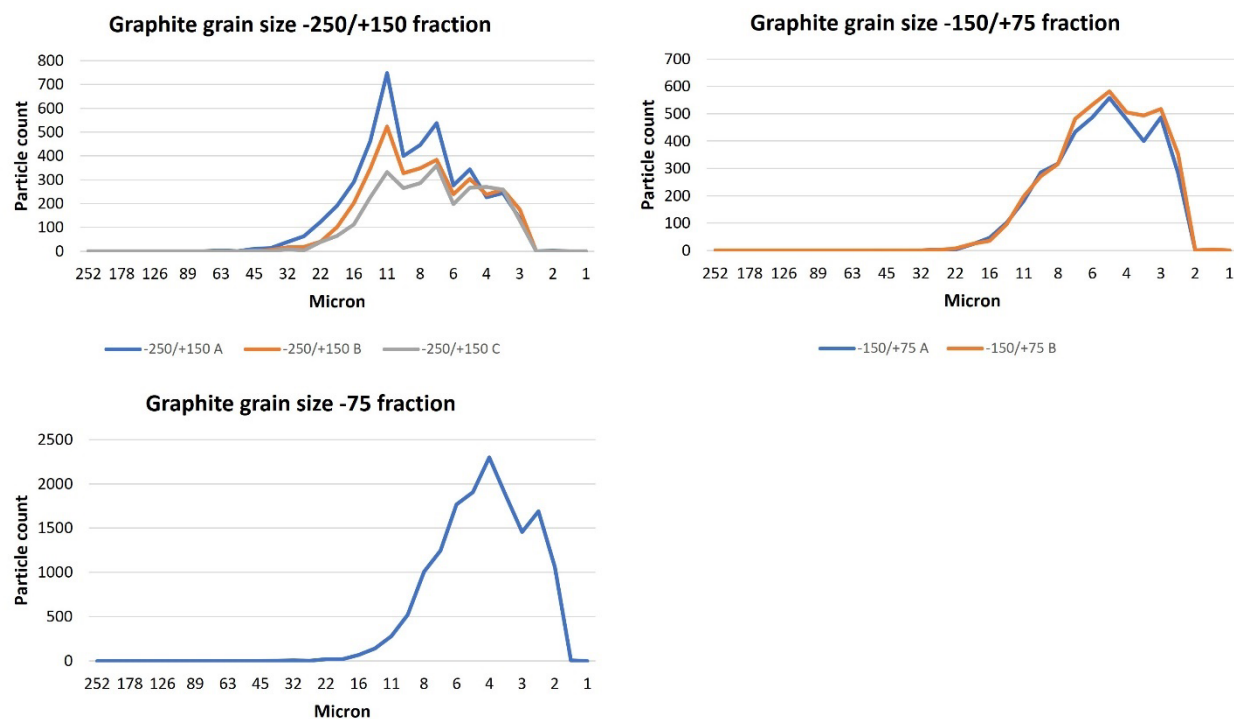


Figure 75. Graphs highlighting the grain size distribution data for graphite in the three size fractions analyzed from Sample YA4-CAM.

(A) SEM-BSE and (B) AMICS particle images sample YA4-CAM A -250/+150 (enlarged)

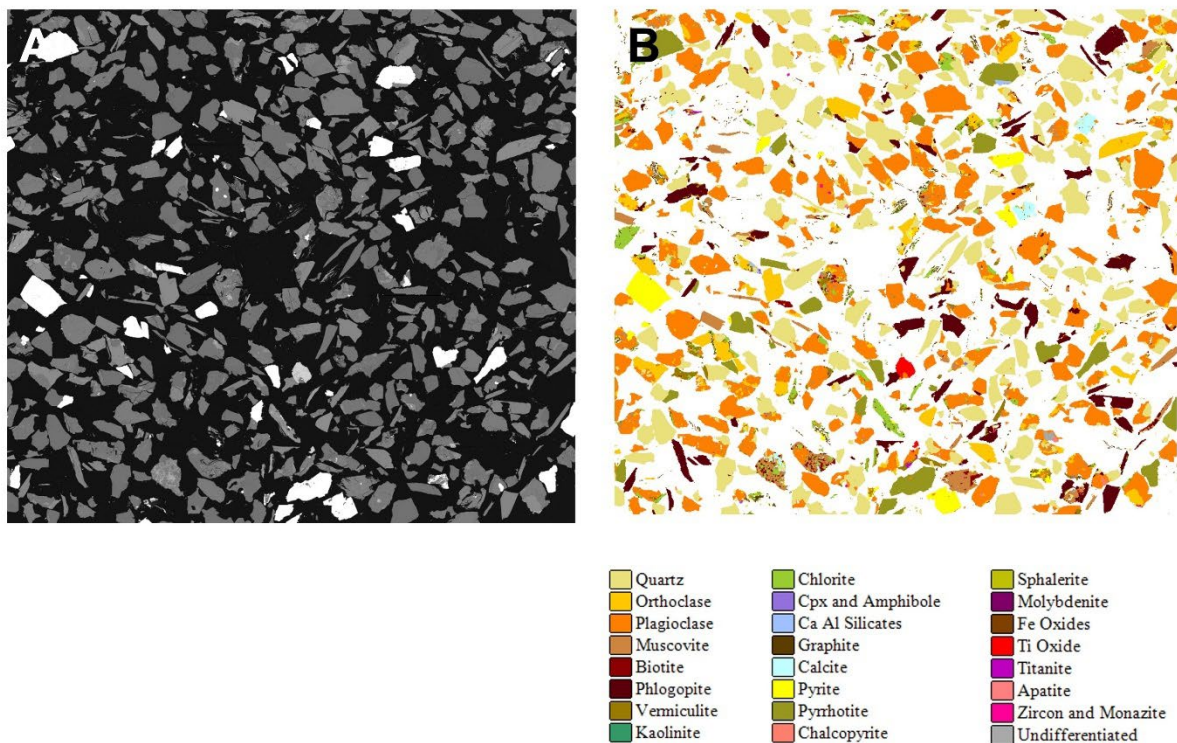


Figure 76. Higher magnification SEM-BSE image (A) and AMICS particle image (B) for the corresponding area Sample YA4-CAM - 250/+150 μm size fraction replicate A. Note the clear correspondence between the AMICS and the SEM-BSE images.

17.6 Sample ZA5-CAM

The modal mineralogy data for Sample ZA5-CAM for the three size fractions and replicate analyses are presented in Table L11 in Appendix L as mass %. In this summary major minerals form >10%, minor minerals 1-10% and trace minerals (<1%).

The -250/+150 µm size fraction for Sample ZA5-CAM is composed of major quartz (24.92-25.55%), plagioclase (22.33-23.68%), phlogopite (11.25-11.68%), and pyrrhotite (15.34-18.30%) along with minor orthoclase, muscovite, biotite, vermiculite, clinopyroxene and amphibole, CaAl silicates, graphite (3.57-5.83%) and pyrite (1.02-1.20%). Trace phases present are: kaolinite, chlorite, calcite, chalcopyrite (0.14-0.31%), sphalerite (0.53-0.90%), molybdenite, Fe oxides, Ti oxides, titanite, apatite, zircon and monazite and “undifferentiated” (Table L11, Figures 79 and 78).

The -150/+75 µm size fraction for Sample ZA5-CAM is composed of major quartz (30.34-30.83%), plagioclase (22.17-22.58%), phlogopite (12.58-12.67%), and pyrrhotite (14.01-14.25%) along with minor orthoclase, muscovite, biotite, vermiculite, clinopyroxene and amphibole, CaAl silicates, graphite (1.03-1.84%) and pyrite (0.93-1.00%). Trace phases present are: kaolinite, chlorite, calcite, chalcopyrite (0.27-0.35%), sphalerite (0.38-0.68%), molybdenite, Fe oxides, Ti oxides, titanite, apatite, zircon and monazite and “undifferentiated” (Table L11, Figures 79 and 78).

The -75 µm size fraction for Sample ZA5-CAM is composed of major quartz (29.58%), plagioclase (22.79%) and pyrrhotite (14.70%) along with minor orthoclase, muscovite, biotite, phlogopite, vermiculite, chlorite, clinopyroxene and amphibole, CaAl silicates and pyrite (1.94%). Trace phases present are: kaolinite, graphite (0.77%), calcite, chalcopyrite (0.35%), sphalerite (0.68%), molybdenite, Fe oxides, Ti oxides, titanite, apatite, zircon and monazite and “undifferentiated” (Table L11, Figures 79 and 78).

(A) SEM-BSE and (B) AMICS particle images sample ZA5-CAM A -250/+150 (enlarged)

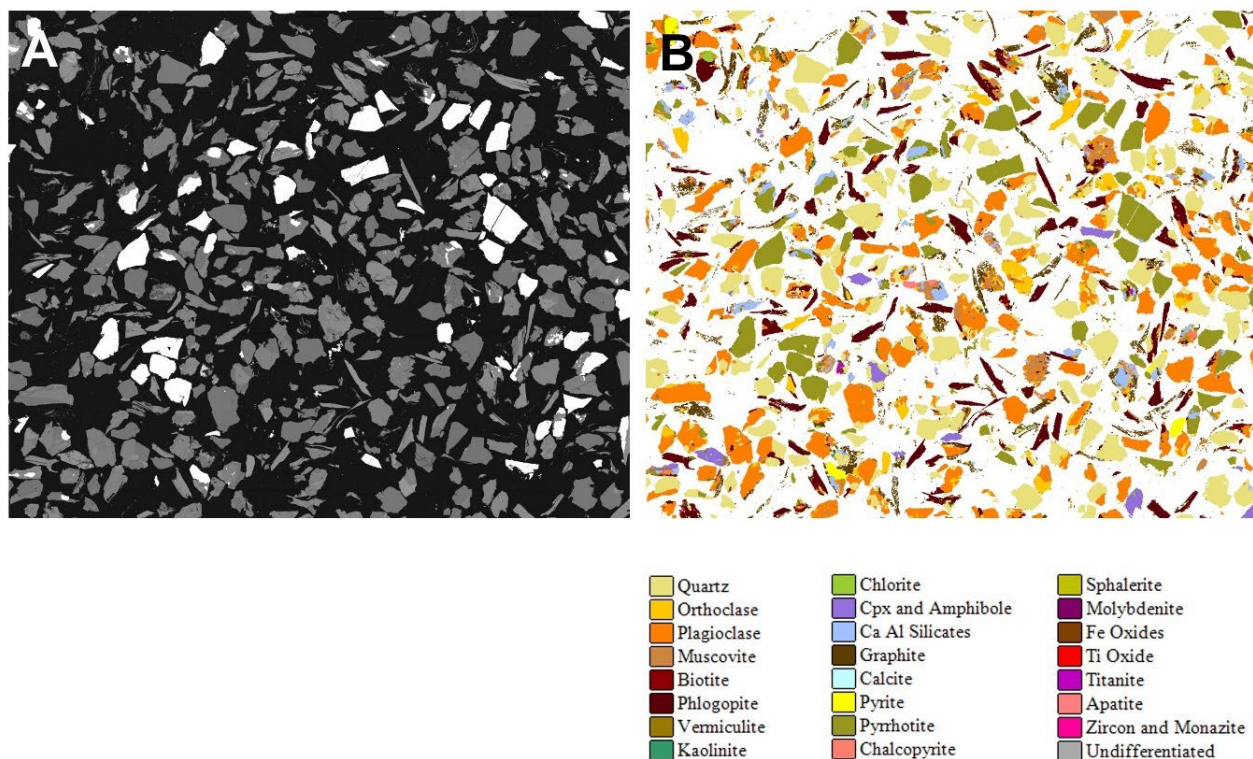


Figure 77. Higher magnification SEM-BSE image (A) and AMICS particle image (B) for the corresponding area Sample ZA5-CAM - 250/+150 µm size fraction replicate A. Note the clear correspondence between the AMICS and the SEM-BSE images.

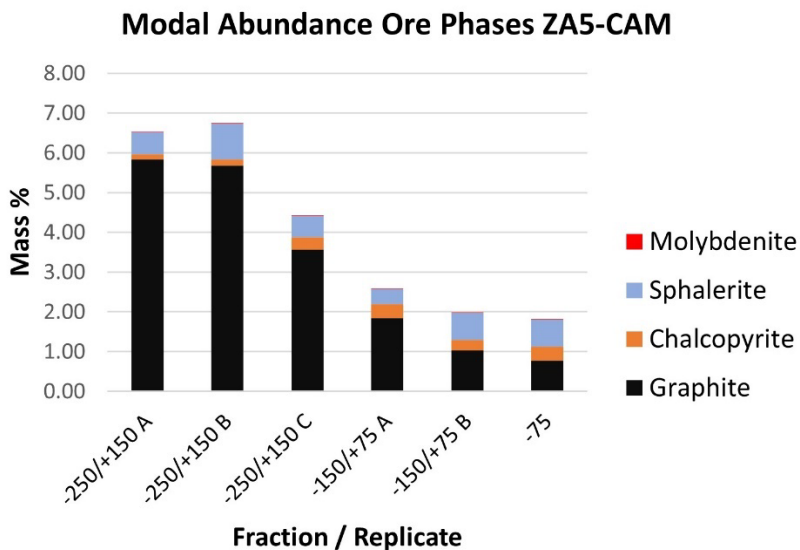


Figure 78. Modal mineralogy (mass %) ore phases for Sample ZA5-CAM.

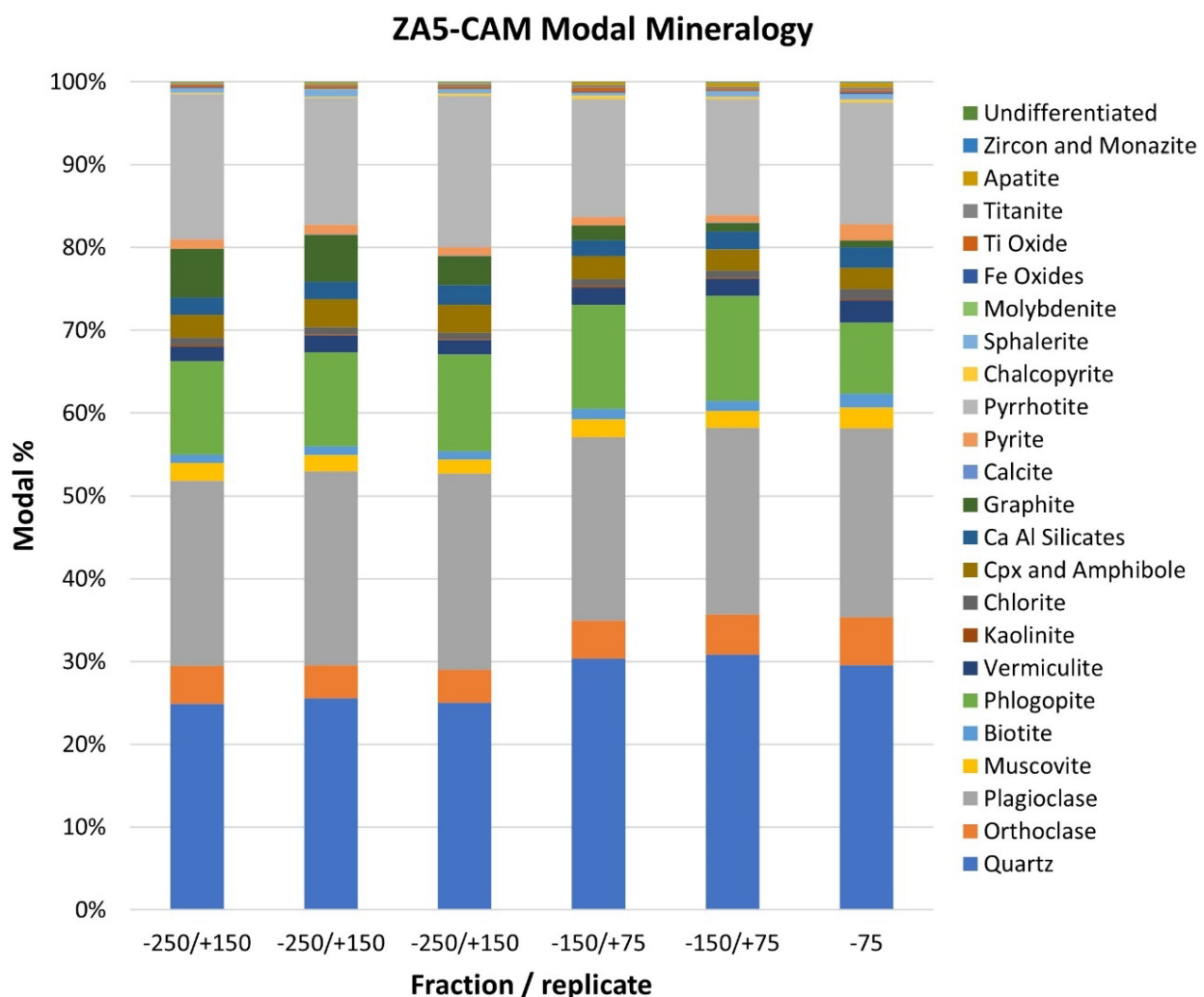


Figure 79. Modal mineralogy (mass %) all phases for Sample ZA5-CAM

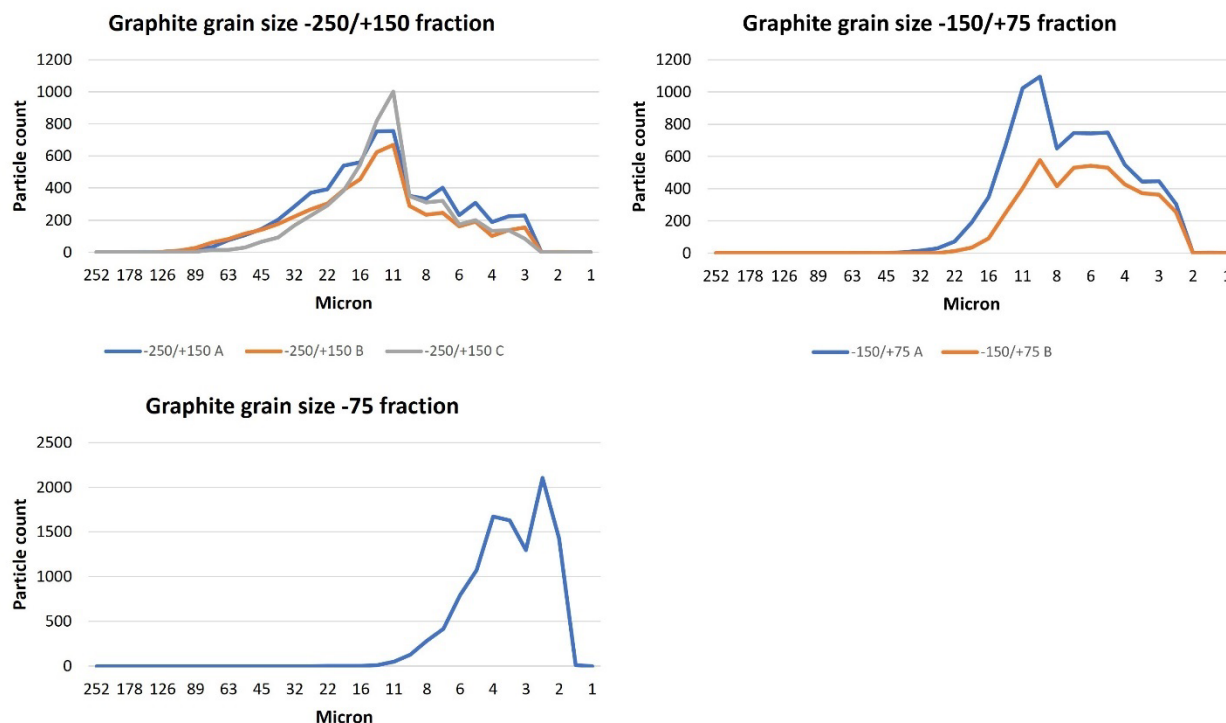


Figure 80. Graphs highlighting the grain size distribution data for graphite in the three size fractions analyzed from Sample ZA5-CAM.

18 ACID MINE DRAINAGE

An environmental impact of doing any industrial action is how that environment interacts with the legacy industrial waste dumps, stockpiles and facilities left behind after the operation has been decommissioned. Acid mine drainage (AMD) is one of those impacts that need to be understood, then managed. The effective management of these historical industrial sites can involve actions to reduce AMD, some of which could result in the recovery of useful metals. Two examples of AMD in Finland could be the historical mine sites Orijärvi and Aijala.

Abandoned mine drainage is conventionally seen as water that is polluted from contact with mining activity, and normally associated with coal mining (United States Environmental Protection Agency). The same principle could apply to any industrial side stream stockpile, that is exposed to the weather, and is in place for a period of time (months to years). This is a common form of water pollution in areas where mining took place in the past. There are several issues with abandoned mines that impact water quality:

- acid mine drainage (the most prevalent)
- alkaline mine drainage (this typically occurs when calcite or dolomite is present)
- metal mine drainage (high levels of lead or other metals drain from these abandoned mines)

Acid mine drainage is the formation and movement of highly acidic water rich in heavy metals. This acidic water forms through the chemical reaction of surface water (rainwater, snowmelt, pond water) and shallow subsurface water with rocks that contain sulfur-bearing minerals, resulting in sulfuric acid. Heavy metals can be leached from rocks that come in contact with the acid, a process that may be substantially enhanced by bacterial action. The resulting fluids may be highly toxic and, when mixed with groundwater, surface water and soil, may have harmful effects on humans, animals, and plants.

AMD has been used as a metric to classify the environmental impact and legacy footprint of industrial sites national governments. It has been useful in classifying the waste plumes of extractive industries like mining, and quarries. AMD has also been a tool to assess industrial sites like foundries, smelters and factories. Conventionally these industries are considered separately. According to the Finnish government (Ministry of the Environment Finland 2013), extractive waste can be classified as inert (extractive waste includes waste rock, soil, topsoil, and tailings), among other criteria, (Rytönen 2022):

- Sulfide sulfur is equal to or less than 0.1 %
- Sulfide sulfur equal to or less than 1%, when neutralization potential ratio (NP/AP) is greater than 3.
- As an addition the aqua regia (AR) extraction rates of semimetals and metals should not exceed the threshold values. AR test ISO 11466 (Luodes *et al.* 2011)
- AR-test is the most used extraction analysis used in Finland which especially dissolve elements bound to sulfide phases (Karlsson *et al.* 2021)
- Sulfidic sulfur can be determined with EN 14582 / ISO 15178 (Luodes *et al.* 2011)
- NP/AP with EN 15875 (Luodes *et al.* 2011)
- If classified as non-inert, the waste usage and deposition require further investigation (Luodes *et al.* 2011)

It becomes clear that the most problematic are the sulfide minerals. Table # (parts 1 and 2) show the threshold and guideline values for the concentrations of some common harmful substances in soil as total concentration per dry matter (Ministry of the Environment Finland 2007). The guideline values have been defined on the basis of either ecological risks (e) or health risks (t). If the risk of groundwater contamination is higher than normal in concentrations below the lower guideline value, the substances are marked with the letter (p).

Traditionally, AMD legacy footprint studies would consider just mining operations in isolation, or industrial site operations in isolation. The reality is the same area of land could interact with many different industrial sites, mines, quarries, factories, and farms, through the movement of water in the water table and regional freshwater catchment movement. Thus, it is recommended that all possible contaminants are examined and considered. Tables 17 and 18 shows all contaminates of interest, with naturally occurring concentrations normally associated with mining and quarrying, shown in blue. Presence of these elements in higher concentrations shown in Table 1 are considered to be a target for removal and/or long-term management.

Table 17. Threshold and guideline values for the concentrations of harmful substances in soil
 (Ministry of the Environment Finland 2007)

Substance (symbol)	Natural concentration ¹ (mg/kg)	Threshold value (mg/kg)	Lower guideline value (mg/kg)	Higher guideline value (mg/kg)
Metals and semimetals²				
Antimony (Sb) (p)	0,02 (0,01-0,2)	2	10 (t)	50 (e)
Arsenic (As) (p)	1 (0,1-25)	5	50 (e)	100 (e)
Mercury (Hg)	0,005 (< 0,005-0,05)	0,5	2 (e)	5 (e)
Cadmium (Cd)	0,03 (0,01-0,15)	1	10 (e)	20 (e)
Cobalt (Co) (p)	8 (1-30)	20	100 (e)	250 (e)
Chrome (Cr)	31 (6-170)	100	200 (e)	300 (e)
Copper (Cu)	22 (5-110)	100	150 (e)	200 (e)
Lead (Pb)	5 (0,1-5)	60	200 (t)	750 (e)
Nickel (Ni)	17 (3-100)	50	100 (e)	150 (e)
Zinc (Zn)	31 (8-110)	200	250 (e)	400 (e)
Vanadium (V)	38 (10-115)	100	150 (e)	250 (e)
Other inorganic				
Cyanide (CN)		1	10	50
Aromatic hydrocarbons				
Benzene (p)		0,02	0,2 (t)	1 (t)
Toluene (p)			5 (t)	25 (t)
Ethylbenzene (p)			10 (t)	50 (t)
Xylenes ³ (p)			10 (t)	50 (t)
TEX ⁴		1		
Polycyclic aromatic hydrocarbons				
Anthracene		1	5 (e)	15 (e)
Benzo(a)anthracene		1	5 (e)	15 (e)
Benzo(a)pyrene		0,2	2 (t)	15 (e)
Benzo(k)fluoranthene		1	5 (e)	15 (e)
Phenanthrene		1	5 (e)	15 (e)
Fluoranthene		1	5 (e)	15 (e)
Naphthalene		1	5 (e)	15 (e)
PAH ⁵		15	30 (e)	100 (e)
Polychlorinated biphenyls (PCB) and polychlorinated dibenzo-p-dioxins and furans (PCDD/F)				
PCB ⁶		0,1	0,5 (t)	5 (e)
PCDD-PCDF-PCB ⁷		0,00001	0,0001 (t)	0,0015 (e)

Table 18. Threshold and guideline values for the concentrations of harmful substances in soil
 (Ministry of the Environment Finland 2007)

Substance (symbol)	Natural concentration ¹ (mg/kg)	Threshold value (mg/kg)	Lower guideline value (mg/kg)	Higher guideline value (mg/kg)
Chlorinated aliphatic hydrocarbons				
Dichloromethane (p)		0,01	1 (t)	5 (t,e)
Vinyl chloride (p)		0,01	0,01 (t)	0,01 (t)
Dichloroethene ³ (p)		0,01	0,05 (t)	0,2 (t)
Trichloroethene (p)		0,01	1 (t,e)	5 (e)
Tetrachloroethene (p)		0,01	0,5 (t)	2 (t)
Chlorobenzenes				
Trichlorobenzenes ³		0,1	5 (t)	20 (e)
Tetrachlorobenzenes ³		0,1	1 (t)	5 (e)
Pentachlorobenzene		0,1	1 (t)	5 (e)
Hexachlorobenzene		0,01	0,05 (t)	2 (e)
Chlorophenols				
Monochlorophenols ³ (p)		0,5	5 (e,t)	10 (e)
Dichlorophenols ³ (p)		0,5	5 (t)	40 (e)
Trichlorophenols ³ (p)		0,5	10 (e,t)	40 (e)
Tetrachlorophenols ⁴ (p)		0,5	10 (e,t)	40 (e)
Pentachlorophenol (p)		0,5	10 (e,t)	20 (e)
Pesticides and biocides				
Atrazine (p)		0,05	1 (e)	2 (e)
DDT-DDD-DDE ⁸		0,1	1 (e)	2 (e)
Dieldrin		0,05	1 (e)	2 (e)
Endosulphan ⁹ (p)		0,1	1 (e)	2 (e)
Heptachlorine		0,01	0,2 (t)	1 (e)
Lindane (p)		0,01	0,2 (t)	2 (e)
TBT-TPT ¹⁰		0,1	1 (e)	2 (e)
Petroleum hydrocarbon fractions and oxygenates				
MTBE-TAME ¹¹		0,1	5 (t)	50 (t)
Petrol fractions (C5-C10 ¹²)			100	500
Middle distillates (>C10 - C21 ¹²)			300	1000
Heavy petroleum fractions (>C21-C40 ¹²)			600	2000
Petroleum fractions (>C10 - C40 ¹²)		300		

Notes for Tables 17 & 18:

1. The median and range of the natural concentration of fines in moraine when defined by extraction with aqua regia, except pyrolytically defined mercury. It must be taken into account in site-specific analyses that especially in clay soils the natural concentrations may be clearly higher than those measured from moraine.
2. The guideline values for metals and semimetals defined on ecological grounds are derived by adding the average natural concentration of the mineral soil to the calculated concentration describing the acceptable ecological risk of the substance. Correspondingly, the natural concentration of the soil in the area can be taken into account in site-specific analyses if it has been analyzed with a reliable method.

3. Total concentration including the structural isomers of the substance.
4. Total concentration including the following compounds: toluene, ethylbenzene and xylene.
5. Total concentration of PAH compounds including the following compounds: anthracene, acenaphthene, acenaphthylene, benzo(a)anthracene, benzo(a)pyrene, benzo(b)fluoranthene, benzo(g,h,i)perylene, benzo(k)fluoranthene, dibenzo(a,h)anthracene, phenanthrene, fluoranthene, fluorene, indeno(1,2,3-c,d)pyrene, chrysene, naphthalene and pyrene.
6. Total concentration including PCB congeners 28, 52, 101, 118, 138, 153, 180.
7. Total concentration stated as WHO toxicity equivalent including PCDD/F compounds and dioxin-like PCB compounds.
8. Total concentration including the following compounds: dichlorodiphenyltrichloroethane (DDT), dichlorodiphenyldichloroethane (DDD) and dichlorodiphenyldichloroethylene (DDE).
9. Total concentration including the following compounds: alpha-endosulphane and beta-endosulphane.
10. Total concentration including the following compounds: tributyl tin (TBT) and triphenyl tin (TPT).
11. Total concentration including the following compounds: methyl tert-butyl ether (MTBE) and tert-amyl methyl ether (TAME).
12. Series of n paraffins in gas-chromatographic analysis.

18.1 Soil contamination

The threshold values shown in Tables 17 and 18 are based on the natural con-centration which are based on the analysis of fines in moraine by extraction with AR. AR-test is the most used extraction analysis method used in Finland which especially dissolve element bound to sulfide phases which are the most problematic and raising concerns in terms of extractive waste (Karlsson, Alakangas, & Kauppila, A Test of Two Methods for Waste Rock Drainage Quality Prediction: Aqua Regia Extraction and Single-addition Net-acid Generation Test Leachate Analysis, 2021). The analysis is recommended to perform for particles smaller than 2 mm / 2000 µm following standards ISO 11466 or EN 13657 and measuring the concentrations of elements with ICP-AES/OES/MS or GFAAS. The Hg should be defined pyrolytically (Luodes *et al.* 2011; Finnish Government, 2007).

18.2 Sulfide sulfur

In extractive waste the sulfur can be present as sulfide (S₂-) or sulfate (SO₄2-) in minerals. Sulfide sulfur limit of 0.1% is set to ensure that the inert waste does not develop any AMD in the waste deposit area (waste rock dump / uncovered TSF) or in applications (e.g., roads). As stated in previous chapter, the major AMD risk is based on the oxidation of sulfide minerals. For the sulfide sulfur determination there is no set global standards and therefore the analyses are based on the total sulfur analysis. When defining total sulfur that should take account that the analyze can overestimate the samples potential to create AMD if major part of the samples sulfur is in other form than sulfide (Luodes, et al., 2011). Different methods of sulfur analysis include bomb combustion (EN 14582), high temperature combustion (ISO 351 or ISO 15178), iodine method (EN 1744-1) and Schöniger apparatus (EN 14582). From these methods the bomb combustion method is the

preferred one in Europe (Punkkinen H., et al., 2019). Luodes, et al. (2011) also stated in the paper that the most “baseline” results are achieved with bomb combustion or high temperature bomb combustion method.

18.3 ABA test

Acid base accounting (ABA) is a static test used for extractive waste. The ABA tests does not give any information of the acid production or neutralization rates and is rather used to get information about the acid generation and neutralization potential. Usually, the static tests are performed first and when more information is needed kinetic tests (which can be measured in months or years) are performed (Punkkinen, et al., 2019; Luodes, et al., 2011). ABA tests include determination of sulfide sulfur (S%) which is used to calculate the acid potential (AP). The neutralization potential (NP) amount of carbonate (C%) and other alkaline material pre-sent in the sample. The ratio of NP and AP (NP/AP: neutralization potential ratio, NPR) or subtraction NP-AP (net neutralization potential, NNP) is then used to estimate the risk for AMD. The results are presented in kg CaCO₃/ton. There are several variations of ABA test, including ABA with Sobek method and modified ABA with modified Sobek method and up-grade of the most used method (EN 15875) (Punkkinen, et al. 2019).

18.4 NAG test

The net acid generation (NAG) test is a static test to determine the waste rock or tailings potential to generate AMD. The NAG test is suitable to use as prediction tool and as combination with ABA test. The NAG test is based on the samples reaction with hydrogen peroxide which work as oxidizing agent for sulfide minerals. During the test when hydrogen peroxide is added, both acid generation and acid neutralization can occur. After the test final pH is recorded (NAG pH) and the sample is back titrated with NaOH to pH 4.5 and 7 and the net acid generation (NAG, H₂SO₄/ton) capacity is calculated (Karlsson, 2019; Weber et al., 2006). If the final NAG pH is higher than 4.5 and NAG is 0 the sample can be classified as non-acid forming (NAF) and when the NAG pH is lower than 4.5 and NAG is higher than 0 potentially acid forming (PAF) (Shaw, 2005).

18.5 NAPP

The net acid production potential (NAPP) can be used together with NAG to have more detailed results and to compare results with ABA tests. The NAPP can be calculated as subtraction between maximum potential acidity (MPA) and acid neutralizing capacity (ANC), NAPP = MPA – ANC (Karlsson, 2019; Weber et al., 2006). According to Amira International (2002), the ANC can be calculated from NP (ANC = NP/50*49) and MPA from the S% (MPA = S%*30.6). All the NAPP, ANC and MPA are expressed in H₂SO₄ equivalent as kg H₂SO₄/ton (Weber et al., 2006).

Table 19. Aitolampi Graphite Ore (PA1) and threshold and guideline values for the concentrations of harmful substances in soil
(Ministry of the Environment Finland 2007)

Contamination threshold AMD Substance (symbol)	Natural concentration (mg/kg)	Threshold value (mg/kg)	Lower guideline value (mg/kg)	Higher guideline value (mg/kg)	Graphite Ore PA1 (mg/kg)
Metals and semimetals					
Antimony (Sb) (p)	0,02 (0,01-0,2)	2	10 (t)	50 (e)	-
Arsenic (As) (p)	1 (0,1-25)	5	50 (e)	100 (e)	-
Mercury (Hg)	0,005 (< 0,005-0,05)	0.5	2 (e)	5 (e)	-
Cadmium (Cd)	0,03 (0,01-0,15)	1	10 (e)	20 (e)	-
Cobalt (Co) (p)	8 (1-30)	20	100 (e)	250 (e)	60.4
Chrome (Cr)	31 (6-170)	100	200 (e)	300 (e)	237.3
Copper (Cu)	22 (5-110)	100	150 (e)	200 (e)	833.8
Lead (Pb)	5 (0,1-5)	60	200 (t)	750 (e)	18.3
Nickel (Ni)	17 (3-100)	50	100 (e)	150 (e)	319
Zinc (Zn)	31 (8-110)	200	250 (e)	400 (e)	2 553.0
Vanadium (V)	38 (10-115)	100	150 (e)	250 (e)	1 276

The guideline values have been defined on the basis of ecological risks (e)

The guideline values have been defined on the basis of health risks (t)

If the risk of groundwater contamination is higher than normal in concentrations below the lower guideline value, the substances are marked with the letter (p)

Table 20. Aitolampi Graphite Ore (PA1) Acid Mine Drainage (AMD) results
(Analysis by Eurofins Environment Testing Finland (Jyväskylä))

Aitolampi Graphite Ore PA1			
Test	Method	Result	Unit
Sulfur (S)	Incl. men., Spectrophotometer (IR)	5.96	(%)
Total Carbon (TC)	Incl. men., Spectrophotometer (IR)	7.87	(%)
C carbonate	Incl. men., Spectrophotometer (IR)	0.56	(%)
C non-carbon	Incl. men., Spectrophotometer (IR)	7.31	(%)
Acid Potential (AP)	Incl. management, Technology [Computational]	190	kg CaCO ₃ /tonne
Neutralization Potential (NP)	Incl. management, Technology [Computational]	-1.2	kg CaCO ₃ /tonne
NNP	Incl. management, Technology [Computational]	<0.3	kg CaCO ₃ /tonne
Neutralization Potential Ratio (NPR)	Incl. management, Technology [Computational]	<0.1	
ANC	Incl. management, Technology [Computational]	<0.3	kg H ₂ SO ₄ /Tonne
MPA	Incl. management, Technology [Computational]	180	kg H ₂ SO ₄ /Tonne
NAPP	Incl. management, Technology [Computational]	180	kg H ₂ SO ₄ /Tonne
NAG pH 4.5	ARD Test Handbook, Project P387A, 2002	27	kg SO ₄ /Tonne
NAG pH 7.0	ARD Test Handbook, Project P387A, 2003	68.000	kg SO ₄ /Tonne
NAG-pH	ARD Test Handbook, Project P387A, 2004	2.5	
Electrical conductivity 25°C	ARD Test Handbook, Project P387A, 2005	292.00	mS/m

Table 21. Aitolampi Graphite Ore (QA2) and threshold and guideline values for the concentrations of harmful substances in soil
(Ministry of the Environment Finland 2007)

Contamination threshold AMD Substance (symbol)	Natural concentration (mg/kg)	Threshold value (mg/kg)	Lower guideline value (mg/kg)	Higher guideline value (mg/kg)	Graphite Ore QA2 (mg/kg)
Metals and semimetals					
Antimony (Sb) (p)	0,02 (0,01-0,2)	2	10 (t)	50 (e)	-
Arsenic (As) (p)	1 (0,1-25)	5	50 (e)	100 (e)	-
Mercury (Hg)	0,005 (< 0,005-0,05)	0.5	2 (e)	5 (e)	-
Cadmium (Cd)	0,03 (0,01-0,15)	1	10 (e)	20 (e)	-
Cobalt (Co) (p)	8 (1-30)	20	100 (e)	250 (e)	35.1
Chrome (Cr)	31 (6-170)	100	200 (e)	300 (e)	229.1
Copper (Cu)	22 (5-110)	100	150 (e)	200 (e)	406.2
Lead (Pb)	5 (0,1-5)	60	200 (t)	750 (e)	17.6
Nickel (Ni)	17 (3-100)	50	100 (e)	150 (e)	284.9
Zinc (Zn)	31 (8-110)	200	250 (e)	400 (e)	1 375
Vanadium (V)	38 (10-115)	100	150 (e)	250 (e)	1 100

The guideline values have been defined on the basis of ecological risks (e)

The guideline values have been defined on the basis of health risks (t)

If the risk of groundwater contamination is higher than normal in concentrations below the lower guideline value, the substances are marked with the letter (p)

Table 22. Aitolampi Graphite Ore (QA2) Acid Mine Drainage (AMD) results
(Analysis by Eurofins Environment Testing Finland (Jyväskylä))

Aitolampi Graphite Ore QA2			
Test	Method	Result	Unit
Sulfur (S)	Incl. men., Spectrophotometer (IR)	4.64	(%)
Total Carbon (TC)	Incl. men., Spectrophotometer (IR)	6.02	(%)
C carbonate	Incl. men., Spectrophotometer (IR)	0.21	(%)
C non-carbon	Incl. men., Spectrophotometer (IR)	5.81	(%)
Acid Potential (AP)	Incl. management, Technology [Computational]	150.0	kg CaCO ₃ /tonne
Neutralization Potential (NP)	Incl. management, Technology [Computational]	4.2	kg CaCO ₃ /tonne
NNP	Incl. management, Technology [Computational]	<0.3	kg CaCO ₃ /tonne
Neutralization Potential Ratio (NPR)	Incl. management, Technology [Computational]	<0.1	
ANC	Incl. management, Technology [Computational]	4.1	kg H ₂ SO ₄ /Tonne
MPA	Incl. management, Technology [Computational]	140	kg H ₂ SO ₄ /Tonne
NAPP	Incl. management, Technology [Computational]	140	kg H ₂ SO ₄ /Tonne
NAG pH 4.5	ARD Test Handbook, Project P387A, 2002	27	kg SO ₄ /Tonne
NAG pH 7.0	ARD Test Handbook, Project P387A, 2003	59	kg SO ₄ /Tonne
NAG-pH	ARD Test Handbook, Project P387A, 2004	2.5	
Electrical conductivity 25°C	ARD Test Handbook, Project P387A, 2005	221	mS/m

Table 23. Aitolampi Graphite Ore (XA3) and threshold and guideline values for the concentrations of harmful substances in soil
(Ministry of the Environment Finland 2007)

Contamination threshold AMD Substance (symbol)	Natural concentration (mg/kg)	Threshold value (mg/kg)	Lower guideline value (mg/kg)	Higher guideline value (mg/kg)	Graphite Ore XA3 (mg/kg)
Metals and semimetals					
Antimony (Sb) (p)	0,02 (0,01-0,2)	2	10 (t)	50 (e)	-
Arsenic (As) (p)	1 (0,1-25)	5	50 (e)	100 (e)	-
Mercury (Hg)	0,005 (< 0,005-0,05)	0.5	2 (e)	5 (e)	-
Cadmium (Cd)	0,03 (0,01-0,15)	1	10 (e)	20 (e)	-
Cobalt (Co) (p)	8 (1-30)	20	100 (e)	250 (e)	39.9
Chrome (Cr)	31 (6-170)	100	200 (e)	300 (e)	144.3
Copper (Cu)	22 (5-110)	100	150 (e)	200 (e)	159.0
Lead (Pb)	5 (0,1-5)	60	200 (t)	750 (e)	8.3
Nickel (Ni)	17 (3-100)	50	100 (e)	150 (e)	157.0
Zinc (Zn)	31 (8-110)	200	250 (e)	400 (e)	524.0
Vanadium (V)	38 (10-115)	100	150 (e)	250 (e)	469.0

The guideline values have been defined on the basis of ecological risks (e)

The guideline values have been defined on the basis of health risks (t)

If the risk of groundwater contamination is higher than normal in concentrations below the lower guideline value, the substances are marked with the letter (p)

Table 24. Aitolampi Graphite Ore (XA3) Acid Mine Drainage (AMD) results
(Analysis by Eurofins Environment Testing Finland (Jyväskylä))

Aitolampi Graphite Ore XA3			
Test	Method	Result	Unit
Sulfur (S)	Incl. men., Spectrophotometer (IR)	4.71	(%)
Total Carbon (TC)	Incl. men., Spectrophotometer (IR)	4.98	(%)
C carbonate	Incl. men., Spectrophotometer (IR)	0.06	(%)
C non-carbon	Incl. men., Spectrophotometer (IR)	4.92	(%)
Acid Potential (AP)	Incl. management, Technology [Computational]	150	kg CaCO ₃ /tonne
Neutralization Potential (NP)	Incl. management, Technology [Computational]	2.0	kg CaCO ₃ /tonne
NNP	Incl. management, Technology [Computational]	<0.3	kg CaCO ₃ /tonne
Neutralization Potential Ratio (NPR)	Incl. management, Technology [Computational]	<0.1	
ANC	Incl. management, Technology [Computational]	2.0	kg H ₂ SO ₄ /Tonne
MPA	Incl. management, Technology [Computational]	140	kg H ₂ SO ₄ /Tonne
NAPP	Incl. management, Technology [Computational]	140	kg H ₂ SO ₄ /Tonne
NAG pH 4.5	ARD Test Handbook, Project P387A, 2002	42	kg SO ₄ /Tonne
NAG pH 7.0	ARD Test Handbook, Project P387A, 2003	75	kg SO ₄ /Tonne
NAG-pH	ARD Test Handbook, Project P387A, 2004	2.3	
Electrical conductivity 25°C	ARD Test Handbook, Project P387A, 2005	314	mS/m

Table 25. Aitolampi Graphite Ore (YA4) and threshold and guideline values for the concentrations of harmful substances in soil
(Ministry of the Environment Finland 2007)

Contamination threshold AMD Substance (symbol)	Natural concentration (mg/kg)	Threshold value (mg/kg)	Lower guideline value (mg/kg)	Higher guideline value (mg/kg)	Graphite Ore YA4 (mg/kg)
Metals and semimetals					
Antimony (Sb) (p)	0,02 (0,01-0,2)	2	10 (t)	50 (e)	11.1
Arsenic (As) (p)	1 (0,1-25)	5	50 (e)	100 (e)	1.8
Mercury (Hg)	0,005 (< 0,005-0,05)	0.5	2 (e)	5 (e)	-
Cadmium (Cd)	0,03 (0,01-0,15)	1	10 (e)	20 (e)	-
Cobalt (Co) (p)	8 (1-30)	20	100 (e)	250 (e)	25.6
Chrome (Cr)	31 (6-170)	100	200 (e)	300 (e)	128.4
Copper (Cu)	22 (5-110)	100	150 (e)	200 (e)	114.6
Lead (Pb)	5 (0,1-5)	60	200 (t)	750 (e)	9.1
Nickel (Ni)	17 (3-100)	50	100 (e)	150 (e)	96.3
Zinc (Zn)	31 (8-110)	200	250 (e)	400 (e)	150.3
Vanadium (V)	38 (10-115)	100	150 (e)	250 (e)	234.0

The guideline values have been defined on the basis of ecological risks (e)

The guideline values have been defined on the basis of health risks (t)

If the risk of groundwater contamination is higher than normal in concentrations below the lower guideline value, the substances are marked with the letter (p)

Table 26. Aitolampi Graphite Ore (YA4) Acid Mine Drainage (AMD) results
(Analysis by Eurofins Environment Testing Finland (Jyväskylä))

Aitolampi Graphite Ore YA4			
Test	Method	Result	Unit
Sulfur (S)	Incl. men., Spectrophotometer (IR)	3.73	(%)
Total Carbon (TC)	Incl. men., Spectrophotometer (IR)	2.81	(%)
C carbonate	Incl. men., Spectrophotometer (IR)	0.13	(%)
C non-carbon	Incl. men., Spectrophotometer (IR)	2.68	(%)
Acid Potential (AP)	Incl. management, Technology [Computational]	120	kg CaCO ₃ /tonne
Neutralization Potential (NP)	Incl. management, Technology [Computational]	8.3	kg CaCO ₃ /tonne
NNP	Incl. management, Technology [Computational]	<0.3	kg CaCO ₃ /tonne
Neutralization Potential Ratio (NPR)	Incl. management, Technology [Computational]	<0.1	
ANC	Incl. management, Technology [Computational]	8.1	kg H ₂ SO ₄ /Tonne
MPA	Incl. management, Technology [Computational]	110	kg H ₂ SO ₄ /Tonne
NAPP	Incl. management, Technology [Computational]	110	kg H ₂ SO ₄ /Tonne
NAG pH 4.5	ARD Test Handbook, Project P387A, 2002	39	kg SO ₄ /Tonne
NAG pH 7.0	ARD Test Handbook, Project P387A, 2003	59	kg SO ₄ /Tonne
NAG-pH	ARD Test Handbook, Project P387A, 2004	2.3	
Electrical conductivity 25°C	ARD Test Handbook, Project P387A, 2005	322	mS/m

Table 27. Aitolampi Graphite Ore (ZA5) and threshold and guideline values for the concentrations of harmful substances in soil
(Ministry of the Environment Finland 2007)

Contamination threshold AMD Substance (symbol)	Natural concentration (mg/kg)	Threshold value (mg/kg)	Lower guideline value (mg/kg)	Higher guideline value (mg/kg)	Graphite Ore ZA5 (mg/kg)
Metals and semimetals					
Antimony (Sb) (p)	0,02 (0,01-0,2)	2	10 (t)	50 (e)	12.2
Arsenic (As) (p)	1 (0,1-25)	5	50 (e)	100 (e)	-
Mercury (Hg)	0,005 (< 0,005-0,05)	0.5	2 (e)	5 (e)	-
Cadmium (Cd)	0,03 (0,01-0,15)	1	10 (e)	20 (e)	-
Cobalt (Co) (p)	8 (1-30)	20	100 (e)	250 (e)	50.6
Chrome (Cr)	31 (6-170)	100	200 (e)	300 (e)	276.4
Copper (Cu)	22 (5-110)	100	150 (e)	200 (e)	873.4
Lead (Pb)	5 (0,1-5)	60	200 (t)	750 (e)	13.0
Nickel (Ni)	17 (3-100)	50	100 (e)	150 (e)	226.2
Zinc (Zn)	31 (8-110)	200	250 (e)	400 (e)	2 595.0
Vanadium (V)	38 (10-115)	100	150 (e)	250 (e)	1 237

The guideline values have been defined on the basis of ecological risks (e)

The guideline values have been defined on the basis of health risks (t)

If the risk of groundwater contamination is higher than normal in concentrations below the lower guideline value, the substances are marked with the letter (p)

Table 28. Aitolampi Graphite Ore (ZA5) Acid Mine Drainage (AMD) results
(Analysis by Eurofins Environment Testing Finland (Jyväskylä))

Aitolampi Graphite Ore ZA5			
Test	Method	Result	Unit
Sulfur (S)	Incl. men., Spectrophotometer (IR)	5.02	(%)
Total Carbon (TC)	Incl. men., Spectrophotometer (IR)	7.30	(%)
C carbonate	Incl. men., Spectrophotometer (IR)	0.29	(%)
C non-carbon	Incl. men., Spectrophotometer (IR)	7.01	(%)
Acid Potential (AP)	Incl. management, Technology [Computational]	160	kg CaCO ₃ /tonne
Neutralization Potential (NP)	Incl. management, Technology [Computational]	2.2	kg CaCO ₃ /tonne
NNP	Incl. management, Technology [Computational]	<0.3	kg CaCO ₃ /tonne
Neutralization Potential Ratio (NPR)	Incl. management, Technology [Computational]	<0.1	
ANC	Incl. management, Technology [Computational]	2.2	kg H ₂ SO ₄ /Tonne
MPA	Incl. management, Technology [Computational]	150	kg H ₂ SO ₄ /Tonne
NAPP	Incl. management, Technology [Computational]	150	kg H ₂ SO ₄ /Tonne
NAG pH 4.5	ARD Test Handbook, Project P387A, 2002	25	kg SO ₄ /Tonne
NAG pH 7.0	ARD Test Handbook, Project P387A, 2003	59	kg SO ₄ /Tonne
NAG-pH	ARD Test Handbook, Project P387A, 2004	2.6	
Electrical conductivity 25°C	ARD Test Handbook, Project P387A, 2005	218	mS/m

19 REFERENCES

- ALS. (2021). Aqua Regia or 4 Acid Digestion.
- Amira International. (2002). ARD Test Handbook: Prediction & Kinetic Control of Acid Mine Drainage, AMIRA P387A. Melbourne: Ian Wark Research Institute and Environmental Geochemistry International Ltd.
- Beowulf Mining. (2022). Aitolampi - Graphite. Retrieved March 14, 2022, from <https://beowulfmining.com/projects/finland/aitolampi/#overview>
- Blowes, D. W., Ptacek, C. J., Jambor, J. L., Weisener, C. G., Paktunc, D., Gould, W. D., & Johnson, D. B. (2014). The Geochemistry of Acid Mine Drainage. doi:10.1016/B978-0-08-095975-7.00905-0
- Damm, S., & Zhou, Q. (2020). Supply and Demand of Natural Graphite. DERA Rohstoffinformationen. Retrieved from <https://www.deutsche-rohstoffagentur.de/DERA/DE/Downloads/Studie%20Graphite%20eng%202020.pdf?blob=publicationFile&v=3>
- INN. (2021). Europe's Graphite Supply Chain — Key Facts. Retrieved from <https://investingnews.com/daily/resource-investing/battery-metals-investing/graphite-investing/europees-graphite-supply-chain/>
- INN. (2021). Types of Graphite: Amorphous, Flake and Vein. Retrieved from <https://investingnews.com/daily/resource-investing/battery-metals-investing/graphite-investing/types-of-graphite-amorphous-flake-and-vein/>
- Karlsson, T., Alakangas, L., & Kauppila, P. (2021). A Test of Two Methods for Waste Rock Drainage Quality Prediction: Aqua Regia Extraction and Single-addition Net-acid Generation Test Leachate Analysis. Mine Water and the Environment 40, p. 736–751. doi:<https://doi.org/10.1007/s10230-021-00784-0>
- Kauppila, P. (2019). NP calculated based on carbonate content (“carbonate NP”). Retrieved from <https://mineclosure gtk.fi/np-calculated-based-on-carbonate-content-carbonate-np/>
- Leco. (2021). 844 Series Combustion Analyzer. Retrieved from <https://www.leco.com/product/844-series>
- Luodes, H., Kauppila, P., Karlsson, T., Nikkarinen, M., Aatos, S., Tornivaara, A., . . . Kaartinen, T. (2011). Kaivannaisjätteen Luokittelu Pysyväksi - Louhinnassa Muodostuvat Sivukivet. Suomen Ympäristö 21/2011.
- Michaux, S. (2019). Graphite Outlook - Opportunities and Challenges.
- Ministry of the Environment Finland (2007): Government Decree on the Assessment of Soil Contamination and Remediation Needs
- Moore, D.M. and Reynolds, R.C. (1997) X-ray diffraction and identification and analysis of clay minerals. 2nd Edition, Oxford University Press, New York.
- Partinen, J. (2019): OPTIMIZATION OF CONVERSION AND ANODE FURNACES IN RELATION TO ELEMENTAL DISTRIBUTIONS, Master's Programme in Chemical, Biochemical and Materials Engineering, Aalto University

Post, J.E. and Bish, D.L. (1989) Rietveld refinement of crystal structures using powder X-ray diffraction data. Modern powder diffraction, 20, pp.277-308.

Punkkinen, H., Karlsson, T., Juvankoski, M., Kaartinen, T., Laine-Ylijoki, J., Merta, E., . . . Wahlström , M. (2019). Sulphur Determinations. Retrieved from <https://mineclosure.gtk.fi/sulphur-determinations/>

Robinson Jr., G. R., Hammarstrom, J. M., & Olson, W. D. (2017). Graphite, chap J. In K. J. Schulz, J. H. DeYoung Jr, R. R. Seal II, & D. C. Bradley, Critical mineral resources of the United States—Economic and environmental geology and prospects for future supply. U.S. Geological Survey Professional Paper 1802, p. J1–J24. doi:<https://doi.org/10.3133/pp1802j>

SCHULTZ, B., SANDMANN, D. and GILBRICHT, S. (2020): SEM-based automated mineralogy and its application in geo- and material sciences. Minerals, 10, 1004; doi:10.3390/min10111004.

Sharma, S. K., Chio, C. H. and Muenow D. W. (2006): Raman spectroscopic investigation of ferrous sulfate hydrates, Lunar and Planetary Science XXXVII (2006), Hawaii Institute of Geophysics and Planetology, University of Hawaii, Honolulu

Singh, R. Yadav, R.S., Kuřitka, I., Vilcakova, J. Jaromir Havlica, Jiri Masilko, Lukas Kalina, Jakub Tkacz, Miroslava Hajdúchová & Vojtěch Enev (2017): Structural, dielectric, electrical and magnetic properties of CuFe₂O₄ nanoparticles synthesized by honey mediated sol–gel combustion method and annealing effect. J Mater Sci: Mater Electron 28, 6245–6261 (2017). <https://doi.org/10.1007/s10854-016-6305-4>

Su Kyoung Park, In Cheol Kwon, Su Jeong Lee, Il Kwon Huh, and Nam Chul Cho (2019): Microstructural analysis of slags using Raman micro spectroscope, Journal of Conservation Science Vol.35, No.2, pp145-152(2019) DOI <https://doi.org/10.12654/JCS.2019.35.2.04> Printed in the Republic of Korea

Tayebi-Khorami, M., Edraki, M., Corder, G., & Golev, A. (2019). Re-Thinking Mining Waste through an Integrative Approach Led by Circular Economy Aspirations. Retrieved from <https://doi.org/10.3390/min9050286>

Törmänen, T., & Tuomela, P. (2021). Analysis of Finnish Battery Mineral Deposits. GTK.

Xiaojian Fu, Guang Yang, Jingbo Sun and Ji Zou (2012): Vibrational spectra of copper hydrates investigated with low temperature Raman spectroscopy and terahertz time domain spectroscopy, J Phys Chem A. 2012 Jul 12;116(27):7314-8. doi: 10.1021/jp302997h. Epub 2012 Jul 2.

X-Ray Minerals Services Ltd. (2021). X-ray Diffraction. Retrieved from <https://www.xrayminerals.co.uk/fi/analytical-services/mineralogical-analysis/x-ray-diffraction/>

20 APPENDIX A – BATCIRCLE 2.0 PROJECT DESCRIPTION

BATCircle 2.0 is a project developed and funded by Business Finland (<https://www.businessfinland.fi/>). The concept includes both primary raw materials, downstream refining and recycling in batteries. Most relevant operators in the existing battery business at all stages of the regional value chain are involved with this project in some form. This project will focus on the circular battery materials value system and changing R&D focus from EV high Co content batteries to high Ni content batteries.

Business Finland has granted the BATCircle 2.0 (Finland-based Circular Ecosystem of Battery Metals) consortium with 10.8 million euros as part of a total funding budget of 19.3 million euros for three years. This funding enables the consortium to continue to build on the first phase of BATCircle which was successfully completed in April 2021. In addition, BATCircle 2.0 is a key project in Business Finland's Smart Mobility and Batteries from Finland programs.

The use and demand for lithium-ion batteries is increasing drastically, as the number of electronic devices and electric vehicles and energy storage continues to rise. These batteries require not only lithium, but also other key metals like cobalt, nickel, manganese, copper, aluminium as well as graphite and other anode materials. Consequently, it is important to create a European-wide battery industry which utilizes the enormous business potential in the lithium-ion batteries throughout the whole value chain. Additionally, European self-sufficiency in the battery sector is one of the major objectives as Europe is currently highly dependent on the supply of both raw materials and battery cells from overseas.

The BATCircle 2.0 project targets adding value to the Finnish battery metals and materials sector. 'We believe that our domestic battery metals ecosystem will enable the growth of a European ecosystem that follows the principles of a circular economy and further strengthens Finland's position in the field,' says Mari Lundström, Principal Investigator of BATCircle and Associate Professor at Aalto University, School of Chemical Engineering.

Established in 2019, the BATCircle consortium aims at improving the manufacturing processes of mining, metals refining and battery chemicals as well as materials industry, and at increasing the recycling efficiency of lithium-ion batteries. 'This ecosystem addresses the targets of the Finnish national battery strategy launched earlier this year, and the targets set in the European battery ecosystem. Our aim is to accelerate Finland's sustainable and low-carbon economic growth and support the achievement of climate objectives in transport by developing skills in the field and by expanding co-operation,' says Tuomas van der Meer, Technology manager, Metso Outotec.



Joint industry-academia project (2021-2024):

- Coordinated by Aalto University
- 15 companies
- 4 universities
- 2 research centers



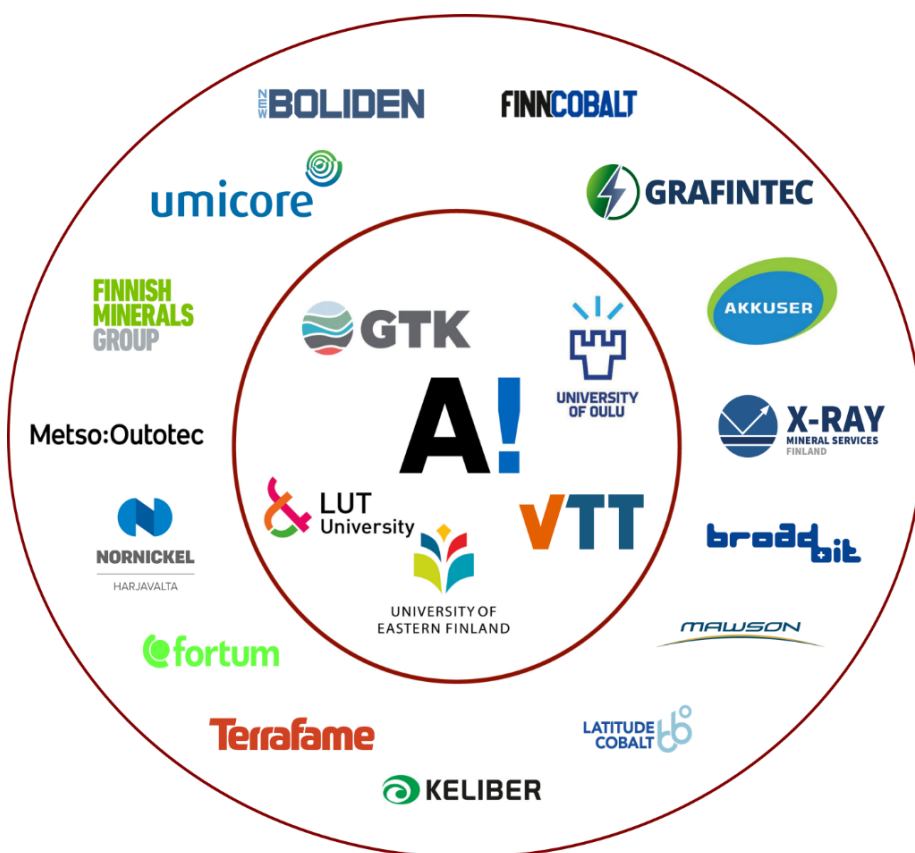


Figure A1. The BATcircle Consortium

Official BATCircle 2.0 Project website: <https://batcircle.aalto.fi/en/batcircle-20-continues-to-lead-battery-metals-and-recycling-research>

20.1 BATcircle Work Package Structure

The BATCircle 2.0 project has seven work packages:



WP1: Battery minerals exploration and responsible mining

- A unique integrated prospectivity approach for new resources and improved battery mineral prospecting methods.
- Development in data mining and statistical findings of potential locations combined with geological structure models.
- New prospectivity indications are developed by exploration of weak geochemical halos, by isotope fingerprints and surveying of deep regional scale geophysical anomalies.
- A regional geophysical & geological model of the Kuusamo schist belt to support battery mineral exploration

WP2: Enhanced battery materials recycling

- Data-driven classification of batteries by non-destructive means, linked to characterization of crushed batteries
- Study the leaching phenomena of real EV battery waste, with low-Co chemistries
- Improve recovery and recycling of currently non- or under-recovered (graphite, Li, impurities) elements present in the battery waste
- Develop dynamic modeling for SX process optimization
- Develop new methods (IX, chromatography) for battery metals recovery
- Develop membrane separation unit processes to enhance hydrometallurgical LIB recycling

WP3: Advanced minerals and metals processing

- Produce high purity graphite products from primary resources
- Develop pyrometallurgical processes for LIB treatment and integration into primary processing
- Study the environmental impacts (LCA) of lithium from virgin vs. multimetal recycled raw materials.
- Industrial integration of battery raw materials into primary hydrometallurgical processing and bench scale piloting the most promising raw material
- Study the possibility to substitute conventional oil industry originated diluents by so-called green diluents in primary battery metals processing

WP4: State-of-the-art battery materials

- Increased knowledge of synthesis of precursors (NMC, LiOH) and cathode active materials, from continuous flow laboratory-scale processing to pilot-scale
- New core competence in the synthesis and purification of anode active material
- Development of new sophisticated tools for the characterization of precursors and active materials
- Increased understanding on the use of secondary material flows and purity requirements in the synthesis of active electrode materials

WP5: Circular battery materials value system

- Increase understanding of circularity in context of battery materials
- Development of engineering parameters to support circular technologies
- Systems level assessment of integrated recycling processes
- Extensive characterization of battery materials from both primary and secondary sources
- Development of mineral characterization standards for Li, Co and Ni
- Assessment of how to develop an e-waste materials characterization standard
- Identification of circular economy related opportunities for battery value chain actors to support decision making. Design for circularity aspects identification to support the Finnish battery ecosystem and investigating circular economy landscape to support circularity business

WP6: Project management

- Facilitate communication within and outside the consortium
- Ensure the project is on schedule and following the Joint research plan
- Organize meetings for the consortium, steering group and Advisory Board
- Compile reports for the funding body
- Represent the ecosystem to external stakeholders

WP7: European network

- The objective of the WP is to further strengthen the position of Finnish organization in the European battery value chains.

20.2 How this report relates to the rest of the BATCircle 2 project

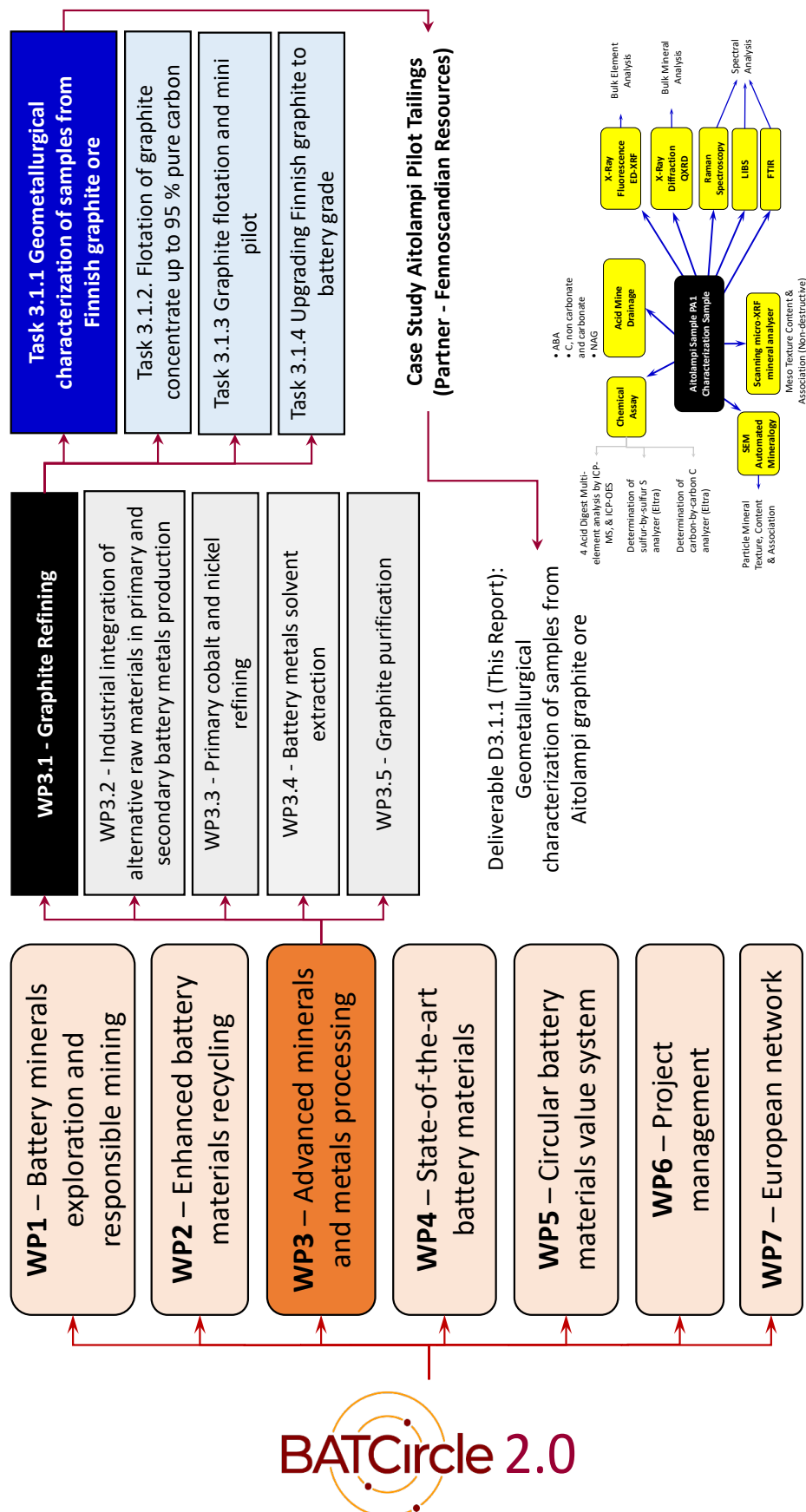


Figure A2. How this report relates to the rest of the BATCircle 2.0 project

21 APPENDIX B - SAMPLE LABELLING PROTOCOL

The following labelling protocol was developed for the Aitolahti geometallurgy campaign within the BATCircle 2.0 project.

21.1 Unique rock type sample tag to help prevent labelling mistakes between sample groups

P, Q, X, Y, Z

21.2 Deposit name

A Aitolahti. Target mineral graphite.

21.3 Rock types selected for study

- 1 High Carbon Low Barium
- 2 High Carbon Low Sulfur
- 3 Medium Carbon Medium Sulfur
- 4 Low Carbon Low Barium
- 5 High Carbon High Barium

21.4 First pass crush -3.35mm sub-sampling

- | | | |
|----|---|------------------|
| AA | } | Samples for Task |
| AB | | 3.1.1 |
| AC | | |
| AD | | |
| AS | } | Samples for Task |
| AT | | 3.1.2 |

21.5 Process path sub-group

- | | |
|-----|-------------------------------------|
| C | Characterization |
| A | Chemical Assay |
| XF | X-Ray Fluorescence |
| XD | X-Ray Diffraction |
| AM | Automated Mineralogy |
| SMX | Scanning Micro-XRF mineral analyzer |
| AMD | Acid Mine Drainage test(s) |

F	Flotation
FC	Flotation Concentrate
FT	Flotation Tailings
L	Leaching
LT	Leaching Tailings
M	Magnetic Separation
LIMS	Low Intensity Magnetic Separation concentrate
MIMS	Medium Intensity Magnetic Separation concentrate
HIMS	High Intensity Magnetic Separation concentrate
NM	Non Magnetic tailings
GS	Gravity Separation – Shaking Table
H	Heavy density fraction
M	Middlings fraction
L	Light density fraction
GK	Gravity Separation - Knelson
VH	Very Heavy density fraction
KL	Knelson Low density fraction

21.6 Examples

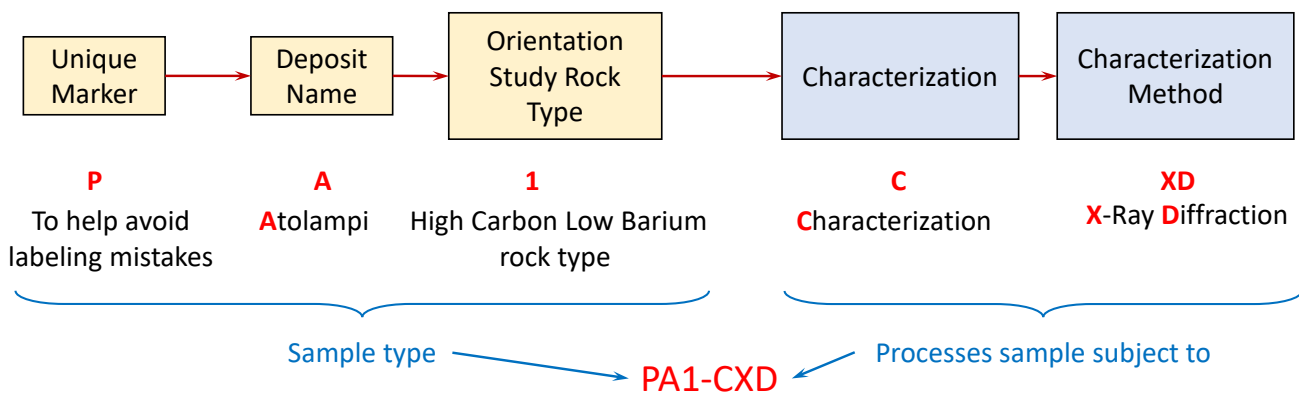


Figure B1. Sample PA1-CXD label explained

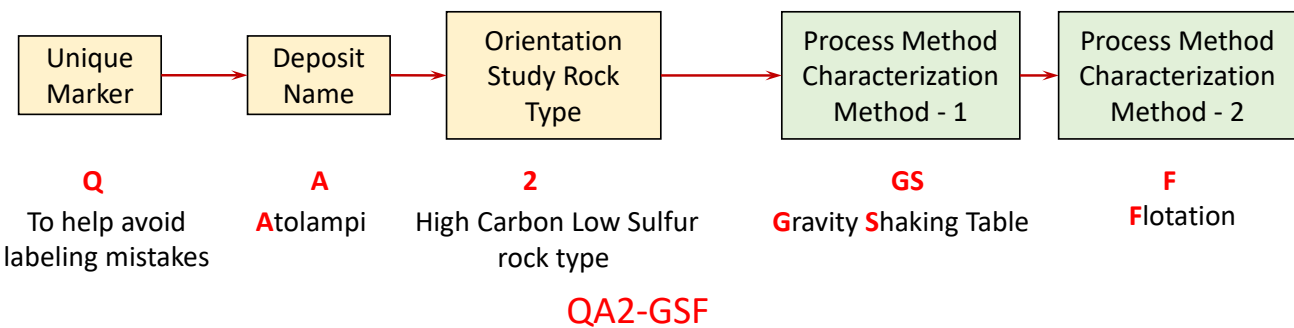


Figure B2. Sample QA2-GSF label explained

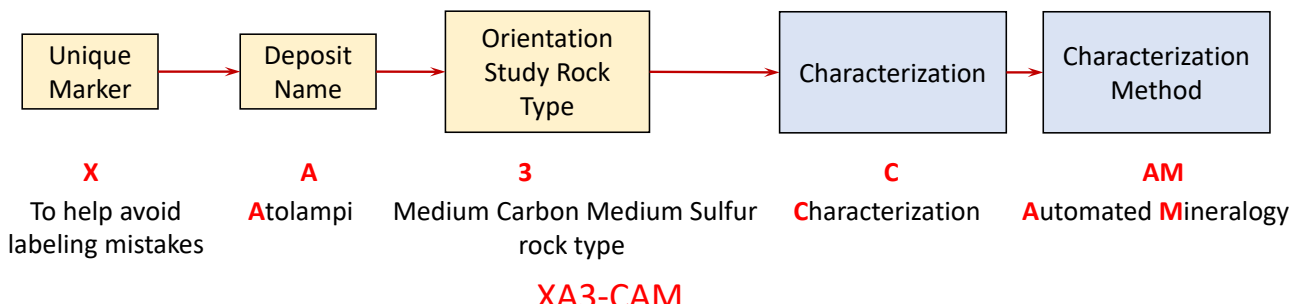


Figure B3. Sample XA3-CAM label explained

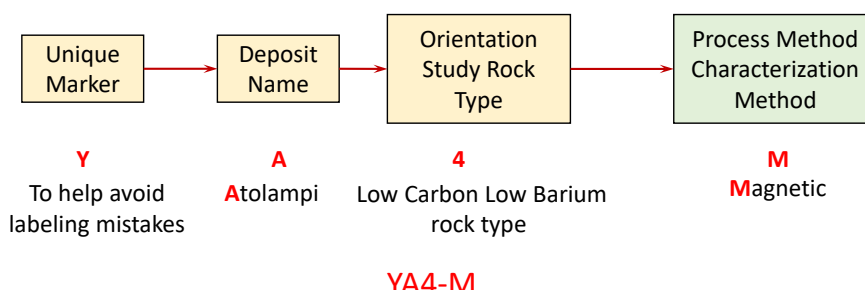


Figure B4. Sample YA4-M label explained

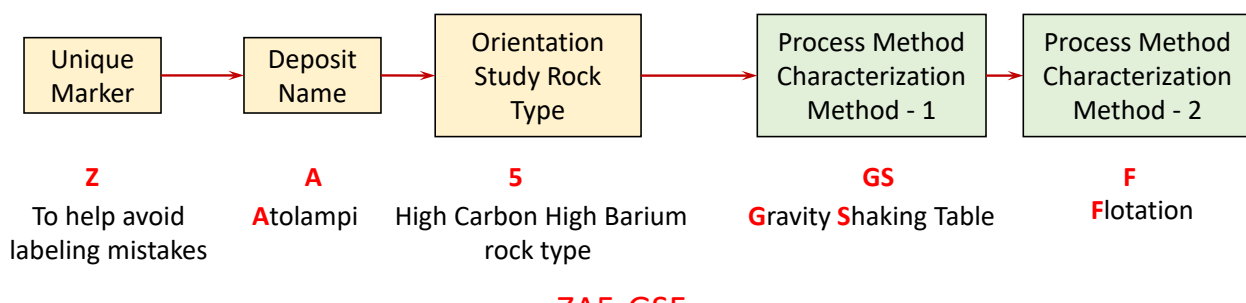
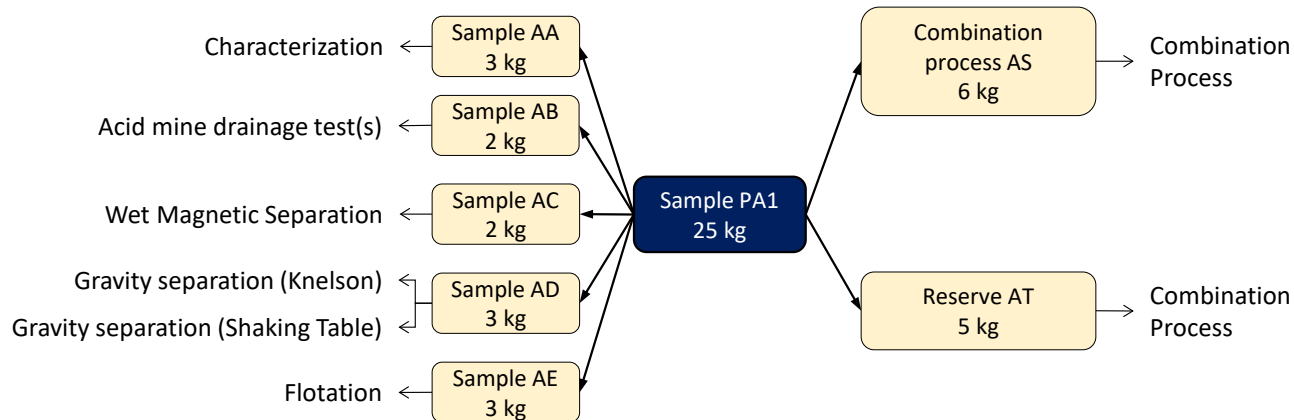


Figure B5. Sample ZA-GSF label explained

22 APPENDIX C - SAMPLE PREPARATION

All sample residues are to be kept and returned to GTK Mintec where possible. All samples that are still representative are to be kept after tests done as an orientation sample specific reserve sample. The following sample preparations were conducted for each of the Aitolahti samples:

- **Step 0:** Clean down all equipment with compressed air and sweep floor.
- **Step 1:** Check label protocol (see Appendix B).
- **Step 2:** Select 2-3 intact core section examples that are reasonably representative of the rest of the sample (say 50 to 100mm long). Weigh, bag and label this sample with the label coding PA1-CSMX (using PA1 rock type as an example). This is to be sent to Espoo office to be analyzed by the Scanning Micro-XRF mineral analyzer.
- **Step 3:** Measure remaining sample mass as received (to 0.1g precision)
- **Step 4:** Crush the sample in large crusher with approximately CSS setting of around 15mm
- **Step 5:** Measure the sample mass (to 0.1g precision), post coarse crush. Aim for 0.5% sample loss or less.
- **Step 6:** Crush the sample to 99% mass passing 3.35mm
- **Step 7:** Measure the sample mass (to 0.1g precision), post fine crush. Aim for 0.5% sample loss or less.
- **Step 8:** Rotary divide or riffle the sample into representative sub-samples that would be tasked to specific characterization and process separation tests. Divide the approximate 25 kg sample into approximate sub-samples as shown:



- **Step 9:** Measure sample mass (to 0.1g precision) of each sub-sample. Mathematically combine all sub-samples and compare to the mass in Step 6. Aim for 0.5% sample loss or less.
- **Step 10:** Label the sub-samples according to the protocol in Appendix B

- **Step 11:** Take Sample AA (approximately 3 kg) and rotary divide it into 4 sub-samples. Measure sample mass (to 0.1g precision) of each sub-sample. Mathematically combine all sub-samples and compare to the mass in Step 9. Aim for 0.5% sample loss or less. Take the four AA sub samples and label them for mailout.
- **Step 12:** Take Sample AB (approximately 2 kg) and rotary divide it into 4 sub-samples. Measure sample mass (to 0.1g precision) of each sub-sample. Mathematically combine all sub-samples and compare to the mass in Step 9. Aim for 0.5% sample loss or less. Take the four AB sub samples and label them for mailout.
- **Step 13:** Mail out the samples in Table C1 to the required destination.

Table C1. Sub-sampling for characterization and acid mine drainage tests

Step	Source Sub-sample	Relabelling	Target Mass	Test	Mail to
2	PA1	PA1-CSMX	2-3 intact core sections	Scanning Micro-XRF mineral analyzer	GTK Espoo office
11	PA1-AA1	PA1-CA	600-700g	Chemical Assay	ALS Finland
11	PA1-AA2	PA1-CXF	600-700g	XRF	X-Ray Mineral Services Finland
11	PA1-AA3	PA1-CXD	600-700g	XRD	X-Ray Mineral Services Finland
11	PA1-AA4	PA1-CAM	600-700g	Automated Mineralogy	-
12	PA1-AB1	PA1-AMD-1		Acid Mine Drainage	-
12	PA1-AB2	PA1-AMD-2		Acid Mine Drainage	-
12	PA1-AB3	PA1-AMD-3		Acid Mine Drainage	-
12	PA1-AB4	PA1-AMD-4		Acid Mine Drainage	-

All sample residues are to be kept and returned to GTK Mintec where possible. All samples that are still representative are to be kept after tests done as an orientation sample specific reserve sample.

23 APPENDIX D – CORRELATION MATRIX ANALYSIS OF AITOLAMPI ASSAY

Table D1-1. Aitolampi Chemical Assay Correlation Matrix

Correlation	Ag_ppm	Al_pct	As_ppm	Au_ppm	B_ppm	Ba_ppm	Be_ppm	Ca_pct	Bi_ppm	Ce_ppb	Cd_ppm	Co_ppm	Cr_ppm	Cs_ppm	Cu_ppm	Fe_pct	Ga_ppm		
Ag_ppm	1	-0.03675	0.3381	-0.2454	-0.00471	-0.4527	0.4169	0.8141	0.1327	0.6763	-0.0172	0.6555	0.4605	0.1063	0.7683	0.4876	-0.1146		
Al_pct	-0.03675	1	-0.2138	0.07607	0.01668	0.6195	0.1354	-0.144	0.06452	0.148	0.1213	0.1757	0.6424	0.2849	0.1192	-0.08268	0.9223		
As_ppm	0.3381	-0.2138	1	-0.1581	0.04111	-0.3314	0.3898	0.2929	0.00121	0.3211	-0.1005	0.3978	0.08383	0.03938	0.3515	0.401	-0.2967	0.1008	
Au_ppm	-0.2454	0.07607	-0.1581	1	-0.00722	0.1016	0.1143	-0.3021	0.1248	-0.05157	0.1416	-0.09005	-0.00833	-0.09881	-0.06387	-0.1232	-0.02061	0.4458	
B_ppm	-0.00471	0.01668	0.04111	-0.00722	1	0.02234	0.08873	-0.02605	0.1065	0.08706	-0.01585	0.02489	0.0532	-0.06591	0.0621	0.04	-0.02061	0.4458	
Ba_ppm	0.4527	0.6195	-0.3314	0.1016	0.002234	1	-0.3502	-0.507	-0.2574	-0.3111	0.02217	-0.2461	0.139	0.185	-0.3337	-0.3724	0.5967	0.44223	
Be_ppm	0.4169	0.1354	0.3898	0.1143	0.08873	-0.3502	1	0.2829	0.4608	0.5758	0.2001	0.4463	0.3275	-0.08513	0.573	0.3464	0.6464	-0.2336	
Bi_ppm	0.8141	-0.144	0.2929	-0.3021	-0.02605	-0.507	0.2829	1	-0.0572	0.4566	-0.1914	0.6207	0.3343	0.1902	0.4958	0.6628	0.8076	0.02405	
Ca_pct	0.1327	0.06452	0.00121	0.1248	0.1065	-0.2574	0.4608	-0.0572	1	0.2944	0.2748	-0.00532	0.02085	-0.4591	0.3069	-0.0887	0.08936	0.4458	
Cd_ppm	0.6763	0.148	0.3211	-0.05157	0.08706	-0.3111	0.5758	0.4566	0.2944	1	0.2452	0.5541	0.71	0.1012	0.8784	0.284	0.02976	0.4458	
Ce_ppb	-0.0172	0.1213	-0.1005	0.1416	-0.01585	0.02217	0.2001	-0.1914	0.2748	0.2452	1	-0.07597	0.115	-0.3577	0.201	-0.2664	0.2283	0.4458	
Co_ppm	0.6555	0.1757	0.3978	-0.09005	0.02489	-0.2461	0.4463	0.6207	-0.00532	0.5541	-0.07597	1	0.5344	0.2301	0.6628	0.8076	0.02405	0.4458	
Cr_ppm	0.4605	0.6424	0.0883	-0.09833	0.0532	0.139	0.3275	0.3343	0.02085	0.71	0.115	0.5344	1	0.3779	0.6342	0.1914	0.5187	0.4458	
Cs_ppm	0.1063	0.2849	0.03938	-0.09881	-0.06591	0.185	-0.08513	0.1902	-0.4591	0.1012	-0.3577	0.2301	0.3779	1	0.08442	0.2287	0.1541	0.4458	
Cu_ppm	0.7683	0.1192	0.3515	-0.06387	0.0621	-0.3337	0.573	0.4958	0.3069	0.8784	0.201	0.6628	0.6342	0.08442	1	0.3552	-0.00943	0.4458	
Fe_pct	0.4876	-0.08268	0.401	-0.1232	0.04	-0.3724	0.3464	0.6464	-0.0887	0.284	-0.2664	0.8076	0.1914	0.2287	0.3552	1	-0.2007	0.4458	
Ga_ppm	-0.1146	0.9223	-0.2967	0.1008	-0.02061	0.5967	0.04223	-0.2336	0.08936	0.02976	0.2283	0.02405	0.5187	0.1541	-0.00943	-0.2007	1	0.4458	
Ge_ppm	0.7166	0.285	0.3233	-0.08297	0.1409	-0.2267	0.5041	0.5606	0.1381	0.8022	0.1336	0.765	0.7386	0.26	0.8265	0.5453	0.1547	0.4458	
Hg_ppm	0.5877	0.04706	0.3832	0.008727	0.09208	-0.3585	0.6147	0.3812	0.2307	0.8981	0.1287	0.5622	0.5909	0.127	0.7785	0.3717	-0.07359	0.4458	
In_ppm	0.5979	0.2439	0.2199	-0.09705	0.05291	-0.116	0.3387	0.4661	0.1098	0.7298	0.09938	0.5497	0.6049	0.1151	0.615	0.3537	0.1959	0.4458	
K_pct	-0.1945	0.6365	-0.2397	-0.00146	-0.06162	0.7255	-0.3387	-0.1336	-0.4987	-0.1836	-0.2438	-0.02376	0.3436	0.6918	-0.2132	-0.107	0.5558	0.4458	
La_ppb	5.90E-04	0.07964	-0.07624	0.1044	0.00473	-0.0475	0.1985	-0.1669	0.2665	0.2444	0.9926	-0.07355	0.0851	-0.352	0.2	-0.2447	0.1959	0.4458	
Li_pct	-0.1165	0.7854	-0.2378	0.1385	-0.03851	0.534	0.03401	-0.1197	-0.1134	-0.01559	3.59E-04	0.0801	0.4678	0.288	-0.07988	-0.031	0.7936	0.4458	
Mg_pct	0.2948	0.8172	-0.06785	0.01614	0.01201	0.25	0.2507	0.2011	0.01927	0.4066	0.03052	0.4087	0.8403	0.3857	0.3662	0.1581	0.7364	0.4458	
Mn_ppm	0.2842	0.2235	-0.01061	-0.08572	-0.1006	0.01875	0.4109	-0.09422	0.01713	-0.156	0.2102	0.2185	0.3312	0.005374	0.317	0.2667	0.4458	0.4458	
Mo_ppm	0.6713	0.04757	0.4075	-0.06339	0.1008	-0.4179	0.6307	0.5872	0.2578	0.9198	0.1628	0.6851	0.6376	0.1372	0.8454	0.5162	-0.1042	0.4458	
Na_pct	0.07178	0.5202	-0.06023	-0.0832	0.05277	0.3005	0.1627	-0.08568	0.1775	0.1983	0.2925	0.05301	0.3307	0.09873	0.2073	-0.165	0.4533	0.4458	
Ni_ppm	0.6298	-0.1132	0.4955	-0.09486	0.06746	-0.479	0.5675	0.6515	0.09836	0.638	-0.07875	0.8257	0.3731	0.1762	0.6788	0.8713	-0.2711	0.4458	
P_ppm	-0.03897	0.00119	-0.1205	0.04508	0.02277	-0.05517	-0.05026	-0.08431	0.1774	-0.01799	0.1168	-0.1496	-0.09563	-0.097	-0.01779	-0.1589	0.0451	0.4458	
Pb_ppm	0.5173	-0.09596	0.3554	0.002921	0.07986	-0.5054	0.6153	0.3337	0.545	0.6321	0.2523	0.4207	0.2655	-0.3825	0.6218	0.2921	-0.135	0.4458	
Rb_ppm	-0.02581	0.5155	-0.134	-0.06423	-0.08289	0.5104	-0.2594	0.06546	-0.5268	-0.04425	-0.3004	0.09798	0.4008	0.8633	-0.08035	0.04502	0.4102	0.4458	
Re_ppm	0.6187	0.1318	0.3516	-0.01737	0.1085	-0.3504	0.6229	0.4748	0.2768	0.9596	0.2286	0.5954	0.7113	0.1485	0.8581	0.3632	-0.0802	0.4458	
S_pct	0.5992	-0.2927	0.4825	-0.1512	0.04436	-0.5914	0.4123	0.7231	0.001618	0.3925	-0.2363	0.7697	0.1369	0.1588	0.4587	0.9454	-0.406	0.4458	
Sb_ppm	0.08776	0.04036	0.02184	0.0797	-0.1185	-0.05201	0.1426	0.005437	0.1135	0.08052	0.07933	0.09808	-1.11E-04	-0.05817	0.1021	0.0461	0.07034	0.4458	
Se_ppm	0.7931	0.06843	0.388	-0.1023	0.06108	-0.3753	0.5532	0.5586	0.2565	0.8994	0.1714	0.6668	0.629	0.1098	0.9452	0.4047	-0.06176	0.4458	
Sn_ppm	0.5283	0.3867	0.217	-0.1625	-0.03005	0.001466	0.3247	0.4369	-0.03393	0.6055	0.2192	0.4499	0.6925	0.4514	0.5738	0.2445	0.2855	0.4458	
Sr_ppm	0.03187	0.1472	-0.04203	0.07402	0.08871	-0.09067	0.2019	-0.07939	0.6077	0.2354	0.1836	-0.07266	0.0761	-0.1624	0.2264	-0.1799	0.06415	0.4458	
Te_ppm	0.3375	0.19	-0.04609	-0.2215	-0.08019	-0.04524	-0.1475	0.4403	-0.1754	-0.04659	-0.1941	0.1409	0.1715	0.112	-0.08844	0.07354	0.1879	0.4458	
Th_ppm	0.3254	0.3054	0.1396	0.1596	0.07762	0.07665	-0.07205	0.4796	0.1692	0.3082	0.6097	0.6487	0.4055	0.5635	-0.1898	0.5677	0.1283	0.2409	
Tl_ppm	0.4458	0.1054	0.2784	-0.2927	0.4825	-0.1512	0.04436	-0.5914	0.4123	0.7231	0.001618	0.3925	0.1714	0.6668	0.517	0.7225	0.517	0.3946	-0.00583
U_ppm	0.6181	0.03568	0.4248	-0.06964	0.1018	-0.4105	0.6498	0.2616	0.8746	0.9868	0.2078	0.6097	0.6846	0.1114	0.8668	0.5001	0.1259	0.8236	0.4458
Zn_ppm	0.6946	0.1155	0.3519	-0.06027	0.07315	-0.3462	0.5936	0.5137	0.06202	0.09895	0.2361	0.4048	-0.1108	0.5491	-0.1456	0.4493	0.517	0.3946	-0.00583

Table D1-2. Aitolampi Chemical Assay Correlation Matrix

Correlation	Ge_ppm	Hg_ppm	In_ppm	K_pct	La_ppb	Li_ppm	Mg_pct	Mn_ppm	Mo_ppm	Na_pct	Ni_ppm	P_ppm	Rb_ppm	Re_ppm	S_pct	Sb_ppm	
Ag_ppm	0.7166	0.5877	0.5979	-0.1945	5.90E-04	0.2948	0.2842	0.6713	0.07178	0.6298	-0.03897	0.5173	-0.02581	0.6187	0.5992	0.08776	
Al_pct	0.285	0.04706	0.2439	0.6365	0.07964	0.7854	0.8172	0.2235	0.04757	0.5202	-0.1132	0.00119	-0.09596	0.5155	0.1318	-0.2927	0.04036
As_ppm	0.3233	0.3832	0.2199	-0.2397	-0.07624	-0.2378	-0.06785	-0.01061	0.4075	-0.06023	0.4955	-0.1205	0.3554	-0.134	0.3516	0.4825	0.02184
Au_ppm	-0.08297	0.008727	-0.09705	-0.00146	0.1044	0.1385	0.01614	-0.08572	-0.06339	-0.0832	-0.09486	0.04508	0.002921	-0.06423	-0.01737	-0.1512	0.07977
B_ppm	0.1409	0.09208	0.05291	-0.06162	0.00473	-0.03851	0.01201	-0.1006	0.1008	0.05277	0.06746	0.02277	0.07986	-0.08289	0.1085	0.04436	-0.1185
Ba_ppm	-0.2267	-0.3585	-0.116	0.7255	-0.00475	0.534	0.25	-0.2069	-0.4179	0.3005	-0.479	-0.05517	-0.5054	0.5104	-0.3504	-0.5914	-0.05201
Be_ppm	0.5041	0.6147	0.3387	-0.3387	0.1985	0.03401	0.2507	0.01875	0.6307	0.1627	0.5675	-0.05026	0.6153	-0.2594	0.6229	0.4123	0.14246
Bi_ppm	0.5606	0.3812	0.4661	-0.1336	-0.1669	-0.1197	0.2011	0.4109	0.5872	-0.08588	0.6515	-0.08431	0.3337	0.06546	0.4748	0.7231	0.005437
Ca_pct	0.1381	0.2307	0.1098	-0.4987	0.2665	-0.1134	0.01927	-0.09422	0.2578	0.1775	0.09836	0.1774	0.545	-0.5268	0.2768	0.001618	0.1135
Cd_ppm	0.8022	0.8981	0.7298	-0.1836	0.2444	-0.01559	0.4066	0.01713	0.9198	0.1983	0.638	-0.01799	0.6321	-0.04425	0.9596	0.3925	0.08052
Ce_ppb	0.1336	0.1287	0.09938	-0.2438	0.9926	3.59E-04	0.03052	-0.156	0.1628	0.2925	-0.07875	0.1168	0.2523	-0.3004	0.2286	-0.2363	0.07933
Co_ppm	0.765	0.5622	0.5497	-0.02376	-0.07355	0.0801	0.4087	0.2102	0.6831	0.05301	0.8257	-0.1496	0.4207	0.09798	0.5954	0.7697	0.09808
Cr_ppm	0.7386	0.5909	0.6049	0.3436	0.0851	0.4678	0.8403	0.2185	0.6376	0.3307	0.3731	-0.09563	0.2655	0.4008	0.7113	0.1369	-1.11E-04
Cs_ppm	0.26	0.1227	0.1151	0.6918	-0.352	0.288	0.3857	0.3312	0.1372	0.09873	0.1762	-0.097	-0.3825	0.8633	0.1485	0.1588	-0.05817
Cu_ppm	0.8265	0.7785	0.615	-0.2132	0.2	-0.07988	0.36662	0.005374	0.8454	0.2073	0.6788	-0.01779	0.6218	-0.08035	0.8581	0.4587	0.1021
Fe_pct	0.5453	0.3717	0.3537	-0.107	-0.2447	-0.031	0.1581	0.317	0.5162	-0.165	0.8713	-0.1589	0.2711	0.0451	-0.135	0.4102	-0.0802
Ga_ppm	0.1547	-0.07359	0.1959	0.5538	0.1959	0.7936	0.7364	0.2667	-0.1042	0.4533	-0.2711	0.0451	-0.09401	0.4098	0.09829	0.6459	0.3603
Ge_ppm	1	0.734	0.6475	-0.01209	0.1366	0.1325	0.5623	0.2083	0.8271	0.1743	0.7351	-0.05959	0.485	0.1244	0.8129	0.562	0.02493
Hg_ppm	0.734	1	0.6683	-0.2224	0.1288	-0.01616	0.3273	0.0214	0.8698	0.03255	0.6954	-0.03522	0.6114	-0.07251	0.8874	0.4765	0.01818
In_ppm	0.6475	0.6683	1	0.01794	0.1043	0.1589	0.4181	0.11797	0.6614	0.08539	0.5047	-0.09401	0.4098	0.09829	0.6459	0.3603	0.08873
K_pct	-0.01209	-0.2224	0.01794	1	-0.2587	0.5874	0.455	0.18	-0.2414	0.2438	-0.2652	-0.1108	-0.6234	0.9447	-0.195	-0.3061	-0.08202
La_ppb	0.1366	0.1288	0.1043	-0.2587	1	-0.03313	-0.00957	-0.1579	0.1672	0.2815	-0.0596	0.08552	0.2556	-0.3051	0.2267	-0.2064	0.084
Li_ppm	0.1325	-0.01616	0.1589	0.5874	-0.03313	1	0.7151	0.4065	-0.08647	0.2351	-0.1474	0.01123	-0.2288	0.491	-0.02518	-0.2389	0.06407
Mg_pct	0.5623	0.3273	0.4181	0.455	-0.00957	0.7151	1	0.4519	0.3347	0.3342	0.1851	0.04958	0.1065	0.4593	0.4108	0.03415	0.05762
Mn_ppm	0.2083	0.0214	0.1797	0.18	-0.1579	0.4065	0.4519	1	0.06274	-0.07567	0.1408	0.09759	-0.02525	0.2898	0.04262	0.275	0.04746
Mo_ppm	0.8271	0.8698	0.6614	-0.2414	0.1672	-0.08647	0.3347	0.06274	1	0.1156	0.8246	-0.04829	0.6647	-0.06529	0.967	0.6116	0.06542
Na_pct	0.1743	0.03255	0.08539	0.2438	0.2815	0.2351	0.3342	-0.07567	0.1156	1	-0.06756	0.06106	0.06911	0.1914	0.1659	-0.1996	0.09906
Ni_ppm	0.7351	0.6954	0.5047	-0.2652	-0.0596	-0.1474	0.1851	0.1408	0.8246	-0.06756	1	-0.136	0.565	-0.07411	0.7153	0.9113	0.07248
P_ppm	-0.05959	-0.03522	-0.09401	-0.1108	0.08552	0.01123	0.04958	0.09759	-0.04829	0.06106	-0.136	0.01807	-0.1132	-0.02227	-0.1053	0.01059	0.1483
Pb_ppm	0.485	0.6114	0.4098	-0.6234	0.2556	-0.2288	0.1065	-0.02525	0.6647	0.06911	0.565	0.01807	1	-0.5581	0.6433	0.4362	0.1483
Rb_ppm	0.1244	-0.07251	0.09829	0.9447	-0.3051	0.491	0.4593	0.2898	-0.06529	0.1914	-0.07411	-0.1132	-0.5581	1	-0.03626	-0.1049	-0.08145
Re_ppm	0.8129	0.8874	0.6459	-0.195	0.2267	-0.02518	0.4108	0.04262	0.967	0.1659	0.7153	-0.02227	0.6433	-0.03626	1	0.4691	0.1483
S_pct	0.562	0.4765	0.3603	-0.3061	-0.2064	-0.2389	0.03415	0.275	0.616	-0.1996	0.9113	-0.1053	0.4362	-0.1049	0.4691	1	0.06005
Sb_ppm	0.02493	0.01818	0.08873	-0.08202	0.084	0.06407	0.05762	0.04746	0.06542	0.09906	0.07248	0.01059	0.1483	-0.08445	0.0681	0.06005	1
Se_ppm	0.8566	0.8122	0.6314	-0.2198	0.1738	-0.1044	0.3419	0.03001	0.8896	0.157	0.7176	-0.03467	0.6379	-0.06652	0.8804	0.5146	0.07085
Sn_ppm	0.7063	0.5073	0.4365	0.2589	0.2182	0.2911	0.5791	0.2896	0.6006	0.3464	0.4134	-0.03476	0.2354	0.3864	0.6244	0.2499	0.06268
Sr_ppm	0.05337	0.0883	0.02426	-0.1876	0.176	-0.1476	0.02048	-0.1536	0.18	0.3285	-0.00849	0.1541	0.234	-0.1893	0.2226	-0.1196	0.06117
Te_ppm	0.0773	-0.1369	0.2284	0.2523	-0.1971	0.2139	0.2348	0.4122	-0.08539	0.0166	-0.08416	-0.07947	-0.09369	0.2613	-0.1119	0.03802	-0.06938
Th_ppm	0.5798	0.5037	0.4422	-0.2279	0.6256	0.1288	0.414	-0.05447	0.6003	0.3097	0.3848	-0.04528	0.5613	-0.22	0.6305	0.1466	0.1367
Tl_ppm	0.5637	0.5607	0.3448	0.2255	-0.1331	0.05194	0.3967	0.5895	0.1449	0.5509	-0.06256	0.1378	0.4709	0.6054	0.4508	0.05271	0.07086
U_ppm	0.8098	0.834	0.5716	-0.2559	0.1847	-0.1026	0.3133	0.02598	0.9624	0.131	0.814	-0.03373	0.6621	-0.08057	0.9355	0.6033	0.07086
Zn_ppm	0.8136	0.9159	0.7546	-0.1978	0.2086	-0.02301	0.3847	0.04386	0.9454	0.1691	0.709	-0.03635	0.6462	-0.04525	0.9558	0.4784	0.07668

Table D1-3. Aitolampi Chemical Assay Correlation Matrix

Correlation	Se_ppm	Sn_ppm	Sr_ppm	Te_ppm	Th_ppm	Tl_ppm	U_ppm	Zn_ppm
Ag_ppm	0.7931	0.5283	0.03187	0.3375	0.3254	0.4458	0.6181	0.6946
Al_pct	0.06843	0.3867	0.1472	0.19	0.3054	0.1054	0.03568	0.1155
As_ppm	0.388	0.217	-0.04203	-0.04609	0.1396	0.2784	0.4248	0.3519
Au_ppm	-0.1023	-0.1625	0.07402	-0.2215	0.07762	-0.08531	-0.06964	-0.06027
B_ppm	0.06108	-0.03005	0.08871	-0.08019	0.07665	0.009955	0.1018	0.07315
Ba_ppm	-0.3753	0.001466	-0.09067	-0.04524	-0.07205	-0.2361	-0.4105	-0.3462
Be_ppm	0.5532	0.3247	0.2019	-0.1475	0.4796	0.3166	0.6498	0.5936
Bi_ppm	0.5586	0.4369	-0.07939	0.4403	0.1692	0.4048	0.5294	0.5137
Ca_pct	0.2565	-0.03393	0.6077	-0.1754	0.3082	-0.1108	0.2616	0.2825
Cd_ppm	0.8994	0.6055	0.2354	-0.04659	0.6097	0.5491	0.8746	0.9868
Ce_ppb	0.1714	0.2192	0.1836	-0.1941	0.6487	-0.1456	0.1775	0.2078
Co_ppm	0.6668	0.4499	-0.07266	0.1409	0.4055	0.4493	0.6462	0.6097
Cr_ppm	0.629	0.6925	0.0761	0.1715	0.5635	0.5179	0.5873	0.6846
Cs_ppm	0.1098	0.4514	-0.1624	0.112	-0.1898	0.7225	0.1437	0.1114
Cu_ppm	0.9452	0.5738	0.2264	-0.00844	0.5677	0.517	0.8236	0.8668
Fe_pct	0.4047	0.2445	-0.1799	0.07354	0.1283	0.3946	0.5001	0.3749
Ga_ppm	-0.06176	0.2855	0.06415	0.1879	0.2409	-0.00583	-0.1259	-0.01154
Ge_ppm	0.8566	0.7063	0.05337	0.0773	0.5798	0.5637	0.8098	0.8136
Hg_ppm	0.8122	0.5073	0.0883	-0.1369	0.5037	0.5607	0.834	0.9159
In_ppm	0.6314	0.4365	0.02426	0.2284	0.422	0.3448	0.5716	0.7546
K_pct	-0.2198	0.2589	-0.1876	0.2523	-0.2279	0.2255	-0.2559	-0.1978
La_ppb	0.1738	0.2182	0.176	-0.1971	0.6256	-0.1331	0.1847	0.2086
Li_ppm	-0.1044	0.2911	-0.1476	0.2139	0.1288	0.05194	-0.1026	-0.02301
Mg_pct	0.3419	0.5791	0.002048	0.2348	0.414	0.3967	0.3133	0.3847
Mn_ppm	0.03001	0.2896	-0.1536	0.4122	-0.05447	0.2983	0.02598	0.04386
Mo_ppm	0.8896	0.6006	0.18	-0.08539	0.6003	0.5895	0.9624	0.9454
Na_pct	0.157	0.3464	0.3285	-0.0166	0.3097	0.1449	0.131	0.1691
Ni_ppm	0.7176	0.4134	-0.00849	-0.08416	0.3848	0.5509	0.814	0.709
P_ppm	-0.03467	-0.03476	0.1541	-0.07947	-0.04528	-0.06256	-0.03373	-0.03635
Pb_ppm	0.6379	0.2354	0.234	-0.09369	0.5613	0.1378	0.6621	0.6462
Rb_ppm	-0.06652	0.3864	-0.1893	0.2613	-0.22	0.4709	-0.08057	-0.04525
Re_ppm	0.8804	0.6244	0.226	-0.1119	0.6305	0.6054	0.9355	0.9558
S_pct	0.5146	0.2499	-0.1196	0.03802	0.1466	0.4508	0.6033	0.4784
Sb_ppm	0.07085	0.06268	0.0617	-0.06938	0.1367	0.05271	0.07086	0.07668
Se_ppm	1	0.5727	0.1875	0.001297	0.5436	0.5454	0.8432	0.8957
Sn_ppm	0.5727	1	-0.01344	0.1279	0.5029	0.5406	0.6379	0.6037
Sr_ppm	0.1875	-0.01344	1	-0.1034	0.1966	0.01706	0.1843	0.2039
Te_ppm	0.001297	0.1279	-0.1034	1	-0.1124	-0.06106	-0.1515	-0.04159
Th_ppm	0.5436	0.5029	0.1966	-0.1124	1	0.1222	0.6225	0.5991
Tl_ppm	0.5454	0.5406	0.01706	-0.06106	0.1222	1	0.5675	0.5607
U_ppm	0.8432	0.6379	0.1843	-0.1515	0.6225	0.5675	1	0.8973
Zn_ppm	0.8957	0.6037	0.2039	-0.04159	0.5991	0.5607	0.8973	1

24 APPENDIX E – PRINCIPLE COMPONENT ANALYSIS OF AITOLAMPI ASSAY DATABASE

One of the methods used to partition a large and varied data matrix into meaningful groups is the application of a statistical technique called Principle Component Analysis (PCA).

PCA is a mature statistical technique that is widely used for finding patterns in data of multiple dimensions. PCA finds a set of orthogonal dimensions, which account for all the variance in a particular dataset, by reducing the dimensionality of a complex system of correlations into a smaller number of dimensions. The first principal component (PC1) accounts for as much data variance as possible and each subsequent principal component accounts for remaining data variance (PC2, PC3, PC4...).

This approach is to spatially model classes created during principal component analysis and attempt to partition the data set into groups that describe the most variability (PC1, PC2, etc.). Each class has a given distribution for each parameter, where the target processing response and variability is examined in each block by association.

24.1 Principal component Method:

1. Subtract the mean from each of the data dimensions in order to create a data set that has a mean of zero.
2. Calculate the covariance matrix for the dataset. The covariance is a measure of how much each dimension varies from the mean with respect to each other (i.e. the relative spread of data in a dataset). The formula for the covariance is:

$$\text{cov}(X, Y) = \frac{\sum_{i=1}^n (X_i - \bar{X})(Y_i - \bar{Y})}{(n-1)} \quad \text{Equation E1}$$

The value obtained from the covariance calculation is not as important as if they sign is positive or negative.

- If the result is positive, it implies that a direct relationship exists between the two datasets.
- If the sign is negative: the data sets are inversely related to each other.
- If the result of the covariance calculation equals zero, the two data dimensions are independent of each other.

As there are multidimensional datasets, a covariance matrix is used. The covariance matrix is defined as:

$$C^{n \times n} = (c_{i,j}, c_{i,j} = \text{cov}(Dim_i, Dim_j)) \quad \text{Equation E2}$$

This equation states that if you have an n-dimensional dataset, then the matrix has n rows and columns and each entry in the matrix is the result of calculating the covariance between two separating dimensions.

3. Calculate the eigenvectors and eigenvalues for the matrix:

Let A be a square matrix. A non-zero vector C is called an eigenvector of A if and only if there exists a number (real or complex) λ such that $AC = \lambda C$. If such a number λ exists, it is called a eigenvalue of A. The vector C is called the eigenvector associated to the eigenvalue associated to the eigenvalue λ .

4. Select components and form a feature vector. A feature vector is an n-dimensional vector of numerical features representing an object.
5. Derive new datasets by condensing multidimensional data into orthogonal dimensions (i.e. Principal Components)

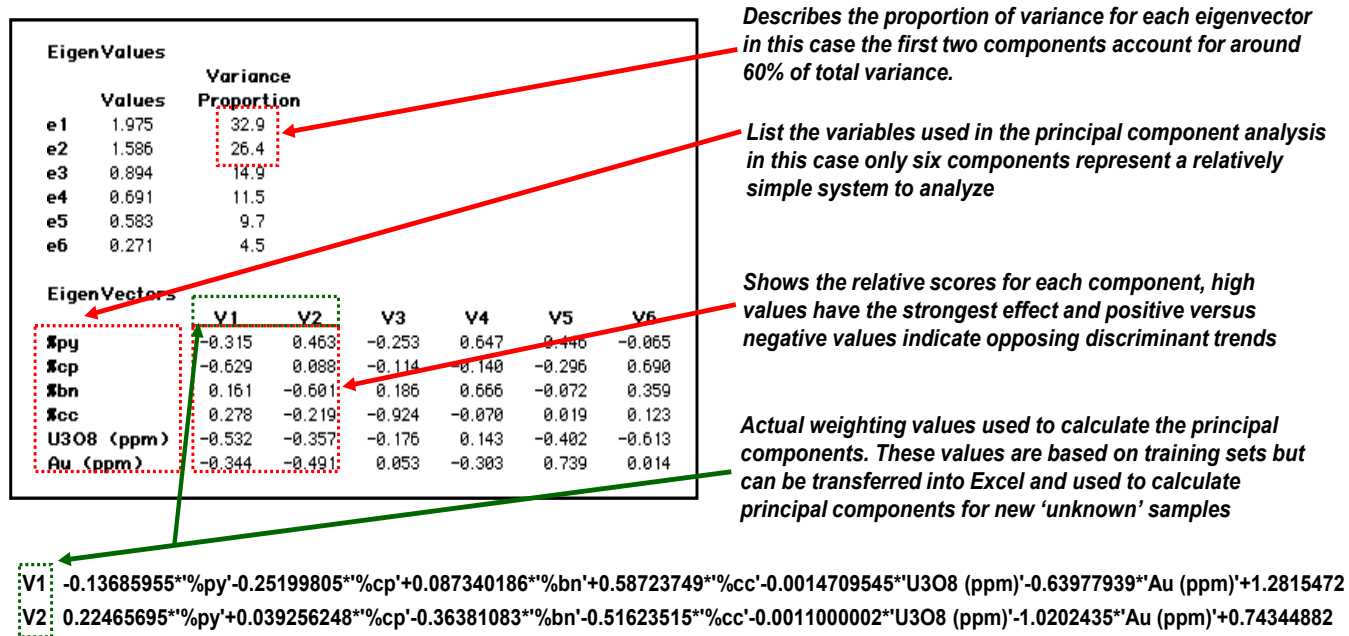
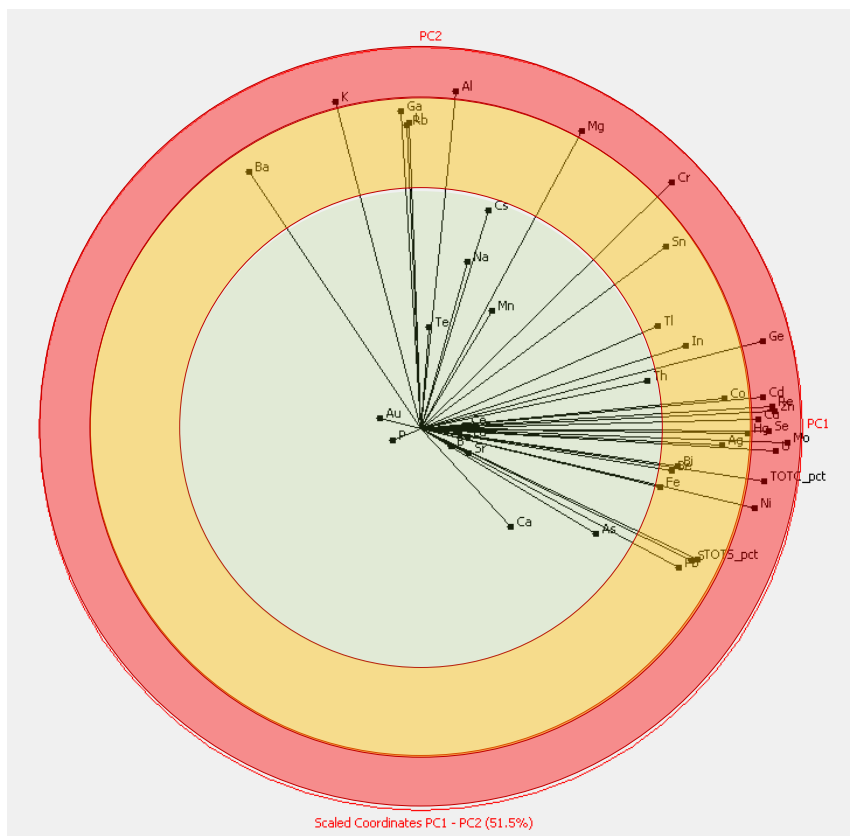


Figure E1. Principle component methodology

PCA expresses the data in such a way as to highlight similarities and differences within the data set. It is well suited to analysis of rock-based attributes using large datasets in geometallurgy.

It is to be remembered that this PCA based characterization has been set up to group based on fundamental multivariate controls of the whole data set, not on constraining the processing response. This can potentially result in large variability within classes that may cover the entire distribution of processing performance results.

It is for this reason that the PCA procedure is not the final analytical goal of a geometallurgical study. The decision of what a Class (or process defined ore type) could or should be is to be guided by patterns found in the target process behavior data with a secondary consideration for what the PCA tool returned and what was learned in the domaining study. Figure E2 shows areas of influence on data variability on a plot of PC1 versus PC2. The closer to the edge of the plot (number 1, positive or negative), the higher the influence. The closer to the center (or value 0), the lesser the influence on the variability of the data set.



Primary Influence: K, Al, Mg, Cr, Ge, Cd, Zn, Cu, Se, Hg, Mo, U, C, Ni,

Secondary Influence: Ba, Ga, Rb, Sn, In, Co, Ag, Bi, Fe, S, Pb

No Influence: Cs, Na, Mn, Te, Th, As, Ca, Au, P, Ce, Sr, B

Figure E2. Principle Component Analysis areas of influence

A Principal Component Analysis was done on the Aitolampi drill hole chemical assay data base. The correlation matrix of this data is shown in Appendix D. This analysis was done using the IoGAS analysis software. The results were shown in Table E1 and Figures E3 to E9.

Table E1. Aitolahti PCA analysis Eigenvalues Proportion

	Eigenvalues	Percent	Cumulative %
PC1	14.69	34.97	34.97
PC2	6.595	15.7	50.68
PC3	4.869	11.59	62.27
PC4	2.033	4.841	67.11
PC5	1.615	3.846	70.96
PC6	1.557	3.706	74.66
PC7	1.301	3.099	77.76
PC8	1.17	2.787	80.55
PC9	1.085	2.583	83.13
PC10	0.8396	1.999	85.13
PC11	0.8199	1.952	87.08
PC12	0.7864	1.872	88.95
PC13	0.6454	1.537	90.49
PC14	0.5492	1.308	91.8
PC15	0.4649	1.107	92.9
PC16	0.3993	0.9506	93.86
PC17	0.3904	0.9295	94.78
PC18	0.3317	0.7898	95.57
PC19	0.2569	0.6116	96.19
PC20	0.2112	0.5027	96.69
PC21	0.201	0.4785	97.17
PC22	0.1683	0.4008	97.57
PC23	0.156	0.3715	97.94
PC24	0.1375	0.3275	98.27
PC25	0.116	0.2763	98.54
PC26	0.104	0.2477	98.79
PC27	0.08525	0.203	98.99
PC28	0.07223	0.172	99.17
PC29	0.06097	0.1452	99.31
PC30	0.05122	0.122	99.43
PC31	0.04592	0.1093	99.54
PC32	0.04322	0.1029	99.65
PC33	0.03654	0.087	99.73
PC34	0.03471	0.08265	99.82
PC35	0.01995	0.0475	99.86
PC36	0.01736	0.04134	99.9
PC37	0.01563	0.03721	99.94
PC38	0.008916	0.02123	99.96
PC39	0.005762	0.01372	99.98
PC40	0.003989	0.009497	99.99
PC41	0.003597	0.008565	99.99
PC42	0.002428	0.00578	100

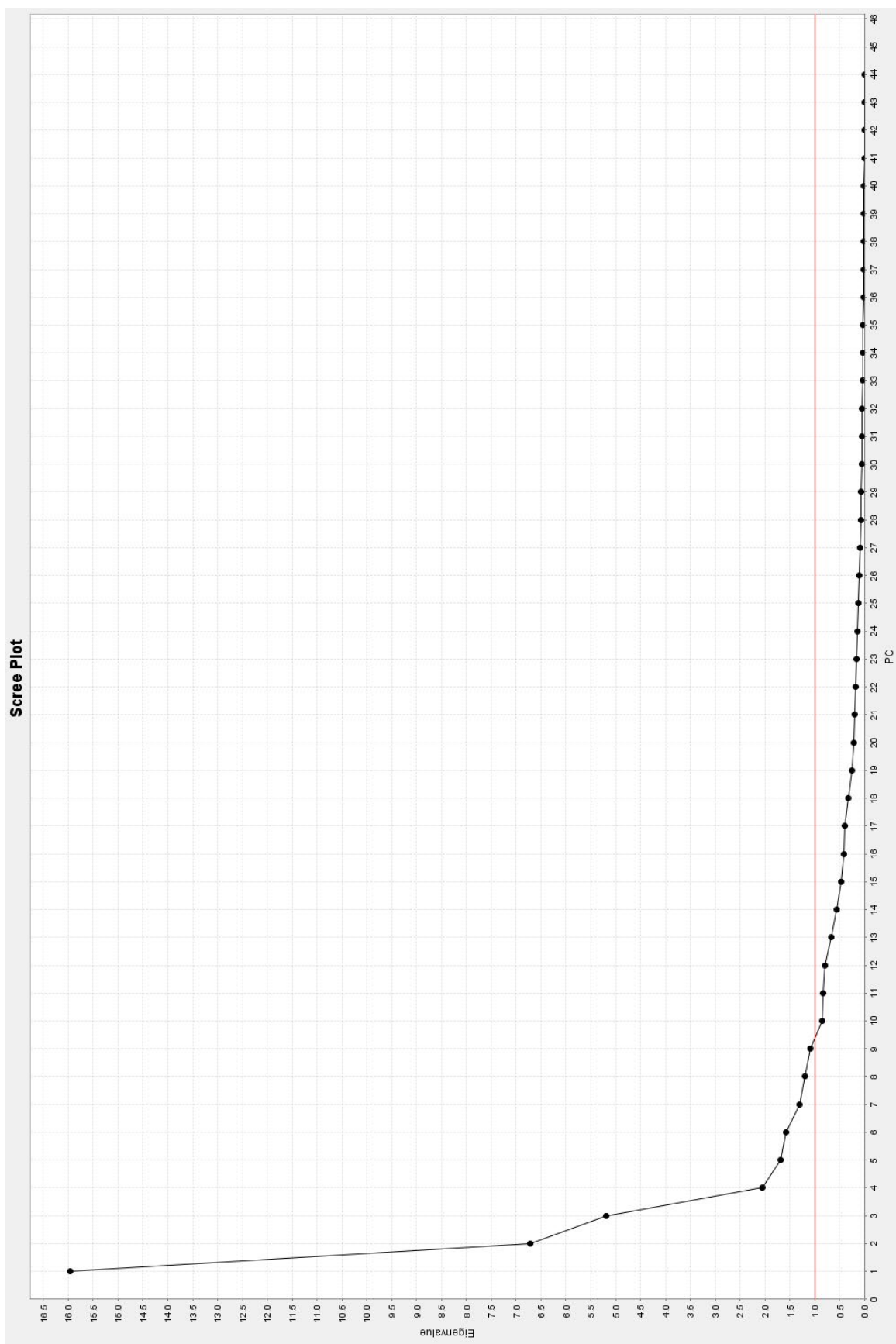


Figure E3. Eigen value distribution in Aitolampi chemical assay data set

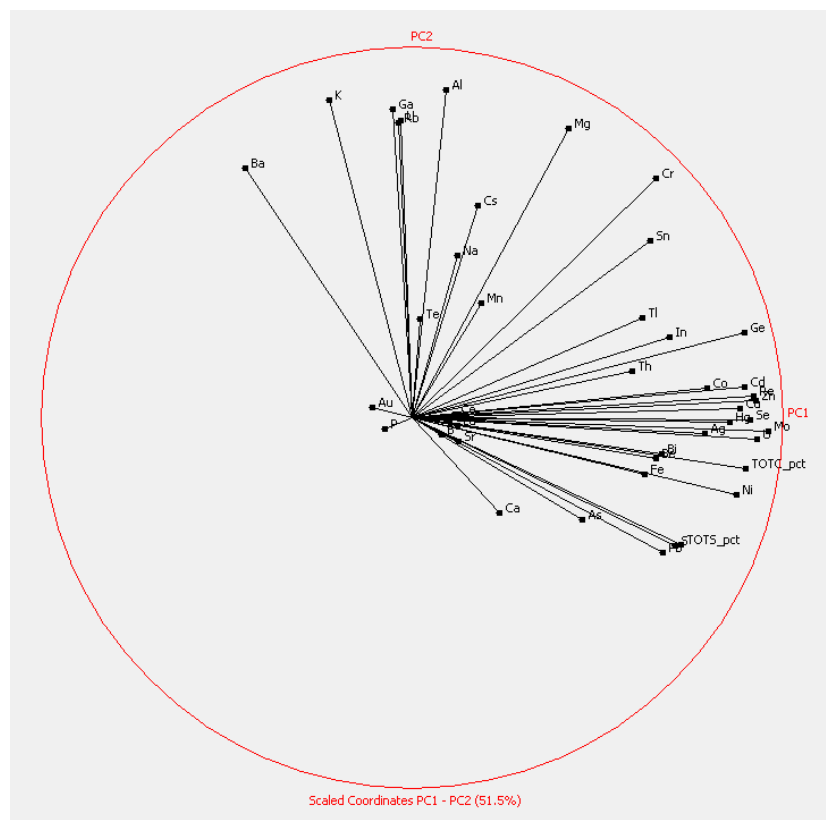


Figure E4. PC1 vs. PC2

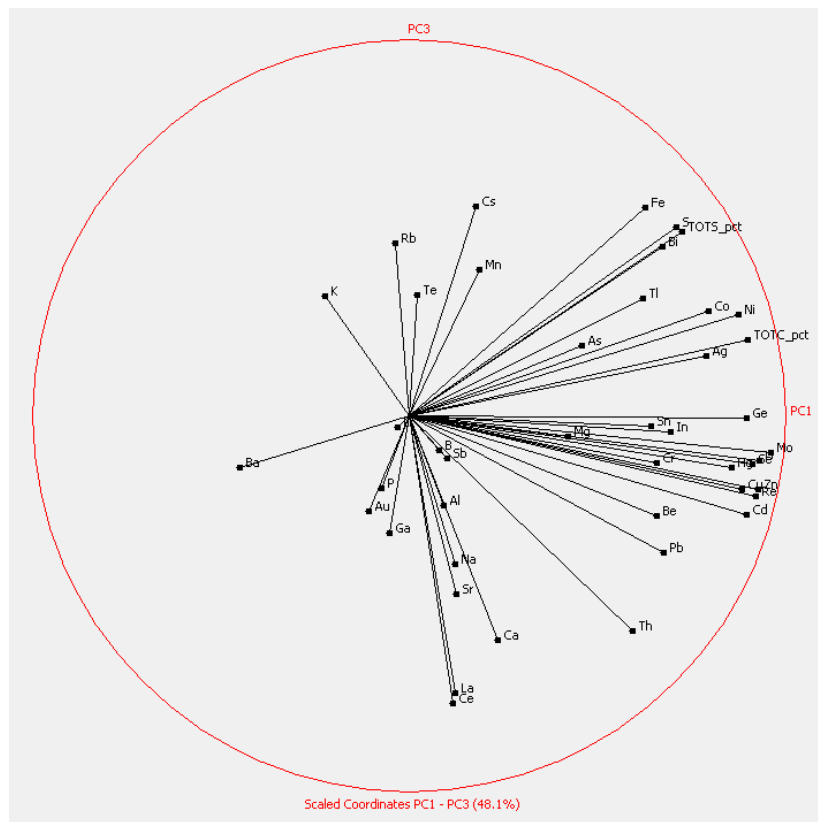


Figure E5. PC1 vs. PC3

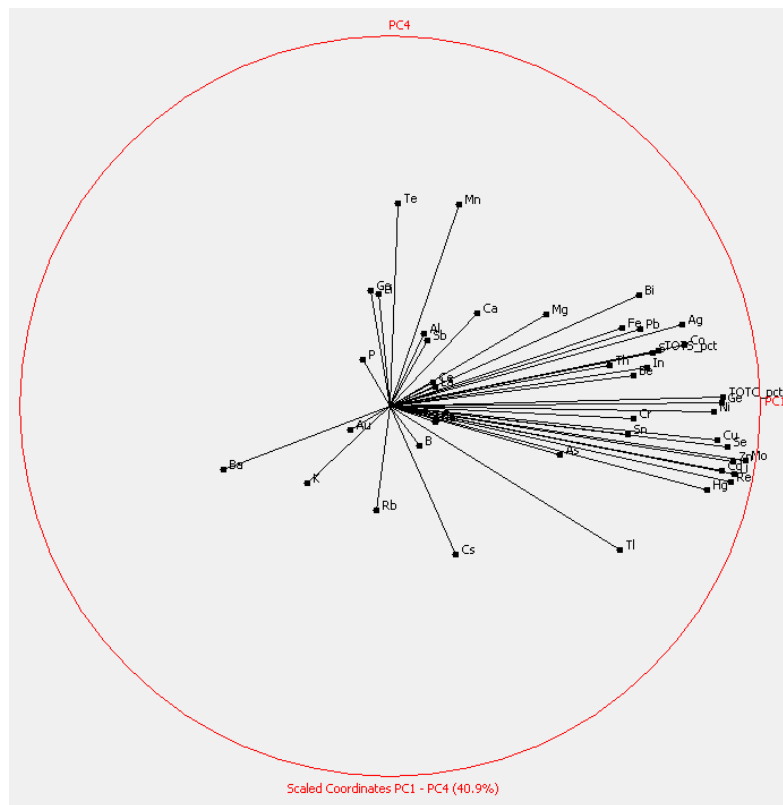


Figure E6. PC1 vs. PC4

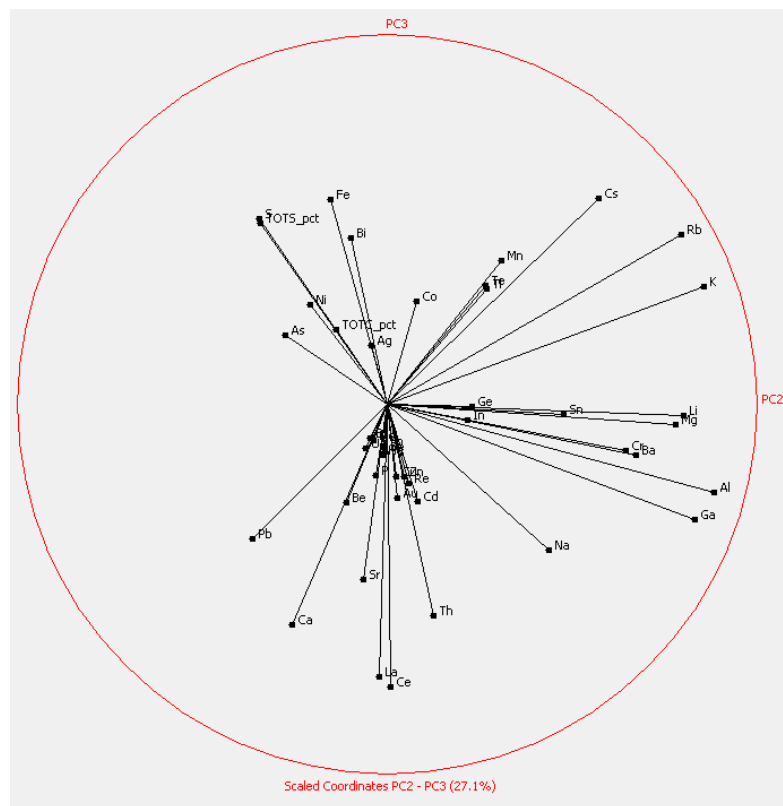


Figure E7. PC2 vs. PC3

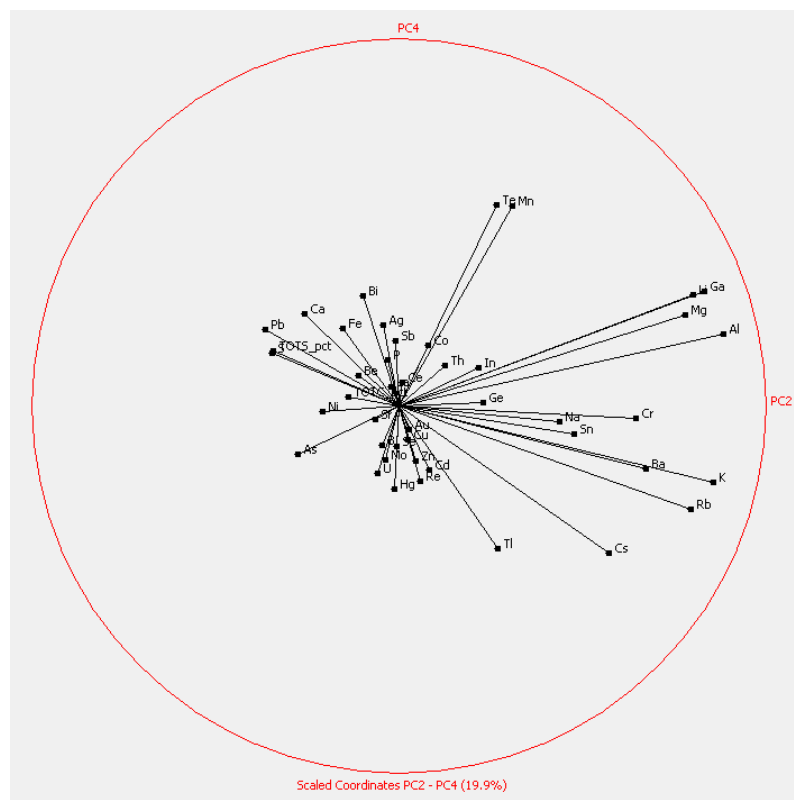


Figure E8. PC2 vs. PC4

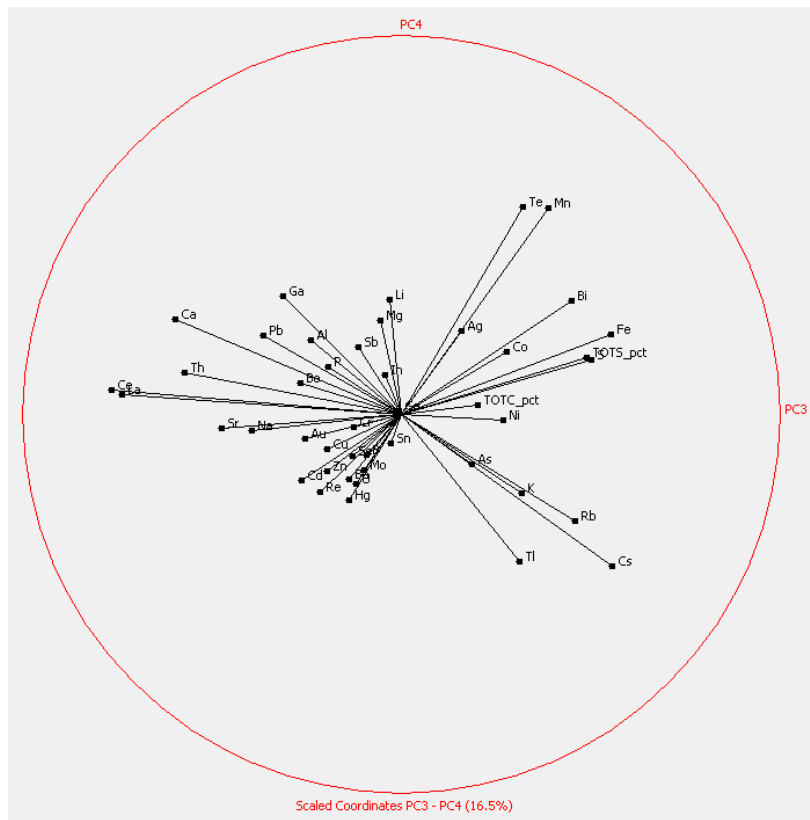


Figure E9. PC3 vs. PC4

25 APPENDIX F - CLASS SELECTION OF ORE TYPES IN AITOLAMPI CHEMICAL ASSAY DATA

Using the PCA plots in Figures F1 to F11, in Appendix E, and the correlation matrix in Appendix D, the elements that had greater influence and control over variability in the data set were extracted from the full data set to be examined more closely. Table F1 shows a second correlation matrix to examine how these influential elements might relate to each other.

Table F1. Correlation matrix of the elements that control variability in the Aitolampi chemical assay set

Correlation	TOTC_pct	TOTS_pct	Co_ppm	Cu_ppm	Fe_pct	Mg_pct	Mo_ppm	Zn_ppm
TOTC_pct	1	0.84	0.78	0.68	0.77	0.28	0.87	0.75
TOTS_pct	0.84	1	0.78	0.48	0.94	0.045	0.63	0.49
Co_ppm	0.78	0.78	1	0.66	0.81	0.41	0.69	0.61
Cu_ppm	0.68	0.48	0.66	1	0.36	0.37	0.85	0.87
Fe_pct	0.77	0.94	0.81	0.36	1	0.16	0.52	0.37
Mg_pct	0.28	0.045	0.41	0.37	0.16	1	0.33	0.38
Mo_ppm	0.87	0.63	0.69	0.85	0.52	0.33	1	0.95
Zn_ppm	0.75	0.49	0.61	0.87	0.37	0.38	0.95	1
Ba_ppm	-0.5	-0.6	-0.25	-0.33	-0.37	0.25	-0.42	-0.35
Bi_ppm	0.7	0.73	0.62	0.5	0.65	0.2	0.59	0.51
Ni_ppm	0.92	0.91	0.83	0.68	0.87	0.19	0.82	0.71
U_ppm	0.85	0.61	0.65	0.82	0.5	0.31	0.96	0.9
Se_ppm	0.73	0.53	0.67	0.95	0.4	0.34	0.89	0.9
Ge_ppm	0.75	0.57	0.77	0.83	0.55	0.56	0.83	0.81
Cd_ppm	0.69	0.41	0.55	0.88	0.28	0.41	0.92	0.99

Correlation	Ba_ppm	Bi_ppm	Ni_ppm	U_ppm	Se_ppm	Ge_ppm	Cd_ppm
TOTC_pct	-0.5	0.7	0.92	0.85	0.73	0.75	0.69
TOTS_pct	-0.6	0.73	0.91	0.61	0.53	0.57	0.41
Co_ppm	-0.25	0.62	0.83	0.65	0.67	0.77	0.55
Cu_ppm	-0.33	0.5	0.68	0.82	0.95	0.83	0.88
Fe_pct	-0.37	0.65	0.87	0.5	0.4	0.55	0.28
Mg_pct	0.25	0.2	0.19	0.31	0.34	0.56	0.41
Mo_ppm	-0.42	0.59	0.82	0.96	0.89	0.83	0.92
Zn_ppm	-0.35	0.51	0.71	0.9	0.9	0.81	0.99
Ba_ppm	1	-0.51	-0.48	-0.41	-0.38	-0.23	-0.31
Bi_ppm	-0.51	1	0.65	0.53	0.56	0.56	0.46
Ni_ppm	-0.48	0.65	1	0.81	0.72	0.74	0.64
U_ppm	-0.41	0.53	0.81	1	0.84	0.81	0.87
Se_ppm	-0.38	0.56	0.72	0.84	1	0.86	0.9
Ge_ppm	-0.23	0.56	0.74	0.81	0.86	1	0.8
Cd_ppm	-0.31	0.46	0.64	0.87	0.9	0.8	1

This smaller set of elements was imported in the IoGAS software, where each element was examined against all other elements in a variety of ways. The purpose was to determine patterns and relationships between elements. This included, cross correlation, probability plots, box & whisker plots and multivariate dimensional analysis. This was also done for the selected PCA outcomes.

Using this information, the data set was split into 5 groupings or classes. Each one was assigned a color. In the IoGAS software, each class was examined as a separate data set attribute, then compared against all other classes. This was done to determine if these classes were genuinely different.

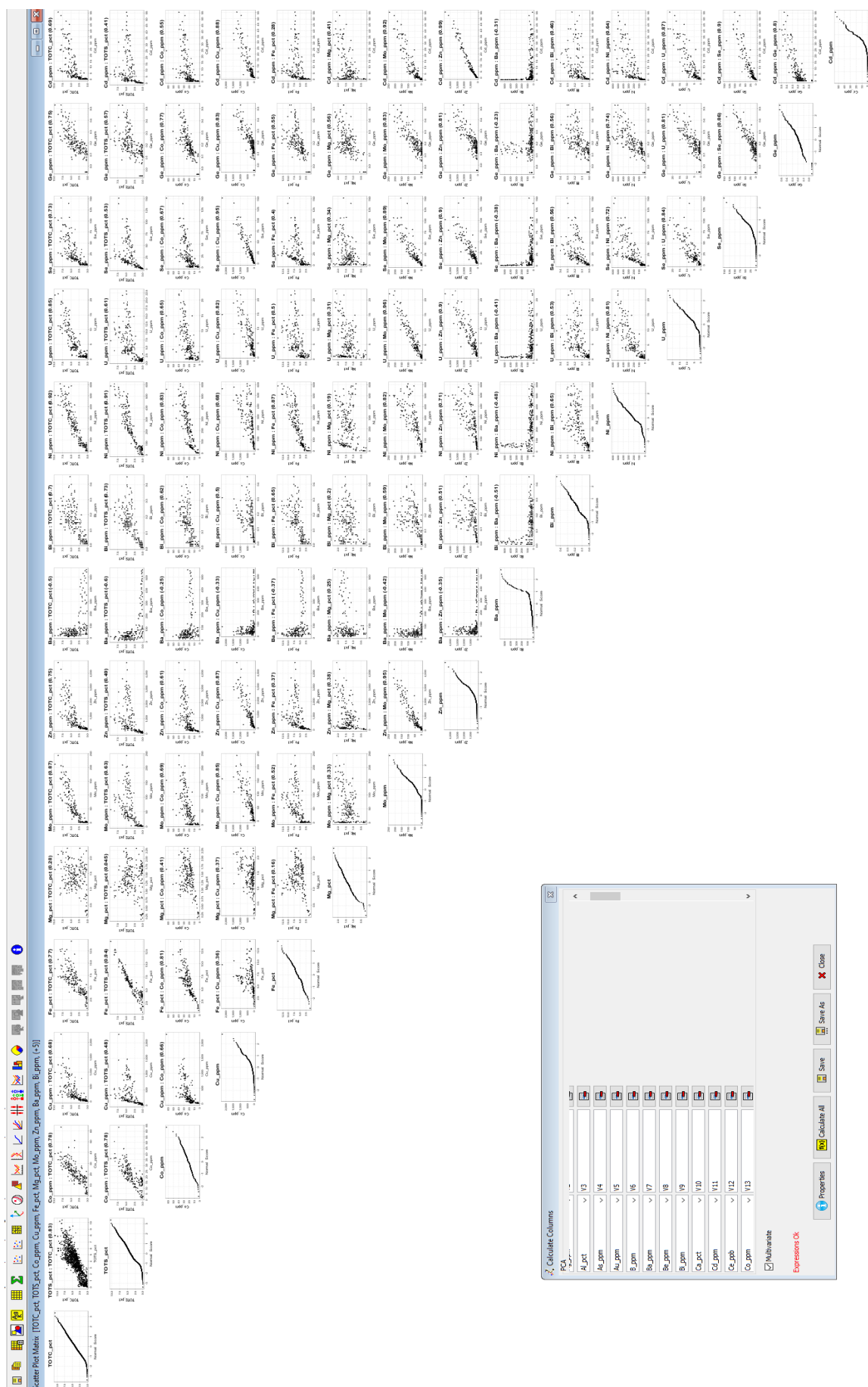


Figure F1. Correlation matrix of the elements that control variability in the Aitolampi chemical assay set

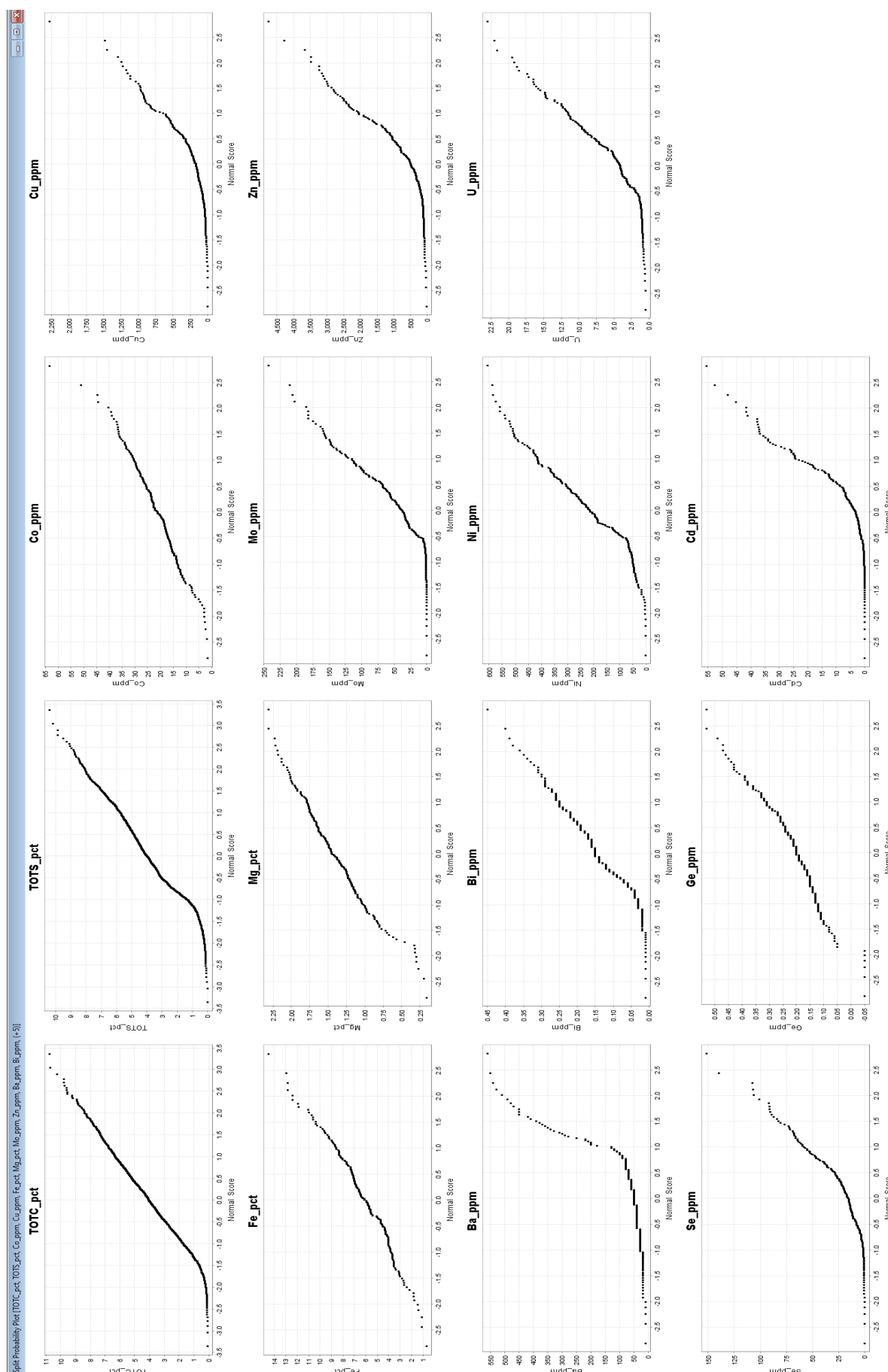


Figure F2. Probability plots of the elements that control variability in the Aitolampi chemical assay set



Figure F3. Correlations between elements by Class - 1

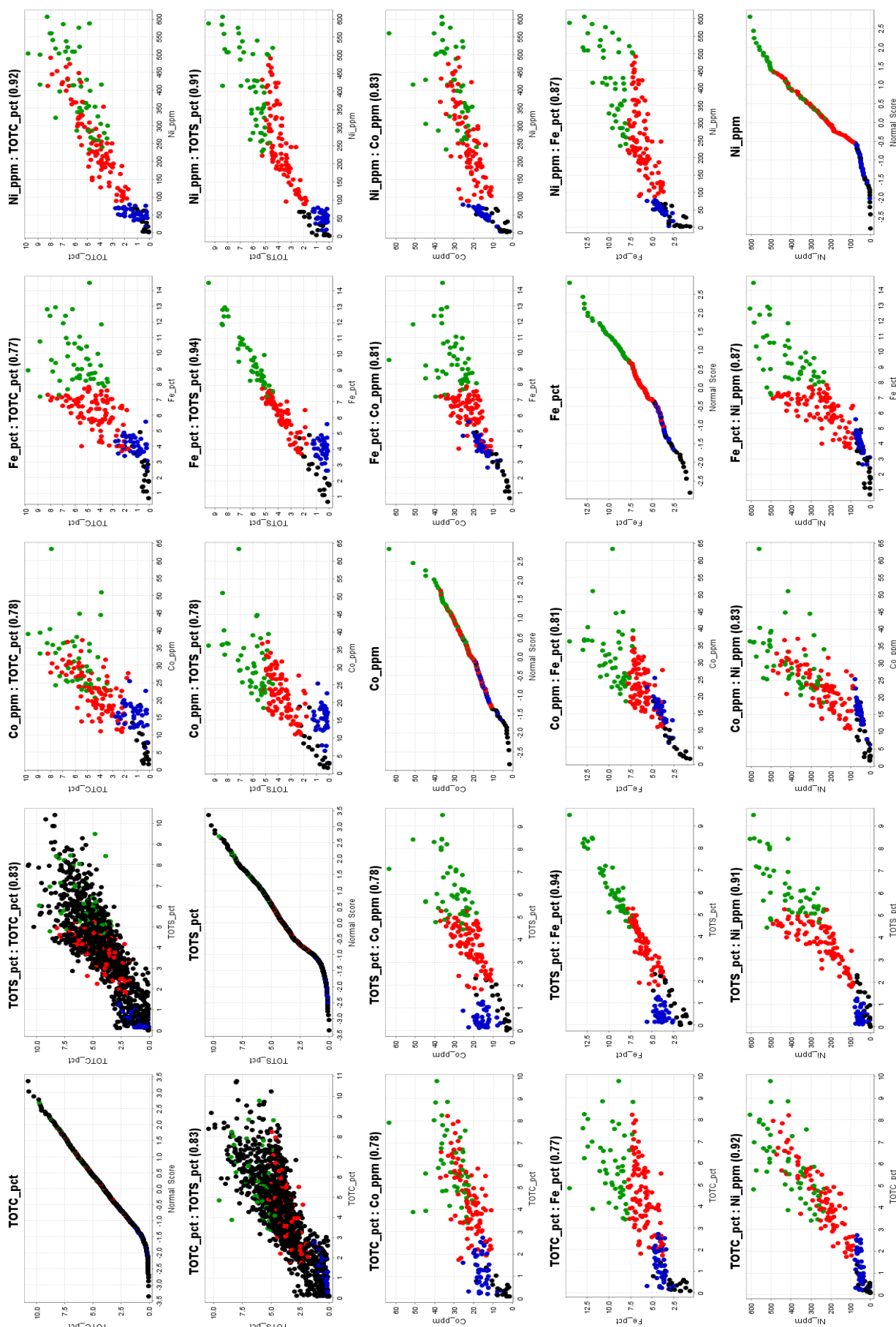


Figure F4. Correlations between elements by Class - 2

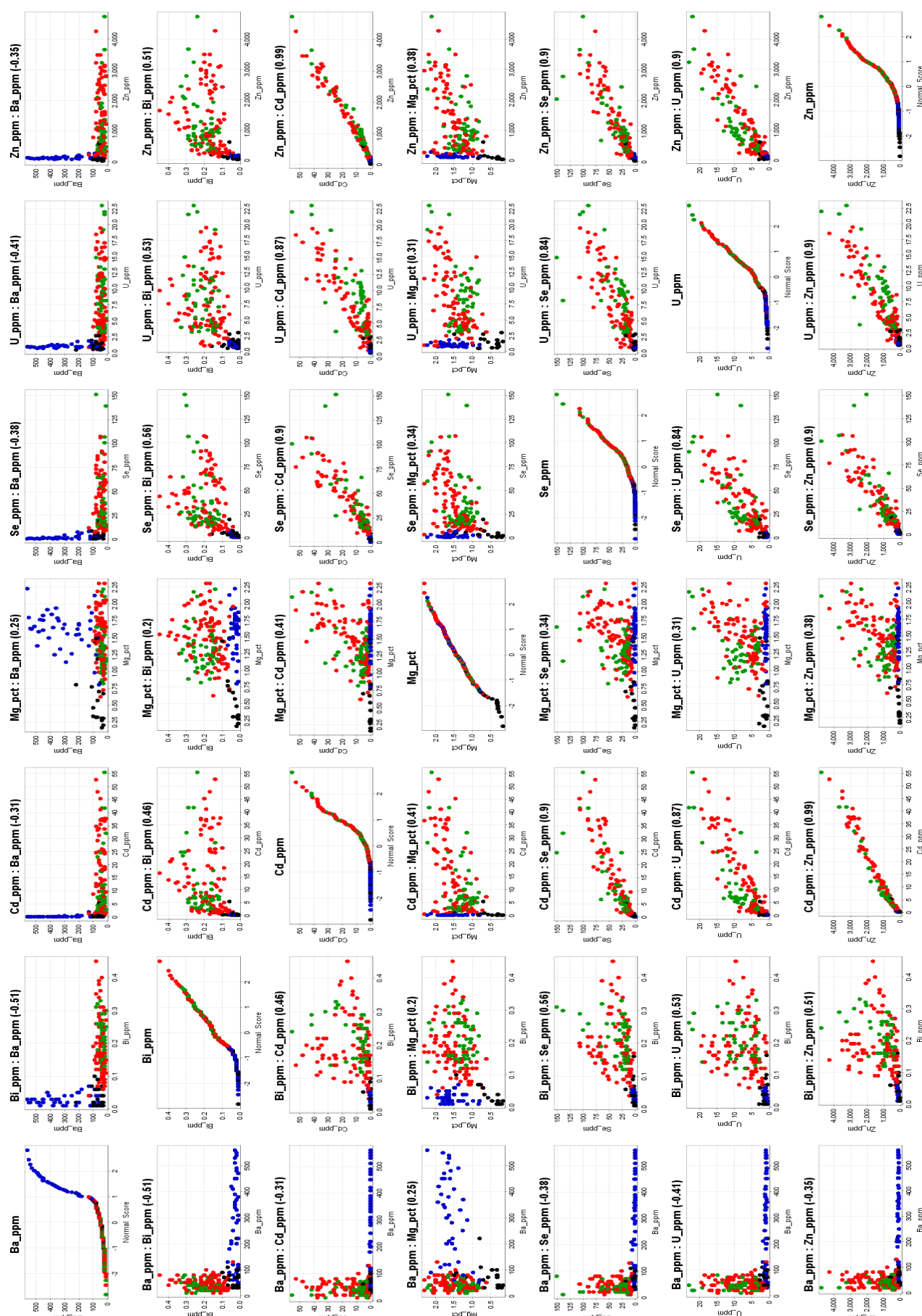


Figure F5. Correlations between elements by Class - 3

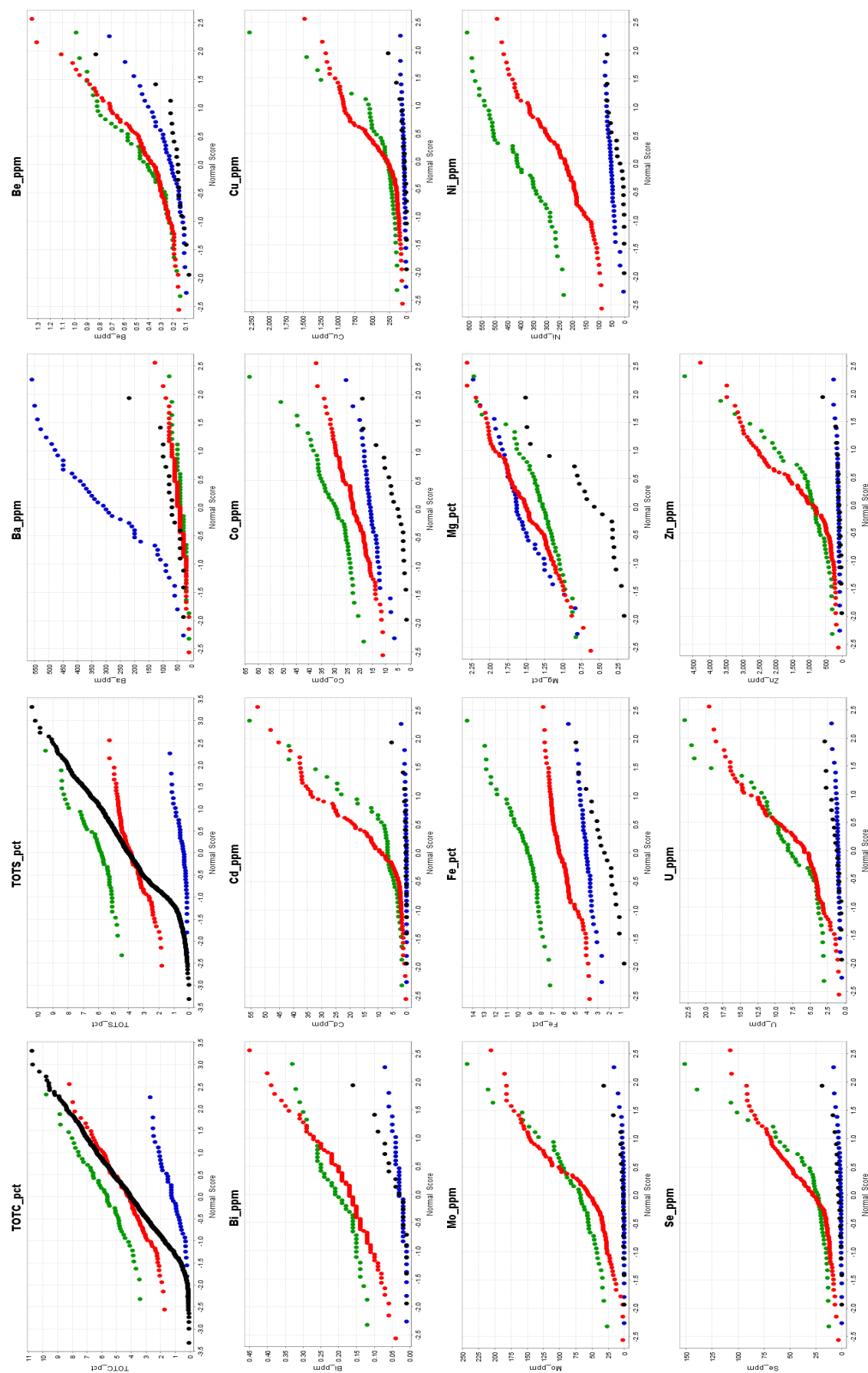


Figure F6. Probability plots of elements by Class

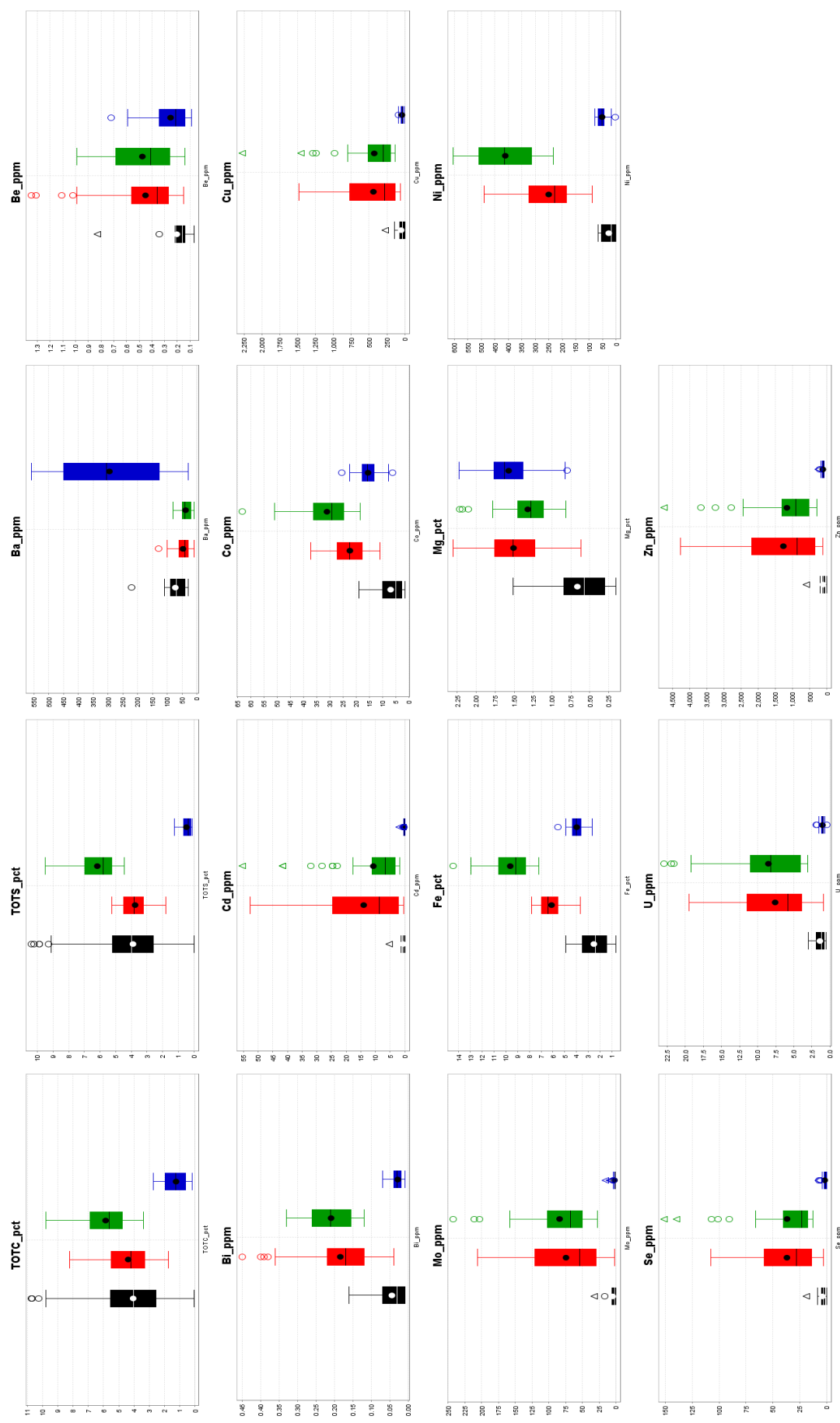


Figure F7. Box & Whisker Plots of elements by Class

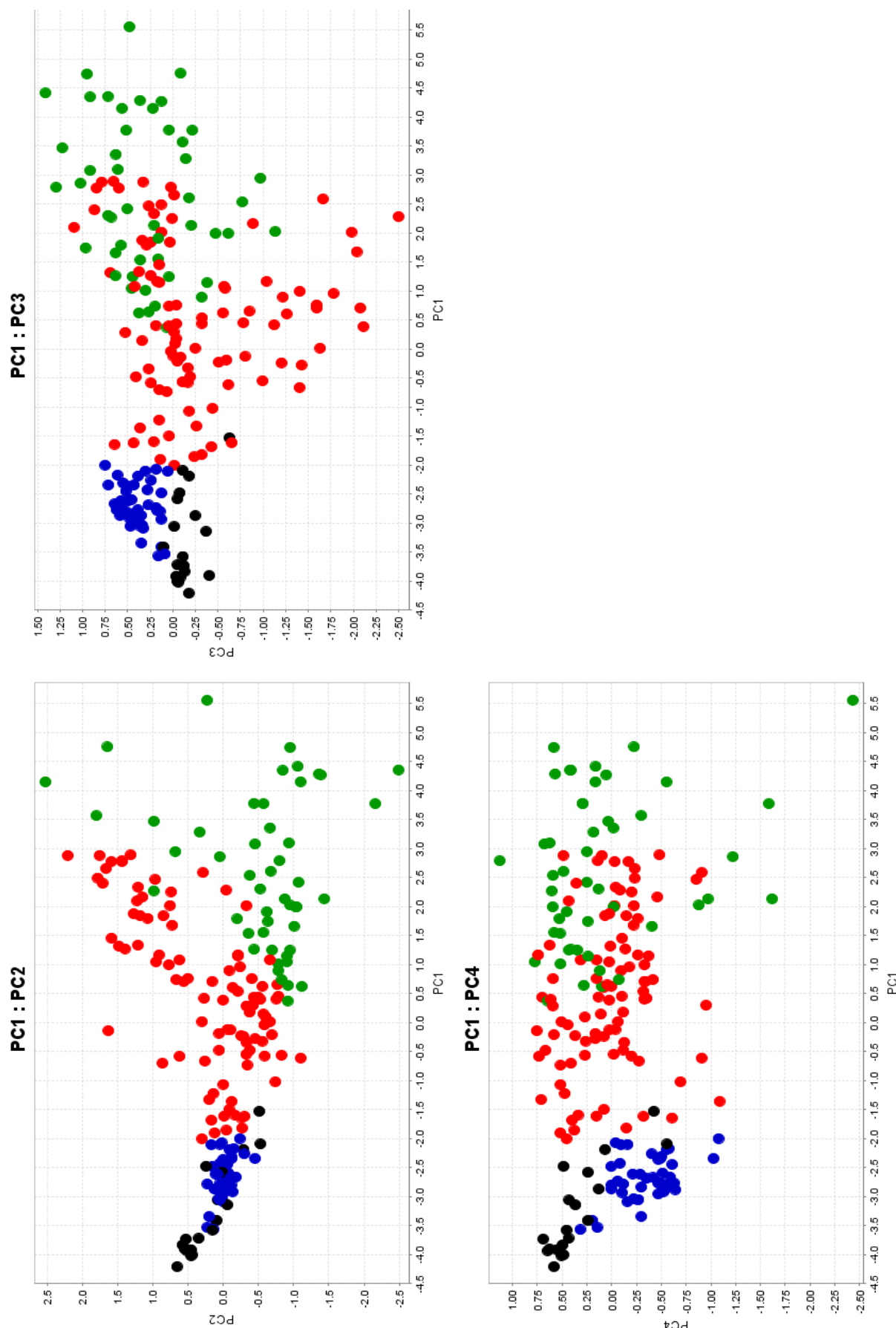


Figure F8. PCA components cross correlation

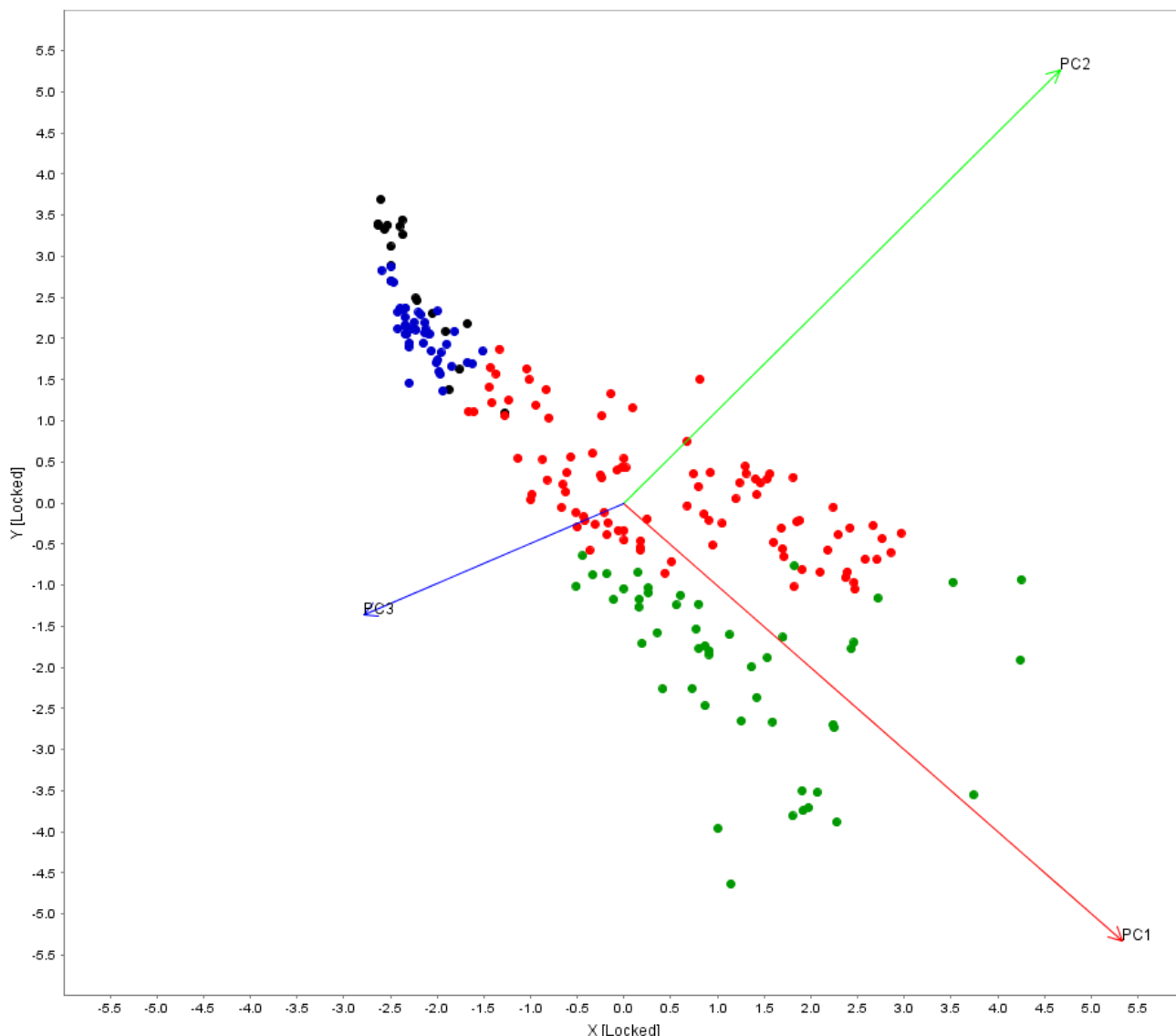


Figure F9. PC1 vs. PC2 vs. PC3 three dimensional plot - 1

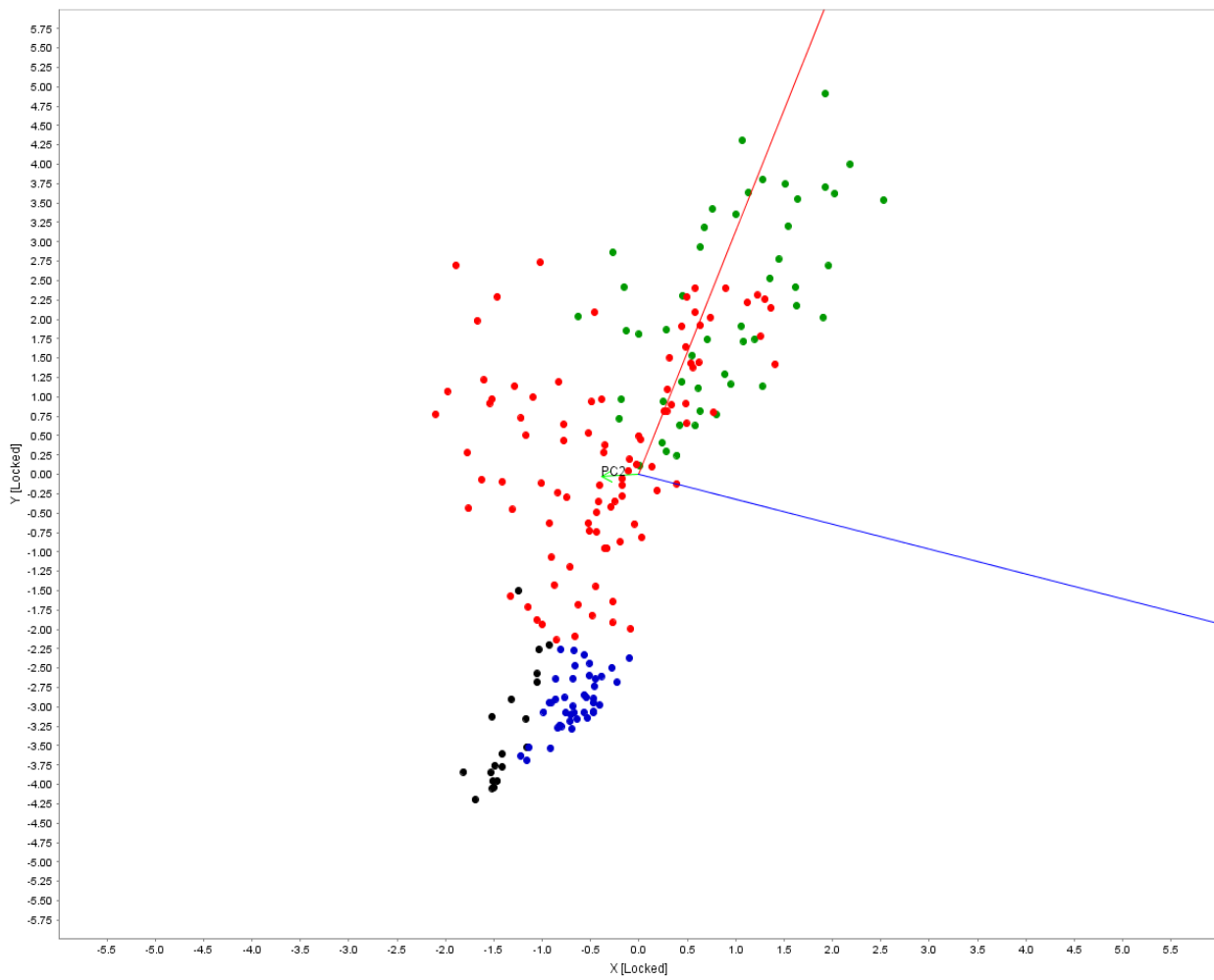


Figure F10. PC1 vs. PC2 vs. PC3 three dimensional plot - 2

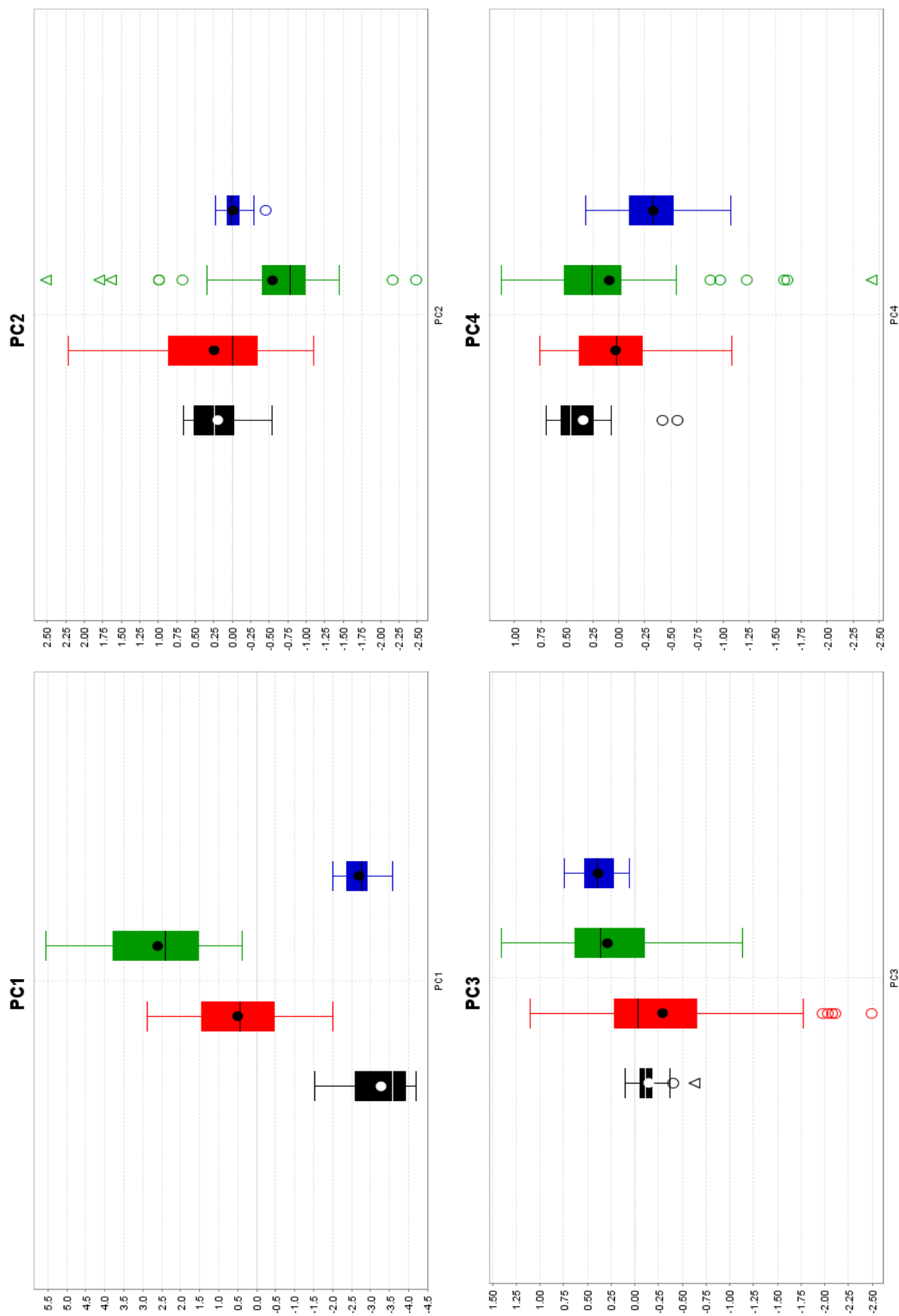
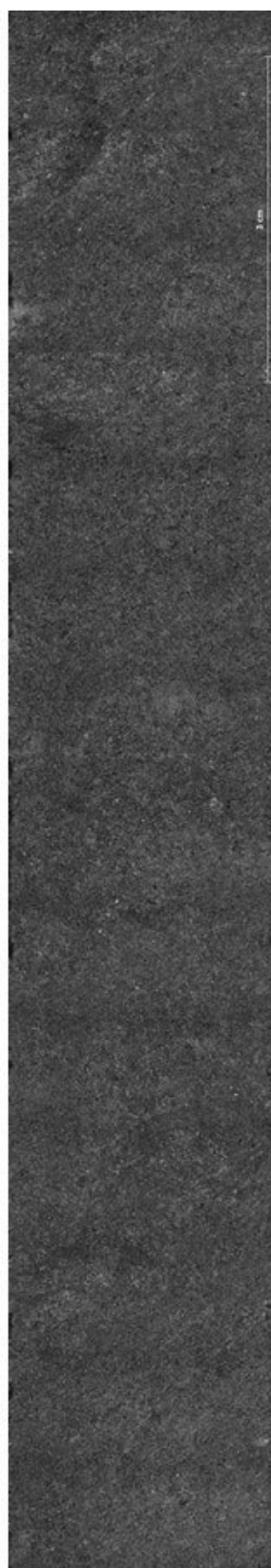


Figure F11. PC1, PC2, PC3 and PC4 according to Class

26 APPENDIX G – SCANNING MICRO-XRF MAPPING

26.1 Sample PA1 Scanning Micro-XRF



Mapping parameters

Width:	5143 pixel
	144 mm
Height:	879 pixel
	24.6 mm
Pixel Size:	28 µm
Total number of pixel:	4520697 pixel

Acquisition parameters

Frame count:	0
Pixel time:	10 ms/pixel
Measure time:	10:15 h
Overall time:	13:30 h
Stage speed:	2.8 mm/s
Stage position (X,Y,Z):	35.875;70.97;111.488 mm

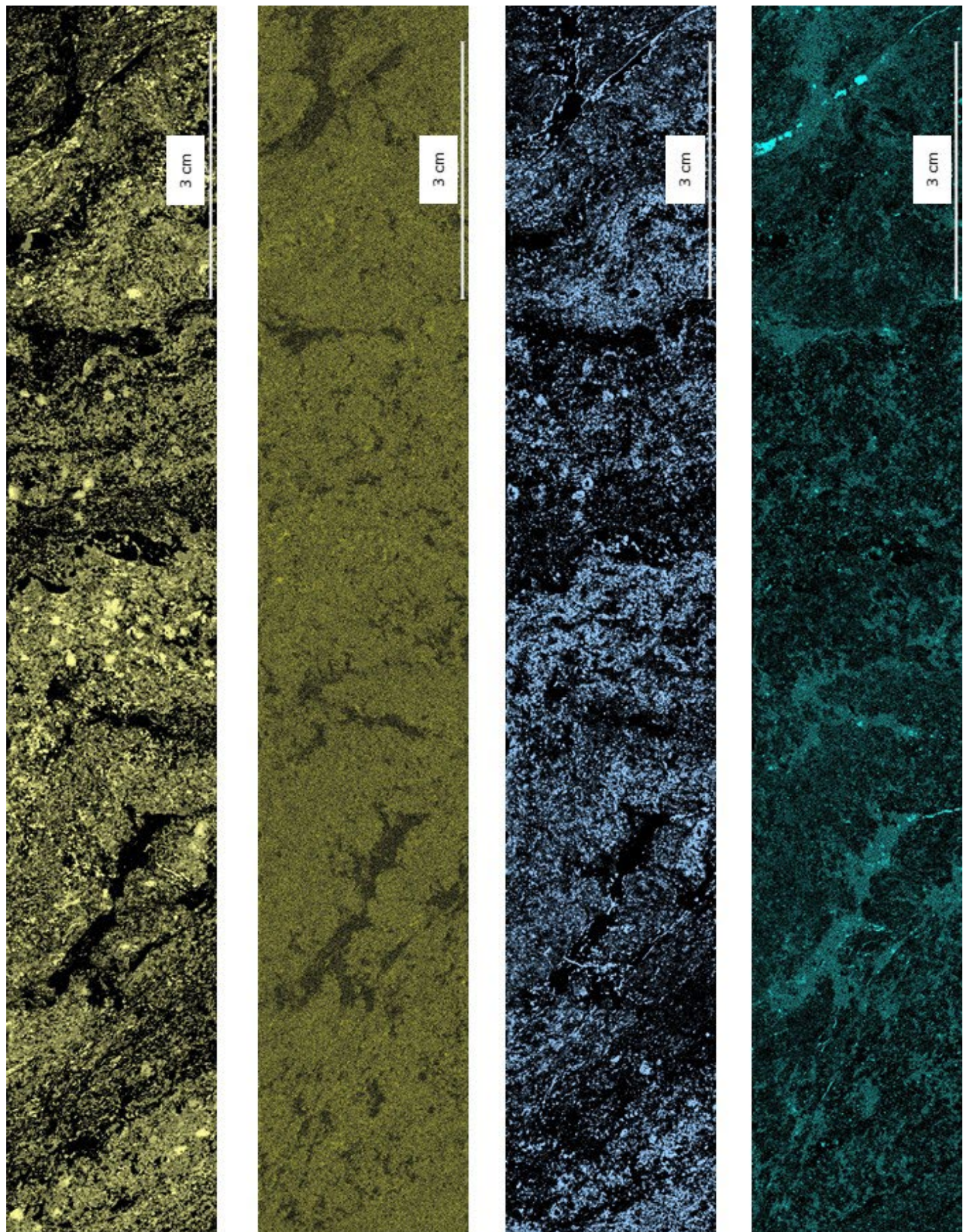
Tube parameter

High voltage:	50 kV
Anode current:	599 µA
Filter:	Empty
Optic:	Lens
Collimator diameter:	0
SpotSize:	20
Chamber at:	Air 1.7 mbar
Flow rate:	--- 1/min
Anode:	Rh

Detector parameters

Selected detectors:	1,2
Max. pulse throughput:	275000 cps

Raw Image – Sample PA1

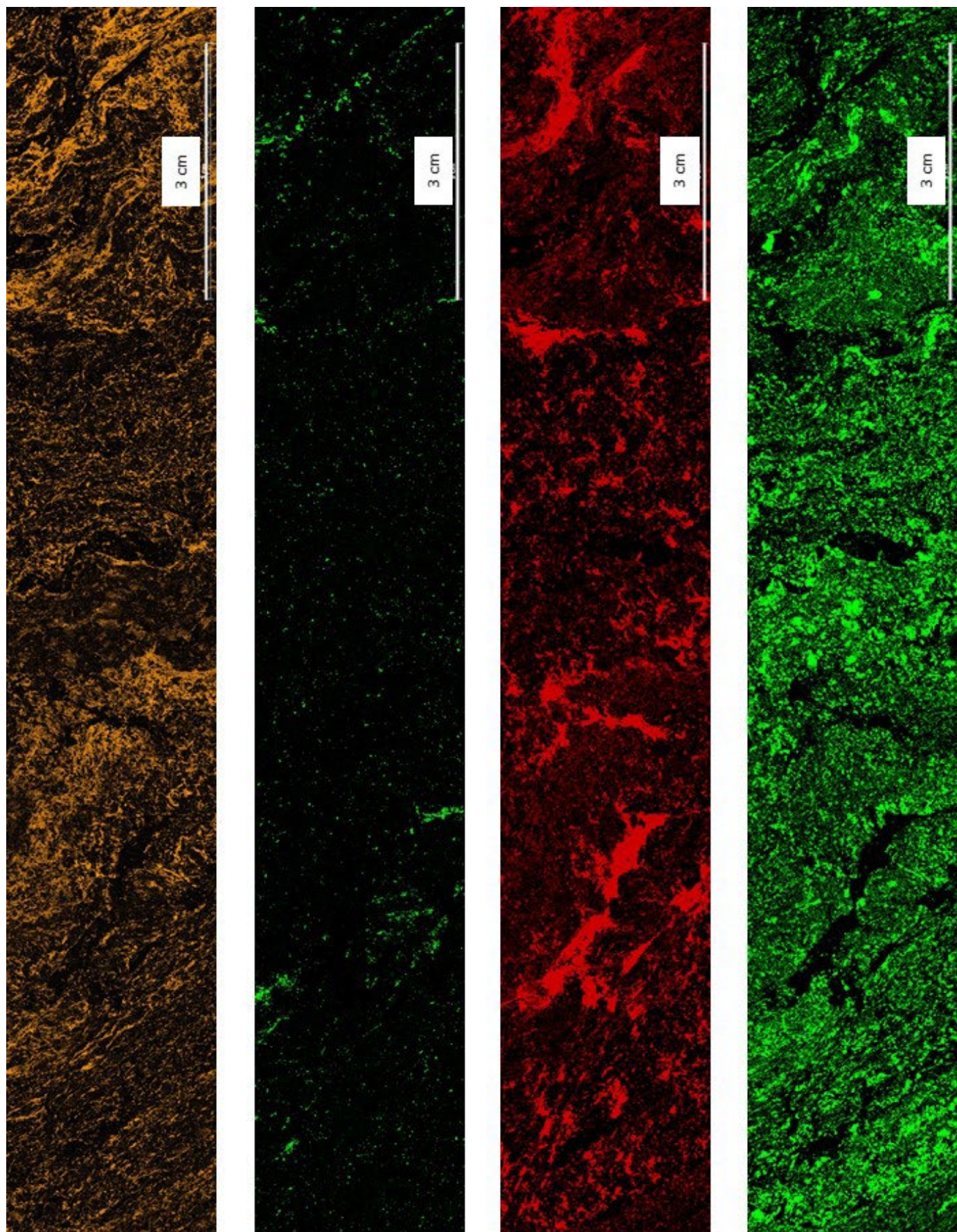


PA1 Element Al

PA1 Element As

PA1 Element Ca

PA1 Element Co

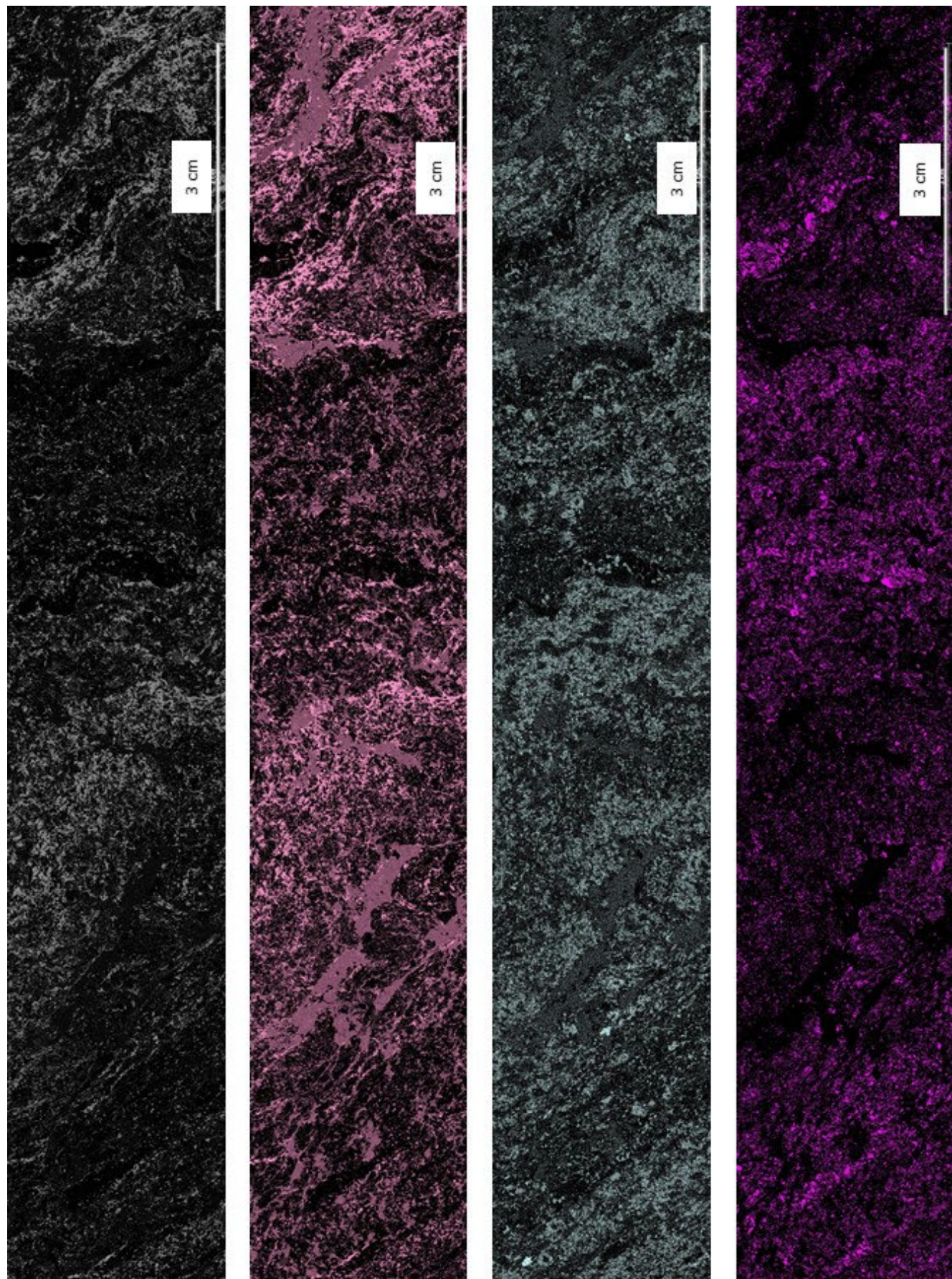


PA1 Element Cr

PA1 Element Cu

PA1 Element Fe

PA1 Element K

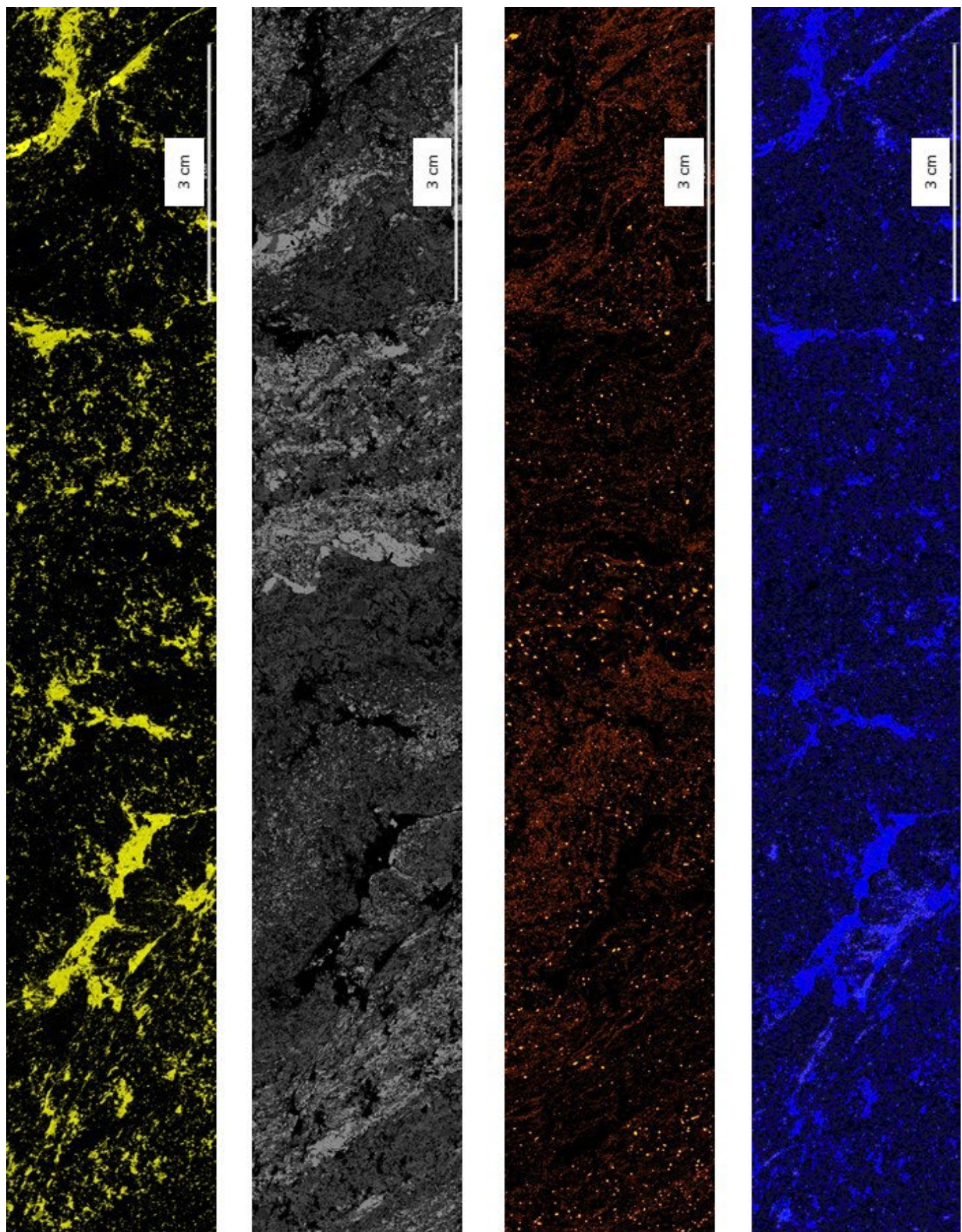


PA1 Element Mg

PA1 Element Mn

PA1 Element Na

PA1 Element Ni

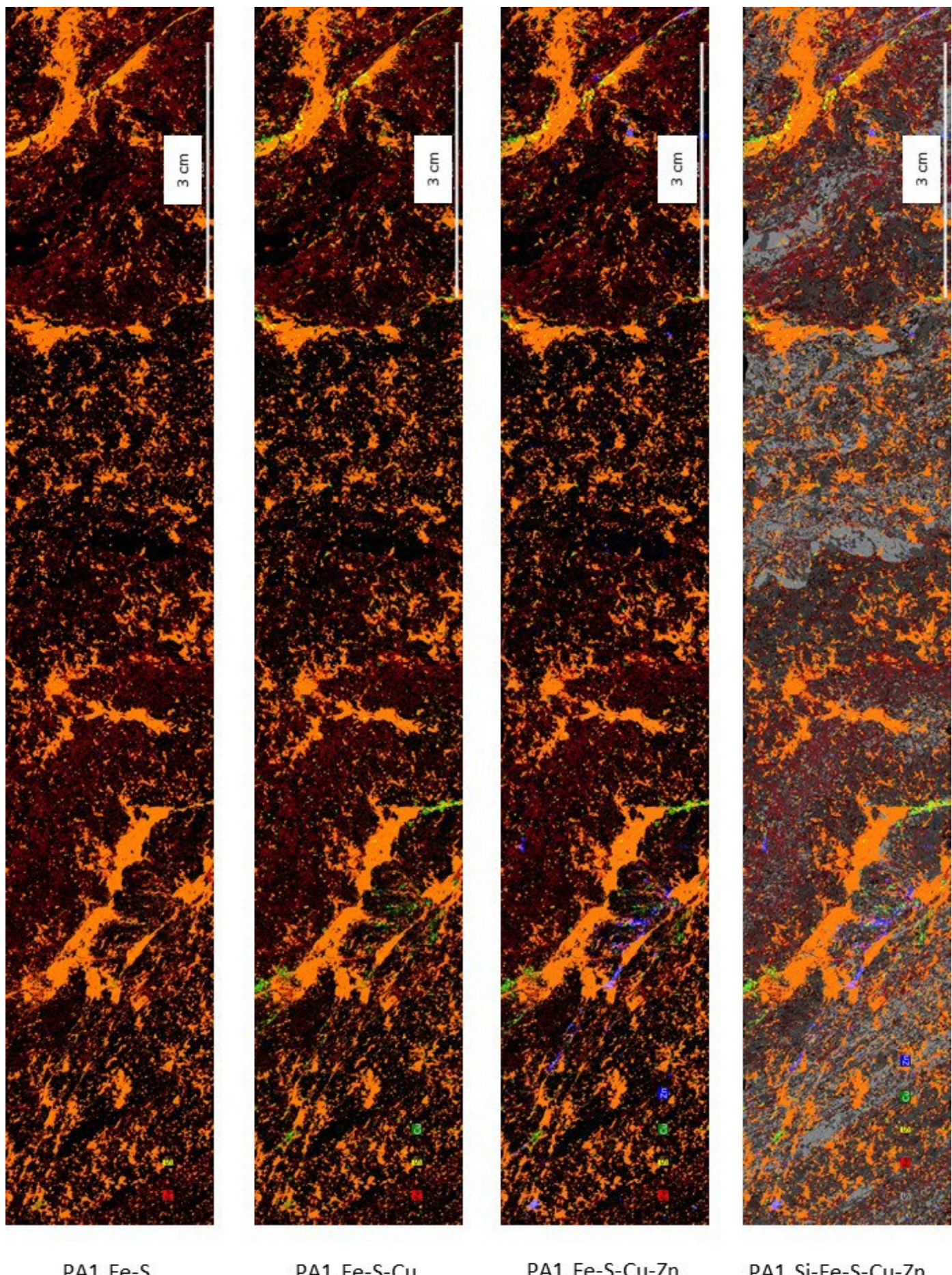


PA1 Element S

PA1 Element Si

PA1 Element Ti

PA1 Element Zn



PA1 Fe-S

PA1 Fe-S-Cu

PA1 Fe-S-Cu-Zn

PA1 Si-Fe-S-Cu-Zn

26.2 Sample QA2 Scanning Micro-XRF



Mapping parameters

Width:	3780 pixel
Height:	155.44 mm
Pixel Size:	1312 pixel
Total number of pixel:	53.795 mm

Acquisition parameters

Frame count:	1
Pixel time:	10 ms/pixel
Measure time:	11:48 h
Overall time:	15:06 h
Stage speed:	4.1 mm/s
Stage position (X,Y,Z):	69.754;72.743;89.916 mm

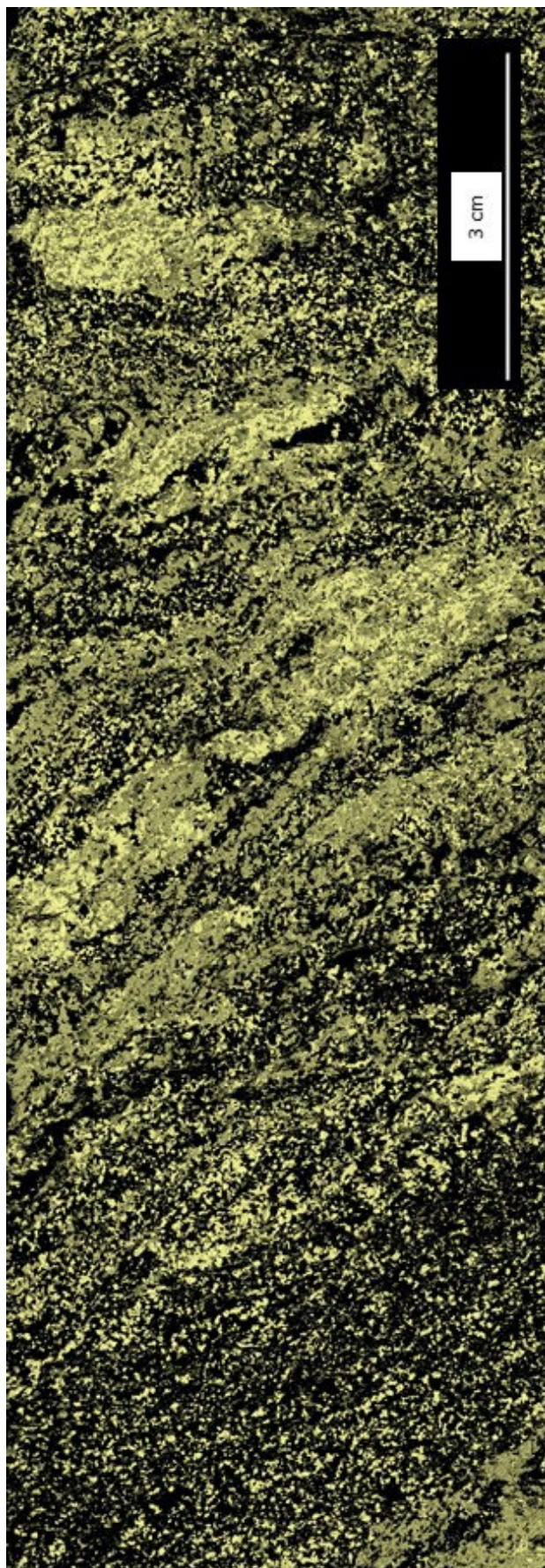
Tube parameter

High voltage:	50 kV
Anode current:	600 µA
Filter:	Empty
Optic:	Lens
Collimator diameter:	0
SpotSize:	20
Chamber at:	Air 2 mbar
Flow rate:	--- l/min
Anode:	Rh

Detector parameters

Selected detectors:	1,2
Max. pulse throughput:	275000 cps

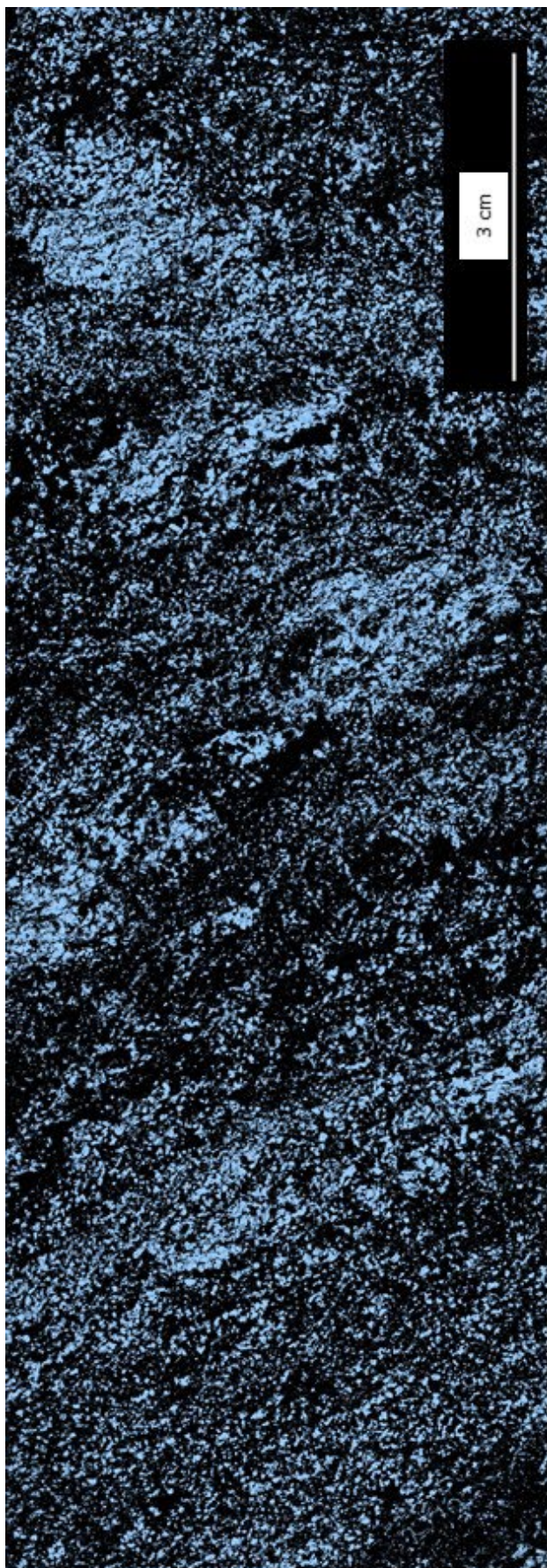
Raw Image - Sample QA2



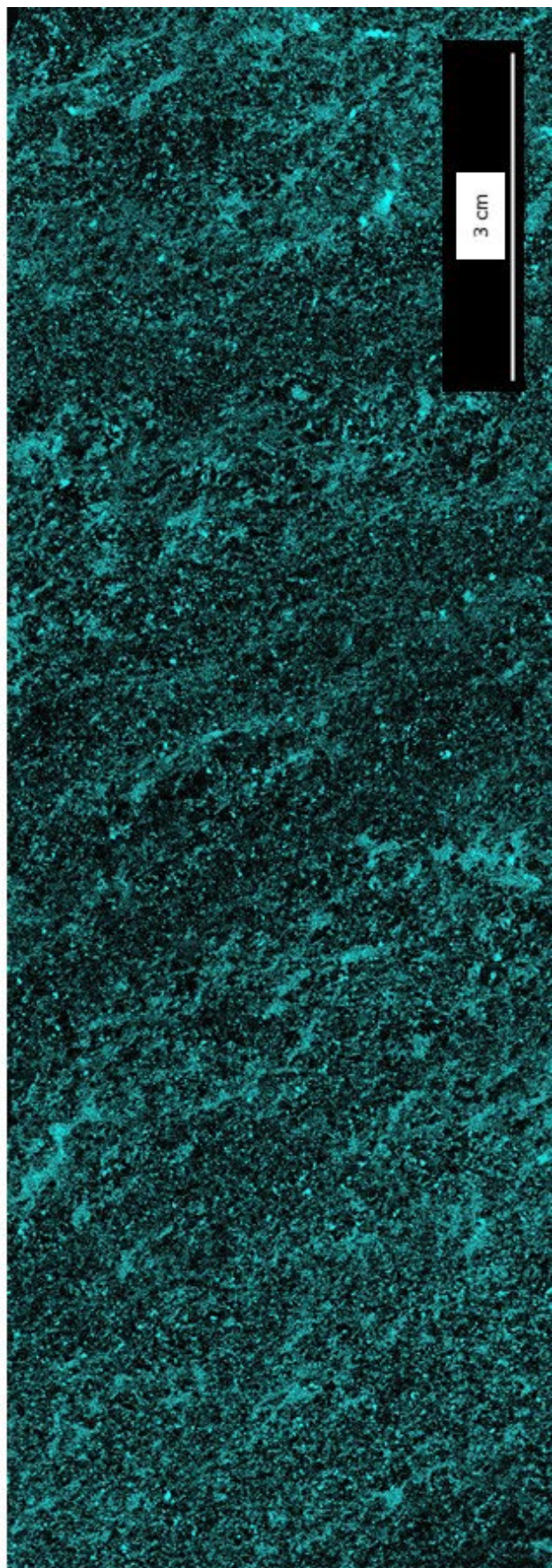
QA2 Element Al



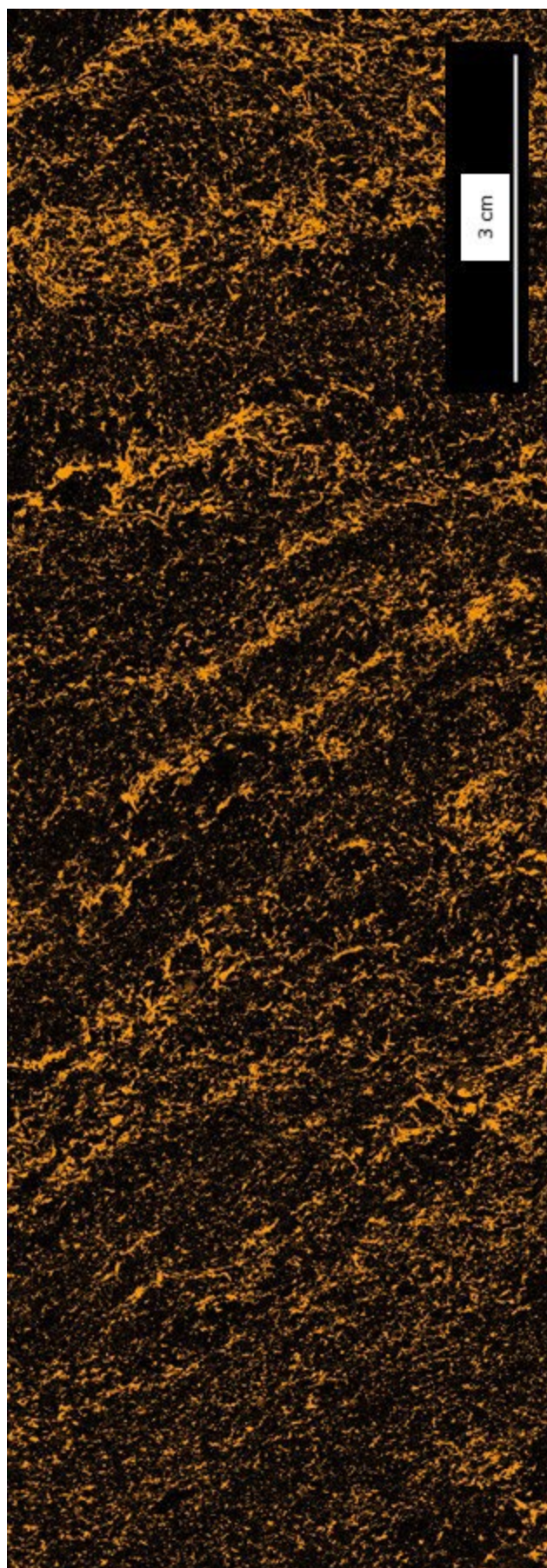
QA2 Element As



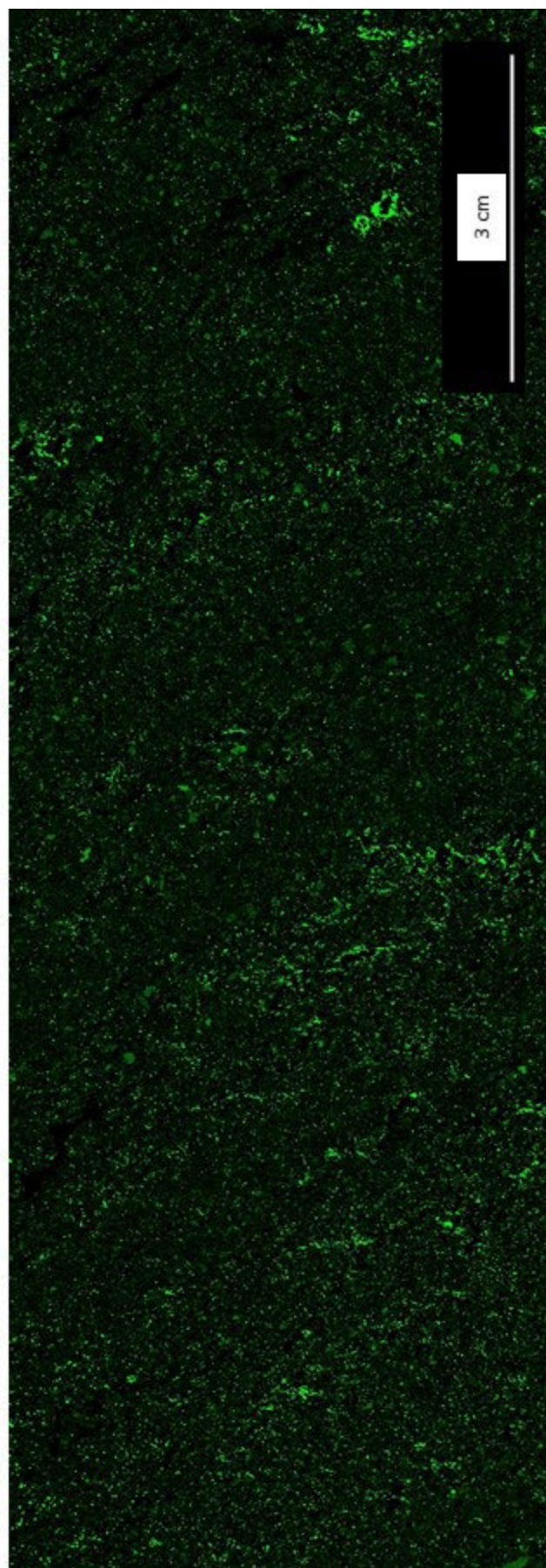
QA2 Element Ca



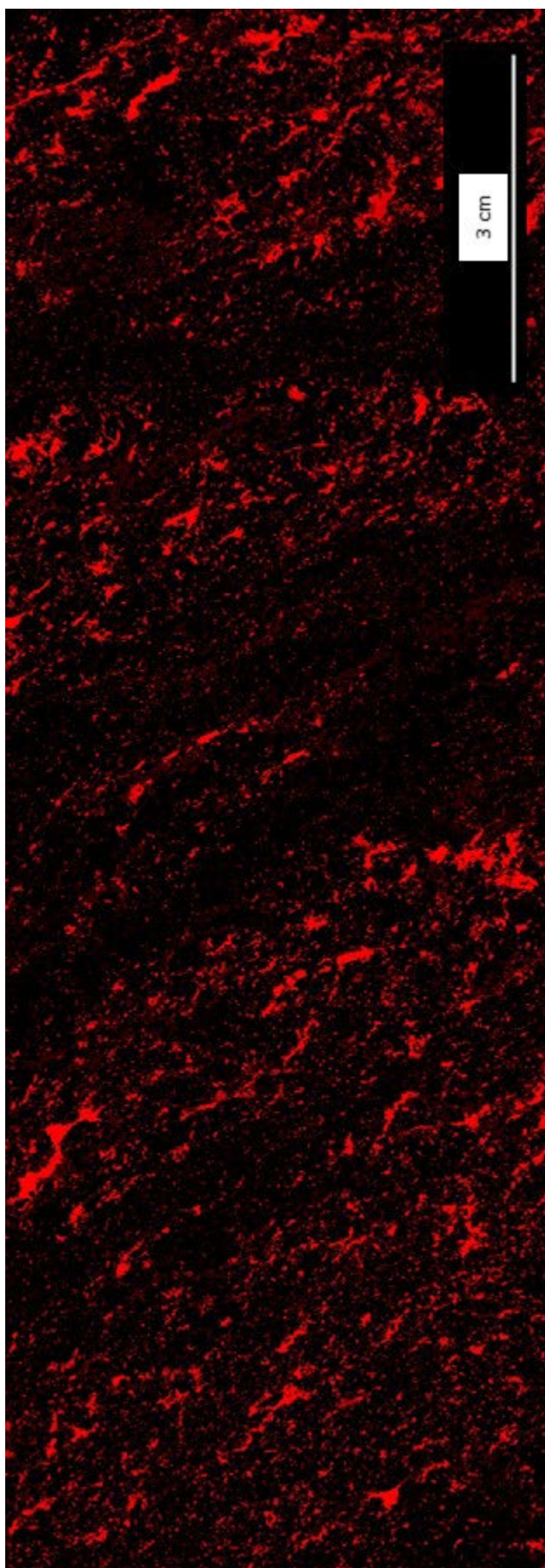
QA2 Element Co



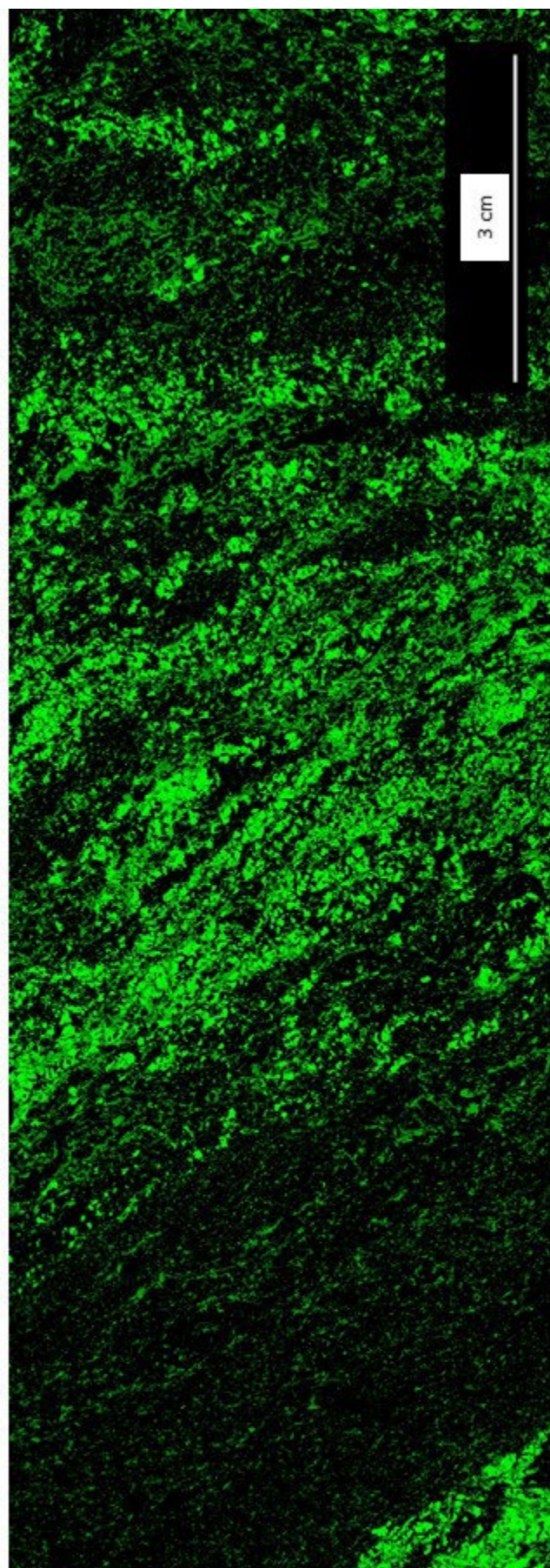
QA2 Element Cr



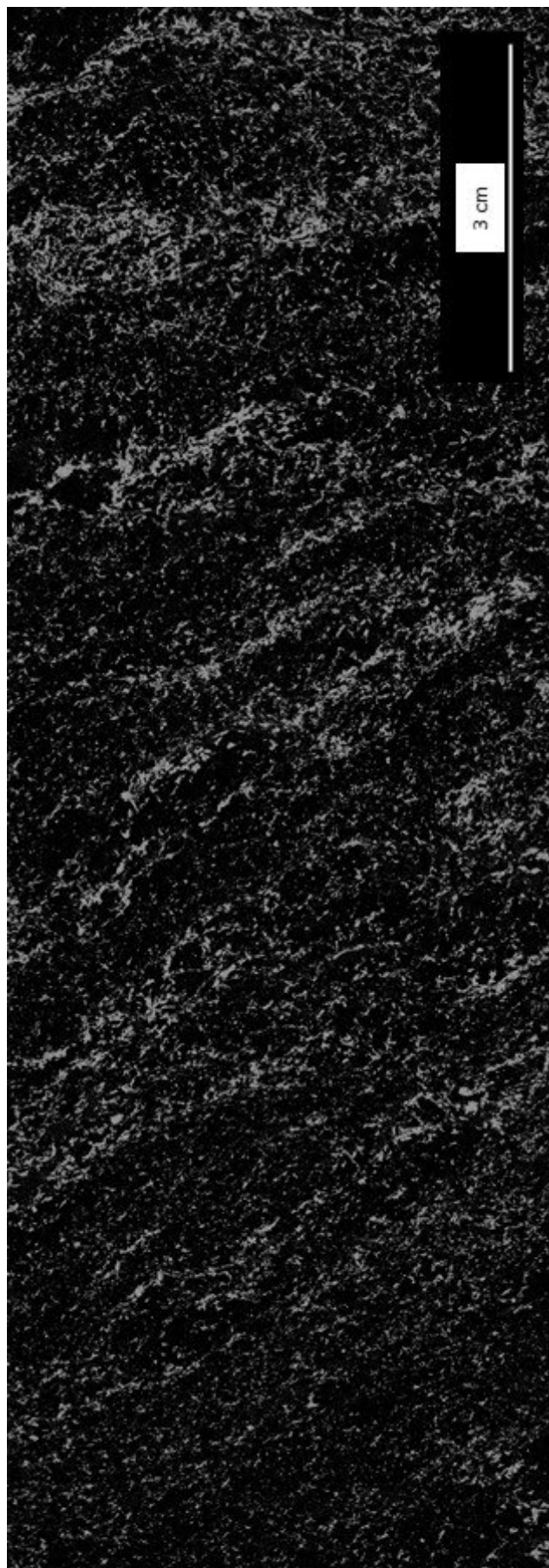
QA2 Element Cu



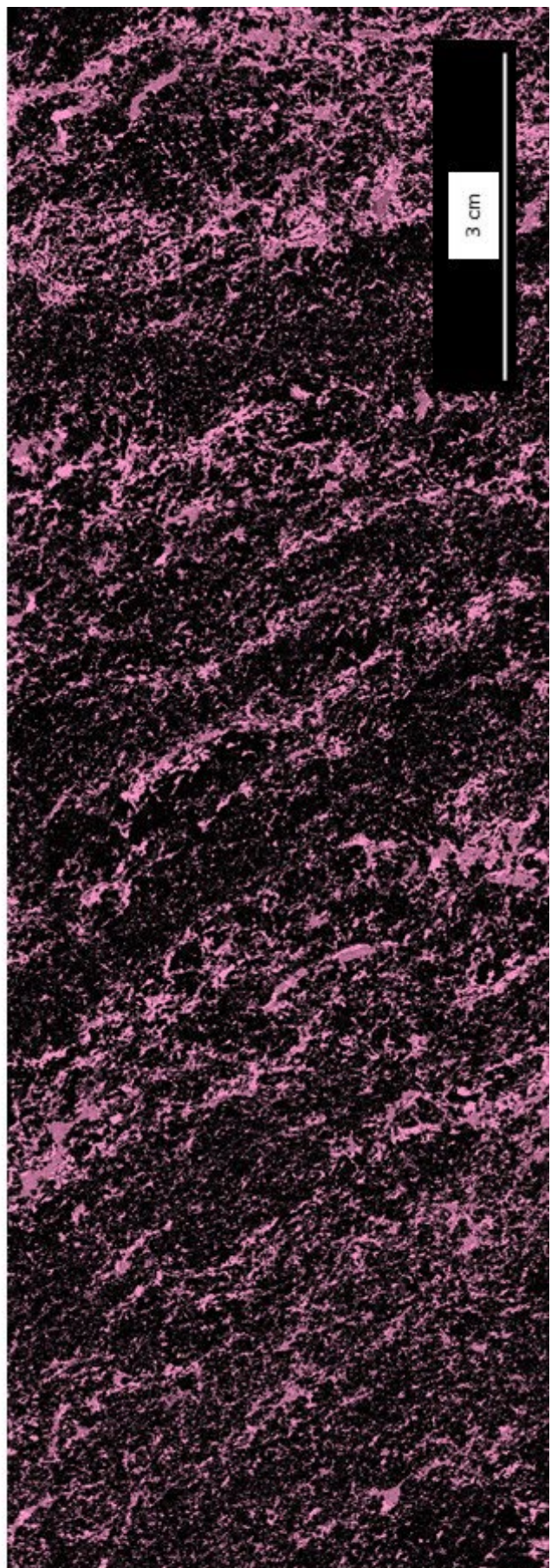
QA2 Element Fe



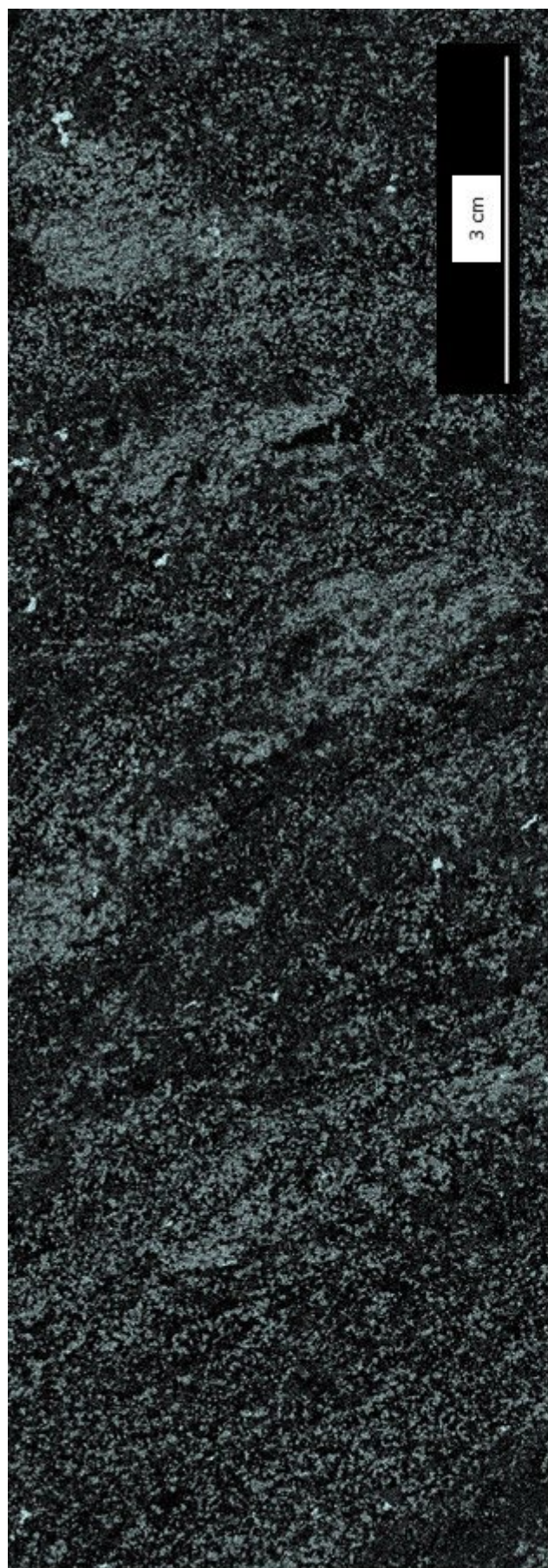
QA2 Element K



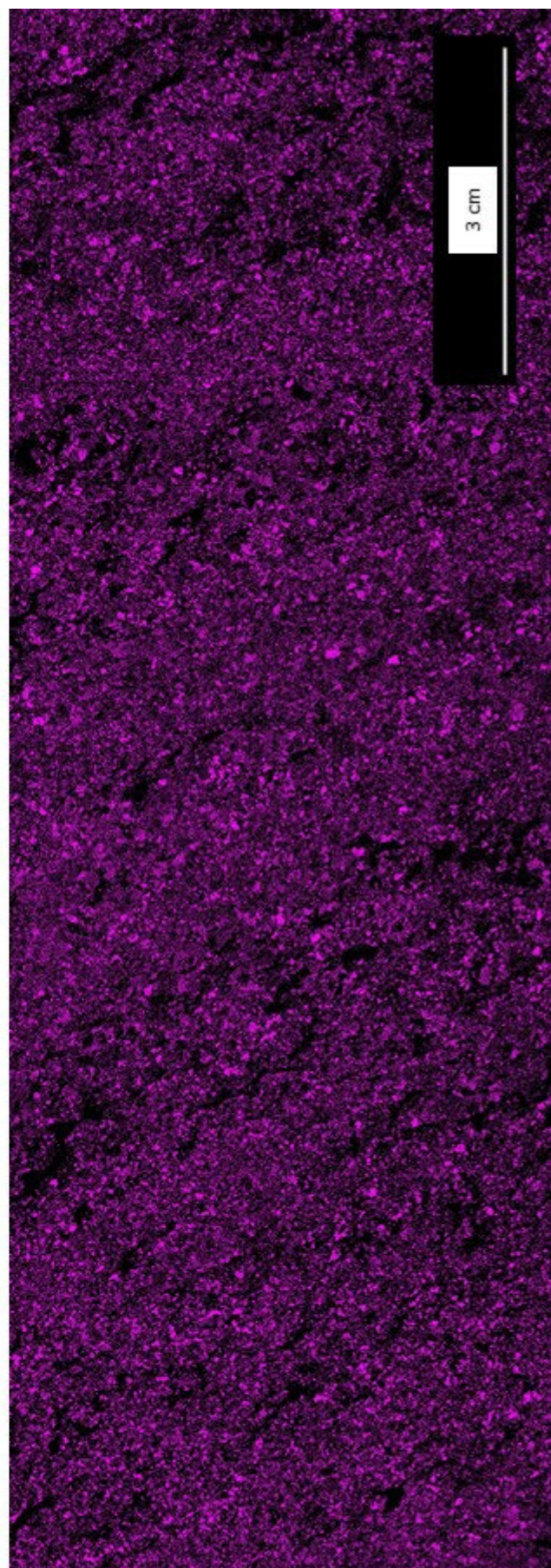
QA2 Element Mg



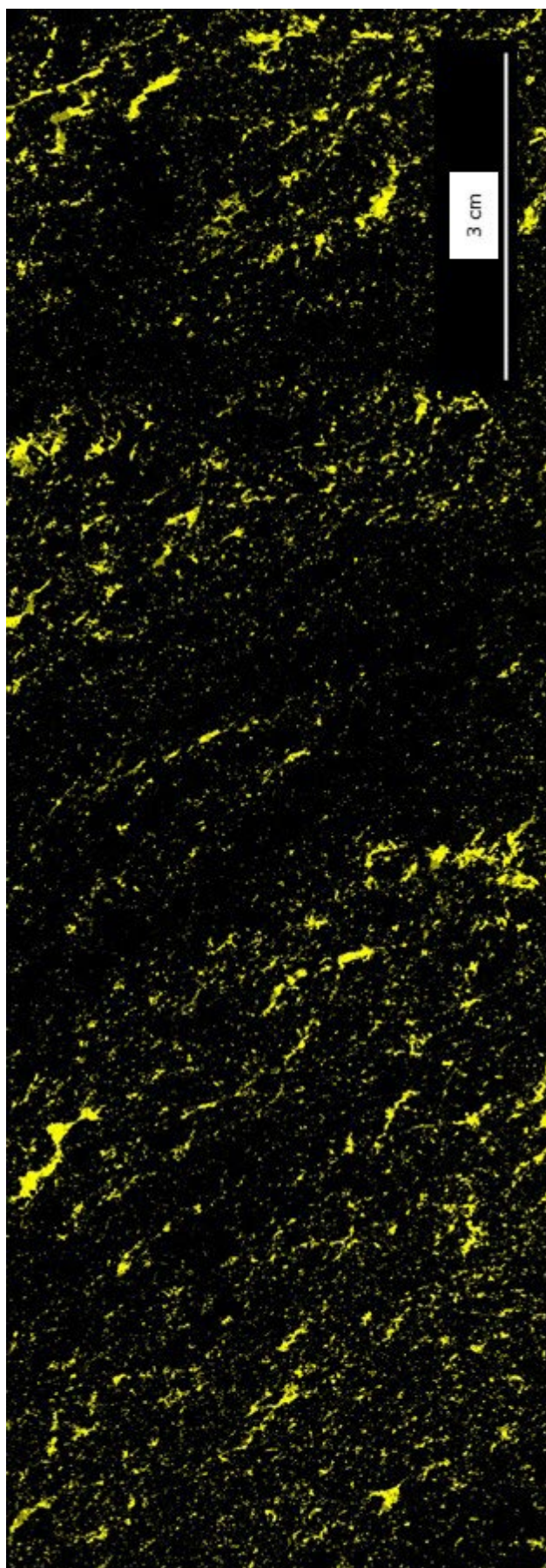
QA2 Element Mn



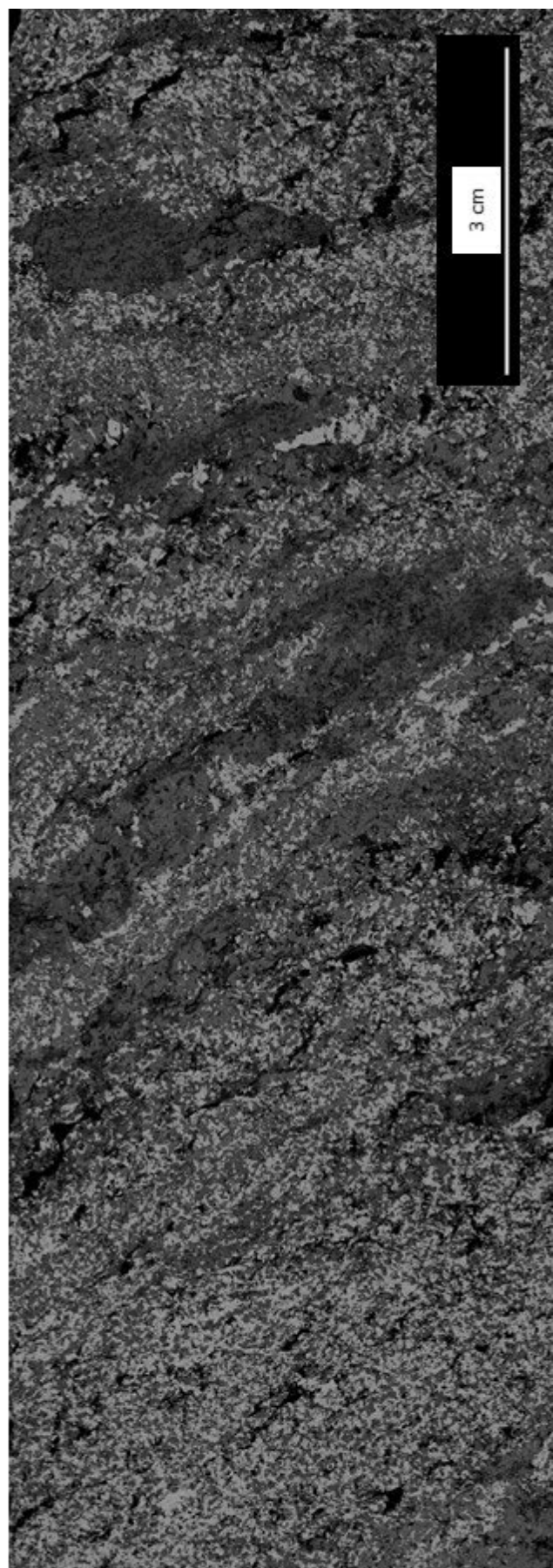
QA2 Element Na



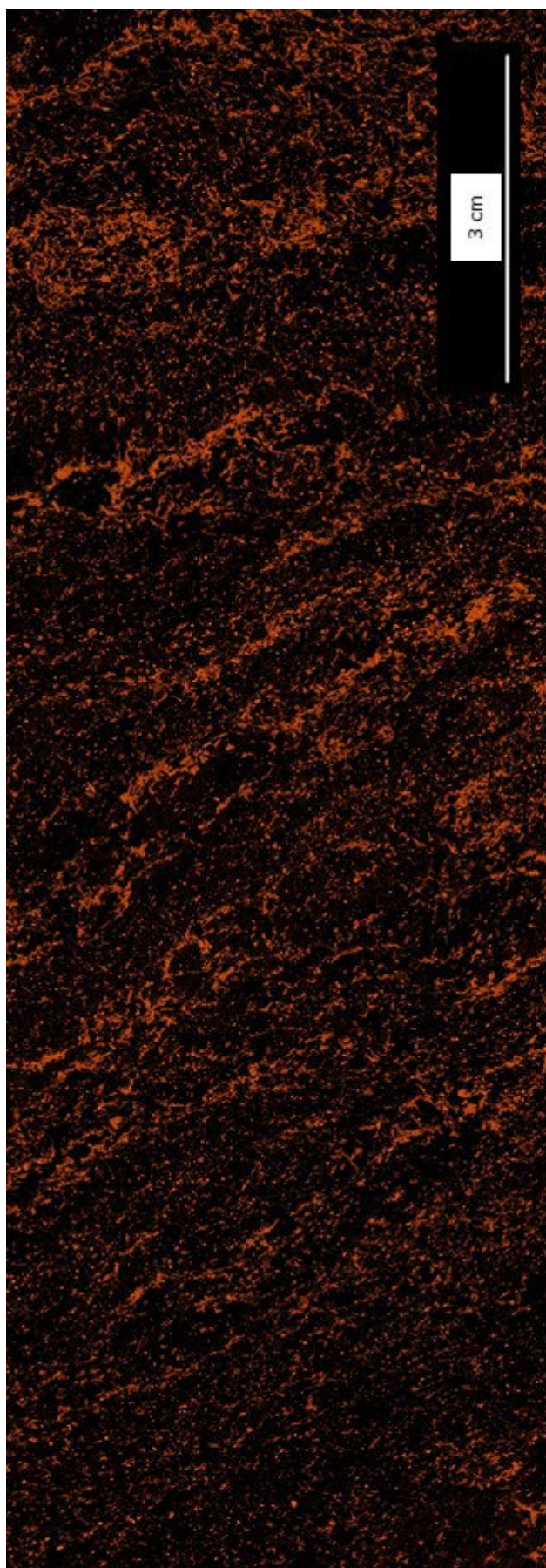
QA2 Element Ni



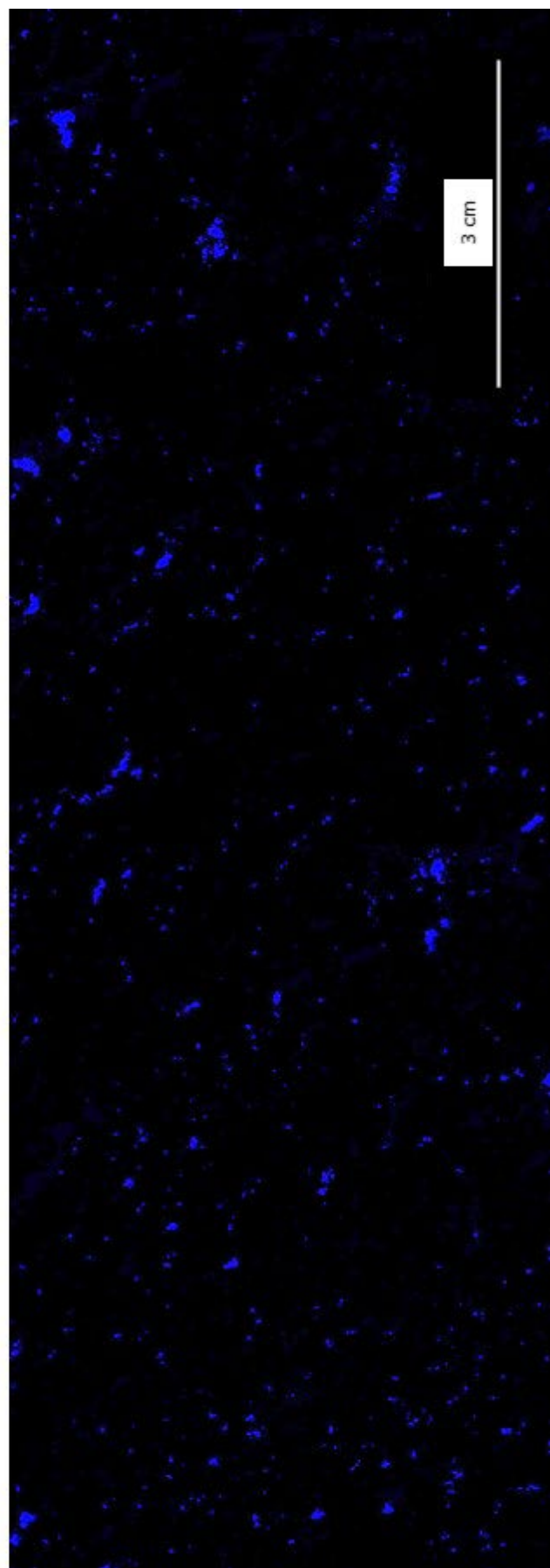
QA2 Element S



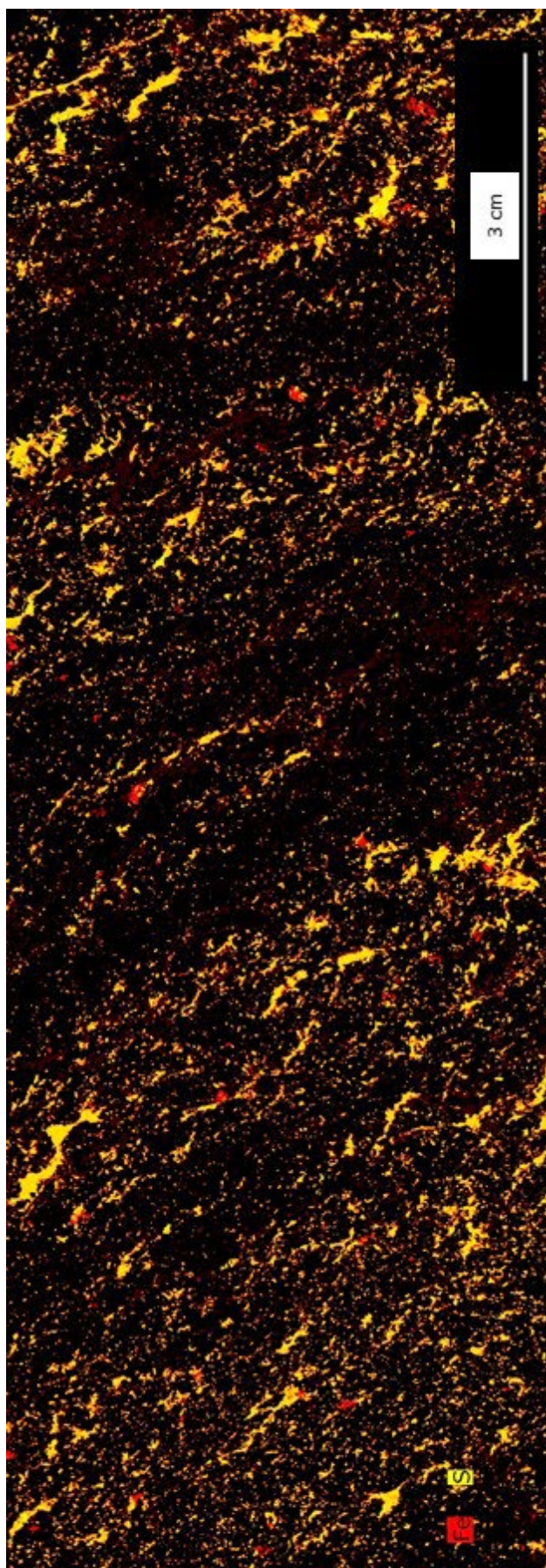
QA2 Element Si



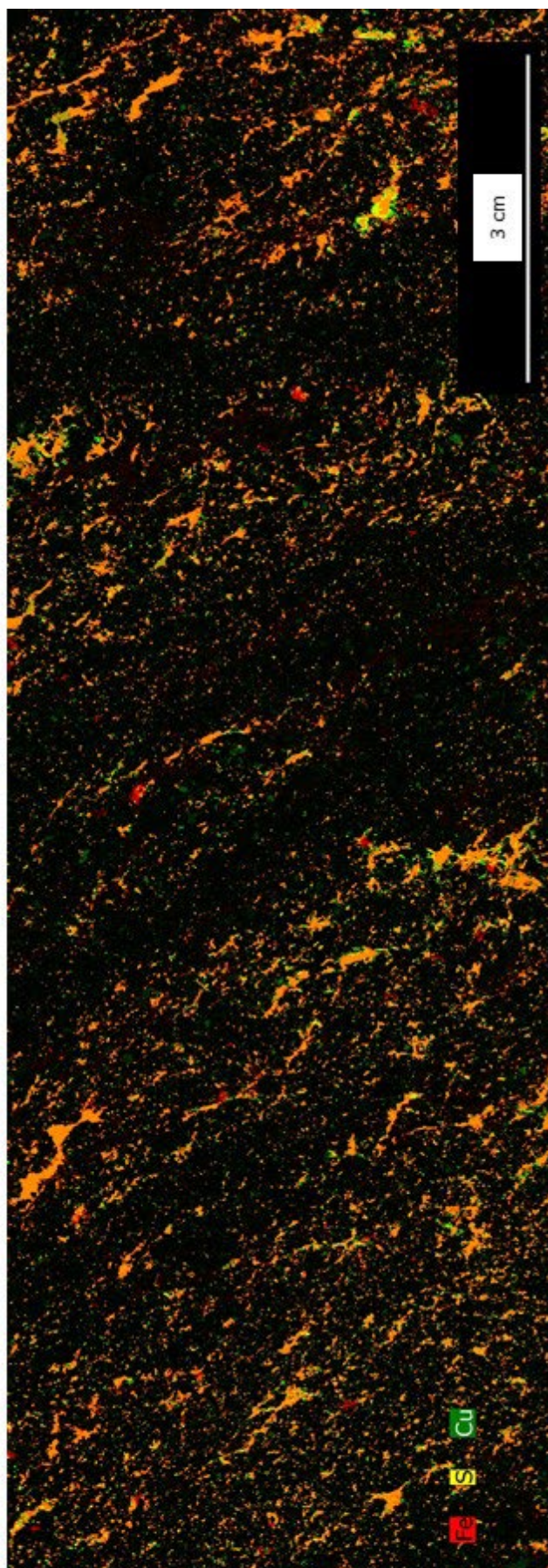
QA2 Element Ti



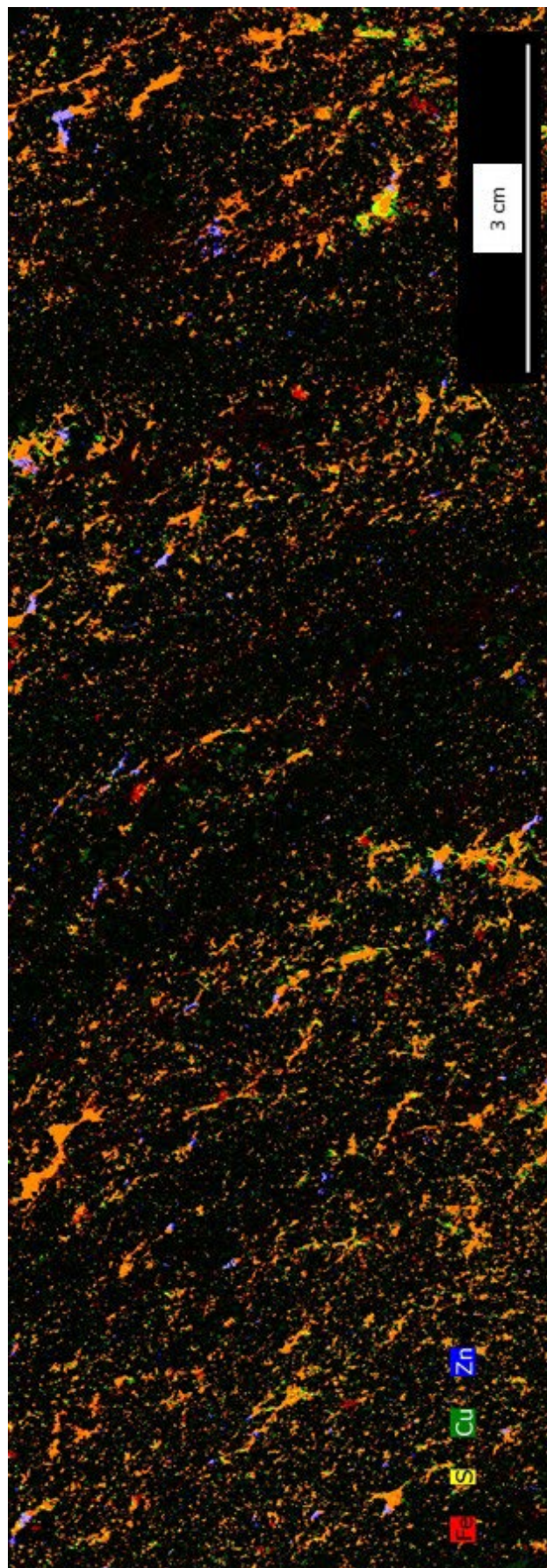
QA2 Element Zn



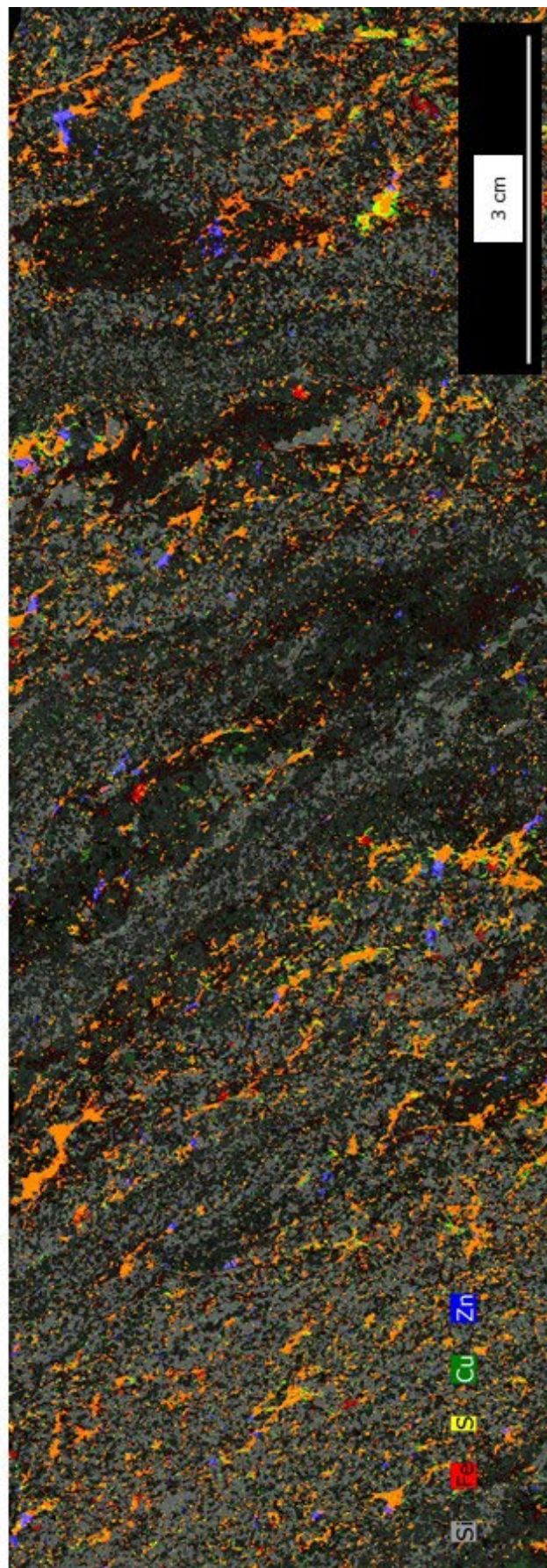
QA2 Fe-S



QA2 Fe-S-Cu

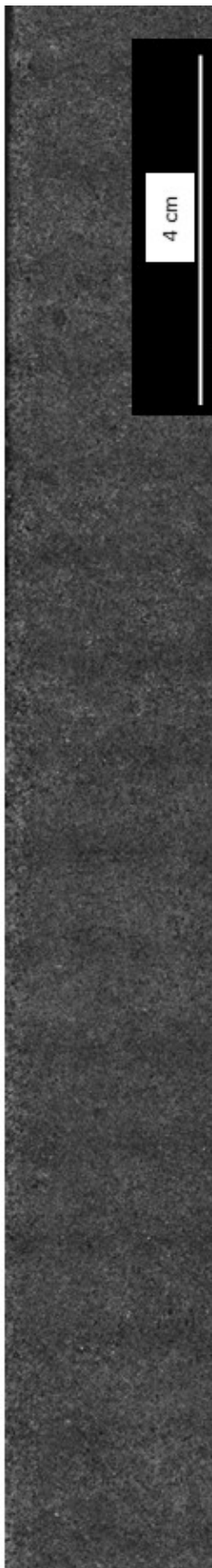


QA2 Fe-S-Cu-Zn



QA2 Si-Fe-S-Cu-Zn

26.3 Sample XA3 Scanning Micro-XRF



Mapping parameters

Width:	5594 pixel
Height:	178.911 mm
Pixel Size:	762 pixel
Total number of pixel:	24.35 mm
	32 μ m
	4262628 pixel

Acquisition parameters

Frame count:	0
Pixel time:	10 ms/pixel
Measure time:	9:59 h
Overall time:	12:43 h
Stage speed:	3.2 mm/s
Stage position (X,Y,Z):	51.616;58.713;103.357 mm

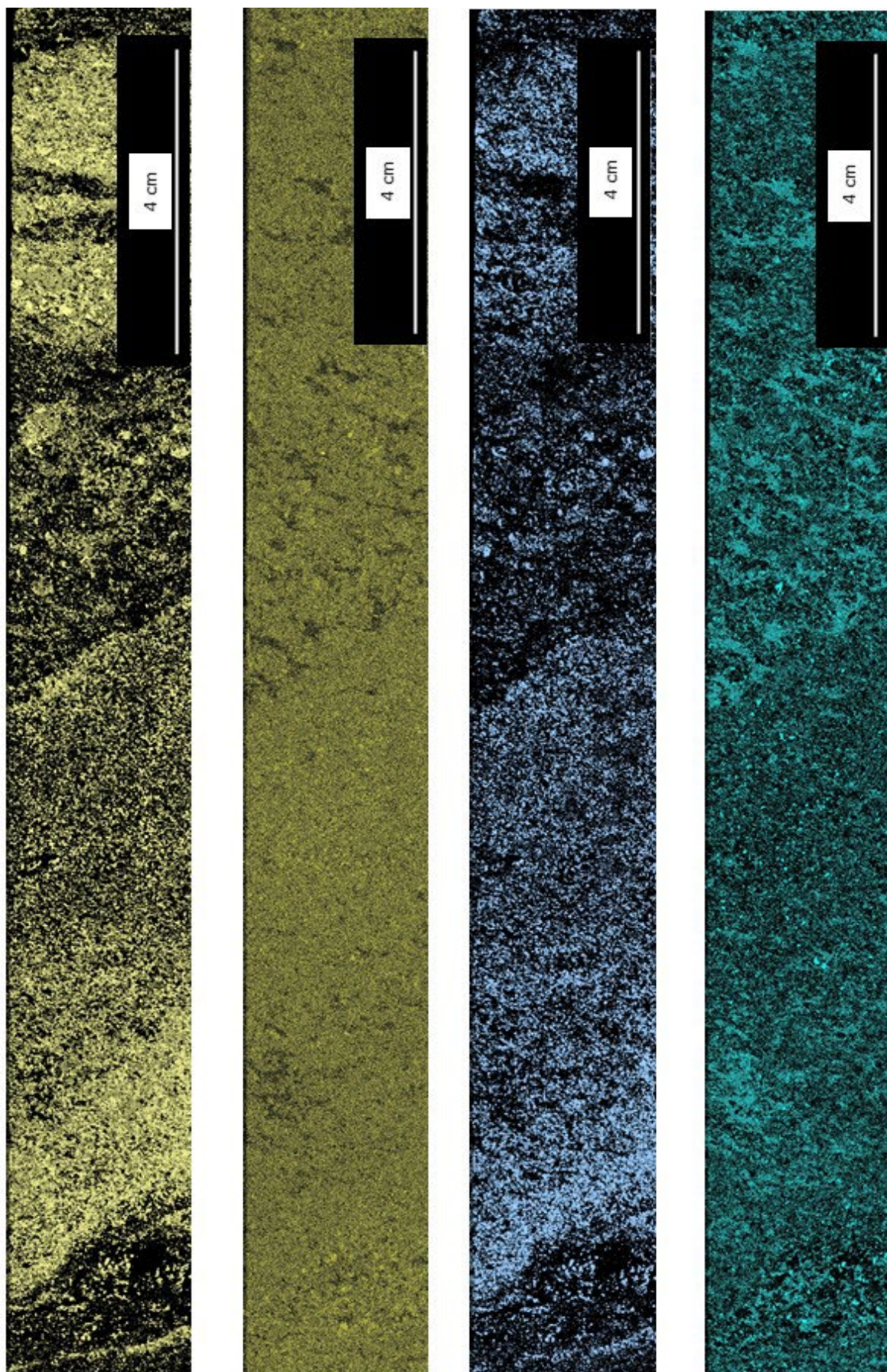
Tube parameter

High voltage:	50 kV
Anode current:	600 μ A
Filter:	Empty
Optic:	Lens
Collimator diameter:	0
SpotSize:	20
Chamber at:	Air 2 mbar
Flow rate:	--- l/min
Anode:	Rh

Detector parameters

Selected detectors:	1,2
Max. pulse throughput:	275000 cps

Raw Image – Sample XA3

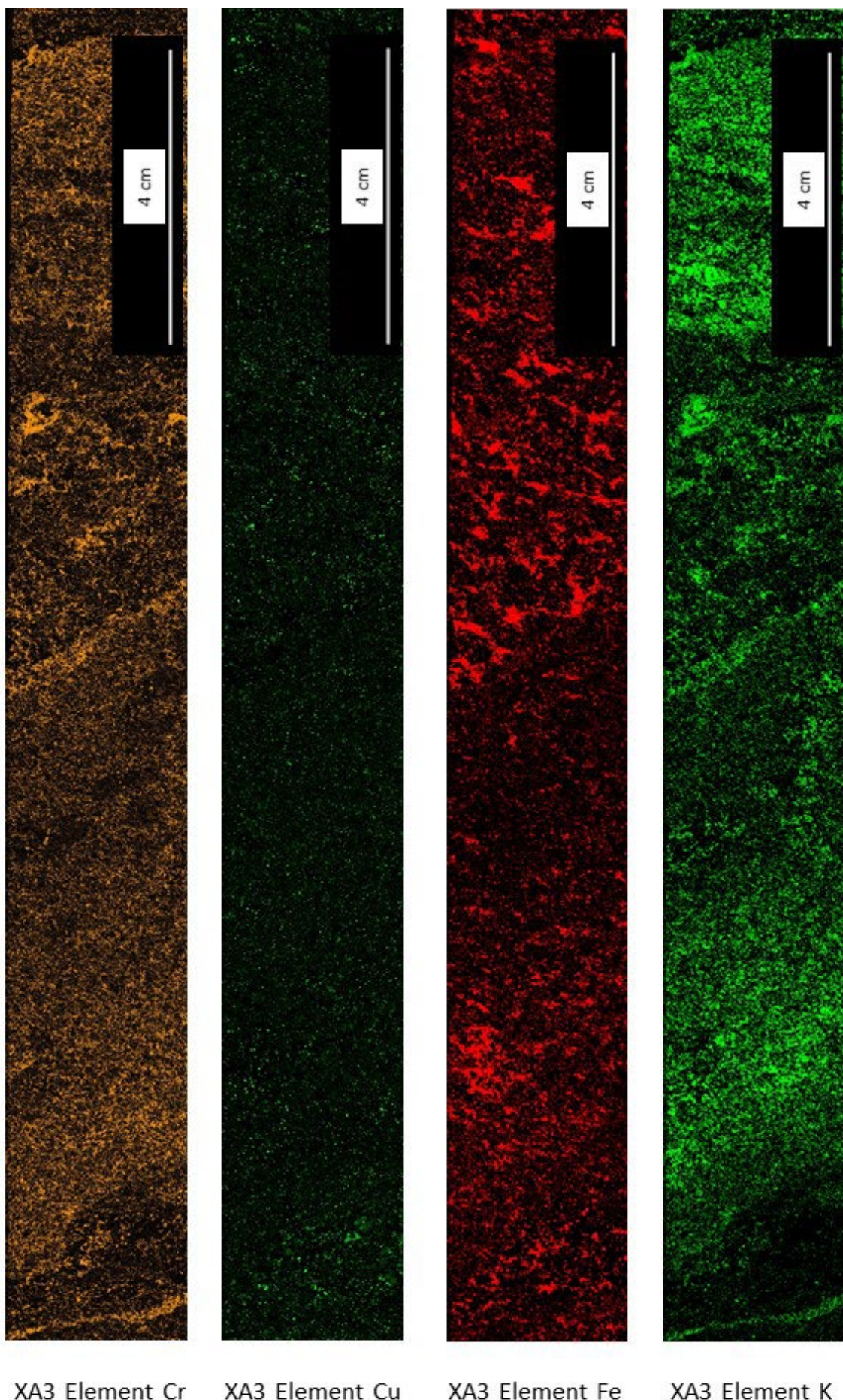


XA3 Element Al

XA3 Element As

XA3 Element Ca

XA3 Element Co

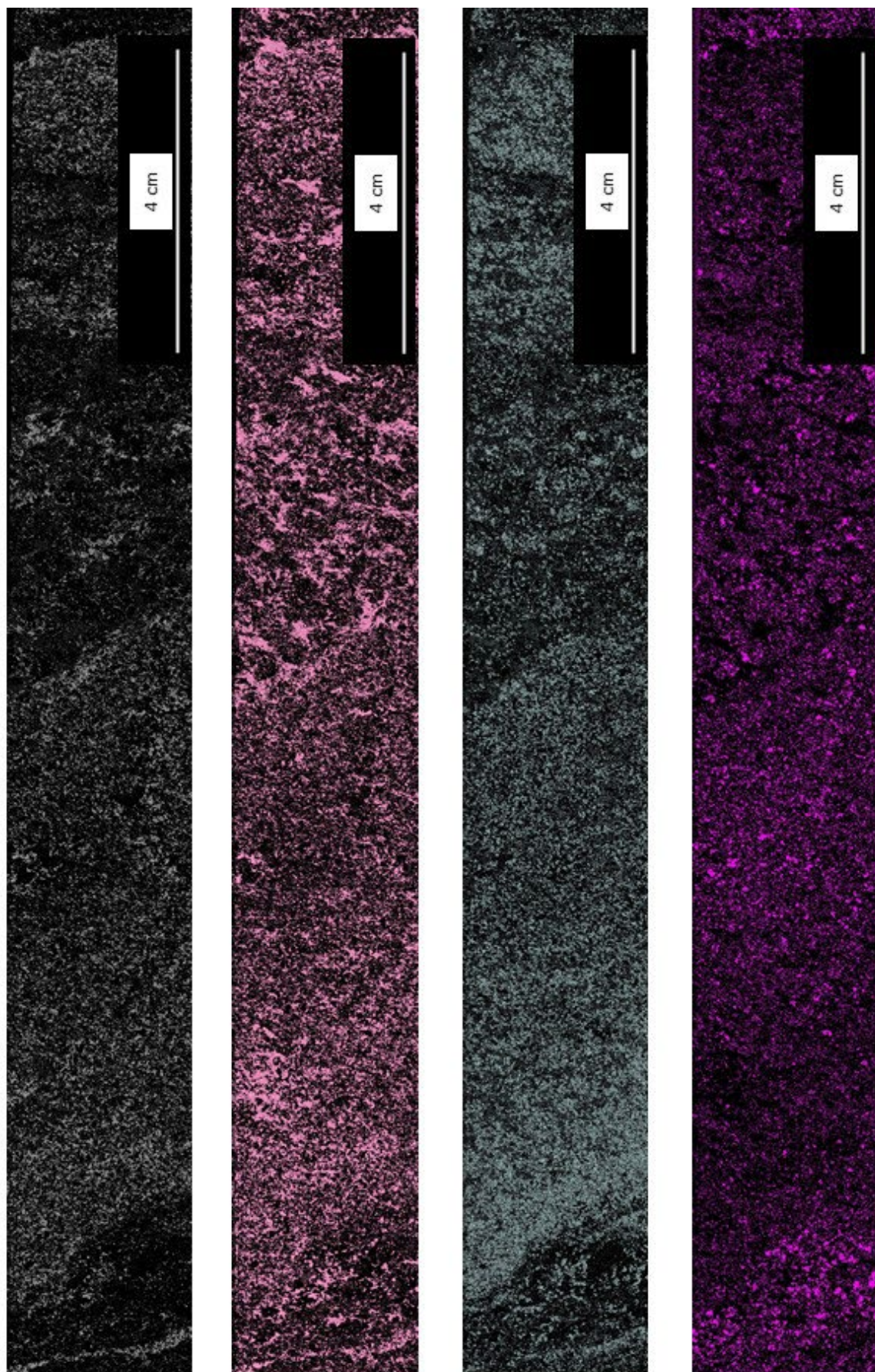


XA3 Element Cr

XA3 Element Cu

XA3 Element Fe

XA3 Element K

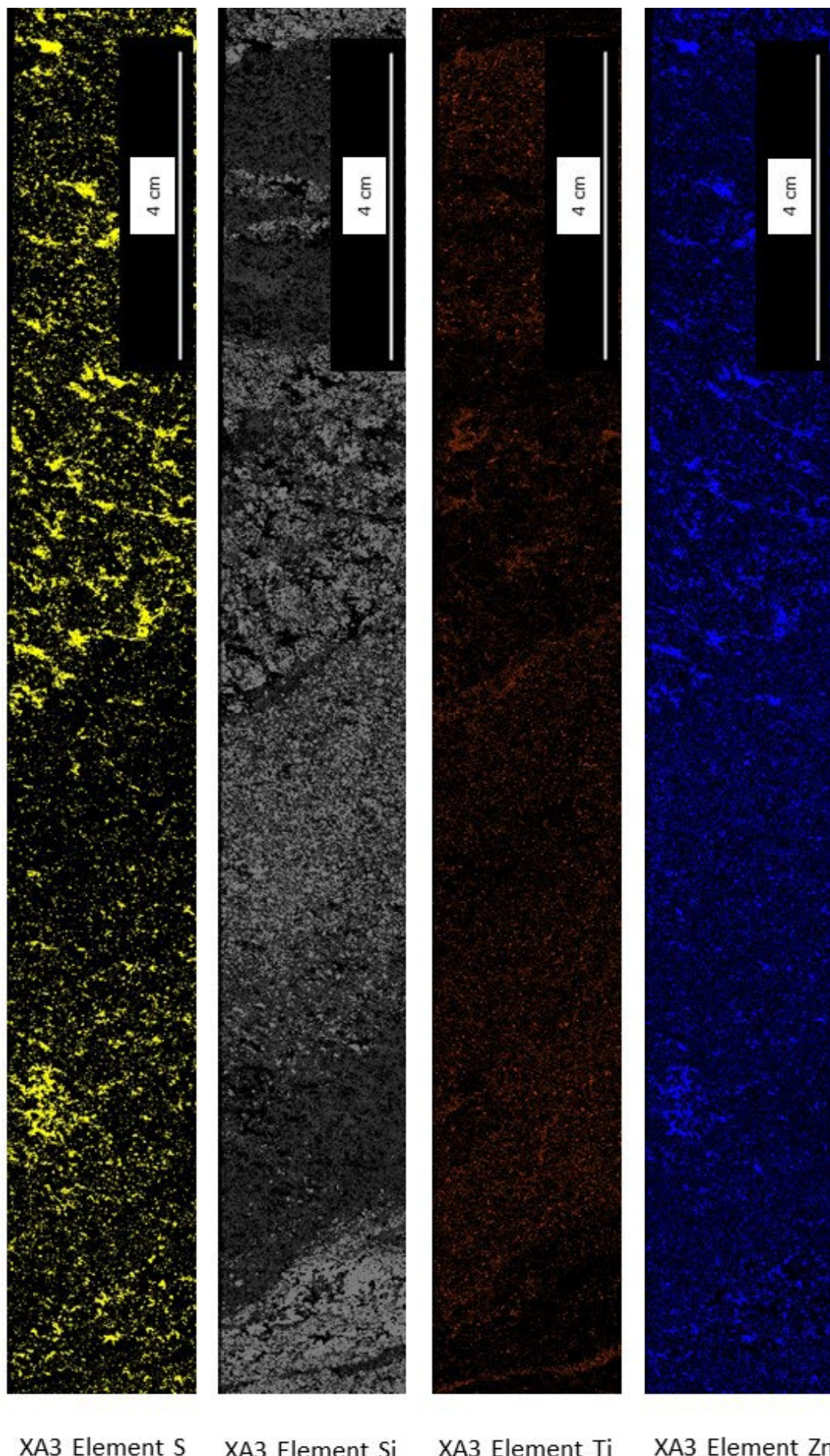


XA3 Element Mg

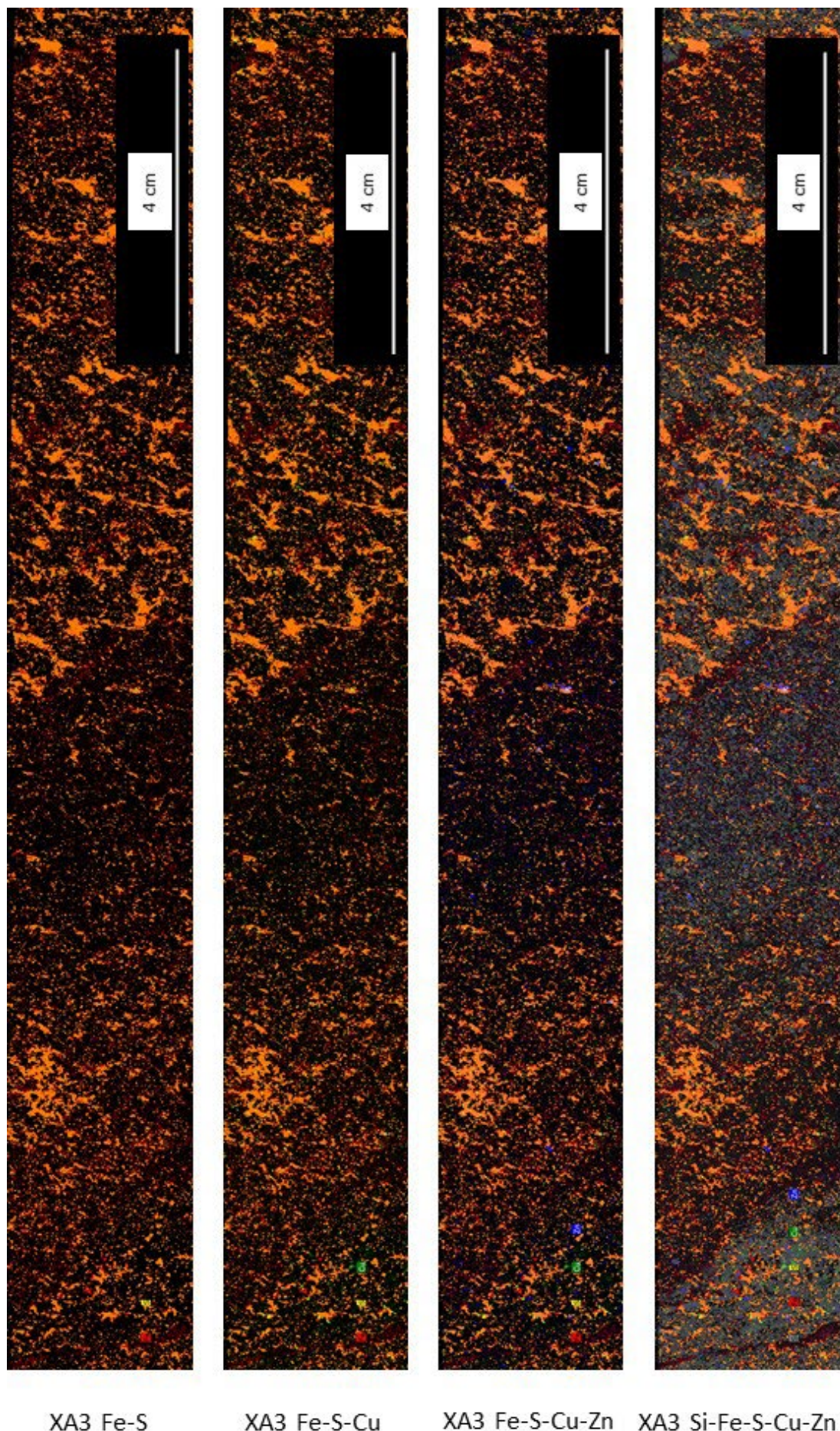
XA3 Element Mn

XA3 Element Na

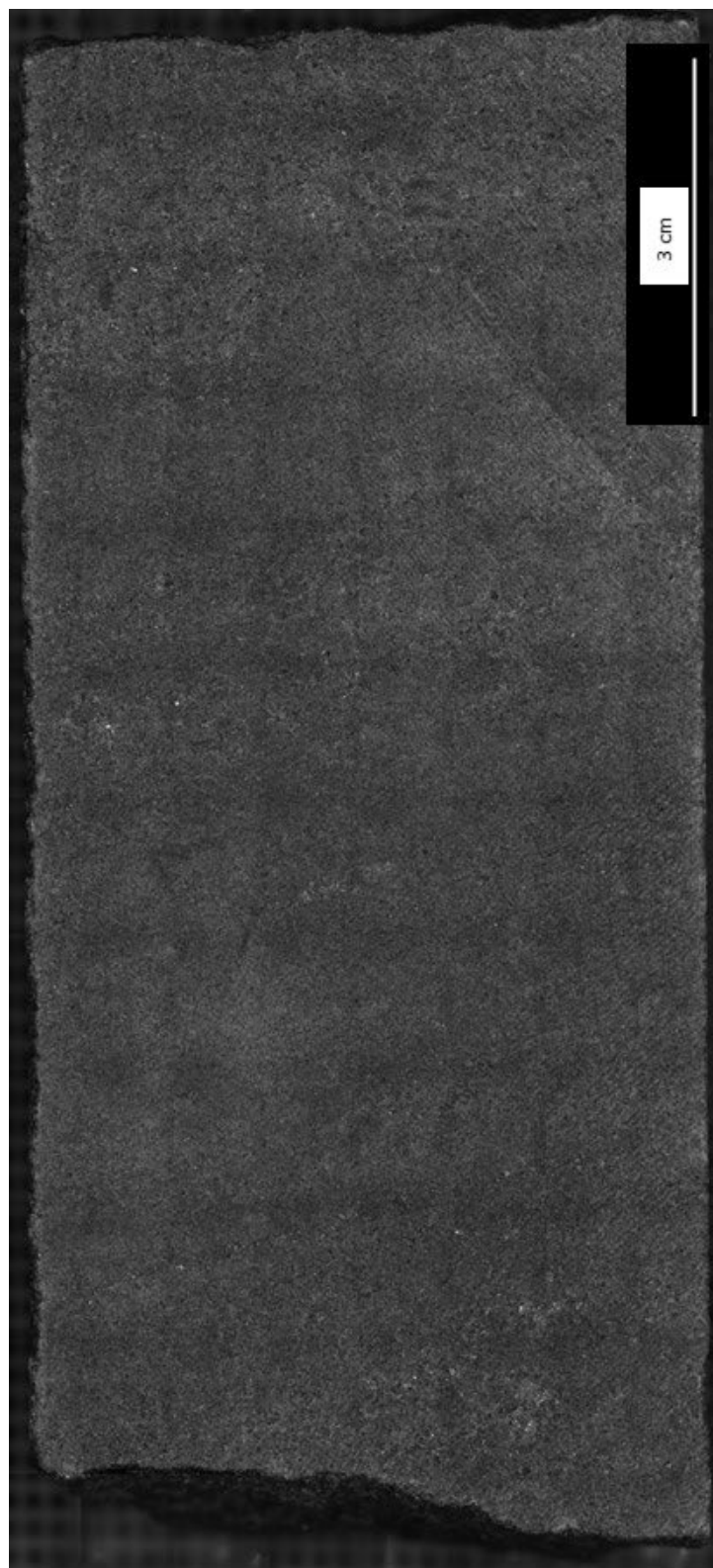
XA3 Element Ni



XA3 Element S XA3 Element Si XA3 Element Ti XA3 Element Zn

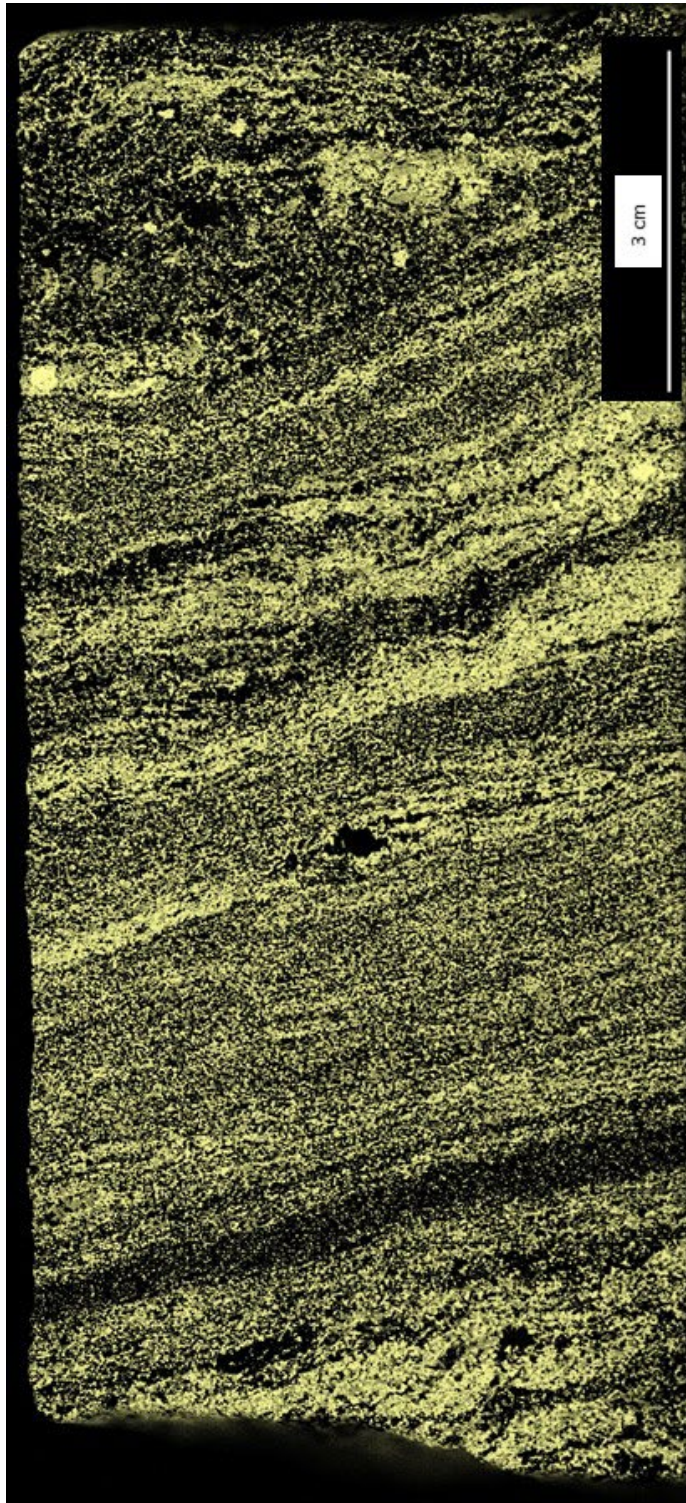


26.4 Sample YA4 Scanning Micro-XRF

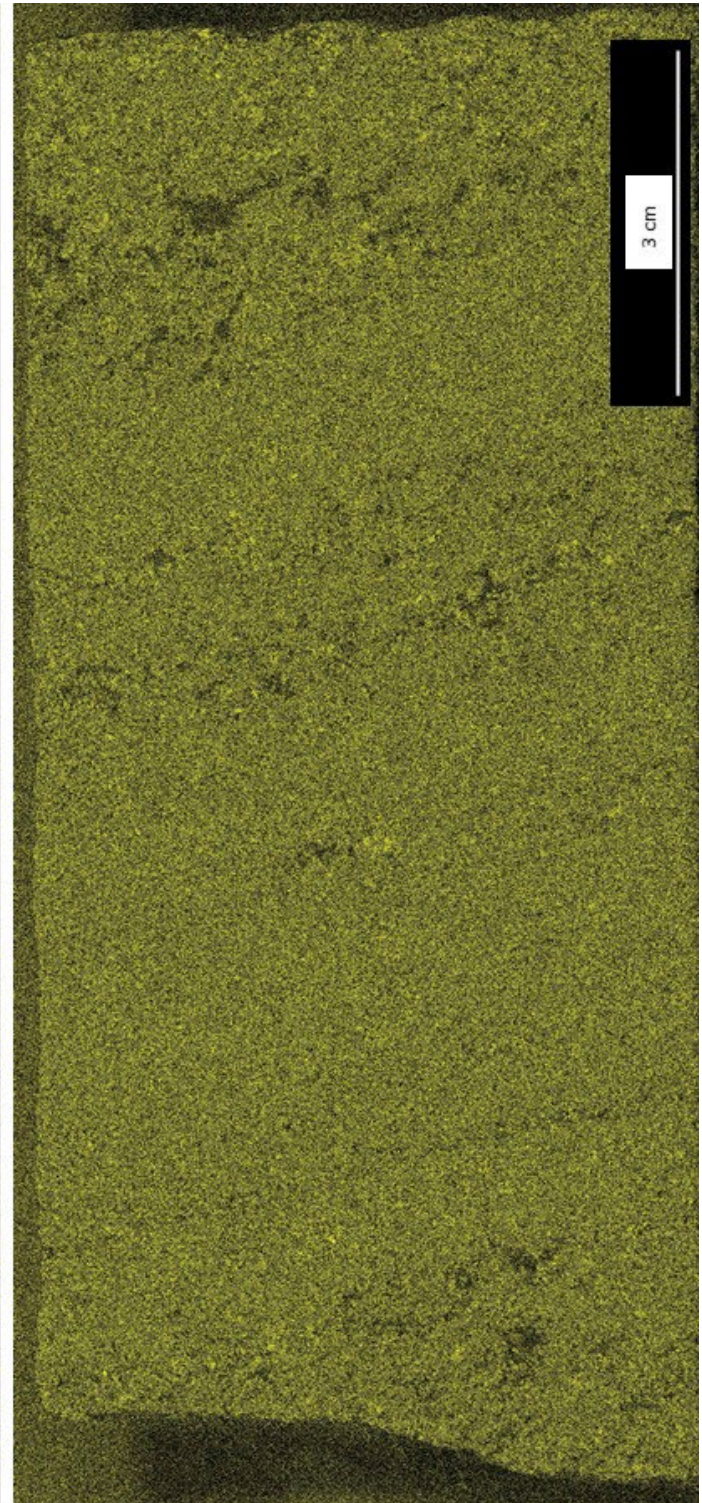


Mapping parameters	
Width:	3250 pixel
Height:	130.303 mm
Pixel Size:	1480 pixel
Total number of pixel:	59.171 mm
	40 µm
Acquisition parameters	
Frame count:	1
Pixel time:	10 ms/pixel
Measure time:	11:37 h
Overall time:	14:48 h
Stage speed:	4.0 mm/s
Stage position (X,Y,Z):	82.244;70.039;89.916 mm
Tube parameter	
High voltage:	50 kV
Anode current:	600 µA
Filter:	Empty
Optic:	Lens
Collimator diameter:	0
SpotSize:	20
Chamber at:	Air 2 mbar
Flow rate:	--- l/min
Anode:	Rh
Detector parameters	
Selected detectors:	1,2
Max. pulse throughput:	275000 cps

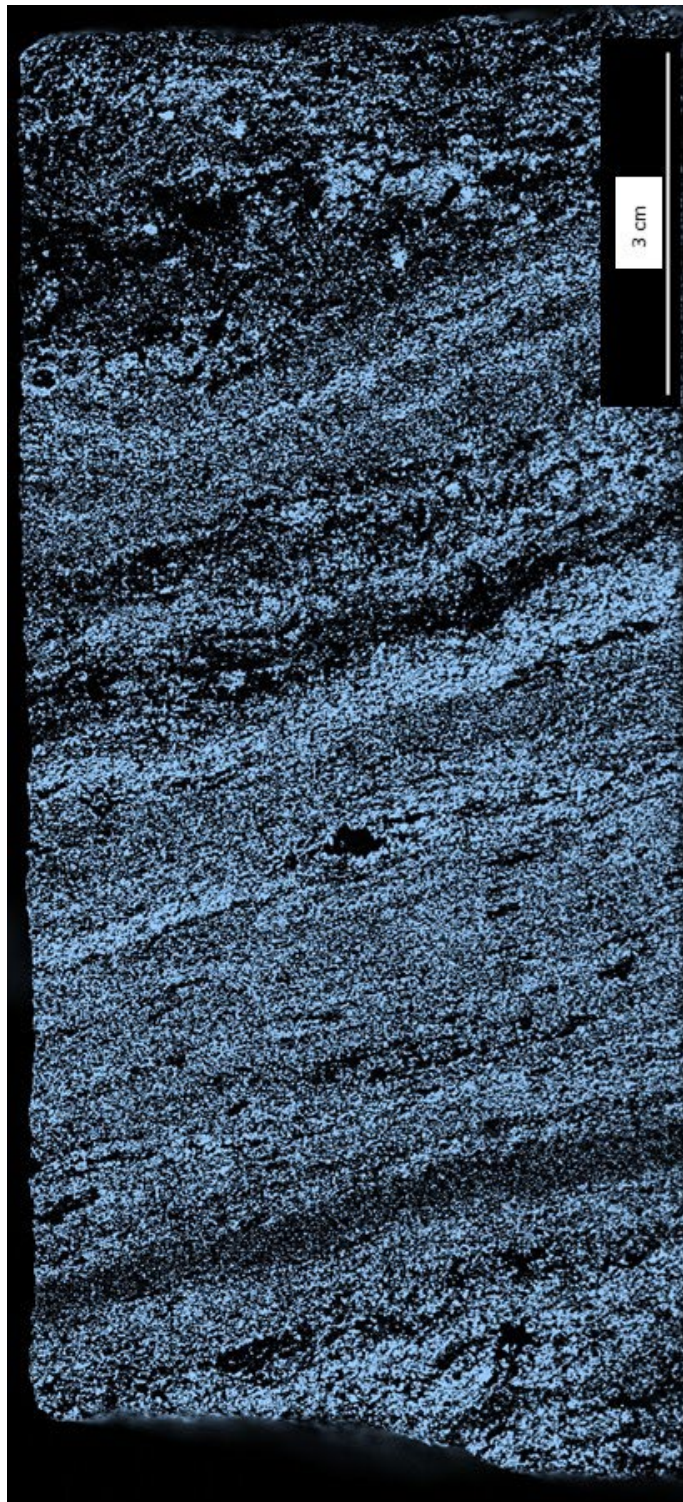
Raw Image - Sample YA4



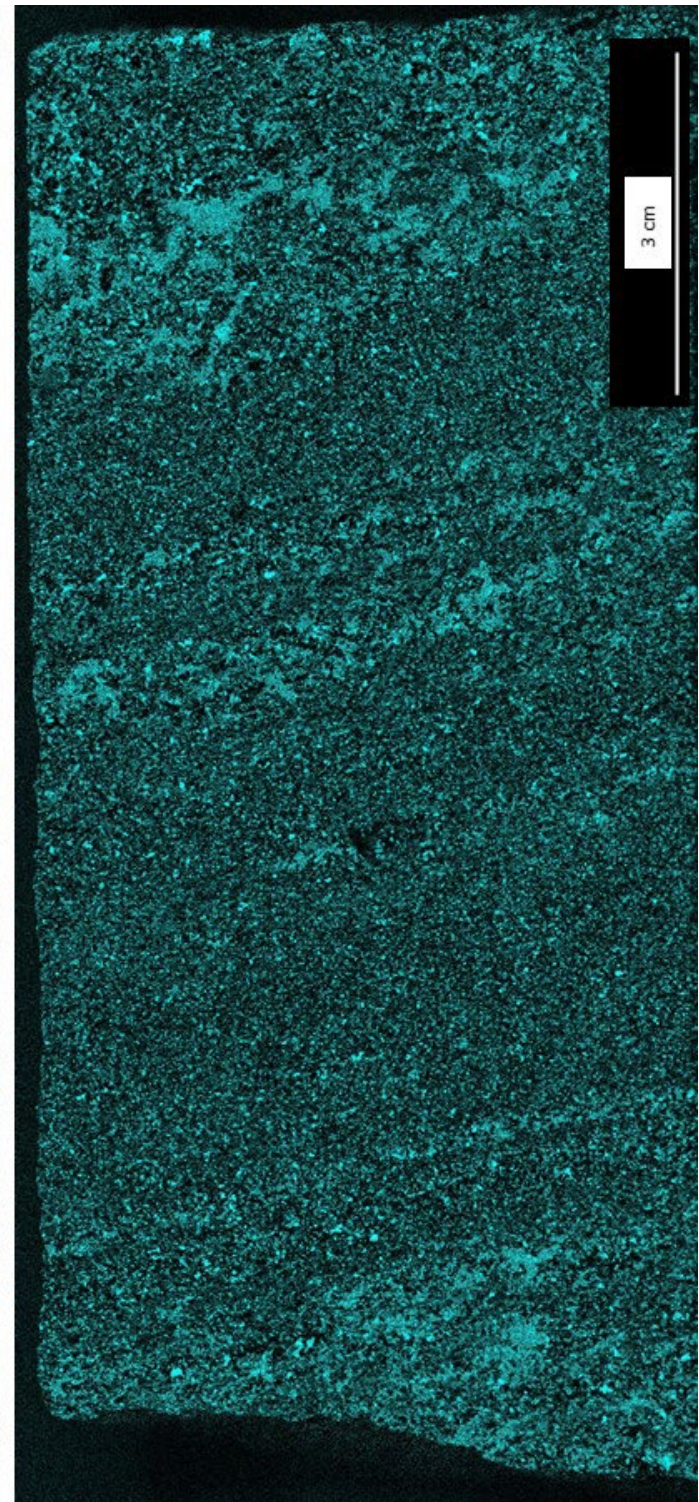
YA4 Element Al



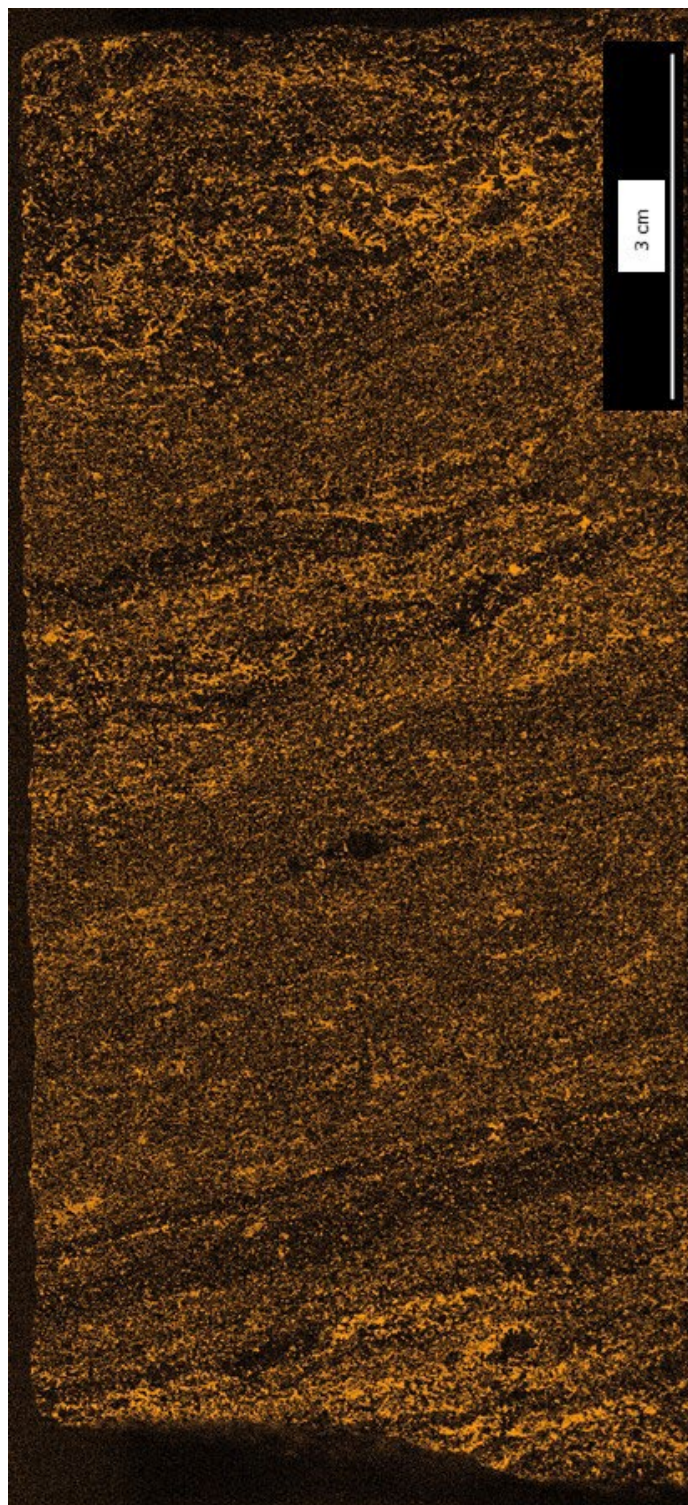
YA4 Element As



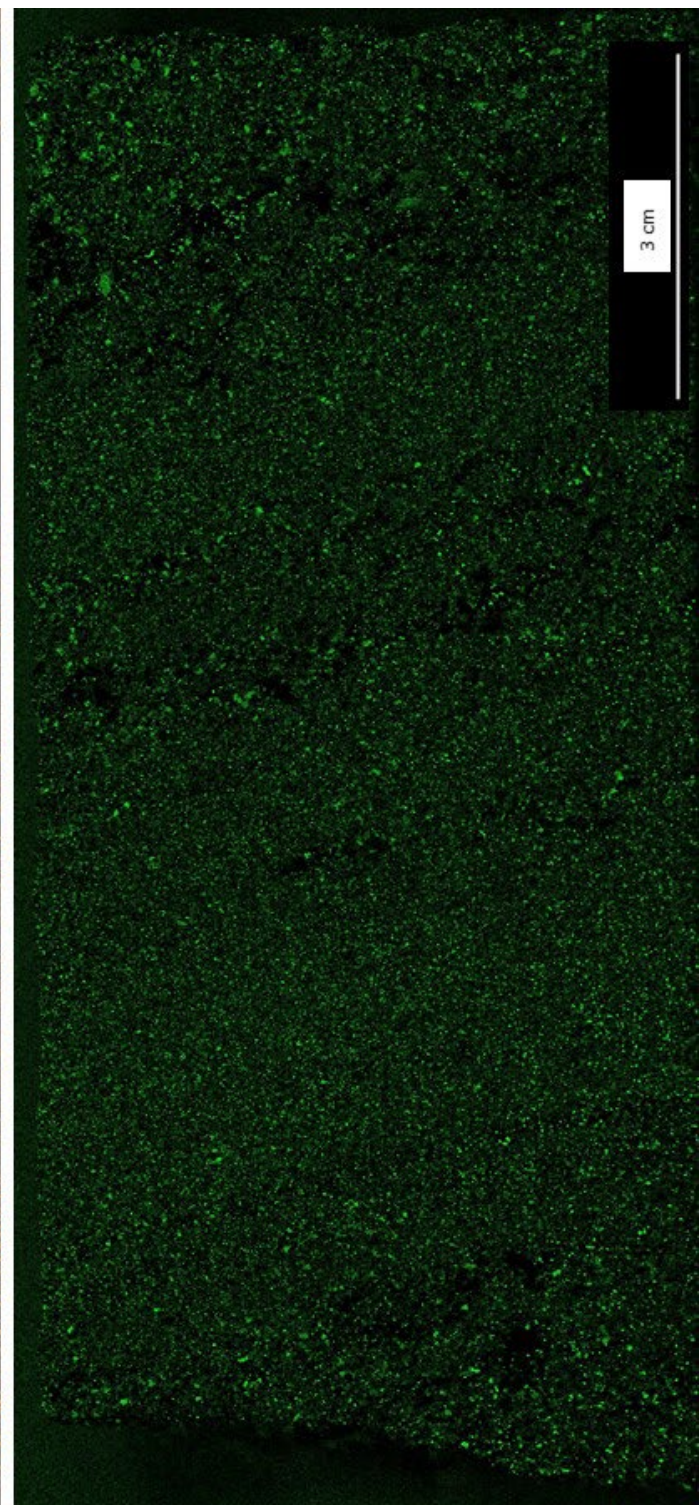
YA4 Element Ca



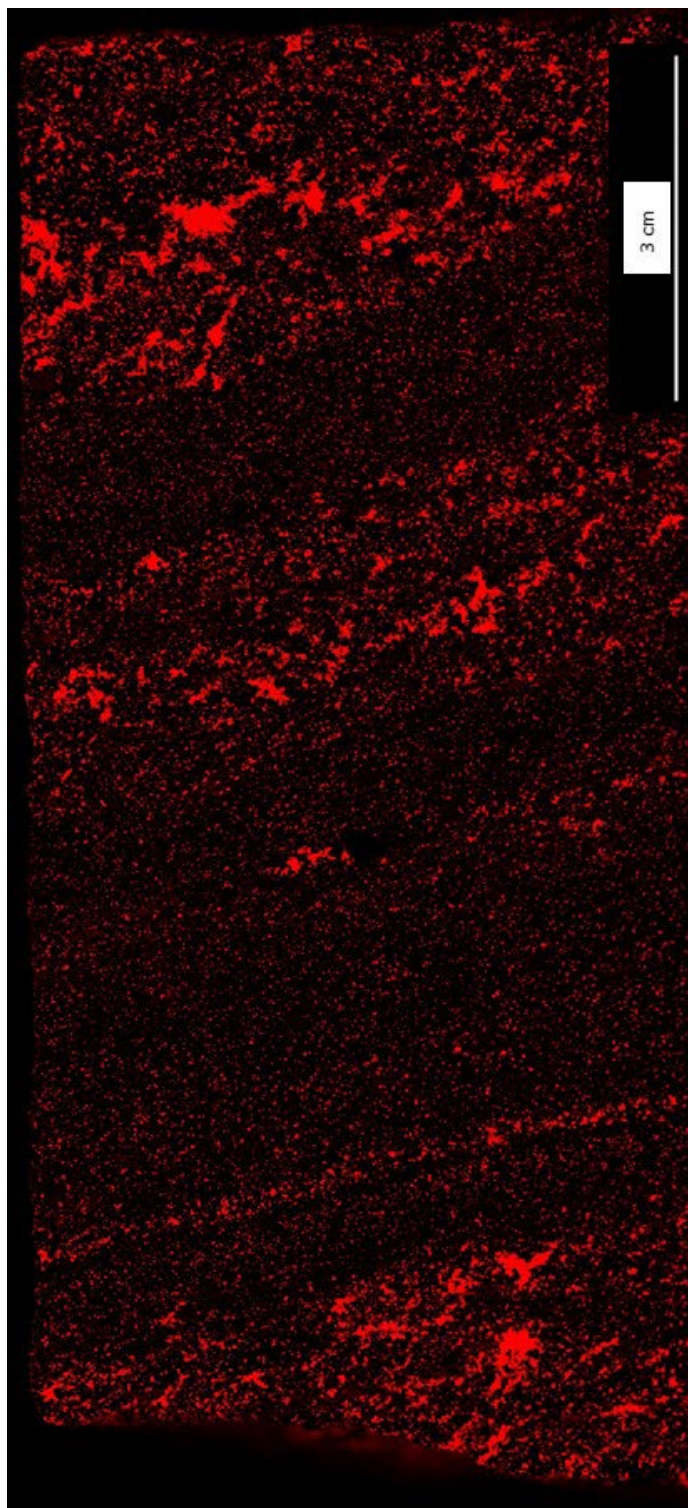
YA4 Element Co



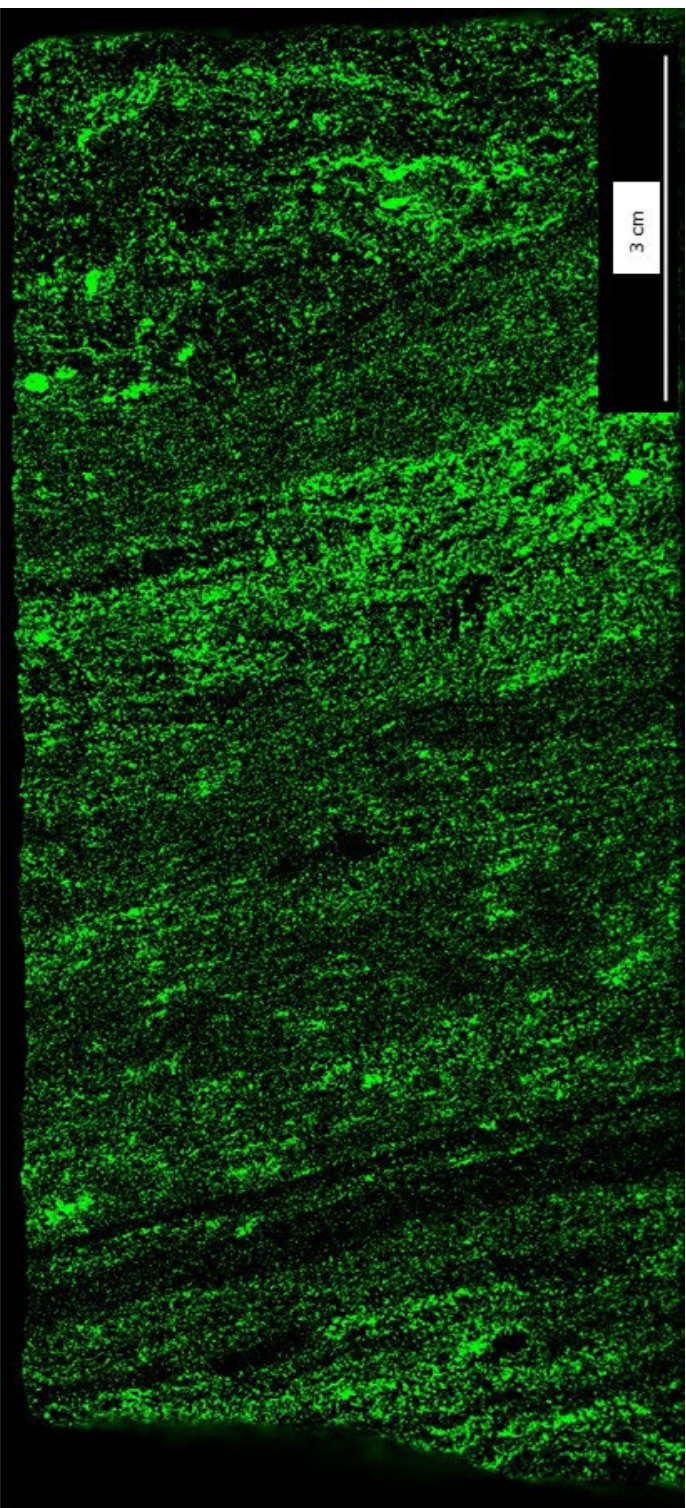
YA4 Element Cr



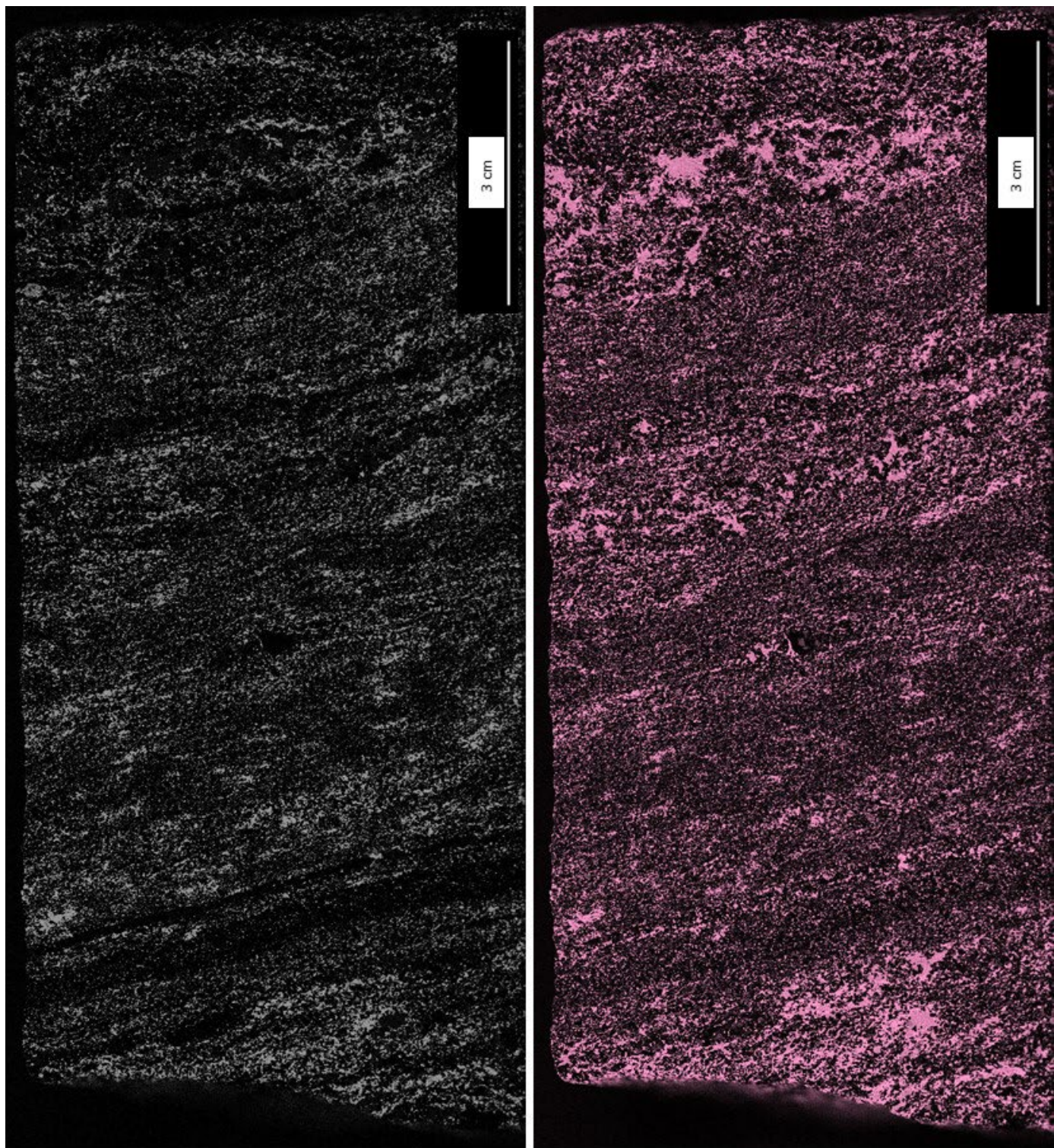
YA4 Element Cu



YA4 Element Fe

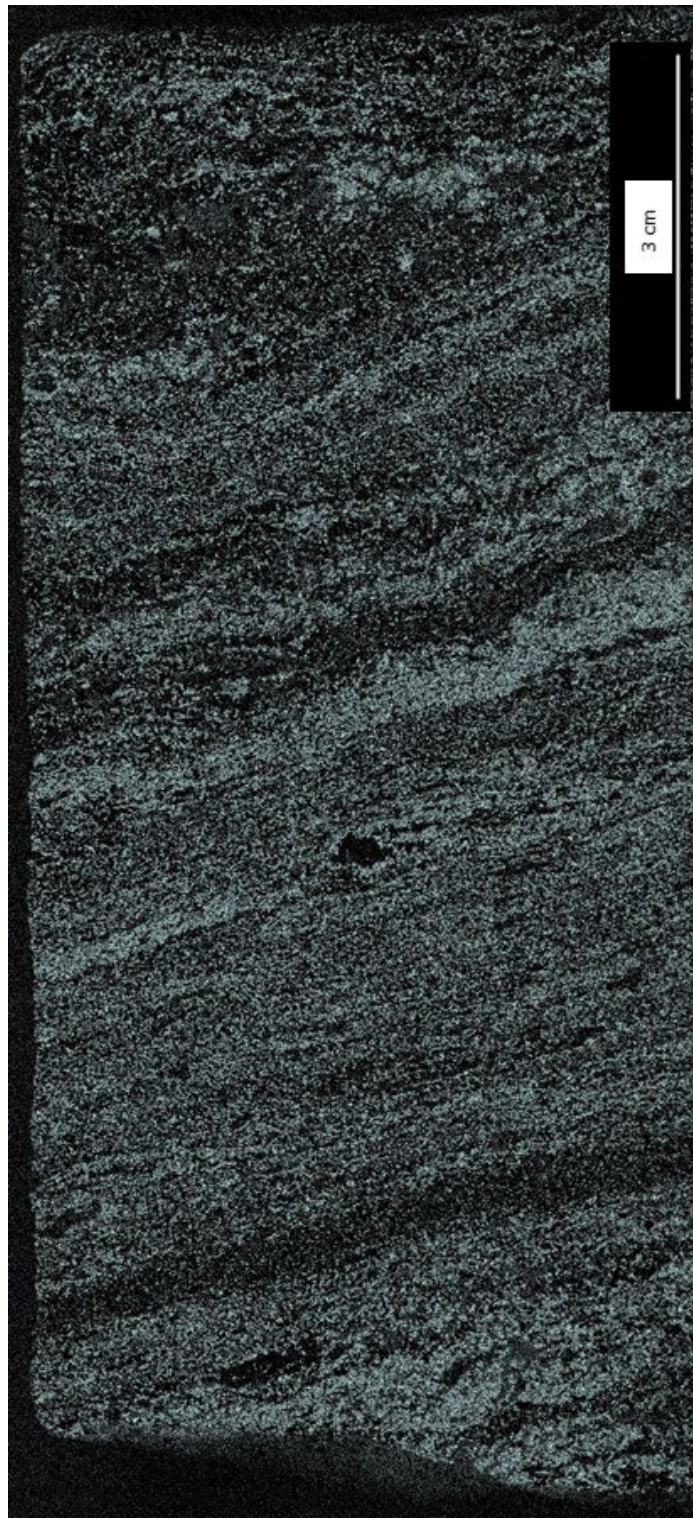


YA4 Element K

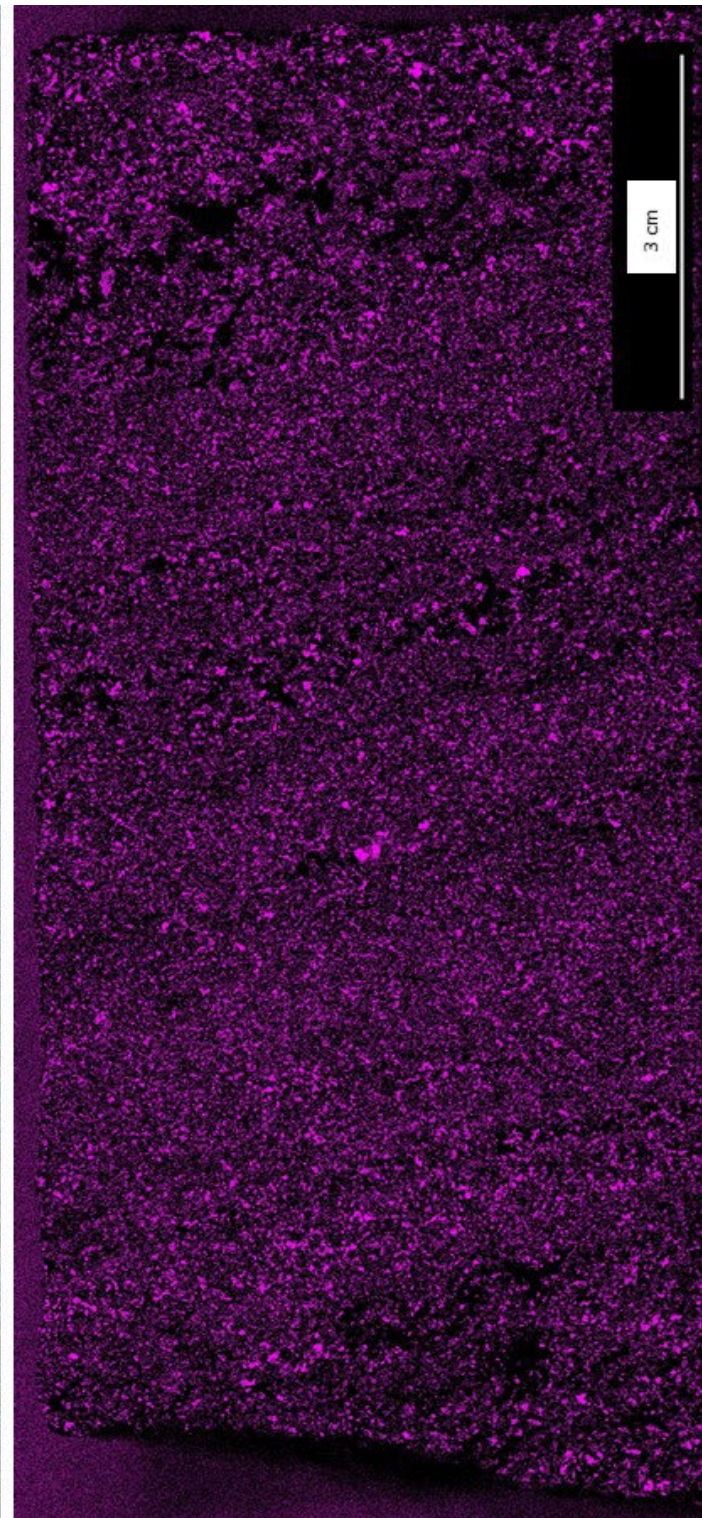


YA4 Element Mg

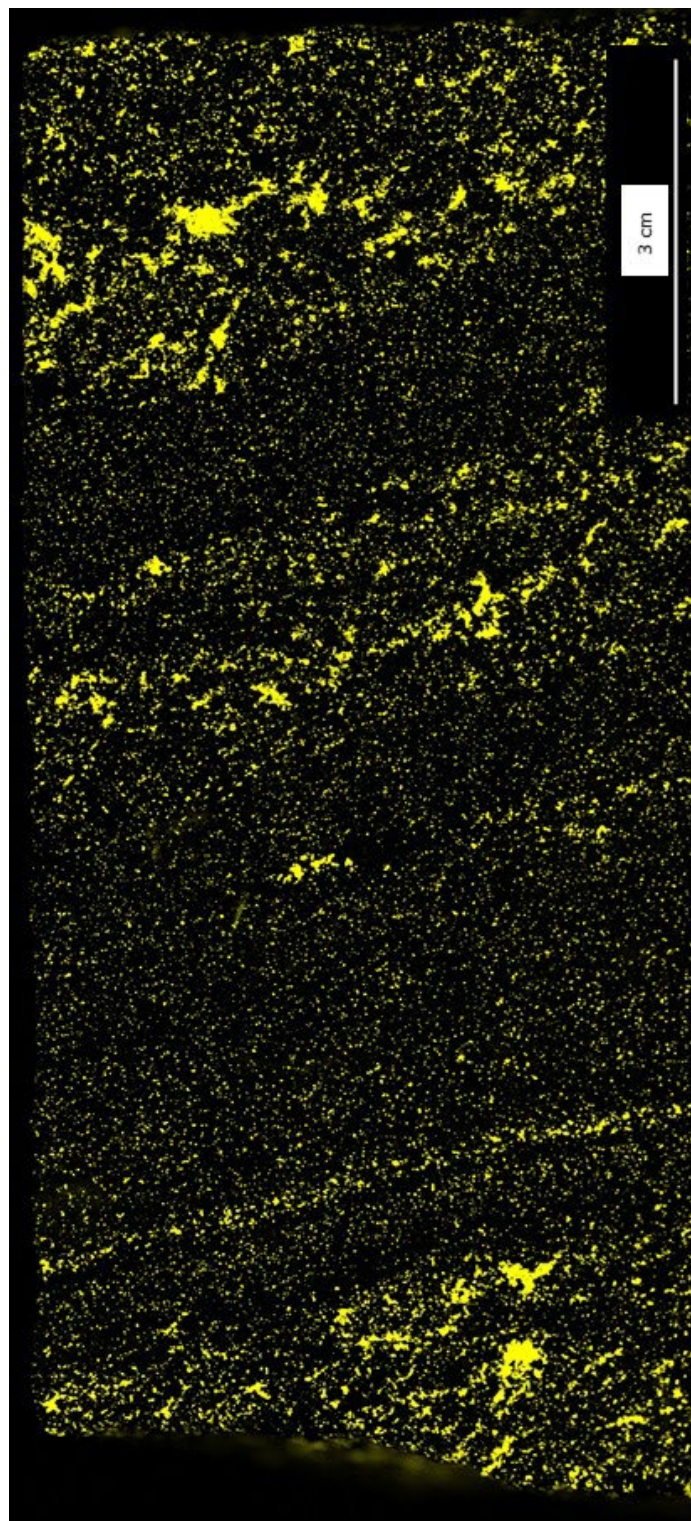
YA4 Element Mn



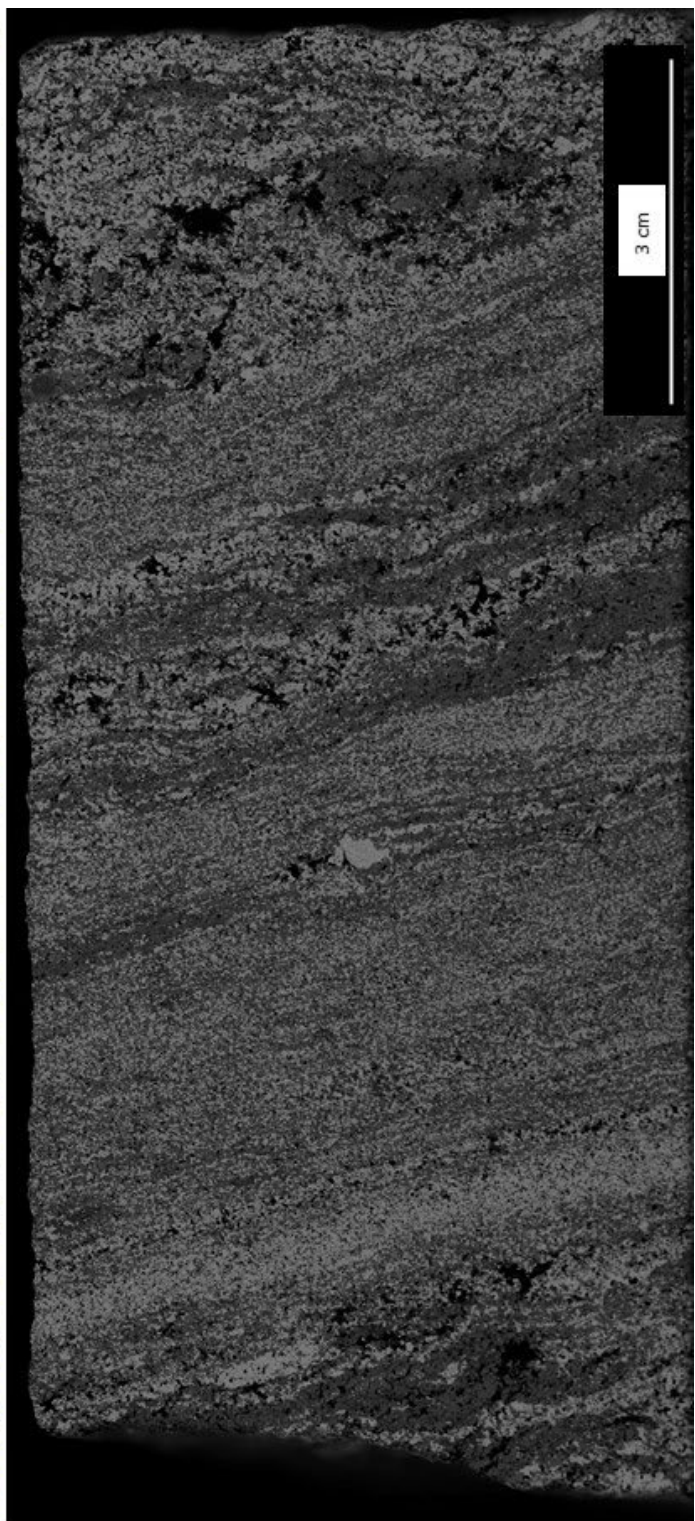
YA4 Element Na



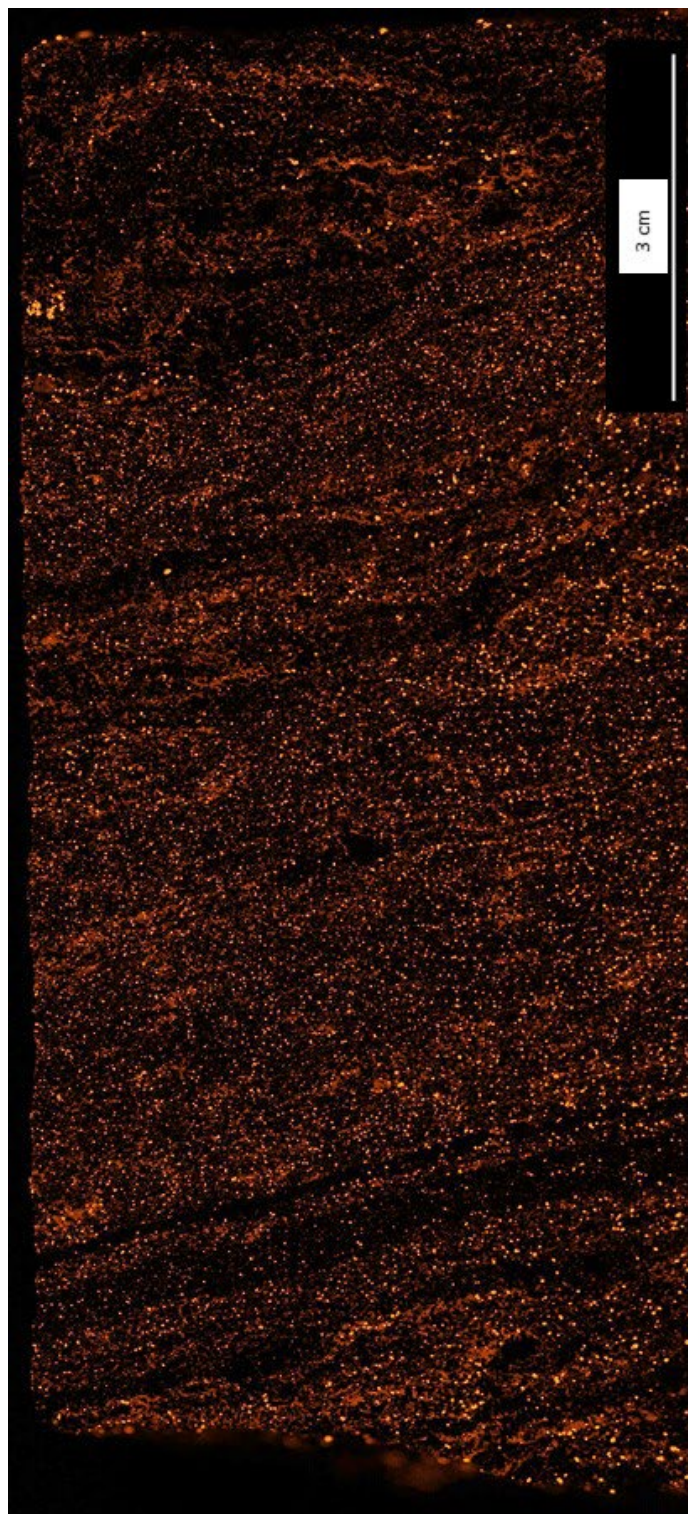
YA4 Element Ni



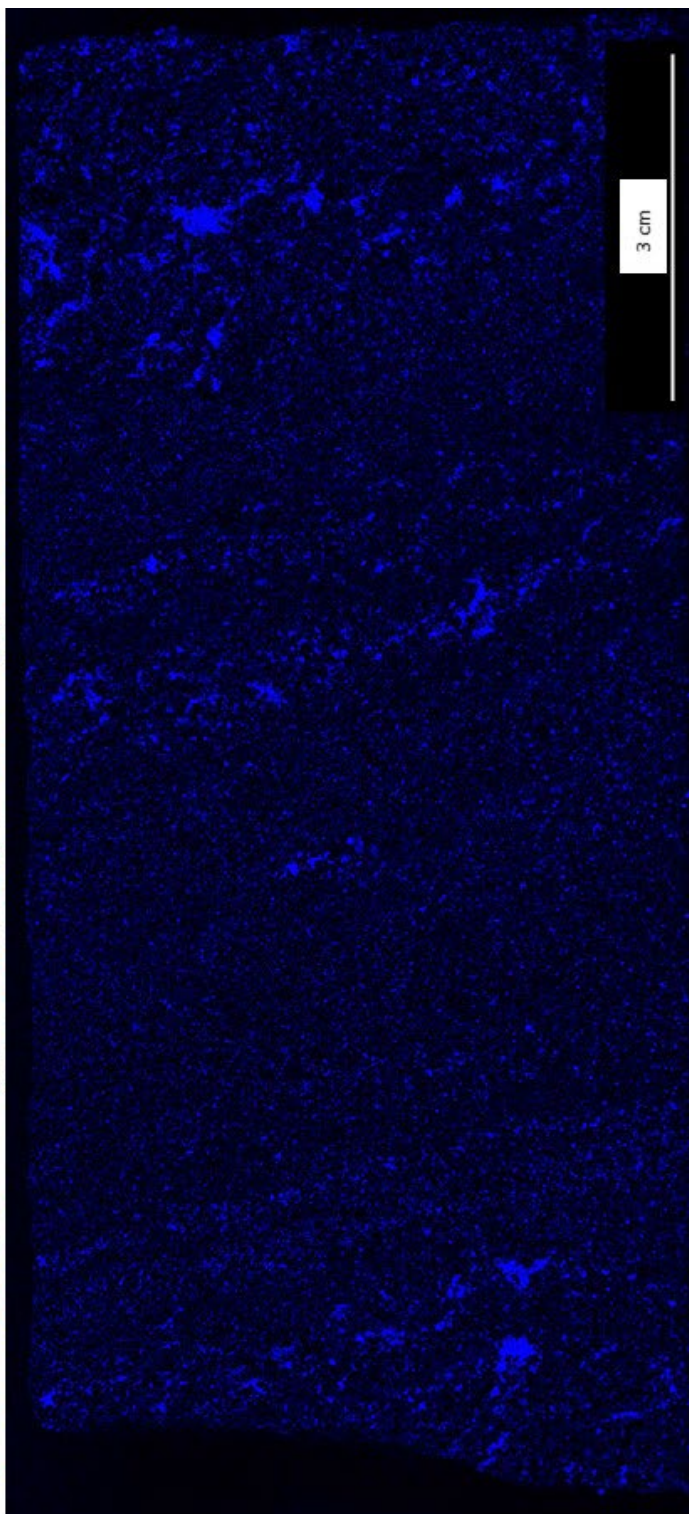
YA4 Element S



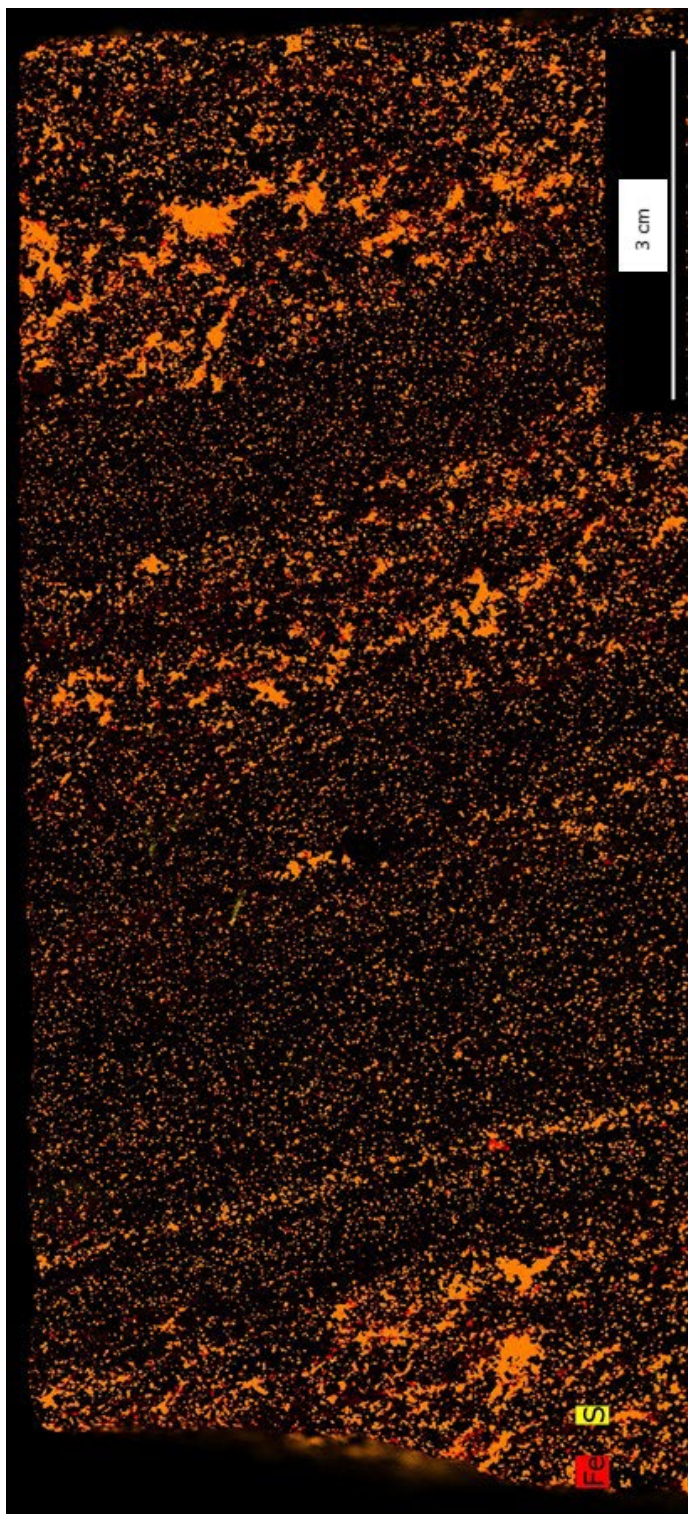
YA4 Element Si



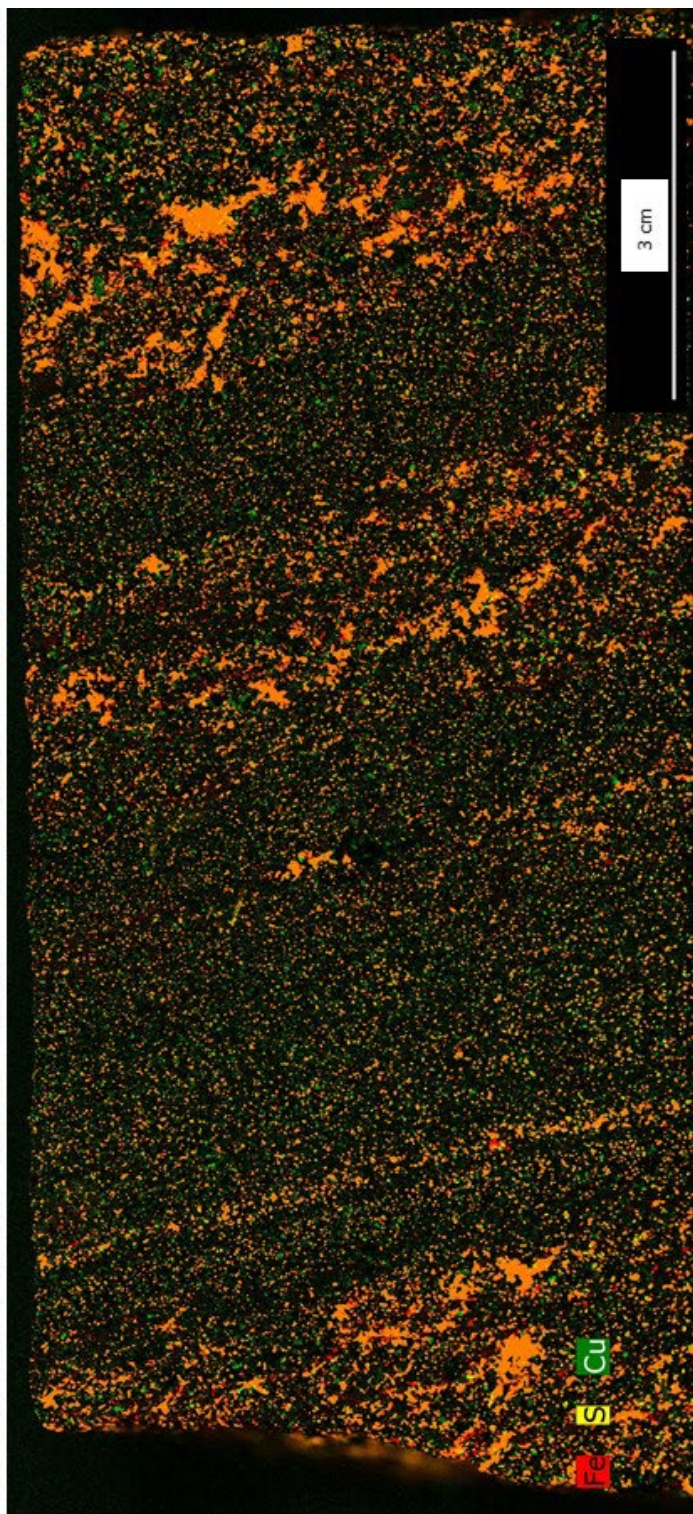
YA4 Element Ti



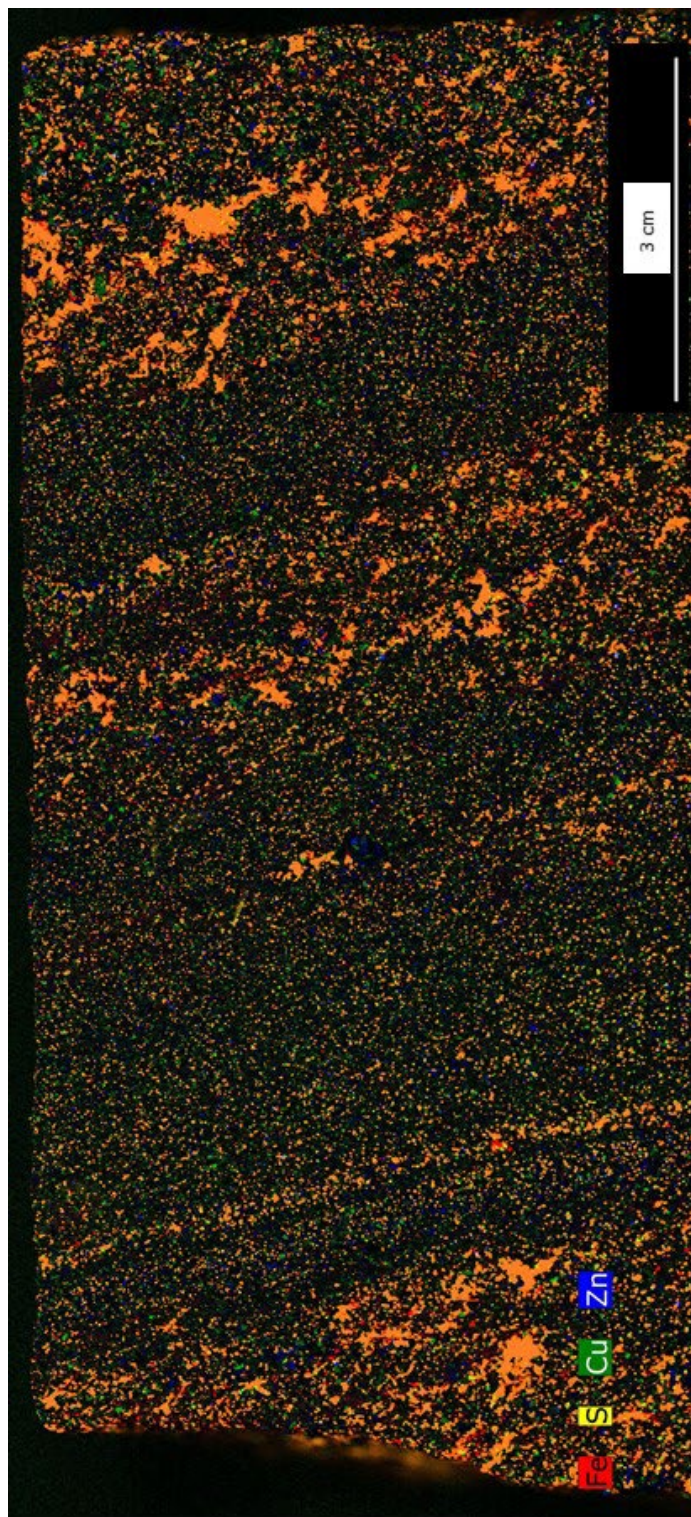
YA4 Element Zn



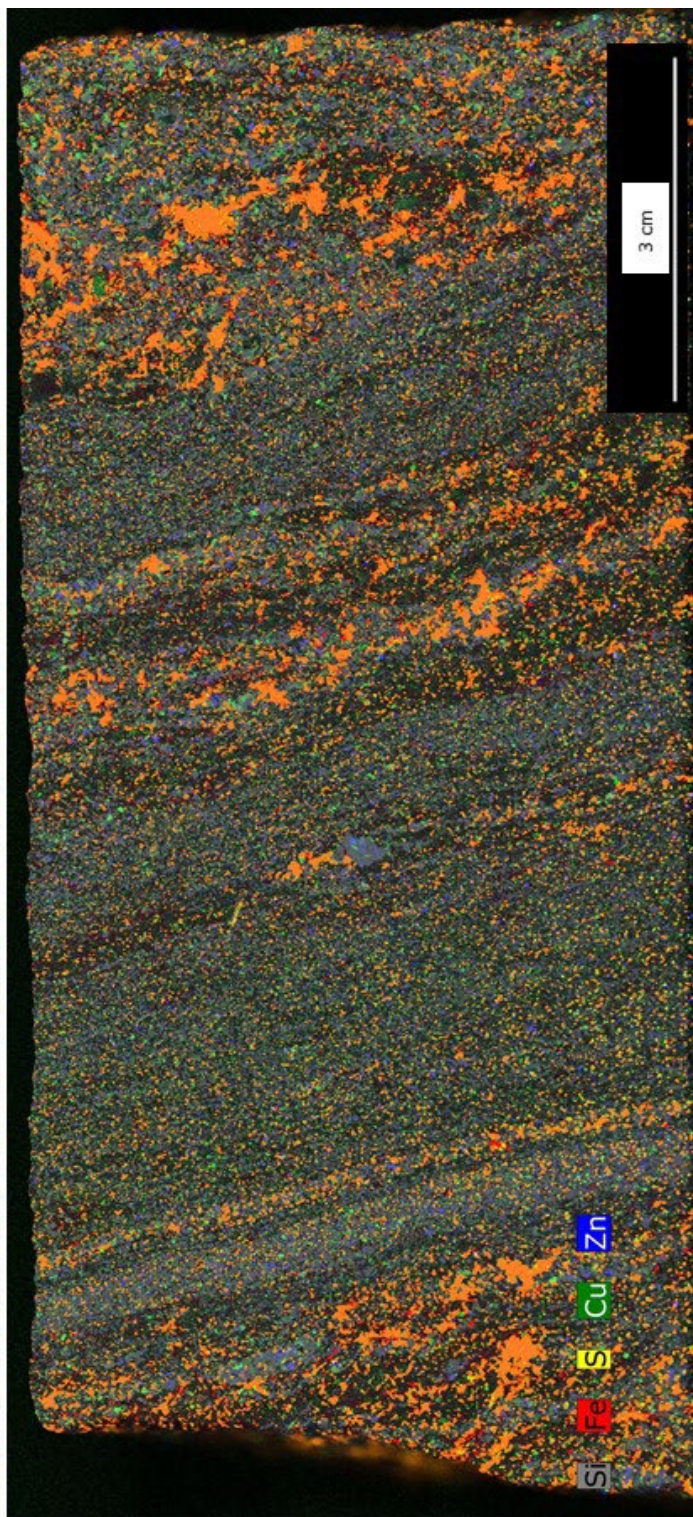
YA4 Fe-S



YA4 Fe-S-Cu

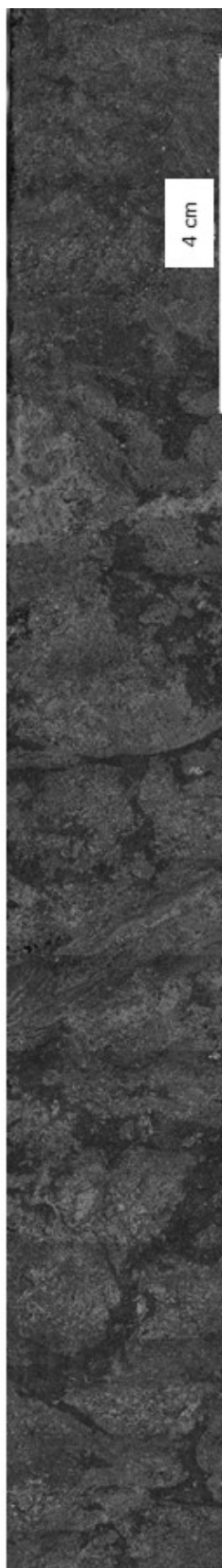


YA4 Fe-S-Cu-Zn



YA4 Si-Fe-S-Cu-Zn

26.5 Sample ZA5 Scanning Micro-XRF



Mapping parameters

Width:	5900 pixel
	177 mm
Height:	830 pixel
	24.9 mm
Pixel Size:	30 µm
Total number of pixel:	4897000 pixel

Acquisition parameters

Frame count:	0
Pixel time:	10 ms/pixel
Measure time:	10:42 h
Overall time:	14:32 h
Stage speed:	3.0 mm/s
Stage position (X,Y,Z):	19.528;65.454;111.814 mm

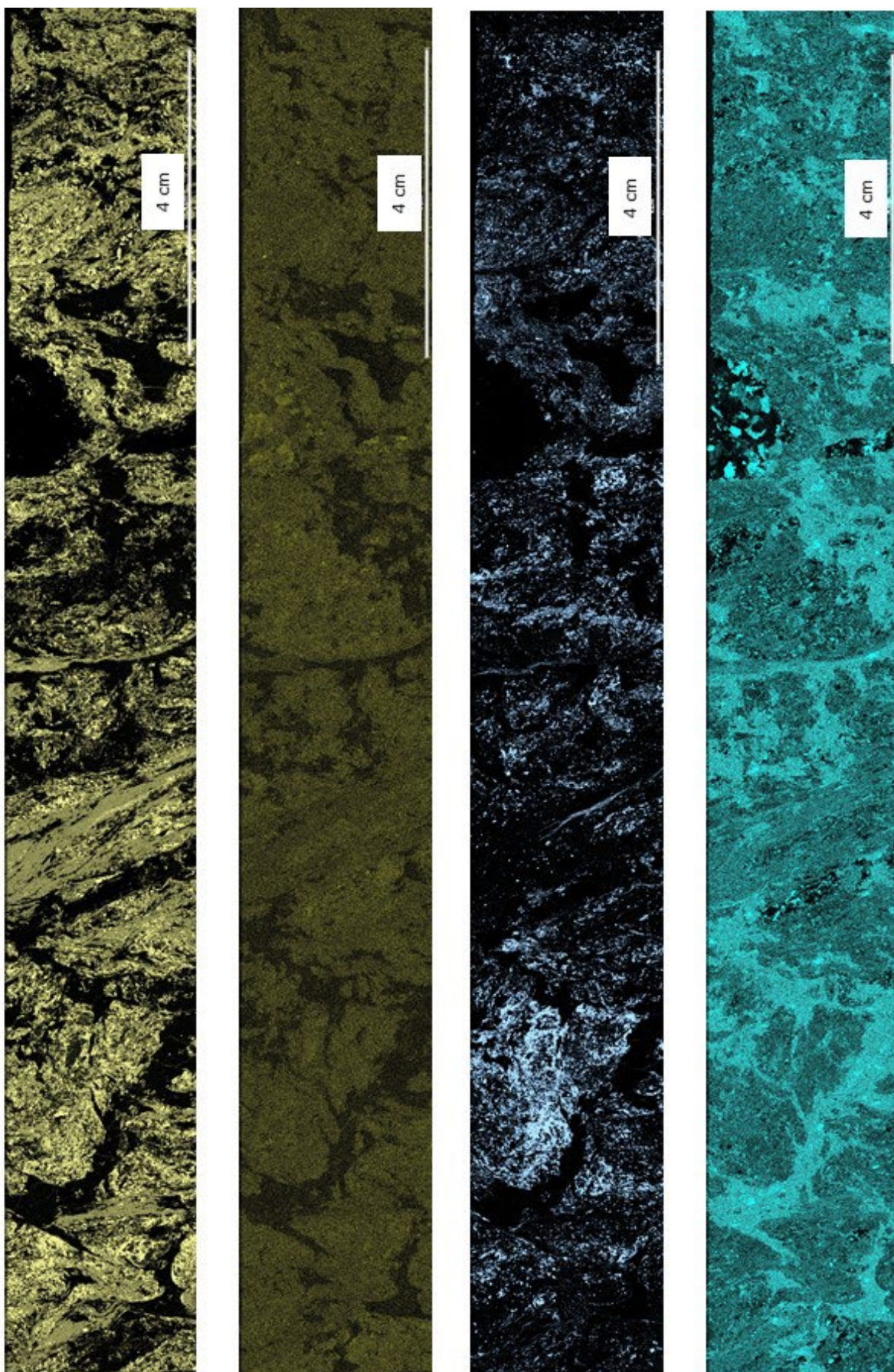
Tube parameter

High voltage:	50 kV
Anode current:	600 µA
Filter:	Empty
Optic:	Lens
Collimator diameter:	0
SpotSize:	20
Chamber at:	Air 2 mbar
Flow rate:	--- l/min
Anode:	Rh

Detector parameters

Selected detectors:	1,2
Max. pulse throughput:	275000 cps

Raw Image – Sample ZA5

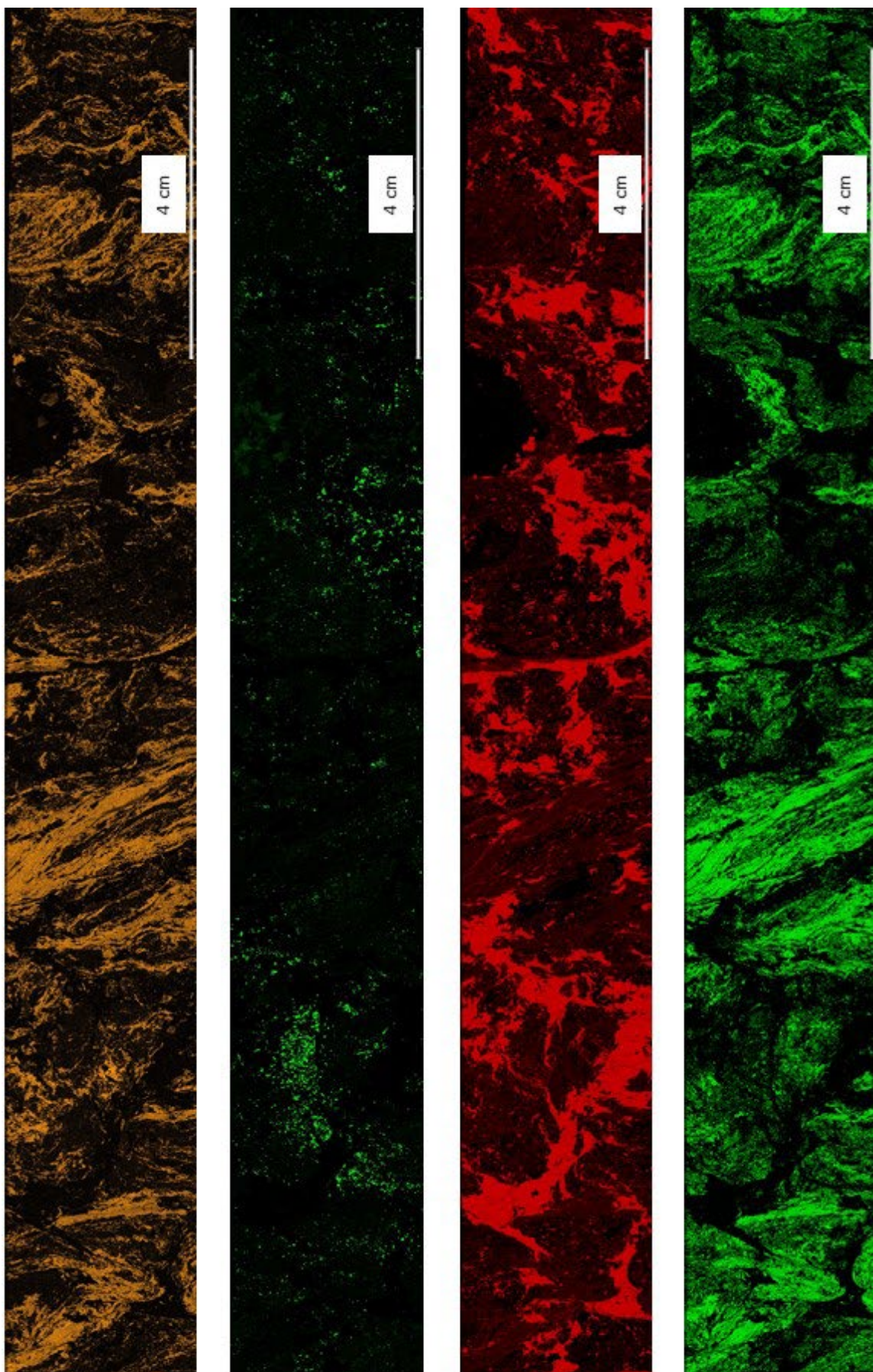


ZA5 Element Al

ZA5 Element As

ZA5 Element Ca

ZA5 Element Co

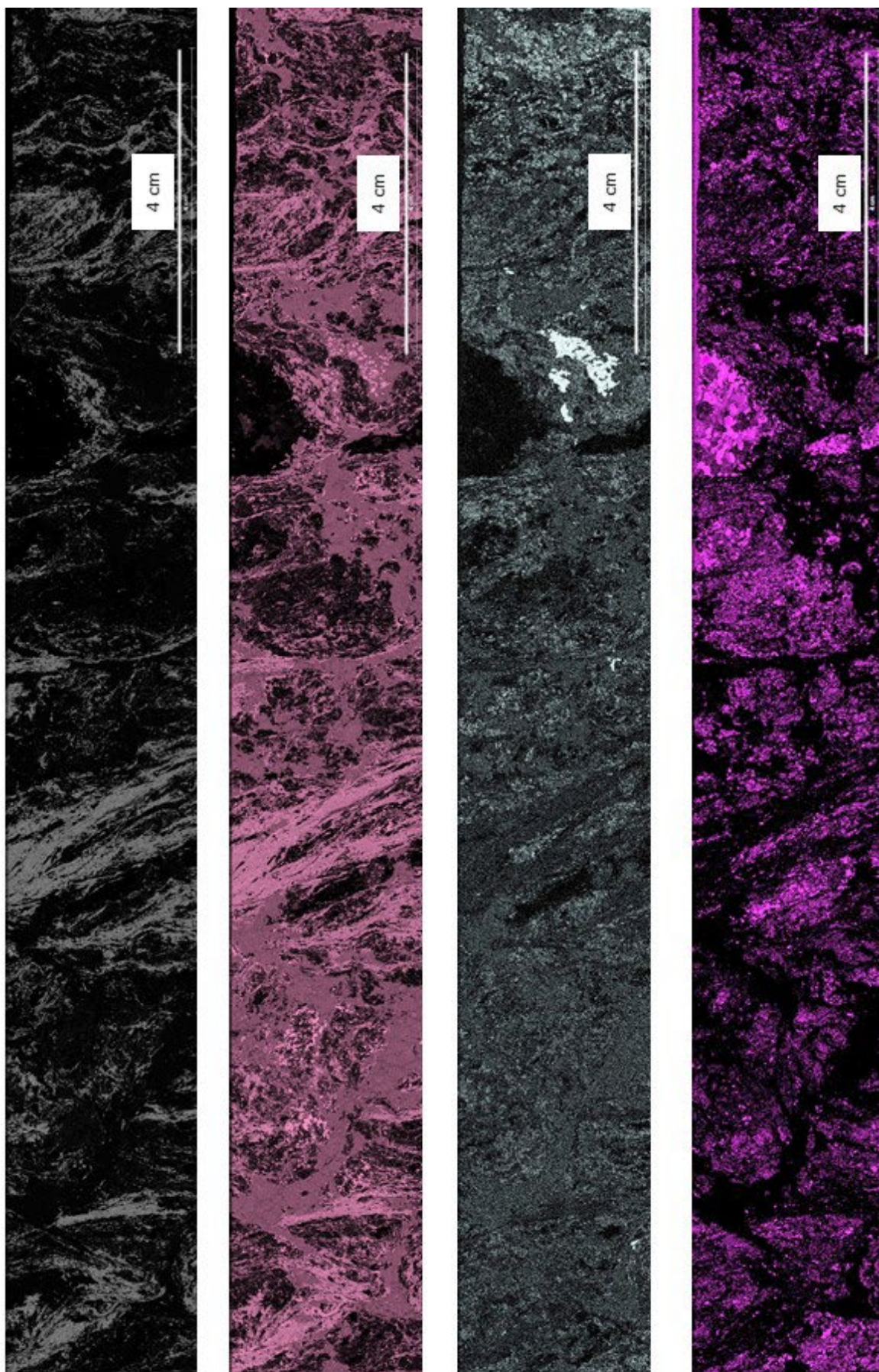


ZA5 Element Cr

ZA5 Element Cu

ZA5 Element Fe

ZA5 Element K

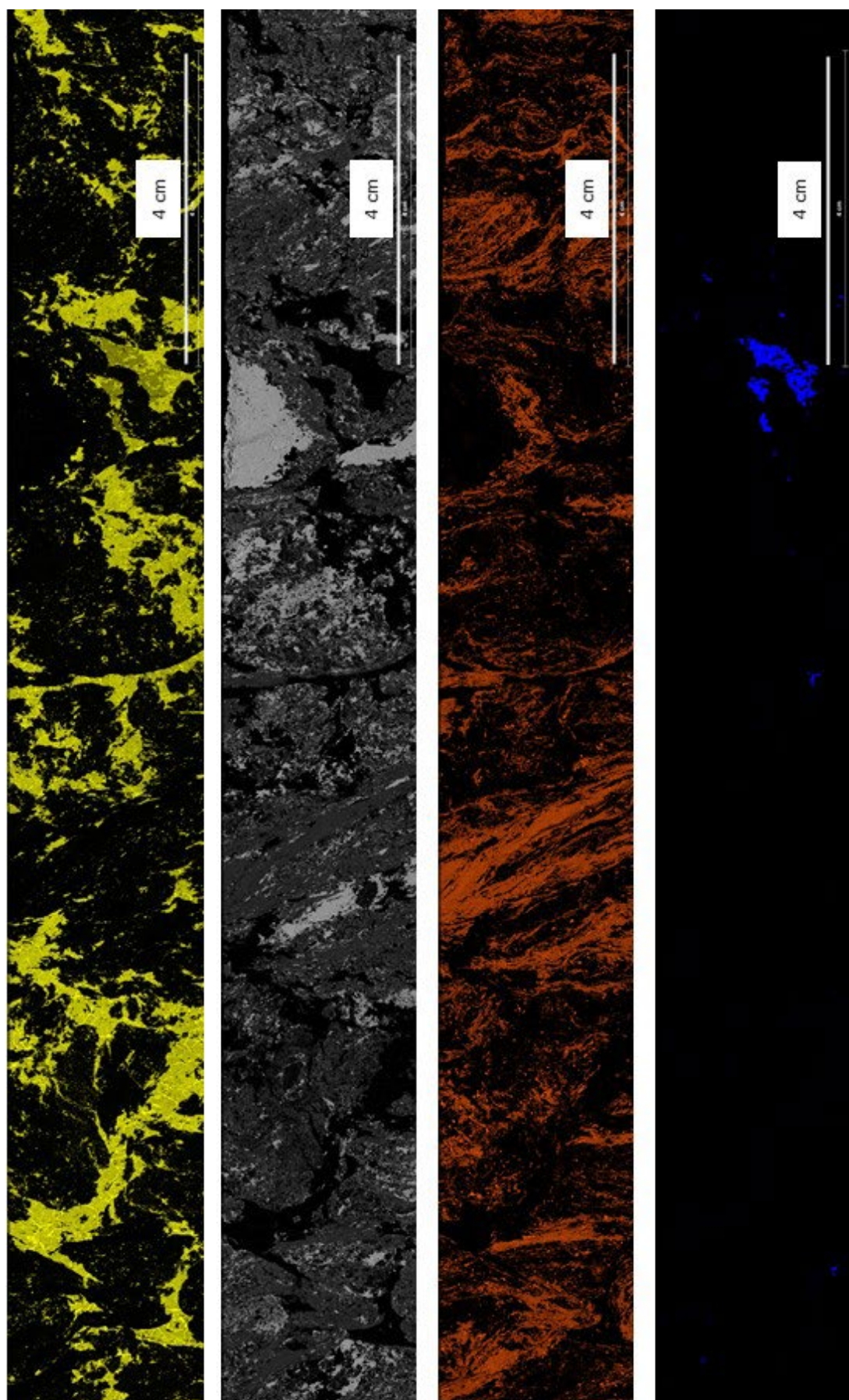


ZA5 Element Mg

ZA5 Element Mn

ZA5 Element Na

ZA5 Element Ni

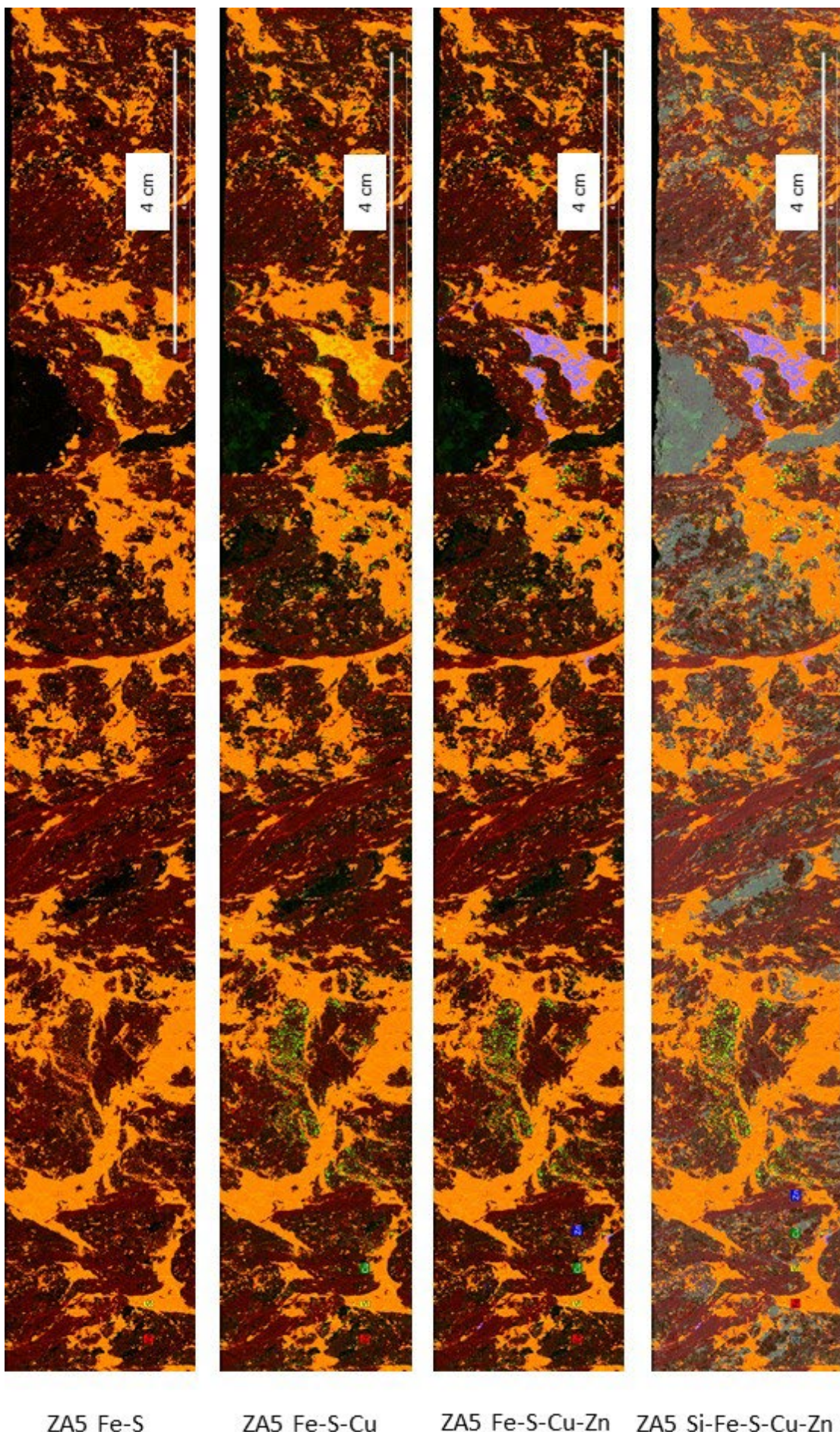


ZA5 Element S

ZA5 Element Si

ZA5 Element Ti

ZA5 Element Zn



27 APPENDIX H - MAJOR AND TRACE ELEMENTS (ICP-OES / MS - XMS)

Table H1. Major elements (ICP-OES/MS-XMS)

Method Sample	Al2O3 ICP-OES %	SiO2 ICP-OES %	TiO2 ICP-OES %	Fe2O3 ICP-OES %	MnO ICP-OES %	MgO ICP-OES %	CaO ICP-OES %	Na2O ICP-OES %	K2O ICP-OES %	P2O5 ICP-OES %
PA1-C	10.95	51.86	0.50	12.34	0.06	3.96	3.04	1.48	2.15	0.13
QA2-C	12.29	55.51	0.55	9.89	0.06	3.44	2.96	1.99	2.49	0.16
XA3-C	11.76	59.71	0.54	9.50	0.05	2.57	2.83	2.43	1.96	0.18
YA4-C	12.34	60.42	0.62	8.62	0.05	2.62	2.41	2.68	2.31	0.18
ZA5-C	11.93	54.24	0.54	10.25	0.06	3.79	2.98	1.81	2.35	0.13
Pilot Tails Eastern	12.51	64.54	0.48	9.53	0.05	2.50	2.51	2.48	2.28	0.15
Pilot Tails Western	12.74	62.02	0.53	9.61	0.06	3.07	2.64	2.38	2.52	0.18

Note: Sulphur values can be treated as semi-quantitative.

Table H2-1. Trace elements (ICP-OES/MS-XMS)

Method Sample	S ICP-OES mg/kg	Be ICP-MS mg/kg	Sc ICP-OES mg/kg	V ICP-MS mg/kg	Cr ICP-MS mg/kg	Co ICP-MS mg/kg	Ni ICP-MS mg/kg	Cu ICP-MS mg/kg	Zn ICP-MS mg/kg	Ga ICP-MS mg/kg	Rb ICP-MS mg/kg
PA1-C	30405.20	2.38	0.70	1313.56	194.10	63.36	238.12	432.36	3084.12	20.33	121.01
QA2-C	27541.70	2.30	0.52	1281.15	181.14	30.71	197.89	262.84	1858.72	21.58	130.70
XA3-C	32047.21	2.27	0.47	644.64	92.54	18.61	128.33	92.90	656.38	18.84	110.56
YA4-C	33156.57	2.45	0.72	399.21	92.01	18.81	99.15	99.14	315.90	22.43	119.59
ZA5-C	39628.49	2.64	0.65	1297.79	206.66	25.19	139.25	348.37	3615.18	22.72	146.13
Pilot Tails Eastern	28122.41	1.99	0.67	564.46	149.40	22.58	169.32	74.04	908.63	18.38	99.63
Pilot Tails Western	26664.62	2.30	0.83	817.16	207.86	29.52	214.88	230.61	1774.52	21.92	121.15

Note: Sulphur values can be treated as semi-quantitative.

Table H2-2. Trace elements (ICP-OES/MS-XMS)

Method Sample	Sr ICP-MS mg/kg	Y ICP-MS mg/kg	Zr ICP-MS mg/kg	Nb ICP-MS mg/kg	Mo ICP-MS mg/kg	Sn ICP-MS mg/kg	Cs ICP-MS mg/kg	Ba ICP-MS mg/kg	La ICP-MS mg/kg	Ce ICP-MS mg/kg	Pr ICP-MS mg/kg
PA1-C	155.37	47.02	147.06	13.10	129.39	0.70	3.03	349.68	50.30	90.21	12.65
QA2-C	209.46	35.91	194.38	15.51	112.06	0.52	3.65	435.93	53.68	99.97	12.92
XA3-C	235.14	40.24	200.13	13.55	42.38	0.47	4.17	350.06	45.45	83.54	10.81
YA4-C	203.18	30.22	220.68	17.98	28.35	0.72	3.46	411.00	49.90	97.21	11.75
ZA5-C	182.78	38.39	161.25	13.12	116.85	0.65	5.29	399.20	44.09	80.31	11.16
Pilot Tails Eastern	204.70	26.66	153.26	13.20	33.10	0.67	3.56	605.63	69.47	110.21	12.05
Pilot Tails Western	230.14	34.73	191.91	12.38	70.11	0.83	3.85	560.79	116.25	179.70	22.64

Note: Sulphur values can be treated as semi-quantitative.

Table H2-3. Trace elements (ICP-OES/MS-XMS)

Method Sample	Nd ICP-MS mg/kg	Sm ICP-MS mg/kg	Eu ICP-MS mg/kg	Gd ICP-MS mg/kg	Tb ICP-MS mg/kg	Dy ICP-MS mg/kg	Ho ICP-MS mg/kg	Er ICP-MS mg/kg	Tm ICP-MS mg/kg	Yb ICP-MS mg/kg
PA1-C	49.30	9.60	2.02	10.31	1.55	9.38	2.09	5.54	0.91	6.09
QA2-C	50.98	9.89	2.26	9.70	1.48	8.41	1.74	4.74	0.79	4.66
XA3-C	42.04	8.36	1.90	8.29	1.30	7.87	1.77	5.09	0.89	4.86
YA4-C	44.92	8.29	1.85	8.04	1.22	6.86	1.45	4.19	0.65	3.97
ZA5-C	43.68	8.79	1.98	9.12	1.42	8.66	1.86	5.09	0.83	5.44
Pilot Tails Eastern	42.08	6.94	1.72	7.11	0.95	5.42	1.16	3.23	0.49	3.21
Pilot Tails Western	73.26	11.60	2.56	11.57	1.50	8.19	1.70	4.48	0.69	4.64

Note: Sulphur values can be treated as semi-quantitative.

Table H2-4. Trace elements (ICP-OES/MS-XMS)

Method Sample	Lu ICP-MS mg/kg	Hf ICP-MS mg/kg	Ta ICP-MS mg/kg	W ICP-MS mg/kg	Tl ICP-MS mg/kg	Pb ICP-MS mg/kg	Th ICP-MS mg/kg	U ICP-MS mg/kg
PA1-C	1.02	5.46	1.70	7.31	4.13	2.86	14.40	21.35
QA2-C	0.78	6.72	1.92	6.10	3.09	1.05	15.41	15.27
XA3-C	0.77	6.81	2.34	3.98	2.33	1.85	12.89	10.57
YA4-C	0.64	8.34	2.05	2.92	3.05	3.17	13.99	6.70
ZA5-C	0.95	5.67	1.87	5.72	5.05	2.67	15.21	23.28
Pilot Tails Eastern	0.52	5.48	1.71	4.21	2.83	4.44	12.39	7.70
Pilot Tails Western	0.72	6.67	1.54	5.45	5.09	5.64	19.93	15.04

Note: Sulphur values can be treated as semi-quantitative.

28 APPENDIX I – X-RAY DIFFRACTION (QXRD) SPECTRA OF SAMPLES MEASURED



Figure I1 - X-Ray Diffraction (XRD) spectra of Sample PA1 – 1

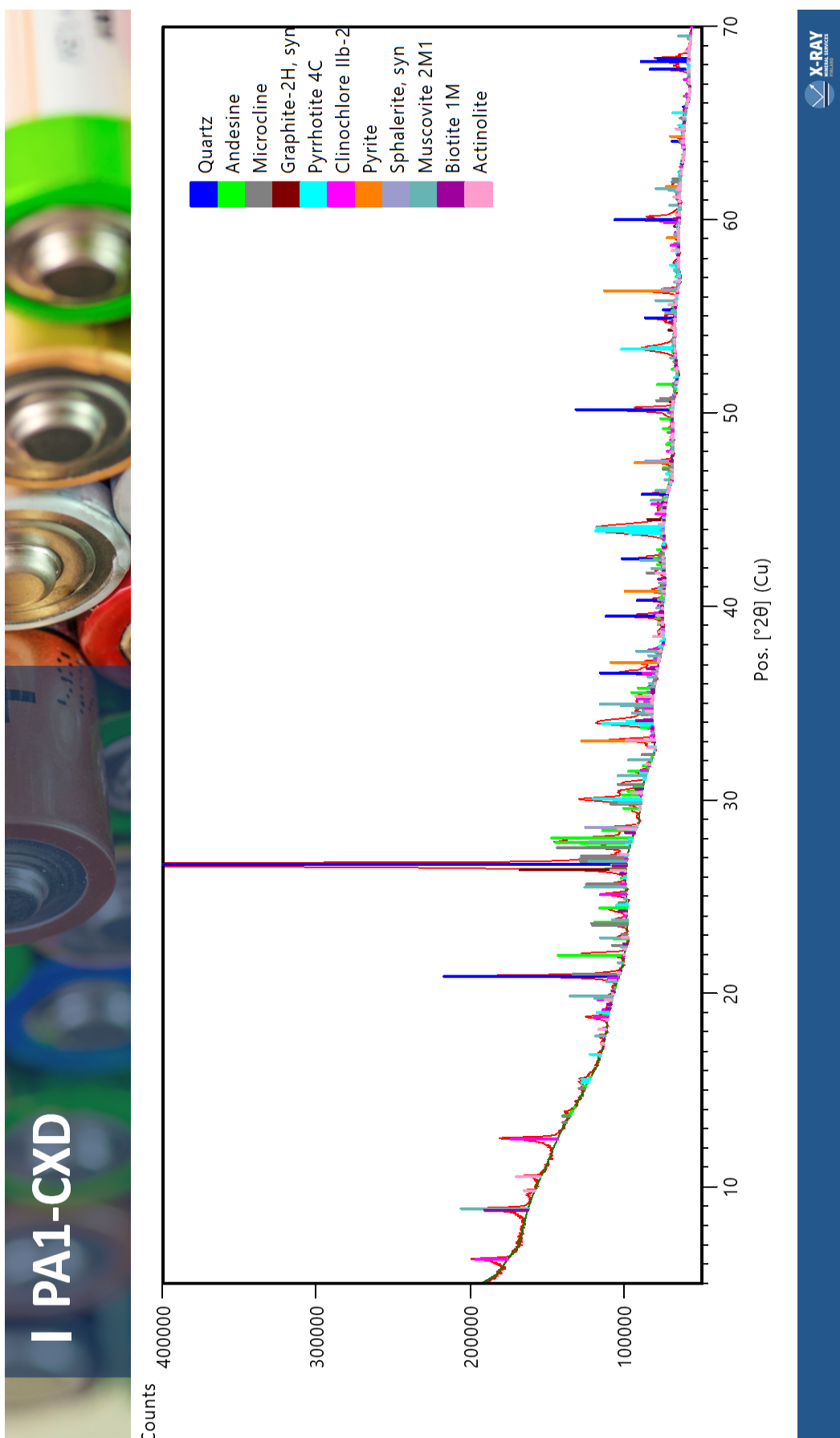


Figure I2 - X-Ray Diffraction (XRD) spectra of Sample PA1 - 2

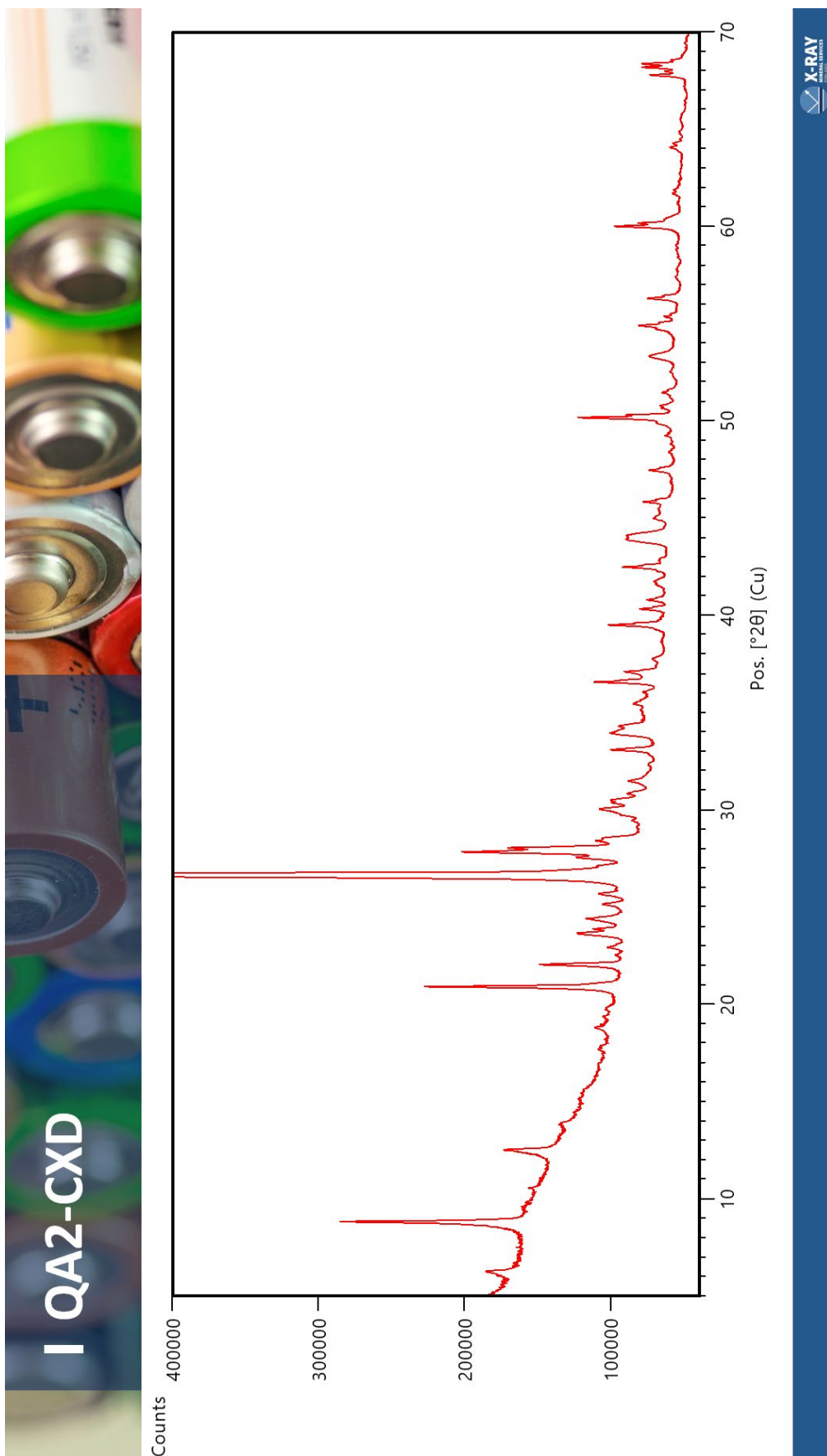


Figure I3 - X-Ray Diffraction (XRD) spectra of Sample QA2 - 1

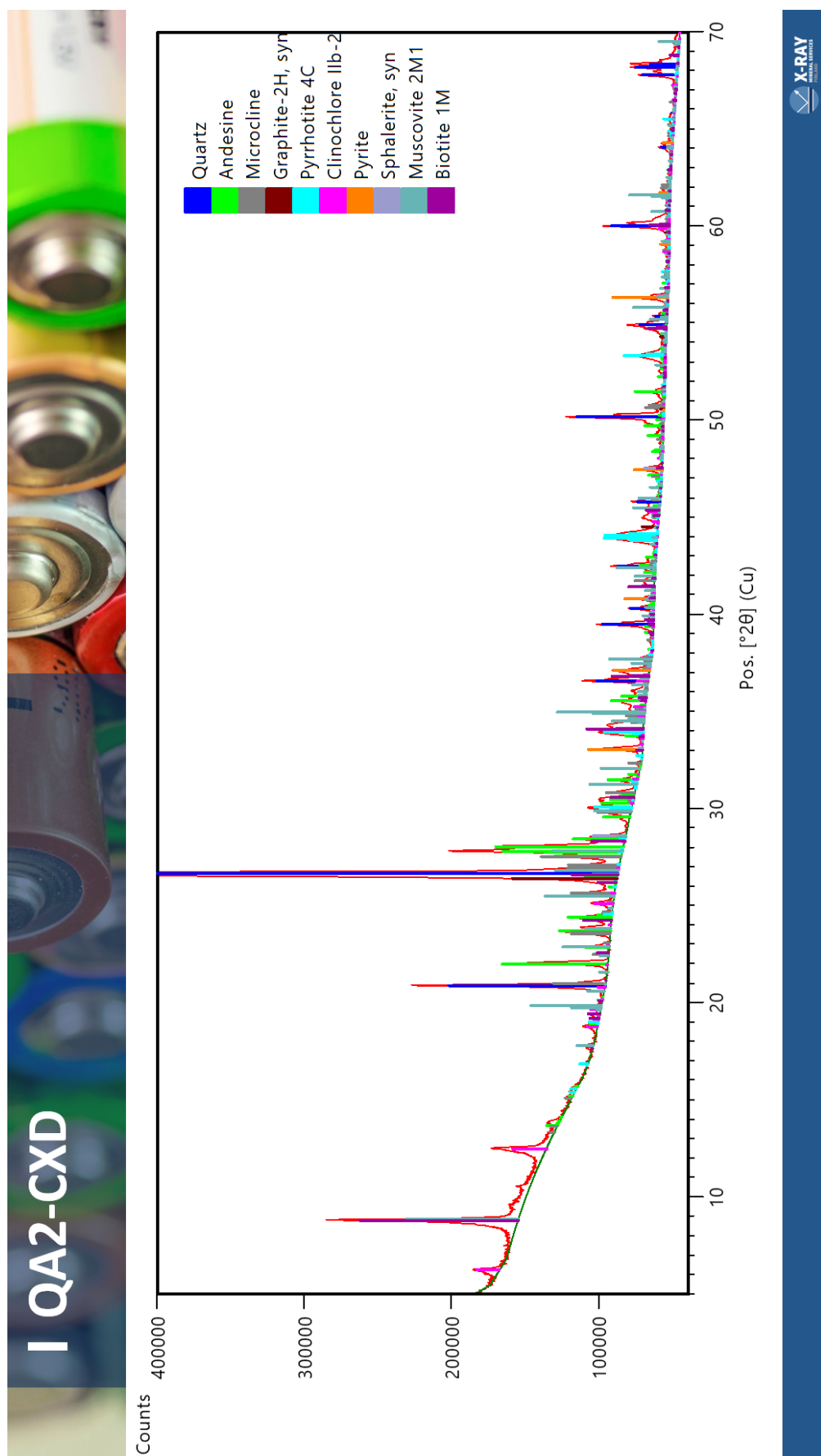


Figure I4 - X-Ray Diffraction (XRD) spectra of Sample QA2 - 2

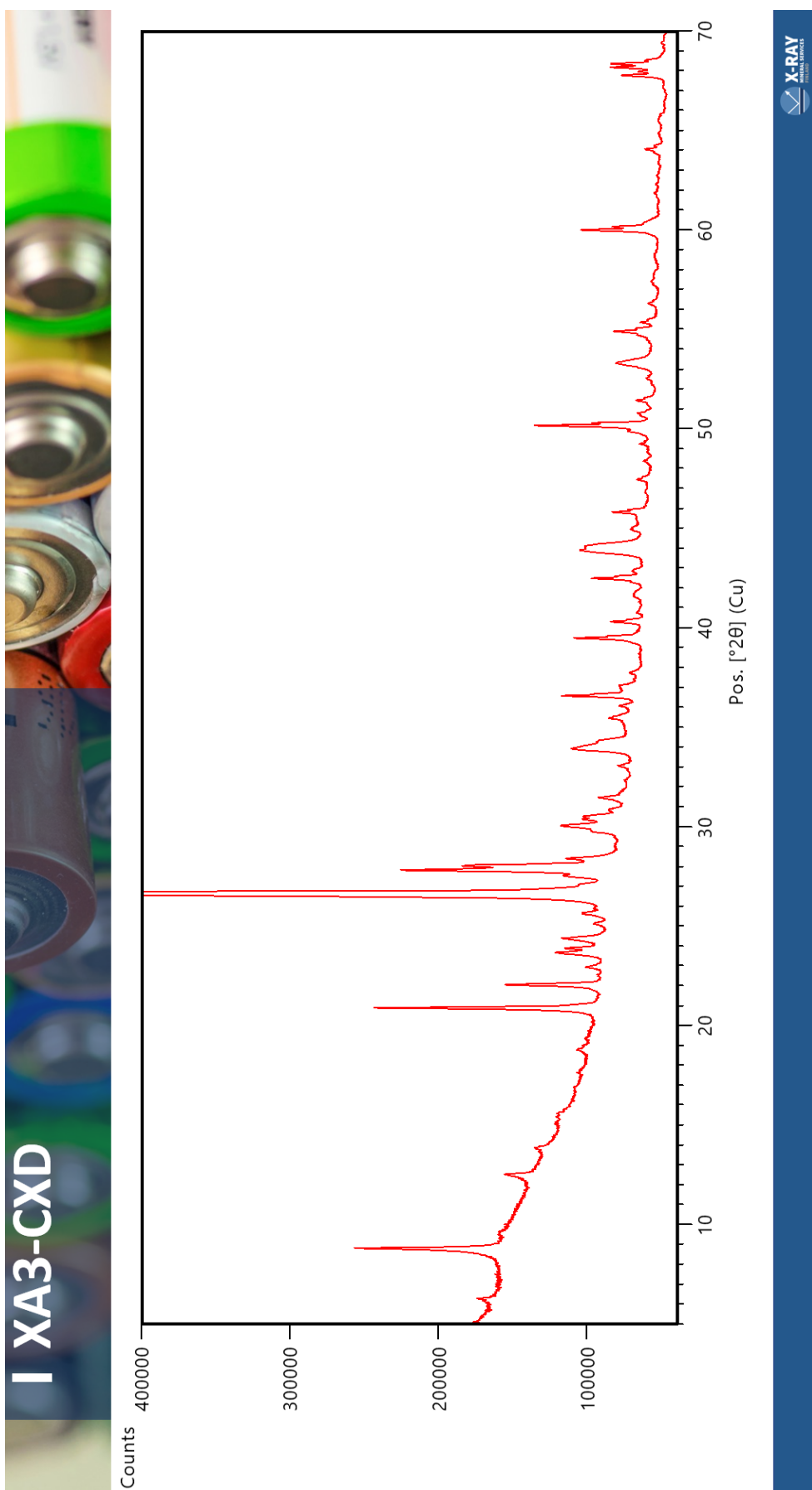


Figure I5 - X-Ray Diffraction (XRD) spectra of Sample XA3 - 1

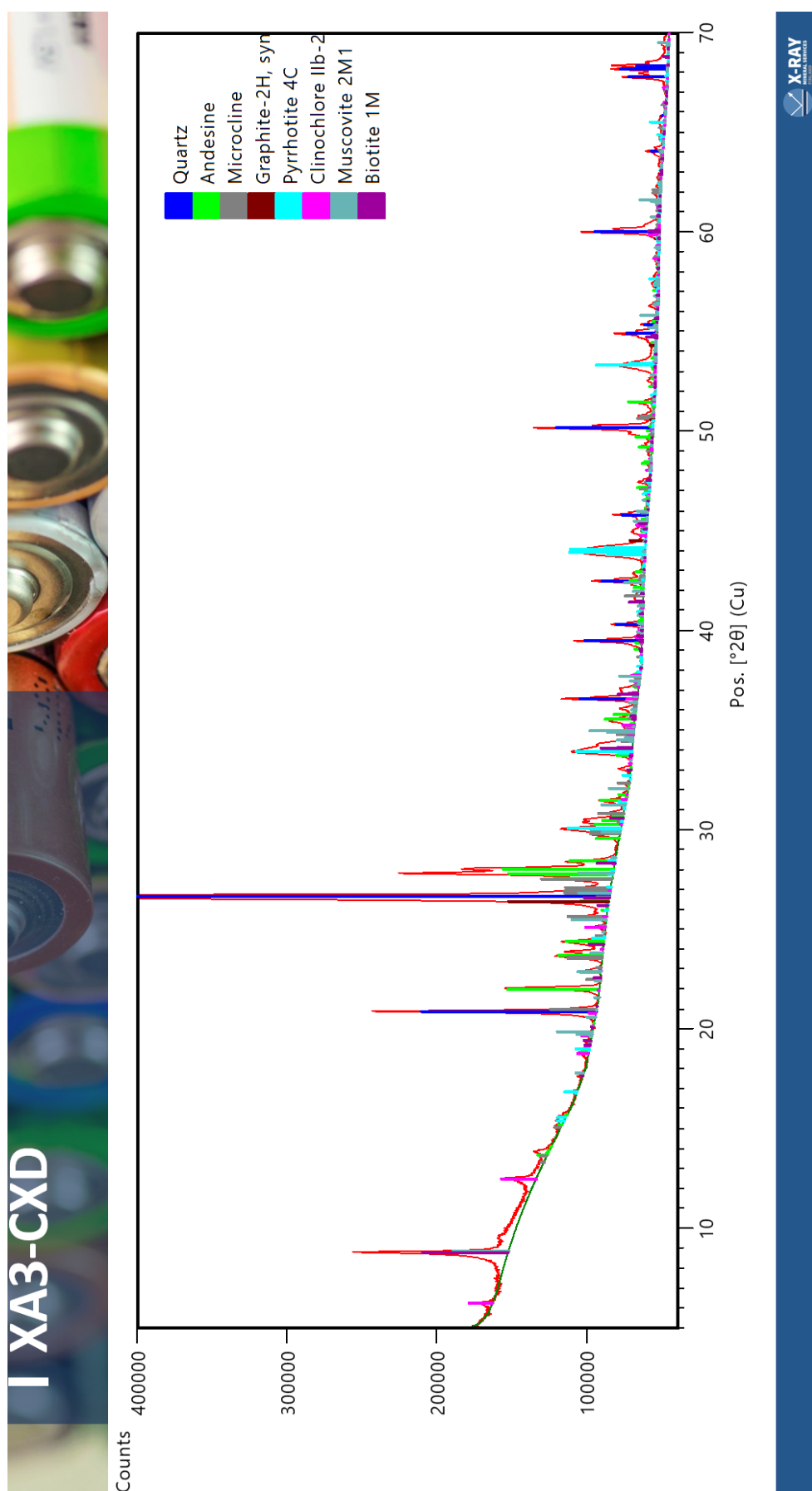


Figure I6 - X-Ray Diffraction (XRD) spectra of Sample XA3 - 2

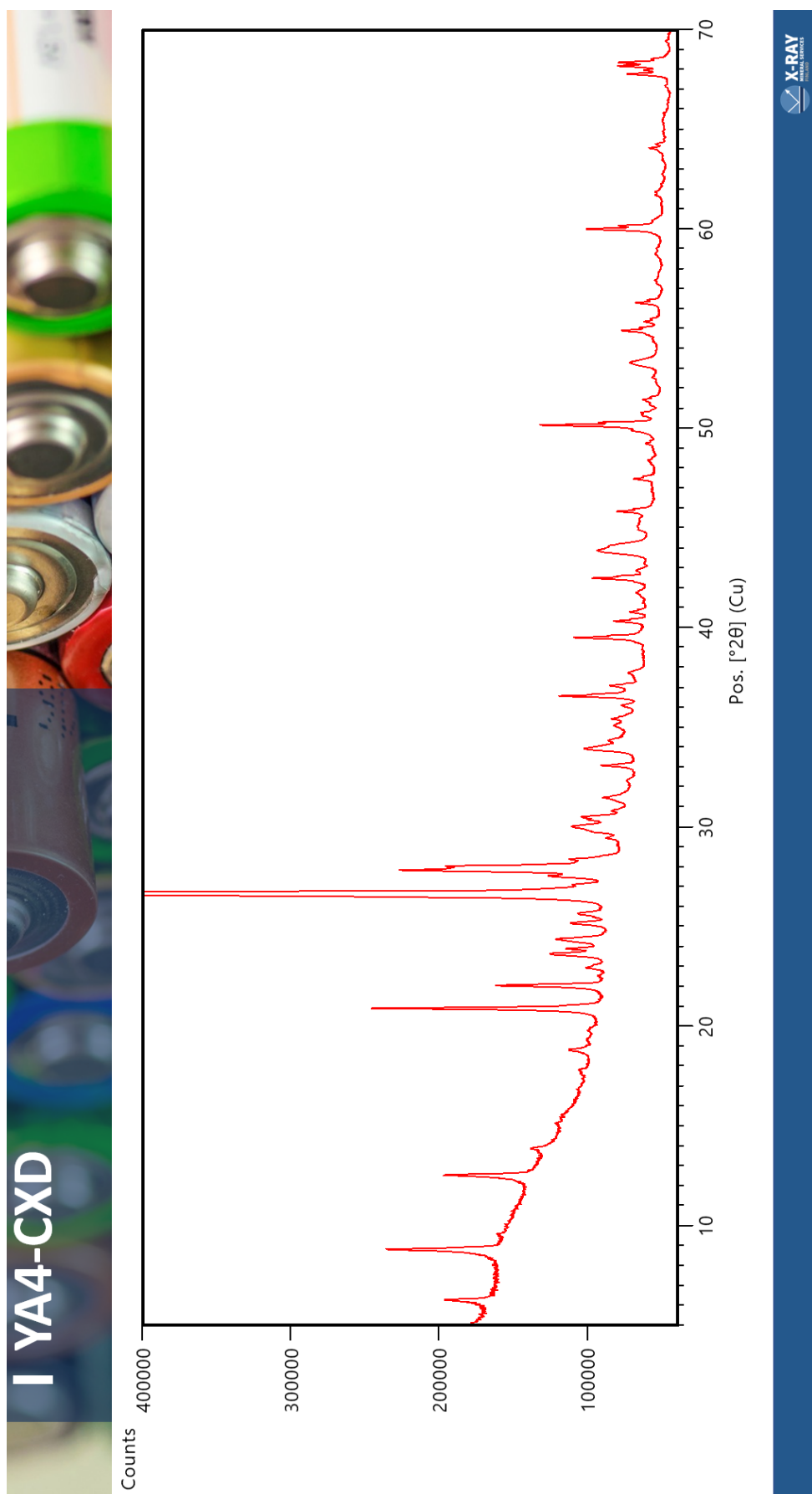


Figure I7 - X-Ray Diffraction (XRD) spectra of Sample YA4 -1

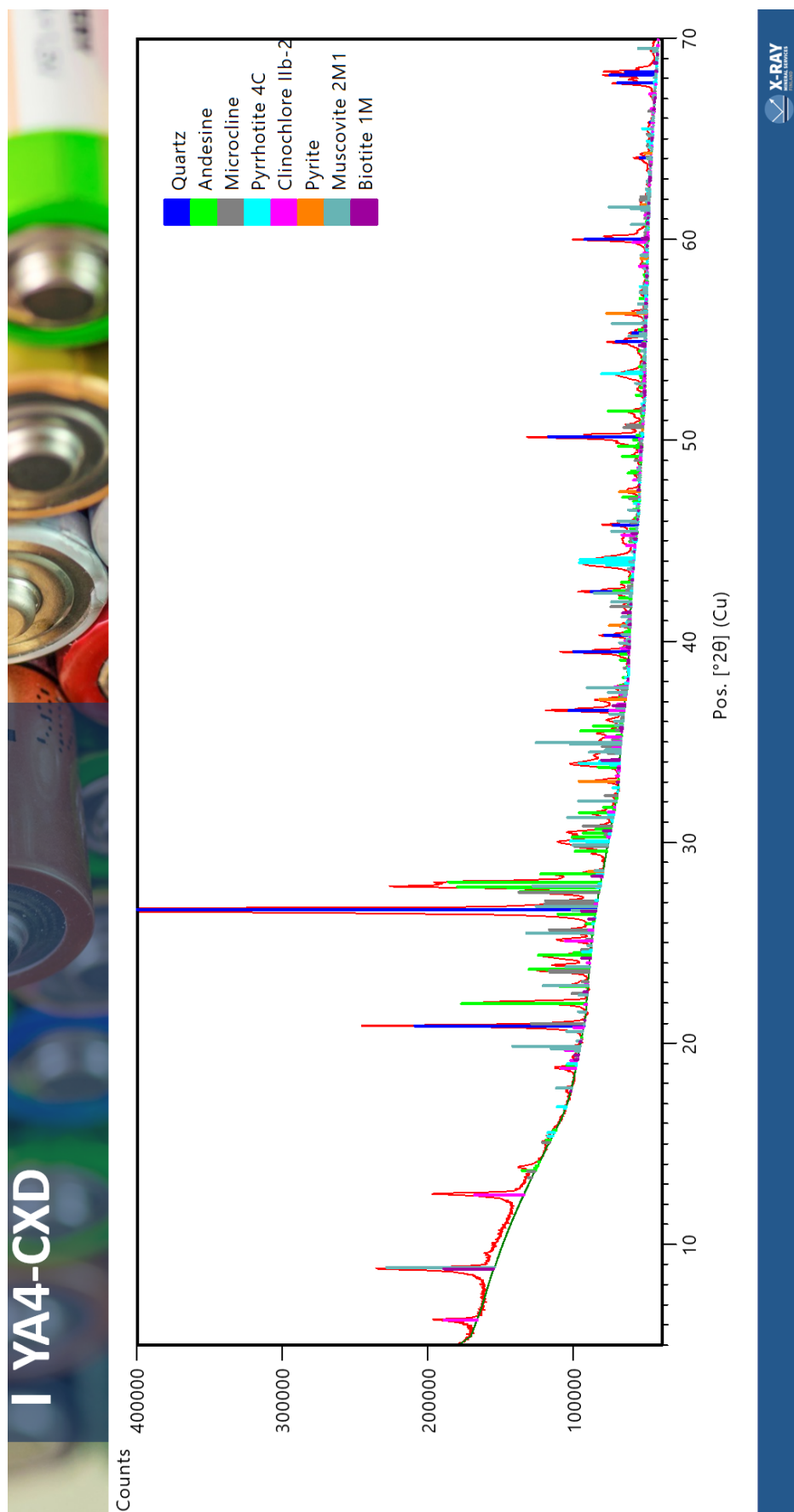


Figure I8 - X-Ray Diffraction (XRD) spectra of Sample YA4 - 2

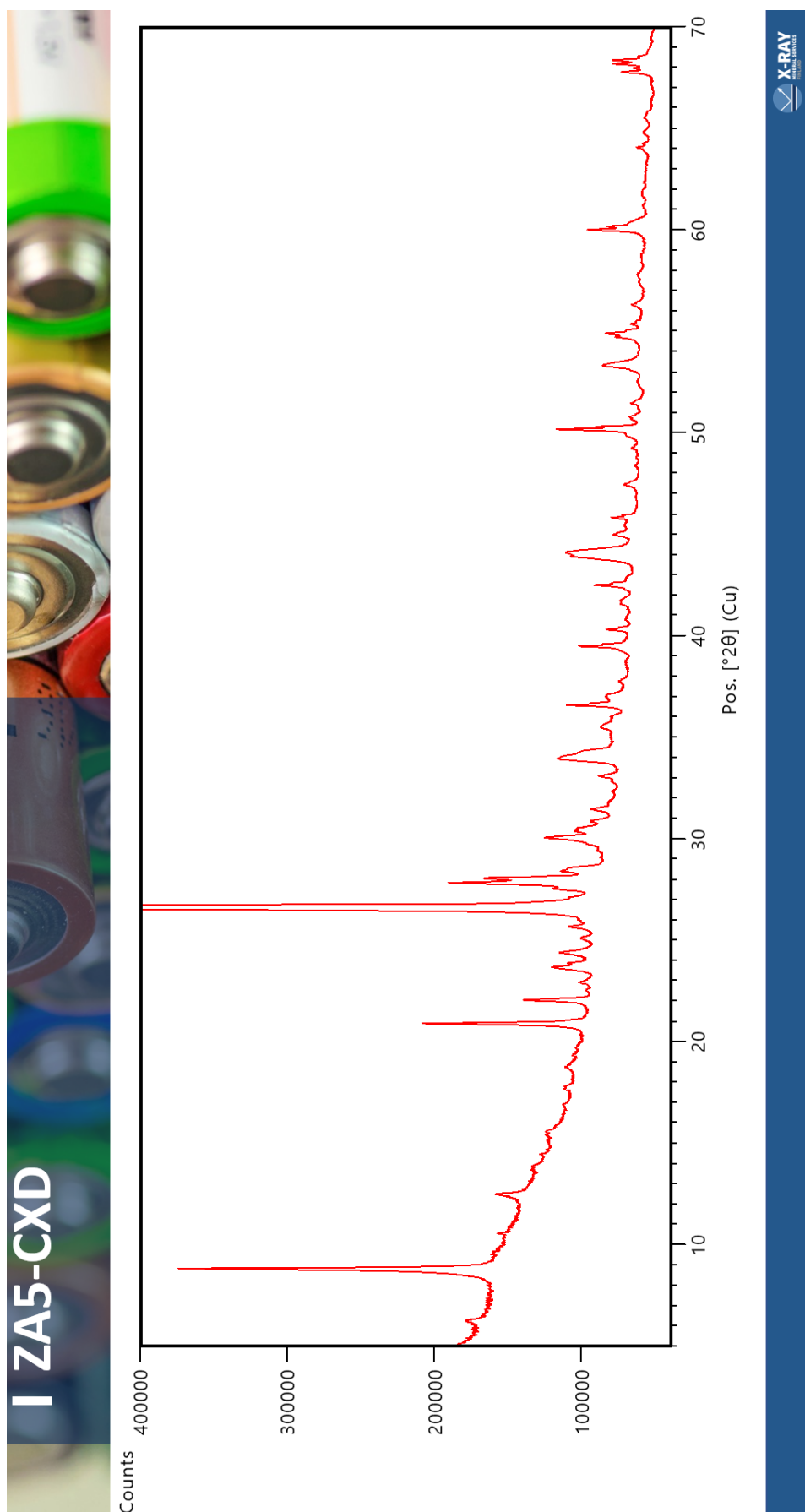


Figure I9 - X-Ray Diffraction (XRD) spectra of Sample ZA5 - 1

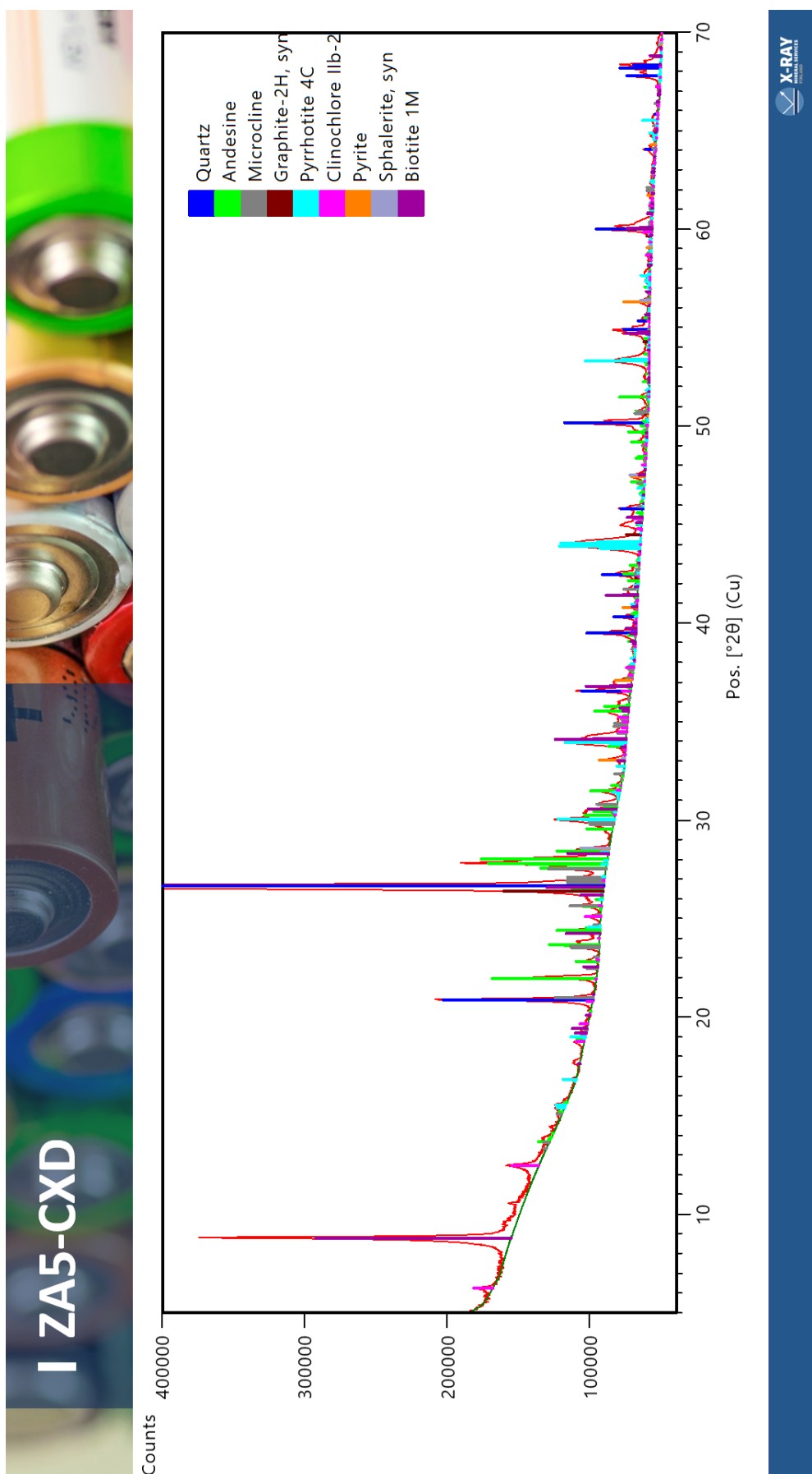


Figure I10 - X-Ray Diffraction (XRD) spectra of Sample ZA5 - 2

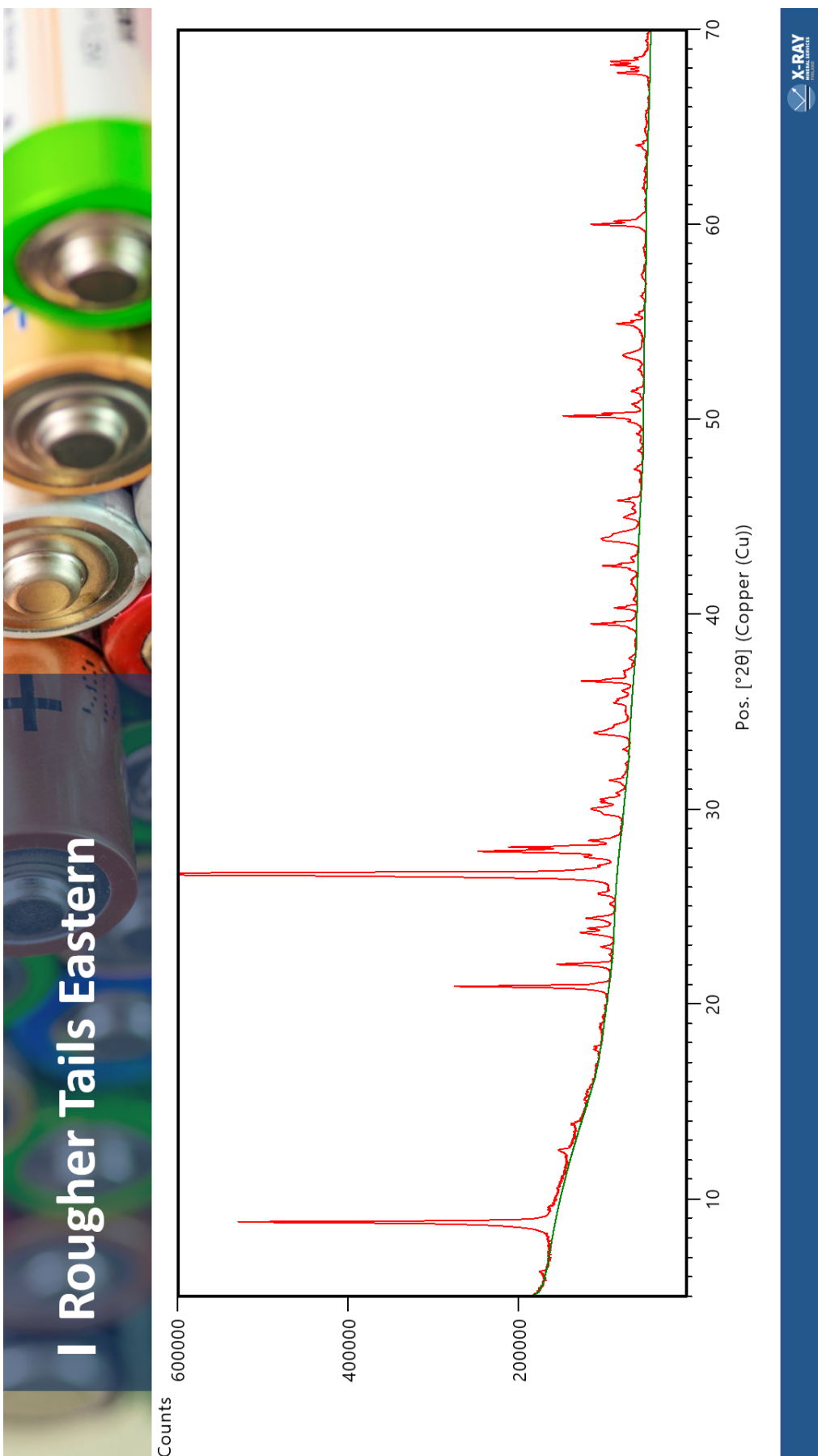


Figure I11 - X-Ray Diffraction (XRD) spectra of Aitolampi Pilot Tailings Eastern - 1

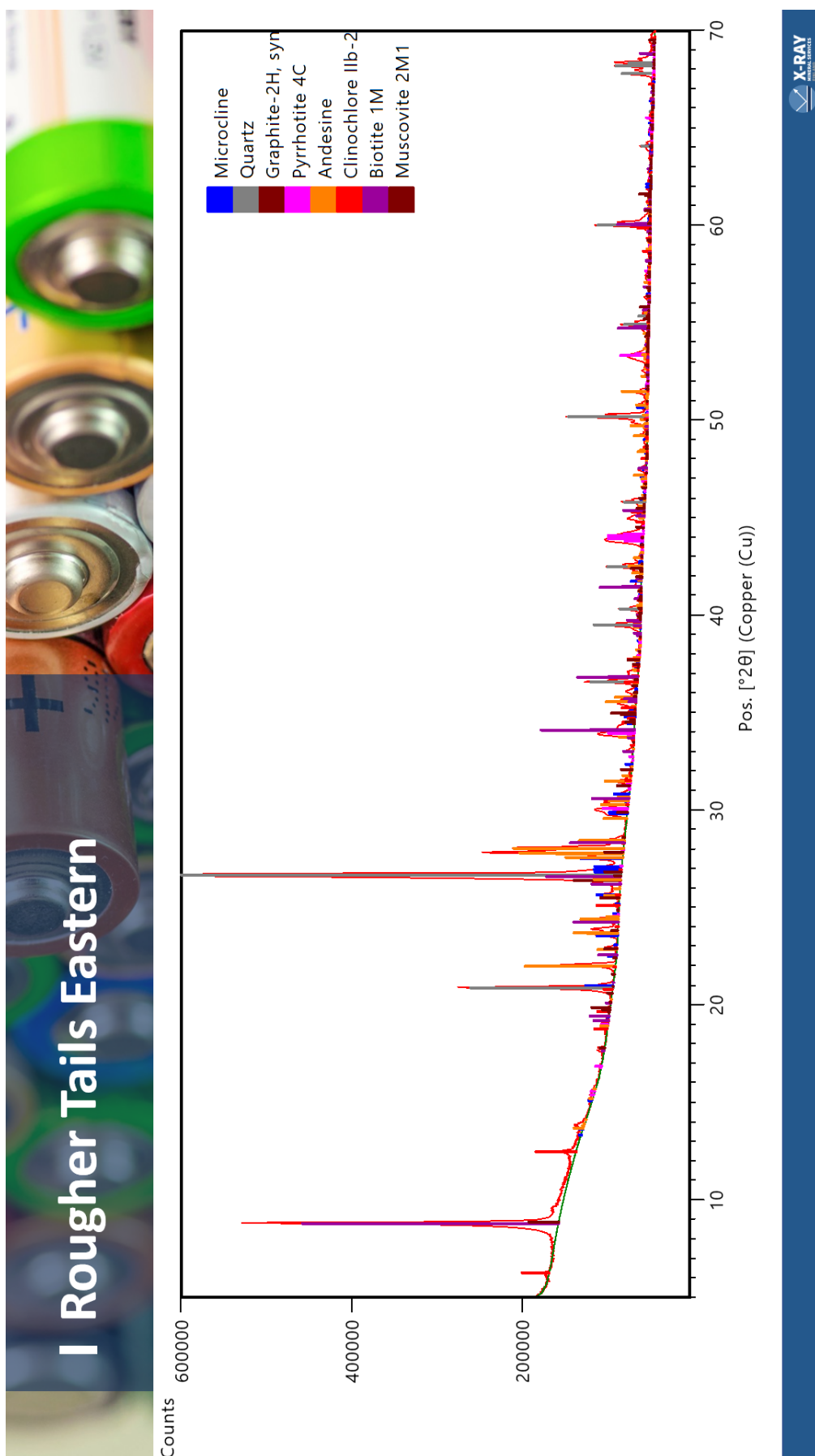


Figure I12 - X-Ray Diffraction (XRD) spectra of Aitolampi Pilot Tailings Eastern - 2

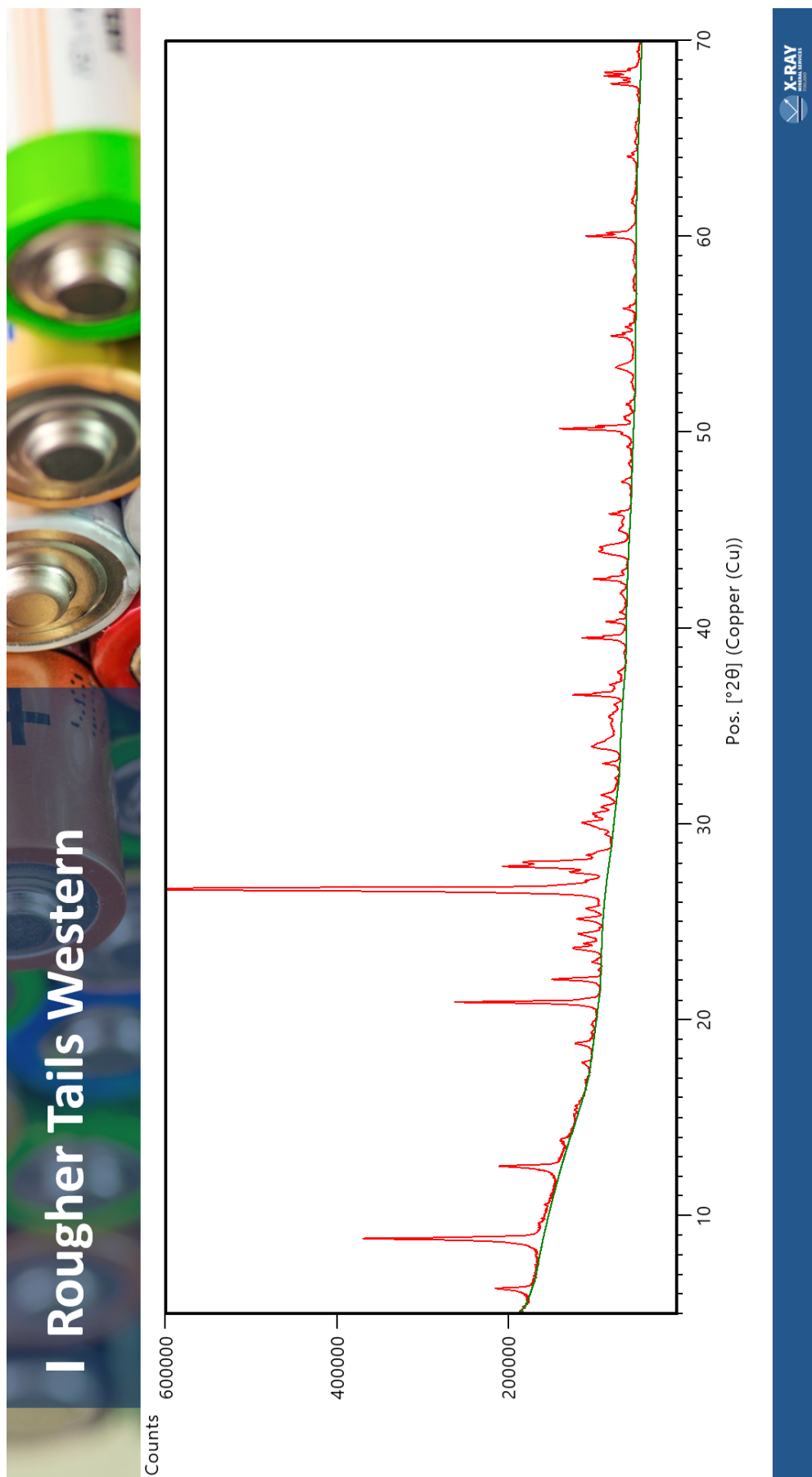


Figure I13 - X-Ray Diffraction (XRD) spectra of Aitolampi Pilot Tailings Western - 1

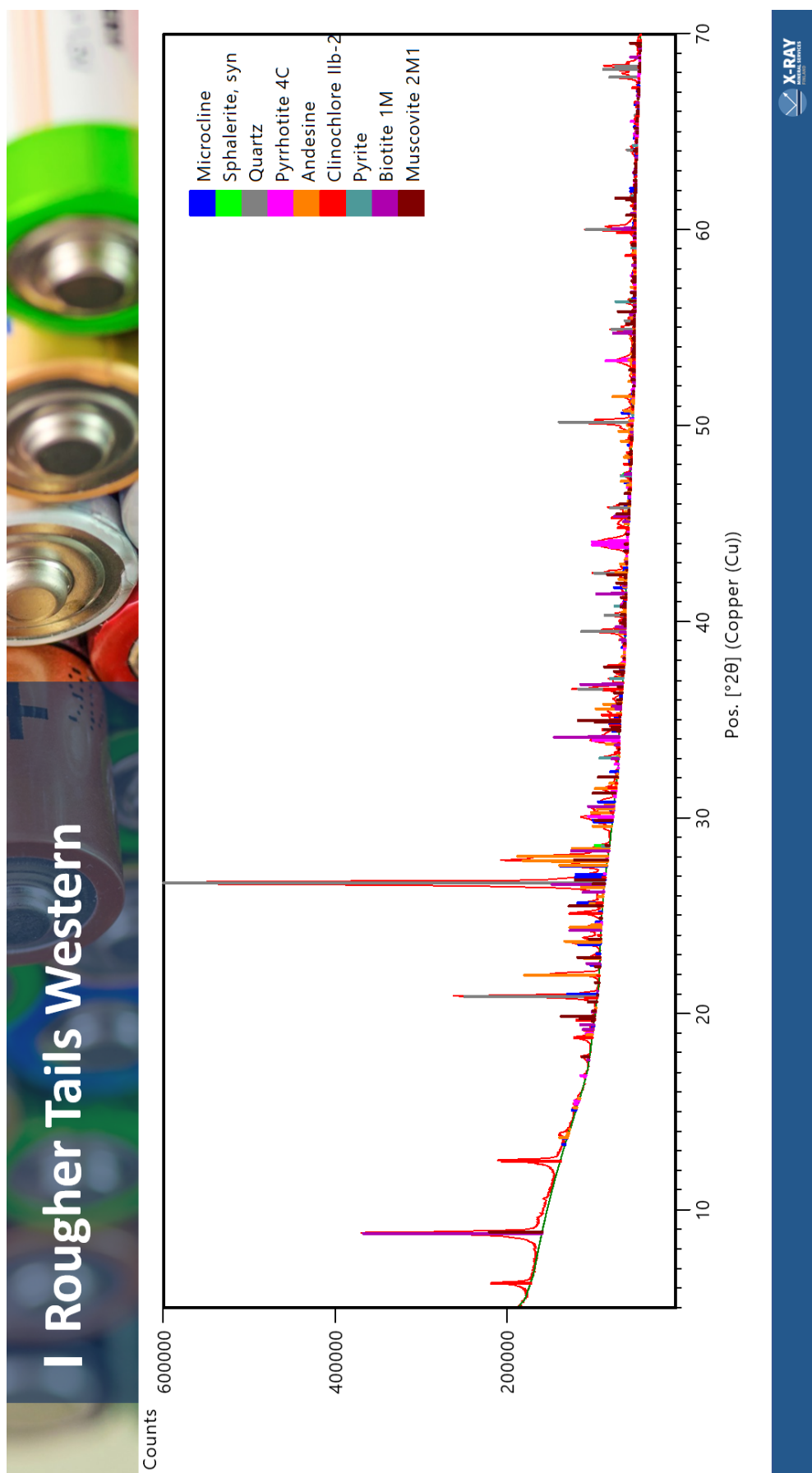
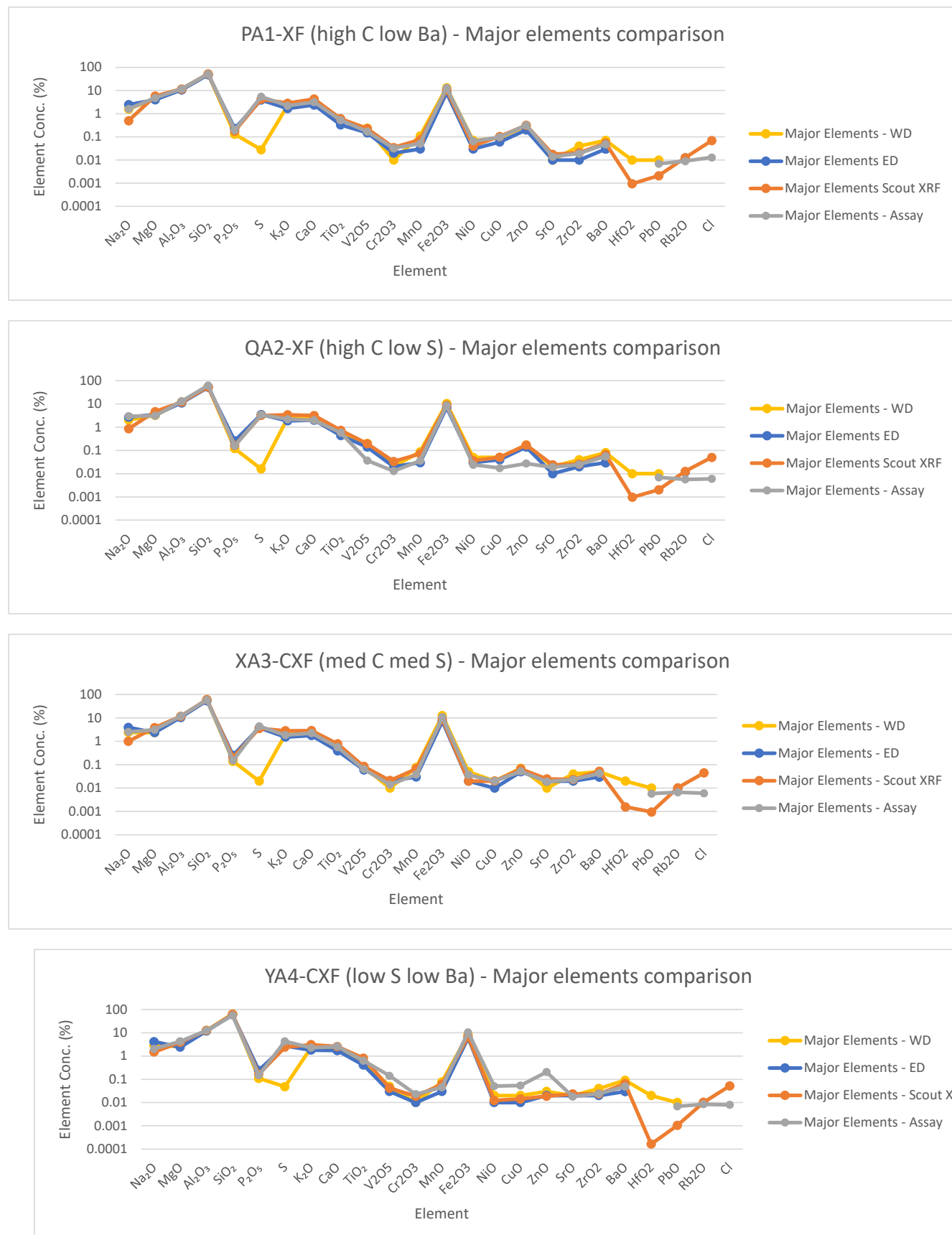
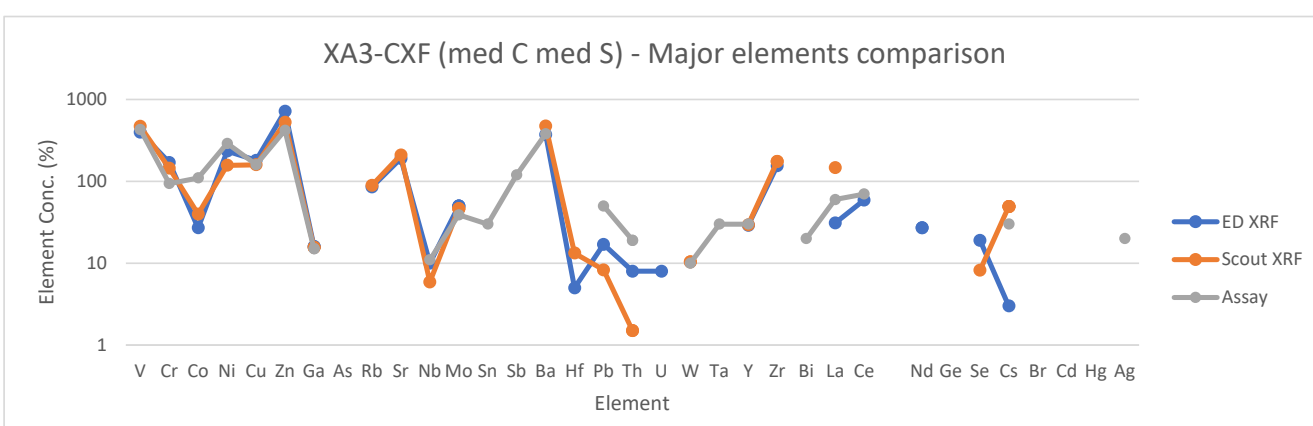
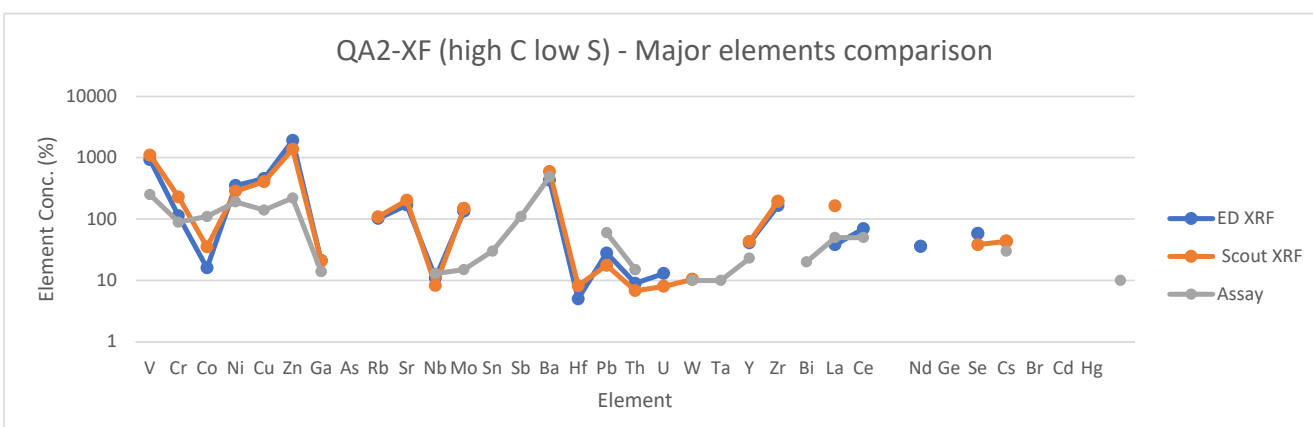
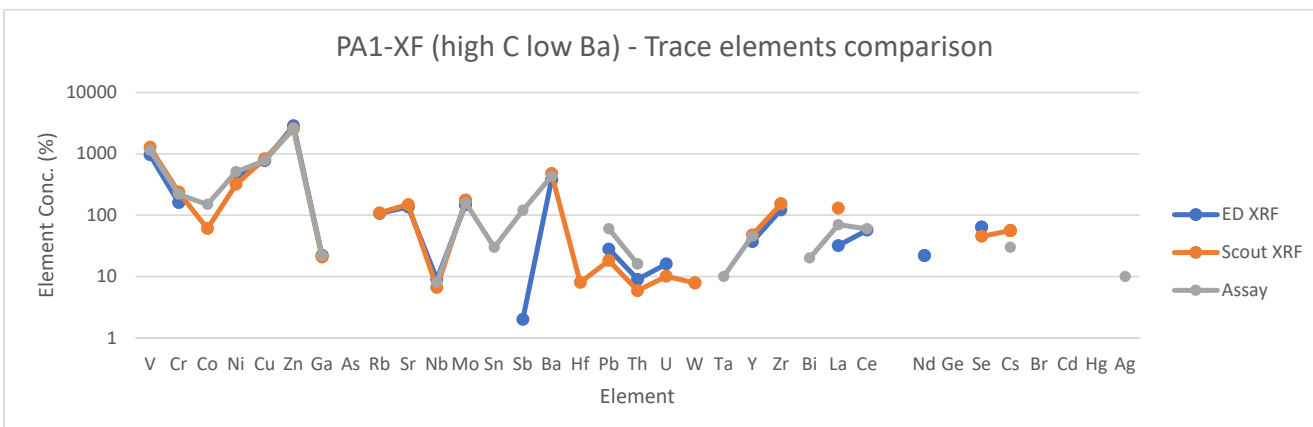
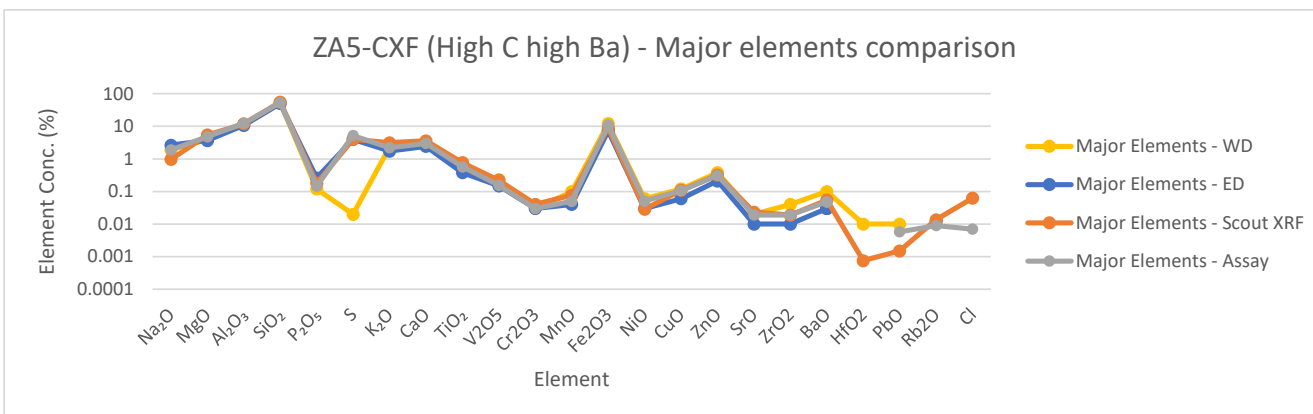


Figure I14 - X-Ray Diffraction (XRD) spectra of Aitolampi Pilot Tailings Western – 2

29 APPENDIX J – COMPARISON OF DIFFERENT XRF METHODS

The same samples were compared with different methods of measurement.





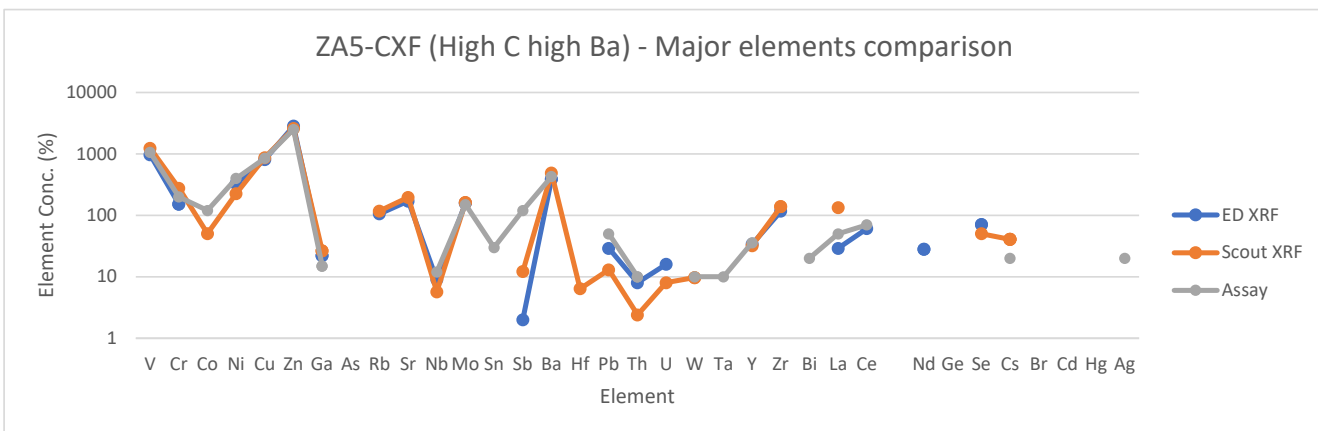
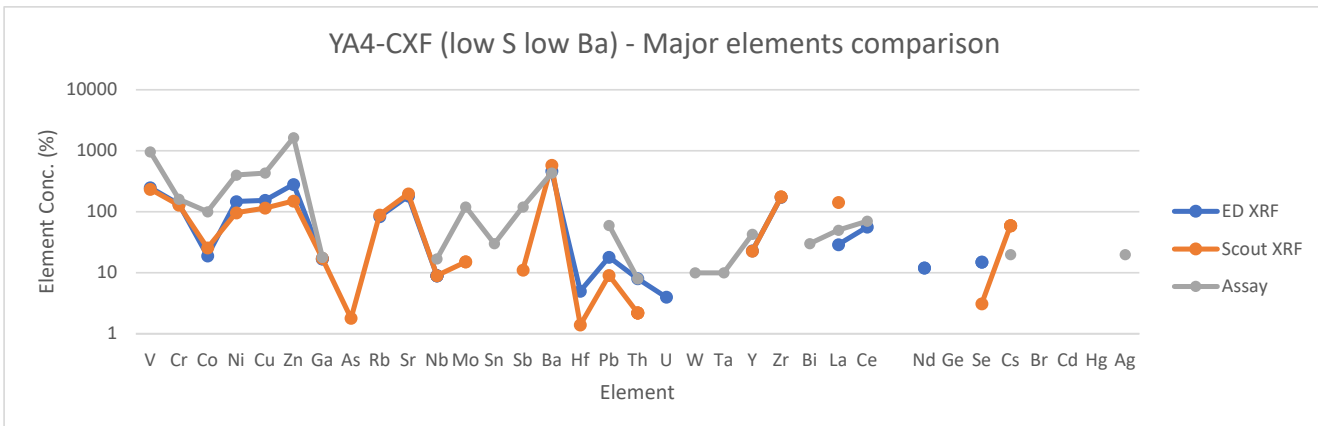


Table J1-1. XRF Fused Disc Li Borate Fusion data compared to XRF Scout data

Major Elements Run Beads (Measured with Fused Disc Li Borate Fusion) (X-Ray Mineral Services Finland)

Label	Content	Na ₂ O	MgO	Al ₂ O ₃	SiO ₂	P ₂ O ₅	S	K ₂ O	CaO	TiO ₂
		%	%	%	%	%	%	%	%	%
PA1-XF	high C low Ba	1.59	4.3	10.99	50.18	0.13	0.03	2.25	3.2	0.53
QA2-XF	high C low S	2.04	3.22	12.08	55.3	0.12	0.02	2.49	2.48	0.61
XA3-CXF	med C med S	2.42	2.35	11.16	58.18	0.14	0.02	1.96	2.11	0.55
YA4-CXF	low S C low Ba	2.88	2.53	12.52	63.01	0.11	0.05	2.29	1.79	0.59
ZA5-CXF	high C high Ba	1.91	3.88	11.64	53.31	0.12	0.02	2.33	2.75	0.52

XRF SCOUT DATA EDXRF Scout (X-Ray Mineral Services Finland)

Label	Content	Method	Na ₂ O	MgO	Al ₂ O ₃	SiO ₂	P ₂ O ₅	S	K ₂ O	CaO	TiO ₂
			%	%	%	%	%	%	%	%	%
PA1-XF	high C low Ba	0.5	5.8	11.7	52.6	0.18	4.23	2.8	4.3	0.6	0.23
QA2-XF	high C low S	0.9	4.7	12.1	54.5	0.16	3.22	3.4	3.2	0.7	0.20
XA3-CXF	med C med S	1.0	3.8	11.7	61.2	0.20	3.59	2.8	2.9	0.8	0.08
YA4-CXF	low S C low Ba	1.5	3.9	12.5	61.2	0.16	2.39	3.1	2.6	0.8	0.04
ZA5-CXF	high C high Ba	1.0	5.5	11.9	55.9	0.18	4.00	3.1	3.6	0.8	0.22

Chemical Assay Data 4 Acid Digest (CRS)

Label	Content	Method	Na ₂ O	MgO	Al ₂ O ₃	SiO ₂	P ₂ O ₅	S	K ₂ O	CaO	TiO ₂
			%	%	%	%	%	%	%	%	%
PA1-XF	high C low Ba	1.6	4.79	11.7	51.6	0.195	5.45	2.2	3.17	0.53	0.169
QA2-XF	high C low S	2.98	3.1	13.1	62.3	0.158	3.39	2.2	1.99	0.58	0.037
XA3-CXF	med C med S	2.5	3.14	11.9	58.9	0.149	4.41	1.85	2.24	0.56	0.064
YA4-CXF	low S C low Ba	2.03	4.26	12.5	56	0.147	4.28	2.25	2.57	0.63	0.141
ZA5-CXF	high C high Ba	1.9	4.8	12.4	53.6	0.145	5.24	2.21	2.99	0.57	0.155

Table J1-2. XRF Fused Disc Li Borate Fusion data compared to XRF Scout data

Major Elements Run Beads (Measured with Fused Disc Li Borate Fusion) (X-Ray Mineral Services Finland)										Major Elements Run Beads (Measured with Fused Disc Li Borate Fusion) (X-Ray Mineral Services Finland)												
Label	Content	Cr2O3	MnO	Fe2O3	NiO	CuO	ZnO	SrO	ZrO2	BaO	HfO2	PbO	%	%	Rb2O	PbO	%	%	Cl	%		
PA1-XF	high C low Ba	0.01	0.11	13.37	0.07	0.09	0.3	0.01	0.04	0.07	0.01	0.01	0.01	0.01	0.01	0.01	0.01	0.01	0.01			
QA2-XF	high C low S	0.02	0.09	10.51	0.05	0.05	0.117	0.02	0.04	0.08	0.01	0.01	0.01	0.01	0.01	0.01	0.01	0.01	0.01			
XA3-CXF	med C med S	0.01	0.08	12.72	0.05	0.02	0.07	0.01	0.04	0.05	0.02	0.02	0.02	0.02	0.02	0.02	0.02	0.02	0.01			
YA4-CXF	low S C low Ba	0.01	0.08	8.24	0.02	0.02	0.03	0.02	0.04	0.09	0.01	0.02	0.02	0.02	0.02	0.02	0.02	0.02	0.01			
ZA5-CXF	high C high Ba	0.03	0.10	12.17	0.06	0.12	0.38	0.02	0.04	0.1	0.01	0.01	0.01	0.01	0.01	0.01	0.01	0.01	0.01			
XRF SCOUT DATA EDXRF Scout (X-Ray Mineral Services Finland)										XRF SCOUT DATA EDXRF Scout (X-Ray Mineral Services Finland)												
Label	Content	V2O3	Cr2O3	MnO	Fe2O3	NiO	CuO	ZnO	SrO	ZrO2	BaO	HfO2	PbO	%	%	Rb2O	PbO	%	%	Cl	%	
PA1-XF	high C low Ba	0.03	0.08	10.82	0.04	0.10	0.32	0.02	0.05	0.00	0.00	0.01	0.07	93.73	93.73	0.07	0.07	0.07	0.07	0.07	0.07	
QA2-XF	high C low S	0.03	0.07	8.79	0.04	0.05	0.117	0.02	0.03	0.07	0.00	0.00	0.01	0.05	91.68	91.68	0.05	0.05	0.05	0.05	0.05	0.05
XA3-CXF	med C med S	0.02	0.07	8.89	0.02	0.02	0.07	0.02	0.02	0.05	0.00	0.00	0.01	0.04	96.98	96.98	0.04	0.04	0.04	0.04	0.04	0.04
YA4-CXF	low S C low Ba	0.02	0.06	6.76	0.01	0.01	0.02	0.02	0.02	0.06	0.00	0.00	0.01	0.05	94.89	94.89	0.05	0.05	0.05	0.05	0.05	0.05
ZA5-CXF	high C high Ba	0.04	0.08	9.07	0.03	0.11	0.32	0.02	0.02	0.05	0.00	0.00	0.01	0.06	95.20	95.20	0.06	0.06	0.06	0.06	0.06	0.06
Chemical Assay Data 4 Acid Digest (CRS)										Chemical Assay Data 4 Acid Digest (CRS)												
Label	Content	V2O3	Cr2O3	MnO	Fe2O3	NiO	CuO	ZnO	SrO	ZrO2	BaO	HfO2	PbO	%	%	Rb2O	PbO	%	%	Cl	%	
PA1-XF	high C low Ba	0.032	0.051	12.98	0.0648975	0.0978404	0.3211584	0.014	0.019	0.048	0	0.0069264	0.009	0.013	0.013	0.013	0.013	0.013	0.013	0.013	26.8	26.8
QA2-XF	high C low S	0.013	0.036	8.547	0.0241775	0.0175252	0.0273856	0.019	0.025	0.055	0	0.0069264	0.0057	0.006	0.006	0.006	0.006	0.006	0.006	0.006	10.2	10.2
XA3-CXF	med C med S	0.014	0.038	10.747	0.0369025	0.0200288	0.0522816	0.019	0.023	0.042	0	0.005772	0.0066	0.006	0.006	0.006	0.006	0.006	0.006	0.006	18.9	18.9
YA4-CXF	low S C low Ba	0.023	0.045	10.406	0.0509	0.0538274	0.2041472	0.018	0.024	0.049	0	0.0069264	0.0084	0.008	0.008	0.008	0.008	0.008	0.008	0.008	22.6	22.6
ZA5-CXF	high C high Ba	0.03	0.05	11.11	0.0509	0.106403	0.3124448	0.019	0.048	0	0.005772	0.009	0.007	0.007	0.007	0.007	0.007	0.007	0.007	0.007	25	25

Table J2-1. XRF Fused Disc Li Borate Fusion data compared to XRF Scout data

XRF SCOUT DATA EDXRF Scout (X-Ray Mineral Services Finland)										Chemical Assay Data 4 Acid Digest (CRS)											
Label	V	Cr	Co	Ni	Cu	Zn	Ga	As	Rb	Sr	Nb	Mo	Sn	ppm							
PA1-XF	1276	237	60	319	834	2553	21	<0.6	109	149	7	174	<1.4								
QA2-XF	1100	229	35	285	406	1375	21	<0.7	109	202	8	148	<1.3								
XA3-CXF	469	144	40	157	159	524	16	<0.6	89	209	6	46	<1.2								
YA4-CXF	234	128	26	96	115	150	17	2	89	198	9	15	<1.1								
ZA5-CXF	1237	276	51	226	873	2595	26	<0.7	118	197	6	163	<1.3								

Table J2-2. XRF Fused Disc Li Borate Fusion data compared to XRF Scout data

Label	Sb	Ba	Hf	Pb	Th	U	W	Ta	Y	Zr	Bi
	ppm	ppm	ppm	ppm	ppm	ppm	ppm	ppm	ppm	ppm	ppm
XRF SCOUT DATA EDXRF Scout (X-Ray Mineral Services Finland)											
PA1-XF	<1.6	478	8	18	6	10	8	<3.9	48	153	<0.9
QA2-XF	<1.4	594	8	18	7	8	10	<3.7	43	194	<0.8
XA3-CXF	<1.4	472	13	8	2	<1.2	10	<3.7	30	175	<0.8
YA4-CXF	11	579	1	9	2	<1.1	<1.9	<3.4	23	175	<0.7
ZA5-CXF	12	489	6	13	2	8	10	<3.7	32	139	<0.8
Chemical Assay Data 4 Acid Digest (CRS)											
Label	Sb	Ba	Hf	Pb	Th	U	W	Ta	Y	Zr	Bi
	ppm	ppm	ppm	ppm	ppm	ppm	ppm	ppm	ppm	ppm	ppm
PA1-XF	120	430		60	16	0	0	10	46		20
QA2-XF	110	490		60	15	0	10	10	23		20
XA3-CXF	120	380		50	19	0	10	30	30		20
YA4-CXF	120	430		60	8	0	10	10	43		30
ZA5-CXF	120	430		50	10	0	10	10	36		20

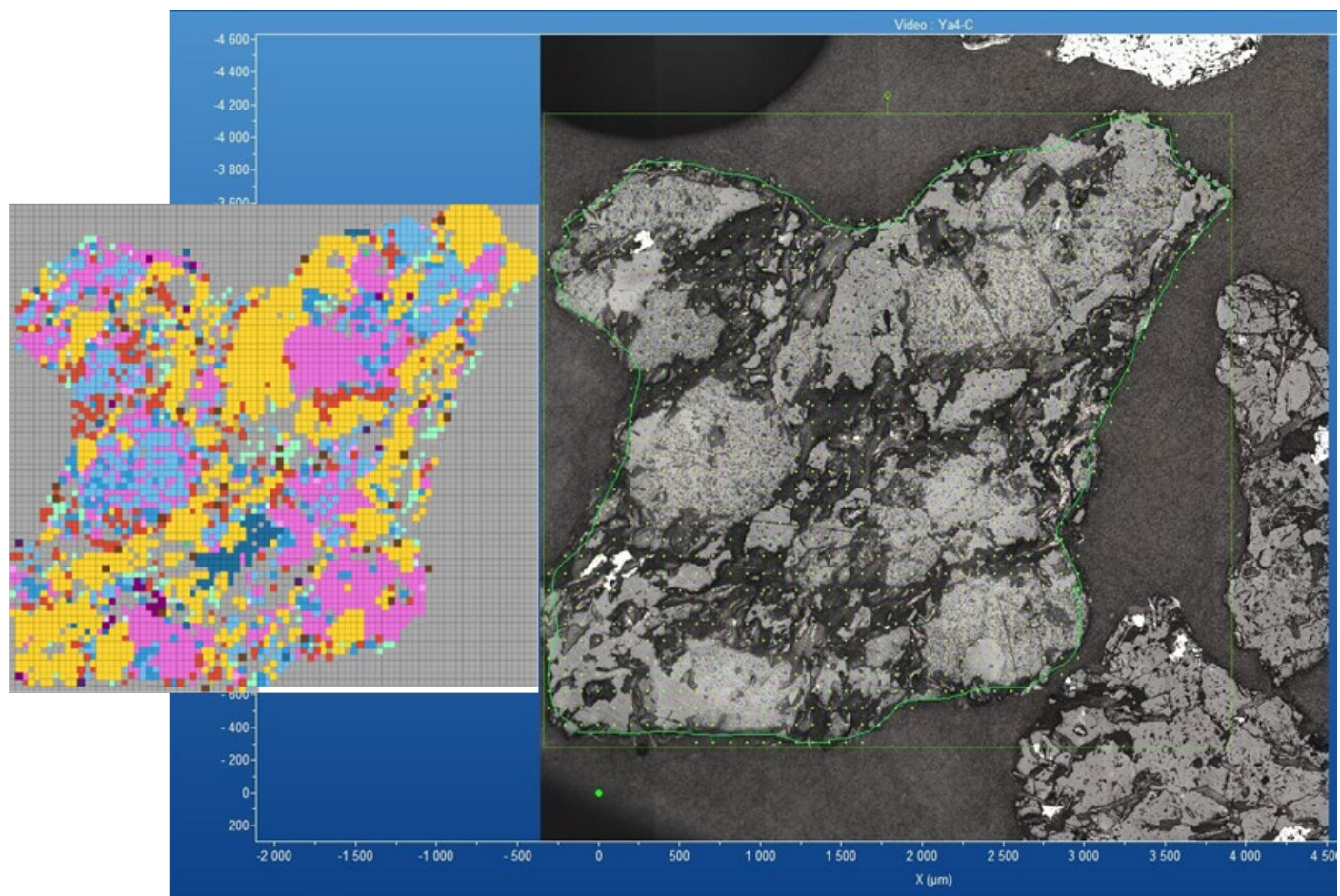
Table J2-3. XRF Fused Disc Li Borate Fusion data compared to XRF Scout data

XRF SCOUT DATA EDXRF Scout (X-Ray Mineral Services Finland)							Chemical Assay Data 4 Acid Digest (CRS)						
Label	La	Ce	Nd	Ge	Se	Cs	Br	Cd	Hg	Ag	ppm		
PA1-XF	130	ppm	ppm	ppm	ppm	45	56	<0.3	0	<2.4			
QA2-XF	164	ppm	ppm	ppm	ppm	38	43	<0.3	0	<2.1			
XA3-CXF	147	ppm	ppm	ppm	ppm	8	49	<0.3	0	<2.1			
YA4-CXF	142	ppm	ppm	ppm	ppm	3	59	<0.3	0	<2.0			
ZA5-CXF	134	ppm	ppm	ppm	ppm	50	41	<0.3	0	<2.2			
PA1-XF	70	ppm	ppm	ppm	ppm	60	60	30	30	10	10		
QA2-XF	50	ppm	ppm	ppm	ppm	50	50	30	30	20	20		
XA3-CXF	60	ppm	ppm	ppm	ppm	70	70	30	30	20	20		
YA4-CXF	50	ppm	ppm	ppm	ppm	70	70	20	20	20	20		
ZA5-CXF	50	ppm	ppm	ppm	ppm	70	70	20	20	20	20		

Table J2-4. XRF Fused Disc Li Borate Fusion data compared to XRF Scout data

Chemical Assay Data 4 Acid Digest (CRS)	Label	S	Te	Si	Ti	Fe	Mn	Mg	Ca
		ppm	ppm	ppm	ppm	ppm	ppm	ppm	ppm
PA1-XF	59800	0	241000	3200	91700	400	28900	22600	
QA2-XF	37800	10	291000	3470	60400	280	18700	14200	
XA3-CXF	50900	0	275000	3340	75900	300	18900	16000	
YA4-CXF	49300	0	262000	3750	73500	350	25700	18400	
ZA5-CXF	53100	0	251000	3400	78700	390	28900	21400	

30 APPENDIX K - RAMAN ANALYSIS OF GRAPHITE ORE SAMPLES AND TAILINGS



Raman microscopy map – X-ray Mineral Services UK

Analysis done

Dr. Max Franzel, Dr. Nikolaos Apeiranthitis, Morven Davidson
X-ray Mineral Services Finland Ltd

30.1 Method

30.1.1 Ore samples

Five ore graphite samples were analysed with Raman microscopy for their spectral fingerprint. PA1-C, QA2-C, XA3-C, YA4-C, ZA5-C were received as smashed rock chips. In order to perform the Raman analysis, resin blocks were prepared and polished for each sample, revealing a granular representation of the rock. Within these grains, it was possible to identify the main mineralogy as well as the presence of graphite. Textural information can also be drawn by the analytical approach developed.

Raman microscopy workflow analysis:

- Point analysis of present mineral phases within 2 grains for each sample
- Map scans of the same two grains for acquiring a cumulative spectrum

Raman analysis parameter setting:

Point and map scan analysis

- Laser: 532 nm
- Energy: 25%
- Acquisition time: 1 sec
- Acquisition accumulation: 1 spectrum
- Magnification lenses: 10X (unless otherwise specified)

In addition to this workflow, 4 high resolution scans were performed only for sample YA4-C. Three of the scans were performed on three different grains under 10X magnification while the fourth scan was performed under 50X for configuring the texture in more detail.

It is important to note that the way all samples were presented for analysis (as centimeter rock chips), introduces a degree of bias to the analysis, as some grains would contain only silicates, while others may have opaque phases or graphite grains. An example of the general view of the ore resin blocks is shown in Figure 1.

30.1.2 Tailings

Two tailings samples, APTE-C and APTE-W, were analysed with Raman microscopy, after preparing resin polished packs. Similarly, to the ore samples, point analysis was performed for acquiring individual mineral phases spectra. Due to the finer grain size of both of these samples, map scans were not possible to acquire, as the resin material would interfere with the grains. For that reason, a higher amount of point analysis was done. These were added to acquire the cumulative spectrum for the non-opaque minerals. A second cumulative spectra for the non-opaque mineral phases are given, where possible.

All spectra presented are corrected for the resin background signal. However, resin material signal interference may still be present.

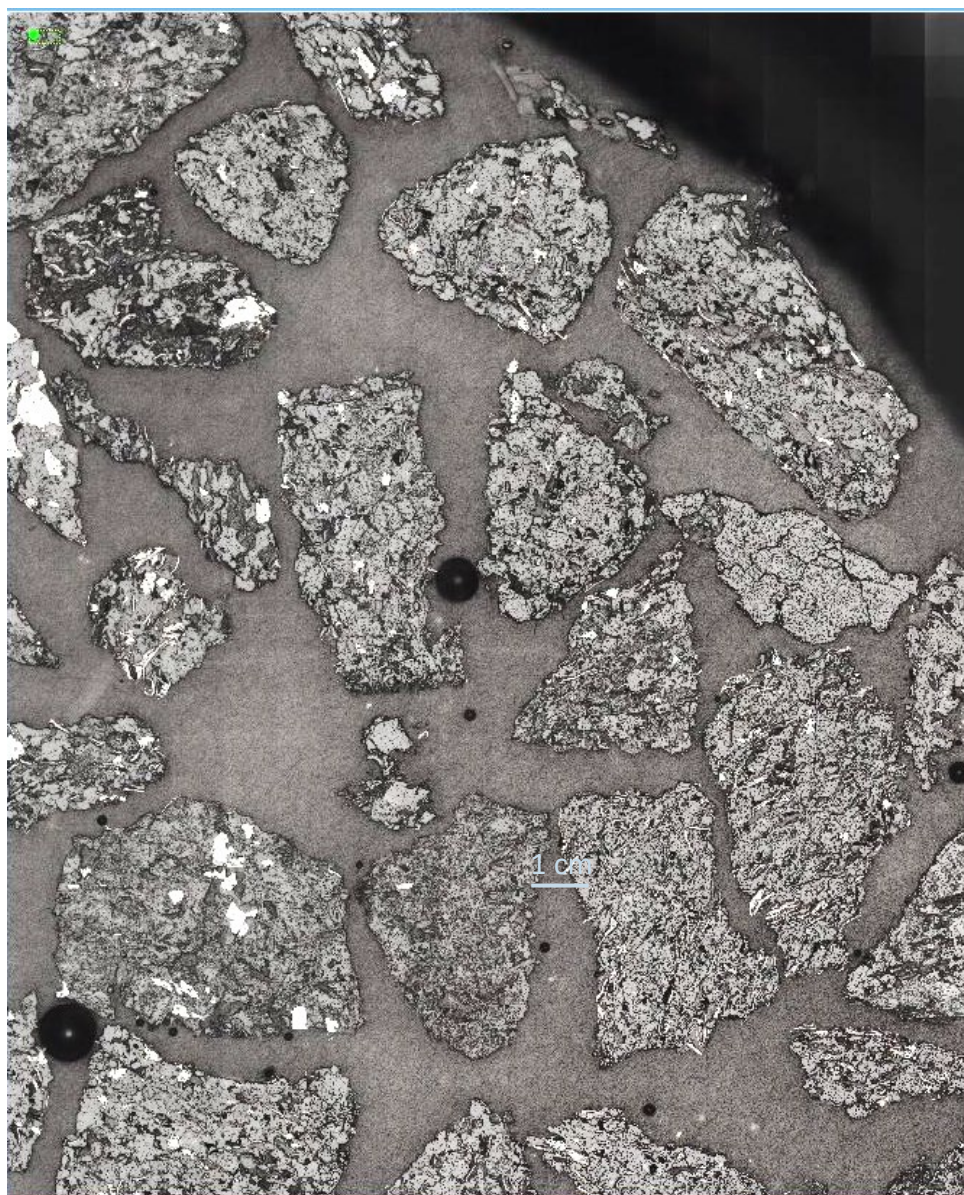


Figure K2. Grain size and sample representation in YA4-C graphite ore sample.

30.2 Results

Results will be presented with the following structure. For each graphite ore and tailing sample, the grain images and the respective cumulative spectra of two grains will be presented, with some basic mineral annotations for specific Raman peaks. In the accompanying Appendix, a breakdown of each cumulative spectrum will be given based on the point analysis conducted on selected grains (best effort was applied in order to present as representative data / spectra as possible given the initial heterogeneity).

Across samples, the cumulative spectra are dominated by the strong presence of quartz and plagioclases/feldspars. These bands occur from $185\text{--}500\text{ cm}^{-1}$ for silicate phases (see Appendix). Graphite, as the phase of interest, occurs as a distinctive band at 1600 cm^{-1} . It was observed that Ti-rich phases, such as anatase, are strongly present in the samples. The individual spectra for anatase have a prominent peak below 185 cm^{-1} , however this is not clearly distinguished in the cumulative spectra. Sulfide phases were also observed in some samples, which have been identified with QXRD, however, the statistical presence of these phases with Raman analysis can not be translated to the total concentration in the whole sample. Mica and chlorite phases have also been observed.

30.2.1 PA1-C

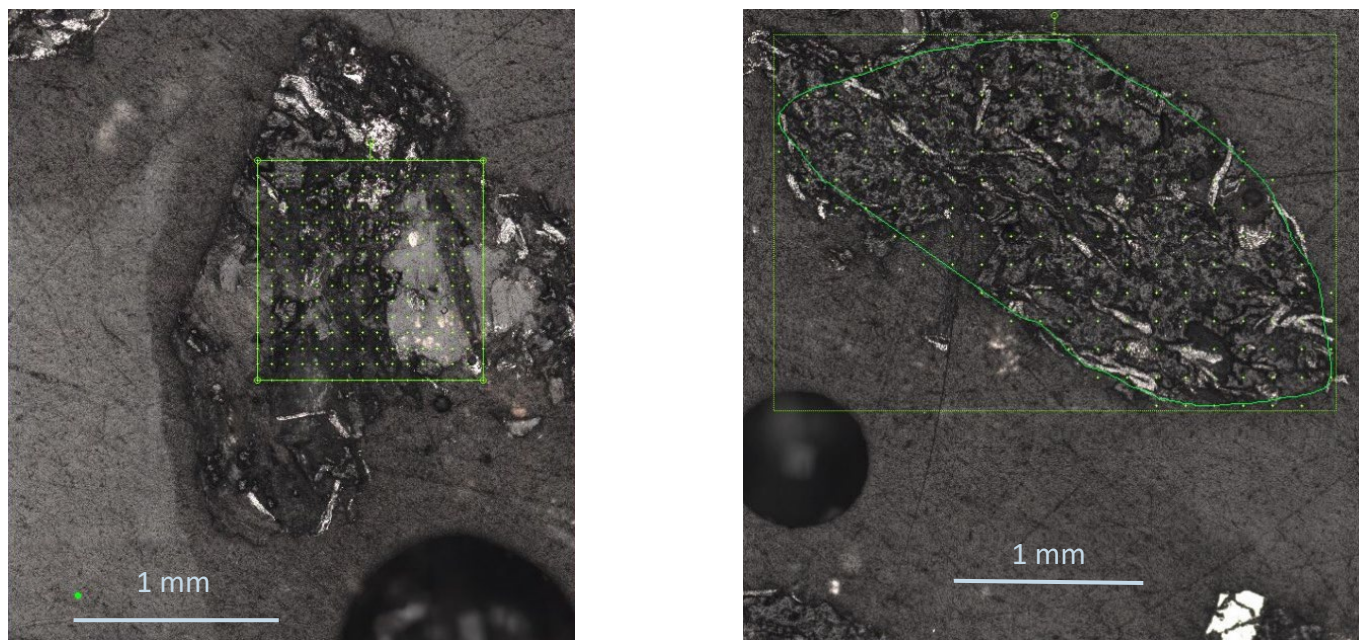


Figure K3. Grain scans in PA1-C samples, producing the two cumulative spectra Map1 (left-hand side grain) and Map2 (right-hand side grain)

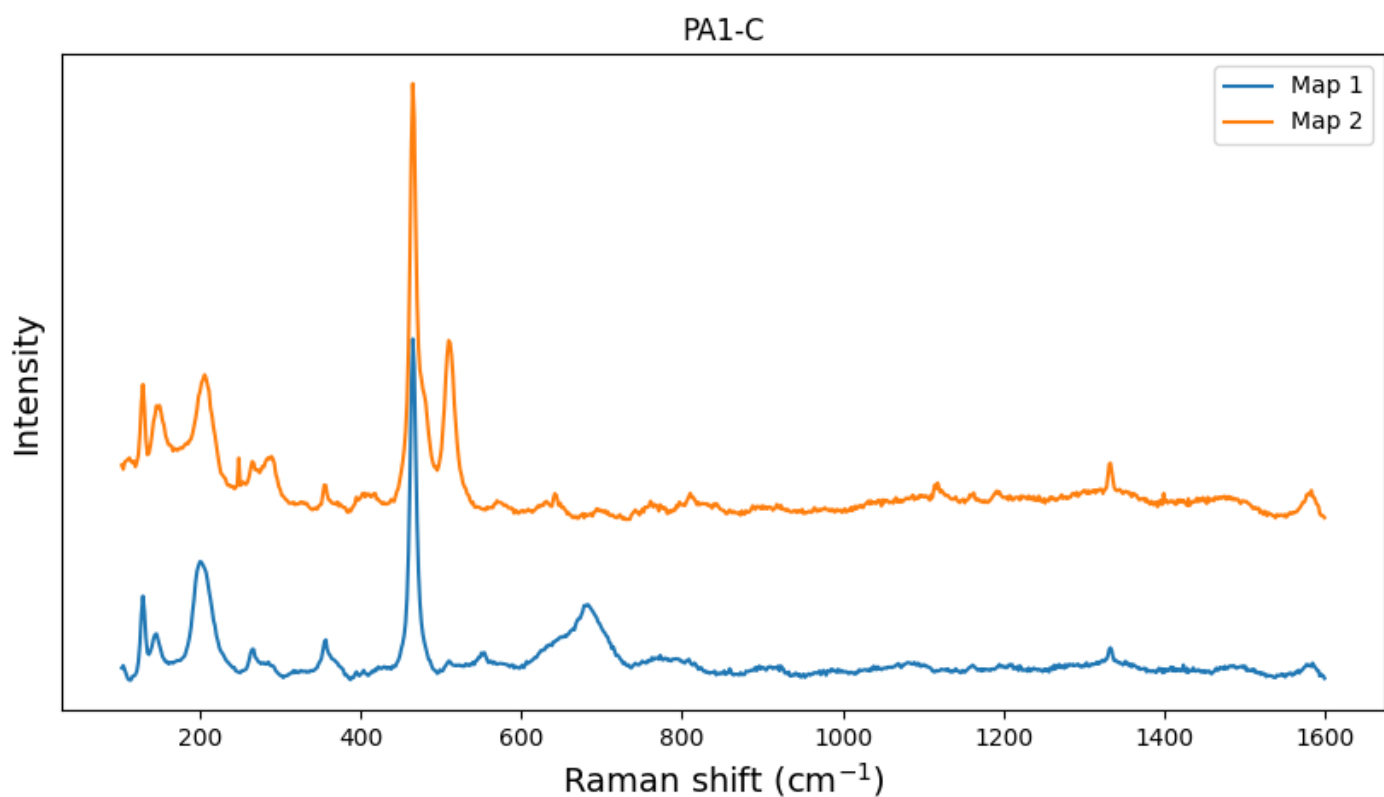
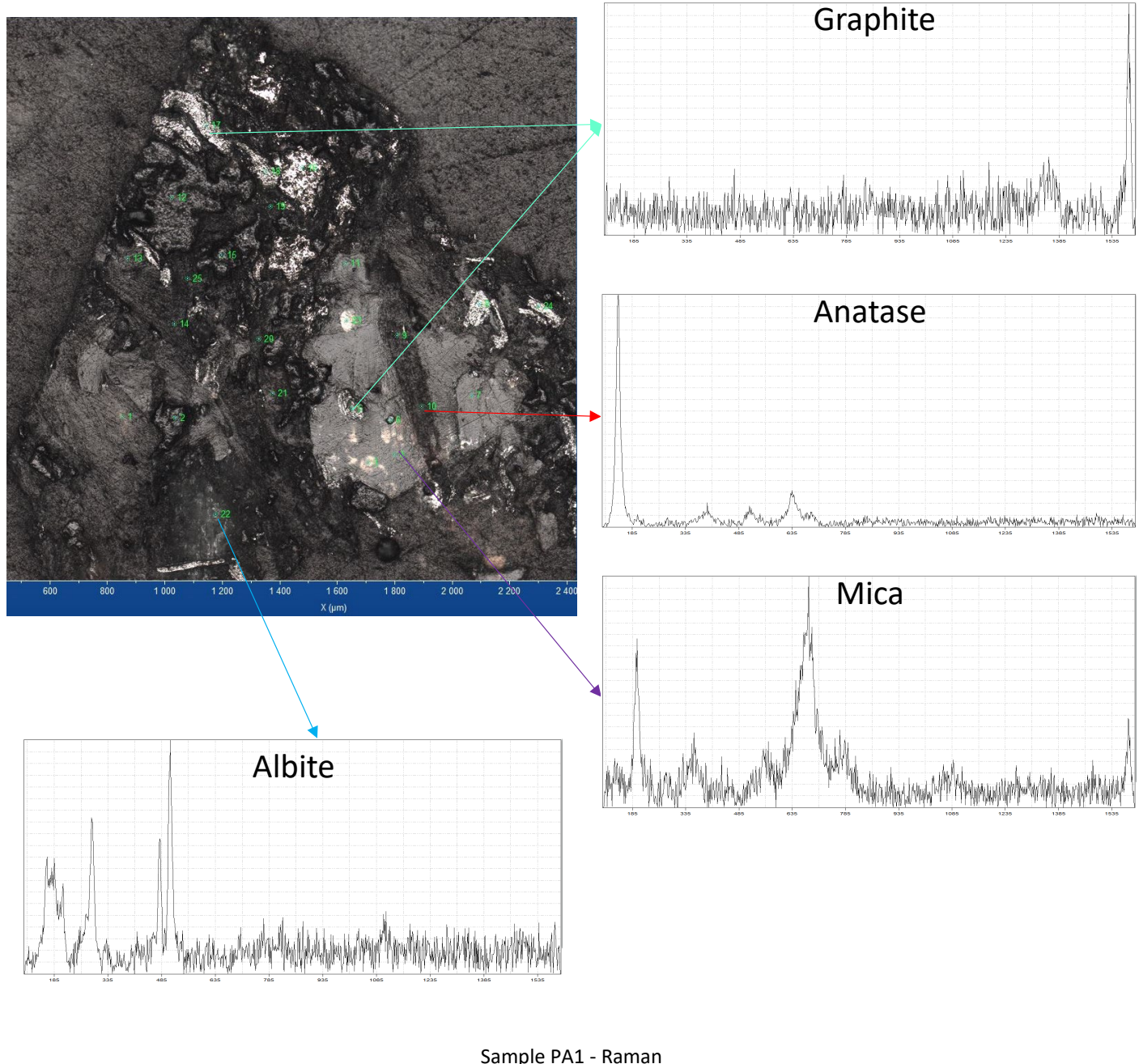


Figure K4. Cumulative spectra for grain scans in Figure 2.



30.2.2 QA2-C

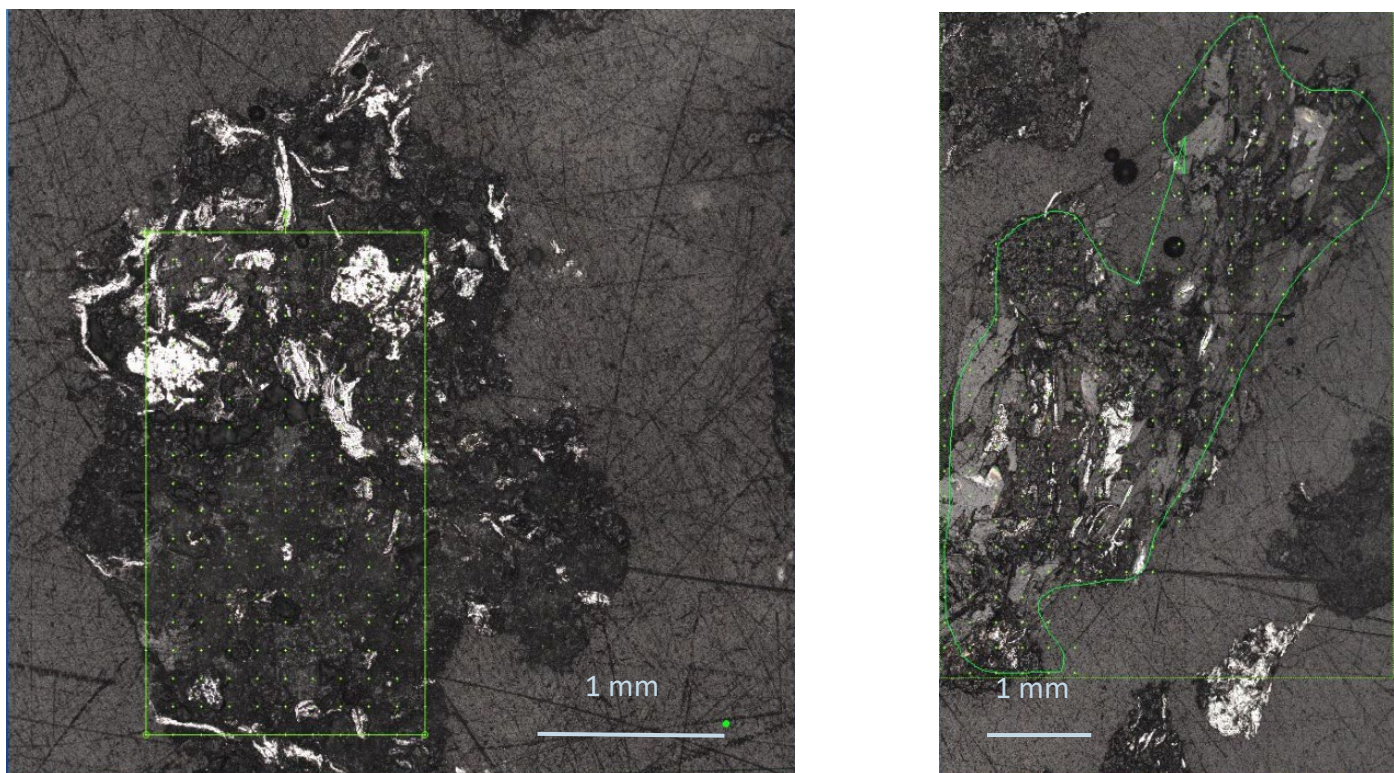


Figure K5. Grain scans in QA2-C samples, producing the two cumulative spectra Map1 (left-hand side grain) and Map2 (right-hand side grain)

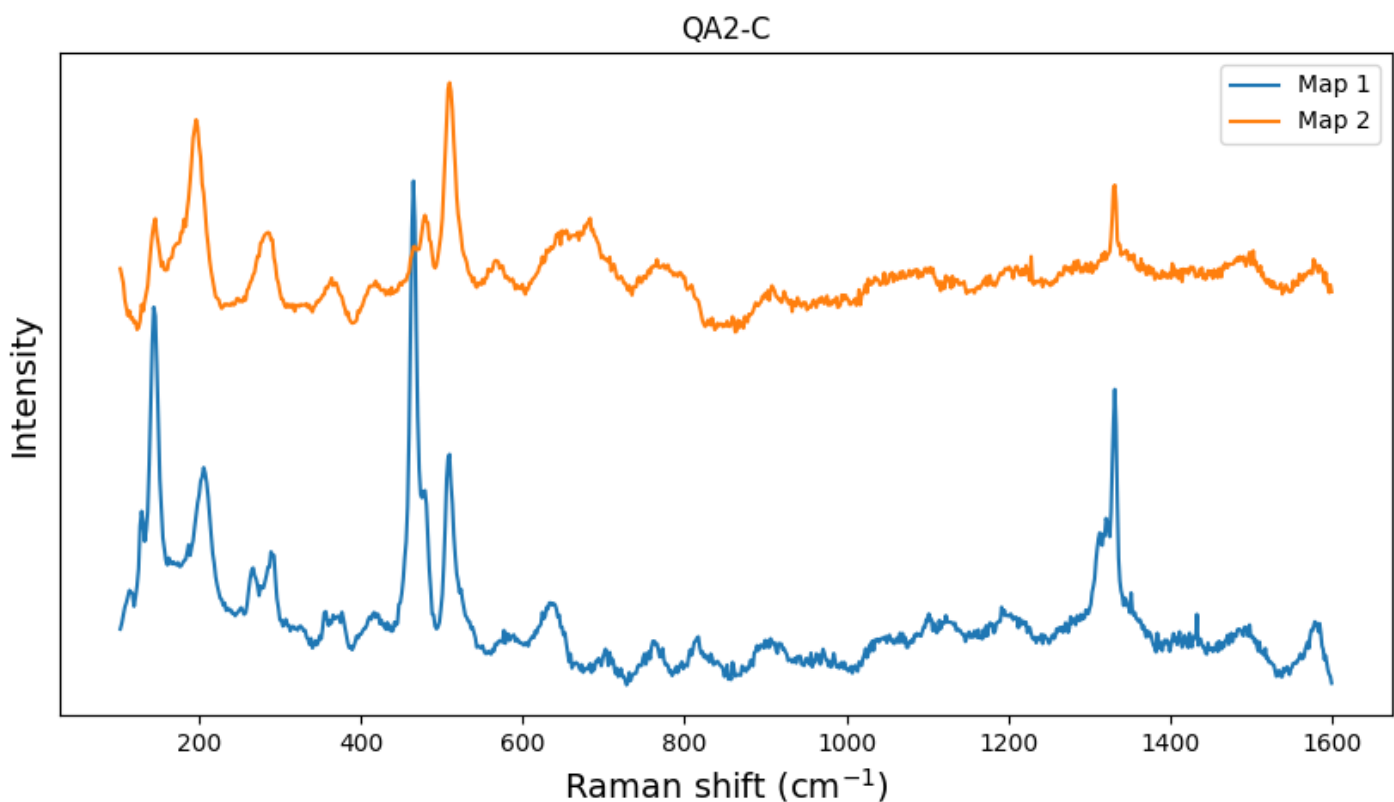
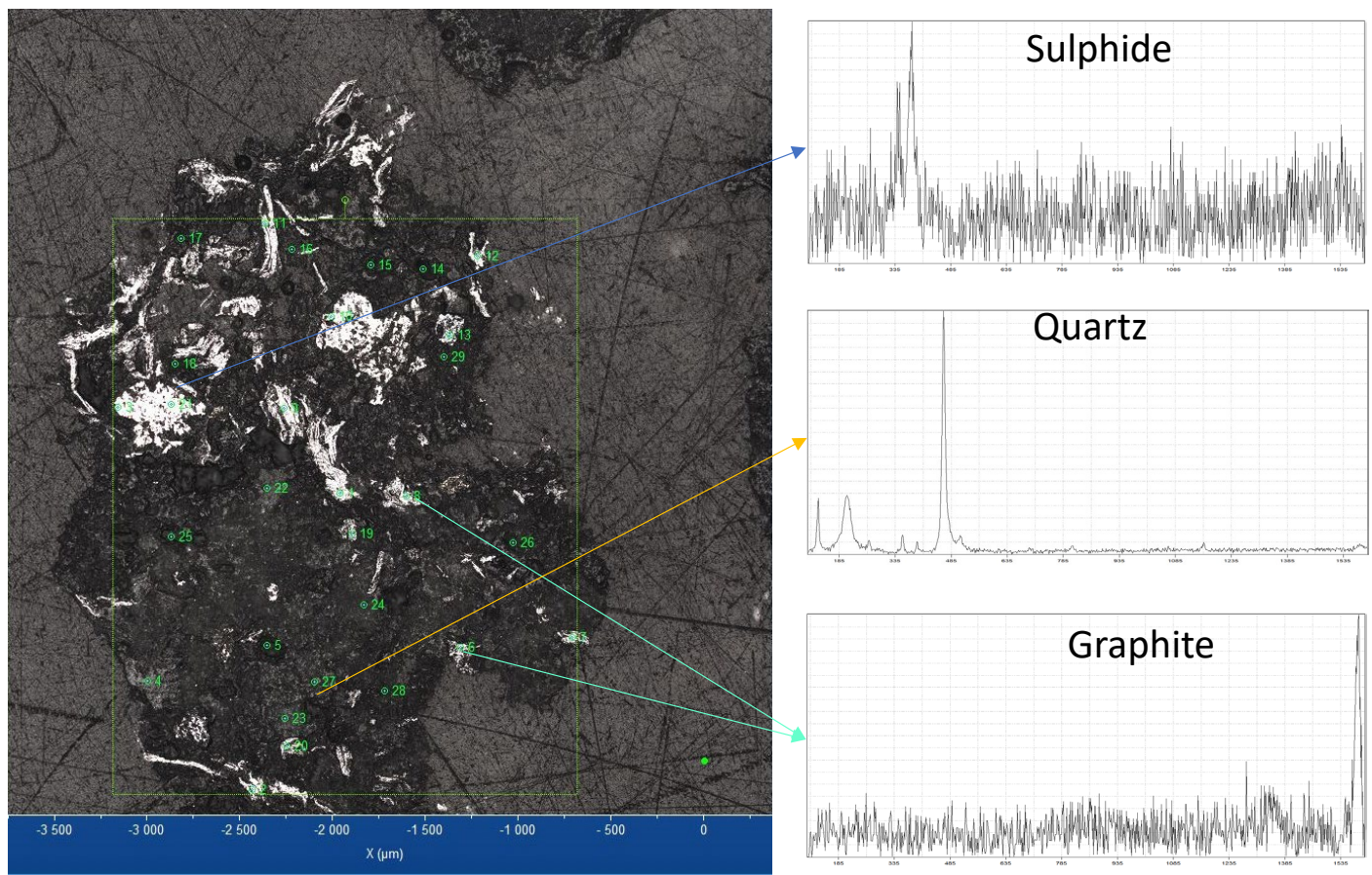


Figure K6. Cumulative spectra for grain scans in Figure K4.



Sample QA2 - Raman

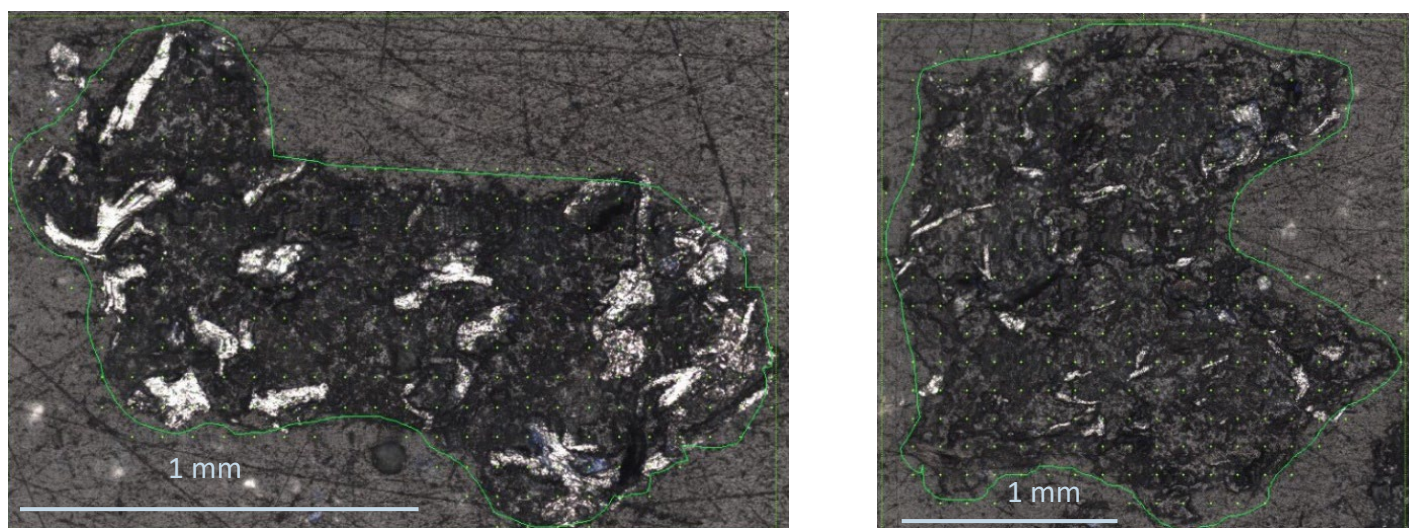
30.2.3 XA3-C

Figure K7. Grain scans in XA3-C samples, producing the two cumulative spectra Map1 (left-hand side grain) and Map2 (right-hand side grain)

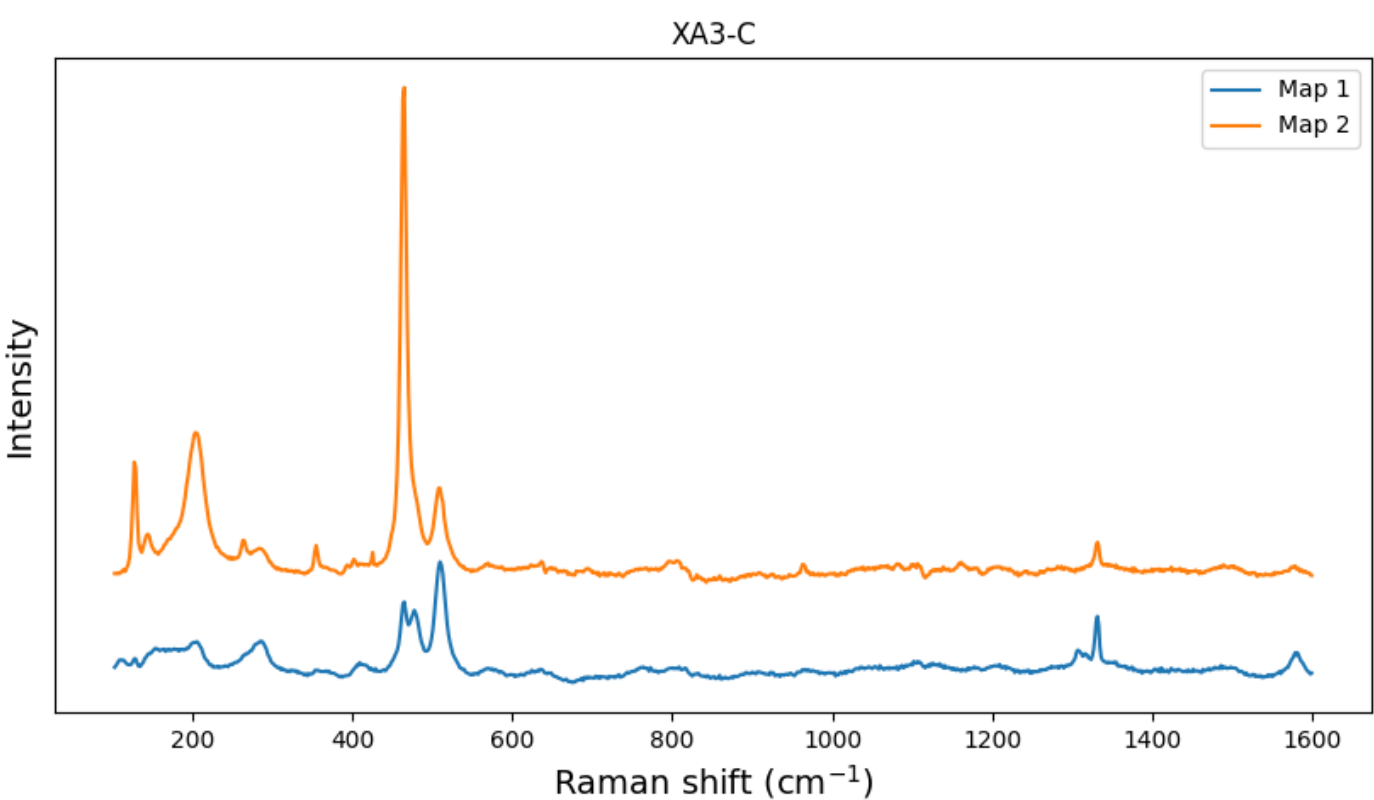
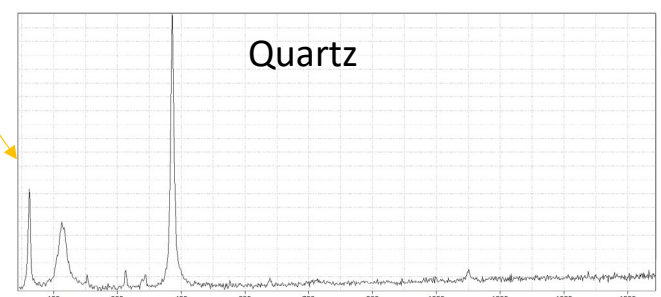
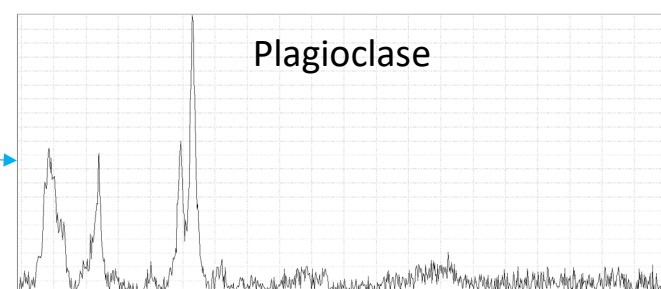
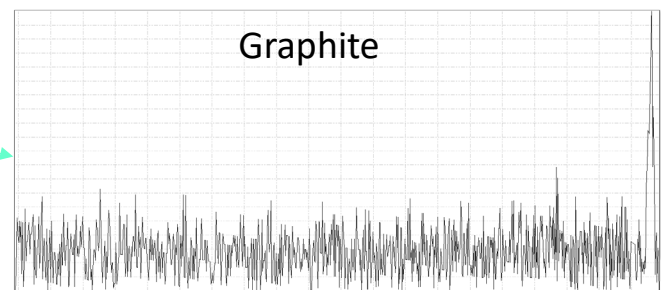
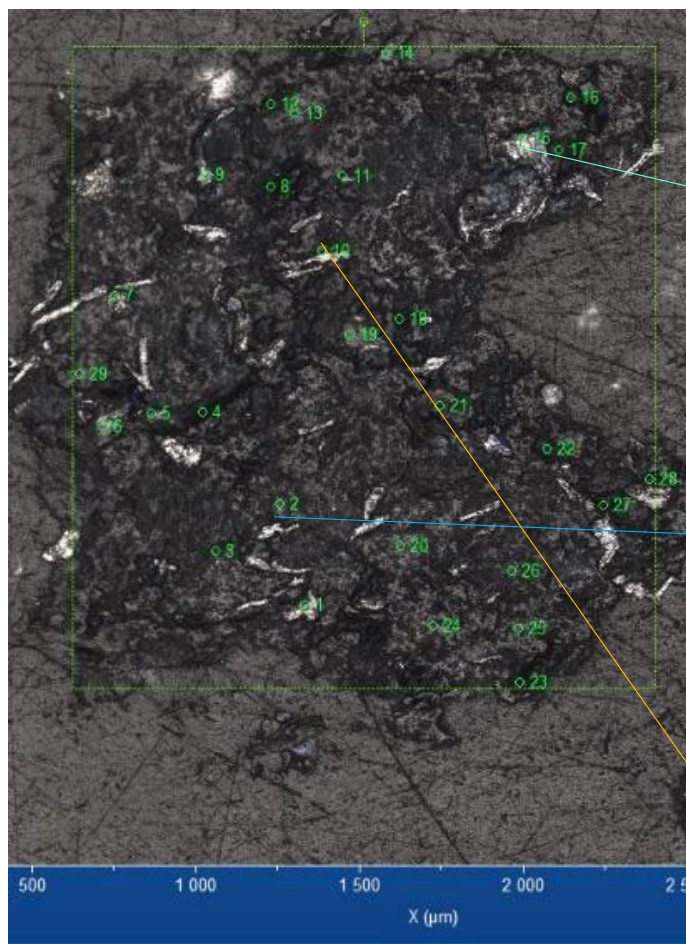


Figure K8. Cumulative spectra for grain scans in Figure K6.



Sample XA3 - Raman

30.2.4 YA4-C

High resolution maps were constructed for the YA4-C ore sample, as an example of textural analysis by Raman microscopy. In this case, three different grains were scanned, using a grid of over 9000 point analyses, producing a mineralogical map. The information of the initial grain, grid, and identified mineral location was compiled in Spotfire, producing a mineralogy map as shown in Figure 8 and Figure 9 and (Appendix slides 5 and 6). This Raman analysis configuration can give the textural context of the analysed area/grain, illustrating the relationship between graphite and other mineral phases present.

It can be observed that graphite has an elongated crystal structure in the majority of the cases, with no preferential proximity to other minerals. It appears to occur adjacent to any of the silicate minerals, e.g. quartz, plagioclases or micas, as well as the Ti-rich phases.

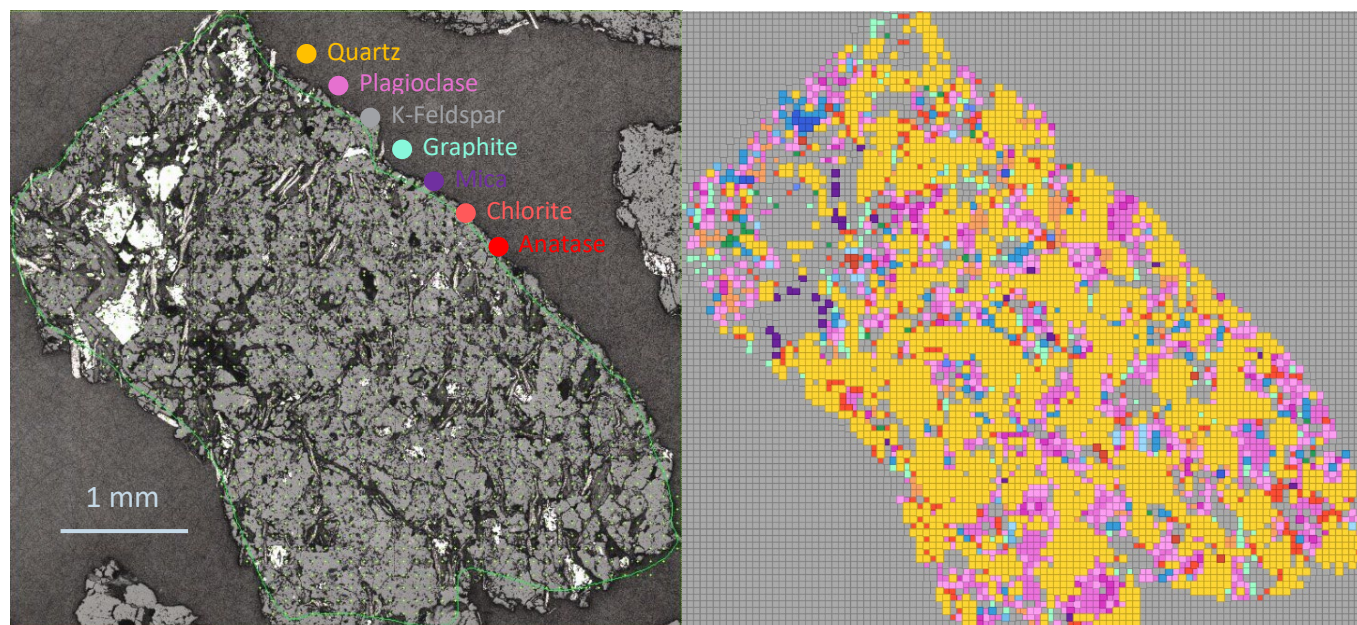


Figure K9. High resolution map scan of a selected grain in YA4-C, under 10X magnification lense, (left-hand side). A compilation of the mineralogy accordindg to the gridding reference of the map scan using Spotfire (right-hand side)

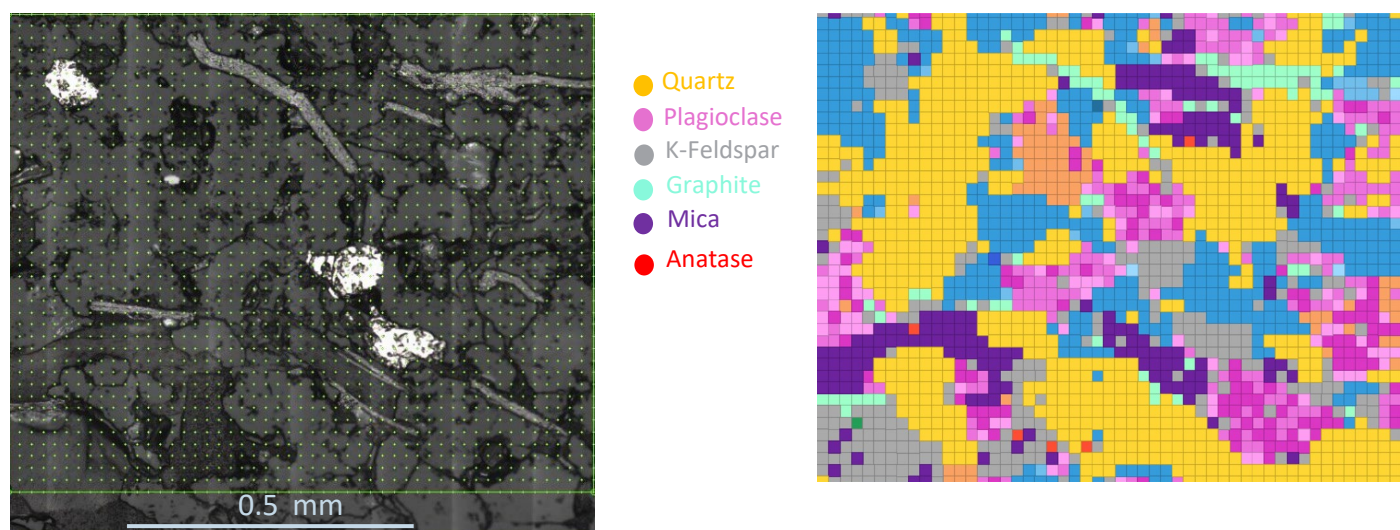
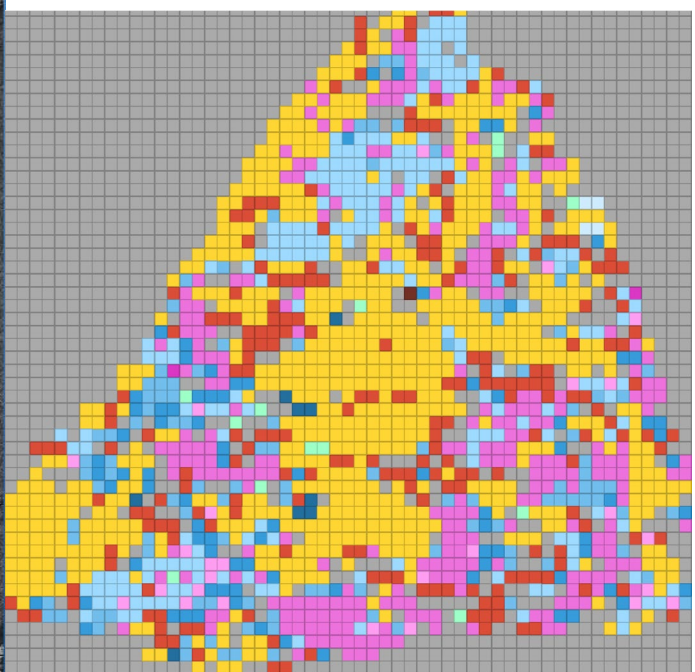
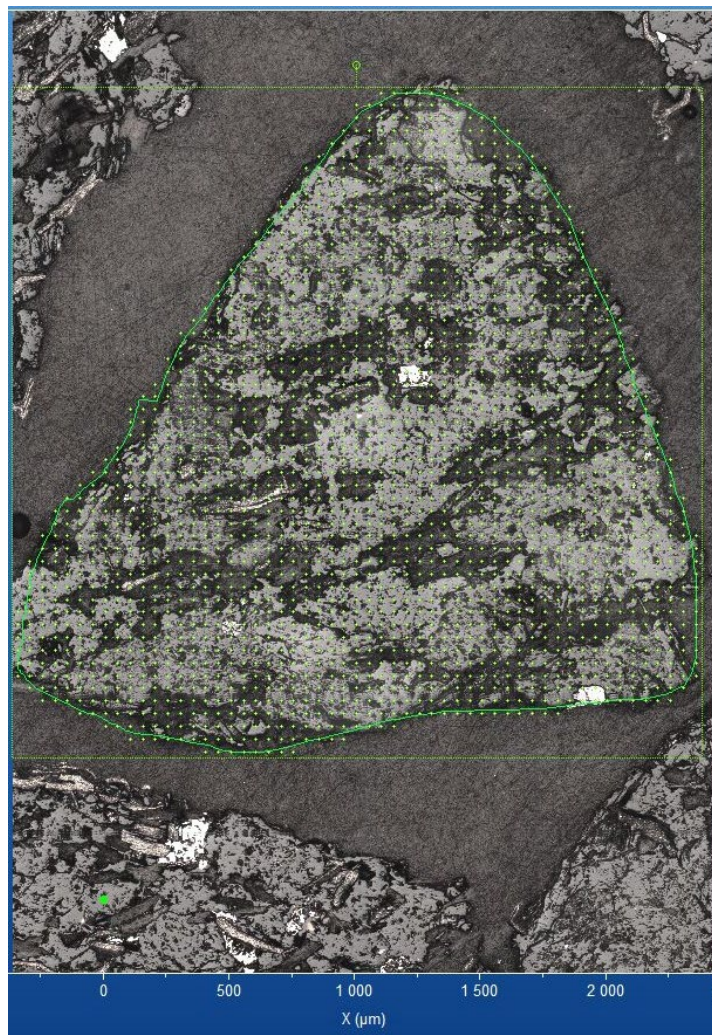


Figure K10. High resolution map scan of a small grain area in YA4-C, under 50X magnification lense, (left-hand side A compilation of the mineralogy accordindg to the gridding reference of the map scan using Spotfire (right-hand side)

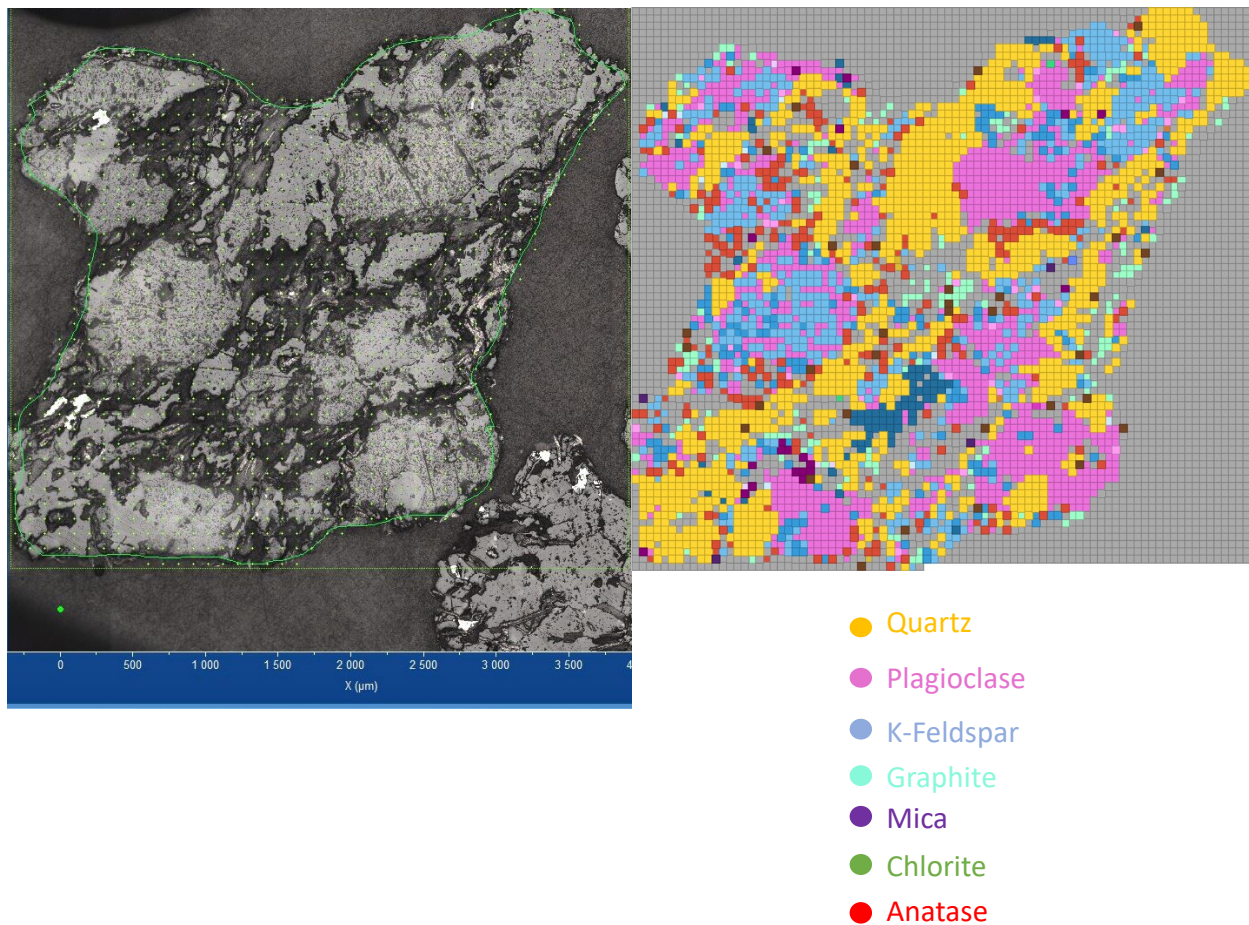
Grain 1



- Quartz
- Plagioclase
- K-Feldspar
- Graphite
- Mica
- Chlorite
- Anatase

Sample YA4 – Raman Grain 1

Grain 2



Sample YA4 – Raman Grain 2

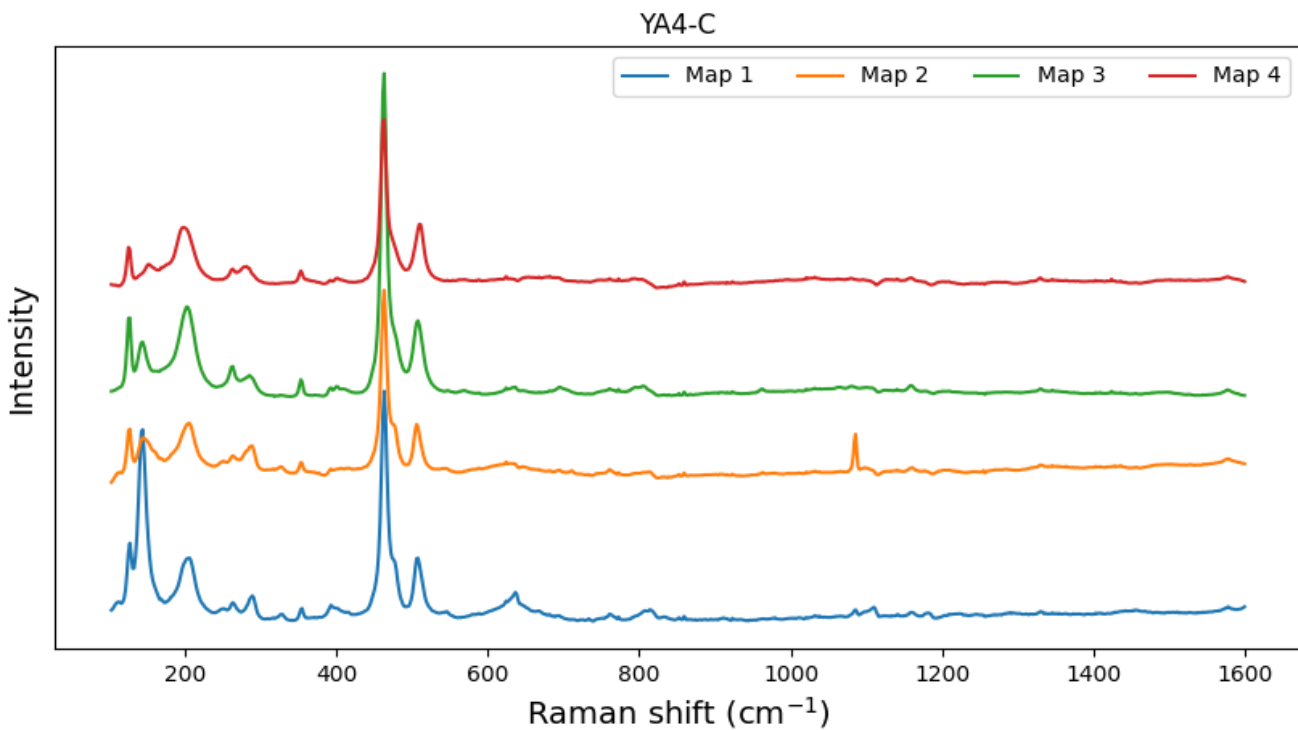


Figure K11. Cumulative spectra for 4 different high resolution grain scans. Map 3 corresponds to scan in Figure 8 and Map 4 from scan shown in Figure K9. See Appendix K for Grain 1 – Map 1, and Grain 2 – Map 2.

30.2.5 ZA5-C

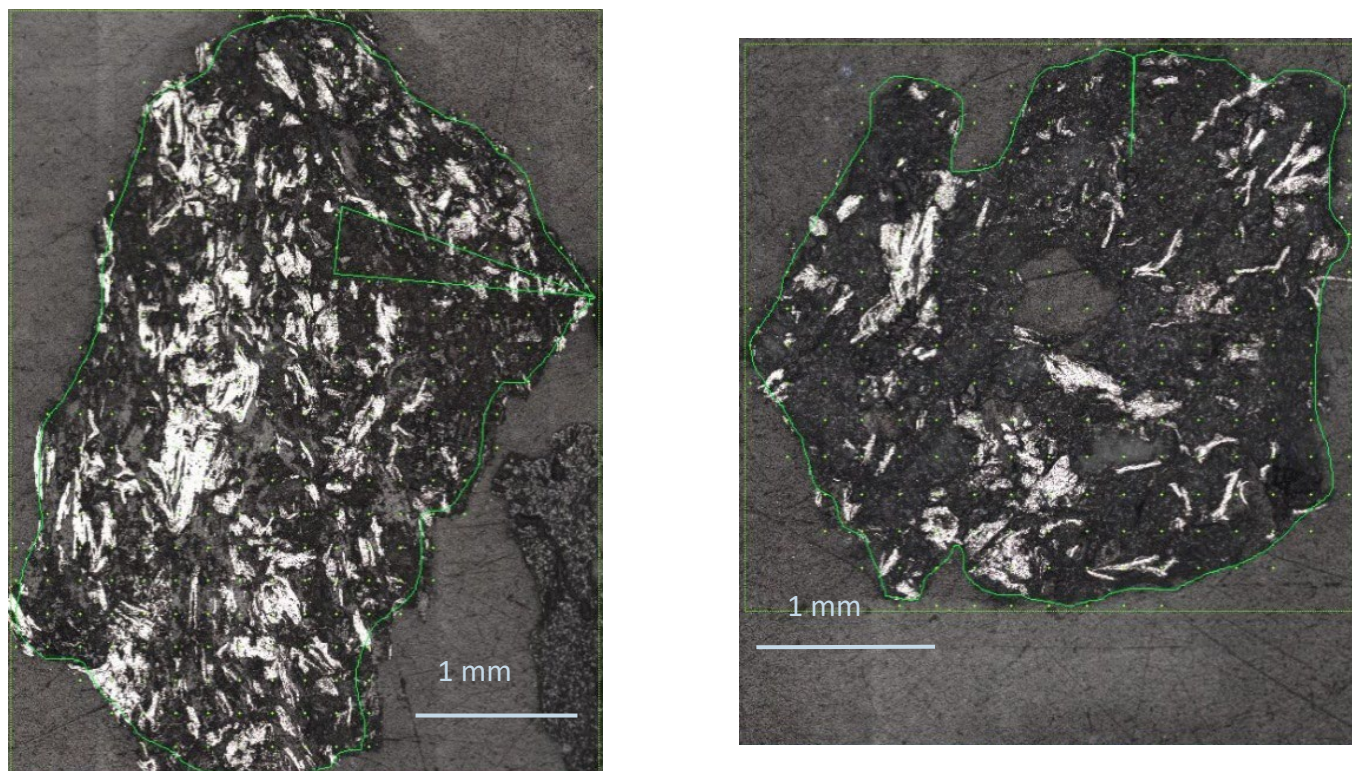


Figure K12. Grain scans in ZA5-C samples, producing the two cumulative spectra Map1 (left-hand side grain) and Map2 (right-hand side grain)

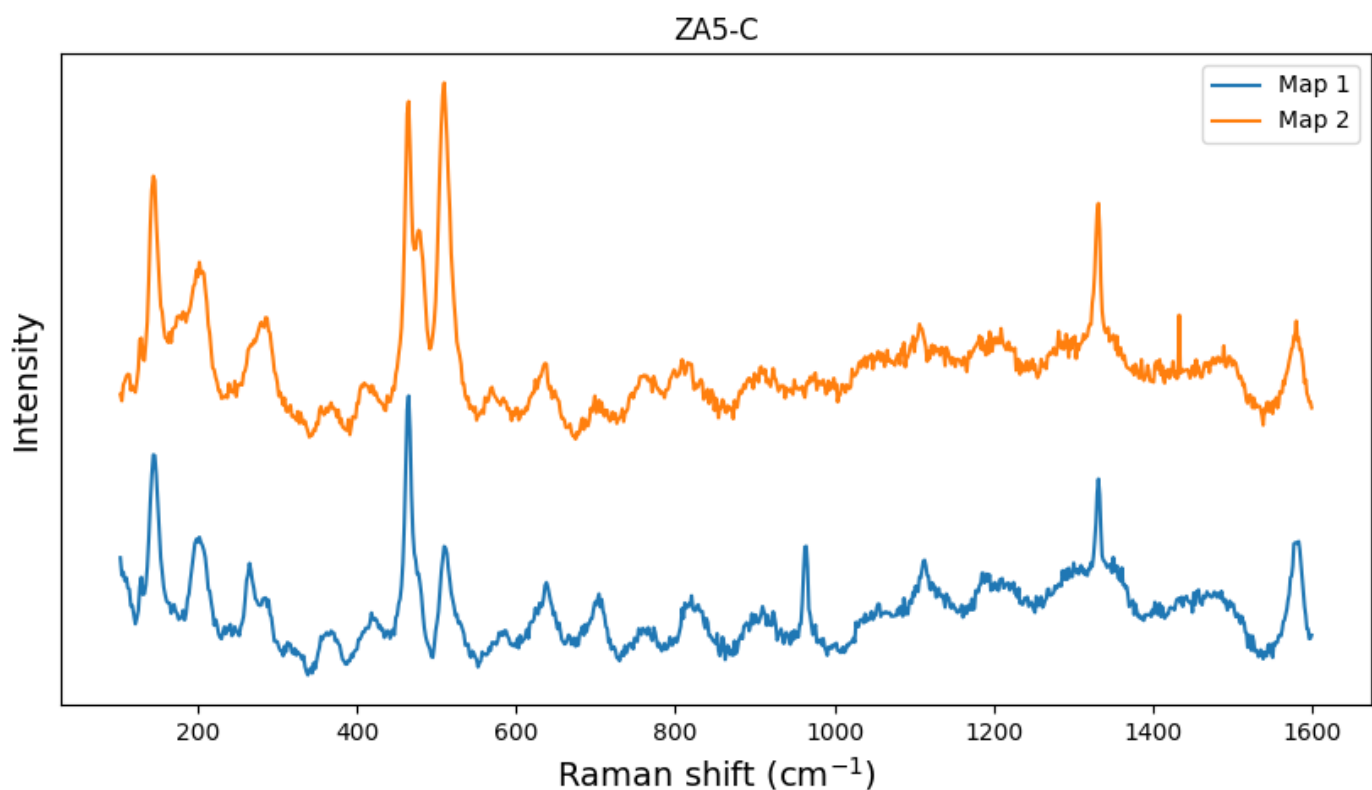
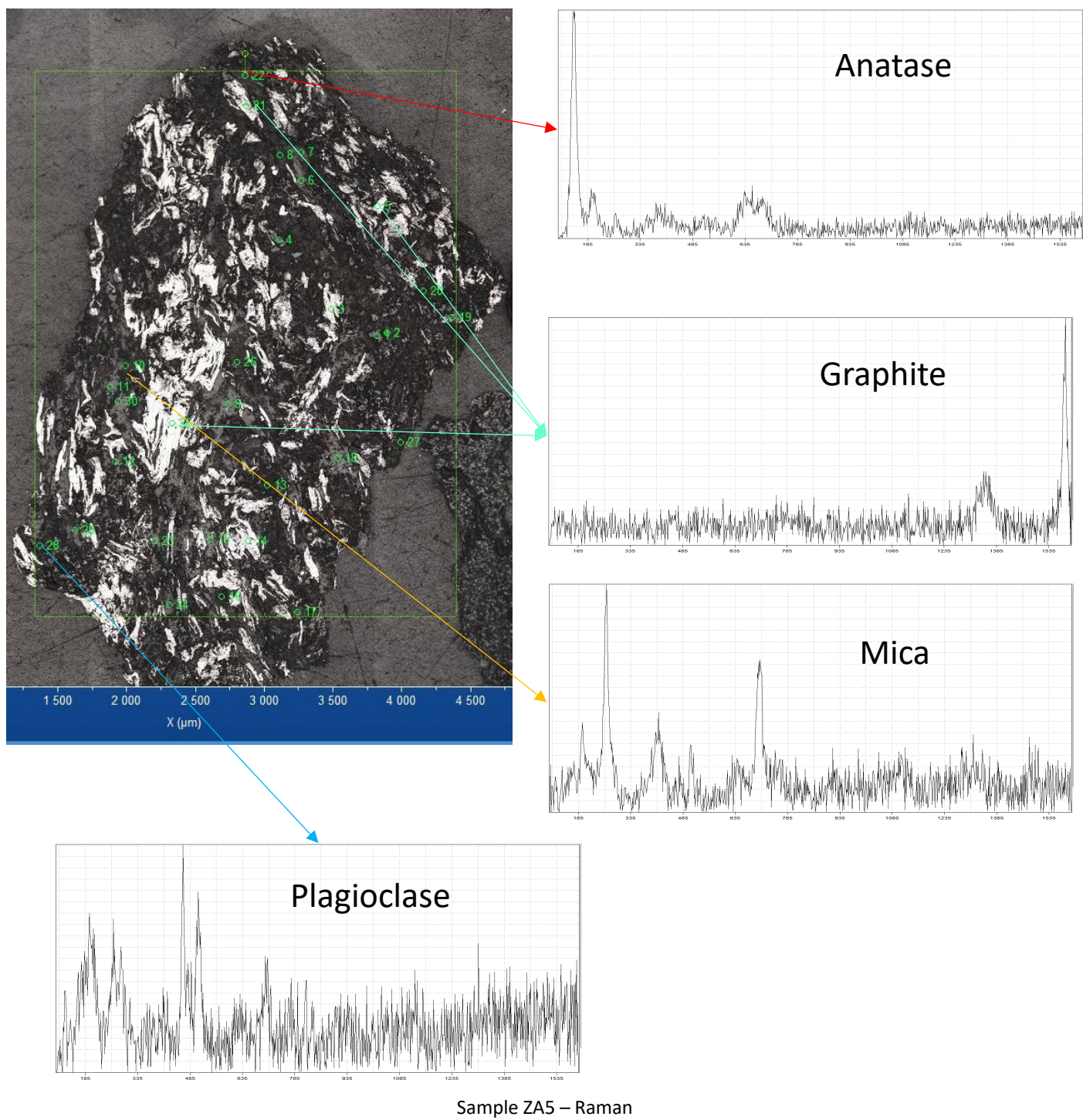


Figure K13. Cumulative spectra for grain scans in Figure K11.



30.2.6 Aitolampi Pilot Tailings West APTW-C

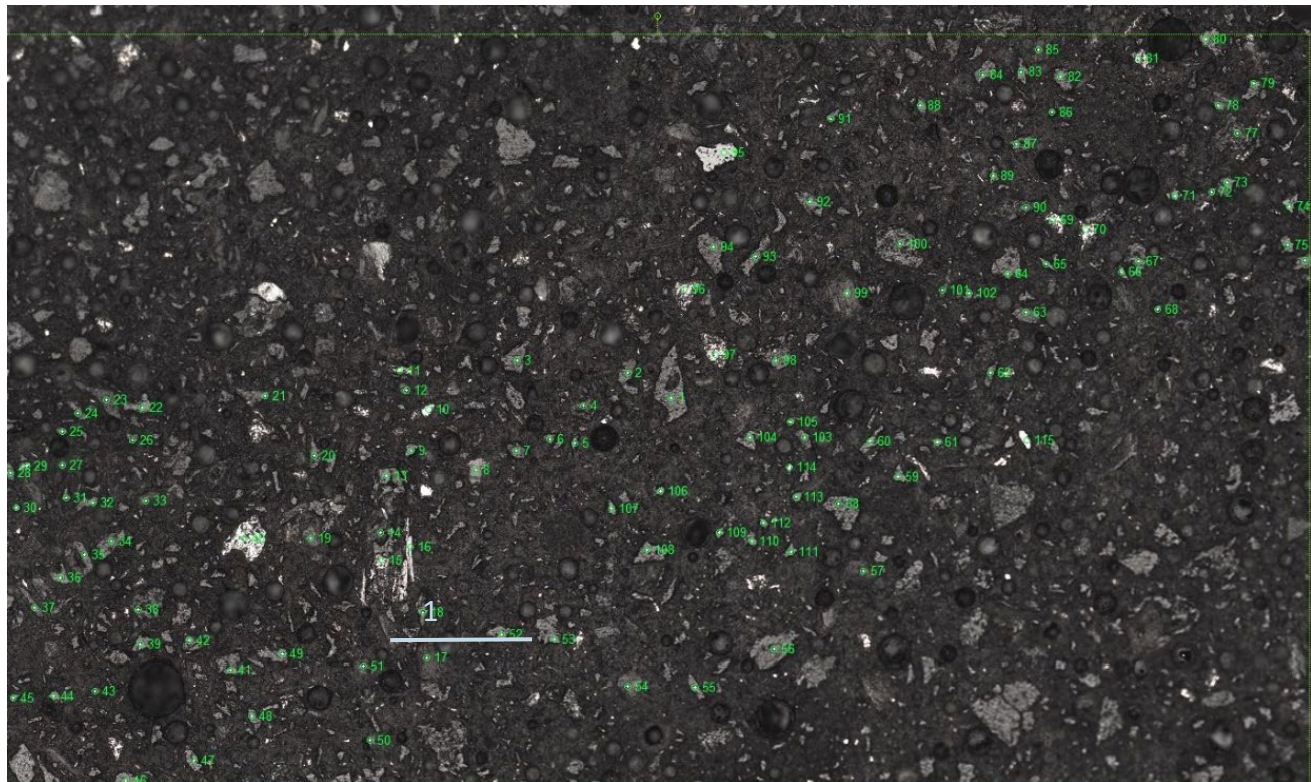


Figure K14. Point analysis of the APTW-C tailing sample resin pack.

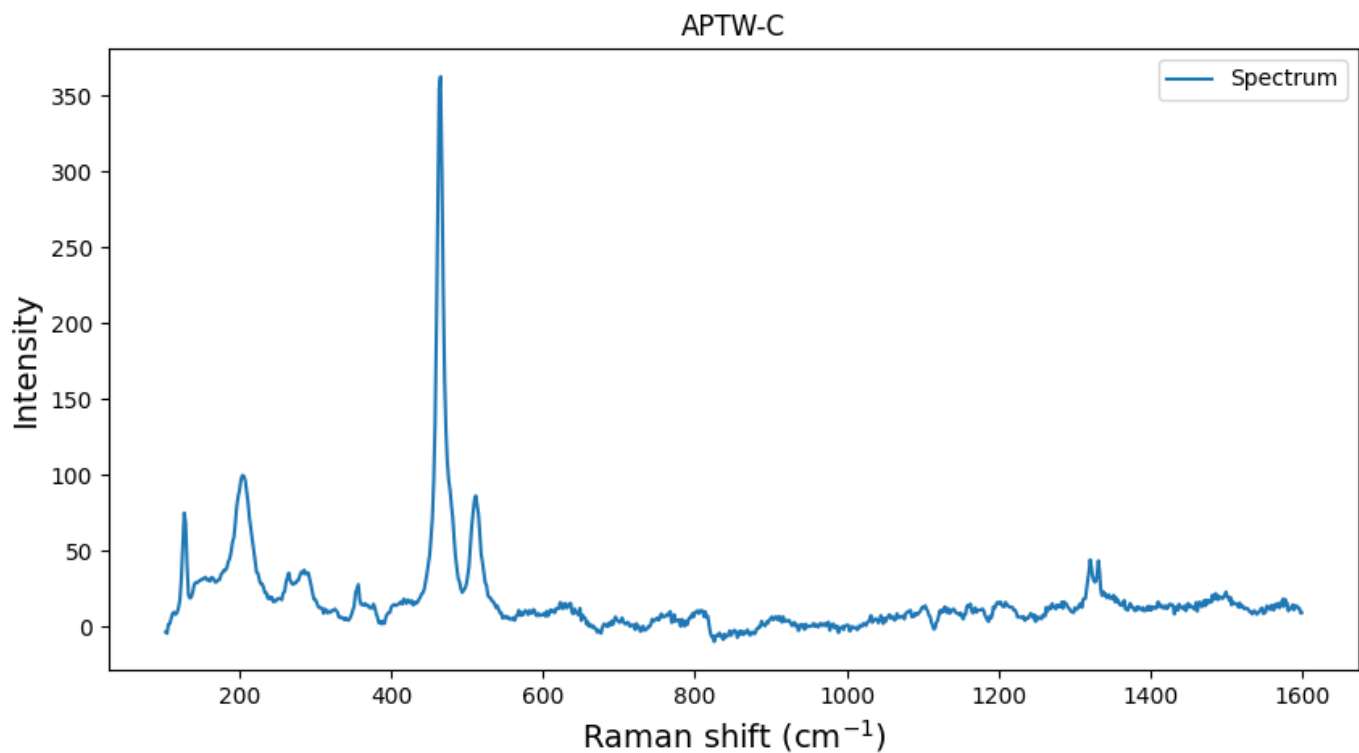
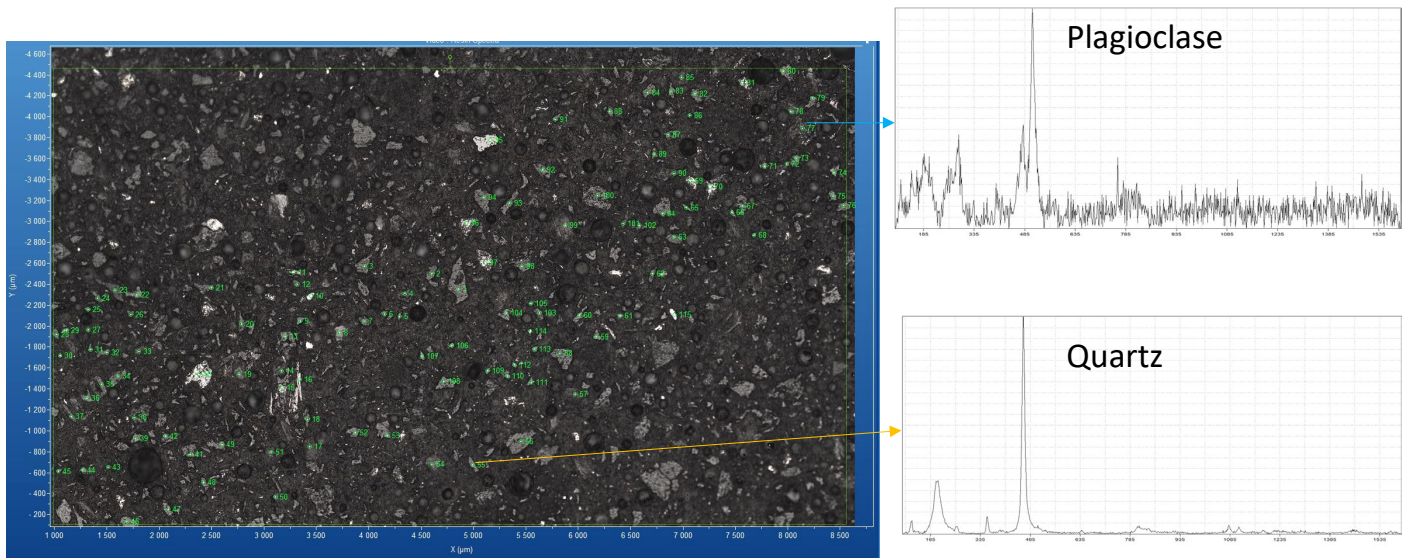


Figure K15. Cumulative spectrum of tailing sample APTW-C, calculated using the point analysis as shown in Figure K13.



Sample Aitolampi Pilot Tailings West APTW-C – Raman

30.2.7 Aitolampi Pilot Tailings East APTE-C

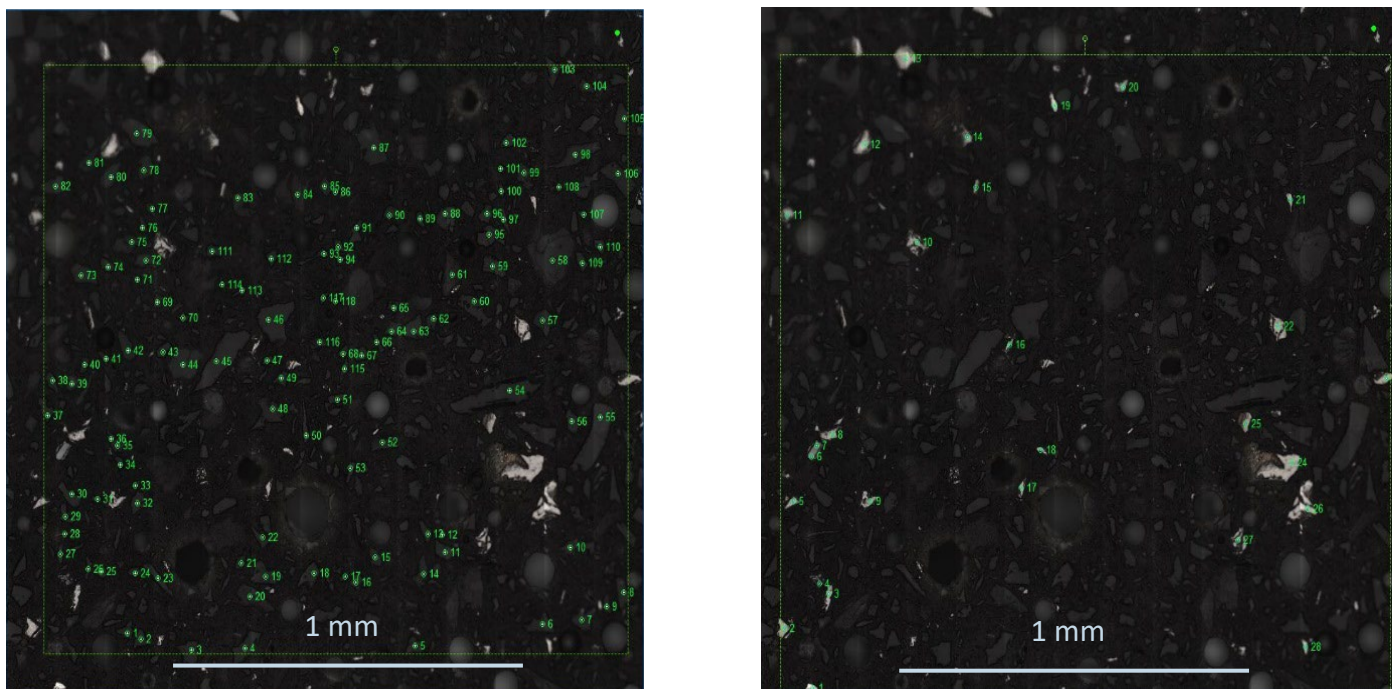


Figure K16. Point analysis of the APTE-C tailing sample resin pack on non-opaque mineral phases (left-hand side) and opaque mineral phases (right-hand side).

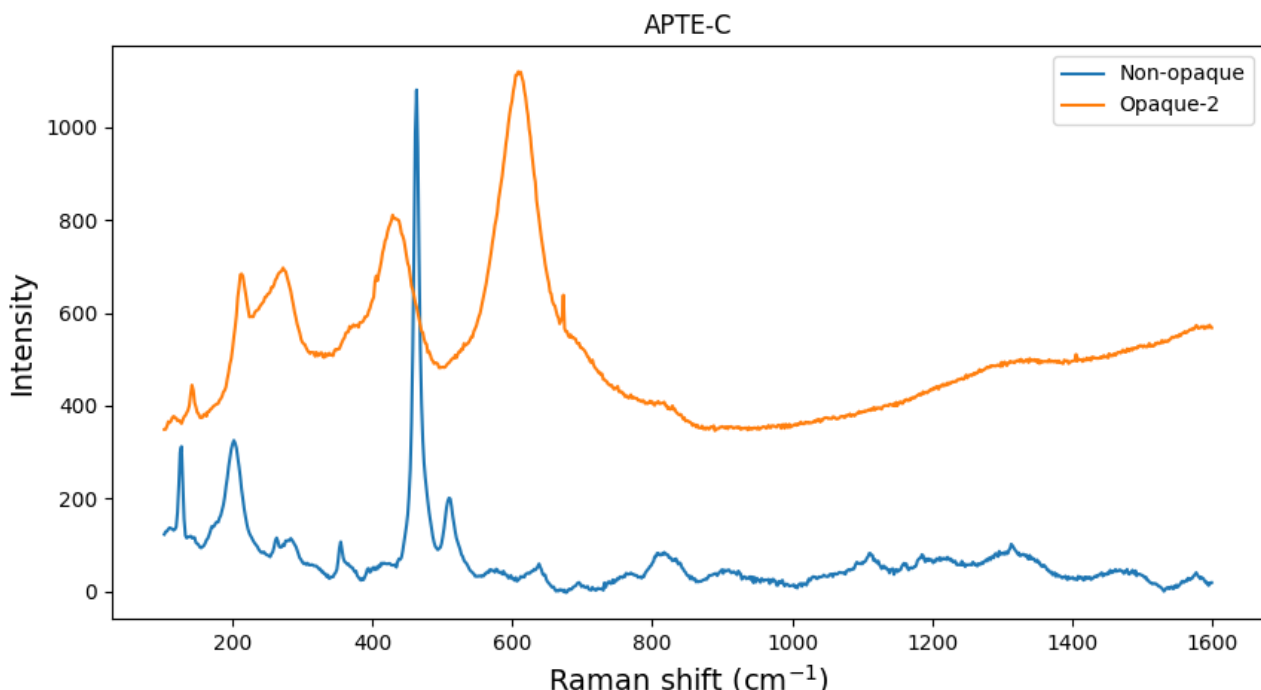
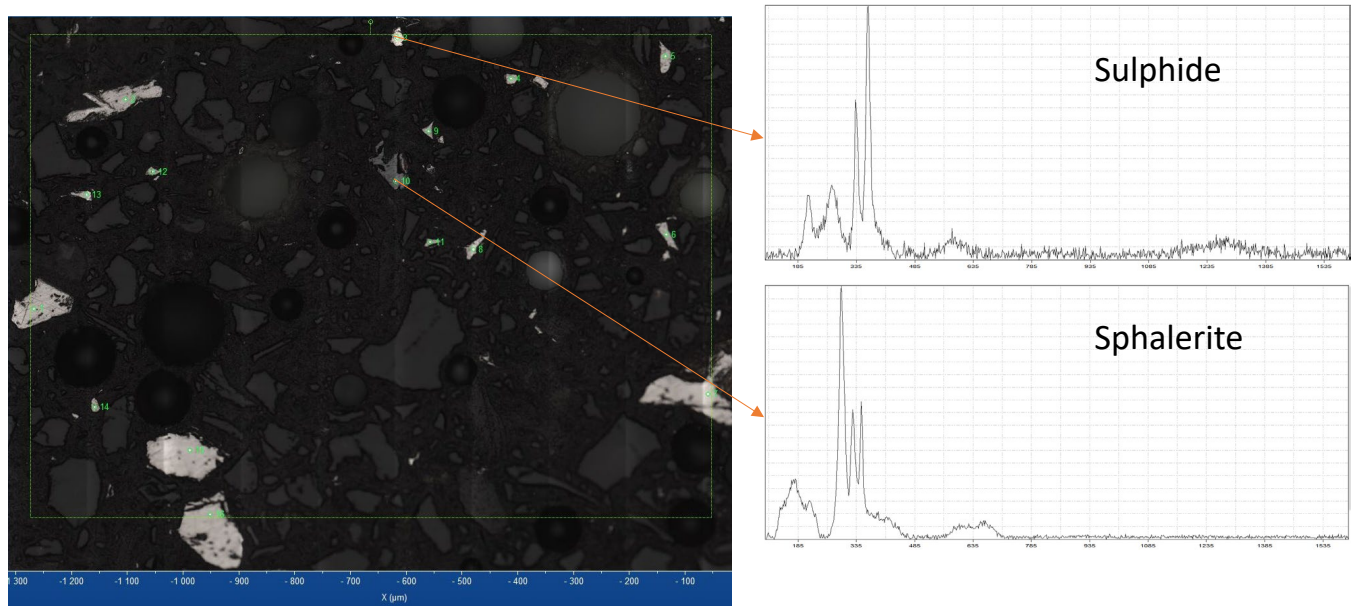


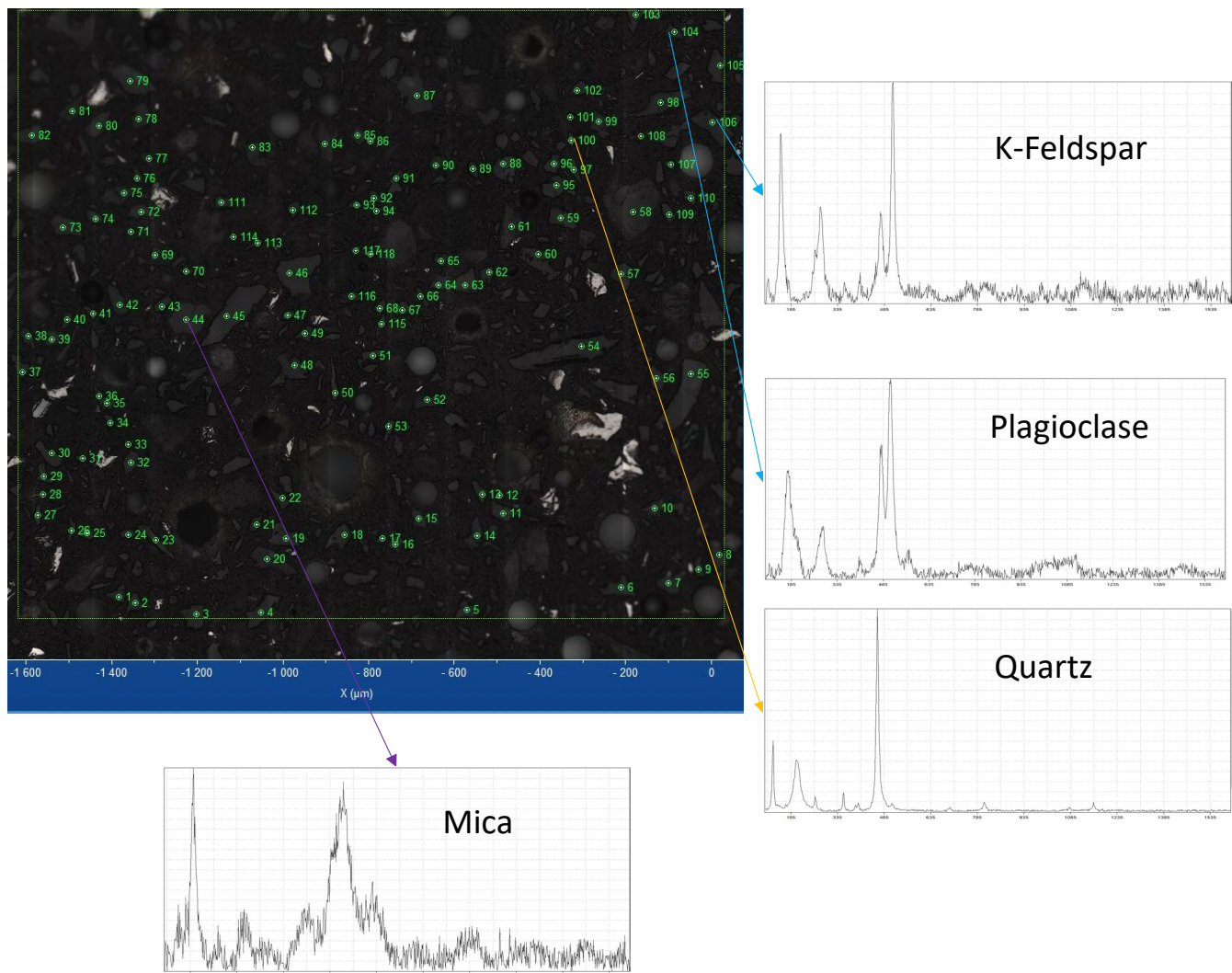
Figure K17. Cumulative spectra of the non-opaque phases and opaque phase derived by the point analysis as shown in Figure K15.

Opaque phases



Sample Aitolahti Pilot Tailings East APTE-C – Raman

Silicates (Non-opaque)



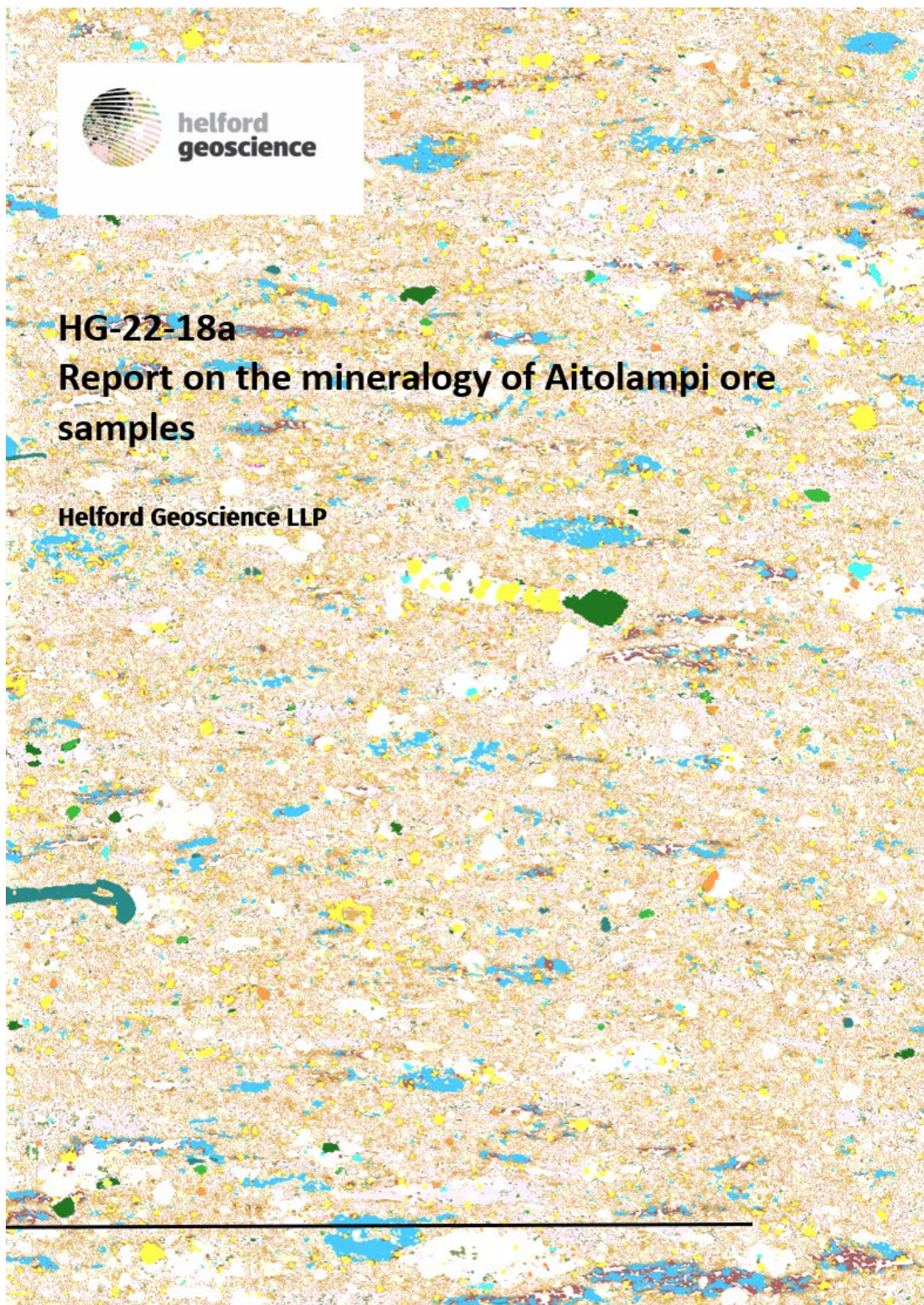
30.3 Appendix K - Conclusions

Graphite ore and tailings samples were analyzed with Raman microscopy, producing individual mineral spectra, as shown in the Appendix, as well as cumulative spectra as shown in this report using (high resolution) scan maps point analyses. This report also demonstrates how Raman microscopy can give a textural analysis of the ore rock chips and/or tailing samples, giving additional information about the presence and relationship of graphite within the rock matrix and the silicate mineral phases.

The mineralogical results follow the findings of the QXRD however in a more qualitative manner. In order to approximate the QXRD results, high resolution scans are required to acquire statistical representation of the mineral phases. However, we found that Raman microscopy can prove robust in terms of data quality and textural analysis, with high resolution optical images accompanied with basic mineral identification. Integrating these two sets of information and compiled it in Spotfire can give a very good representation and summary of the analyzed sample for minerals of interest, their distribution and relationships to the matrix.

31 APPENDIX L - AUTOMATED MINERALOGY SEM

Samples were prepared and investigated by Duncan Pirrie, Helford Geoscience LLP. using automated SEM-EDS along with individual spot chemical analyses using EDS (this work was conducted as a subcontractor through X-Ray Mineral Services Oy). The aim of the analysis is to gain an understanding of how the metals are occurring within the sample along with what form any Br, Bi and Se present is occurring in.



L1. Introduction

Five samples, each subdivided into three size fractions (-250/+150 µm, -150/+75 µm and -75 µm) from the Aitolampi project were submitted to Helford Geoscience LLP for mineralogical analysis using automated SEM-EDS (Table L1). The analysis of three replicate blocks from the coarsest size fraction, two from the middle fraction and one from the finest size fraction of each sample was requested, so that in total 30 blocks were prepared and measured. Automated SEM-EDS is a widely used methodology for the characterization of the mineralogy of exploration samples, processed ore concentrates and waste streams (e.g. Schultz *et al.*, 2020).

Table L1. Samples submitted for analysis and laboratory code

Sample Number	Size fractions	Replicate blocks	Lab codes
PA1-CAM	-250/+150 µm	3	VL-22198:001 A, B, C
	-150/+75 µm	2	VL-22198:002 A, B
	-75 µm	1	VL-22198:003
QA2-CAM	-250/+150 µm	3	VL-22198:004 A, B, C
	-150/+75 µm	2	VL-22198:005 A, B
	-75 µm	1	VL-22198:006
XA3-CAM	-250/+150 µm	3	VL-22198:007 A, B, C
	-150/+75 µm	2	VL-22198:008 A, B
	-75 µm	1	VL-22198:009
YA4-CAM	-250/+150 µm	3	VL-22198:010 A, B, C
	-150/+75 µm	2	VL-22198:011 A, B
	-75 µm	1	VL-22198:012
ZA5-CAM	-250/+150 µm	3	VL-22198:013 A, B, C
	-150/+75 µm	2	VL-22198:014 A, B
	-75 µm	1	VL-22198:015

L2. Analytical techniques

On receipt the samples were sealed within plastic zip lock sample bags containing a dry sized sample (Figure 1). The samples were digitally photographed and then subsampled and prepared for analysis as resin impregnated polished blocks and given unique laboratory codes (Table L1). A representative aliquot of each sample was dispersed with a filler and then resin impregnated. On curing, the resin block was then cross sectioned and the cross sectioned surfaces remounted within a resin block, and then polished, so that both area of the cross section were within the polished face for analysis. This preparation method was used to test for particle segregation within the resin. For each of the five samples, three replicates were analyzed from the -250/+150 µm size fraction, two replicates were analyzed from the -150/+75 µm size fraction and one sample was prepared and measured from the -75 µm size fraction. The data for each separate subsample are provided. The mineralogy and texture of the samples was quantified through automated SEM-EDS mineral analysis (Schultz *et al.*, 2020). Analysis was undertaken using a Hitachi SU3900 scanning electron microscope fitted with a single large area (60 mm²) Bruker SDD energy dispersive spectrometer and

running the AMICS automated mineralogy software package. Beam conditions are optimized for analysis and therefore an accelerating voltage of 20kV coupled with a beam current of approximately 15 nA were used. The samples were measured with a segmented field image mode of analysis. This analytical mode subdivides the BSE image into domains (segments) of similar brightness which represent different mineral grains / crystals and then acquires a representative EDS X-ray spectrum from a point within the segment; the mineral identified is then assigned to the entire segment. Measurements are optimized to highlight both textural and modal mineralogical information and so an effective image resolution of 2.12 µm is achieved.

The EDS spectra acquired during the measurement are compared with a library of measured and synthetic standards and a mineral identification is made on a closest match basis. Phases which are not represented in the standards list at the time of measurement are added either by acquiring reference spectra directly from the sample, or by creating a reference spectrum from the measurement itself. As the standards list can comprise hundreds of reference spectra, the data are grouped into a final, reported mineral list (Table L2). Modal data, expressed as both mass % and area % are provided (excel file HG-22-18b) along with mineral association data (excel file HG-22-18c), mineral size distribution data (excel file HG-22-18d) and mineral liberation data (excel file HG-22-18e) for the potential ore phases. The mineral size data are the individual "grains" of the mineral of interest which are mostly enclosed within a larger particle or, if liberated, are particles themselves. In the mineral size data the size groupings are the virtual screen mesh size (in microns) converted from imperial or mesh units. The retained wt % data is the calculated mass of particles or grains retained on the virtual screen. The cumulative passing is the inverse. For the grain size data, the particle count should really be "grain count" as it is the number of individual grains measured (there may be more than one grain in a particle). During the automated mineralogy analysis, a full area SEM-BSE montage is also captured of the analyzed area. AMICS particle images and SEM-BSE images are summarized in powerpoint files HG-22-18f (PA1-CAM), HG-22-18g (QA2-CAM), HG-22-18h (XA3-CAM), HG-22-18i (YA4-CAM) and HG-22-18j (ZA5-CAM).



Figure L1. Representative digital image of sample submitted for analysis.

Table L2. Mineral groupings used to process the data.

Mineral	Description
Quartz	Silica group of minerals (e.g. quartz, cristobalite, etc). Includes opal and chert.
Orthoclase	K-rich alkali feldspar including orthoclase, sanidine & microcline.
Plagioclase	Plagioclase compositions ranging from albite to anorthite.
Muscovite	Muscovite and other aluminous micas. For brevity, also includes illite.
Biotite	Biotite and other Fe-rich micas. May include Ti-bearing mica varieties.
Phlogopite	Mg-rich mica varieties such as phlogopite.
Vermiculite	Mg-rich, K-poor aluminosilicates such as vermiculite. May include orthorhombic amphiboles such as anthophyllite.
Kaolinite	Kaolinite and other aluminosilicates such as kyanite, topaz etc.
Chlorite	Chlorite and other Mg-bearing aluminosilicates.
Cpx and Amphibole	Diopside, hornblende and other Ca-bearing Mg silicates.
Ca Al Silicates	Ca Al silicate phases such as epidote and zoisite.
Graphite	Graphite.
Calcite	Calcite. Dolomite and ankerite are included.
Pyrite	Pyrite, marcasite and other S-rich Fe sulphides.
Pyrrhotite	Pyrrhotite and other Fe-rich Fe sulphides.
Chalcopyrite	Cu sulphides. Primarily chalcopyrite but may also include bornite, covellite etc.
Sphalerite	Zn sulphides such as sphalerite.
Molybdenite	Molybdenite. May also include minor galena and / or elemental sulphur.
Fe Oxides	Fe oxides and hydroxides. May also include iron / steel. Can contain minor amounts of Mn.
Ti Oxide	Ti oxides such as rutile, anatase and ilmenite.
Titanite	Ca Ti silicates such as titanite. May also include perovsite.
Apatite	Ca phosphates.
Zircon and Monazite	Zircon, monazite and xenotime.
Undifferentiated	Undifferentiated mineral phases (trace quantities).

L3. Sample Descriptions

L3.1 Sample PA1-CAM

L3.1.1 Modal mineralogy

The modal mineralogy data for Sample PA1-CAM for the three size fractions and replicate analyses are presented in Table 3 as mass %; the data presented as both mass % and also area % are also provided within excel file HG-22-18b. Mineral association data (excel file HG-22-18c), mineral size distribution data (excel file HG-22-18d) and mineral liberation data (excel file HG-22-18e) for the potential ore phases are also provided. In this summary major minerals form >10%, minor minerals 1-10% and trace minerals (<1%).

The -250/+150 µm size fraction for Sample PA1-CAM is composed of major quartz (22.79-23.50%), plagioclase (15.08-15.62%) and pyrrhotite (14.56-17.57%) along with minor orthoclase, muscovite, biotite, phlogopite, vermiculite, chlorite, clinopyroxene and amphibole, CaAl silicates, graphite (2.07-6.11%) and pyrite (1.62-2.11%). Trace phases present are: kaolinite, calcite, chalcopyrite (0.13-0.29%), sphalerite (0.42-0.56%), molybdenite (0.01%), Fe oxides, Ti oxides, titanite, apatite, zircon and monazite and “undifferentiated” (Table L3, Figures L2 and L3).

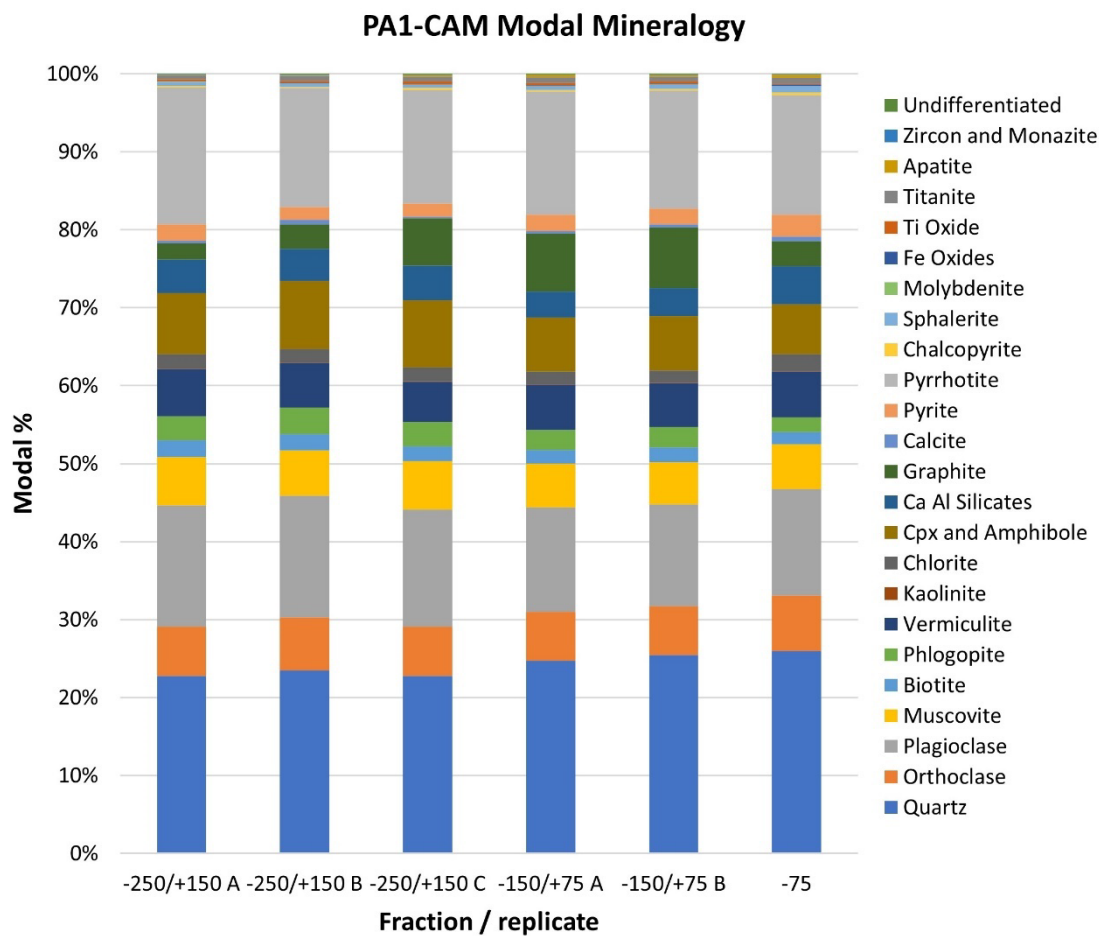
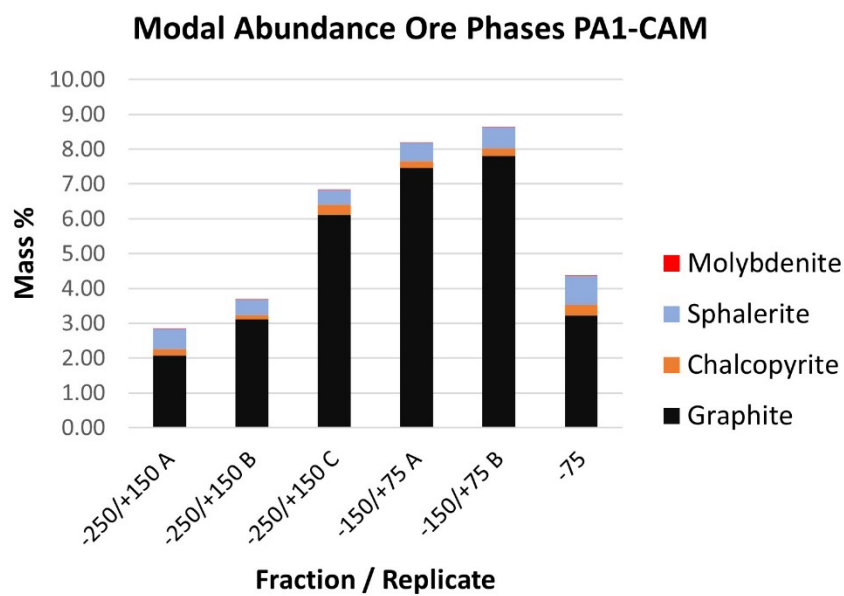
The -150/+75 µm size fraction for Sample PA1-CAM is composed of major quartz (24.74-25.47%), plagioclase (13.07-13.40%) and pyrrhotite (15.11-15.84%) along with minor orthoclase, muscovite, biotite, phlogopite, vermiculite, chlorite, clinopyroxene and amphibole, CaAl silicates, graphite (7.47-7.81%) and pyrite (2.02-2.06%). Trace phases present are: kaolinite, calcite, chalcopyrite (0.19-0.21%), sphalerite (0.53-0.61%), molybdenite (0.02%), Fe oxides, Ti oxides, titanite, apatite, zircon and monazite and “undifferentiated” (Table L3, Figures L2 and L3).

The -75 µm size fraction for Sample PA1-CAM is composed of major quartz (25.97%), plagioclase (13.68%) and pyrrhotite (15.38%) along with minor orthoclase, muscovite, biotite, phlogopite, vermiculite, chlorite, clinopyroxene and amphibole, CaAl silicates, graphite (3.22%) and pyrite (2.81%). Trace phases present are: kaolinite, calcite, chalcopyrite (0.31%), sphalerite (0.83%), molybdenite (0.02%), Fe oxides, Ti oxides, titanite, apatite, zircon and monazite and “undifferentiated” (Table L3, Figures L2 and L3).

Table L3. Quantitative mineralogy based on automated mineralogy Sample PA1-CAM.

Sample Number	PA1-CAM	PA1-CAM	PA1-CAM	PA1-CAM	PA1-CAM	PA1-CAM
Size Fraction (Microns)	-250/+150	-250/+150	-250/+150	-150/+75	-150/+75	-75
Replicate	A	B	C	A	B	
Quartz	22.80	23.50	22.79	24.74	25.47	25.97
Orthoclase	6.28	6.79	6.29	6.26	6.22	7.12
Plagioclase	15.55	15.62	15.08	13.40	13.07	13.68
Muscovite	6.22	5.81	6.17	5.60	5.47	5.70
Biotite	2.19	2.04	1.90	1.77	1.89	1.60
Phlogopite	3.06	3.44	3.13	2.55	2.61	1.90
Vermiculite	6.02	5.73	5.20	5.82	5.60	5.85
Kaolinite	0.12	0.06	0.06	0.06	0.08	0.07
Chlorite	1.79	1.72	1.74	1.60	1.56	2.12
Cpx and Amphibole	7.83	8.77	8.59	6.92	6.98	6.45
Ca Al Silicates	4.35	4.12	4.44	3.35	3.56	4.87
Graphite	2.07	3.12	6.11	7.47	7.81	3.22
Calcite	0.30	0.59	0.18	0.31	0.40	0.55
Pyrite	2.11	1.62	1.69	2.06	2.02	2.81
Pyrrhotite	17.57	15.28	14.56	15.84	15.11	15.38
Chalcopyrite	0.20	0.13	0.29	0.19	0.21	0.31
Sphalerite	0.56	0.43	0.42	0.53	0.61	0.83
Molybdenite	0.01	0.01	0.01	0.02	0.02	0.02
Fe Oxides	0.01	0.09	0.04	0.06	0.03	0.18
Ti Oxide	0.28	0.29	0.39	0.33	0.36	0.19
Titanite	0.49	0.60	0.54	0.71	0.54	0.67
Apatite	0.11	0.12	0.25	0.31	0.25	0.40
Zircon and Monazite	0.04	0.03	0.04	0.03	0.06	0.07
Undifferentiated	0.04	0.11	0.09	0.07	0.08	0.04
Total	100.00	100.00	100.00	100.00	100.00	100.00

Figure L2 demonstrates that there is very little variance in the modal mineralogy between both the different size fractions and the different replicates of the same size fraction. Figure L3 shows the abundance of graphite, chalcopyrite, sphalerite and molybdenite in the analysed fractions / replicates. Graphite abundance varies between 2.07 and 7.81% and is most abundant within the -150/+75 µm size fraction for Sample PA1-CAM. Chalcopyrite abundance varies between 0.13 and 0.31%, whilst sphalerite ranges between 0.42 and 0.83%.

**Figure L2.** Modal mineralogy (mass %) all phases for Sample PA1-CAM**Figure L3.** Modal mineralogy (mass %) ore phases for Sample PA1-CAM.

L3.1.2 AMICS and SEM-BSE imaging

AMICS particle textural images for Sample PA1-CAM are provided in powerpoint file HG-22-18f; high resolution images are provided electronically. The particle images provide the mineralogical data in overall textural context. Individual particles may be small rock fragments, or effectively liberated individual mineral grains. As can be seen in Figure L4, even within the -250/+150 µm size fraction for Sample PA1-CAM, the mineral phases are typically well liberated.

AMICS particle images sample PA1-CAM A -250/+150 µm

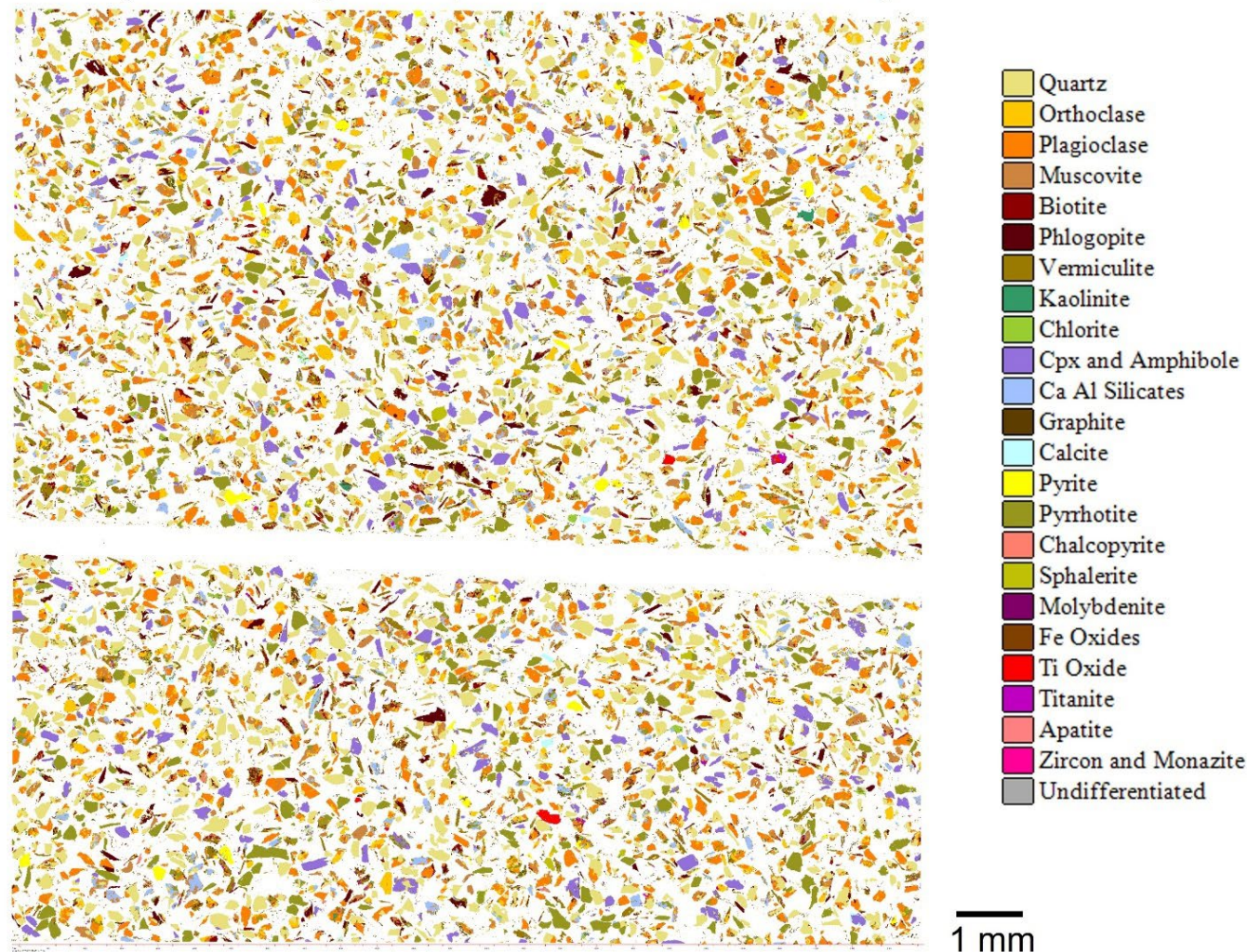


Figure L4. Representative example of AMICS particle images Sample PA1-CAM -250/+150 µm size fraction replicate A. Note that even within this, the coarsest size fraction, the mineral phases are characteristically well liberated.

During AMICS measurement, a scanning electron microscope backscatter electron (SEM-BSE) image of the area measured is also collected. The SEM-BSE images are provided in powerpoint file HG-22-18f, along with the corresponding AMICS mineral images. An example is provided in Figure L5. High resolution “zoomable” images are also provided electronically. THE SEM-BSE images provide additional textural information and show the correspondence between the AMICS mineral “map” and the SEM-BSE image. Note the apparent high degree of mineral liberation.

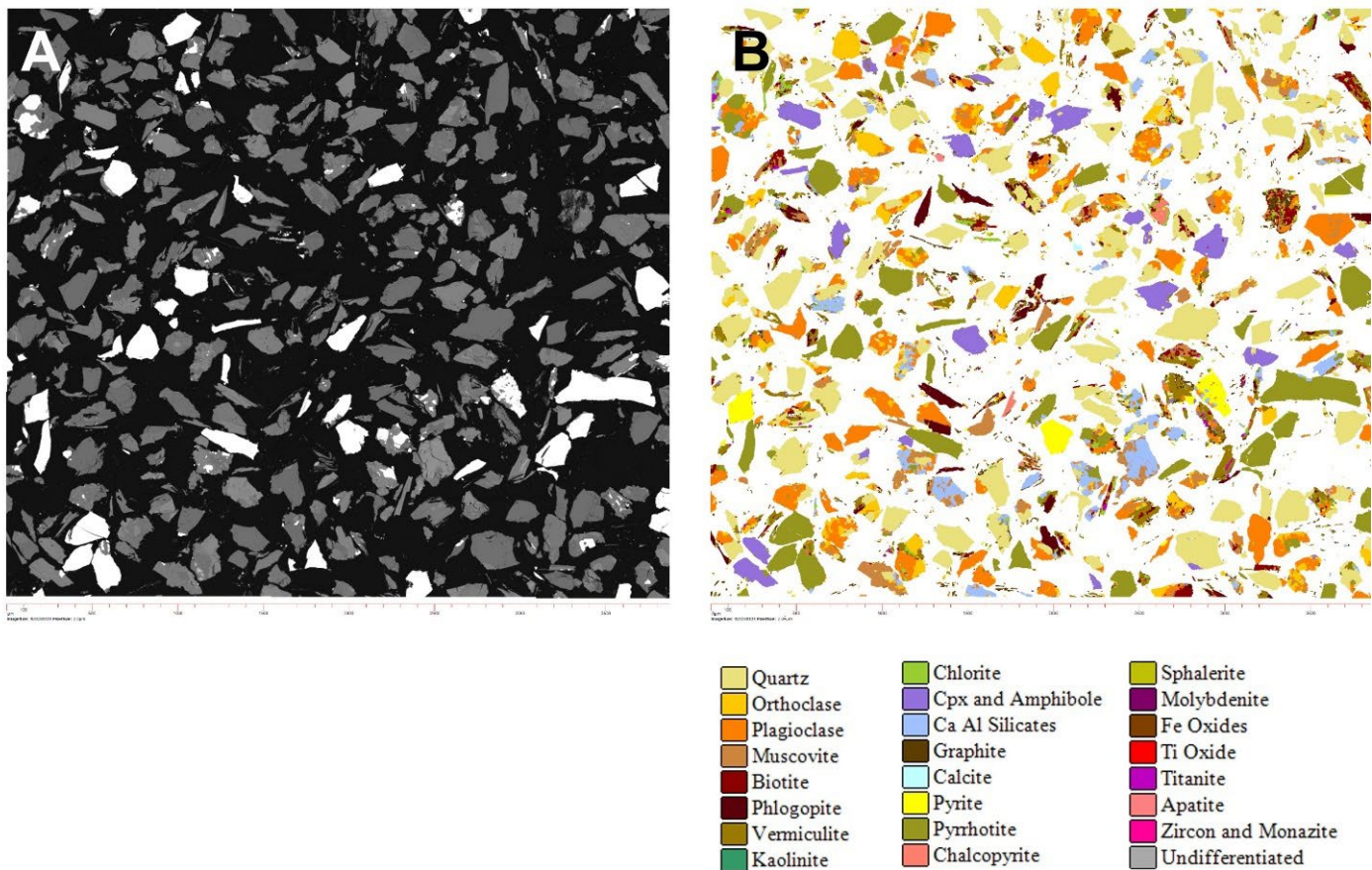


Figure L5. Higher magnification SEM-BSE image (A) and AMICS particle image (B) for the corresponding area Sample PA1-CAM - 250/+150 µm size fraction replicate A. Note the clear correspondence between the AMICS and the SEM-BSE images.

L3.1.3 Mineral size, mineral liberation, and mineral association data

Based on the AMICS analyses, three additional data sets are provided: mineral association data are provided for all phases and all samples within excel file HG-22-18c. These data are based on the observed transitions from one mineral to the adjoining mineral. Where there is a transition to “background” it shows that the mineral phase is surrounded by the resin i.e. the mineral grain is liberated. Mineral association data for graphite are summarized in Table L4. Graphite is predominantly (64-80.5%) associated with “background” i.e. is liberated or is associated with vermiculite (4.8-8.5%), muscovite (2.5-4.5%), quartz (2.4-3.6%), plagioclase (2.0-4.0%), orthoclase (1.8-3.2%) and chlorite (1.4-3.3%). Mineral associations for all other phases are <2%.

Table L4. Graphite mineral association data Sample PA1-CAM.

Mineral	-250/+150 A	-250/+150 B	-250/+150 C	-150/+75 A	-150/+75 B	-75
Background	64.2	70.2	75.0	80.5	78.4	71.7
Quartz	3.6	3.3	3.3	2.4	2.7	2.6
Orthoclase	3.2	2.8	2.5	1.8	1.8	2.1
Plagioclase	4.0	3.4	2.7	2.0	2.1	3.0
Muscovite	4.5	3.4	3.1	2.5	2.5	3.3
Biotite	2.2	1.6	1.5	1.0	1.1	1.4
Phlogopite	1.9	1.3	1.3	0.9	1.2	1.4
Vermiculite	8.5	6.9	5.2	4.8	5.3	7.8
Kaolinite	0.1	0.1	0.1	0.1	0.1	0.1
Chlorite	3.3	2.7	1.8	1.4	1.4	2.7
Cpx and Amphibole	1.2	1.1	0.9	0.6	0.9	0.8
Ca Al Silicates	1.1	1.2	1.1	0.5	0.6	0.7
Graphite	0.0	0.0	0.0	0.0	0.0	0.0
Calcite	0.2	0.2	0.1	0.1	0.1	0.2
Pyrrite	0.4	0.3	0.3	0.3	0.3	0.4
Pyrrhotite	0.8	0.8	0.6	0.6	0.8	0.8
Chalcopyrite	0.1	0.0	0.0	0.1	0.0	0.1
Sphalerite	0.1	0.1	0.1	0.1	0.1	0.1
Molybdenite	0.0	0.0	0.0	0.0	0.0	0.0
Fe Oxides	0.0	0.0	0.0	0.0	0.0	0.1
Ti Oxide	0.0	0.0	0.1	0.0	0.1	0.1
Titanite	0.4	0.4	0.3	0.3	0.2	0.3
Apatite	0.1	0.1	0.1	0.0	0.1	0.1
Zircon and Monazite	0.0	0.0	0.0	0.0	0.0	0.0
Undifferentiated	0.0	0.1	0.1	0.1	0.0	0.0

Mineral size distribution data are provided for graphite, chalcopyrite, pyrite, pyrrhotite and sphalerite within excel file HG-22-18d; size data for other reported phases are available on request. This provides mineral size data irrespective of whether or not the mineral phase is liberated. The grain size data for graphite are summarized in Figure L6. Within both the -250/+150 and -150/+75 μm size fractions, the graphite particles have a grain size ranging between 63 and 2 μm size, with a mode of 11 μm . This reduces in the -75 μm size fraction with a range between 16 and 2 μm , with a mode of 4 μm . It should be noted that the AMICS grain size data are based on the measured 2D sample.

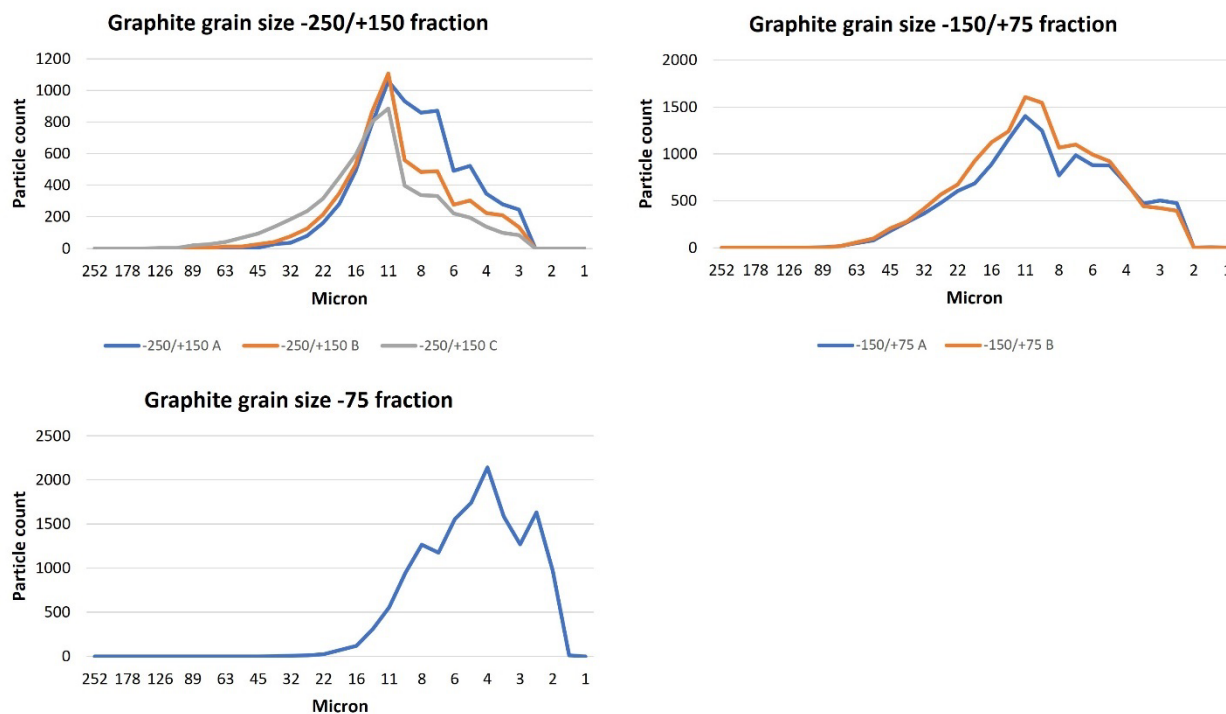


Figure L6. Graphs highlighting the grain size distribution data for graphite in the three size fractions analyzed from Sample PA1-CAM.

Mineral liberation data are provided for graphite, chalcopyrite, pyrite, pyrrhotite and sphalerite within excel file HG-22-18e. For graphite, the liberation data show that in the -250/+150 μm size fraction graphite liberation >70% ranges between 24-48%, 56-58% in the -150/+75 μm size fraction and 37% in the -75 μm size fraction.

L3.2 Sample QA2-CAM

L3.2.1 Modal mineralogy

The modal mineralogy data for Sample QA2-CAM for the three size fractions and replicate analyses are presented in Table 5 as mass %; the data presented as both mass % and also area % are also provided within excel file HG-22-18b. Mineral association data (excel file HG-22-18c), mineral size distribution data (excel file HG-22-18d) and mineral liberation data (excel file HG-22-18e) for the potential ore phases are also provided. In this summary major minerals form >10%, minor minerals 1-10% and trace minerals (<1%). The -250/+150 μm size fraction for Sample QA2-CAM is composed of major quartz (27.38-29.52%), plagioclase (23.21-24.66%), phlogopite (11.00-12.36%) and pyrrhotite (9.55-11.55%) along with minor orthoclase, muscovite, biotite, vermiculite, chlorite, clinopyroxene and amphibole, CaAl silicates, graphite (1.68-1.95%) and pyrite (2.09-2.82%). Trace phases present are: kaolinite, calcite, chalcopyrite (0.09-0.27%), sphalerite (0.27-0.73%), molybdenite (0.01-0.02%), Fe oxides, Ti oxides, titanite, apatite, zircon and monazite and "undifferentiated" (Table K5, Figures K7 and K8). The -150/+75 μm size fraction for Sample QA2-CAM is composed of major quartz (32.18-32.58%), plagioclase (21.07-22.54%), phlogopite (10.60-10.62%) and pyrrhotite (9.45-11.11%) along with minor orthoclase, muscovite, biotite, vermiculite, chlorite, clinopyroxene and amphibole, CaAl silicates, graphite (1.44-1.53%) and pyrite (1.76-1.96%). Trace phases

present are: kaolinite, calcite, chalcopyrite (0.12-0.18%), sphalerite (0.42-0.72%), molybdenite (0.01-0.02%), Fe oxides, Ti oxides, titanite, apatite, zircon and monazite and “undifferentiated” (Table L5, Figures L7 and L8). The -75 µm size fraction for Sample QA2-CAM is composed of major quartz (30.69%), plagioclase (22.68%) and pyrrhotite (10.98%) along with minor orthoclase, muscovite, biotite, phlogopite, vermiculite, chlorite, clinopyroxene and amphibole, CaAl silicates, graphite (1.60%) and pyrite (3.24%). Trace phases present are: kaolinite, calcite, chalcopyrite (0.28%), sphalerite (0.52%), molybdenite (0.02%), Fe oxides, Ti oxides, titanite, apatite, zircon and monazite and “undifferentiated” (Table L5, Figures L7 and L8).

Table L5. Quantitative mineralogy based on automated mineralogy Sample QA2-CAM.

Sample Number	QA2-CAM	QA2-CAM	QA2-CAM	QA2-CAM	QA2-CAM	QA2-CAM
Size Fraction (Microns)	-250/+150	-250/+150	-250/+150	-150/+75	-150/+75	-75
Replicate	A	B	C	A	B	
Quartz	27.80	27.38	29.52	32.18	32.58	30.69
Orthoclase	5.83	6.57	6.06	5.87	6.10	7.17
Plagioclase	24.66	24.27	23.21	22.54	21.07	22.68
Muscovite	2.67	2.51	2.59	3.00	2.67	3.05
Biotite	1.40	1.46	1.42	1.62	1.69	1.72
Phlogopite	11.00	12.36	12.35	10.60	10.62	6.40
Vermiculite	2.62	2.90	2.38	2.70	2.32	2.69
Kaolinite	0.20	0.16	0.16	0.18	0.19	0.22
Chlorite	2.35	2.70	2.39	2.57	2.58	3.19
Cpx and Amphibole	2.77	2.02	1.98	2.41	2.00	1.75
Ca Al Silicates	1.24	1.43	1.26	1.29	1.13	1.69
Graphite	1.95	1.81	1.68	1.44	1.53	1.60
Calcite	0.25	0.21	0.22	0.32	0.28	0.48
Pyrite	2.30	2.82	2.09	1.76	1.96	3.24
Pyrrhotite	11.55	9.55	10.83	9.45	11.11	10.98
Chalcopyrite	0.09	0.11	0.27	0.12	0.18	0.28
Sphalerite	0.29	0.73	0.27	0.42	0.72	0.52
Molybdenite	0.01	0.02	0.01	0.01	0.02	0.02
Fe Oxides	0.06	0.02	0.02	0.06	0.08	0.14
Ti Oxide	0.56	0.47	0.52	0.51	0.59	0.51
Titanite	0.21	0.24	0.28	0.39	0.17	0.31
Apatite	0.12	0.20	0.23	0.39	0.34	0.53
Zircon and Monazite	0.05	0.05	0.22	0.12	0.04	0.11
Undifferentiated	0.03	0.02	0.02	0.04	0.04	0.03
Total	100.00	100.00	100.00	100.00	100.00	100.00

Figure L7 demonstrates that there is very little variance in the modal mineralogy between both the different size fractions and the different replicates of the same size fraction. Figure L8 shows the abundance of graphite, chalcopyrite, sphalerite and molybdenite in the analyzed fractions / replicates. Graphite abundance ranges between 1.44 and 1.95%. Chalcopyrite abundance varies between 0.09 and 0.28%, whilst sphalerite ranges between 0.27 and 0.73%.

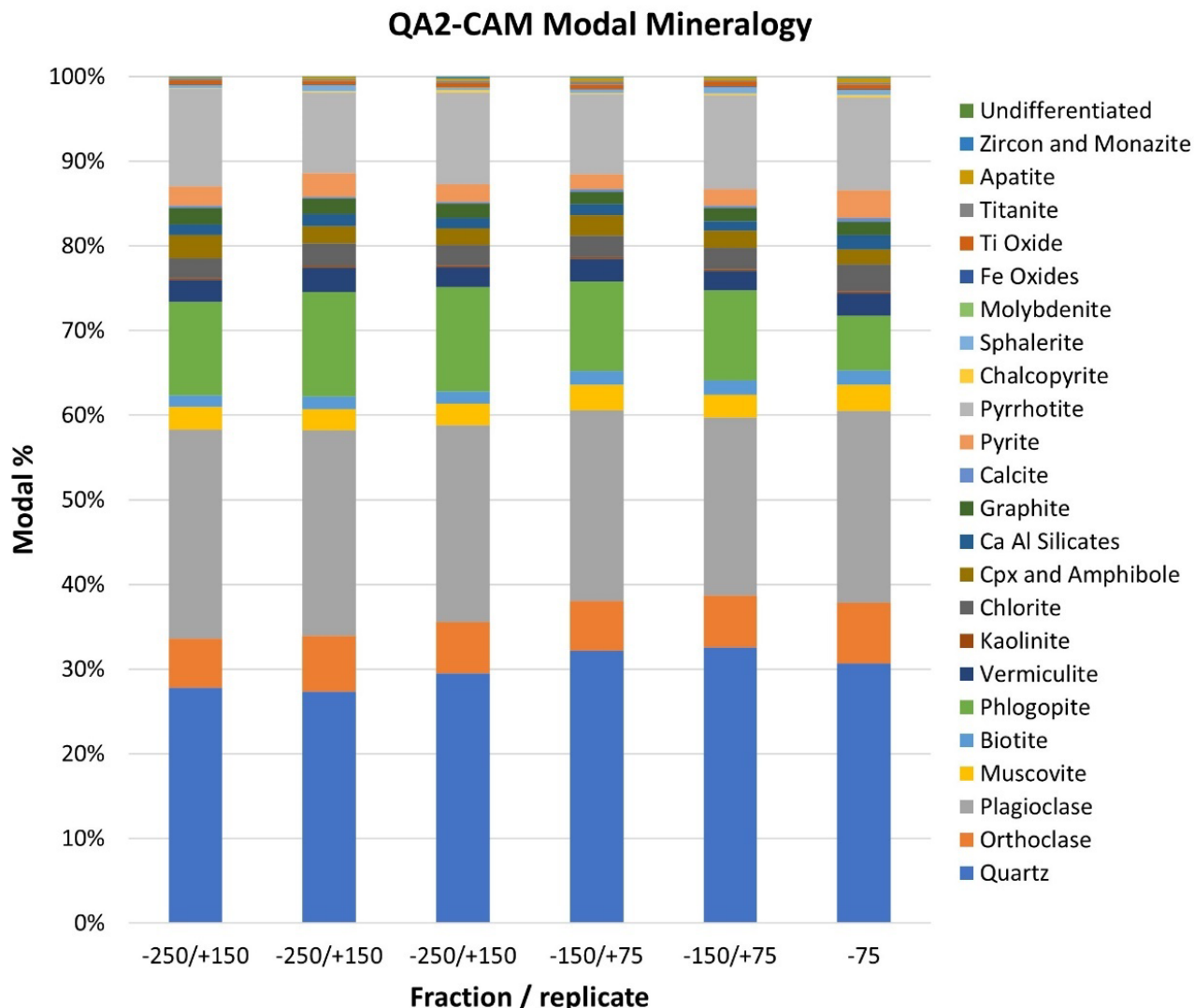


Figure L7. Modal mineralogy (mass %) all phases for Sample QA2-CAM

AMICS particle textural images for Sample QA2-CAM are provided in powerpoint file HG-22-18g; high resolution images are provided electronically. The particle images provide the mineralogical data in overall textural context. Individual particles may be small rock fragments, or effectively liberated individual mineral grains. As can be seen in Figure L9, even within the -250/+150 µm size fraction for Sample QA2-CAM, the mineral phases are typically well liberated.

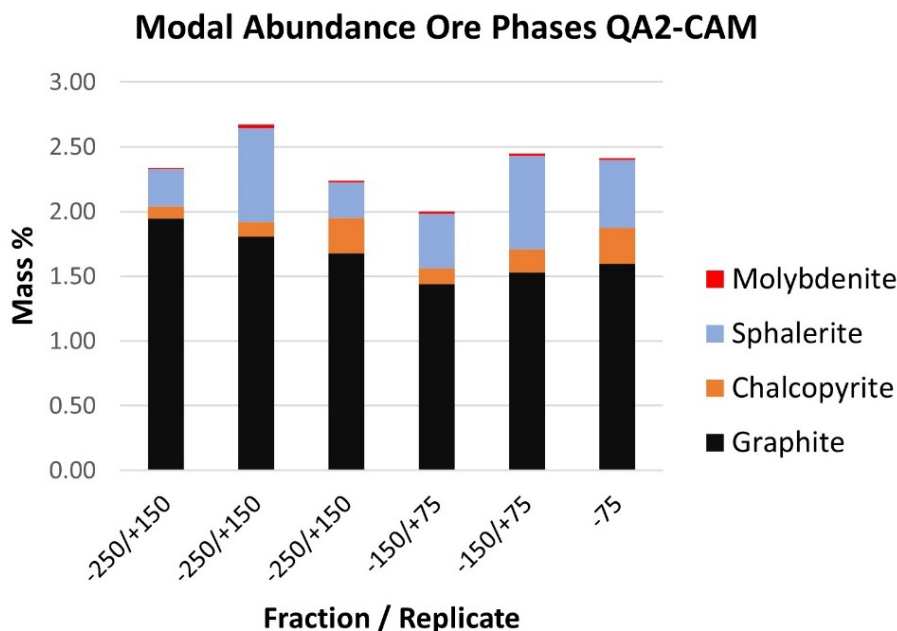


Figure L8. Modal mineralogy (mass %) ore phases for Sample QA2-CAM.

L3.2.2 AMICS and SEM-BSE imaging

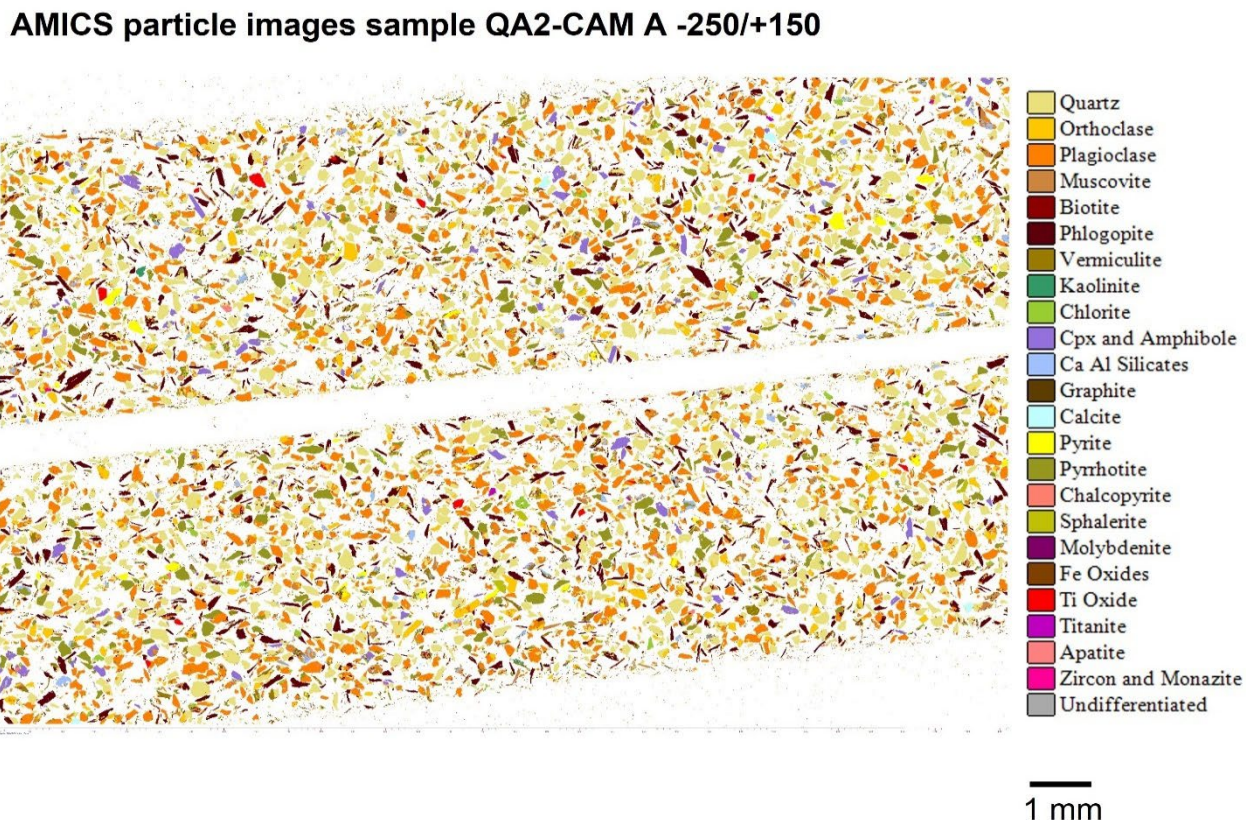


Figure L9. Representative example of AMICS particle images Sample QA2-CAM -250/+150 μm size fraction replicate A. Note that even within this, the coarsest size fraction, the mineral phases are characteristically well liberated.

During AMICS measurement, a scanning electron microscope backscatter electron (SEM-BSE) image of the area measured is also collected. The SEM-BSE images are provided in powerpoint file HG-22-18g, along with the corresponding AMICS mineral images. An example is provided in Figure L10. High resolution “zoomable” images are also provided electronically. THE SEM-BSE images provide additional textural information and show the correspondence between the AMICS mineral “map” and the SEM-BSE image. Note the apparent high degree of mineral liberation.

(A) SEM-BSE and (B) AMICS particle images sample QA2-CAM A -250/+150 (enlarged)

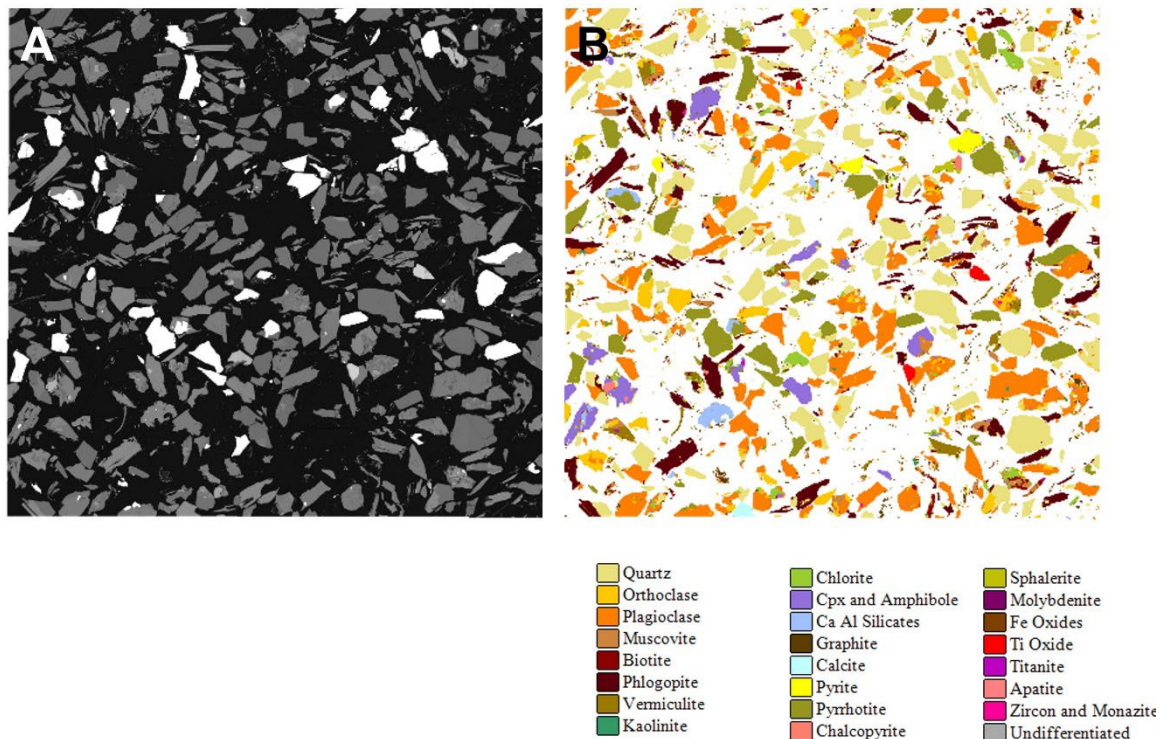


Figure L10. Higher magnification SEM-BSE image (A) and AMICS particle image (B) for the corresponding area Sample QA2-CAM -250/+150 µm size fraction replicate A. Note the clear correspondence between the AMICS and the SEM-BSE images.

K3.2.3 Mineral size, mineral liberation and mineral association data

Based on the AMICS analyses, three additional data sets are provided: mineral association data are provided for all phases and all samples within excel file HG-22-18c. These data are based on the observed transitions from one mineral to the adjoining mineral. Where there is a transition to “background” it shows that the mineral phase is surrounded by the resin i.e. the mineral grain is liberated. Mineral association data for graphite are summarized in Table L6. Graphite is predominantly (64.4-72.1%) associated with “background” i.e. is liberated or is associated with phlogopite (3.3-7.2%), vermiculite (4.1-5.1%), muscovite (2.5-3.2%), quartz (2.4-3.5%), plagioclase (3.7-4.9%), orthoclase (2.0-2.8%), chlorite (3.2-4.1%) and biotite (1.7-2.6%). Mineral associations for all other phases are <1%.

Table L6. Graphite mineral association data Sample QA2-CAM.

Mineral	-250/+150 A	-250/+150 B	-250/+150 C	-150/+75 A	-150/+75 B	-75
Background	64.4	64.7	70.7	71.4	65.3	72.1
Quartz	3.5	3.3	2.9	2.4	2.7	2.5
Orthoclase	2.5	2.6	2.0	2.0	2.8	2.1
Plagioclase	4.9	4.6	3.7	3.7	4.2	4.1
Muscovite	3.0	2.9	2.6	2.8	3.2	2.5
Biotite	2.3	2.3	2.1	2.1	2.6	1.7
Phlogopite	7.0	7.2	5.8	4.6	6.9	3.3
Vermiculite	4.9	5.1	4.1	4.8	5.1	4.6
Kaolinite	0.7	0.5	0.6	0.6	0.6	0.3
Chlorite	3.7	3.9	3.2	3.4	4.1	3.9
Cpx and Amphibole	0.6	0.5	0.4	0.4	0.3	0.3
Ca Al Silicates	0.6	0.7	0.4	0.3	0.4	0.3
Graphite	0.0	0.0	0.0	0.0	0.0	0.0
Calcite	0.1	0.1	0.1	0.2	0.1	0.3
Pyrite	0.5	0.4	0.4	0.2	0.4	0.4
Pyrrhotite	0.8	0.6	0.6	0.5	0.6	0.6
Chalcopyrite	0.0	0.0	0.0	0.0	0.0	0.1
Sphalerite	0.1	0.1	0.0	0.1	0.1	0.1
Molybdenite	0.0	0.0	0.0	0.0	0.0	0.0
Fe Oxides	0.1	0.0	0.1	0.1	0.1	0.1
Ti Oxide	0.1	0.1	0.0	0.1	0.1	0.1
Titanite	0.2	0.3	0.2	0.2	0.2	0.2
Apatite	0.1	0.1	0.0	0.1	0.1	0.1
Zircon and Monazite	0.0	0.0	0.0	0.0	0.1	0.0
Undifferentiated	0.0	0.0	0.0	0.0	0.0	0.0

Mineral size distribution data are provided for graphite, chalcopyrite, pyrite, pyrrhotite and sphalerite within excel file HG-22-18d; size data for other reported phases are available on request. This provides mineral size data irrespective of whether or not the mineral phase is liberated. The grain size data for graphite are summarized in Figure L11. Within the -250/+150 µm size fraction, the graphite particles have a grain size ranging between 32 and 2 µm size, with a mode of 11 µm. Within the -150/+75 µm size fraction, the graphite particles have a grain size ranging between 32 and 2 µm size, with a mode of 6 µm. This reduces in the -75 µm size fraction with a range between 22 and 2 µm, with a mode of 4 µm. It should be noted that the AMICS grain size data are based on the measured 2D sample.

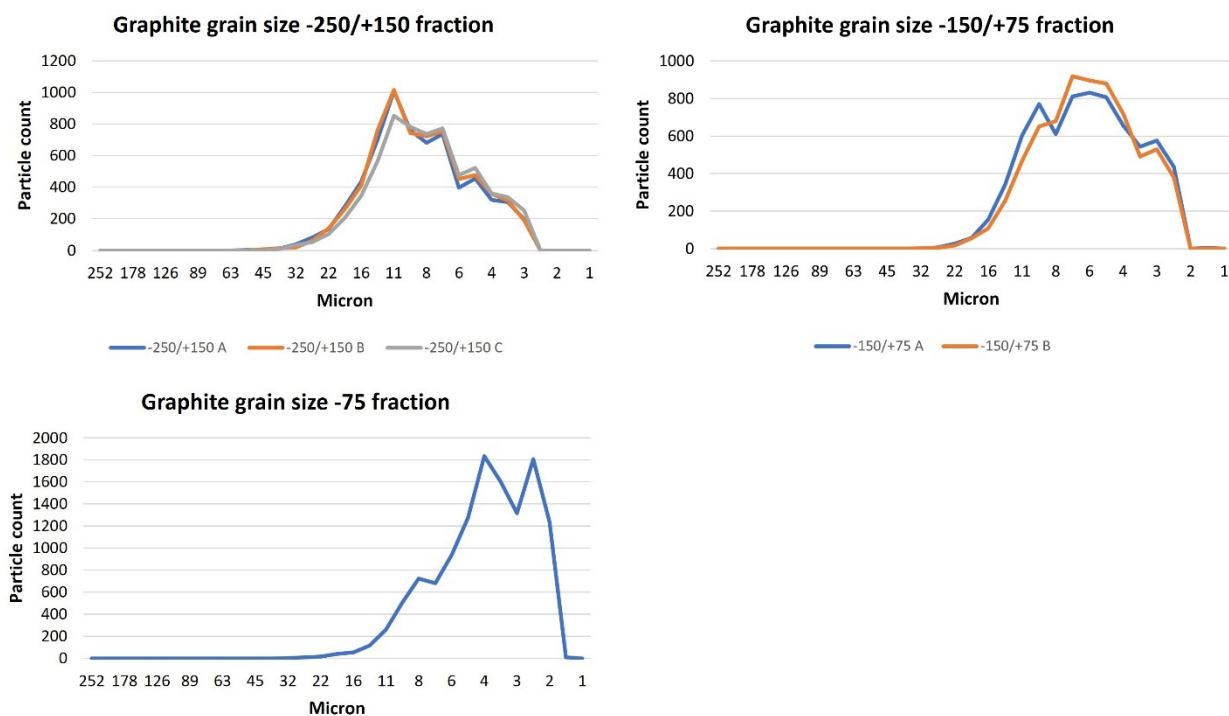


Figure L11. Graphs highlighting the grain size distribution data for graphite in the three size fractions analyzed from Sample QA2-CAM.

Mineral liberation data are provided for graphite, chalcopyrite, pyrite, pyrrhotite and sphalerite within excel file HG-22-18e. For graphite, the liberation data show that in the -250/+150 μm size fraction graphite liberation >70% ranges between 28.7-31.2%, 23.4-35.3% in the -150/+75 μm size fraction and 33.7% in the -75 μm size fraction.

L3.3 Sample XA3-CAM

L3.3.1 Modal mineralogy

The modal mineralogy data for Sample XA3-CAM for the three size fractions and replicate analyses are presented in Table L7 as mass %; the data presented as both mass % and also area % are also provided within excel file HG-22-18b. Mineral association data (excel file HG-22-18c), mineral size distribution data (excel file HG-22-18d) and mineral liberation data (excel file HG-22-18e) for the potential ore phases are also provided. In this summary major minerals form >10%, minor minerals 1-10% and trace minerals (<1%).

The -250/+150 μm size fraction for Sample XA3-CAM is composed of major quartz (30.53-30.93%), plagioclase (27.96-30.48%) and pyrrhotite (14.07-16.67%) along with minor orthoclase, muscovite, phlogopite, vermiculite, graphite (2.81-5.51%) and pyrite (0.76-1.12%). Trace phases present are: biotite, kaolinite, chlorite, clinopyroxene and amphibole, CaAl silicates, calcite, chalcopyrite (0.03-0.04%), sphalerite (0.01-0.21%), molybdenite (0.01%), Fe oxides, Ti oxides, titanite, apatite, zircon and monazite and "undifferentiated" (Table L7, Figures L12 and L13).

The -150/+75 µm size fraction for Sample XA3-CAM is composed of major quartz (35.05-35.35%), plagioclase (25.06-25.47%) and pyrrhotite (13.12-13.99%) along with minor orthoclase, muscovite, phlogopite, vermiculite and graphite (4.20-4.60%). Trace phases present are: biotite, kaolinite, chlorite, clinopyroxene and amphibole, CaAl silicates, calcite, pyrite (0.79%) chalcopyrite (0.02-0.08%), sphalerite (0.07-0.09%), molybdenite (0.01%), Fe oxides, Ti oxides, titanite, apatite, zircon and monazite and “undifferentiated” (Table L7, Figures L12 and L13).

The -75 µm size fraction for Sample XA3-CAM is composed of major quartz (34.31%), plagioclase (27.10%) and pyrrhotite (13.71%) along with minor orthoclase, muscovite, biotite, phlogopite, vermiculite, chlorite, CaAl silicates, graphite (1.66%) and pyrite (1.81%). Trace phases present are: kaolinite, clinopyroxene and amphibole, calcite, chalcopyrite (0.08%), sphalerite (0.14%), Fe oxides, Ti oxides, titanite, apatite, zircon and monazite and “undifferentiated” (Table L7, Figures L12 and L13).

Table L7. Quantitative mineralogy based on automated mineralogy Sample XA3-CAM.

Sample Number	XA3-CAM	XA3-CAM	XA3-CAM	XA3-CAM	XA3-CAM	XA3-CAM
Size Fraction (Microns)	-250/+150	-250/+150	-250/+150	-150/+75	-150/+75	-75
Replicate	A	B	C	A	B	
Quartz	30.53	30.76	30.93	35.05	35.35	34.31
Orthoclase	4.79	4.10	4.74	4.78	4.35	6.16
Plagioclase	29.04	30.48	27.96	25.06	25.47	27.10
Muscovite	1.30	1.26	1.24	1.35	1.42	1.61
Biotite	0.69	0.71	0.82	0.99	0.88	1.30
Phlogopite	8.60	9.23	9.52	9.41	9.13	6.36
Vermiculite	1.41	1.35	1.52	1.55	1.46	1.93
Kaolinite	0.15	0.15	0.11	0.14	0.12	0.18
Chlorite	0.73	0.82	0.85	0.91	0.79	1.07
Cpx and Amphibole	0.27	0.23	0.20	0.16	0.15	0.23
Ca Al Silicates	0.74	0.85	0.77	0.76	0.67	1.12
Graphite	2.81	3.73	5.51	4.60	4.20	1.66
Calcite	0.01	0.01	0.01	0.01	0.01	0.03
Pyrite	1.12	0.76	0.86	0.79	0.79	1.81
Pyrrhotite	16.67	14.56	14.07	13.12	13.99	13.71
Chalcopyrite	0.04	0.04	0.03	0.02	0.08	0.08
Sphalerite	0.11	0.01	0.21	0.09	0.07	0.14
Molybdenite	0.00	0.01	0.01	0.00	0.01	0.00
Fe Oxides	0.04	0.03	0.03	0.07	0.07	0.13
Ti Oxide	0.68	0.61	0.33	0.64	0.62	0.36
Titanite	0.09	0.08	0.07	0.11	0.07	0.11
Apatite	0.09	0.13	0.10	0.32	0.22	0.43
Zircon and Monazite	0.05	0.08	0.06	0.03	0.05	0.13
Undifferentiated	0.04	0.01	0.06	0.03	0.03	0.03
Total	100.00	100.00	100.00	100.00	100.00	100.00

Figure L12 demonstrates that there is very little variance in the modal mineralogy between both the different size fractions and the different replicates of the same size fraction, other than an apparent increase in quartz abundance in the -150/-75 and -75 µm size fractions relative to the -250/+150 µm size fraction. Figure L13 shows the abundance of graphite, chalcopyrite, sphalerite and molybdenite in the analyzed fractions / replicates. Graphite abundance ranges between 1.66 and 5.51%. Chalcopyrite abundance varies between 0.02 and 0.08%, whilst sphalerite ranges between 0.01 and 0.21%.

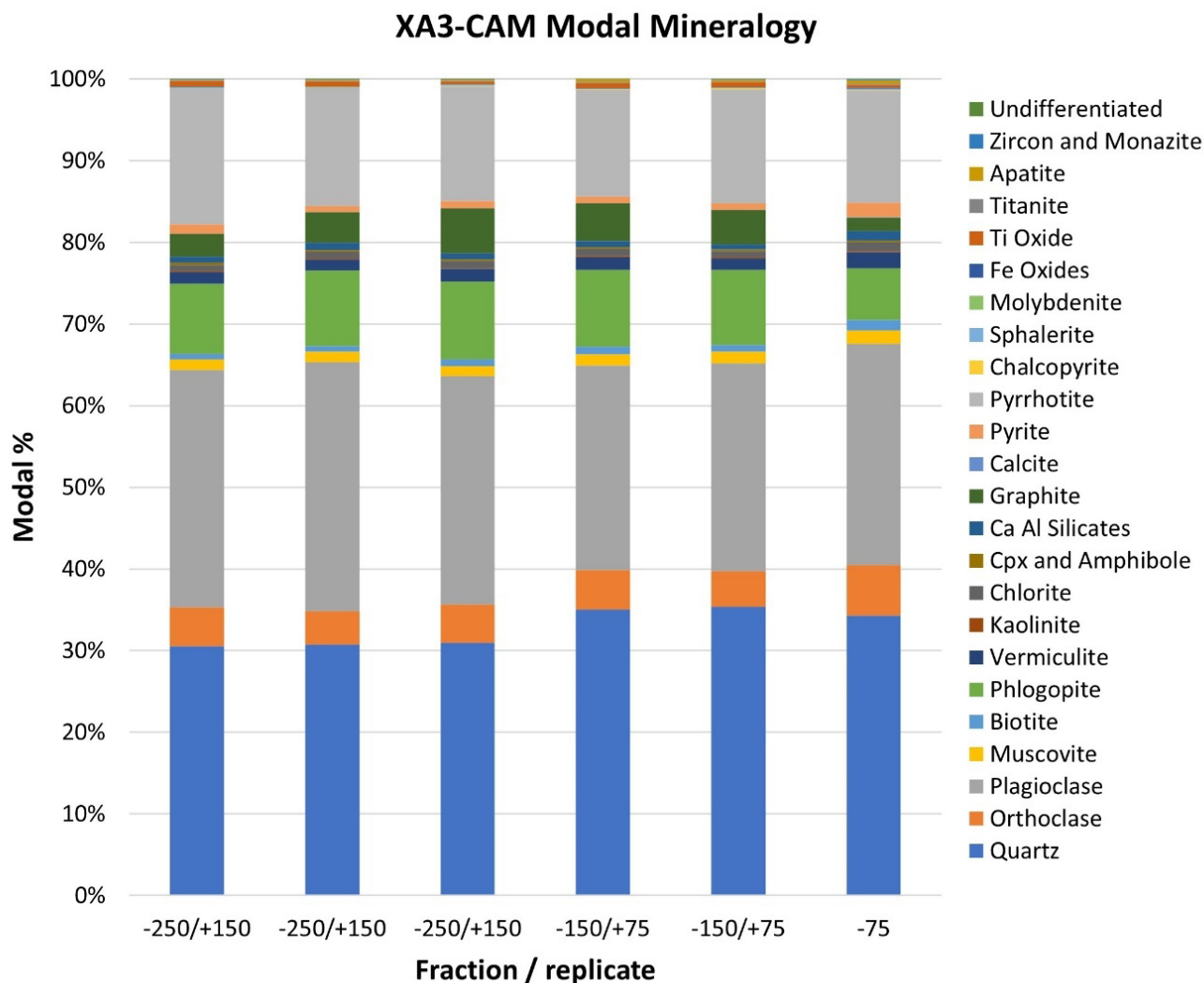


Figure L12. Modal mineralogy (mass %) all phases for Sample XA3-CAM

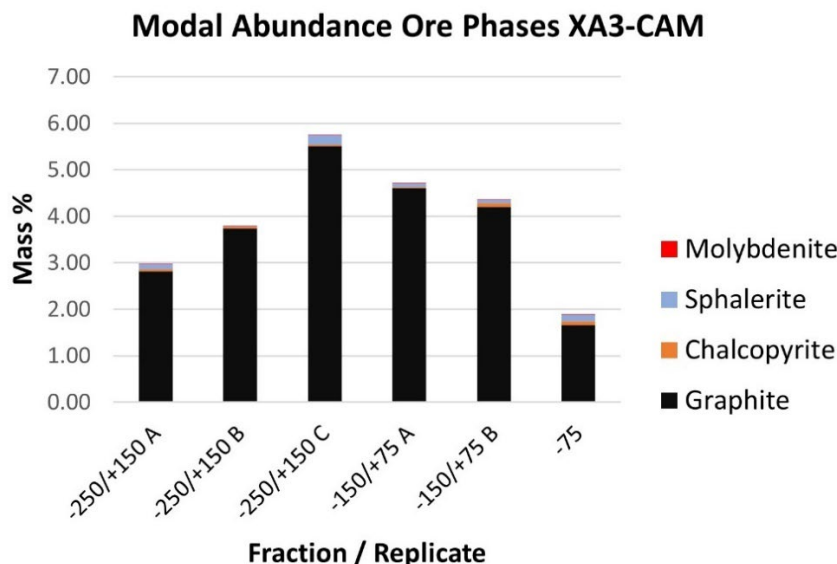


Figure L13. Modal mineralogy (mass %) ore phases for Sample XA3-CAM.

L3.3.2 AMICS and SEM-BSE imaging

AMICS particle images sample XA3-CAM A -250/+150

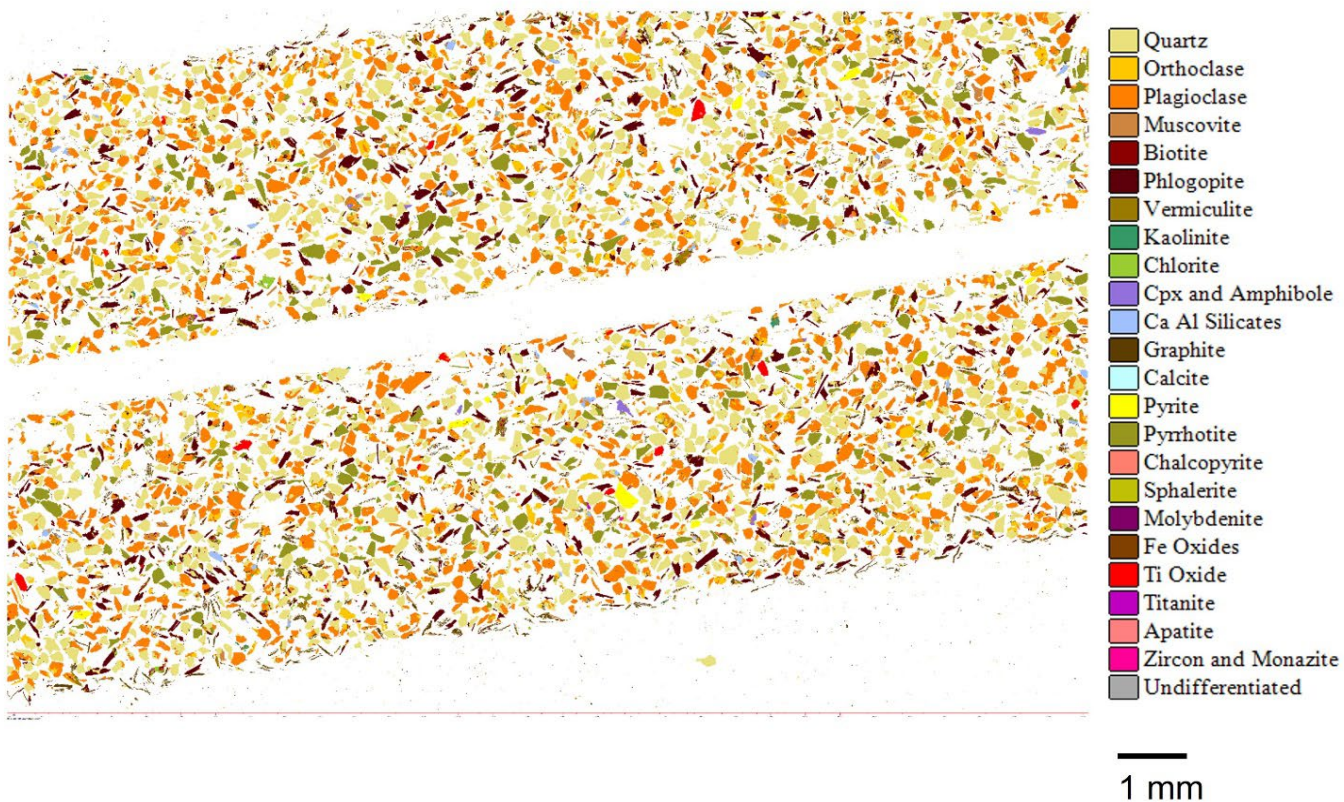


Figure L14. Representative example of AMICS particle images Sample XA3-CAM -250/+150 μm size fraction replicate A. Note that even within this, the coarsest size fraction, the mineral phases are characteristically well liberated.

AMICS particle textural images for Sample XA3-CAM are provided in powerpoint file HG-22-18h; high resolution images are provided electronically. The particle images provide the mineralogical data in overall textural context. Individual particles may be small rock fragments, or effectively liberated individual mineral grains. As can be seen in Figure L14, even within the -250/+150 µm size fraction for Sample XA3-CAM, the mineral phases are typically well liberated.

During AMICS measurement, a scanning electron microscope backscatter electron (SEM-BSE) image of the area measured is also collected. The SEM-BSE images are provided in powerpoint file HG-22-18h, along with the corresponding AMICS mineral images. An example is provided in Figure L15. High resolution “zoomable” images are also provided electronically. THE SEM-BSE images provide additional textural information and show the correspondence between the AMICS mineral “map” and the SEM-BSE image. Note the apparent high degree of mineral liberation.

(A) SEM-BSE and (B) AMICS particle images sample XA3-CAM A -250/+150 (enlarged)

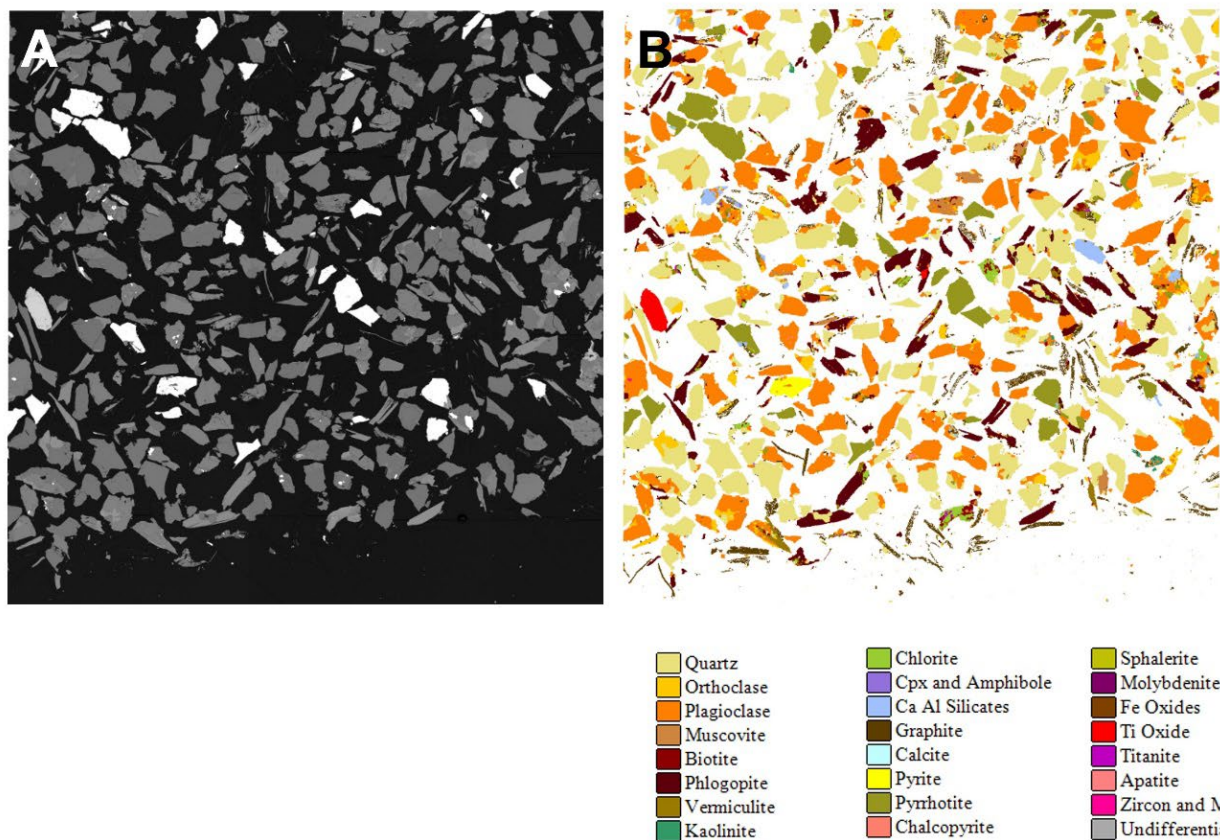


Figure L15. Higher magnification SEM-BSE image (A) and AMICS particle image (B) for the corresponding area Sample XA3-CAM -250/+150 µm size fraction replicate A. Note the clear correspondence between the AMICS and the SEM-BSE images.

L3.3.3 Mineral size, mineral liberation and mineral association data

Based on the AMICS analyses, three additional data sets are provided: mineral association data are provided for all phases and all samples within excel file HG-22-18c. These data are based on the observed transitions from one mineral to the adjoining mineral. Where there is a transition to “background” it shows that the mineral phase is surrounded by the resin i.e. the mineral grain is liberated. Mineral association data for graphite are summarised in Table 8. Graphite is predominantly (73.2-85.3%) associated with “background” i.e. is liberated or is associated with phlogopite (2.6-4.3%), vermiculite (1.8-4.3%), muscovite (1.0-1.2%), quartz (2.1-3.4%), plagioclase (2.3-5.0%), orthoclase (1.4-2.6%) and biotite (0.8-1.8%). Mineral associations for all other phases are <1%.

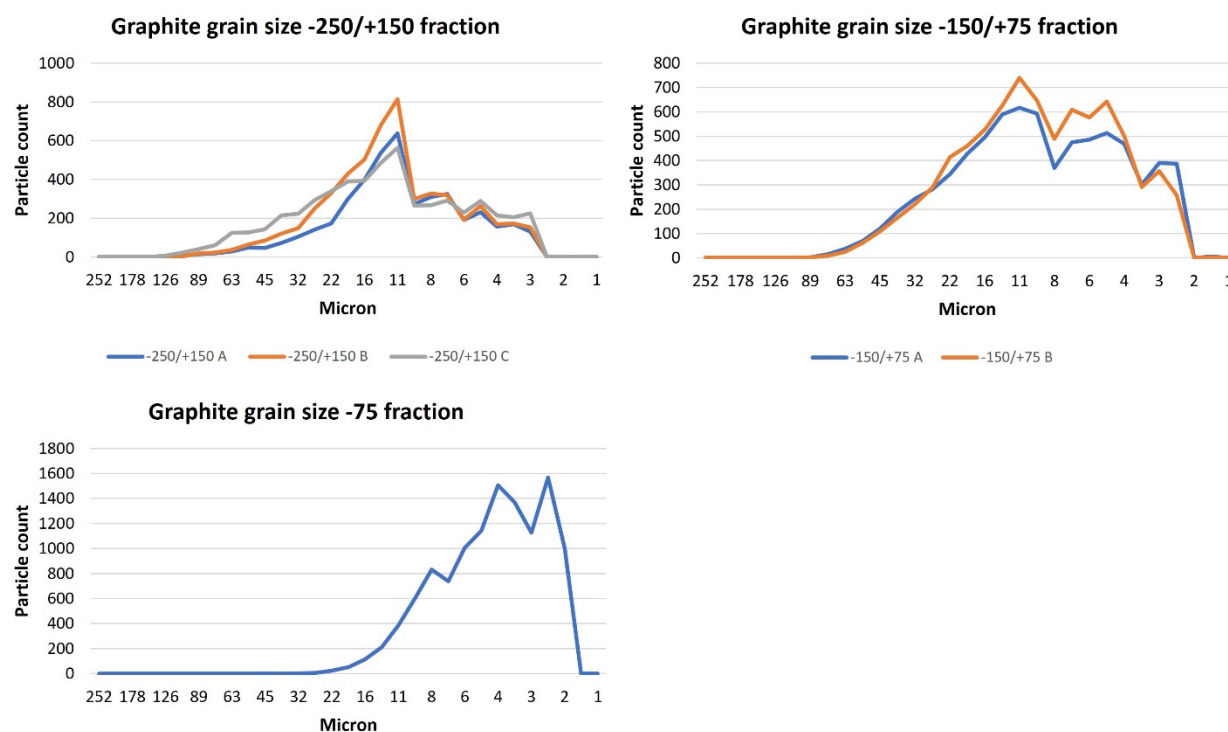


Figure L16. Graphs highlighting the grain size distribution data for graphite in the three size fractions analysed from Sample XA3-CAM.

Table L8. Graphite mineral association data Sample XA3-CAM.

Mineral	-250/+150 A	-250/+150 B	-250/+150 C	-150/+75 A	-150/+75 B	-75
Background	78.7	82.3	80.7	85.2	85.3	73.2
Quartz	3.2	2.7	3.3	2.1	2.1	3.4
Orthoclase	2.6	1.8	2.2	1.6	1.4	2.1
Plagioclase	3.9	3.4	3.7	2.3	2.4	5.0
Muscovite	1.2	1.1	1.1	1.1	1.0	1.6
Biotite	1.1	0.8	1.1	1.0	0.8	1.8
Phlogopite	4.1	3.0	3.4	2.6	3.1	4.3
Vermiculite	2.3	2.1	2.1	2.0	1.8	4.3
Kaolinite	0.4	0.4	0.2	0.2	0.2	0.2
Chlorite	0.9	0.9	0.9	0.7	0.7	1.8
Cpx and Amphibole	0.1	0.1	0.1	0.1	0.1	0.1
Ca Al Silicates	0.3	0.3	0.3	0.2	0.1	0.2
Graphite	0.0	0.0	0.0	0.0	0.0	0.0
Calcite	0.0	0.0	0.0	0.0	0.0	0.0
Pyrite	0.2	0.1	0.2	0.1	0.2	0.3
Pyrrhotite	0.7	0.6	0.5	0.4	0.5	0.8
Chalcopyrite	0.0	0.0	0.0	0.0	0.0	0.0
Sphalerite	0.0	0.0	0.0	0.0	0.0	0.0
Molybdenite	0.0	0.0	0.0	0.0	0.0	0.0
Fe Oxides	0.1	0.0	0.0	0.1	0.0	0.1
Ti Oxide	0.1	0.1	0.1	0.1	0.1	0.2
Titanite	0.1	0.1	0.1	0.1	0.0	0.1
Apatite	0.0	0.0	0.0	0.1	0.0	0.2
Zircon and Monazite	0.0	0.0	0.0	0.0	0.0	0.1
Undifferentiated	0.0	0.0	0.1	0.0	0.0	0.0

Mineral size distribution data are provided for graphite, chalcopyrite, pyrite, pyrrhotite and sphalerite within excel file HG-22-18d; size data for other reported phases are available on request. This provides mineral size data irrespective of whether or not the mineral phase is liberated. The grain size data for graphite are summarized in Figure L16. Within the -250/+150 µm size fraction, the graphite particles have a grain size ranging between 126 and 2 µm size, with a mode of 11 µm. Within the -150/+75 µm size fraction, the graphite particles have a grain size ranging between 89 and 2 µm size, with a mode of 11 µm. This reduces in the -75 µm size fraction with a range between 22 and 2 µm, with a mode of 2 µm. It should be noted that the AMICS grain size data are based on the measured 2D sample.

Mineral liberation data are provided for graphite, chalcopyrite, pyrite, pyrrhotite and sphalerite within excel file HG-22-18e. For graphite, the liberation data show that in the -250/+150 µm size fraction graphite liberation >70% ranges between 52-60.5%, 68.2-68.4% in the -150/+75 µm size fraction and 37.8% in the -75 µm size fraction.

L3.4 Sample YA4-CAM

L3.4.1 Modal mineralogy

The modal mineralogy data for Sample YA4-CAM for the three size fractions and replicate analyses are presented in Table 9 as mass %; the data presented as both mass % and also area % are also provided within excel file HG-22-18b. Mineral association data (excel file HG-22-18c), mineral size distribution data (excel file HG-22-18d) and mineral liberation data (excel file HG-22-18e) for the potential ore phases are also provided. In this summary major minerals form >10%, minor minerals 1-10% and trace minerals (<1%).

The -250/+150 µm size fraction for Sample YA4-CAM is composed of major quartz (29.95-30.57%) and plagioclase (30.52-31.15%) along with minor orthoclase, muscovite, phlogopite, vermiculite, chlorite, graphite (0.71-1.31%), pyrite (1.97-2.62%) and pyrrhotite (9.76-11.07%). Trace phases present are: biotite, kaolinite, clinopyroxene and amphibole, CaAl silicates, calcite, chalcopyrite (0.03-0.07%), sphalerite (0-0.08%), Fe oxides, Ti oxides, titanite, apatite, zircon and monazite and “undifferentiated” (Table L9, Figures L17 and L18).

The -150/+75 µm size fraction for Sample YA4-CAM is composed of major quartz (32.98-34.06%), plagioclase (25.86-28.04%) and pyrrhotite (8.91-10.78%) along with minor orthoclase, muscovite, phlogopite, vermiculite, chlorite and pyrite (1.80-2.09%). Trace phases present are: biotite, kaolinite, clinopyroxene and amphibole, CaAl silicates, graphite (0.56-0.57%) calcite, chalcopyrite (0.04%), sphalerite (0.03-0.04%), Fe oxides, Ti oxides, titanite, apatite, zircon and monazite and “undifferentiated” (Table L9, Figures L17 and L18).

The -75 µm size fraction for Sample YA4-CAM is composed of major quartz (31.96%) and plagioclase (27.71%) along with minor orthoclase, muscovite, biotite, phlogopite, vermiculite, chlorite, graphite (1.91%), calcite, pyrite (2.81%) and pyrrhotite (8.41%). Trace phases present are: kaolinite, clinopyroxene and amphibole, CaAl silicates, chalcopyrite (0.11%), sphalerite (0.10%), Fe oxides, Ti oxides, titanite, apatite, zircon and monazite and “undifferentiated” (Table L9, Figures L17 and L18).

Table L9. Quantitative mineralogy based on automated mineralogy Sample YA4-CAM.

Sample Number	YA4-CAM	YA4-CAM	YA4-CAM	YA4-CAM	YA4-CAM	YA4-CAM
Size Fraction (Microns)	-250/+150	-250/+150	-250/+150	-150/+75	-150/+75	-75
Replicate	A	B	C	A	B	
Quartz	29.95	29.97	30.57	32.98	34.06	31.96
Orthoclase	6.86	6.71	6.41	6.49	6.36	8.86
Plagioclase	31.13	30.52	31.15	25.86	28.04	27.71
Muscovite	3.19	3.00	3.37	3.18	3.01	3.26
Biotite	0.76	0.70	0.71	0.75	0.75	1.01
Phlogopite	7.45	7.66	8.01	8.85	8.63	4.47
Vermiculite	1.98	2.32	2.43	2.54	2.50	2.65
Kaolinite	0.04	0.04	0.03	0.04	0.02	0.07
Chlorite	3.10	2.86	3.28	3.59	3.52	3.77
Cpx and Amphibole	0.15	0.16	0.15	0.12	0.12	0.17
Ca Al Silicates	0.17	0.11	0.10	0.14	0.09	0.19
Graphite	1.31	0.84	0.71	0.57	0.56	1.91
Calcite	0.58	0.50	0.76	0.66	0.58	1.07
Pyrite	2.57	2.62	1.97	2.09	1.80	2.81
Pyrrhotite	9.97	11.07	9.76	10.78	8.91	8.41
Chalcopyrite	0.07	0.04	0.03	0.04	0.04	0.11
Sphalerite	0.00	0.08	0.00	0.04	0.03	0.10
Molybdenite	0.00	0.00	0.00	0.00	0.00	0.00
Fe Oxides	0.08	0.04	0.01	0.10	0.04	0.12
Ti Oxide	0.32	0.47	0.23	0.70	0.54	0.55
Titanite	0.09	0.09	0.11	0.10	0.12	0.13
Apatite	0.13	0.14	0.11	0.27	0.18	0.38
Zircon and Monazite	0.06	0.04	0.06	0.04	0.07	0.22
Undifferentiated	0.04	0.02	0.03	0.06	0.02	0.05
Total	100.00	100.00	100.00	100.00	100.00	100.00

Figure L17 demonstrates that there is very little variance in the modal mineralogy between both the different size fractions and the different replicates of the same size fraction. Figure L18 shows the abundance of graphite, chalcopyrite, sphalerite and molybdenite in the analyzed fractions / replicates. Graphite abundance ranges between 0.56 and 1.91%. Chalcopyrite abundance varies between 0.03 and 0.11%, whilst sphalerite ranges between 0 and 0.10%.

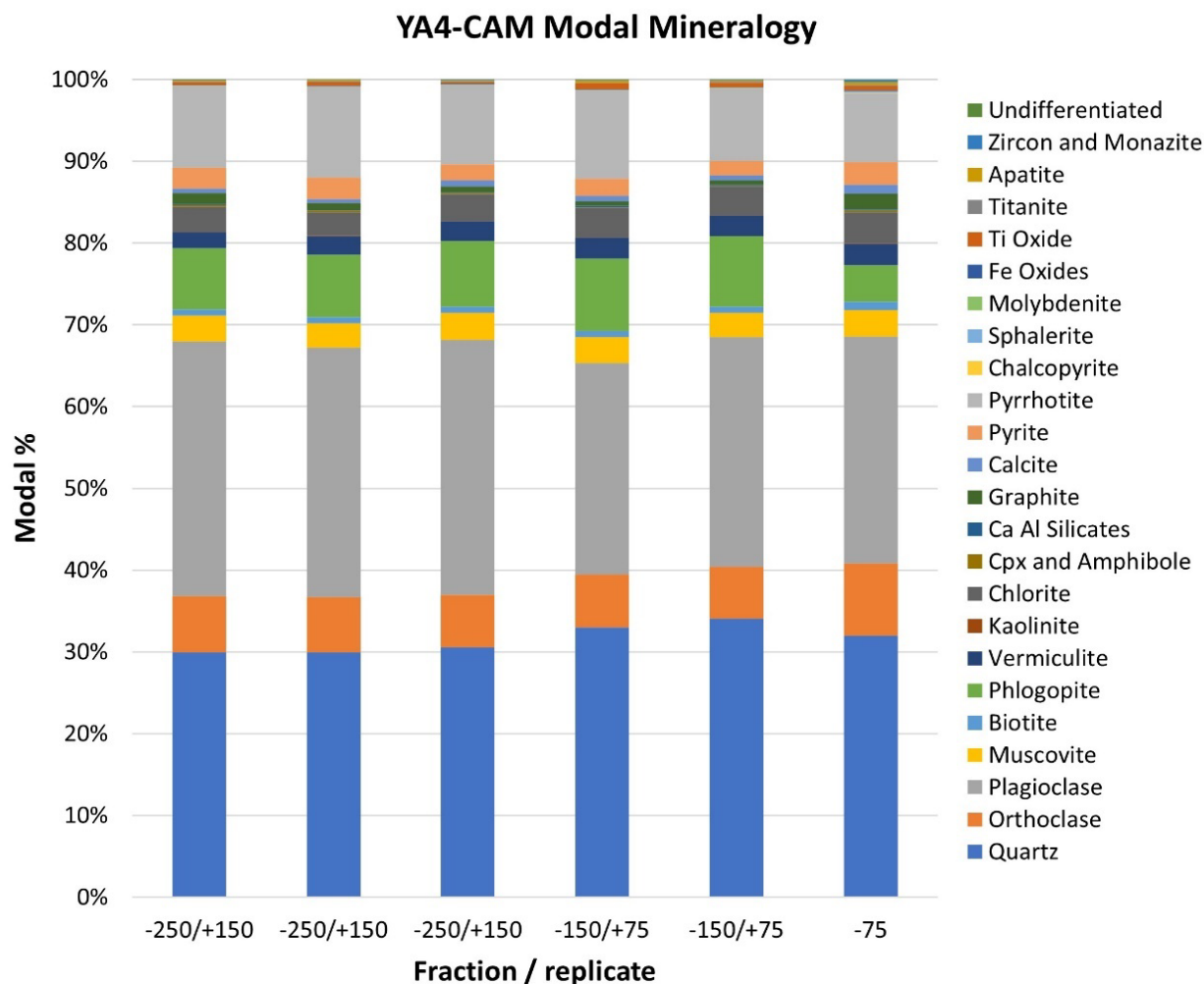


Figure L17. Modal mineralogy (mass %) all phases for Sample YA4-CAM

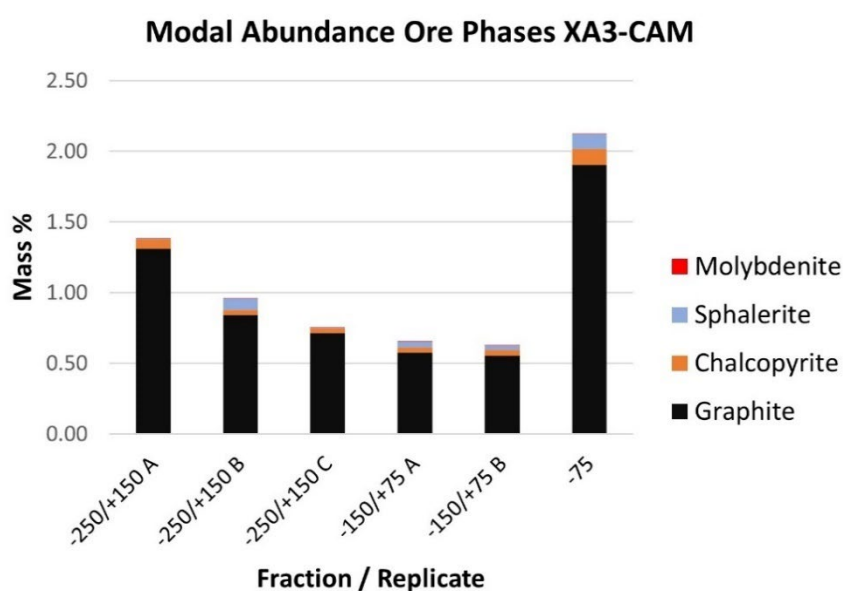


Figure L18. Modal mineralogy (mass %) ore phases for Sample YA4-CAM.

L3.4.2 AMICS and SEM-BSE imaging

AMICS particle textural images for Sample YA4-CAM are provided in powerpoint file HG-22-18i; high resolution images are provided electronically. The particle images provide the mineralogical data in overall textural context. Individual particles may be small rock fragments, or effectively liberated individual mineral grains. As can be seen in Figure L19, even within the -250/+150 µm size fraction for Sample YA4-CAM, the mineral phases are typically well liberated.

AMICS particle images sample YA4-CAM A -250/+150

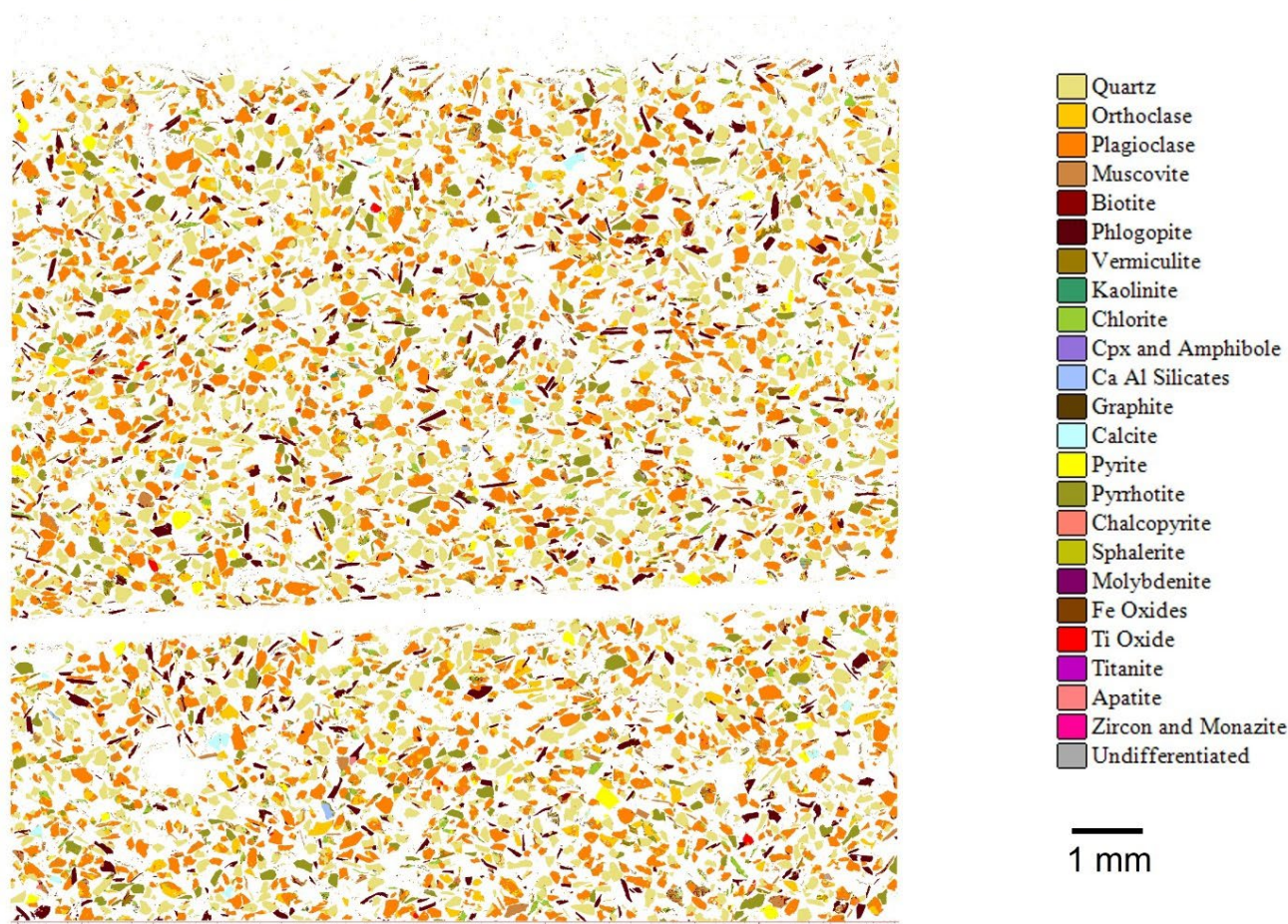


Figure L19. Representative example of AMICS particle images Sample YA4-CAM -250/+150 µm size fraction replicate A. Note that even within this, the coarsest size fraction, the mineral phases are characteristically well liberated.

During AMICS measurement, a scanning electron microscope backscatter electron (SEM-BSE) image of the area measured is also collected. The SEM-BSE images are provided in powerpoint file HG-22-18i, along with the corresponding AMICS mineral images. An example is provided in Figure L20. High resolution “zoomable” images are also provided electronically. THE SEM-BSE images provide additional textural information and show the correspondence between the AMICS mineral “map” and the SEM-BSE image. Note the apparent high degree of mineral liberation.

(A) SEM-BSE and (B) AMICS particle images sample YA4-CAM A -250/+150 (enlarged)

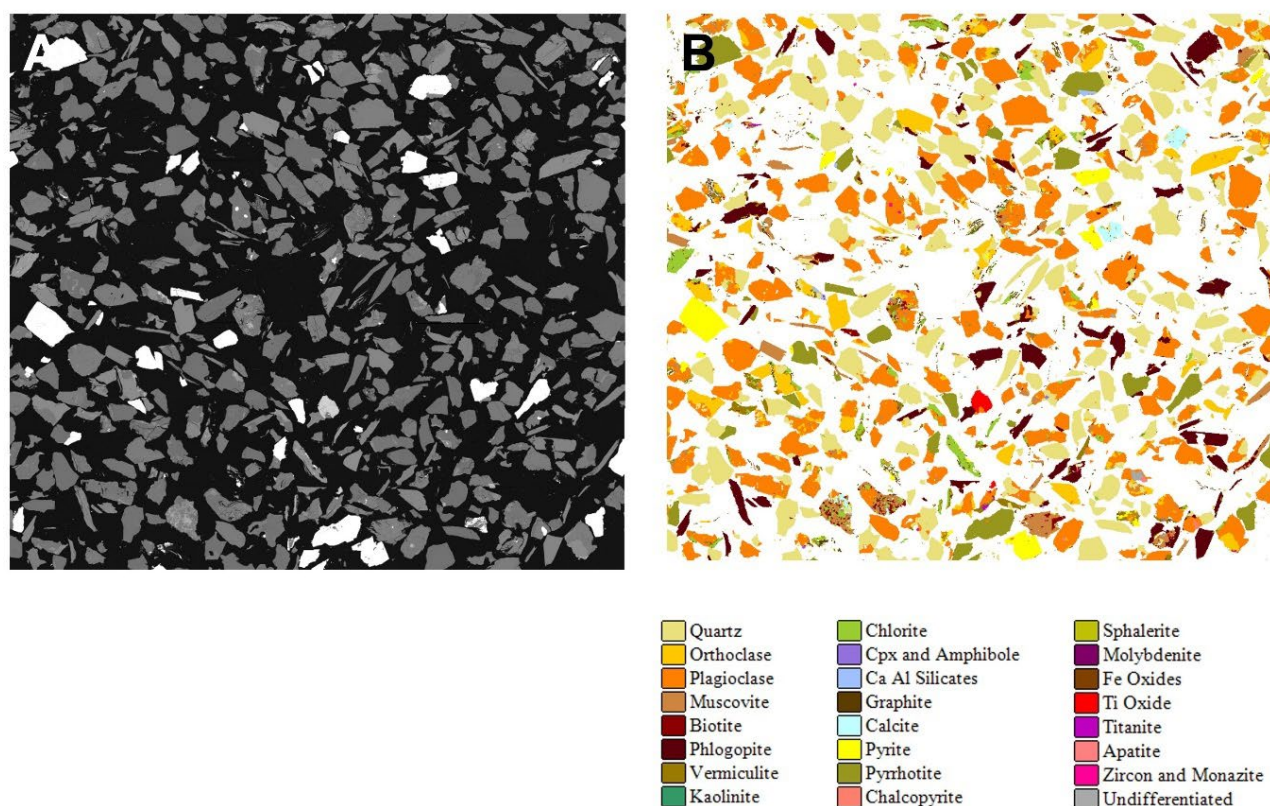


Figure L20. Higher magnification SEM-BSE image (A) and AMICS particle image (B) for the corresponding area Sample YA4-CAM -250/+150 µm size fraction replicate A. Note the clear correspondence between the AMICS and the SEM-BSE images.

L3.4.3 Mineral size, mineral liberation and mineral association data

Based on the AMICS analyses, three additional data sets are provided: mineral association data are provided for all phases and all samples within excel file HG-22-18c. These data are based on the observed transitions from one mineral to the adjoining mineral. Where there is a transition to “background” it shows that the mineral phase is surrounded by the resin i.e. the mineral grain is liberated. Mineral association data for graphite are summarized in Table K10. Graphite is predominantly (62.2-69%) associated with “background” i.e. is liberated or is associated with chlorite (6.8-9.4%), phlogopite (2.9-5.6%), vermiculite (4.6-6.6%), muscovite (3.0-3.9%), quartz (2.5-4.2%), plagioclase (4.2-6.4%), orthoclase (2.6-3.3%) and biotite (1.1-1.5%). Mineral associations for all other phases are <1%.

Table L10. Graphite mineral association data Sample YA4-CAM.

Mineral	-250/+150 A	-250/+150 B	-250/+150 C	-150/+75 A	-150/+75 B	-75
Background	68.0	69.0	63.1	62.4	62.2	63.2
Quartz	2.9	2.7	2.5	2.6	2.5	4.2
Orthoclase	2.9	3.2	3.3	2.6	2.7	3.1
Plagioclase	4.4	4.4	4.4	4.2	4.6	6.4
Muscovite	3.1	3.1	3.9	3.9	3.5	3.0
Biotite	1.1	1.1	1.5	1.2	1.3	1.2
Phlogopite	4.2	3.6	4.7	5.1	5.6	2.9
Vermiculite	4.6	4.7	5.7	6.6	6.6	5.6
Kaolinite	0.1	0.1	0.1	0.1	0.0	0.1
Chlorite	6.9	6.8	9.0	9.4	9.2	7.1
Cpx and Amphibole	0.1	0.1	0.1	0.1	0.1	0.1
Ca Al Silicates	0.1	0.0	0.1	0.1	0.1	0.1
Graphite	0.0	0.0	0.0	0.0	0.0	0.0
Calcite	0.3	0.2	0.3	0.2	0.3	1.0
Pyrite	0.3	0.4	0.5	0.2	0.3	0.6
Pyrrhotite	0.5	0.3	0.4	0.5	0.6	0.6
Chalcopyrite	0.0	0.0	0.0	0.0	0.0	0.0
Sphalerite	0.0	0.0	0.0	0.0	0.0	0.0
Molybdenite	0.0	0.0	0.0	0.0	0.0	0.0
Fe Oxides	0.0	0.0	0.0	0.1	0.1	0.1
Ti Oxide	0.1	0.1	0.1	0.2	0.2	0.2
Titanite	0.1	0.1	0.2	0.2	0.2	0.1
Apatite	0.0	0.1	0.0	0.1	0.1	0.2
Zircon and Monazite	0.0	0.0	0.0	0.0	0.0	0.1
Undifferentiated	0.0	0.0	0.0	0.1	0.0	0.1

Mineral size distribution data are provided for graphite, chalcopyrite, pyrite, pyrrhotite and sphalerite within excel file HG-22-18d; size data for other reported phases are available on request. This provides mineral size data irrespective of whether or not the mineral phase is liberated. The grain size data for graphite are summarized in Figure L21. Within the -250/+150 µm size fraction, the graphite particles have a grain size ranging between 45 and 3 µm size, with a mode of 11 µm. Within the -150/+75 µm size fraction, the graphite particles have a grain size ranging between 22 and 2 µm size, with a mode of 5 µm. Within the -75 µm size fraction the graphite particles have a grain size ranging between 22 and 2 µm, with a mode of 5 µm. It should be noted that the AMICS grain size data are based on the measured 2D sample.

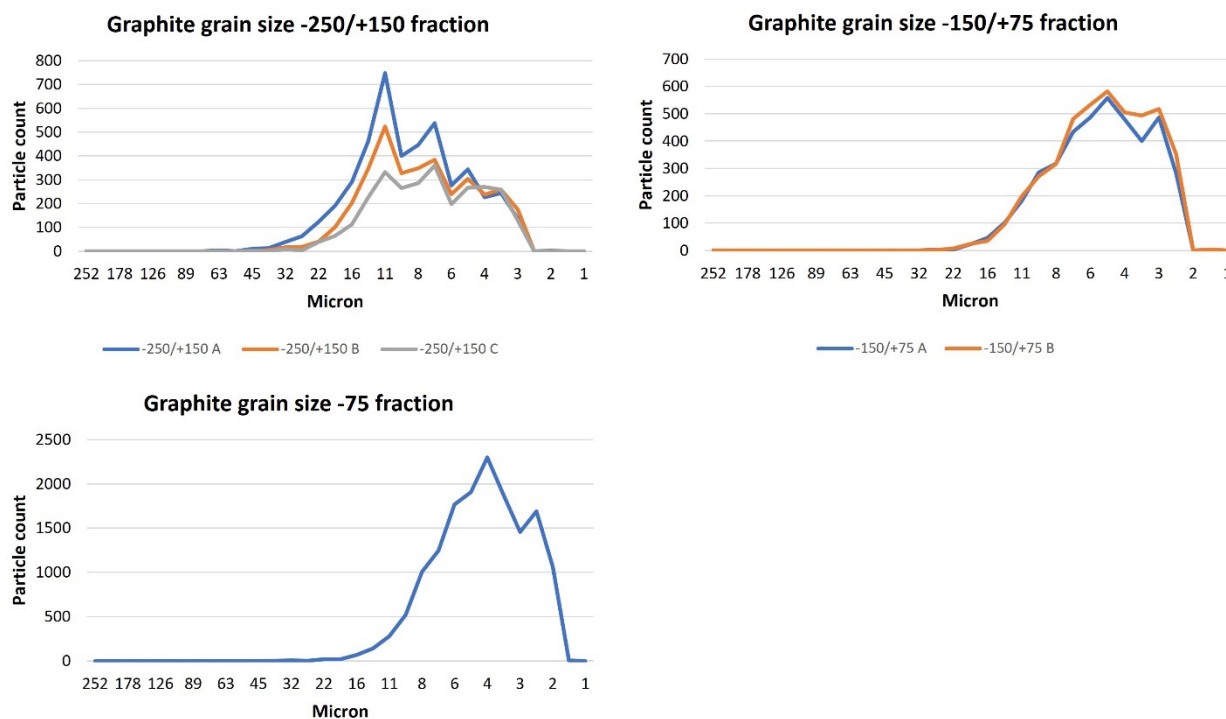


Figure L21. Graphs highlighting the grain size distribution data for graphite in the three size fractions analyzed from Sample YA4-CAM.

Mineral liberation data are provided for graphite, chalcopyrite, pyrite, pyrrhotite and sphalerite within excel file HG-22-18e. For graphite, the liberation data show that in the -250/+150 μm size fraction graphite liberation >70% ranges between 25.9-33.8%, 20.1-21.3% in the -150/+75 μm size fraction and 16.5% in the -75 μm size fraction.

L3.5 Sample ZA5-CAM

L3.5.1 Modal mineralogy

The modal mineralogy data for Sample ZA5-CAM for the three size fractions and replicate analyses are presented in Table K11 as mass %; the data presented as both mass % and also area % are also provided within excel file HG-22-18b. Mineral association data (excel file HG-22-18c), mineral size distribution data (excel file HG-22-18d) and mineral liberation data (excel file HG-22-18e) for the potential ore phases are also provided. In this summary major minerals form >10%, minor minerals 1-10% and trace minerals (<1%).

The -250/+150 μm size fraction for Sample ZA5-CAM is composed of major quartz (24.92-25.55%), plagioclase (22.33-23.68%), phlogopite (11.25-11.68%), and pyrrhotite (15.34-18.30%) along with minor orthoclase, muscovite, biotite, vermiculite, clinopyroxene and amphibole, CaAl silicates, graphite (3.57-5.83%) and pyrite (1.02-1.20%). Trace phases present are: kaolinite, chlorite, calcite, chalcopyrite (0.14-0.31%), sphalerite (0.53-0.90%), molybdenite, Fe oxides, Ti oxides, titanite, apatite, zircon and monazite and “undifferentiated” (Table L11, Figures L22 and L23).

The -150/+75 μm size fraction for Sample ZA5-CAM is composed of major quartz (30.34-30.83%), plagioclase (22.17-22.58%), phlogopite (12.58-12.67%), and pyrrhotite (14.01-14.25%) along with minor orthoclase, muscovite, biotite, vermiculite, clinopyroxene and amphibole, CaAl silicates, graphite (1.03-1.84%) and

pyrite (0.93-1.00%). Trace phases present are: kaolinite, chlorite, calcite, chalcopyrite (0.27-0.35%), sphalerite (0.38-0.68%), molybdenite, Fe oxides, Ti oxides, titanite, apatite, zircon and monazite and “undifferentiated” (Table L11, Figures L22 and L23).

The -75 µm size fraction for Sample ZA5-CAM is composed of major quartz (29.58%), plagioclase (22.79%) and pyrrhotite (14.70%) along with minor orthoclase, muscovite, biotite, phlogopite, vermiculite, chlorite, clinopyroxene and amphibole, CaAl silicates and pyrite (1.94%). Trace phases present are: kaolinite, graphite (0.77%), calcite, chalcopyrite (0.35%), sphalerite (0.68%), molybdenite, Fe oxides, Ti oxides, titanite, apatite, zircon and monazite and “undifferentiated” (Table L11, Figures L22 and L23).

Table L11. Quantitative mineralogy based on automated mineralogy Sample ZA5-CAM.

Sample Number	ZA5-CAM	ZA5-CAM	ZA5-CAM	ZA5-CAM	ZA5-CAM	ZA5-CAM
Size Fraction (Microns)	-250/+150	-250/+150	-250/+150	-150/+75	-150/+75	-75
Replicate	A	B	C	A	B	
Quartz	24.92	25.55	25.03	30.34	30.83	29.58
Orthoclase	4.55	3.98	4.00	4.60	4.86	5.78
Plagioclase	22.33	23.48	23.68	22.17	22.58	22.79
Muscovite	2.21	1.95	1.70	2.16	2.00	2.50
Biotite	1.00	1.04	1.00	1.27	1.23	1.70
Phlogopite	11.25	11.39	11.68	12.58	12.67	8.58
Vermiculite	1.77	1.98	1.77	2.10	2.02	2.68
Kaolinite	0.19	0.18	0.12	0.17	0.14	0.19
Chlorite	0.91	0.82	0.77	0.82	0.87	1.16
Cpx and Amphibole	2.72	3.38	3.31	2.78	2.60	2.59
Ca Al Silicates	2.13	2.14	2.36	1.86	2.13	2.51
Graphite	5.83	5.68	3.57	1.84	1.03	0.77
Calcite	0.01	0.02	0.02	0.03	0.04	0.05
Pyrite	1.20	1.14	1.02	1.00	0.93	1.94
Pyrrhotite	17.52	15.34	18.30	14.25	14.01	14.70
Chalcopyrite	0.14	0.15	0.31	0.35	0.27	0.35
Sphalerite	0.55	0.90	0.53	0.38	0.68	0.68
Molybdenite	0.01	0.01	0.01	0.01	0.01	0.01
Fe Oxides	0.08	0.06	0.04	0.12	0.07	0.17
Ti Oxide	0.28	0.31	0.28	0.46	0.23	0.27
Titanite	0.16	0.21	0.25	0.32	0.25	0.34
Apatite	0.16	0.17	0.16	0.34	0.48	0.56
Zircon and Monazite	0.03	0.07	0.03	0.02	0.03	0.07
Undifferentiated	0.05	0.04	0.06	0.05	0.06	0.04
Total	100.00	100.00	100.00	100.00	100.00	100.00

Figure L22 demonstrates that there is very little variance in the modal mineralogy between both the different size fractions and the different replicates of the same size fraction. Figure L23 shows the abundance of graphite, chalcopyrite, sphalerite and molybdenite in the analyzed fractions / replicates. Graphite abundance ranges between 0.77 and 5.83%. Chalcopyrite abundance varies between 0.14 and 0.35%, whilst sphalerite ranges between 0.38 and 0.90%.

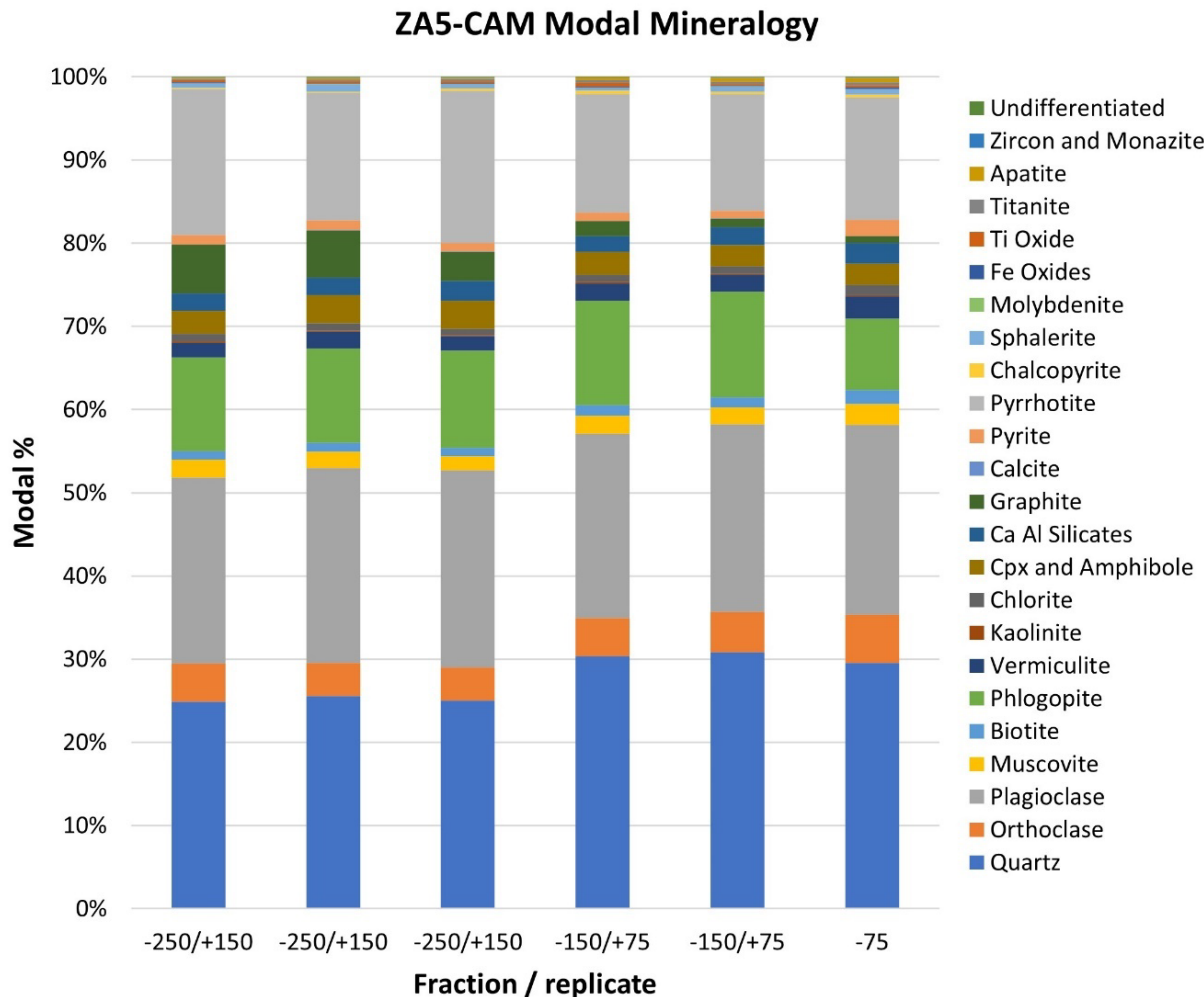


Figure L22. Modal mineralogy (mass %) all phases for Sample ZA5-CAM

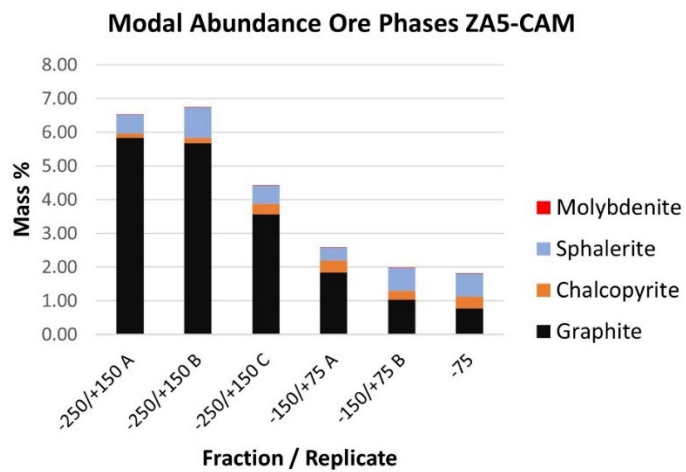


Figure L23. Modal mineralogy (mass %) ore phases for Sample ZA5-CAM.

L3.5.2 AMICS and SEM-BSE imaging

AMICS particle textural images for Sample ZA5-CAM are provided in powerpoint file HG-22-18j; high resolution images are provided electronically. The particle images provide the mineralogical data in overall textural context. Individual particles may be small rock fragments, or effectively liberated individual mineral grains. As can be seen in Figure L24, even within the -250/+150 µm size fraction for Sample ZA5-CAM, the mineral phases are typically well liberated.

AMICS particle images sample ZA5-CAM A -250/+150

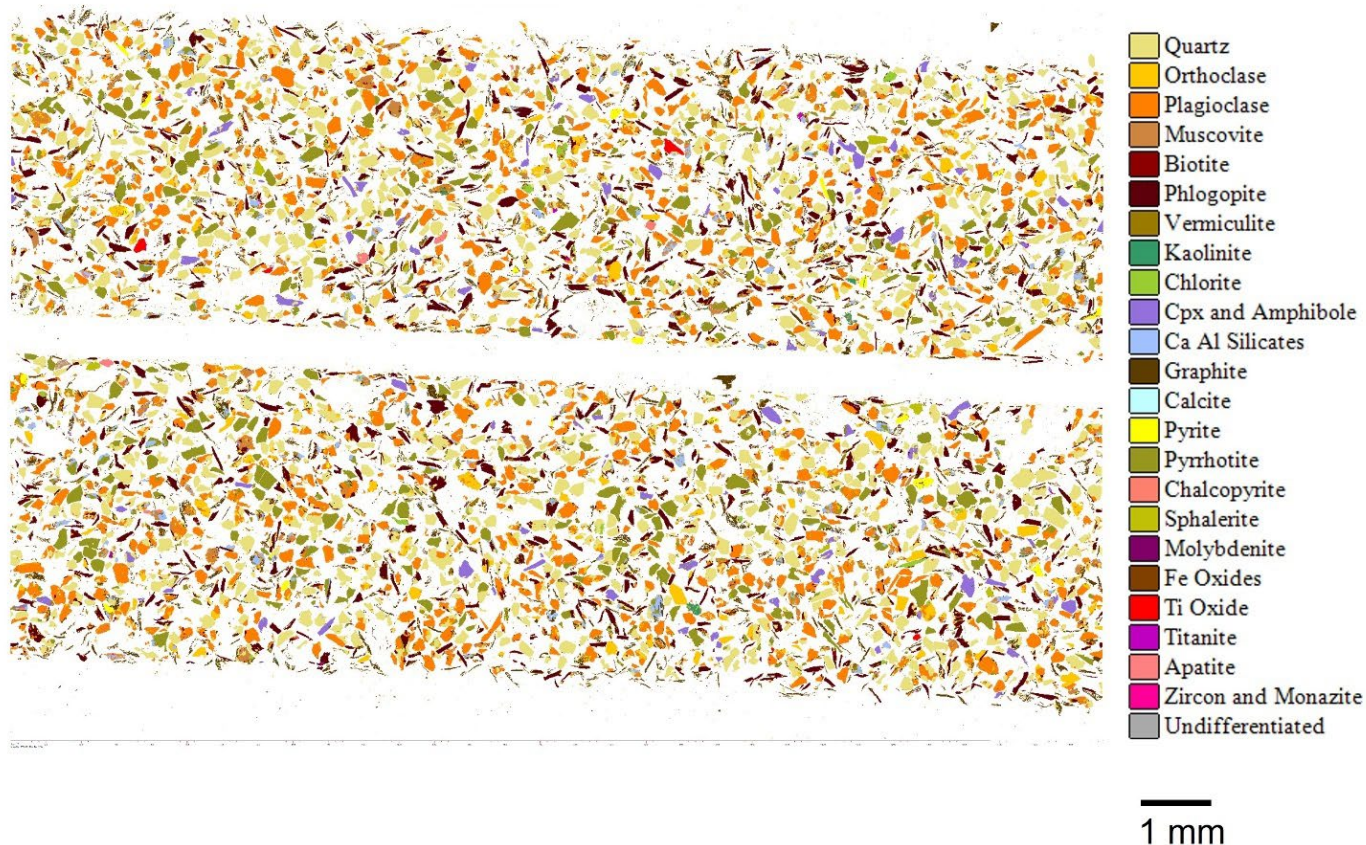


Figure L24. Representative example of AMICS particle images Sample ZA5-CAM -250/+150 µm size fraction replicate A. Note that even within this, the coarsest size fraction, the mineral phases are characteristically well liberated.

During AMICS measurement, a scanning electron microscope backscatter electron (SEM-BSE) image of the area measured is also collected. The SEM-BSE images are provided in powerpoint file HG-22-18j, along with the corresponding AMICS mineral images. An example is provided in Figure K25. High resolution “zoomable” images are also provided electronically. THE SEM-BSE images provide additional textural information and show the correspondence between the AMICS mineral “map” and the SEM-BSE image. Note the apparent high degree of mineral liberation.

(A) SEM-BSE and (B) AMICS particle images sample ZA5-CAM A -250/+150 (enlarged)

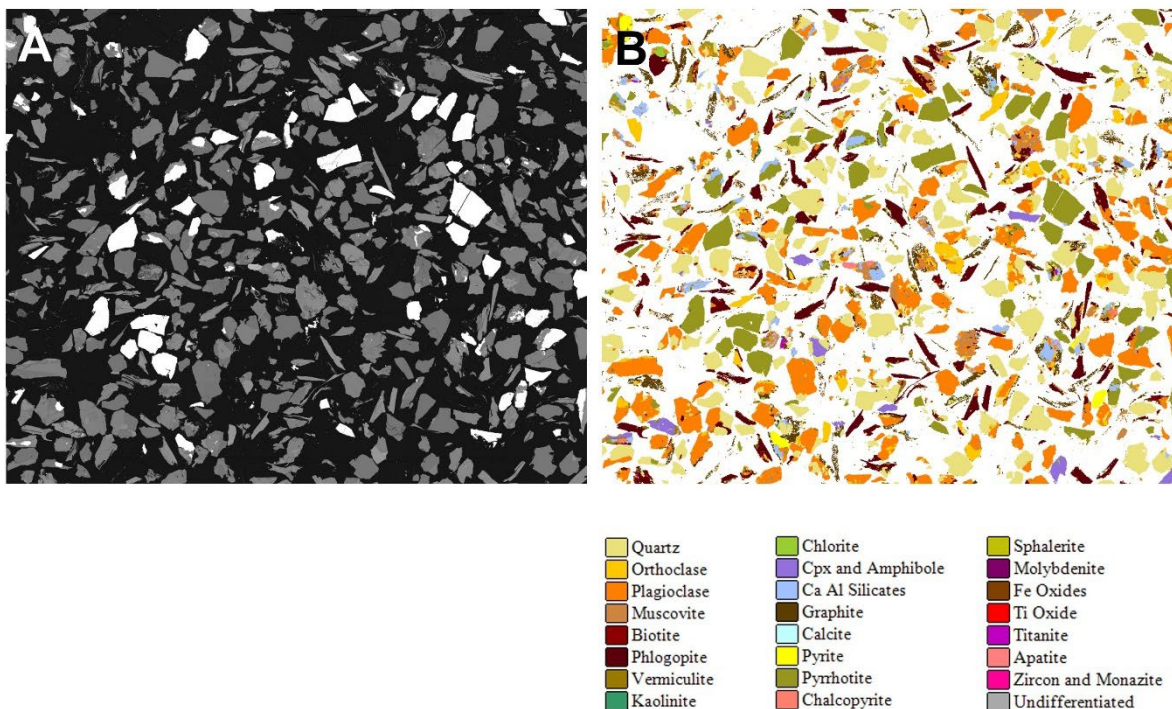


Figure L25. Higher magnification SEM-BSE image (A) and AMICS particle image (B) for the corresponding area Sample ZA5-CAM - 250/+150 µm size fraction replicate A. Note the clear correspondence between the AMICS and the SEM-BSE images.

L3.5.3 Mineral size, mineral liberation and mineral association data

Based on the AMICS analyses, three additional data sets are provided: mineral association data are provided for all phases and all samples within excel file HG-22-18c. These data are based on the observed transitions from one mineral to the adjoining mineral. Where there is a transition to “background” it shows that the mineral phase is surrounded by the resin i.e. the mineral grain is liberated. Mineral association data for graphite are summarized in Table L12. Graphite is predominantly (64.4-80.5%) associated with “background” i.e. is liberated or is associated with chlorite (0.9-2.4%), phlogopite (3.7-6.6%), vermiculite (2.3-6.1%), muscovite (1.2-2.6%), quartz (2.1-3.0%), plagioclase (3.3-5.8%), orthoclase (1.5-2.4%) and biotite (1.1-2.6%). Mineral associations for all other phases are <1%.

Table L12. Graphite mineral association data Sample ZA5-CAM.

Mineral	-250/+150 A	-250/+150 B	-250/+150 C	-150/+75 A	-150/+75 B	-75
Background	78.9	80.5	80.0	77.7	70.7	64.4
Quartz	2.9	2.5	2.4	2.1	2.3	3.0
Orthoclase	1.8	1.5	1.6	1.5	2.0	2.4
Plagioclase	3.9	3.5	3.7	3.3	4.4	5.8
Muscovite	1.5	1.2	1.2	1.7	2.6	2.3
Biotite	1.2	1.2	1.1	1.6	2.0	2.6
Phlogopite	3.8	3.7	4.0	5.0	6.6	6.6
Vermiculite	2.4	2.5	2.3	3.4	4.3	6.1
Kaolinite	0.3	0.3	0.2	0.5	0.3	0.3
Chlorite	0.9	0.8	0.9	1.2	1.7	2.4
Cpx and Amphibole	0.3	0.3	0.3	0.4	0.6	0.6
Ca Al Silicates	0.8	0.6	0.9	0.5	0.8	0.7
Graphite	0.0	0.0	0.0	0.0	0.0	0.0
Calcite	0.0	0.0	0.0	0.0	0.0	0.0
Pyrite	0.3	0.3	0.2	0.3	0.3	0.5
Pyrrhotite	0.6	0.6	0.6	0.5	0.8	1.2
Chalcopyrite	0.0	0.0	0.1	0.0	0.0	0.1
Sphalerite	0.1	0.1	0.1	0.0	0.1	0.2
Molybdenite	0.0	0.0	0.0	0.0	0.0	0.0
Fe Oxides	0.0	0.0	0.0	0.0	0.1	0.2
Ti Oxide	0.0	0.0	0.1	0.1	0.1	0.1
Titanite	0.1	0.1	0.2	0.1	0.1	0.2
Apatite	0.0	0.0	0.0	0.0	0.1	0.2
Zircon and Monazite	0.0	0.0	0.0	0.0	0.0	0.0
Undifferentiated	0.1	0.0	0.0	0.0	0.0	0.0

Mineral size distribution data are provided for graphite, chalcopyrite, pyrite, pyrrhotite and sphalerite within excel file HG-22-18d; size data for other reported phases are available on request. This provides mineral size data irrespective of whether or not the mineral phase is liberated. The grain size data for graphite are summarized in Figure L26. Within the -250/+150 µm size fraction, the graphite particles have a grain size ranging between 89 and 3 µm size, with a mode of 11 µm. Within the -150/+75 µm size fraction, the graphite particles have a grain size ranging between 32 and 2 µm size, with a mode of 9 µm. Within the -75 µm size fraction the graphite particles have a grain size ranging between 16 and 2 µm, with a mode of 4 µm. It should be noted that the AMICS grain size data are based on the measured 2D sample.

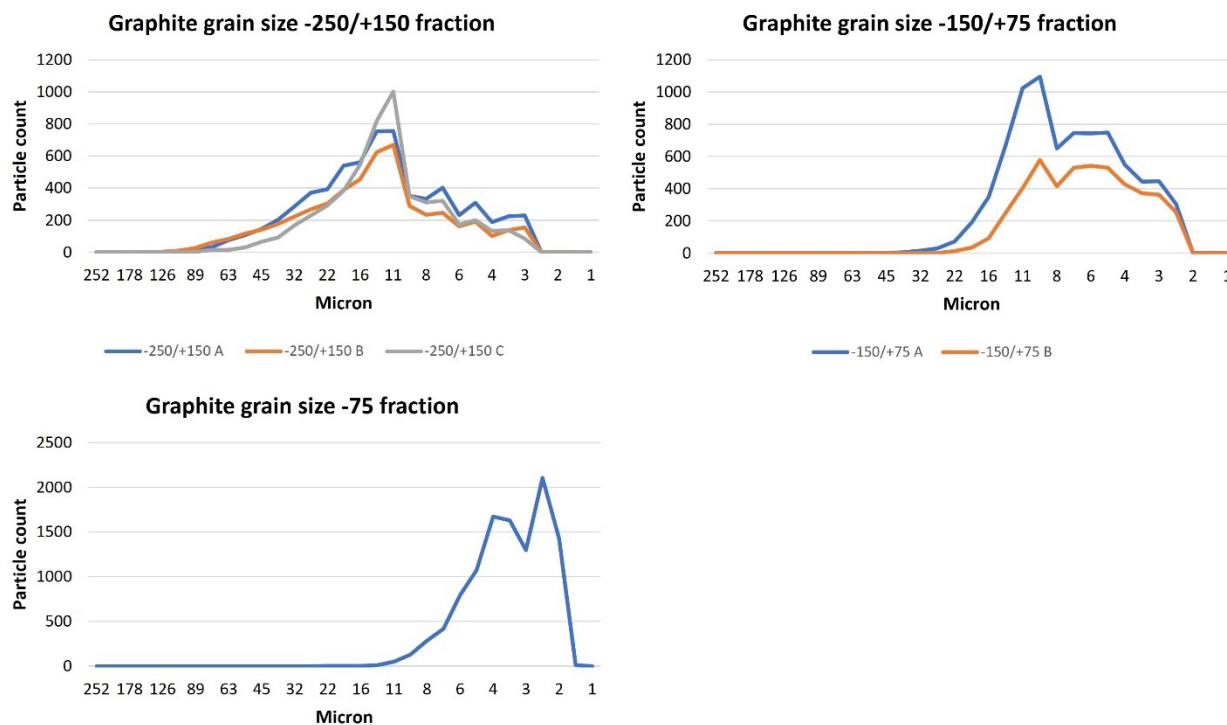


Figure L26. Graphs highlighting the grain size distribution data for graphite in the three size fractions analyzed from Sample ZA5-CAM.

Mineral liberation data are provided for graphite, chalcopyrite, pyrite, pyrrhotite and sphalerite within excel file HG-22-18e. For graphite, the liberation data show that in the -250/+150 μm size fraction graphite liberation >70% ranges between 52-54.5%, 33.8-46.4% in the -150/+75 μm size fraction and 12.2% in the -75 μm size fraction.

L4. References

SCHULTZ, B., SANDMANN, D. & GILBRICHT, S. 2020. SEM-based automated mineralogy and its application in geo- and material sciences. *Minerals*, **10**, 1004; doi:10.3390/min10111004.